

Geological Fieldwork 2025

A Summary of Field Activities and Current Research

BRITISH COLUMBIA
Ministry of Mining and Critical Minerals

Paper 2026-01

BRITISH COLUMBIA

Ministry of Mining and Critical Minerals

Geological Fieldwork 2025

A Summary of Field Activities and Current Research

Ministry of Mining and Critical Minerals
British Columbia Geological Survey

Paper 2026-01

Ministry of Mining and Critical Minerals
Mines Competitiveness and Authorizations Division
British Columbia Geological Survey

Recommended citation format for individual papers:

Ootes, L., Wall, C., and Mihalynuk, M.G., 2026. Rossland Group extends north: Detrital zircon U-Pb ages allow supracrustal unit reassignments in southern British Columbia and have tectonic implications. In: Geological Fieldwork 2025, British Columbia Ministry of Mining and Critical Minerals, British Columbia Geological Survey Paper 2026-01, pp. 119-130.

Front Cover:
Traversing along treeline on the Scud River stock (185 Ma; Cone Mountain plutonic suite), looking north to the Scud glacier, near the Galore Creek deposit. See Campbell, R.W., Gibson, K., van Straaten, B.I., Creaser, R.A., and Oliver, J., 2026. Paleozoic to Eocene intrusions in the Golden Triangle, northwestern British Columbia: A project update. In: Geological Fieldwork 2025, British Columbia Ministry of Mining and Critical Minerals, British Columbia Geological Survey Paper 2026-01, this volume. **Photo by Benjamin Johnstone.**

Back Cover:
Traversing along the eastern slope of Mt. Johnny, studying lower Hazelton Group stratigraphy in northwestern British Columbia. See van Straaten, B.I., 2026. A Triassic-Jurassic stratigraphic framework for the Golden Triangle, northwestern British Columbia: A project update. In: Geological Fieldwork 2025, British Columbia Ministry of Mining and Critical Minerals, British Columbia Geological Survey Paper 2026-01, this volume. **Photo by Rafael Bacha.**

This publication is available, free of charge, from the British Columbia Geological Survey website:
https://www2.gov.bc.ca/gov/content/industry/mineral-exploration-mining/british-columbia-geological-survey/publications

British Columbia Cataloguing in Publication Data

Main entry under title:

Geological Fieldwork: - 1974 -

Annual.

Issuing body varies

Vols. for 1978-1996 issued in series: Paper / British Columbia. Ministry of Energy, Mines and Petroleum Resources; vols. for 1997 - 1998, Paper / British Columbia. Ministry of Employment and Investment; vols. for 1999-2004, Paper / British Columbia. Ministry of Energy and Mines; vols. for 2005-2009, Paper / British Columbia. Ministry of Energy, Mines and Petroleum Resources; vols. for 2010, Paper / British Columbia. Ministry of Forests, Mines and Lands; vols. for 2011, Paper / British Columbia. Ministry of Energy and Mines; vols. for 2012- , Paper / British Columbia. Ministry of Energy, Mines and Natural Gas; vols. for 2014- , Paper / British Columbia. Ministry of Energy and Mines; vols. for 2018- , Paper / British Columbia. Ministry of Energy, Mines and Petroleum Resources; vols. for 2021- , Paper / British Columbia. Ministry of Energy, Mines and Low Carbon Innovation.

Includes Bibliographical references.

ISSN 0381-243X=Geological Fieldwork

1. Geology - British Columbia - Periodicals. 2. Mines and mineral resources - British Columbia - Periodicals. 3. Geology - Fieldwork - Periodicals. 4. Geology, Economic - British Columbia - Periodicals. 5. British Columbia. Geological Survey Branch - Periodicals. I. British Columbia. Geological Division. II. British Columbia. Geological Survey Branch. III. British Columbia. Geological Survey Branch. IV. British Columbia. Dept. of Mines and Petroleum Resources. V. British Columbia. Ministry of Energy, Mines and Petroleum Resources. VI. British Columbia. Ministry of Employment and Investment. VII. British Columbia Ministry of Energy and Mines. VIII. Series: Paper (British Columbia. Ministry of Energy, Mines and Petroleum Resources). IX. Series: Paper (British Columbia. Ministry of Employment and Investment). X. Series: Paper (British Columbia Ministry of Energy and Mines). XI. Series: Paper (British Columbia Ministry of Energy, Mines and Petroleum Resources). XII. Series: Paper (British Columbia Ministry of Forests, Mines and Lands). XIII. Series: Paper (British Columbia Ministry of Energy and Mines). XIV. Series: Paper (British Columbia Ministry of Energy, Mines and Natural Gas). XV. Series: Paper (British Columbia Ministry of Energy and Mines). XVI. Series: Paper (British Columbia Ministry of Energy, Mines and Petroleum Resources). XVII. Series: Paper (British Columbia Ministry of Energy, Mines and Low Carbon Innovation).

QE187.46 622.1’09711 C76-083084-3 (Rev.)

Victoria
British Columbia
Canada

April 2026

Preface

Geological Fieldwork 2025

Geological Fieldwork 2025 is the fifty-first edition of the annual volume that presents peer-reviewed papers detailing the results of British Columbia Geological Survey (BCGS) geoscience activities. This work is freely available through the online BCGS Publication Catalogue. The Survey also produces a wide range of reports, maps, and databases, and contributes to peer-reviewed journals and partner publications throughout the year. In addition, BCGS releases a companion volume, Mining and Exploration in British Columbia, the latest in a series of annual reviews that dates back to 1874.

As is tradition, the first paper in the volume, by Brideau et al., provides an overview of Survey activities in 2025. The second paper, by Hickin, highlights the contributions made by the Survey in the last five years to the Pan-Canadian Geoscience Strategy, a federal, provincial, and territorial collaboration that articulates the common needs and goals of geoscience organizations in Canada. Through its engagement program, BCGS is connecting Indigenous groups, local communities, government, the minerals industry, and the public to the geology and mineral resources of the province. Bacha outlines the developing data sharing initiatives that the Survey is using to build trust and exchange knowledge with Indigenous communities.

The continued importance of critical minerals research at the Survey is reflected by several papers in this volume. Ootes et al. summarize the workflow to identify mineralogic controls on critical companion metal distribution using samples from the historical Sullivan lead-zinc-silver deposit as an example. Wei et al. continued to examine critical metal concentrations and partitioning in volcanogenic massive sulphide deposits from across the province. Graham et al. examine critical companion metals at the Schaft Creek, Mount Polley, and New Afton porphyry deposits, and Bain et al. focus on platinum group minerals at the New Afton deposit. Rukhlov et al., take a multi-analytical approach to test exploration tools that use stream-sediment samples to fingerprint upstream carbonatite-hosted niobium, tantalum, rare earth element, and other critical mineral deposits.



Foundational mapping, geochronology, and geochemistry are also reflected in numerous papers. In a second paper, Ootes et al. use detrital zircon U-Pb data to reassess the distribution of rock units at the transition between Quesnellia and Ancestral North America to propose a provocative but testable tectonic model that challenges conventional views. Working in the Golden Triangle, which hosts numerous porphyry, epithermal, and VMS deposits, Campbell et al. give a progress report on continued work to establish a regional framework for intrusive rocks, and van Straaten reports on a study of stratigraphic relationships aimed at better understanding the tectonic and metallogenic evolution of the region. Zagorevski et al. use radiolarian biostratigraphy to re-evaluate terranes in the northern Cordillera of British Columbia and Yukon. Mihalynuk and Gabites confirm an Oligocene age of ca. 24 Ma for polymetallic porphyry-related breccias at the Giant Copper deposit using $^{40}Ar/^{39}Ar$ biotite data. Two Emeritus Scientists contributed to the volume this year, releasing previously unpublished geochronologic data. Nelson provides precise U-Pb zircon ages from samples of the Wark-Colquitz complex in downtown Victoria, and Ferri and Friedman report vintage U-Pb zircon data from the central part of the province in two papers, one from the Lay Range assemblage, one from the Snowshoe Group.

The British Columbia geoscience Spatial Data Infrastructure (BCgSDI) project represents the most significant enhancement being carried out at the Survey related to information systems and data delivery. Cui et al. profile this project, which is integrating geoscience and mineral resource databases into a single unified system ready for advanced analytics and emerging technology such as large language models and artificial intelligence. The approach being used by the Survey offers a practical template for similar modernizations at other agencies. The Survey continues to integrate bedrock maps into BC Digital Geology, and Elia and Ferbey report on a complementary project to compile digital surficial geology mapping in the Interior Plateau. Brideau et al. present a preliminary iteration of a landslide database for British Columbia, providing initial desktop-level information of known landslides to local governments, practitioners, and researchers. Zhang et al. provide a preliminary version of a geoscience knowledge index map, the first geospatial compilation of publicly available geoscience information footprints for British Columbia.

This year marks the conclusion of three years of significant provincial investment in critical minerals geoscience at BCGS. These funds have effectively levered major federal programs, such as Geomapping for Energy and Minerals (GEM-GeoNorth) and the Critical Minerals and Geoscience Data (CMGD) initiative, substantially strengthening the Survey's capacity to evaluate and better understand British Columbia's critical minerals potential. Alongside the many publications released during this period, we look forward to sharing the substantial new data, ongoing research, and value added insights that this investment continues to make possible.

The year has not been without its challenges. Although the Survey has experienced modest growth in recent years, efforts to replace departing staff have been hindered by ongoing provincial fiscal restraint. Job action by the British Columbia General Employees' Union (BCGEU) and the Professional Employees Association (PEA) in the fall of 2025 led to a two month strike that delayed numerous publications, slowed sample submissions and analytical work, and resulted in the cancellation of the BCGS annual Open House. Despite these setbacks, BCGS staff rose to the occasion and still delivered 75 publications in 2025, a testament to their professionalism, resilience, and commitment to public geoscience.

The need for strong, trusted public geoscience has never been more important. In a world marked by geopolitical instability, conflicts that disrupt global energy and mineral supply chains, and unpredictable trade barriers, securing sustainable access to raw materials is essential. British Columbia, and Canada as a whole, stand out as stable, mineral-rich jurisdictions capable of supplying the resources needed to advance clean technologies, support national defense, and bolster economic security. Public geoscience underpins successful mineral exploration. Continued investment in the British Columbia Geological Survey will help sustain a healthy pipeline of early-stage projects, ensuring a resilient, innovative, and prosperous mineral exploration and mining sector for the province.



Adrian S. Hickin
Chief Geologist and Executive Director
British Columbia Geological Survey

Table of Contents

Brideau, M-A., Cui, Y., Clarke, G., and Hickin, A.S.: British Columbia Geological Survey annual program review 2025-2026 1

Hickin, A.S.: British Columbia Geological Survey's contributions to the Pan-Canadian Geoscience Strategy 2021-2026 17

Bacha, R.R.B.: Data sharing for Indigenous Peoples engagement: What and how 37

Ootes, L., Graham, A.C., Whitmore, K., Goudie, D., Piercey, S.J., Barker, S., Milne, S., and McFarlane, C.: Mineralogical control on critical companion metal distribution: Expanded workflow, with examples from the Sullivan Pb-Zn-Ag deposit... 45

Wei, C., Pietruszka, D.K., Piercey, S.J., Aylward, W., Kommescher, S., Scanlan, E., and Layton-Matthews, D.: Critical metal distributions in volcanogenic massive sulphide (VMS) deposits in British Columbia: A progress report 53

Graham, A.C., Vaughan Forrester, K., Ootes, L., Bain, W., Campbell, R.W., and Goudie, D.: Critical companion metals in porphyry deposits in British Columbia: Lithogeochemistry and scanning electron microscopy-mineral liberation analysis (SEM-MLA) from the Schaft Creek, Mount Polley, and New Afton deposits 69

Bain, W., Joudrie, R., de Waal, F., Mihalynuk, M.G., and Goudie, D.: Distribution and texture of platinum group minerals in the C and West Cave zones of the New Afton Cu-Au deposit, British Columbia 85

Rukhlov, A.S., Ootes, L., Cunningham, Q.F., Goudie, D., von der Handt, A., Spence, J., Wall, C., and Barker, S.: A multi-analytical approach to stream-sediment samples from modern drainages enhances the search for REE and rare metals 97

Ootes, L., Wall, C., and Mihalynuk, M.G.: Rossland Group extends north: Detrital zircon U-Pb ages allow supracrustal unit reassignments in southern British Columbia and have tectonic implications 119

Campbell, R.W., Gibson, K., and van Straaten, B.I.: Paleozoic to Eocene intrusions in the Golden Triangle, northwestern British Columbia: A project update..... 131

van Straaten, B.I.: A Triassic-Jurassic stratigraphic framework for the Golden Triangle, northwestern British Columbia: A project update..... 143

Zagorevski, A., Cordey, F., Mihalynuk, M.G., and Vaillancourt, A.: Application of radiolarian biostratigraphy in constraining the geology of the northern Canadian Cordillera, British Columbia and Yukon 153

Mihalynuk, M.G., and Gabites, J.E.: 24 Ma Giant Copper polymetallic porphyry-related breccia of the ancestral Cascades, southwest British Columbia..... 163

Nelson, J.: Early Jurassic intrusion and deformation in the Wark-Colquitz complex, Victoria, British Columbia 175

Ferri, F., and Friedman, R.: Age and geochemistry of middle to late Paleozoic volcanism along the western edge of Ancestral North America in north-central British Columbia 183

Table of Contents continued

Ferri, F., and Friedman, R.: Geochemistry of volcanic rocks in the Snowshoe Group (Neoproterozoic-Cambrian) and geochronology, Sm-Nd isotopic data, and geochemistry of crosscutting Permian intrusions: Episodic back-arc magmatism along the western edge of Ancestral North America in Kootenay terrane 203

Cui, Y., Norris, J., and Fortin, G.: British Columbia geoscience Spatial Data Infrastructure (BCgSDI): A progress report..... 221

Elia, E.A., and Ferbey, T.: Interior Plateau surficial geology compilation: Selection and standardization of maps and data 227

Brideau, M-A., Brayshaw, D., and Hancock, C-A.: Highlights for British Columbia from the preliminary Canadian Landslide Database..... 239

Zhang, P., Brideau, M-A., and Szponarski, K.: Geoscience knowledge density map of British Columbia, Version 1.0..... 247

Appendix: British Columbia Geological Survey Publications 2025, including peer-reviewed external papers co-authored by BCGS staff..... 253

British Columbia Geological Survey annual program review 2025-2026

Marc-André Brideau[1], Yao Cui[1], Gordon Clarke[2], and Adrian S. Hickin[1]

[1] British Columbia Geological Survey, Ministry of Mining and Critical Minerals, Victoria, BC, V8W 9N3
[2] British Columbia Geological Survey, Ministry of Mining and Critical Minerals, Vancouver, BC, V6Z 2G3
[a] corresponding author: Adrian.Hickin@gov.bc.ca

Recommended citation: Brideau, M-A., Cui, Y., Clarke, G., and Hickin, A.S., 2026. British Columbia Geological Survey annual program review 2025-2026. In: Geological Fieldwork 2025, British Columbia Ministry of Mining and Critical Minerals, British Columbia Geological Survey Paper 2026-01, pp. 1-16.

Abstract

Headquartered in Victoria, the British Columbia Geological Survey generates geoscience knowledge and data to inform land use and resource management decisions, and to support the growth of British Columbia as a competitive jurisdiction for mineral exploration. Geoscience outreach and public engagement are core functions of the Survey. Given intersecting and diverse interests about mineral resource development in the province, the Survey engagement program provides unbiased geoscience information to British Columbians to balance exploration and mining, environmental and heritage concerns, and economic realities. There continues to be an increased demand for geoscience information needed to guide land-use decisions and co-management of mineral resources by increased delivery of Mineral Lands Assessment reports that evaluate the significance of mineral resources in an area and the likelihood of mineral exploration and mining continuing in the future. These reports are aided by renewed mineral potential maps that also serve mineral exploration by indicating areas that are more likely and less likely to host mineralization.

The Cordilleran Geoscience Section conducts field, laboratory, and office-based research including bedrock and surficial geology mapping programs, regional geochemical surveys, and targeted mineral deposit studies. Critical minerals continued to be a major theme for the Survey in 2025. One stream of projects evaluates the availability of critical minerals to be added to production as co-products or byproducts in the short term. A second stream uses foundational mapping, geochronology, geochemistry, and geophysics to focus on longer term goals to identify new deposits and to encourage investment in under-explored critical mineral systems. The Resource Information Section is responsible for developing and updating provincial geoscience databases and disseminating data online through our geospatial web service (MapPlace). The Section is also responsible for reviewing mineral assessment reports, compiling mineral occurrences, archiving exploration technical documents, and updating mineral resource inventory data. To improve efficiency in data management, the Survey continues to modernize its information systems as part of the British Columbia geoscience Spatial Data Infrastructure (BCgSDI). The Mineral Development Office (MDO) is the Vancouver base of the Survey. It provides investment intelligence to government and global business and publishes the annual Mining and Exploration in British Columbia overview volume.

Keywords: Public geoscience, geology, information management, mineral exploration, engagement

1. Introduction

The British Columbia Geological Survey (BCGS, the Survey), a branch in the Mines Competitiveness and Authorizations Division of the British Columbia Ministry of Mining and Critical Minerals, has provided public geoscience services since 1895. The BCGS provides objective, reliable, evidence-based geoscience to many modern societal issues centred on the Earth sciences. Credible unbiased geoscience is of value for the exploration and mining of critical minerals, building relationships with Indigenous Peoples, and informing everyone living in the province about geoscience-related issues. Headquartered in Victoria, the Survey generates and disseminates public geoscience information that supports effective mineral exploration, sound land use management, and responsible governance. The Survey is the primary repository for provincial geoscience data and knowledge. Maps, reports, and databases are freely available online and are public resources for Indigenous groups, local communities, the minerals industry, public safety agencies, environmental scientists, research organizations, and other government agencies. Current research programs and publications (Figs. 1, 2) continue to define the geological evolution and mineral resources of the province, generating knowledge and data to support decisions that balance economic, environmental, and community interests. Virtually all Survey activities contribute to the Pan-Canadian Geoscience Strategy, a federal, provincial, and territorial collaboration that articulates the common needs and goals of geoscience organizations in Canada (Hickin, 2026).

The BCGS consists of three sections: 1) Cordilleran Geoscience; 2) Resource Information; and 3) the Mineral Development Office. The Cordilleran Geoscience Section generates new knowledge through field, laboratory, and office-based research activities including geological mapping programs, regional geochemical surveys, and targeted geological and mineral deposit studies. The Cordilleran Geoscience Section also curates the provincial sample archive

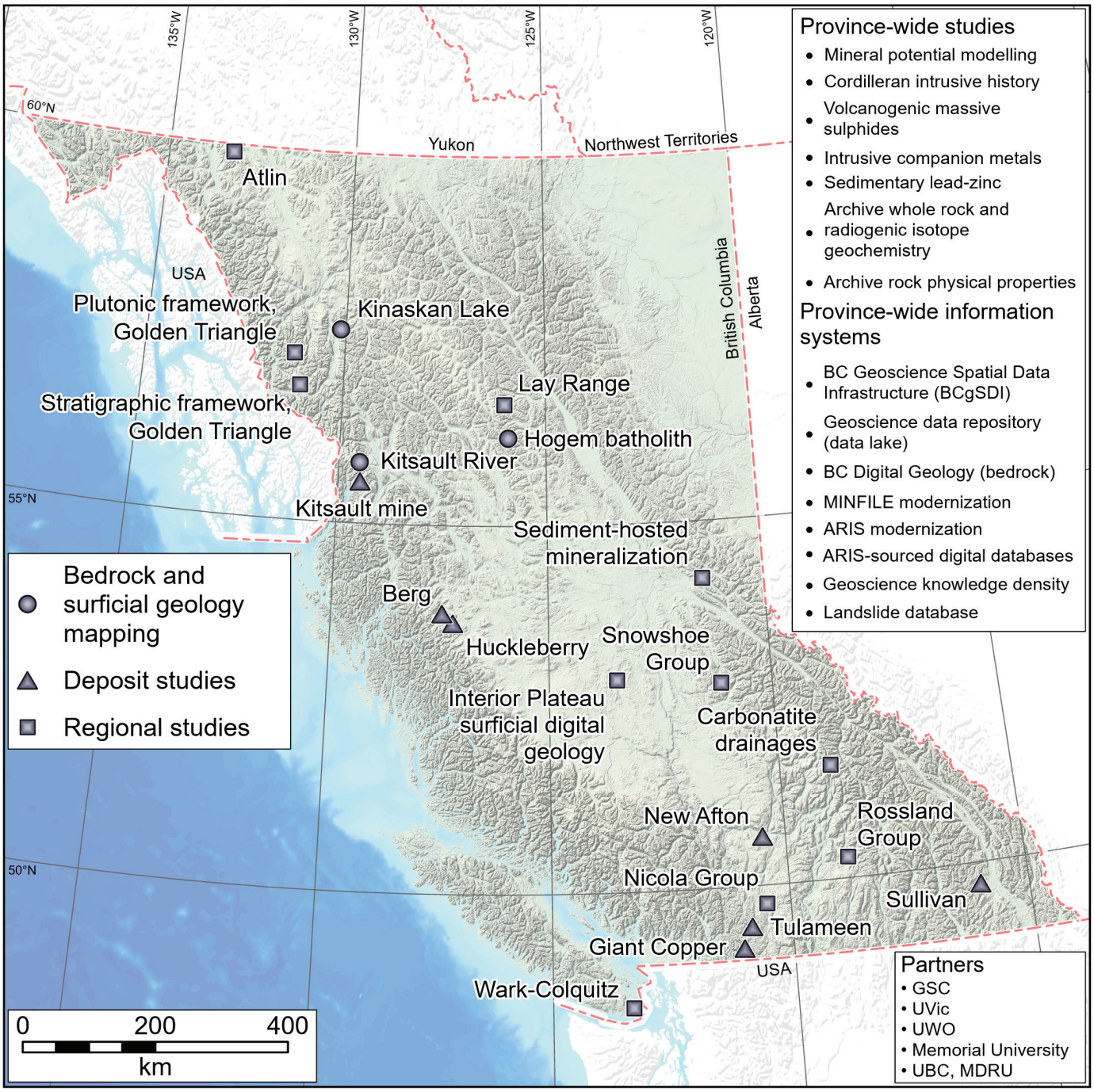
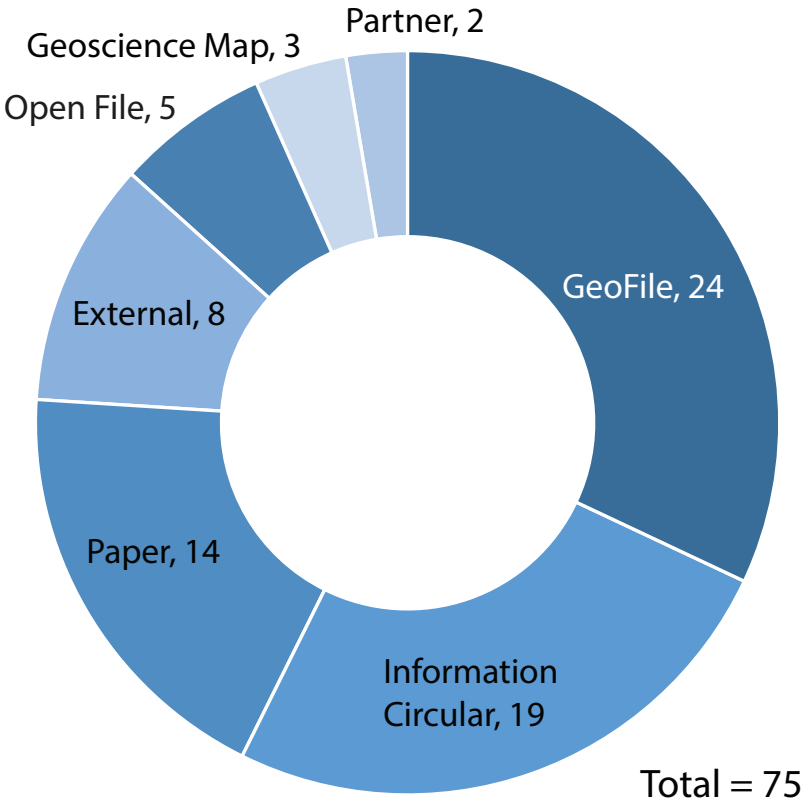


Fig. 1. British Columbia Geological Survey projects in 2025.

samples, enabling the Survey to re-examine legacy specimens as analytical techniques evolve. The Resource Information Section is responsible for developing and updating provincial geoscience databases and disseminating data online through our geospatial web service (MapPlace). The Resource Information Section is also responsible for reviewing mineral assessment reports, compiling mineral occurrences, archiving exploration technical documents, and updating mineral resource inventory data. The Mineral Development Office (MDO) is the Vancouver base of the Survey and provides investment intelligence to government and global business. The MDO is staffed by a group of Regional Geologists who, stationed in exploration centres across the province, track mineral exploration activities and provide geoscience expertise in their regions. The MDO publishes the annual Mining and Exploration in British Columbia overview volume (Clarke et al., 2026).



Papers*: This series is reserved for reviews and final thematic or regional works. Geological Fieldwork, our annual review of field activities and current research, is released as the first Paper of each year.

Geoscience Maps: This series is the BCGS vehicle for publishing final maps.

Open Files: These maps and reports present the interim results of ongoing research, particularly mapping projects.

GeoFiles: These publications enable rapid release of extensive data tables from ongoing geochemical, geochronologic, and geophysical work. As such, they serve the same function as data repositories provided by many journals, providing immediate access to raw data from specific projects.

Information Circulars*: These publications provide accessible geoscience information to a broad audience in government, industry, and the general public. Included in the Information Circular series is the annual Provincial Overview of Exploration and Mining in British Columbia. Starting in 2026, the volume will be released as the second in the Paper series, with the title Mining and Exploration in British Columbia.

Contributions to partner publications: This category includes reports, maps, and other products published by another agency such as the Geological Survey of Canada or Geoscience BC, but have received contributions from British Columbia Geological Survey staff.

External publications: These are contributions to the peer reviewed literature and published in a recognized national or international scientific journal.

*The count refers to the total number of articles.

Fig. 2. Type and numbers of publication produced by the British Columbia Geological Survey in 2025.

2. Critical minerals

Critical minerals continue to be a major theme for the Survey. In 2025-2026, the Survey advanced new multi-year projects to address knowledge gaps and gain insights into the mineral systems that contain critical minerals, the origin, age, and geographic distribution of mineralized rocks, and the spatial distribution of critical minerals within ore bodies (Fig. 1). One stream of projects examines the mineral systems that host significant deposits and mines, past and present. These projects are assessing if critical minerals could conceivably be added to production as co-products or byproducts in the short term. The workflow developed by the BCGS to support this stream is described in Ootes et al. (2026a) with examples from the historical Sullivan lead-zinc-silver deposit (Fig. 3).

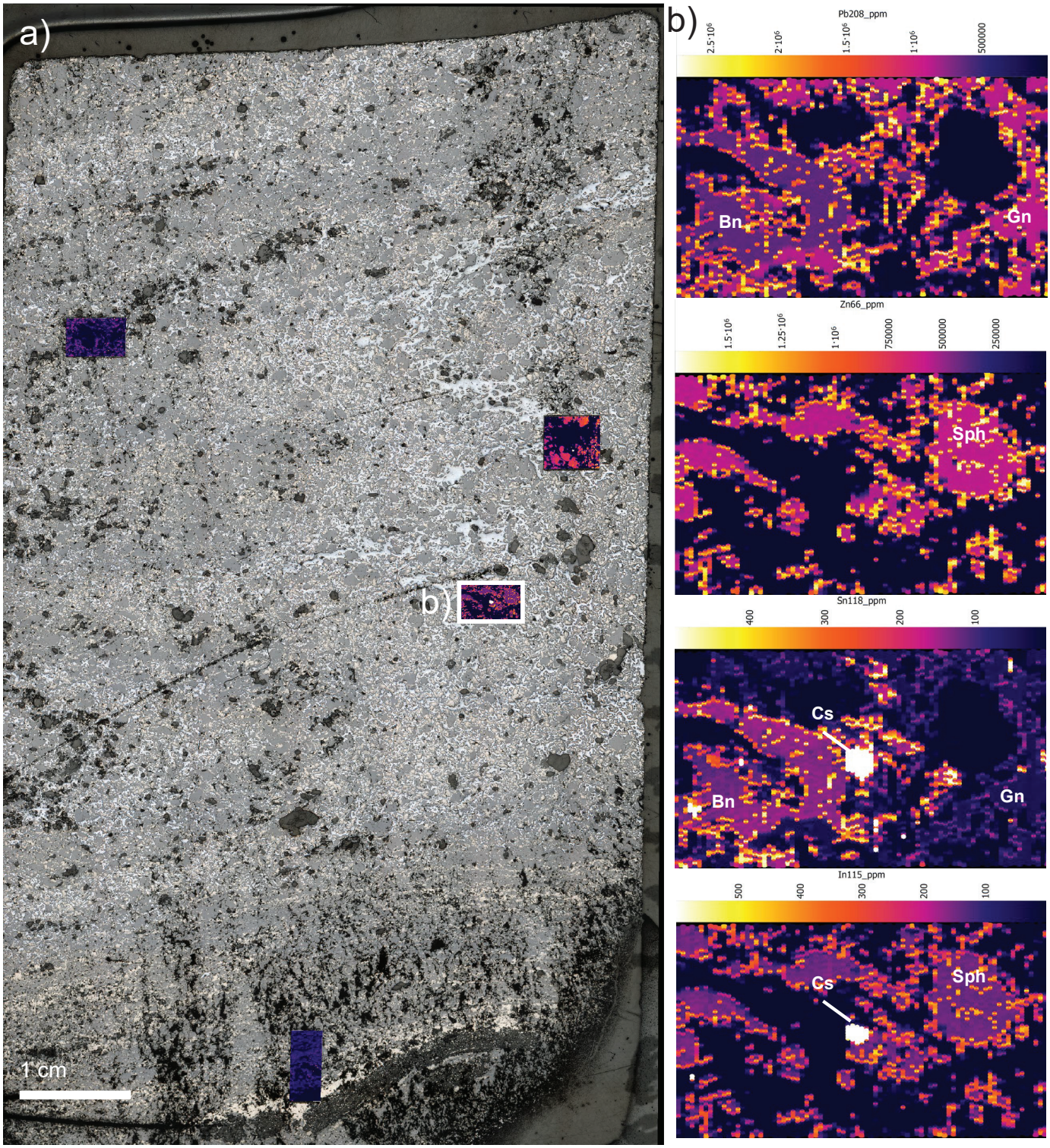


Fig. 3. a) Thin section photomicrograph of the past-producing Sullivan mine 'Main band' (reflected light). The four coloured boxes denote locations of laser ablation-inductively coupled-plasma mass spectrometry (LA-ICP-MS) maps. **b)** Examples of elemental distribution of one of these maps. From top to bottom are elemental distributions on Pb^{208}, Zn^{66}, Sn^{118}, and In^{115}. The circular white mineral in the Sn and In maps is cassiterite. Colour ramps are in parts per million (ppm). See Ootes et al. (2026a).

Additional projects from this stream include selected porphyry deposit studies in the Golden Triangle (Lawley et al., 2025) and specific deposit studies such as Schaft Creek, Huckleberry, Berg, Mount Polley, and New Afton (Graham et al., 2025, 2026; Bain et al., 2026).

A second stream focuses on the longer term to identify new deposits and to encourage investment in under-explored critical mineral systems. These projects include foundational mapping, geochronology, geochemistry, and geophysics. Some of these studies were regional, such as work in the Golden Triangle focused on better understanding the intrusive (Campbell et al., 2026) and stratigraphic (van Straaten, 2026) frameworks that control mineralization and a project that examined volcanogenic massive sulphide (VMS), porphyry, and epithermal deposits in the Kitsault area (Miller et al., 2025a, b). In the eastern part of the province, Rukhlov et al. (2026) took a multi-analytical approach to test exploration tools (Rukhlov et al., 2024, 2025a) that use stream-sediment samples to fingerprint upstream carbonatite-hosted niobium, tantalum, rare earth element (REE), and other critical mineral deposits. Many projects are province wide in scope, such as: 1) developing a modernized magmatic framework for critical mineral-bearing intrusive systems using high-precision age and isotopic tracer data to establish the age, emplacement setting, and geographic distribution of both fertile and barren intrusions (Ootes and Wall, 2024); 2) re-analyzing archived samples using modern whole-rock, trace element, and isotopic methods to understand the geological settings important for mineralization (British Columbia Geological Survey, 2025a; Rukhlov et al., 2025b); 3) measuring physical properties of archived rock samples; 4) mineral potential modelling of critical mineral-bearing systems (Wearmouth et al., 2024a, b); 5) examining critical minerals in volcanogenic massive sulphide (VMS) deposits (Wei et al., 2026); 6) examining critical minerals in deposits related to sedimentary rocks (Graham et al., 2025); 7) digitizing assessment reports and creating databases to enable easy extraction of critical mineral occurrences that may have been overlooked in original work (Fortin and Silva, 2025, 2026); and 8) creating a geoscience data repository (data lake) of historical records to enable machine learning and artificial intelligence interrogation for unrecognized critical mineral-bearing mineral occurrences.

3. Engagement

Public engagement is an important theme for the Survey because geoscience literacy helps British Columbians understand how geoscience underpins economic development, climate change adaptation, and public safety. Strengthening communication and outreach makes geoscience data and concepts more accessible to the public, policymakers, stakeholders, and rightsholders, thus supporting informed decisions that balance resource development with environmental, cultural, and economic priorities. BCGS efforts also emphasize inclusive engagement with Indigenous communities and diverse audiences to foster shared knowledge and responsible management of geological resources in the province.

The Survey's public engagement program provides unbiased geological information to address the varied interests concerning mineral resource development. By connecting Indigenous Peoples, local communities, government, industry, and the broader public to provincial geology and mineral resources, the program supports land-use planning, co-management, and relationship building. Bacha (2026) outlines the developing data sharing initiatives that the Survey is using to build trust and exchange knowledge with Indigenous communities.

BCGS engagement activities in 2025-2026 included providing information to and interacting with Indigenous Peoples, elected officials, students, and the general public. The BCGS took part in Mining Day at the Legislature, an event sponsored by the British Columbia Mining Association (MABC), where the Survey provided experiential learning opportunities to the sitting government, opposition members, and their staff (Fig. 4). The Survey participated in the annual Discovery Day at the Association of Mineral Exploration Roundup Convention in Vancouver, and Geodiversity Fest at the Royal British Columbia Museum in Victoria. BCGS staff



Fig. 4. Engagement with government. David Eby, Premier, and Jagrup Brar, Minister of Mining and Critical Minerals, Mining Day at the Legislature, May 2025.

are also active in the professional geoscience community by organizing and presenting technical talks, delivering guest lectures at universities, co-supervising graduate student projects, and being on organizing committees of conferences and professional groups.

Collaboration between the Citxw Nlaka'pamux Assembly (CNA) of south-central British Columbia and the Survey led to a successful short course and fieldtrip in which CNA staff visited active exploration sites and experienced first-hand how geological research is carried out, and Survey and industry geologists learned about CNA values, worldviews, and understandings of nature (Bacha, 2025). At the invitation of Tl'azt'en Nation, the BCGS and the Geological Survey of Canada (GSC) held an in-person meeting in December 2025 to review the available public geoscience information for their territory and discuss how it can be accessed and used (Fig. 5). Discussions also covered critical minerals and mineral exploration projects in their territory.



Fig. 5. Engagement with Tl'azt'en Nation, central interior of British Columbia.

4. Land-use planning and mineral potential modelling

Land-use decisions and co-management of natural resources require high-quality information, including geological data. These data are necessary to establish the mineral interests in an area and to evaluate potential economic opportunities. The Survey is meeting a heightened demand for these data by increased delivery of intra- and inter-Ministry Mineral Lands Assessment and industry intelligence reports. In support of four ongoing land-use planning consultations with Indigenous Peoples, the BCGS used previous mineral potential modelling work (Wearmouth, 2024a, b) to generate a series of more consumable publications (British Columbia Geological Survey, 2025b, c, d, e).

BCGS co-organized a pan-Canadian mineral potential modelling workshop where federal, provincial, territorial and international practitioners met to foster and coordinate innovation, discuss past, present, and future methods, explore emerging tools in artificial intelligence and geospatial analysis, and begin addressing shared challenges such as data integration, gaps in data coverage, model uncertainty and interpretation, and communicating results to non-specialists (British Columbia Geological Survey, 2025f). The Survey is now expanding its mineral potential modelling program to extend across the entire province and include additional mineral systems.

5. Partnerships

Partnerships continue to be an effective way for the Survey to lever its resources. Working with other industry, other geoscience agencies, and universities, these partnerships extend across a wide spectrum of collaboration, all with the aim of enhancing public geoscience.

BCGS partnerships with industry are key to support mineral exploration and mining in the province. The Survey has nine agreements and memoranda of understanding with companies ranging from grassroots explorers to major operating mines. These agreements allow for site access by BCGS project geologists, logistical support, exchange of knowledge, sample collection and analyses, and release of data. The partnerships provide companies with improved regional frameworks for their data, and the Survey gets access to resources (e.g., drill core and ore concentrate samples) that would be difficult to independently collect.

The Geological Survey of Canada (GSC) and BCGS continue to benefit from strong ties. One joint project is examining rock physical properties from archived samples. Analyses include density, magnetic susceptibility, and porosity measurements. These physical properties provide the link between remote geophysical surveys and in-situ bedrock, thus improving geophysical and geological interpretations. The physical properties database now incorporates more than 24,000 samples with the intention of reaching a total of 29,000 by April 2027. This large dataset will enhance the accuracy of geophysical inversions and provide a classification tool to help assess bedrock fertility remotely.

The Critical Minerals Geoscience and Data (CMGD) program is a Natural Resources Canada initiative launched in 2023 to provide essential knowledge and data to support the development of Canada's critical minerals resources. BCGS was successful in getting CMGD funding to complete four projects by April 2027. One project (Rukhlov et al., 2026) builds on work by Rukhlov et al. (2024) to evaluate areas prospective for rare metals such as niobium, tantalum, and rare earth elements (REE) through re-analysis of archived stream-sediment samples (Rukhlov et al., 2025a). Another project (Fortin and Silva, 2025) is directed at populating a province-wide drillhole database by extracting information from assessment reports submitted by the mineral exploration industry. This project will generate a provincially maintained database of drillholes and assays, which will enable explorationists to minimize duplicating work. A third CMGD-funded project focuses on understanding the temporal and spatial relation between intrusions and mineralized systems across the province. Many mineralized systems formed during relatively narrow geological time windows; thus high-precision

geochronology is needed to increase exploration success (e.g., Ootes and Wall, 2024; British Columbia Geological Survey, 2025a). This project will triple the amount of modern, high-precision U-Pb zircon age data using chemical abrasion isotope dilution mass spectrometry (CA-TIMS) and associated trace elements and isotopes (hafnium, oxygen). The fourth CMGD project is a geoscience data repository (data lake) initiative for the Canadian Cordillera. Under this project, British Columbia is collaborating with Yukon to develop a new, comprehensive, integrated database that will contain scanned historical data with optical character recognition (OCR) to enable machine learning applications search for unrecognized critical mineral-bearing occurrences contained in assessment reports. To date, approximately 6500 documents have been scanned and indexed.

As co-investigator, BCGS and collaborators are part of two National Science and Engineering Research Council (NSERC) Alliance Grants. These grants enable research activities that advance Canadian knowledge, models, processes, tools, and technologies to support data-driven decisions of domestic critical mineral value chains and grow Canadian expertise. One grant, focusing on the mineralogy and genesis of critical mineral-bearing volcanogenic massive sulphide (VMS) deposits, the enrichment of critical elements in these deposits, and the processes that lead to enrichment, was awarded to Memorial University of Newfoundland. The work, reported on by Piercey et al. (2025), Pietruska et al. (2026), and Wei et al. (2026), provide information on critical element mineral residence, siting, and textures. The end goal of this project will be to provide refined descriptive, genetic, exploration, and development models for critical metal-bearing VMS deposits and in so doing provide an updated metallogenic model for this deposit type. Complementing ongoing BCGS activities (Graham et al., 2025; Northcote, 2025; Ootes et al., 2026a), a second grant led by the Mineral Deposit Research Unit (MDRU), University of British Columbia and focuses on sedimentary exhalative (SEDEX) and Mississippi Valley Type (MVT) mineral systems across the Selwyn Basin (southeastern Yukon), Kechika trough (northeastern British Columbia), and Purcell Basin (southeastern British Columbia).

Collaborations between BCGS and university researchers have always been an important and productive activity of the Survey. Since 2003, the Survey has had a formal partnership with the School of Earth and Ocean Science, University of Victoria. In 2026, BCGS and Western University (London, Ontario) entered a formal research agreement to continue research collaborations critical companion metals occurrences in porphyries (Bain et al., 2026; Graham et al., 2026) and skarn mineral deposits (Bain et al., 2025). The Survey also has informal collaborations with students and faculty at University of the Fraser Valley, Simon Fraser University, The University of British Columbia, British Columbia Institute of Technology, The University of British Columbia-Okanagan, Thompson Rivers University, University of Alberta, University of Calgary, University of Manitoba, Queen's University, Darthmouth University, Colorado School of Mines, and Laoshan Laboratory (China).

6. Cordilleran Geoscience Section

Cordilleran Section geologists collect geoscience data through single and multi-year field-based programs complemented by laboratory and office-based studies. These programs include regional-scale mapping, mineral deposit studies, and developing new mineral exploration methods. Section expertise encompasses tectonics, structural geology, stratigraphy, petrology, metallogeny, critical minerals, geochemistry, Quaternary and surficial geology, and geohazards.

6.1. Framework geoscience

Framework geoscience projects better our understanding of provincial geology and can be regional in extent or focus on detailed mapping with ancillary geochemical and geochronologic work.

Field mapping is the most fundamental form of geological research and remains core to BCGS activities. Miller et al. (2025a) released a preliminary bedrock geology map of the Kitsault River map area in northwestern BC; the final map release is anticipated for summer 2026. Höy and DeFields (2025) released the results of 1:50,000-bedrock mapping in the Lightning Peak area in southeastern BC. Ferbey and Elia (2025a, b, 2026a, b) released a series of four 1:50,000-scale surficial geology maps of the northern Hogem batholith areas in north central BC (Fig. 6) that are companions to the bedrock geology by Ootes et al. (2020). In 2025, the Survey started work on a digital compilation of surficial geology for the Interior Plateau, where thick packages of glacial drift can add complexity to mineral exploration, land-use planning, forestry, and infrastructure projects. Elia and Ferbey (2026) describe how they selected, ranked, and compiled source maps, present methods for converting surficial data to a uniform standard, and provide details about how the compilations may be used. Initial data release for the central portion of the Interior Plateau is anticipated for summer 2026.



Fig. 6. Mesilinka intrusive suite (Middle Jurassic to Early Cretaceous), exposed in the glacially carved U-shaped Klakring Creek valley. View towards the northeast. See Ferbey and Elia (2026a).

In 2025-2026, the Survey continued work to establish a regional framework for Paleozoic to Eocene intrusions (Campbell et al., 2026) and Triassic-Jurassic stratigraphy (van Straaten, 2026) in the Golden Triangle. Campbell et al. (2026) investigated rocks of the Texas Creek plutonic suite (Early Jurassic) in the Bronson corridor near Iskut River (Fig. 7) and in the Salmon Glacier area to understand their potential control on Au (±Ag) and Au-Cu mineralization. Complementing this work, van Straaten (2026) is examining stratigraphic relationships of Triassic-Jurassic units to better constrain the tectonic and metallogenic evolution of the region, which hosts numerous porphyry, epithermal, and VMS deposits (Fig. 8). Mihalynuk et al. (2024) released a 1:50,000-scale map of the western Gladys Lake area near Atlin. Based in part from samples collected during the last few years, Zagorevski et al. (2026a) used radiolarian (Fig. 9) and conodont biostratigraphy to re-evaluate terranes in the northern Cordillera of British Columbia and Yukon, suggesting that Mesozoic rock units are more widespread than previously recognized and potentially represent a disrupted overlap assemblage. Cordey et al. (2025) released a supporting radiolaria dataset; Zagorevski et al. (2026b) compiled radiolarian and conodont data.



Fig 7. Texas Creek plutonic suite quartz monzonite to granodiorite unit (EJTgd), Lehto pluton cut by a biotite-phyric mafic dike. See Campbell et al. (2026).



Fig. 8. Angular unconformity between Stuhini Group sedimentary rocks (Upper Triassic) and the Jack Formation of the lower Hazelton Group (uppermost Triassic to Lower Jurassic) in the Golden Triangle region of northwestern British Columbia. See van Straaten (2026).



Fig. 9. Well-bedded radiolaria-bearing grey chert with orange argillaceous interbeds, Atlin area. See Zagorevski et al. (2026a).

In the north-central part of the province, Ferri and Friedman (2026a) provided Permian U-Pb zircon ages from Lay Range assemblage and Cassiar terrane felsic metavolcanic rocks (Fig. 10). Lithogeochemical data (whole rock, trace, and rare earth element) for the Lay Range assemblage are consistent with eruption in an arc setting. Farther south, Ferri and Friedman (2026b) provide U-Pb zircon and geochemical data on Permian intrusive bodies (Fig. 11) in the Snowshoe Group.

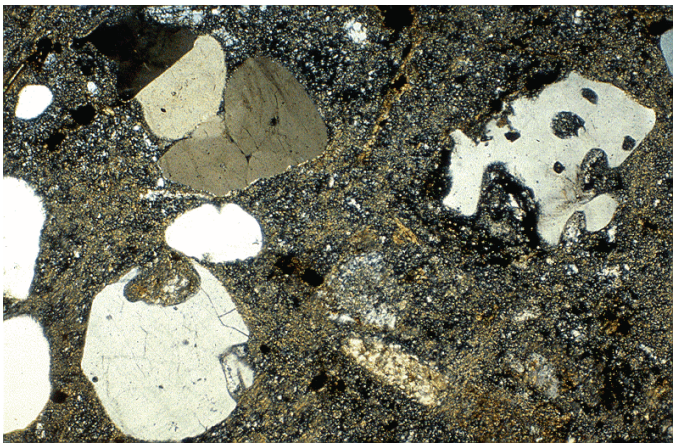


Fig. 10. Photomicrograph of Gilliland tuff from the Wasi Lake area with resorbed quartz grains; crossed polarizers, width of view ~10 mm. See Ferri and Friedman (2026a).



Fig. 11. Pillowed mafic volcanic rocks from the Harveys Ridge succession ~1.5 km southwest of Frank Creek. See Ferri and Friedman (2026b).

The results are consistent with a Permian back-arc along the western margin of Ancestral North America. Lithogeochemical analysis of mafic volcanic rocks in the Snowshoe Group are predominantly alkali basalts indicating a within-plate setting, but some contain basalt to alkali basalt with both E-MORB and arc signatures, and others are alkali basalts displaying within-plate abundances. Southern Quesnel terrane, which contains most of the currently producing mines in the province remains an area of active mineral exploration and of particular focus for the Survey. U-Pb zircon results from Nicola Group samples taken during regional mapping were summarized by Mihalynuk et al. (2025a), $^{40}Ar/^{39}Ar$ results were presented by Gabites and Mihalynuk (2025) and Orchard et al. (2025) determined that conodonts faunas from the Nicola Group near Merritt identify the lower-middle Norian boundary. These publications provide the source data of the time of deposition and maximum deposition age for refinements of key stratigraphic intervals in the Nicola Group proposed by Mihalynuk et al. (2025b).

Ootes et al. (2026b) use detrital zircon U-Pb data to reassess the distribution of rock units at the transition between Quesnellia and Ancestral North America (Fig. 12). In contrast to previous models, the data indicate that the Nicola, Rossland, and Slocan groups formed independently of continental North America as it is currently positioned. Using the new data Ootes et al. (2026b) propose a novel tectonic model that envisages deposition in an east-facing forearc above a west-dipping subduction zone.

In the Southwest Region, Mihalynuk and Gabites (2026) confirmed an Oligocene age of ca. 24 Ma for polymetallic porphyry-related breccias at the Giant Copper deposit using $^{40}Ar/^{39}Ar$ biotite data. Nelson (2026) provides a precise U-Pb zircon date from deformed and post-kinematic intrusive samples of the Wark-Colquitz complex in downtown Victoria (Fig. 13). Both are ca. 193 Ma and agree within error, indicating that the voluminous plutonism and possibly ductile deformation in the complex were short-lived, and coincided in timing with a

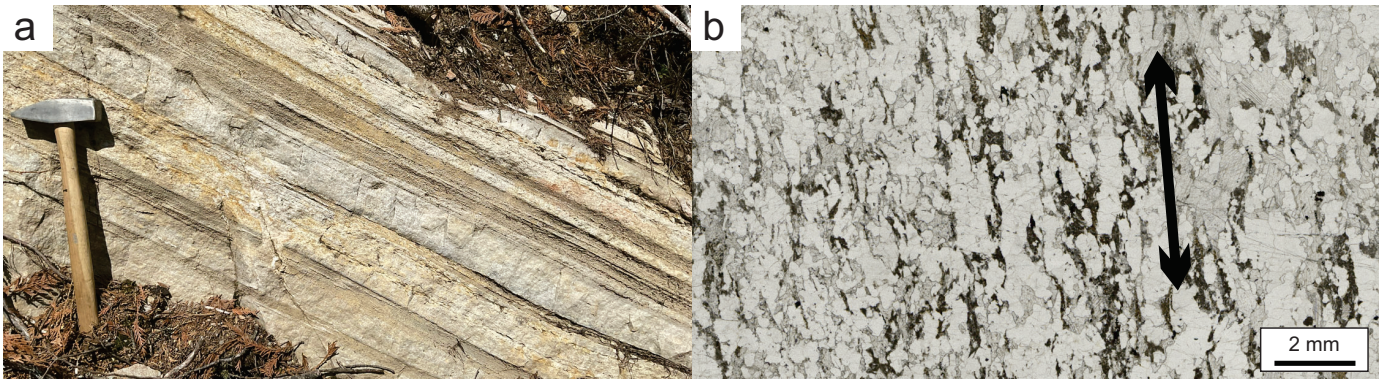


Fig. 12. a) Chase Formation quartzite with layering that is tectonic rather than depositional. **b)** Thin section photomicrograph (plane polarized light) illustrating recrystallized quartz ribbons that define a lineation (parallel to the arrow), supporting that this rock unit is no longer a sedimentary rock but a mylonite in which primary depositional features were transposed into a tectonic fabric during ductile strain. See Ootes et al. (2026b).

major pulse of the Island Intrusions, which are thought to have fed the Bonanza arc. This supports the interpretation that the Wark-Colquitz complex is an exhumed deep-crustal portion of Wrangellia that exposes the roots of the Triassic-Jurassic Bonanza magmatic arc.



Fig. 13. Well-layered Wark-Colquitz gneiss at Mount Tolmie Park, Victoria. See Nelson (2026).

6.2. Economic geology and geochemistry

BCGS economic geology and geochemistry projects focus on better understanding the distribution and origin of precious, base, and critical metals in British Columbia. Northcote (2025) reviewed the inventory of SEDEX, MVT, and related lead-zinc occurrences in the province. Autochthonous and parautochthonous terranes in the eastern part of the Canadian Cordillera in British Columbia are among the few global settings prospective for sedimentary-hosted lead-zinc deposits. These deposits contain most of the provincial zinc inventory and have the potential to host critical-mineral companion metals. Graham and Ootes (2025) investigated the bulk-rock geochemical data for 40 mineralized samples retrieved from the British Columbia Geological Survey rock archive from SEDEX and related deposits and mineral occurrences in Belt-Purcell basin, south Kootenay arc, Monashee-Shuswap region, Germansen Landing area, and the Kechika trough. To support the current priority on critical minerals and metals research, Ootes et al. (2026a) developed a workflow to identify mineralogic controls on critical companion metal distribution using archived samples from the historical Sullivan lead-zinc-silver deposit as an example.

Porphyry deposits are major global sources of copper and molybdenum, both on the 2024 version of the Canadian critical minerals list (NRCan, 2024). These deposits may also contain minor amounts of companion metals that are on the critical minerals lists of many jurisdictions and that could conceivably be byproducts of primary commodity mining (e.g., bismuth, the platinum group elements, rhenium, tellurium, and tungsten). Graham et al. (2025, 2026) examined how the geochemistry of critical companion metals in porphyry deposits in the province relates to the deportment of critical companion metals. Lawley et al. (2025) presented lithogeochemical and detailed mineralogic and trace element mapping analyses from several porphyry copper-gold projects in the Golden Triangle and the Brucejack epithermal gold-silver project to consider the origins of mineralization and the deportment of critical materials (e.g., antimony, bismuth, palladium, tellurium) that could conceivably be recovered as companion metals. Levering its partnerships with industry (see Section 5), the BCGS obtained ore concentrate samples from six operating porphyry mines in British Columbia and analyzed them for presence of critical minerals not currently being recovered. Analysis of these samples, along with work by Lawley et al. (2025), Graham (2025, 2026), Bain et al. (2026), will improve our understanding of critical minerals in the processing chain from mineralized rock to ore concentrate.

Piercey et al. (2025), Wei et al. (2026) and Pietruszka et al. (2026) continued their research partnership with the BCGS studying the mineralogy and genesis of critical mineral-bearing VMS deposits, the enrichment of critical elements in these deposits, and the processes that lead to enrichment. They used a suite of quantitative analysis of major and minor elements using electron probe microanalyzer (EPMA), determination of trace elements using laser ablation-inductively coupled plasma-mass spectrometry (LA-ICP-MS) and scanning electron microscopy-mineral liberation analysis (SEM-MLA) techniques to examine critical metal concentrations and partitioning in mineral phases.

The British Columbia alkaline province, which extends along the length of the eastern part of Cordillera for at least 1000 km, was the focus of numerous studies. Carbonatites and related rock types host niobium-tantalum-rare earth elements (REE) deposits and are under-explored in the region. Rukhlov et al. (2026) used several techniques on stream-sediment samples to test the ‘carbonatite geochemical index’ (Rukhlov et al., 2024, 2025a), which was derived from a drainage study that considered pathfinders for niobium, rare earth element, and other critical minerals in carbonatites and related silica-undersaturated and alkaline silicate rocks. Rukhlov et al. (2026) concluded that indicator minerals identified in catchment basins with data from qualitative X-ray diffraction analysis, quantitative evaluation of minerals by scanning electron microscopy (QEMSCAN®), scanning electron microscopy-mineral liberation analysis (SEM-MLA), micro-X-ray fluorescence (μXRF), detrital zircon and apatite trace-element analysis, and U-Pb detrital zircon geochronology confirm the occurrence of carbonatites in bedrock upstream. Abdale et al. (2025) provided new U-Pb zircon ages and hafnium data from carbonatites and syenites in the Blue River area and Monashee complex of southeastern BC. They identified two distinct pulses of carbonatite

magmatism: Early Cambrian (ca. 505 Ma) associated with continental margin extension, and Upper Devonian (ca. 358 Ma) linked to back-arc extension. Further analysis by Abdale et al. (2026) of the integrated U-Th-Pb geochronology, textural observations, trace element analysis, and Pb isotope data from the Monashee complex was able to resolve timing of the initial magmatism activity and subsequent younger Jurassic hydrothermal processes.

The BCGS archive is home to rock, mineral, and geochemical samples collected from across the province (Rukhlov et al., 2023). These collections represent a valuable resource for public geoscience, supporting re-analysis using modern comprehensive and high-precision analytical methods for new geoscience initiatives. The British Columbia Geological Survey (2025a) released initial results of a province-wide geochemical re-analysis project, providing whole rock and mineral Sr-Nd-Hf-Pb and galena Pb isotopic data from about 1400 archive samples.

6.3. Thematic geoscience

In 2025-2026, the Cordilleran Section also advanced work on two thematic geoscience projects to understand the how geoscience information and landslide hazards are distributed across the province. Zhang et al. (2026) generated a series of geoscience knowledge density map, the first geospatial compilation of publicly available geoscience information footprints for British Columbia. These maps display the spatial distribution of bedrock and surficial map, thematic, geophysical, geochemical, geochronological, and mineral resource information and include a derivative cumulative density map that provides a first-order characterization of all geoscience information in the province. Maps depicting the spatial distribution of geoscience information are of value for establishing information needed for making land-use decisions, planning new projects, mineral potential modelling, and increasing public awareness of geoscience activities. Brideau et al. (2026a) released a publicly available preliminary Canadian Landslide Database which is a compilation of existing landslide inventories and new mapping. Version 13 of the database contains 28,000 national entries of which 14,520 are from British Columbia. Brideau et al. (2026b) highlights how, within the limitations of an ongoing work, the database fills a gap in our overall understanding of landslide processes and provides common baseline knowledge to local governments, practitioners, and researchers. It also provides interested parties with initial desktop-level information of known landslides in an area and helps to identify priorities for further work.

7. Resource Information Section

The British Columbia Geological Survey is the steward of all provincial public geoscience and mineral resource data. Through the Resource Information Section, the Survey preserves, archives, and provides free online access to information gathered for more than 130 years. Delivered through web portals and MapPlace, the BCGS geospatial web service, province-wide databases and web applications include: digital coverage of bedrock geology (BC Digital Geology); the assessment report index system (ARIS); the mineral inventory (MINFILE); coal information (COALFILE); geochronologic data; geochemical and geophysical surveys; and collections of previously unpublished private documents donated by government, universities, industry, and individuals (Property File).

The public-facing end of BCGS databases and web services have been well-received. Like at many public geoscience agencies however, the back end is a patchwork of legacy systems lacking a common interface, which resulted from rapid advancements in computing technology outpacing enterprise-wide system architecture design and integration standards (Cui et al., 2026). Consequently, the databases are a challenge to maintain, inefficient to update, and a significant impediment to delivering Survey programs and support machine learning and natural language processing. Addressing these problems, the Survey has initiated the BCgSDI (BC geoscience Spatial Data Infrastructure) project to modernize our databases and applications and bring them into an integrated system (Cui et al., 2026). The approach being used by the Survey offers a practical template for similar modernizations in other agencies, and development of the BCgSDI is an important contribution to the Pan Canadian Geoscience Strategy (see Hickin, 2026).

7.1. MapPlace

MapPlace is the Survey's geospatial web service that allows users to discover, visualize, search, and generate summary reports and maps from our databases. Easy access to geoscience maps and data is crucial for making informed decisions on mineral exploration, mining, environmental protection, and land-use management. MapPlace serves as a platform to facilitate data mining and analysis of geoscience information in the context of other data such as mineral titles, assessment reports, land ownership, public infrastructure, and topographic base maps. Some of the data layers and applications are specifically developed to enable research and analytics for mineral exploration.

7.2. ARIS assessment reports and database

Results of mineral exploration are submitted by industry as assessment reports to the government in compliance with the Mineral Tenure Act Regulation. After a one-year confidentiality period, the assessment reports become freely available to the public. ARIS contains more than 41,600 reports dating back to 1947. The Survey manages these reports in the Assessment Report Indexing System (ARIS) database, which has a web interface to search by location, mineral occurrence, commodities, claims, and work types. All the assessment reports are available online as PDF documents and more than 1000 contain data (e.g., geochemical analyses and geophysical surveys) in common digital data formats that can be readily used. New derivative products are being created by capturing data sourced in ARIS documents, including geochemical (Norris and Fortin, 2019; Fortin and Silva, 2026) and drillhole (Fortin and Silva, 2025) databases.

7.3. MINFILE mineral occurrence database

MINFILE is a database containing location, geological, and economic information for more than 16,200 mineral, coal, and industrial mineral mines, deposits, and occurrences in British Columbia. In addition to spatial and non-spatial search and visualization on MapPlace, a dedicated web interface is available to query the database and retrieve details such as geological setting, deposit type, mineralogy, age, commodity, host rock, resources, production, and information sources. Query results are available to download as summary reports, spreadsheets, and GIS data format in KML. MINFILE/pc is a portable extract of the MINFILE database with a built-in search interface and printable reports. The Survey has transformed part of the MINFILE mineral occurrence data to be compliant with the Open Geospatial Consortium (OGC) standard EarthResourceML Lite schema and mapped the contents using the vocabularies adopted by the International Union of Geological Sciences Commission for the Management and Application of Geoscience Information. The EarthResourceML Lite-compliant mineral occurrence data is accessible via the OneGeology portal and open standard-based interface such as the OGC Web Mapping Service (WMS) and Web Feature Service (WFS) specification. These OGC compliant web services are available to be part of the Canadian adoption of the EarthResourceML Lite standard with other Canadian jurisdictions.

7.4. BC Digital Geology

The Survey offers province-wide digital coverage of bedrock geology including details from field mapping, with a typical regional compilation at a scale of 1:50,000. A geospatial frame data (GFD) model is used to simplify the compilation and integration of new regional mapping into the BC Digital Geology database (Cui, 2021). Bedrock geology is standardized with consistent stratigraphic coding, ages, and rock types to enable computations, and is available for download in GeoPackage and Esri shapefile formats. Customized bedrock geological maps and legends can be explored, and data downloaded as KML by spatial and non-spatial queries via MapPlace. The BCGS has transformed digital geology to the GeoSciML Lite schema and mapped the contents using the vocabularies adopted by the International Union of Geological Science Commission for the Management and Application of Geoscience Information.

7.5. Other databases

COALFILE includes a collection of assessment reports, dating back to 1900. Property File is a collection of spatially referenced archived reports, maps, photos, and technical notes documenting mineral exploration activities in British Columbia since the late 1800s. The provincial geochemical databases hold field and geochemical data from multi-media surveys by the Geological Survey of Canada, the BCGS, and Geoscience BC. The databases are updated regularly and contain results from the Regional Geochemical Survey program, till surveys, and lithogeochemical samples. As part of the Critical Minerals Geoscience and Data (CMGD) program (see above), the Survey is also creating a geoscience data repository (data lake) of historical records to enable machine learning and artificial intelligence interrogation of unrecognized critical mineral-bearing mineral occurrences.

8. Mineral Development Office (MDO)

Mining contributes greatly to the economy of British Columbia, and exploration is the backbone of mining. More than 1000 exploration and mining companies are headquartered in Vancouver. In addition, the exploration and mining industry is particularly important for northern communities and some Indigenous groups, employing more than 40,000 people. Between 2020 and 2024, the total value of mining production was $71.89 billion, and the exploration expenditure was $3.0 billion. For 2025, the forecast value of mine production is $16.42 billion, and the exploration expenditure is estimated at $750.9 million (Clarke et al., 2026).

The Mineral Development Office (MDO) is the Vancouver base of the British Columbia Geological Survey. Regional Geologists (Table 1) are part of the MDO and are stationed at exploration centres across the province (Smithers, Prince George, Kamloops, Vancouver) where they provide geoscience expertise and monitor local industry activities. Public geoscience is one of the principal enablers of grassroots mineral exploration, the backbone of mining. The MDO provides technical information and investment intelligence to global business, government, and Indigenous groups.

The Mineral Development Office serves mineral resource decision making by: linking exploration and mining companies to provincial mineral and coal information; conducting an annual expenditure and drilling survey to analyze short- and long-term industry trends (EY LLP, 2026); producing the annual Mining and Exploration volume, a summary of mining and exploration projects, activities, production and expenditures (Fig. 14; Clarke et al., 2026), responding to requests from government and Indigenous groups for mineral resource data needed for land-use planning and to support decision makers; and providing mineral resource, project, and technical data to government groups.

Table 1. British Columbia Regional Geologists.

Regional Geologist	Office	Region
Nate Corcoran	Smithers	Northwest
Hassan Heidarian	Prince George	Northeast and North Central
Cary Pothorin	Kamloops	South Central
BCGS	Cranbrook	Southeast
Bruce Northcote	Vancouver	Southwest

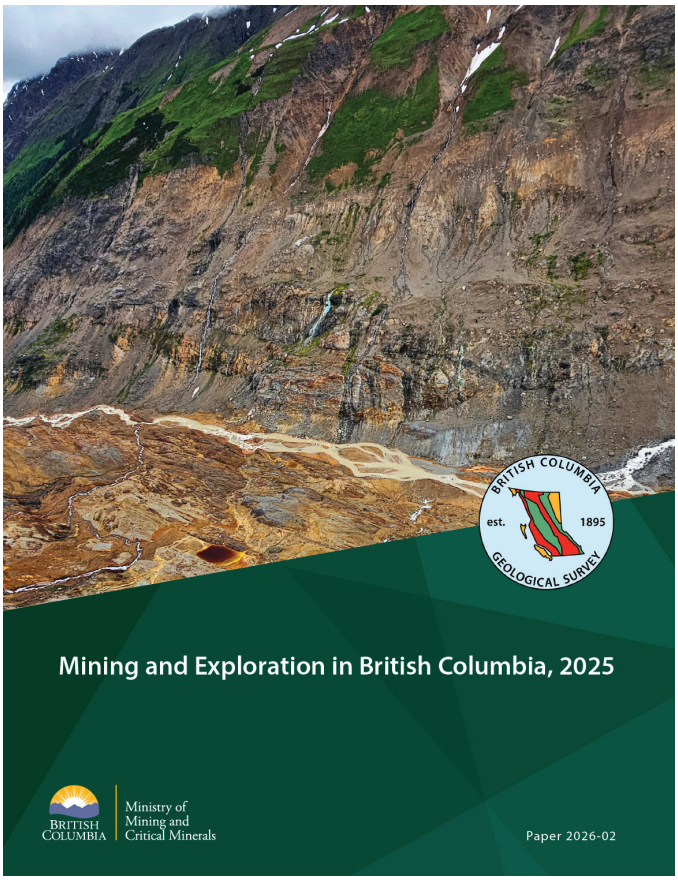


Fig. 14. Mining and Exploration in British Columbia annual volume. See Clarke et al. (2026).

9. Staffing

BCGS is currently staffed by 34 permanent employees (Fig. 15) but vacancies remain from retirements and departures. Building a strong pipeline of skilled geoscientists is needed to sustain Canada's resource development and energy transition and is one of the priority areas of the Pan Canadian Geoscience Strategy (Hickin, 2026). To help train the next generation of geoscientists, the Survey hires 8-12 seasonal or term employees each year, usually university students or recent graduates, to aid safe fieldwork or to assist in targeted projects (Fig. 16).



Fig. 15. British Columbia Geological Survey staff, 2025.



Fig. 16. Training the next generation. Project geologist and geoscience assistants leaving for a helicopter-supported bedrock mapping traverse.

BCGS had several personnel changes in 2025. Kaleigh Szponarski joined the Survey as geomatics specialist and Quinn Cunningham returned to the Survey for a two-year mineral deposits geoscience assistant position funded by Natural Resources Canada's Critical Minerals and Data (CMGD) program. David Zhang has joined the Survey on a one-year assignment as a geomatics specialist to provide leave cover. Di Tang and Ryan Grundy are now pursuing opportunities outside the Survey.

Acknowledgments

We thank George Owsiacki of Total Earth Science Services (Victoria) for desktop publishing this volume, David Zhang, BCGS geomatics specialist, for cartographic support, and to the reviewers of the individual papers for their time sharing their expertise with the authors.

References cited

Abdale, L., Millonig, L., Nelson, J., Groat, L.A., and Gerdes, A., 2025. Temporal evolution of enriched mantle sources in the southeastern Canadian Cordillera revealed by zircon geochronology and Hf isotopes in carbonatites. Chemical Geology, 695, article 123044. <https://doi.org/10.1016/j.chemgeo.2025.123044>

Abdale, L., Nelson, J., Millonig, L.J., Groat, L.A., and Gerdes, A., 2026. Magmatic and hydrothermal histories recorded by altered zircon in carbonatites from Selkirk allochthon and Monashee complex, British Columbia. Geological Society of America Bulletin. <https://doi.org/10.1130/B38415.1>

Bacha, R.R.B., 2025. Field trip guidebook to the geology near Merritt, south-central British Columbia, for the Citxw Nlaka'pamux Assembly. British Columbia Ministry of Mining and Critical Minerals, British Columbia Geological Survey GeoFile 2025-22, 14 p.

Bacha, R.R.B., 2026. Data sharing for Indigenous Peoples engagement: What and how. In: Geological Fieldwork 2025, British Columbia Ministry of Mining and Critical Minerals, British Columbia Geological Survey Paper 2026-01, pp. 37-43.

Bain, W.M., de Waal, F., and Goudie, D.J., 2025. Co-Te mineralization in iron skarns on Vancouver Island and Texada Island. In: Geological Fieldwork 2024, British Columbia Ministry of Mining and Critical Minerals, British Columbia Geological Survey Paper 2025-01, pp. 153-175.

Bain, W., Joudrie, R., Mihalynuk, M., de Waal, F., and Goudie, D., 2026. Distribution and texture of platinum group minerals in the C and West Cave zones of the New Afton Cu-Au deposit, British Columbia. In: Geological Fieldwork 2025, British Columbia Ministry of Mines and Critical Minerals, British Columbia Geological Survey Paper 2026-01, pp. 85-95.

Brideau, M-A., Brayshaw, D., Hancock, C-A., Lipovsky, P., Cronmiller, D., Lewkowicz, A., Blais-Stevens, A., Guthrie, R., Geertsema, M., Goetz, J., McGregor, C., Tannant, D., Friele, P., Clarke, J., Steelquist, A., Wong-Teichroeb, H., Ring, C., and Wells, G., 2026a. Preliminary Canadian Landslide Database (Version 13.0) [Dataset]. Zenodo. <https://doi.org/10.5281/zenodo.18216956>

Brideau, M-A., Brayshaw, D., and Hancock, C-A., 2026b. Highlights for British Columbia from the preliminary Canadian Landslide Database. In: Geological Fieldwork 2025, British Columbia Ministry of Mining and Critical Minerals, British Columbia Geological Survey Paper 2026-01, pp. 239-245.

British Columbia Geological Survey, 2025a. British Columbia radiogenic isotope compilation (Sr-Nd-Hf-Pb). British Columbia Ministry of Mining and Critical Minerals, British Columbia Geological Survey, GeoFile 2025-08, 1 p.

British Columbia Geological Survey, 2025b. Tahltan Land Use Planning area mineral potential map for porphyry, volcanogenic massive sulphide (VMS), and magmatic mafic-ultramafic deposits. British Columbia Ministry of Mining and Critical Minerals, British Columbia Geological Survey Information Circular 2025-10, 2 p.

British Columbia Geological Survey, 2025c. Kaska Land Use Planning area mineral potential map for porphyry, volcanogenic massive sulphide (VMS), magmatic mafic-ultramafic, sedimentary exhalative (SEDEX) and Mississippi Valley Type (MVT) deposits. British Columbia Ministry of Mining and Critical Minerals, British Columbia Geological Survey Information Circular 2025-11, 2 p.

British Columbia Geological Survey, 2025d. Meziadin Land Use Planning area mineral potential map for porphyry, volcanogenic massive sulphide (VMS), and magmatic mafic-ultramafic deposits. British Columbia Ministry of Mining and Critical Minerals, British Columbia Geological Survey Information Circular 2025-12, 2 p.

British Columbia Geological Survey, 2025e. TRT Land Use Planning area mineral potential map for porphyry, volcanogenic massive sulphide (VMS), and magmatic mafic-ultramafic deposits. British Columbia Ministry of Mining and Critical Minerals, British Columbia Geological Survey Information Circular 2025-13, 2 p.

British Columbia Geological Survey, 2025f. Pan-Canadian workshop on mineral potential modelling, September 23, 2025, program with extended abstracts. British Columbia Ministry of Mining and Critical Minerals, British Columbia Geological Survey GeoFile 2025-24, 37 p.

Campbell, R.W., Gibson, K., and van Straaten, B.I., 2026. Paleozoic to Eocene intrusions in the Golden Triangle, northwestern British Columbia: A project update. In: Geological Fieldwork 2025, British Columbia Ministry of Mining and Critical Minerals, British Columbia Geological Survey Paper 2026-01, pp. 131-142.

Clarke, G., Northcote, B.K., Corcoran, N.L., Pothorin, C., Heidarian, H., and Hancock, K., 2026. Mining and Exploration in British Columbia, 2025: A summary. British Columbia Ministry of Mining and Critical Minerals, British Columbia Geological Survey Paper 2026-02, 73 p.

Cordey, F., Zagorevski, A., and Mihalynuk, M.G., 2025. Report on samples collected for radiolaria identification, Atlin area, northwest British Columbia. British Columbia Ministry of Mining and Critical Minerals, British Columbia Geological Survey GeoFile 2025-17, 3 p.

Cui, Y., 2021. A geospatial frame data model to simplify digital map compilation and integration. British Columbia Ministry of Energy, Mines and Low Carbon Innovation, British Columbia Geological Survey Paper 2021-03, 20 p.

Cui, Y., Norris, J., and Fortin, G., 2026. British Columbia geoscience Spatial Data Infrastructure (BCgSDI): A progress report. In: Geological Fieldwork 2025, British Columbia Ministry of Mining and Critical Minerals, British Columbia Geological Survey Paper 2026-01, pp. 221-226.

Elia, E.A., and Ferbey, T., 2026. Interior Plateau surficial geology compilation: Selection and standardization of maps and data. In: Geological Fieldwork 2025, British Columbia Ministry of Mining and Critical Minerals, British Columbia Geological Survey Paper 2026-01, pp. 227-237.

EY LLP, 2026. British Columbia mineral and coal exploration survey 2025 report, in press.

Ferbey, T., and Elia, E.A., 2025a. Surficial geology of the Nanitsch Lake area (NTS 94D/1), British Columbia. British Columbia Ministry of Mining and Critical Minerals, British Columbia Geological Survey Geoscience Map 2025-02, 1:50,000 scale.

Ferbey, T., and Elia, E.A., 2025b. Surficial geology of the Carruthers Pass area (NTS 94D/8), British Columbia. British Columbia Ministry of Mining and Critical Minerals, British Columbia Geological Survey Geoscience Map 2025-03, 1:50,000 scale.

Ferbey, T., and Elia, E.A., 2026a. Surficial geology of the Notch Peak area (NTS 94C/4), British Columbia. British Columbia Ministry of Mining and Critical Minerals, British Columbia Geological Survey Geoscience Map 2026-01, 1:50,000 scale.

Ferbey, T., and Elia, E.A., 2026b. Surficial geology of the Aiken Lake area (NTS 94C/5), British Columbia. British Columbia Ministry of Mining and Critical Minerals, British Columbia Geological Survey Geoscience Map 2026-02, 1:50,000 scale.

Ferri, F., and Friedman, R., 2026a. Age and geochemistry of middle to late Paleozoic volcanism along the western edge of Ancestral North America in north-central British Columbia. In: Geological Fieldwork 2025, British Columbia Ministry of Mining and Critical Minerals, British Columbia Geological Survey Paper 2026-01, pp. 183-201.

Ferri, F., and Friedman, R., 2026b. Geochemistry of volcanic rocks in the Snowshoe Group (Neoproterozoic-Cambrian) and geochronology, Sm-Nd isotopic data, and geochemistry of crosscutting Permian intrusions: Episodic back-arc magmatism along the western edge of Ancestral North America in Kootenay terrane. In: Geological Fieldwork 2025, British Columbia Ministry of Mining and Critical Minerals, British Columbia Geological Survey Paper 2026-01, pp. 203-219.

Fortin, G., and Silva, P.L., 2025. Assessment report drillhole database: Development and initial data release. British Columbia Ministry of Mining and Critical Minerals, British Columbia Geological Survey GeoFile 2025-11, 9 p.

Fortin, G., and Silva, P.L., 2026. Assessment report-sourced surface-sediment geochemistry database: Data update. British Columbia. British Columbia Ministry of Mining and Critical Minerals, British Columbia Geological Survey GeoFile 2026-02, 8 p.

Gabites, J.E., and Mihalynuk, M.G., 2025. $^{40}Ar/^{39}Ar$ geochronologic data from samples collected as part of the Southern Nicola Arc Project. British Columbia Ministry of Mining and Critical Minerals, British Columbia Geological Survey GeoFile 2025-16, 9 p.

Graham, A.C., and Ootes, L., 2025. Geochemical analyses of SEDEX deposits in eastern British Columbia. British Columbia Ministry of Mining and Critical Minerals, British Columbia Geological Survey GeoFile 2025-13, 9 p.

Graham, A.C., Orovan, E., Wall, C., Goudie, D., Creaser, R., Layton-Matthews, D., and Ootes, L., 2025. Data release from critical mineral studies of the Kitsault, Huckleberry, and Berg porphyry deposits. British Columbia Ministry of Mining and Critical Minerals, British Columbia Geological Survey GeoFile 2025-23, 7 p.

Graham, A.C., Vaughan Forrester, K., Ootes, L., Bain, W., Campbell, R., and Goudie, D., 2026. Critical companion metals in porphyry deposits in British Columbia: Lithogeochemistry and scanning electron microscopy-mineral liberation analysis (SEM-MLA) from the Schaft Creek, Mount Polley, and New Afton deposits. In: Geological Fieldwork 2025, British Columbia Ministry of Mining and Critical Minerals, British Columbia Geological Survey Paper 2026-01, pp. 69-83.

Hickin, A.S., 2026. British Columbia Geological Survey's contributions to the Pan-Canadian Geoscience Strategy 2021-2026. In: Geological Fieldwork 2025, British Columbia Ministry of Mining and Critical Minerals, British Columbia Geological Survey Paper 2026-01, pp. 17-36.

Höy, T., and DeFields, G.M., 2025. Geology of the Lightning Peak map area (NTS 082E/15). British Columbia Ministry of Mining and Critical Minerals, British Columbia Geological Survey Open File 2025-02, 1:50,000 scale.

Lawley, C.J.M., Petts, D.C., Lee, W.-S., Cajal, Y., Carrasco-Godoy, C., Campbell, I., Dlugosz, J., Larson, K., Savard, D., Kjarsgaard, I., and van Straaten, B., 2025. Critical raw material potential of porphyry copper-gold deposits in the Golden Triangle, British Columbia, Canada, Ore Geology Reviews, 178, article 106463. <https://doi.org/10.1016/j.oregeorev.2025.106463>

Mihalynuk, M.G., and Gabites, J.E., 2026. 24 Ma Giant Copper polymetallic porphyry-related breccia of the ancestral Cascades, southwest British Columbia. In: Geological Fieldwork 2025, British Columbia Ministry of Mining and Critical Minerals, British Columbia Geological Survey Paper 2026-01, pp. 163-174.

Mihalynuk, M.G., Zagorevski, A., Campbell, R.W., Vaillancourt, A., and Haji Egeh, A., 2024. Geology of the western Gladys Lake area (NTS 104N/13E, 14). British Columbia Ministry of Mining and Critical Minerals, British Columbia Geological Survey Open File 2024-02, 1:50,000 scale.

Mihalynuk, M.G., Friedman, R.M., and Wall, C., 2025a. U-Pb geochronologic data from samples collected as part of the Southern Nicola Arc Project. British Columbia Ministry of Mining and Critical Minerals, British Columbia Geological Survey GeoFile 2025-15, 7 p.

Mihalynuk, M.G., Wall, C., and Zagorevski, A., 2025b. Time of deposition refinements for key stratigraphic intervals of the Nicola Group, southern British Columbia. In: Geological Fieldwork 2024, British Columbia Ministry of Mining and Critical Minerals, British Columbia Geological Survey Paper 2025-01, pp. 105-118.

Miller, E.A., van Straaten, B.I., Ferri, M.D., and Hunter, R., 2025a. Preliminary bedrock geology of the Kitsault River area, northwestern British Columbia: GIS data. British Columbia Ministry of Mining and Critical Minerals, British Columbia Geological Survey GeoFile 2025-20, 3 p.

Miller, E.A., Ferri, M.D., Wall, C., Creaser, R.A., van Straaten, B.I., and Graham, A.C., 2025b. New geochronologic data, Kitsault River area, northwestern British Columbia: Igneous zircons (high-precision CA-TIMS), detrital zircons (LA-ICP-MS), and molybdenite (Re-Os). British Columbia Ministry of Mining and Critical Minerals, British Columbia Geological Survey GeoFile 2025-21, 6 p.

NRCan (Natural Resources Canada), 2024. Critical Minerals List. Government of Canada. <https://www.canada.ca/en/campaign/critical-minerals-in-canada/critical-minerals-an-opportunity-for-canada.html> (last accessed March 17, 2026).

Nelson, J.L., 2026. Early Jurassic intrusion and deformation in the Wark-Colquitz complex, Victoria, British Columbia. In: Geological Fieldwork 2025, British Columbia Ministry of Mining and Critical Minerals, British Columbia Geological Survey Paper 2026-01, pp. 175-181.

Norris, J., and Fortin, G., 2019. Assessment report-sourced surface sediment geochemical database: Development and initial data release from the Interior Plateau. British Columbia Ministry of Energy, Mines and Petroleum Resources, British Columbia Geological Survey GeoFile 2019-04, 10 p.

Northcote, B.K., 2025. Sedimentary hosted lead-zinc deposits in British Columbia. British Columbia Ministry of Mining and Critical Minerals, British Columbia Geological Survey GeoFile 2025-19, 23 p.

Ootes, L., and Wall, C., 2024. High-precision U-Pb zircon igneous crystallization and detrital zircon maximum depositional ages from the Toodoggone region, north-central British Columbia. British Columbia Ministry of Energy, Mines and Low Carbon Innovation, British Columbia Geological Survey Open File 2024-06, 10 p.

Ootes, L., Bergen, A.L., Milidragovic, D., and Jones, G.O., 2020. Geology of the northern Hogem batholith and its surroundings, north-central British Columbia. British Columbia Ministry of Energy and Mines and Petroleum Resources, British Columbia Geological Survey Open File 2020-02, 1:50,000 scale.

Ootes, L. Graham, A.C., Whitmore, K., Goudie, D., Piercey, S.J., Barker, S., Milne, S., and McFarlane, C., 2026a. Mineralogical control on critical companion metal distribution: Expended workflow, with examples from the Sullivan Pb-Zn-Ag deposit. In: Geological Fieldwork 2025, British Columbia Ministry of Mining and Critical Minerals, British Columbia Geological Survey Paper 2026-01, pp. 45-52.

Ootes, L., Wall, C., and Mihalynuk, M.G., 2026b. Rossland Group extends north: Detrital zircon U-Pb ages allow supracrustal unit reassignments in southern British Columbia and have tectonic implications. In: Geological Fieldwork 2025, British Columbia Ministry of Mining and Critical Minerals, British Columbia Geological Survey Paper 2026-01, pp. 119-130.

Orchard, M.J., Friedman, R.M., and Mihalynuk, M.G., 2025. Conodonts identify the lower-middle Norian boundary in association with ~224 Ma U-Pb dates from the Nicola Group, southern British Columbia, Canada. Journal of the Geological Society, 182. <https://doi.org/10.1144/jgs2024-299>

Piercey, S.J., Pietruszka, D., and Goudie, D., 2025. Critical metals in volcanogenic massive sulphide (VMS) deposits in British Columbia: A progress report. In: Geological Fieldwork 2024, British Columbia Ministry of Mining and Critical Minerals, British Columbia Geological Survey Paper 2025-01, pp. 189-201.

Pietruska, D.K., Wei, C., Piercey, S.J., Aylward, W., and Kommescher, S., 2026. Supplementary data for 'Critical metal distributions in volcanogenic massive sulphide (VMS) deposits in British Columbia: A progress report'. British Columbia Ministry of Mining and Critical Minerals, British Columbia Geological Survey GeoFile 2026-01, 3 p.

Rukhlov, A.S., Coats, B., Van der Vlugt, J., Beaupre-Olsen, I.J., and Zaborniak, K., 2023. British Columbia Geological Survey Sample Archive: An emerging resource for public geoscience. In: Geological Fieldwork 2022, British Columbia Ministry of Energy, Mines and Low Carbon Innovation, British Columbia Geological Survey Paper 2023-01, pp. 85-90.

Rukhlov, A.S., Cui, Y., Cunningham, Q., Fortin, G., and Anderson, C., 2024. Geochemical signals of carbonatite-related critical metals in provincial stream sediments. In: Geological Fieldwork 2023, British Columbia Ministry of Energy, Mines and Low Carbon Innovation, British Columbia Geological Survey Paper 2024-01, pp. 97-122.

Rukhlov, A.S., Ootes, L., Creaser, R.A., Cunningham, Q.F., de Waal, F.S., and Wenger, D.K., 2025a. British Columbia carbonatites revisited: New whole rock Sr-Pb-Nd isotopic insights and drainage prospectivity trends. In: Geological Fieldwork 2024, British Columbia Ministry of Mining and Critical Minerals, British Columbia Geological Survey Paper 2025-01, pp. 119-139.

Rukhlov, A.S., Ootes, L., and Han, T., 2025b. British Columbia radiogenic isotope compilation (Sr-Nd-Hf-Pb): Introduction and examples of utility. In: Geological Fieldwork 2024, British Columbia Ministry of Mining and Critical Minerals, British Columbia Geological Survey Paper 2025-01, pp. 177-188.

Rukhlov, A.S., Ootes, L., Cunningham, Q.F., Goudie, D., von der Handt, A., Spence, J., Wall, C., and Barker, S., 2026. A multi-analytical approach to stream-sediment samples from modern drainages enhances the search for REE and rare metals. In: Geological Fieldwork 2025, British Columbia Ministry of Mining and Critical Minerals, British Columbia Geological Survey Paper 2026-01, pp. 97-117.

van Straaten, B.I., 2026. A Triassic-Jurassic stratigraphic framework for the Golden Triangle, northwestern British Columbia: A project update. In: Geological Fieldwork 2025, British Columbia Ministry of Mining and Critical Minerals, British Columbia Geological Survey Paper 2026-01, pp. 143-151.

Wearmouth, C.D., Czertowicz, T.A., Peters, K.J., and Orovan, E.A., 2024a. Preliminary mineral potential maps for the porphyry, volcanic massive sulphide, and magmatic mafic-ultramafic mineral systems, northwest British Columbia. British Columbia Ministry of Energy, Mines and Low Carbon Innovation, British Columbia Geological Survey Open File 2024-05, 1:800,000 scale.

Wearmouth, C.D., Czertowicz, T.A., and Peters, K.J., 2024b. Preliminary mineral potential maps for the SEDEX and MVT mineral systems, northwest British Columbia. British Columbia Ministry of Energy, Mines and Low Carbon Innovation, British Columbia Geological Survey Open File 2024-11, 1:500,000 scale.

Wei, Ch., Pietruszka, D.K., Piercey, S.J., Aylward, W., Kommescher, S., Scanlan, E., and Layton-Matthews, D., 2026. Critical metal distributions in volcanogenic massive sulphide (VMS) deposits in British Columbia: A progress report. In: Geological Fieldwork 2025, British Columbia Ministry of Mining and Critical Minerals, British Columbia Geological Survey Paper 2026-01, pp. 53-67.

Zagorevski, A., Cordey, F., Mihalynuk, M.G., and Vaillancourt, A., 2026a. Application of radiolarian biostratigraphy in constraining geology of the northern Canadian Cordillera, British Columbia and Yukon. In: Geological Fieldwork 2025, British Columbia Ministry of Mining and Critical Minerals, British Columbia Geological Survey Paper 2026-01, pp. 153-162.

Zagorevski, A., Cordey, F., Mihalynuk, M.G., and Vaillancourt, A., 2026b. Compilation of micropaleontological data from the northern Canadian Cordillera, British Columbia and Yukon. British Columbia Ministry of Mining and Critical Minerals, British Columbia Geological Survey GeoFile 2026-05, 4 p.

Zhang, P., Brideau, M-A., and Szponarski, K., 2026. Geoscience knowledge density map of British Columbia, Version 1.0. In: Geological Fieldwork 2025, British Columbia Ministry of Mining and Critical Minerals, British Columbia Geological Survey Paper 2026-01, pp. 247-251.

British Columbia Geological Survey's contributions to the Pan-Canadian Geoscience Strategy 2021-2026

Adrian S. Hickin[1, a]

[1] British Columbia Geological Survey, Ministry of Mining and Critical Minerals, Victoria, BC, V8W 9N3
[a] corresponding author: Adrian.Hickin@gov.bc.ca

Recommended citation: Hickin, A.S., 2026. British Columbia Geological Survey's contributions to the Pan-Canadian Geoscience Strategy 2021-2026. In: Geological Fieldwork 2025, British Columbia Ministry of Mining and Critical Minerals, British Columbia Geological Survey Paper 2026-01, pp. 17-36.

Abstract

With the goal of strengthening cross-jurisdiction coordination of public geoscience to support responsible resource development and the public good, the Pan-Canadian Geoscience Strategy was established as a collaboration among federal, provincial, and territorial geological survey organizations and is coordinated through the National Geological Surveys Committee. Through five priority areas (advancing framework geoscience, improving mineral and energy potential modelling, enhancing data accessibility, supporting geoscience training, promoting public literacy in Earth sciences), the Strategy aims to coordinate efforts to deliver accessible, high-quality geoscience data that supports resource development, land-use planning, climate action, and public safety while fostering innovation and training to strengthen Canada's role in the global energy transition and critical minerals supply chain. The Strategy encapsulates common objectives of Canadian jurisdictions and is intended to enhance collaboration and incrementally advance geoscience knowledge across the country. Since the Strategy was endorsed by federal, provincial, and territorial mines and energy Ministers in 2021, the British Columbia Geological Survey has made significant contributions to each of the priority areas, in large part related to critical mineral research, and has served to co-lead or champion related activities at the national level.

Keywords: Pan-Canadian Geoscience Strategy, National Geological Surveys Committee, Intergovernmental Geoscience Accord, public geoscience, critical minerals, framework geoscience, mineral potential modelling, geoscience data, training geoscientists, geoscience outreach, geoscience engagement

1. Introduction

Canada's mineral and energy sectors are vital to its economy, and public geoscience underpins investment, exploration, and environmental stewardship. High-quality geoscience data reduces exploration risk, informs land-use planning, and supports Indigenous self-determination and decision making. As global demand for critical minerals accelerates, Canada faces challenges in reversing declining reserves and identifying new opportunities. Coordinated public geoscience efforts are essential to maintain national competitiveness and meet environmental, social, and governance (ESG) expectations.

With a goal of strengthening cross-jurisdiction coordination of public geoscience to support responsible resource development and the public good, the Pan-Canadian Geoscience Strategy (Fig. 1) was established as a collaboration among federal, provincial, and territorial geological survey organizations and is coordinated through the National Geological Surveys Committee (NGSC; National Geological Survey Committee, 2025). Advances in science and technology offer expanded opportunities for data acquisition, predictive modeling, digital integration, and modernization of geoscience digital data systems and applications. The Strategy provides a framework for geological survey organizations to lever innovations, share expertise, and collectively enhance Canada's geoscience knowledge base. The strategy outlines five priority areas: 1) advancing framework geoscience; 2) improving mineral and energy potential modelling; 3) enhancing data accessibility; 4) supporting geoscience training; and 5) promoting public literacy in Earth sciences. These priority areas were identified as elements paramount to advance the Canadian economy and support evolving societal needs.

The present contribution describes each of these priority areas and details how the British Columbia Geological Survey (BCGS) has advanced each of them in the province, in large part through critical mineral research, and served to co-lead or champion related activities at the national level.

2. Strategy context and funding

The Strategy was developed in response to the Canadian Minerals and Metals Plan (Natural Resources Canada, 2019) and was endorsed by jurisdiction Ministers in 2021. It is coordinated through the National Geological Surveys Committee a federal-provincial-territorial body that facilitates cooperation among geological surveys and operates under the Intergovernmental Geoscience Accord (National Geological Survey Committee, 2022), which sets out principles for shared responsibilities in geoscience across Canadian jurisdictions. The Accord is signed by all sitting federal, provincial, and territorial mines and energy ministers except for Québec and Prince Edward Island. Québec participates in the spirit of the

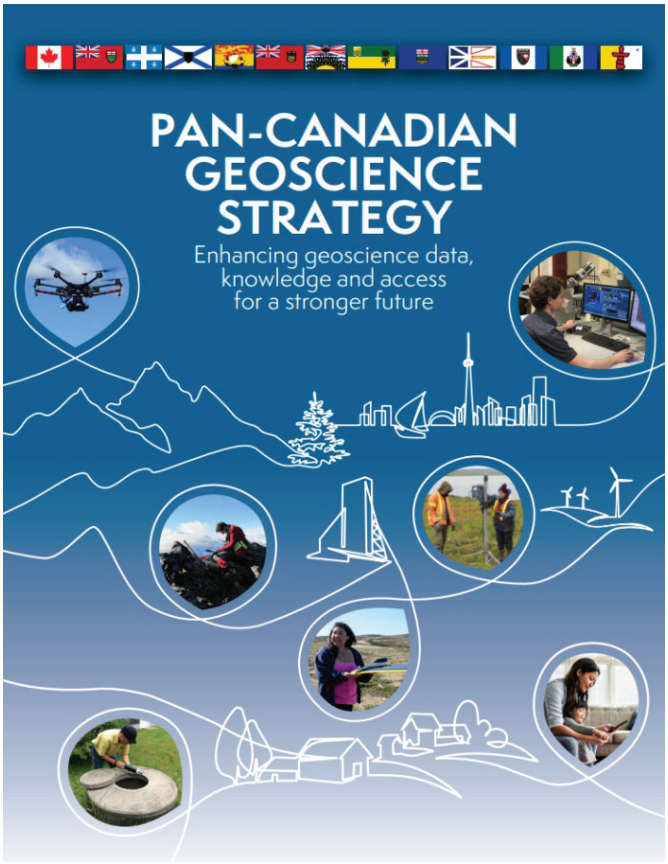


Fig. 1. Cover of Pan-Canadian Geoscience Strategy document. National Geological Surveys Committee of Canada (2022a).

accord, but Prince Edward Island does not have a geological survey organization. First signed in 1996, the accord is typically renewed every five years.

Although endorsed by mines and energy Ministers in Canada, the Strategy is not formally funded. This lack of funding is in marked contrast to large dedicated investment programs in Australia (Geoscience Australia, 2024, 2026), the United States (e.g., United States Geological Survey, 2026), and Europe (EuroGeoSurveys Secretariat, 2025; GeoERA, 2026) and to past coordinated federal-provincial funding frameworks in Canada such as the Mineral Development Agreements (MDAs) of the 1980s and 1990s. The MDAs were federal-provincial partnerships intended to stimulate mineral exploration, technological development, and regional economic growth. MDAs functioned as cooperative frameworks through which the federal government aligned its scientific and technological capabilities with provincial resource strategies (e.g., Janke, 1990). The primary goals included modernizing mineral research, strengthening geoscience programs, and promoting private-sector exploration during a decade characterized by depressed global commodity prices.

Since the MDAs, most federal funding flows to provinces and territories by cost sharing and contribution agreements through programs like Targeted Geoscience Initiative (TGI), Geomapping for Energy and Minerals-GeoNorth (GEM-GeoNorth) and Critical Minerals Geoscience and Data (CMGD). BCGS has benefitted from dedicated provincial funding since 2022 through CleanBC and the provincial Critical Mineral Strategy. These resources have been significantly levered by federal funding through programs like TGI, GEM-GeoNorth, and CMGD and partnerships with universities through Natural Sciences and Engineering Research Council of Canada (NSERC) grants. The injection of these new funds has stimulated projects and activities that have advanced the Strategy priority areas in British Columbia. In the absence of a formally funded strategy, these federal programs have been essential to bring resources into provincial and territorial geoscience organizations that advance the goals of the Strategy.

Although these programs are important for advancing federal, provincial, and territorial priorities, they remain in silos that are not specifically tied to the Strategy. Given massive, dedicated investments by competitors such as Australia, the USA, and the European Union, federal, provincial, and territorial geoscience programs have an opportunity to evolve and consider specific funding that would advance and optimize Strategy goals, objectives, and activities as the Pan-Canadian Geoscience Strategy matures into its second five years.

3. Advancing framework geoscience (priority 1)

Framework geoscience encompasses most of the traditional research by geological surveys and is the foundation for understanding Earth and its history. This work includes elements such as bedrock and surficial geology mapping, the most fundamental form of geoscience research, and ancillary petrographic, stratigraphic, structural, geochronologic, isotopic, lithogeochemical, regional geochemical, geophysical studies and metallogenic and tectonic syntheses. Since the inception of the Strategy, the Survey has been active across the province, carrying out local, regional, and province-wide framework geoscience work (Fig. 2).

Survey geologists have carried out mapping projects in the northwest part of the province in an area known informally as the ‘Golden Triangle’ (Fig. 3; e.g., van Straaten et al., 2022; Miller et al., 2023, 2025a), the Atlin area (e.g., Mihalynuk et al., 2021, 2024) and elsewhere (e.g., Schiarizza, 2022, 2024; Höy and Jackaman, 2024a, b; Veness et al., 2024; Höy and DeFields, 2025; Sauvé et al., 2025). Other studies have focused on regional stratigraphic, magmatic, geochronological, and isotopic frameworks (Table 1). Some of these studies have benefited from emerging technology such as data collection from remotely piloted aircraft systems (RPAS) popularly referred to as drones (Fig. 4; e.g., Elia et al., 2023, 2024a, b; Ferbey et al., 2024).

Like many jurisdictions in Canada and around the world, BCGS has recently focused on foundational work devoted to critical minerals (e.g., Hickin et al., 2023, 2024). The Survey’s approach has been to assess the critical mineral deportment in British Columbia’s primary mineral systems and mines and to provide data, tools, and knowledge that will encourage investment of underexplored resources. These studies have been



Fig 2. Sites of field-based framework geoscience activities by the British Columbia Geological Survey, 2021-2026.

directed at porphyry (e.g., Orovan et al. 2024, 2025; Graham et al., 2025b, 2026), volcanogenic massive sulphide (VMS, e.g., Piercey, 2025; Piercey et al., 2025; Wei et al., 2026), sedimentary exhalative (SEDEX; e.g. Northcote, 2025; Graham and Ootes, 2025; Graham et al., 2025a, b; Ootes et al., 2026a), magnetite skarn (e.g., Bain, 2024; Bain et al., 2025), mafic-ultramafic intrusive (e.g., Spence et al., 2022; Brzozowski and Zaborniak, 2024), and carbonatite (e.g. Rukhlov et al., 2024, 2025a, b, 2026) mineral systems.

In support of other critical minerals projects, the Survey has dedicated considerable resources to upgrading its rock and sediment sample archive (Rukhlov et al., 2023) and geochemical dataset. Of particular importance for understanding the geologic settings in which critical metals mineralize, archived samples have been reanalyzing using modern whole-rock, trace element, and stable and radiogenic isotopic methods (e.g. Van der Vlugt et al., 2022; Han and Rukhlov, 2024; British Columbia Geological Survey, 2025e;



Fig. 3. Field mapping of rocks in the 'Golden Triangle' of northwestern British Columbia.

Rukhlov et al., 2025c). In addition, work continues to establish the timing, emplacement setting, and geographic distribution of both fertile and barren intrusions using high-precision chemical abrasion isotope dilution-thermal ionization mass spectrometry (CA-TIMS) age and isotopic tracer data (e.g., Ootes et al., 2022, 2026b; Ootes and Wall, 2024), and evaluating geochemistry and indicator minerals in modern surface water drainages to develop exploration tools for fingerprinting upstream carbonatite-hosted niobium, rare earth element, and other critical mineral deposits (e.g., Rukhlov et al., 2024, 2025a, b, 2026). Many new and archived samples are being examined to reveal critical metal distributions and element partitioning behaviors between mineral phases by combining petrographic images with methods including scanning electron microscope-mineral liberation analysis (SEM-MLA; Fig. 5), electron probe microanalysis (EPMA); laser ablation-inductively coupled plasma-mass spectrometry (LA-ICP-MS) and micro x-ray fluorescence analysis (e.g., Graham and Ootes, 2025;



Fig. 4. Remotely piloted aircraft system (RPAS), also know as a drone, deployed by British Columbia Geological Survey. **a)** DJI Matrice 600 Pro aircraft help investigate surface sediment composition in the Interior Plateau. **b)**, **c)**, and **d)** drone crew operating and maintaining equipment.

Table 1. Selected BCGS framework geoscience publications since 2021.

Category	Title	Reference
Geochronology	U-Pb geochronological data for intrusive rocks near the Schaft Creek and Galore Creek deposits (southern Telegraph Creek area, NTS 104G), northwestern British Columbia	Bailey et al., 2025
	U-Pb geochronologic data from samples collected as part of the Southern Nicola Arc Project	Mihalynuk et al., 2025a
	$^{40}Ar/^{39}Ar$ geochronologic data from samples collected as part of the Southern Nicola Arc Project	Gabites and Mihalynuk, 2025
	New geochronologic data, Kitsault River area, northwestern British Columbia: Igneous zircons (high-precision CA-TIMS), detrital zircons (LA-ICP-MS), and molybdenite (Re-Os)	Miller et al., 2025b
	High-precision U-Pb zircon igneous crystallization and detrital zircon maximum depositional ages from the Toodoggone region, north-central British Columbia	Ootes and Wall, 2024
	Rossland Group extends north: Detrital zircon U-Pb ages allow supracrustal unit reassignments in southern British Columbia and have tectonic implications	Ootes et al., 2026b
	U-Pb zircon dates for rhyolite and sandstone of Cadwallader terrane, lower Chilcotin River area, south-central British Columbia	Schiarizza and Friedman, 2023
	Conodonts and detrital zircons from Triassic and Jurassic rocks above the Salmon River unconformity, Thompson Plateau, south-central British Columbia	Schiarizza et al., 2022
	The age and provenance of the Lay Range assemblage provides an indirect record of basement to north-central Quesnellia, British Columbia	Ootes et al., 2022
	Geochronologic data from the Kitsault River area, northwest British Columbia	Hunter et al., 2022a
	Geochronology of northern Hogem batholith, Quesnel terrane, north-central British Columbia	Jones et al., 2021
	U-Pb zircon date for Eocene volcanic rocks on Mount Timothy, southcentral British Columbia	Schiarizza and Friedman, 2021
Magmatic	New data on Late Triassic to late Early Jurassic plutonic suites in the northern Golden Triangle region of northwest British Columbia	Campbell and van Straaten, 2025
	Apatite fission track data from northern Hogem batholith, Quesnel terrane, north-central British Columbia: A progress report	Wang, et al., 2025
	Geology and geochemistry of the Kamloops Group (Eocene) in its type area, Kamloops, British Columbia	Van Wagoner and Ootes, 2022
	Volcanism and geochemistry of the Kamloops Group, south-central British Columbia	Van Wagoner et al., 2021a
	Geochemical data from the Kamloops Group	Van Wagoner et al., 2021b
	Mineralogical control on critical companion metal distribution: Expanded workflow, with examples from the Sullivan Pb-Zn-Ag deposit	Ootes et al., 2026a
	Critical companion metals in porphyry deposits in British Columbia: Lithogeochemistry and scanning electron microscopy-mineral liberation analysis (SEM-MLA) from the Schaft Creek, Mount Polley, and New Afton deposits	Graham et al., 2026
	Critical metal distributions in volcanogenic massive sulphide (VMS) deposits in British Columbia: A progress report	Wei et al., 2026
	A multi-analytical approach to stream-sediment samples from modern drainages enhances the search for REE and rare metals	Rukhlov et al., 2026
	Critical minerals at the Berg and Huckleberry porphyry deposits, British Columbia, using scanning electron microscopy-mineral liberation analysis (SEM-MLA)	Orovan et al., 2025

Table 1. Continued.

Category	Title	Reference
Magmatic	A preliminary assessment of critical companion metals in SEDEX deposits of eastern British Columbia: Examples from the historic Sullivan mine and the Cirque project	Graham et al., 2025a
	Co-Te mineralization in iron skarns on Vancouver Island and Texada Island	Bain et al., 2025
	Critical metals in volcanogenic massive sulphide (VMS) deposits in British Columbia: A progress report	Piercey et al., 2025
	Geochemical analyses of SEDEX deposits in eastern British Columbia	Graham and Ootes, 2025
	Textural evidence for ore fluid transport and the magmatic to hydrothermal transition at the past-producing Kitsault Mo-Ag mine	Orovan et al., 2024
	Sulphide mineralization at the E&L magmatic Ni-Cu-PGE deposit: Textural evidence for contamination, vapour saturation, fluid immiscibility, and metal remobilization	Brzowski and Zaborniak, 2024
	Ore and alteration textures of limestone-hosted magnetite-sulphide mineralization at the Merry Widow deposit, Vancouver Island, British Columbia	Bain, 2024
	Did epithermal mineralization in the northern Toodoggone region develop synchronously with large-scale folding?	Ootes, 2023
	Geology of the Tatogga property: Geologic framework for the Saddle North porphyry Cu-Au deposit and the Saddle South epithermal Au-Ag vein system, Iskut district, northwestern British Columbia	Greig et al., 2021
Stratigraphy	Stratigraphic framework, structural setting, and timing of VMS, epithermal, and porphyry mineralization in the Kitsault River area, northwestern British Columbia	Miller et al., 2025c
	Upper Hazelton Group stratigraphy along the Stikine arch, northwestern British Columbia	van Straaten, 2024
	Stratigraphy of the Stuhini Group (Upper Triassic) in the Galore Creek area, northwestern British Columbia	van Straaten et al., 2023
	Time of deposition refinements for key stratigraphic intervals of the Nicola Group, southern British Columbia	Mihalynuk et al., 2025b
	Revised stratigraphy and geochronology of the Hazelton Group, host rocks for volcanogenic mineralization in the Kitsault River area, northwest British Columbia	Hunter et al., 2022b
	Revised stratigraphy of the Stuhini and Hazelton groups and LA-ICP MS zircon geochronology of the Scottie gold mine area, northwestern British Columbia	Stanley and Nelson, 2022
Surficial geology	Interior Plateau surficial geology compilation: Selection and standardization of maps and data	Elia and Ferby, 2026
	Surficial geology of the Nanitsch Lake area (NTS 94D/1)	Ferbey and Elia, 2025a
	Surficial geology of the Carruthers Pass area (NTS 94D/8), British Columbia	Ferbey and Elia, 2025b

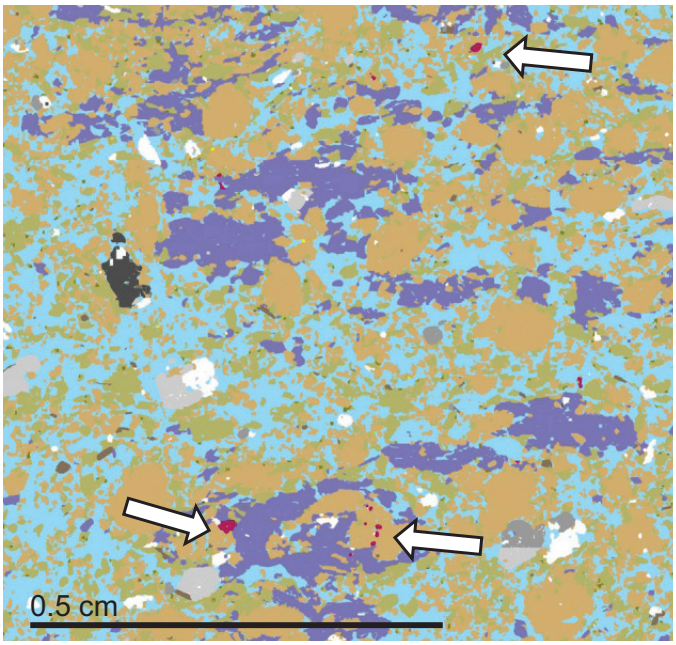


Fig. 5. False colour scanning electron microscope-mineral liberation analysis (SEM-MLA) to find trace minerals such as cassiterite (SnO_2; arrows). See Ootes et al. (2026a).

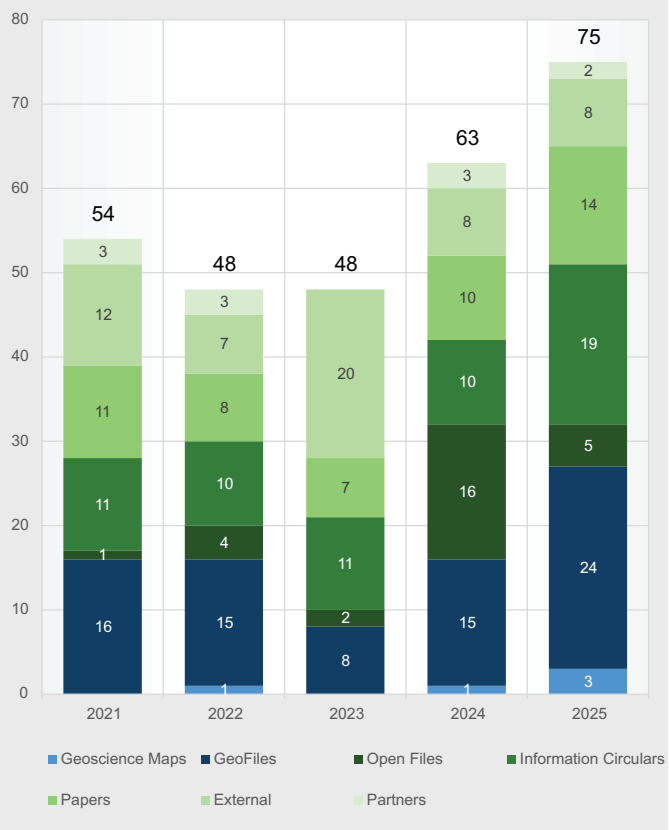


Fig. 6. British Columbia Geological Survey releases 2021-2025 broken down by publication series.

Orovan et al., 2025; Piercey et al., 2025; Ootes et al., 2026a; Wei et al., 2026).

In conjunction with the Geological Survey of Canada, the BCGS has partnered to examining the physical properties of archived samples (density, magnetic susceptibility, porosity) to improve geophysical interpretations and enhance potential fertility assessments remotely (Enkin et al., 2020). The surveys also released new province-wide compilations of high-resolution aeromagnetic data (Oneschuk et al., 2024).

As with all geological survey organizations, releasing the results of research carried out with public funds is essential, and the Survey strives for immediate publication of new foundational geoscience projects. Since 2021, BCGS has produced 288 publications (Fig. 6), most of which are related to the Strategy. Recent growth reflects the injection of new funding from sources not dedicated to the Strategy. Currently, the Survey is beginning to compile the footprint of publicly available geoscience publications in the province in a series geospatial geoscience knowledge density map (Zhang et al., 2026). These maps increase public awareness of geoscience activities and identify potential knowledge gaps for making land-use decisions, planning new projects, and mineral potential modelling.

4. Mineral and energy potential modelling (priority 2)

Mineral and energy resource potential modelling is a tool that uses diverse datasets to consider the likelihood of resources occurring in a given area by using advances in computer science, spatial analysis, and statistical predictive techniques. These models guide land-use and policy decisions, inform Indigenous self-determination processes, reduce exploration risk, attract investment, and support the discovery of critical minerals.

Mineral deposits and natural energy resources form in specific geological settings during distinct periods of Earth history, offering a certain level of predictability. The modelling process combines geological knowledge with spatial datasets such as geological maps, geophysical and geochemical surveys, and known occurrences, which are analyzed using statistical and Geographic Information System (GIS) tools. The main outputs are potential maps showing relative prospectivity for individual resource systems that can be integrated for comprehensive regional assessments. The goal of this priority area is to develop consistent, nation-wide predictive tools that integrate geological data and lever machine learning and data analytics. By coordinating efforts across jurisdictions, this priority area ensures standardized approaches, shared data, and innovative methods.

British Columbia was the first jurisdiction in Canada to complete a province-wide mineral potential assessment (Kilby, 1995, 2004). After a hiatus of about 30 years, the Survey has revitalized its mineral potential mapping program that builds on decades of new geological data, improved exploration techniques, new developments in programming languages and increases in computing power, which have led to significant advances in applying GIS platforms and using computerized

statistical methods. The Survey currently applies the weights of evidence method to integrate multiple geological proxies and training data, evaluate predictability, and generate probability models (Wearmouth, et al., 2024a, b). Modelling in northern British Columbia has focused on porphyry, volcanogenic massive sulphide (VMS), and mafic-ultramafic systems, which host critical minerals like copper, molybdenum, nickel, cobalt, and rare earth elements (Wearmouth et al., 2024c) and sedimentary exhalative (SEDEX) and Mississippi Valley-type (MVT) systems which host primary commodity critical metals such as lead, zinc and companions gallium, germanium, indium (Wearmouth et al., 2024d). These preliminary maps largely corroborate the 1990s assessments but benefit from new data and knowledge. Unlike the labour-intensive original work, the revitalized modelling uses automated spatial analysis, enabling easier updates and future expansion to additional mineral systems. Because of inherent uncertainties and limitations, these technical maps can easily be misunderstood, so the Survey has created more consumable versions for use by non-experts (British Columbia Geological Survey, 2025a, b, c). The Survey is now expanding its modelling program to extend across the entire province and include additional mineral systems.

British Columbia is not alone in advancing tools to predict mineral opportunities. Geological surveys in Canada are well-positioned to lead mineral potential modelling because of their expertise, extensive datasets, and digital infrastructure. As the National Geological Surveys Committee lead for this priority area, BCGS co-organized a workshop in the fall of 2025 (Fig. 7; British Columbia Geological Survey, 2025d) in which federal, provincial, territorial and international practitioners met to foster and coordinate innovation, discuss past, present, and future methods, explore emerging tools in artificial intelligence and geospatial analysis, and begin addressing shared challenges such as data integration, gaps in data coverage, model uncertainty and interpretation, and communicating results to non-specialists.

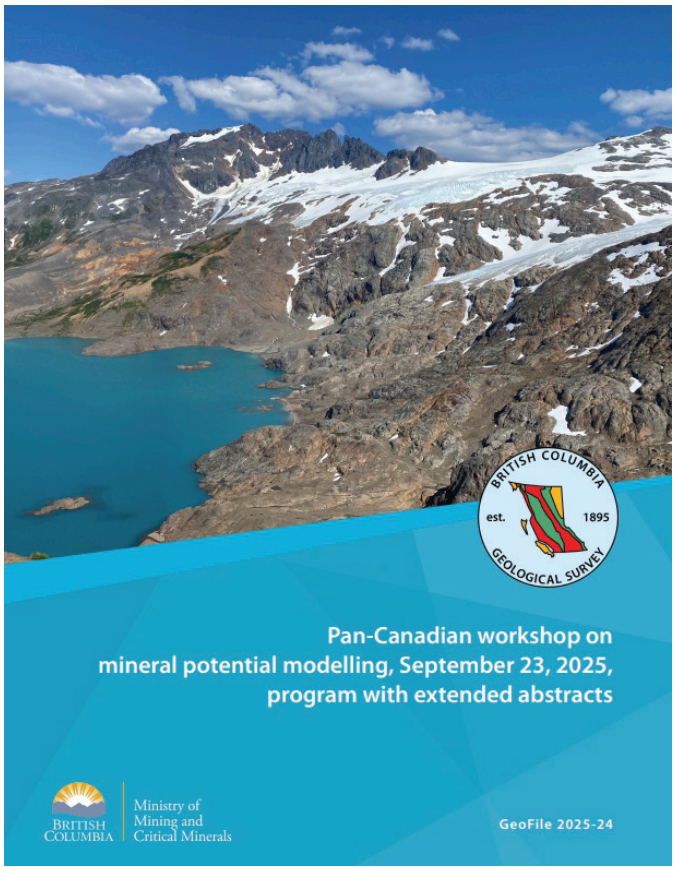


Fig. 7. Mineral potential modelling workshop, fall 2025 (British Columbia Geological Survey, 2025d).

5. Data delivery (priority 3)

Delivering high-quality geoscience data is essential for all publicly funded geological surveys. The data delivery priority of the Strategy is focused on making Canada's geoscience information easily discoverable, interoperable, and openly accessible through modern digital platforms. The goal is to integrate federal, provincial, and territorial datasets into standardized, user-friendly systems that support advanced analytics. This includes improving data quality, harmonizing formats, levering cloud technologies, and developing applications to enable sharing. By enhancing accessibility, this priority reduces duplication, accelerates innovation, and ensures that geoscience information is supporting emerging technology in the public and private sectors. As the steward of all provincial public geoscience and mineral resource data, the BCGS continues to deliver data through its geospatial web service (MapPlace), its digital coverage of bedrock geology (BC Digital Geology), and a suite of databases. Because much of the data are stored in a patchwork of legacy or obsolete systems, the Survey has initiated a project to modernize our databases and applications and bring them into an integrated system referred to as the BC geoscience Spatial Data Infrastructure (BCgSDI; Cui et al., 2026).

MapPlace, the Survey's geospatial web service, is a cornerstone of data accessibility. It enables users to query multiple databases simultaneously and is designed for ease of use, speed, and scalability, allowing anyone with internet access to visualize and access BCGS geoscience datasets and generate custom reports. Through continuous updates and upgrades, this platform significantly reduces the cost and complexity of accessing geoscience. The Survey also maintains a comprehensive catalogue of published reports, maps, and technical papers that can be freely accessed and downloaded online.

BC Digital Geology provides dynamic, province-wide geological coverage that evolves as new field mapping is completed. The coverage includes attributed bedrock geology as spatial data (lines, points, and polygons) that can be queried. BCGS has adopted a geospatial frame model (Cui, 2021) as a means of expediting map updates and strives to continuously enhance the accuracy and attributes for an

analytic-ready provincial bedrock geology data source. To support interoperable exchange of geological information, the BC Digital Geology has adopted the GeoSciML Lite schema and mapped the contents with the vocabularies used by the International Union of Geological Science Commission for the Management and Application of Geoscience Information. The Survey has recently undertaken a compilation of digital Quaternary geology focused on the Interior Plateau (Elia and Ferbey, 2026).

The Survey delivers raw information using a broad suite of databases that are routinely updated and available through the BCGS database webpage (British Columbia Geological Survey, 2026). The MINFILE mineral occurrence database catalogs more than 16,000 mineral occurrences and is currently being modernized and migrated to PostgreSQL/PostGIS; COALFILE contains extensive coal exploration data. The Assessment Report Indexing System (ARIS) database houses more than 41,500 assessment reports submitted since 1947. ARIS was recently modernized by migrating data from FoxPro to PostgreSQL/PostGIS. Because traditional paper or PDF assessment report formats make data extraction challenging, the Survey has a project to digitize older reports using Optical Character Recognition (OCR) to be machine-readable and has created assessment report-sourced databases in a GIS-ready GeoPackage format, thus transforming decades of hard-to-extract information into usable tools. One database contains surface-sediment geochemistry from the Interior Plateau and includes coordinates, sampling details, lab and analytical methods, and results from 34,000 samples with 1.45 million determinations (Norris and Fortin, 2019; Fortin and Silva, 2026). A second database includes drill hole information from the Interior Plateau and includes the locations and geometry of drill holes, core descriptions, sampling parameters, and geochemical assay results for more than 6000 drill holes, 80,000 samples, and 3.8 million determinations from 1300 assay certificates (Fortin and Silva, 2025). Property File is a unique collection of unpublished private documents donated by government, universities, industry, and individuals dating back to the late 19th century. In partnership with the Yukon Geological Survey, BCGS has initiated a Data Lake project, which includes scanning, indexing, and digitizing raw data and historical technical documents to a centralized repository that holds raw, structured, semi-structured, and unstructured data. The Data Lake will be available for interrogation through machine learning and natural language models to discover previously overlooked exploration information. The Survey geochemical database now includes five million determinations from more than 86,000 samples, and the geochronologic database contains about 8700 age determinations, including recent high-precision dating.

The British Columbia geoscience Spatial Data Infrastructure (BCgSDI) project (Cui et al., 2026) is perhaps the most significant enhancement being carried out at the Survey related to the data delivery priority. Although the public-facing end of the Survey databases have been well received, the back end is a patchwork of legacy systems, largely developed in-house, that are siloed and lack a common interface and coherent data management. These systems, many of which are decades-old, have resulted in several enduring challenges such as maintaining similar data in multiple systems and the cost of supporting disparate systems and obsolete technologies. In addition, the systems and applications are not immediately amenable to support AI (artificial intelligence) and LLM (large language models) for advanced data access and modelling. The general term ‘SDI’ (Spatial Data Infrastructure) refers to groups of logically arranged information systems that link data sources to products, are connected via a common interface, and facilitate data sharing and services. Adopting SDI concepts, the BCgSDI project is now making progress to eliminate current database-related service delivery impediments by linking currently disparate databases for better data access and updating. The Survey aspires to advance modern analytics by deploying an architecture on a Cloud platform. Ultimately, the BCgSDI supports efficient publication of analytic ready datasets and maps, improves discoverability through standardized metadata and services, and reduces friction in collaborative projects that span jurisdictions. The approach being used by the Survey also offers a practical template for similar modernizations in other agencies.

6. Training the next generation geoscientists (priority 4)

Building a strong pipeline of skilled geoscientists is needed to sustain Canada’s resource development and energy transition. This priority concentrates on promoting geoscience education and career pathways, strengthening collaboration with academic institutions to align training with emerging industry needs, and expanding experiential learning opportunities through employment and graduate work within geological survey organizations. Additionally, it aims to equip geoscientists with digital and data science skills to foster innovation and ensure a workforce that can lever advanced technologies for evidence-based decision making.

Although not part of its official mandate, BCGS has both formally and informally supported Earth Science post-secondary student projects and typically hires students, recent graduates, or early-career geoscientists as seasonal term geological assistants. Between 2021 and 2026, BCGS has been involved in training more than 30 graduate students and post-doctoral fellows through direct funding and/or through staff supervision. Staff are supporting or have supported student projects at the University of British Columbia, Simon Fraser University, University of Victoria, University of the Fraser Valley, University of Alberta, University of Manitoba, British Columbia Institute of Technology, Western University, Queen’s University, Memorial University of Newfoundland, Canterbury University (New Zealand), and Laoshan Laboratory (China). Projects include a variety of degree levels including PhD (20%), MSc (50%), and undergraduate (15%) as well as post-doctoral projects (15%). BCGS staff roles include supervisor or co-supervisor, advisor,

committee members, and external examiner. Upon request and as part of its general client focus, the Survey provides advice on how to access and use BCGS data and consultations to help students projects succeed.

The Survey contributes to the development of early career geoscientists by hiring them as geological assistants for seasonal term positions. These geological assistants are essential to geological surveys for the safe, efficient and cost-effective collection of field data while providing future geoscientists with hands-on field training that contributes to a highly skilled workforce. Since 2021, BCGS has provided 47 term positions (Fig. 8) mainly to geoscience undergraduate, graduate, and recently graduated university students from across Canada.

7. Geoscience literacy and outreach (priority 5)

Enhancing public literacy is intended to ensure Canadians understand the importance of how geoscience supports the economy, climate change adaptation, and public safety. This includes improving communication and outreach to make geoscience concepts, data, and expertise accessible to the public, policymakers, stakeholders, and rightsholders and be used to help balance resource development with environmental, cultural, and economic considerations. It also emphasizes engagement with Indigenous communities and diverse audiences to promote inclusivity and shared knowledge in managing Canada's geological resources responsibly. In 2023, BCGS hired a dedicated geoscientist to advance the Survey's engagement activities. Through its Engagement Program the Survey is connecting Indigenous Peoples, local communities, government, industry, and the public with the geology and mineral resources of the province. This work supports land-use planning, resource co-management, and relationship building.

Engagement with Indigenous Peoples is a central focus (Bacha, 2026). Many Indigenous Peoples seek a better understanding of the mineral endowment in their



Fig. 8. Training the next generation of geoscientists. **a)** BCGS-supported geological assistant hires. **b)** and **c)** Students being mentored in the field.

territories, recognizing its importance for self-determination and land-use discussions. As an unbiased public geoscience agency, the Survey strives to build trust with the more than 200 First Nations in the province by being an unbiased broker of information, sharing geological knowledge, and working collaboratively with Indigenous governments, leaders, and communities. Through the Engagement Program, BCGS works with Indigenous communities to raise awareness of research on their lands, identify opportunities and challenges, and explore partnerships.

The Survey has adopted, and is working to apply, dialogue and participatory models of engagement that are rooted in mutual respect, two-way communication, collaboration, and participation and strives to overcome barriers inherent in integrating Western geoscience with Traditional Knowledge (Bacha, 2026). The need to foster stronger relationships as an integral part of new fieldwork programs led the Survey to develop its Indigenous Peoples Engagement Policy, which ensures that all BCGS field projects go through multiple engagement sessions before, during, and after boots-on-the-ground activities (Fig. 9). BCGS has also enshrined archaeological and heritage considerations into fieldwork. While conducting work on the land, geologists may inadvertently encounter sites of Indigenous historical value, and the Survey has adopted a protocol that must be followed when finding unreported archaeological materials, commonly referred to as a 'chance finds'.

To date, the Engagement Geologist has worked with more than 50 Indigenous Nations in the province, with interactions ranging from addressing simple requests for information to multi-year partnerships. The geosciences can serve as a neutral and constructive entry point in land-use discussions because Traditional Knowledge and Western science intersections can be the foundation for dialogue. Fieldtrips provide unrivaled opportunities for Indigenous Peoples and geoscientists to come together on the land to build a common understanding of natural history and mineral resources. Collaboration between the Citxw Nlaka'pamux Assembly (CNA) of south-central British Columbia and the Survey led to a successful short course and fieldtrip in which CNA staff visited active exploration sites and experienced first-hand how geological research is carried out, and Survey and industry geologists learned about CNA values, worldviews, and understandings of nature (Fig. 10; Bacha, 2025).

Although focused on partnerships with Indigenous Peoples, the Engagement Program has a broader scope to bring geoscience knowledge to the public and to government groups. The Survey has provided public lectures and participated in events such as the Geodiversity Fest at the Royal British Columbia Museum (Fig. 11) and Discovery Day at the annual Association of Mineral Exploration Roundup convention that offered free, family-focused learning activities to spark interest in the Earth sciences, mineral exploration, and mining. Directed towards all natural resource ministry employees, the Survey

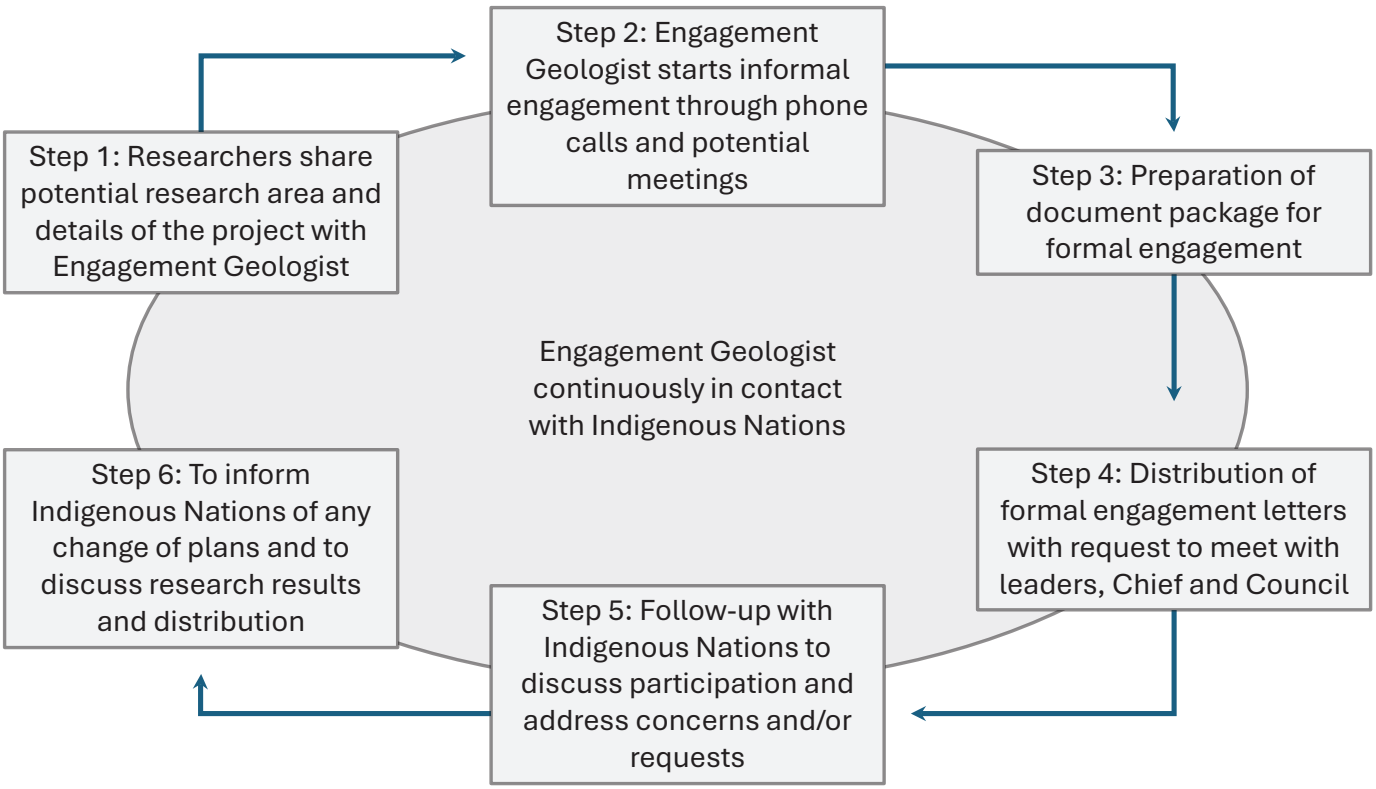


Fig. 9. Diagram depicting ideal Indigenous engagement timelines and workflow cycle for BCGS projects (see Bacha, 2026).



Fig. 10. a) Guidebook for field trip co-developed by BCGS and the Citxw Nlaka'pamux Assembly. **b)** Staff from the Citxw Nlaka'pamux Assembly at short course and **c)** on field trip.



Fig. 11. Engagement with the public. Lecture at the Royal British Columbia Museum, November 2025.

has repeatedly delivered a learning series encompassing topics such as the geological and tectonic history of the province, advances in geoscience, critical minerals, the exploration and mining life cycle, and environmental reclamation. In addition, at Mining Day at the Legislature, an event sponsored by the British Columbia Mining Association (MABC), the Survey provided experiential learning opportunities to the sitting government (Fig. 12), opposition members, and their staff.

8. National level

BCGS has been active at the national level. In 2020, the National Geological Surveys Committee, through a BCGS initiative, established the National Information and Data Management Working Group (IDM), with a goal to enhance the value of available and emerging geoscience data that remains isolated in provincial, territorial and federal repositories by enabling accessibility and interoperability for stakeholders internal and external to governments. The IDM is tasked with breaking down technical and jurisdiction barriers and finding solutions to data integration while recognizing that each jurisdiction must maintain its independence (Fig. 13). Since inception, BCGS has co-chaired or co-sponsored the working group.



Fig. 12. Engagement with government. Premier David Eby, and Minister of Mining and Critical Minerals Jagrup Brar, Mining Day at the Legislature, May 2025.

Following the release of the Strategy and after assessing federal, province and territorial readiness to deliver integrated geoscience data, the IDM was tasked to develop a method of delivering interoperable geoscience or mineral source information via a common portal. The IDM Working Group selected mineral occurrence data as a pilot project, co-led by the Geological Survey of Canada and BCGS, to successfully demonstrate the implementation of an open-standards-based, interoperable web service for accessing data across Canada. These data were networked in 2024 (Fig. 14). The project is continuing with bedrock geology as the next dataset, and a beta version is anticipated to be released to the public.

9. Conclusion

The Pan-Canadian Geoscience Strategy is a federal, provincial, and territorial collaboration that articulates the common needs and goals of geoscience organizations in Canada. All jurisdictions are delivering activities that are advancing the mission and vision of the Strategy and working together through the National Geological Survey Committee to enhance geoscience knowledge in Canada.

British Columbia, through the BCGS, has been active delivering projects and products that substantially advance each of the Strategy priority areas: 1) advancing framework geoscience; 2) improving mineral and energy potential modelling; 3) enhancing data accessibility; 4) supporting geoscience training; and 5) promoting public literacy in Earth sciences. In addition, the Survey has strived to lead at the national level, championing several areas and activities. The Survey will continue to develop geoscience programs to advance the Strategy while meeting the needs and objective of British Columbia.

Despite the contributions that British Columbia and the other Canadian jurisdictions have made, the Pan-Canadian Geoscience Strategy lacks dedicated funding, in contrast to competitors in Australia, the United States and the European Union. If Canada is committed to harnessing the country's mineral resources to contribute to the economy, mitigate external geopolitical threats like tariffs, compete with other nations, and combat climate change, then dedicated funding would help provinces and territories develop new collaborative programs that lever economies of scale. As the next five years of the Strategy is considered, Canada has an opportunity to embrace a national approach to funding Pan-Canadian Geoscience Strategy priority areas.

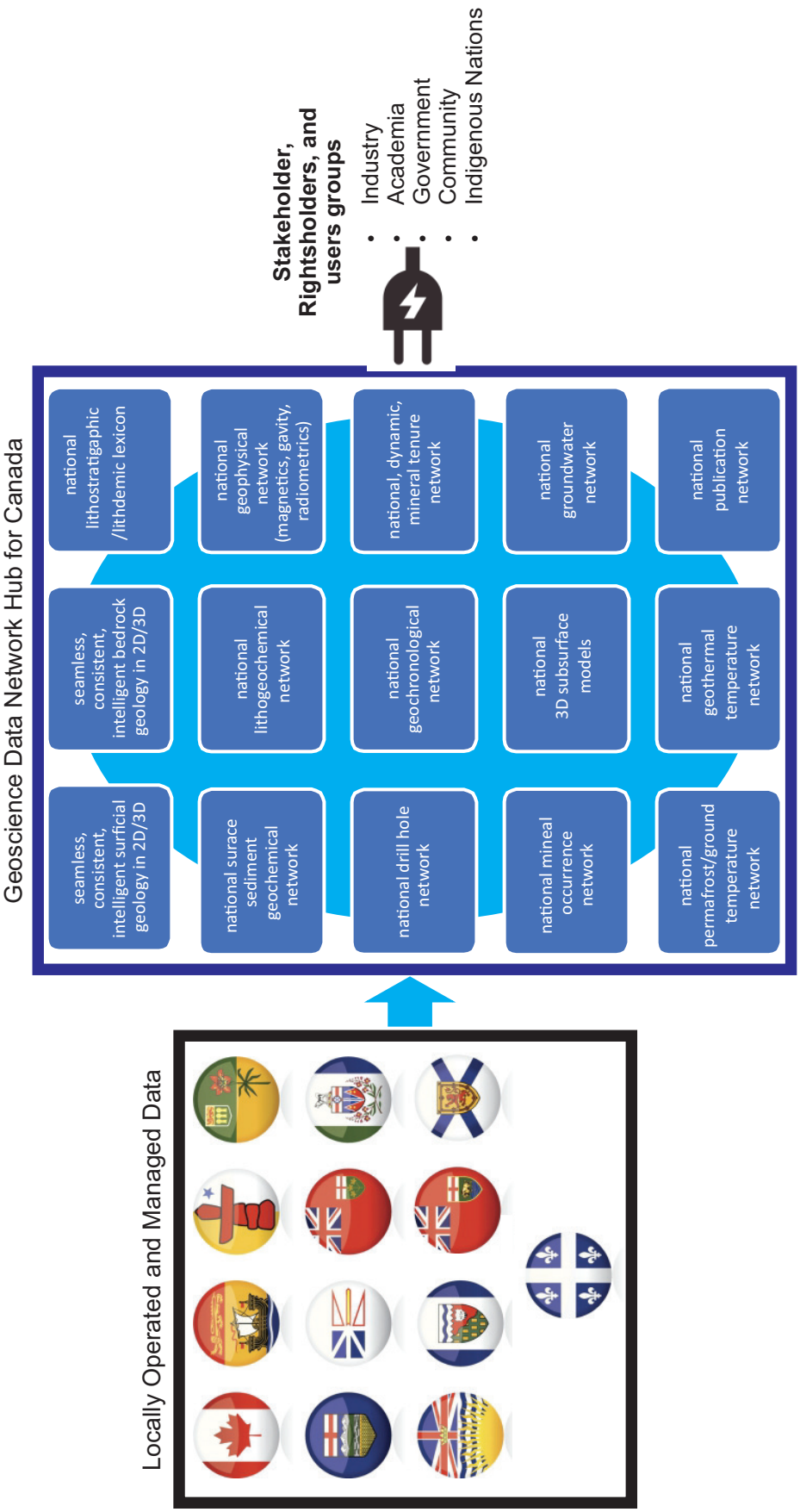


Fig. 13. National Geological Surveys Committee conceptual model for cross-jurisdiction data integration.

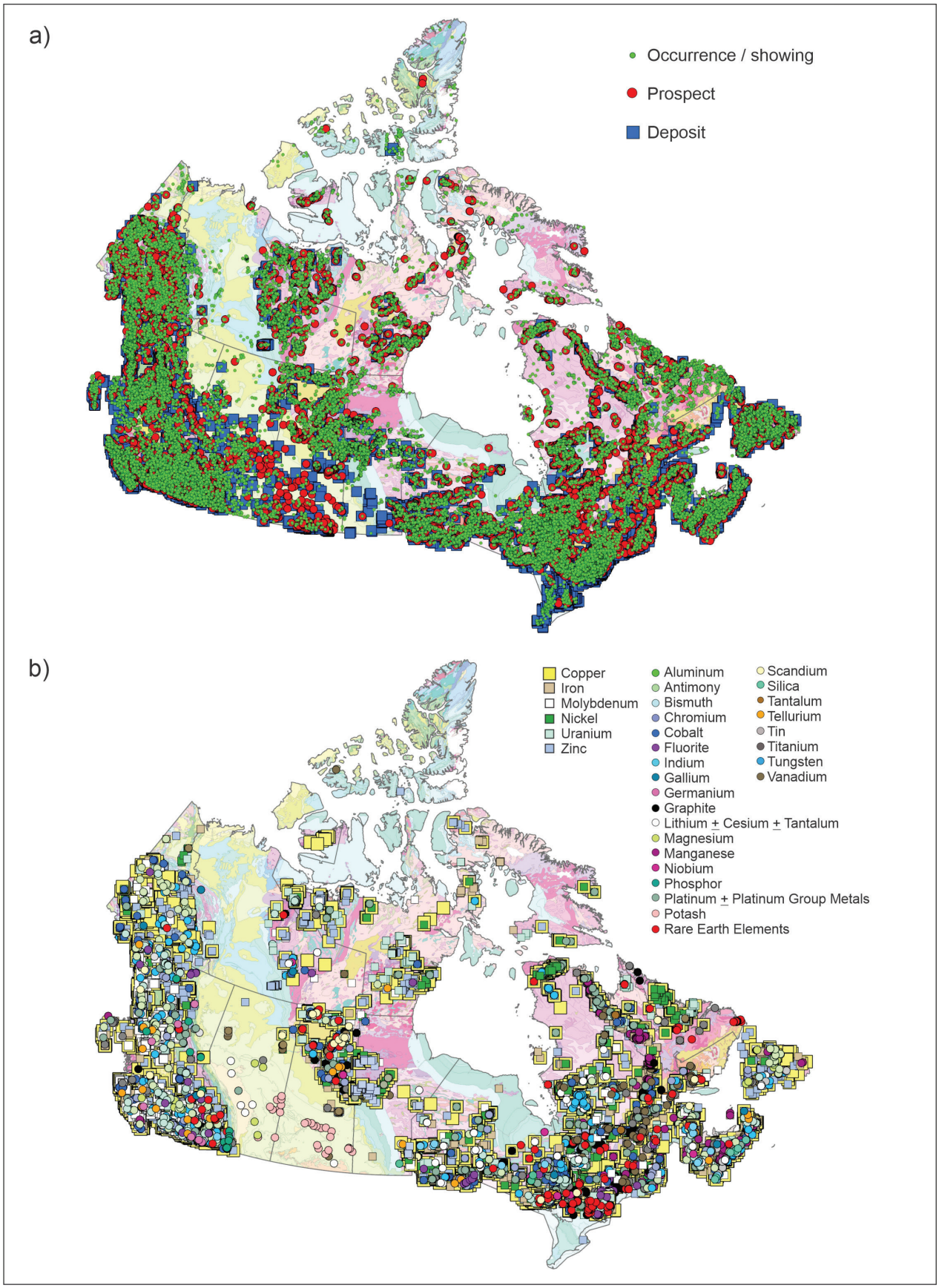


Fig. 14. Pan-Canadian mineral inventory pilot project. **a)** General inventory. **b)** Critical minerals. Base map from Wheeler et al. (1996).

Acknowledgments

British Columbia would like to express gratitude to all members of the National Geological Surveys Committee (NGSC) and to NGSC Secretariat for their collegial and collaborative engagement in advancing geoscience across Canada. The author also recognizes the dedication and immense and tireless contributions made by the British Columbia Geological Survey staff. This paper benefitted from the editorial guidance of Larry Aspler and review by Marc-André Brideau. We thank George Owsiacki of Total Earth Science Services for formatting and layout of the manuscript.

References cited

Bacha, R.R.B., 2025. Field trip guidebook to the geology near Merritt, south-central British Columbia, for the Citxw Nlaka'pamux Assembly. British Columbia Ministry of Mining and Critical Minerals, British Columbia Geological Survey GeoFile 2025-22, 14 p.

Bacha, R.R.B., 2026. Data sharing for Indigenous Peoples engagement: What and how. In: Geological Fieldwork 2025, British Columbia Ministry of Mining and Critical Minerals, British Columbia Geological Survey Paper 2026-01, this volume.

Bailey, L., Kim, R., Takaichi, M., Logan, J., Crowley, J., Friedman, R., Wall, C., van Straaten, B.I., and Campbell, R., 2025. U-Pb geochronological data for intrusive rocks near the Schaft Creek and Galore Creek deposits (southern Telegraph Creek area, NTS 104G), northwestern British Columbia. British Columbia Ministry of Mining and Critical Minerals, British Columbia Geological Survey GeoFile 2025-14, 16 p.

Bain, W.M., 2024. Ore and alteration textures from Co-bearing iron skarns: Examples from Vancouver and Texada islands. British Columbia Ministry of Energy, Mines and Low Carbon Innovation, British Columbia Geological Survey GeoFile 2024-11 (poster).

Bain, W.M., de Waal, F., and Goudie, D.J., 2025. Co-Te mineralization in iron skarns on Vancouver Island and Texada Island. In: Geological Fieldwork 2024, British Columbia Ministry of Mining and Critical Minerals, British Columbia Geological Survey Paper 2025-01, pp. 153-175.

British Columbia Geological Survey, 2026. BC Geological Survey Digital Geoscience Data. <https://www2.gov.bc.ca/gov/content/industry/mineral-exploration-mining/british-columbia-geological-survey/publications/digital-geoscience-data> (last accessed January, 2026).

British Columbia Geological Survey, 2025a. Kaska Land Use Planning area mineral potential map for porphyry, volcanogenic massive sulphide (VMS), magmatic mafic-ultramafic, sedimentary exhalative (SEDEX) and Mississippi Valley Type (MVT) deposits. British Columbia Ministry of Mining and Critical Minerals, British Columbia Geological Survey Information Circular 2025-11, 2 p.

British Columbia Geological Survey, 2025b. Tahltan Land Use Planning area mineral potential map for porphyry, volcanogenic massive sulphide (VMS), and magmatic mafic-ultramafic deposits. British Columbia Ministry of Mining and Critical Minerals, British Columbia Geological Survey Information Circular 2025-10, 2 p.

British Columbia Geological Survey, 2025c. TRT Land Use Planning area mineral potential map for porphyry, volcanogenic massive sulphide (VMS), and magmatic mafic-ultramafic deposits. British Columbia Ministry of Mining and Critical Minerals, British Columbia Geological Survey Information Circular 2025-13, 2 p.

British Columbia Geological Survey, 2025d. Pan-Canadian workshop on mineral potential modelling, September 23, 2025, program with extended abstracts. British Columbia Ministry of Mining and Critical Minerals, British Columbia Geological Survey GeoFile 2025-24, 37 p.

British Columbia Geological Survey, 2025e. British Columbia radiogenic isotope compilation (Sr-Nd-Hf-Pb). British Columbia Ministry of Mining and Critical Minerals, British Columbia Geological Survey, GeoFile 2025-08, 1 p.

Brzozowski, M.J., and Zaborniak, K., 2024. Sulphide mineralization at the E&L magmatic Ni-Cu-PGE deposit: Textural evidence for contamination, vapour saturation, fluid immiscibility, and metal remobilization. In: Geological Fieldwork 2023, British Columbia Ministry of Energy, Mines and Low Carbon Innovation, British Columbia Geological Survey Paper 2024-01, pp. 65-78.

Campbell, R.W., and van Straaten, B.I., 2025. New data on Late Triassic to late Early Jurassic plutonic suites in the northern Golden Triangle region of northwest British Columbia. In: Geological Fieldwork 2024, British Columbia Ministry of Mining and Critical Minerals, British Columbia Geological Survey Paper 2025-01, pp. 49-72.

Cui, Y., 2021. A geospatial frame data model to simplify digital map compilation and integration. British Columbia Ministry of Energy, Mines and Low Carbon Innovation, British Columbia Geological Survey Paper 2021-03, 20 p.

Cui, Y., Norris, J., and Fortin, G., 2026. British Columbia geoscience Spatial Data Infrastructure (BCgSDI): A progress report. In: Geological Fieldwork 2025, British Columbia Ministry of Mining and Critical Minerals, British Columbia Geological Survey Paper 2026-01, pp. 221-226.

Elia, E.A., and Ferbey, T., 2026. Interior Plateau surficial geology compilation: Selection and standardization of maps and data. In: Geological Fieldwork 2025, British Columbia Ministry of Mining and Critical Minerals, British Columbia Geological Survey Paper 2026-01, pp. 227-237.

Elia, E.A., Ferbey, T., Ward, B.C., Shives, R.B.K., Best, M., and Martin-Burtart, N., 2023. Remotely piloted aircraft system (RPAS) for investigating surface sediments in the Interior Plateau of British Columbia: Methods, data, and products. British Columbia Ministry of Energy, Mines and Low Carbon Innovation, British Columbia Geological Survey GeoFile 2023-07, 22 p.

Elia, E.A., Ferbey, T., and Ward, B.C., 2024a. Mapping surficial sediments in the Interior Plateau using remotely piloted aircraft system lidar. British Columbia Ministry of Energy, Mines and Low Carbon Innovation, British Columbia Geological Survey Open File 2024-03, 12 p.

Elia, E.A., Ferbey, T., Campagne, T., Best, M., Shives, R.B.K., and Ward, B.C., 2024b. Investigating surface sediment composition in the Interior Plateau using a remotely piloted aircraft system magnetometer. British Columbia Ministry of Energy, Mines and Low Carbon Innovation, British Columbia Geological Survey Open File 2024-07, 11 p.

Enkin, R.J., Hamilton, T.S., and Morris, W., 2020. The Henkel petrophysical plot: Mineralogy and lithology from physical properties. Geochemistry, Geophysics, Geosystems, 20, article e2019GC008818. <https://agupubs.onlinelibrary.wiley.com/doi/10.1029/2019GC008818>

EuroGeoSurveys Secretariat, 2025. Strategic research and innovation agenda (SRIA) 2025-2034. Building a geological service for Europe. The Geological Surveys of Europe, Brussels, Belgium, 94 p.

Ferbey, T., and Elia, E.A., 2025a. Surficial geology of the Nanitsch Lake area (NTS 94D/1), British Columbia. British Columbia Ministry of Mining and Critical Minerals, British Columbia Geological Survey Geoscience Map 2025-02, 1:50,000 scale.

Ferbey, T., and Elia, E.A., 2025b. Surficial geology of the Carruthers Pass area (NTS 94D/8), British Columbia. British Columbia Ministry of Mining and Critical Minerals, British Columbia Geological Survey Geoscience Map 2025-03, 1:50,000 scale.

Ferbey, T., Elia, E.A., Shives, R.B.K., Martin-Burtart, N., Best, M., and Ward, B.C., 2024. Quantifying potassium concentrations in Interior Plateau surface sediments using remotely piloted aircraft system gamma-ray spectrometry. British Columbia Ministry of Energy, Mines and Low Carbon Innovation, British Columbia Geological Survey Open File 2024-04, 19 p.

Fortin, G., and Silva, P.L., 2025. Assessment report drillhole database: Development and initial data release. British Columbia Ministry of Mining and Critical Minerals, British Columbia Geological Survey GeoFile 2025-11, 9 p.

Fortin, G., and Silva, P.L., 2026. Assessment report-sourced surface-sediment geochemistry database: Data update. British Columbia. British Columbia Ministry of Mining and Critical Minerals, British Columbia Geological Survey GeoFile 2026-02, 8 p.

Gabites, J.E., and Mihalynuk, M.G., 2025. $^{40}Ar/^{39}Ar$ geochronologic data from samples collected as part of the Southern Nicola Arc Project. British Columbia Ministry of Mining and Critical Minerals, British Columbia Geological Survey GeoFile 2025-16, 9 p.

GeoERA, 2026. Establishing the European Geological Surveys Research Area to deliver a Geological Service for Europe. <https://geoera.eu/about-geoera/> (last accessed January, 2026).

Geoscience Australia, 2024 Exploring for the Future-Australia's transformational geoscience program. Commonwealth of Australia (Geoscience Australia). <https://dx.doi.org/10.26186/149743>

Geoscience Australia, 2026. Resourcing Australia's Prosperity. Commonwealth of Australia (Geoscience Australia). <https://www.ga.gov.au/scientific-topics/resourcing-australias-prosperity/data-and-publications/resourcing-australias-prosperity-10-year-roadmap/Resourcing-Australias-Prosperity-Roadmap.pdf> (last accessed January, 2026).

Graham, A.C., and Ootes, L., 2025. Geochemical analyses of SEDEX deposits in eastern British Columbia. British Columbia Ministry of Mining and Critical Minerals, British Columbia Geological Survey GeoFile 2025-13, 9 p.

Graham, A.C., Wearmouth, C.D., Northcote, B., and Ootes, L., 2025a. A preliminary assessment of critical companion elements in SEDEX deposits of eastern British Columbia: Examples from the historic Sullivan mine and the Cirque project. In: Geological Fieldwork 2024, British Columbia Ministry of Mining and Critical Minerals, British Columbia Geological Survey Paper 2025-01, pp. 141-152.

Graham, A.C., Orovan, E., Wall, C., Goudie, D., Creaser, R., Layton-Matthews, D., and Ootes, L., 2025b. Data release from critical mineral studies of the Kitsault, Huckleberry, and Berg porphyry deposits. British Columbia Ministry of Mining and Critical Minerals, British Columbia Geological Survey GeoFile 2025-23, 7 p.

Graham, A.C., Vaughan Forrester, K., Ootes, L., Bain, W., Campbell, R., and Goudie, D., 2026. Critical companion metals in porphyry deposits in British Columbia: Lithogeochemistry and scanning electron microscopy-mineral liberation analysis (SEM-MLA) from the Schaft Creek, Mount Polley, and New Afton deposits. In: Geological Fieldwork 2025, British Columbia Ministry of Mines and Critical Minerals, British Columbia Geological Survey Paper 2026-01, pp. 69-83.

Greig, C.J., Dudek, N.P., ver Hoeve, T.J., Quinn, T.D.M., Newton, G., Makin, S.A., and Greig, R.E., 2021. Geology of the Tatogga property: Geologic framework for the Saddle North porphyry Cu-Au deposit and the Saddle South epithermal Au-Ag vein system, Iskut district, northwestern British Columbia. In: Geological Fieldwork 2020, British Columbia Ministry of Energy, Mines and Low Carbon Innovation, British Columbia Geological Survey Paper 2021-01, pp. 89-111.

Han, T. and Rukhlov, A.S., 2024. Update of rock geochemical database at the British Columbia Geological Survey. British Columbia Ministry of Energy, Mines and Low Carbon Innovation, British Columbia Geological Survey GeoFile 2024-09, 5 p.

Hickin, A.S., Orovan, E.A., Brzozowski, M.J., McLaren, K., Shaw, K.L., and Van der Vlugt, J., 2023. Critical minerals in British Columbia: An atlas of occurrences and producing mines, 2023. British Columbia Ministry of Energy, Mines and Low Carbon Innovation, British Columbia Geological Survey Open File 2023-02 102 p.

Hickin, A.S., Ootes, L., Orovan, E.A., Brzozowski, M.J., Northcote, B.K., Rukhlov, A.S., and Bain, W.M., 2024. Critical minerals and mineral systems in British Columbia. In: Geological Fieldwork 2023, British Columbia Ministry of Energy, Mines and Low Carbon Innovation, British Columbia Geological Survey Paper 2024-01, pp. 13-51.

Höy, T., and DeFields, G.M., 2025. Geology of the Lightning Peak map area (NTS 082E/15). British Columbia Ministry of Mining and Critical Minerals, British Columbia Geological Survey Open File 2025-02, 1:50,000 scale.

Höy, T., and Jackaman, W., 2024a, Geology of the Rossland-Trail map sheet (NTS 082F/04). Geoscience BC Map 2024-02-01. British Columbia Ministry of Mining and Critical Minerals, British Columbia Geological Survey Open File 2024-12, 1:50,000 scale.

Höy, T., and Jackaman, W., 2024b, Geology of the Castlegar map sheet (NTS 082F/05). Geoscience BC Map 2024-02-02. British Columbia Ministry of Mining and Critical Minerals, British Columbia Geological Survey Open File 2024-13, 1:50,000 scale.

Hunter, R.C., Sebert, C.F.B., Friedman, R., and Wall, C., 2022a. Geochronologic data from the Kitsault River area, northwest British Columbia. Ministry of Energy, Mines and Low Carbon Innovation, British Columbia Geological Survey GeoFile 2022-13, 4 p.

Hunter, R.C., Sebert, C.F.B., Friedman, R., and Wall, C., 2022b. Revised stratigraphy and geochronology of the Hazelton Group, host rocks for volcanogenic mineralization in the Kitsault River area, northwest British Columbia. In: Geological Fieldwork 2021, British Columbia Ministry of Energy, Mines and Low Carbon Innovation, British Columbia Geological Survey Paper 2022-01, pp. 63-81.

Janke, B., 1990. Summary Report on the Canada/British Columbia Mineral Development Agreement (1985-1990). Energy, Mines and Resources Canada and British Columbia Ministry of Energy, Mines and Petroleum Resources, MDA 1985-90, 100 p. <https://cmscontent.nrs.gov.bc.ca/geoscience/PublicationCatalogue/Miscellaneous/BCGS_MP-01.pdf>

Jones, G., Ootes, L., Milidragovic, D., Friedman, R., Camacho, A., Luo, Y., Vezinet, A., Pearson, D.G., and Schiarizza, P., 2021. Geochronology of northern Hogem batholith, Quesnel terrane, north-central British Columbia. In: Geological Fieldwork 2020, British Columbia Ministry of Energy, Mines and Low Carbon Innovation, British Columbia Geological Survey Paper 2021-01, pp. 37-56.

Kilby, W.E., 1995. Mineral Potential Project-overview. In: Geological Fieldwork 1994, Ministry of Energy, Mines and Petroleum Resources, British Columbia Geological Survey Paper 1995-01, pp. 411-416.

Kilby, W.E., 2004. The British Columbia Mineral Project 1992-1997 methodology and results. British Columbia Ministry of Energy and Mines, British Columbia Geological Survey GeoFile 2004-2, 324 p.

Mihalynuk, M.G., Milidragovic, D., Tsekhmistrenko, M., and Zagorevski, A., 2021. Turtle Lake area geology (NTS 104M/16). British Columbia Ministry of Energy, Mines and Low Carbon Innovation, British Columbia Geological Survey Open File 2021-02; Geological Survey of Canada Open File 8757, 1:50,000 scale.

Mihalynuk, M.G., Zagorevski, A., Campbell, R.W., Vaillancourt, A., and Haji Egen, A., 2024. Geology of the Western Glady's Lake area (NTS 104N/13E, 14) British Columbia Ministry of Mining and Critical Minerals, British Columbia Geological Survey Open File 2014-02, 1:50,000 scale.

Mihalynuk, M.G., Friedman, R.M., and Wall, C., 2025a. U-Pb geochronologic data from samples collected as part of the Southern Nicola Arc Project. British Columbia Ministry of Mining and Critical Minerals, British Columbia Geological Survey GeoFile 2025-15, 7 p.

Mihalynuk, M.G., Wall, C., and Zagorevski, A., 2025b. Time of deposition refinements for key stratigraphic intervals of the Nicola Group, southern British Columbia. In: Geological Fieldwork 2024, British Columbia Ministry of Mining and Critical Minerals, British Columbia Geological Survey Paper 2025-01, pp. 105-118.

Miller, E.A., van Straaten, B.I., and Hunter, R.C., 2023. Update on bedrock mapping in the Kitsault River area, northwestern British Columbia. In: Geological Fieldwork 2022, British Columbia Ministry of Energy, Mines and Low Carbon Innovation, British Columbia Geological Survey Paper 2023-01, pp. 23-32.

Miller, E.A., van Straaten, B.I., Ferri, M.D., and Hunter, R.C., 2025a. Preliminary bedrock geology of the Kitsault River area, northwestern British Columbia: GIS data. British Columbia Ministry of Mining and Critical Minerals, British Columbia Geological Survey GeoFile 2025-20, 3 p.

Miller, E.A., Ferri, M.D., Wall, C., Creaser, R.A., van Straaten, B.I., and Graham, A.C., 2025b. New geochronologic data, Kitsault River area, northwestern British Columbia: Igneous zircons (high-precision CA-TIMS), detrital zircons (LA-ICP-MS), and molybdenite (Re-Os). British Columbia Ministry of Mining and Critical Minerals, British Columbia Geological Survey GeoFile 2025-21, 6 p.

Miller, E.A., Ferri, M.D., van Straaten, B.I., and Wall, C., 2025c. Stratigraphic framework, structural setting, and timing of VMS, epithermal, and porphyry mineralization in the Kitsault River area, northwest British Columbia. In: Geological Fieldwork 2024, British Columbia Ministry of Mining and Critical Minerals, British Columbia Geological Survey Paper 2025-01, pp. 17-47.

National Geological Surveys Committee, 2022. Intergovernmental Geoscience Accord. <https://www.geologicalsurveys.ca/sites/ngsc-admin/files/2022-08/intergovernmental-geoscience-accord-2022-bilingual.pdf>

National Geological Surveys Committee, 2025. Who we are. <https://www.geologicalsurveys.ca/who-we-are> (last accessed January, 2026). <https://openlibrary.org/books/OL10357307M/Toward_a_Coordinated_Spatial_Data_Infrastructure_for_the_Nation>

Natural Resources Canada, 2019. The Canadian Minerals and Metals Plan. Natural Resources Canada, Paper MA-175/2019E, 46 p.

Norris, J., and Fortin, G., 2019. Assessment report-sourced surface sediment geochemical database: Development and initial data release from the Interior Plateau. British Columbia Ministry of Energy, Mines and Petroleum Resources, British Columbia Geological Survey GeoFile 2019-04, 10 p.

Northcote, B.K., 2025. Sedimentary hosted lead-zinc deposits in British Columbia. British Columbia Ministry of Mining and Critical Minerals, British Columbia Geological Survey GeoFile 2025-19, 23 p.

Oneschuk, D., Hayward, N., Fortin, G., and Hickin, A.S., 2024. Residual total magnetic field and first vertical derivative of the magnetic field: Compilations of British Columbia. British Columbia Ministry of Energy, Mines and Low Carbon Innovation, British Columbia Geological Survey Open File 2024-08. Also published as Geological Survey of Canada Open File 9222, 1:500,000 scale. <https://doi.org/10.4095/p1xpddgswc>

Ootes, L., 2023. Did epithermal mineralization in the northern Toodoggone region develop synchronously with large scale folding? In: Geological Fieldwork 2022, British Columbia Ministry of Energy, Mines and Low Carbon Innovation, British Columbia Geological Survey Paper 2023-01, pp. 13-21.

Ootes, L., and Wall, C., 2024. High-precision U-Pb zircon igneous crystallization and detrital zircon maximum depositional ages from the Toodoggone region, north-central British Columbia. British Columbia Ministry of Energy, Mines and Low Carbon Innovation, British Columbia Geological Survey Open File 2024-06, 10 p.

Ootes, L., Ferri, F., Milidragovic, D., and Wall, C., 2022. The age and provenance of the Lay Range assemblage provides an indirect record of basement to north-central Quesnellia, British Columbia. In: Geological Fieldwork 2021, British Columbia Ministry of Energy, Mines and Low Carbon Innovation, British Columbia Geological Survey Paper 2022-01, pp. 31-44.

Ootes, L., Graham, A.C., Whitmore, K., Goudie, D., Piercey, S.J., Barker, S., Milne, S., and McFarlane, C., 2026a. Mineralogical control on critical companion metal distribution: Expanded workflow, with examples from the Sullivan Pb-Zn-Ag deposit. In: Geological Fieldwork 2025, British Columbia Ministry of Mining and Critical Minerals, British Columbia Geological Survey Paper 2026-01, pp. 45-52.

Ootes, L., Wall, C., and Mihalynuk, M.G., 2026b. Rossland Group extends north: Detrital zircon U-Pb ages allow supracrustal unit reassignments in southern British Columbia and have tectonic implications. In: Geological Fieldwork 2025, British Columbia Ministry of Mining and Critical Minerals, British Columbia Geological Survey Paper 2026-01, pp. 119-130.

Orovan, E.A., Zaborniak, K., and Hooker, K., 2024. Textural evidence for ore fluid transport and the magmatic to hydrothermal transition at the past-producing Kitsault Mo-Ag mine. In: Geological Fieldwork 2023, British Columbia Ministry of Energy, Mines and Low Carbon Innovation, British Columbia Geological Survey Paper 2024-01, pp. 53-64.

Orovan, E.A., Ebert, S., Baldazzi, P., Saxton, D., and Goudie, D.J., 2025. Critical minerals at the Berg and Huckleberry porphyry deposits, British Columbia, using scanning electron microscropy-mineral liberation analysis (SEM-MLA). In: Geological Fieldwork 2024, British Columbia Ministry of Mining and Critical Minerals, British Columbia Geological Survey Paper 2025-01, pp. 73-84.

Piercey, S.J., 2025. Assay data for volcanogenic massive sulphide (VMS) deposit samples from British Columbia. British Columbia Ministry of Mining and Critical Minerals, British Columbia Geological Survey GeoFile 2025-12, 3 p.

Piercey, S.J., Pietruszka, D., and Goudie, D., 2025. Critical metals in volcanogenic massive sulphide (VMS) deposits in British Columbia: A progress report. In: Geological Fieldwork 2024, British Columbia Ministry of Mining and Critical Minerals, British Columbia Geological Survey Paper 2025-01, pp. 189-201.

Rukhlov, A.S., Coats, B., Van der Vlugt, J., Beaupre-Olsen, I.J., and Zaborniak, K., 2023. British Columbia Geological Survey Sample Archive: An emerging resource for public geoscience. In: Geological Fieldwork 2022, British Columbia Ministry of Energy, Mines and Low Carbon Innovation, British Columbia Geological Survey Paper 2023-01, pp. 85-90.

Rukhlov, A.S., Cui, Y., Cunningham, Q., Fortin, G., and Anderson, C., 2024. Geochemical signals of carbonatite related critical metals in provincial stream sediments. In: Geological Fieldwork 2023, British Columbia Ministry of Energy, Mines and

Low Carbon Innovation, British Columbia Geological Survey Paper 2024-01, pp. 97-122.
Rukhlov, A.S., Ootes, L., Creaser, R.A., Cunningham, Q.F., de Waal, F.S., and Wenger, D.K., 2025a. British Columbia carbonatites revisited: New whole rock Sr-Pb-Nd isotopic insights and drainage prospectivity trends. In: Geological Fieldwork 2024, British Columbia Ministry of Mining and Critical Minerals, British Columbia Geological Survey Paper 2025-01, pp. 119-139.
Rukhlov, A.S., Ootes, L., Creaser, R.A., Cunningham, Q.F., de Waal, F.S., and Wenger, D.K., 2025b. Supplementary data for British Columbia carbonatites revisited: New whole rock Sr-Pb-Nd isotopic insights and drainage prospectivity trends. British Columbia Ministry of Mining and Critical Minerals, British Columbia Geological Survey GeoFile 2025-09, 4 p.
Rukhlov, A.S., Ootes, L., and Han, T., 2025c. British Columbia radiogenic isotope compilation (Sr-Nd-Hf-Pb): Introduction and examples of utility. In: Geological Fieldwork 2024, British Columbia Ministry of Mining and Critical Minerals, British Columbia Geological Survey Paper 2025-01, pp. 177-188.
Rukhlov, A.S., Ootes, L., Cunningham, Q.F., Goudie, D., von der Handt, A., Spence, J., Wall, C., and Barker, S., 2026. A multi-analytical approach to stream-sediment samples from modern drainages enhances the search for REE and rare metals. In: Geological Fieldwork 2025, British Columbia Ministry of Mining and Critical Minerals, British Columbia Geological Survey Paper 2026-01, pp. 97-117.
Sauvé, M., Ward, B., and Ferbey, T., 2025. Surficial geology of the Kinaskan Lake area, British Columbia (parts of NTS 104G/08, 09, 16, and 104H/12, 13).
Schiarizza, P., 2022. Bedrock geology, Stump Lake-Salmon River (parts of NTS 82L/05 and 921/08). British Columbia Ministry of Energy, Mines and Low Carbon Innovation, British Columbia Geological Survey Open File 2022-03, 1:50,000 scale.
Schiarizza, P., 2024. Bedrock geology, Bonaparte Lake-Quesnel River, Parts of NTS 92P, 93A, 93B. British Columbia Ministry of Energy, Mines and Low Carbon Innovation, British Columbia Geological Survey Geoscience Map 2024-01, 1:125,000 scale.
Schiarizza, P., and Friedman, R.M., 2021. U-Pb zircon date for Eocene volcanic rocks on Mount Timothy, southcentral British Columbia. In: Geological Fieldwork 2020, British Columbia Ministry of Energy, Mines and Low Carbon Innovation, British Columbia Geological Survey Paper 2021-01, pp. 15-21.
Schiarizza, P., and Friedman, R.M., 2023. U-Pb zircon dates for rhyolite and sandstone of Cadwallader terrane, lower Chilcotin River area, south-central British Columbia. In: Geological Fieldwork 2022, British Columbia Ministry of Energy, Mines and Low Carbon Innovation, British Columbia Geological Survey Paper 2023-01, pp. 65-84.
Schiarizza, P., Orchard, M.J., and Friedman, R.M., 2022. Conodonts and detrital zircons from Triassic and Jurassic rocks above the Salmon River unconformity, Thompson Plateau, south-central British Columbia. In: Geological Fieldwork 2021, British Columbia Ministry of Energy, Mines and Low Carbon Innovation, British Columbia Geological Survey Paper 2022-01, pp. 17-30.
Spence, D.W., Crawford, H., Scoates, J.S., Nott, J.A., Nixon, G.T., and Milidragovic, D., 2022. Mapping ultramafic cumulates at the Tulameen ultramafic-mafic Alaskan-type intrusion, south-central British Columbia, aided by remotely piloted aircraft system photogrammetry. In: Geological Fieldwork 2021, British Columbia Ministry of Energy, Mines and Low Carbon Innovation, British Columbia Geological Survey Paper 2022-01, pp. 103-122.
Stanley, B., and Nelson, J., 2022. Revised stratigraphy of the Stuhini and Hazelton groups and LA-ICP-MS zircon geochronology of the Scottie gold mine area, northwestern British Columbia. In: Geological Fieldwork 2021, British Columbia Ministry of Energy, Mines and Low Carbon Innovation, British Columbia Geological Survey Paper 2022-01, pp. 83-102.
United States Geological Survey, 2026. Earth Mapping Resources Initiative (Earth MRI). <https://www.usgs.gov/special-topics/earth-mri> (last accessed February 2, 2026).
Van der Vlugt, J., Rukhlov, A.S., and van Straaten, B.I., 2022. Lithogeochemical reanalysis of British Columbia Geological Survey archived rock samples from northwestern British Columbia. British Columbia Ministry of Energy, Mines and Low Carbon Innovation, British Columbia Geological Survey GeoFile 2022-14, 15 p.
van Straaten, B.I., 2024. Upper Hazelton Group stratigraphy along the Stikine arch, northwestern British Columbia. In: Geological Fieldwork 2023, British Columbia Ministry of Energy, Mines and Low Carbon Innovation, British Columbia Geological Survey Paper 2024-01, pp. 149-177.
van Straaten, B.I., Logan, J.M., Nelson, J.L., Moynihan, D.P., Diakow, L.J., Gibson, R., Bichlmaier, S.J., Wearmouth, C.D., Friedman, R.M., Golding, M.L., Miller, E.A., and Poulton, T.P., 2022. Bedrock geology of the Dease Lake area, British Columbia Ministry of Energy, Mines and Low Carbon Innovation, British Columbia Geological Survey, Geoscience Map 2022-01, 1:100,000 scale.
van Straaten, B.I., Friedman, R.M., and Camacho, A., 2023. Stratigraphy of the Stuhini Group (Upper Triassic) in the Galore Creek area, northwestern British Columbia. In: Geological Fieldwork 2022, British Columbia Ministry of Energy, Mines and Low Carbon Innovation, British Columbia Geological Survey Paper 2023-01, pp. 33-49.
Van Wagoner, N., Ootes, L., and Thomson-Gladish, J., 2021a. Volcanism and geochemistry of the Kamloops Group, south-central British Columbia. In: Geological Fieldwork 2020, British Columbia Ministry of Energy, Mines and Low Carbon Innovation, British Columbia Geological Survey Paper 2021-01, pp. 65-88.
Van Wagoner, N., Ootes, L., and Sutcliffe, B., 2021b. Geochemical data from the Kamloops Group. British Columbia Ministry of Energy, Mines and Low Carbon Innovation, British Columbia Geological Survey GeoFile 2021-16, 2 p.
Van Wagoner, N., and Ootes, L., 2022. Geology and geochemistry of the Kamloops Group (Eocene) in its type area, Kamloops, British Columbia. In: Geological Fieldwork 2021, British Columbia Ministry of Energy, Mines and Low Carbon Innovation, British Columbia Geological Survey Paper 2022-01, pp. 45-62.
Veness, H., Elia, E.A., and Ferbey, T., 2024. A digital update of Open File 1992-13: Surficial geology map index of British Columbia. British Columbia Ministry of Mining and Critical Minerals, British Columbia Geological Survey Open File 2024-09, 2 p.
Wang, X., Jiao, R., and Ootes, L., 2025. Apatite fission track data from northern Hogem batholith, Quesnel terrane, north-central British Columbia: A progress report. In: Geological Fieldwork 2024, British Columbia Ministry of Mining and Critical Minerals, British Columbia Geological Survey Paper 2025-01, pp. 85-91.
Wearmouth, C.D., Peters, K.J., Czertowicz, T.A., and Orovan, E.A., 2024a. Mineral potential modelling results for northwestern British Columbia, a comparison between past and current work at the British Columbia Geological Survey. In: Geological Fieldwork 2023, British Columbia Ministry of Energy, Mines and Low Carbon Innovation, British Columbia Geological Survey Paper 2024-01, pp. 79-95.
Wearmouth, C., Czertowicz, T., Peters, K.J., and Orovan, E., 2024b. Mineral potential modelling at the British Columbia Geological Survey: Renewed methods with application to northwestern British Columbia. British Columbia Ministry of Energy, Mines and Low Carbon Innovation, British Columbia Geological Survey Paper 2024-02, 28 p.

Wearmouth, C.D., Czertowicz, T.A., Peters, K.J., and Orovan, E.A., 2024c. Preliminary mineral potential maps for the porphyry, volcanic massive sulphide, and magmatic mafic-ultramafic mineral systems, northwest British Columbia. British Columbia Ministry of Energy, Mines and Low Carbon Innovation, British Columbia Geological Survey Open File 2024-05, 1:800,000 scale.

Wearmouth, C.D., Czertowicz, T.A., and Peters, K.J., 2024d. Preliminary mineral potential maps for the SEDEX and MVT mineral systems, northwest British Columbia. British Columbia Ministry of Energy, Mines and Low Carbon Innovation, British Columbia Geological Survey Open File 2024-11, 1:500,000 scale.

Wei, C., Pietruszka, D.K., Piercey, S.J., Aylward, W., Kommescher, S., Scanlan, E., and Layton-Matthews, D., 2026. Critical metal distributions in volcanogenic massive sulphide (VMS) deposits in British Columbia: A progress report. In: Geological Fieldwork 2025, British Columbia Ministry of Mining and Critical Minerals, British Columbia Geological Survey Paper 2026-01, pp. 53-67.

Wheeler, J.O., Hoffman, P.F., Card, K.D., Davidson, A., Sanford, B.V., Okulitch, A.V., and Roest, W.R., 1996. Geological map of Canada Geological Survey of Canada, Map 1860A.

Zhang, P., Brideau, M-A., and Szponarski, K., 2026. Geoscience knowledge density map of British Columbia, Version 1.0. In: Geological Fieldwork 2025, British Columbia Ministry of Mining and Critical Minerals, British Columbia Geological Survey Paper 2026-01, pp. 247-251.

Data sharing for Indigenous Peoples engagement: What and how

Rafael R.B. Bacha[1, a]

[1] British Columbia Geological Survey, Ministry of Mining and Critical Minerals, Victoria, BC, V8W 9N3
[a] corresponding author: Rafael.Bacha@gov.bc.ca

Recommended citation: Bacha, R.R.B., 2026. Data sharing for Indigenous Peoples engagement: What and how. In: Geological Fieldwork 2025, British Columbia Ministry of Mining and Critical Minerals, British Columbia Geological Survey Paper 2026-01, pp. 37-43.

Abstract

As a science agency, the British Columbia Geological Survey strives to be an unbiased broker of information and to build trust and facilitate knowledge exchange with Indigenous Peoples through its Engagement Program. Recognizing the value of better understanding the mineral endowment of their traditional territories for self-determination and decision making, interest in the geosciences from Indigenous communities and leadership has grown. However, several obstacles can impede geoscience information being immediately received, understood, and incorporated into decision-making processes. To ensure that Indigenous Nations can access, absorb, and use geoscience information, the Survey is moving away from the historic deficit model of communication where one-way statements from the researcher to the public prevail. Instead, since 2023 the Survey has adopted, and is working to apply, dialogue and participatory models rooted in mutual respect and collaboration. The Survey addresses initial information barriers by reaching out to Indigenous groups with invitations to participate in knowledge-sharing activities and by preparing compilations highlighting key pieces of information and how the material might be used. If barriers related to the language of geoscience exist, the Survey offers personal consultations, hands-on experiences such as field trips, and makes terminology-filled documents containing foreign concepts more straightforward. Given that Indigenous peoples should be meaningfully engaged in scholarship that concerns them, the Survey works to foster stronger relationships with Indigenous communities as an integral part of new fieldwork programs. Through the BCGS Indigenous Peoples Engagement Policy, new Survey projects undergo multiple engagement sessions before, during, and after studies are carried out. Opportunities exist to use geology as a neutral and constructive entry point into land-use discussions because Traditional Knowledge and Western science intersections can serve as a foundation for dialogue to build a common understanding of the natural and geological history of the province. Geology field trips provide valuable opportunities for Indigenous community members and geoscientists to come together in a powerful but depoliticized setting to build a common understanding of the land, as exemplified by a collaboration between the Citxw Nlaka'pamux Assembly in south-central British Columbia and the Survey.

Keywords: Engagement, data sharing, reconciliation, Indigenous Peoples, Traditional Knowledge, Western science, free prior and informed consent, FPIC

1. Introduction

Through its Engagement Program, which started in 2023, the British Columbia Geological Survey (BCGS) is connecting Indigenous Peoples, local communities, government, the minerals industry, and the public to the geology and mineral resources of the province. This work enhances land-use planning and resource co-management and is particularly important for fostering relationships with Indigenous Peoples. There is growing interest from Indigenous communities and leadership to better understand the mineral endowment of their lands, recognizing the value of this knowledge for self-determination and decision making. As a science agency, the Survey is an unbiased broker of information that serves to build trust and facilitate knowledge exchange. The Survey is striving to connect with Indigenous groups to raise awareness of research projects on their lands, identify opportunities and challenges, and explore partnerships. However, numerous barriers can impede geoscience information being immediately received, understood, and incorporated into decision-making processes.

This paper details the approach the Survey takes in its Engagement Program, which is rooted in mutual respect, two-way communication, and collaboration. It describes how barriers to effective transfer of existing information and historical data can be overcome, particularly those related to the language of geoscience, illustrates the practices the Survey currently uses when conducting new research programs, underscores how a common understanding of the natural history and geological resources in the province can be attained by sharing Traditional Knowledge and Western science, and concludes with an engagement example in which the Citxw Nlaka'pamux Assembly of south-central British Columbia and the Survey successfully co-designed a short course and field trip.

2. The approach

To ensure that Indigenous Nations can access, absorb, and use geoscience information, the Survey has moved away from the historic 'deficit' model of communication (see review by Onstad and van der Flier-Keller, 2025) where one-way communication from the researcher to the public prevails. Instead, the Survey has adopted dialogue and participatory models. The dialogue

model entails two-way communication in which scientists and Indigenous groups communicate early and often to co-produce knowledge by being connected throughout the process (Onstad and van der Flier-Keller, 2025). Participatory models take advantage of fieldwork being inherent to geoscience research, which provides opportunities for first-hand experiences of Western science and Traditional Knowledge. The premise of this process is that research involving Indigenous communities is based on respectful relationships with intensive collaboration and participation.

Establishing partnerships with Indigenous Nations to conduct research might be seen as an obstacle for some researchers. Nonetheless, proper engagement is beneficial to all parties, especially when appropriate engagement mechanisms are in place (Bharadwaj, 2014). Charlene George, artist and band member of the T'Sou-Ke Nation (T'Sou-Ke is the name of the Stickleback fish that lives in the estuary of the Sooke River), says parties should be willing to listen in a different way and work around their differences (pers. comm., August 20, 2024).

The S'tenistolw Conference that was held at Camosun College in 2024 had a particular focus on advances in the field of Indigenous education. Conference Elder Graham Hingangaroa Smith reflected on the metaphor of 'where the waters meet'. He underscored that understanding water not as a divider but as a connector is consistent with the way many Pacific peoples find their knowledge. Applying this metaphor to the geosciences, active data sharing should be seen as one more stream of water connecting and increasing existing channels of knowledge.

Also at the 2024 S'tenistolw Conference, Copper Joe Jack described the importance of respectful interactions and data sovereignty and laid out some rules of engagement (Fig. 1). To paraphrase Jack's words, consent-based decision-making tools using traditional ways and Western knowledge should be based on three key principles: respect, caring, and sharing. When used in combination, these rules form a sacred space to bring and rebuild healthy relationships between peoples and lands.

Respecting different worldviews but with same objectives can support positive transformations. Alongside these rules, the United Nations Declaration on the Rights of Indigenous Peoples (UNDRIP) requires states to consult and cooperate with Indigenous Peoples through free, prior, and informed consent (FPIC) before adopting measures that may affect them. In this context, consultation and participation of Indigenous Peoples before developments must be free of coercion, intimidation, or manipulation, must initiate well before any authorization or commencement of activities, and proponents must provide enough information to address a range of aspects such as nature, size, pace, reversibility, scope, duration, locality, and affected areas of any project or activity. It must also include assessments of the likely economic, cultural, social, and environmental impacts of proposed projects, and finally, the consent.

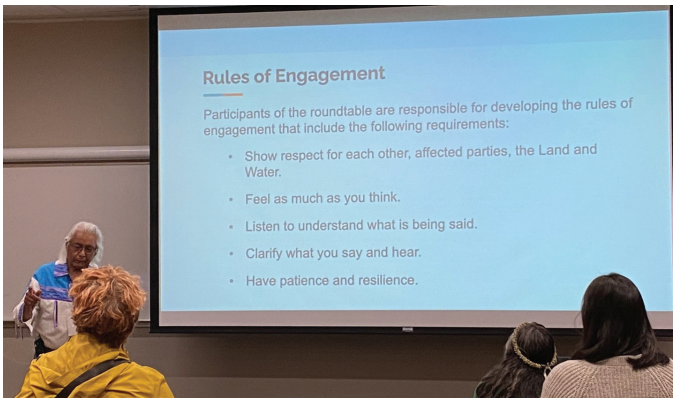


Fig. 1. Copper Joe Jack presenting the Land and People's Relationship model at the S'tenistolw Conference in Victoria, 2024.

Using work such as by Berger (1977) and Booth and Skelton (2011) for guidance, we aspire to work proactively to find mutually acceptable resolutions to Indigenous concerns and giving priority to appreciating perspectives and needs, understanding apprehensions, building positive and respectful community-government relationships, enhancing mutual education, fixing procedural issues, and respecting existing rights.

Although technology now enables us to communicate in real time across the entire planet, there is an enormous difference between remote and in-person interactions. Geoscientists are motivated by a keen desire to investigate how the Earth formed and the changes it has seen through time. So, spending time in Indigenous communities to share neutral information and ideas is an important part of the Engagement Program, as modelled after the internationally recognized benchmark of engagement carried out in the 1970s by Justice Thomas Berger (Berger, 1977) as part of the Mackenzie Valley Pipeline Inquiry. Only by visiting Indigenous communities and listening to how individuals understand their land and paying attention to their concerns about how mineral exploration and development can impact the land and waters can one learn about how people have lived and hunted for thousands of years, understand their connection to the land, and be in a position to conduct meaningful dialogue and communicate neutral information in a non-politicized context. Rather than geoscientists merely providing one-way information sessions about the work they do, community visits, including field trips, encourage a free interchange of ideas, thus serving to enhance intercultural understanding, empathy, and mutual respect.

3. Existing information and historical data

The BCGS is the custodian of all public provincial geoscience data. Between 1874 and 2025, the Survey has released about 6,000 publications, including Papers, Open Files, GeoFiles, Geoscience Maps, Information Circulars, Digital Geoscience Data, Bulletins, Land Use Maps, and Annual Reports (British Columbia Geological Survey, 2026). Survey staff also have a long history of publishing about provincial geoscience in the national and international peer-reviewed literature. The Geological Survey of Canada (the federal geoscience agency) also has a long history of working in the province, publishing internally and externally, and universities such as Simon Fraser

University, University of British Columbia, University of Victoria, Queen's University, and McGill University conduct research that is commonly released in the form of graduate student theses. However, most of the Nations contacted at the start of the Engagement Program were unaware that such a vast assortment of materials was available to them. Furthermore, it can be a daunting task for those unfamiliar with the BCGS publication catalogue, journal catalogues, or research activities at universities to simply access materials then understand how and why studies were done, establish which ones are relevant, and then determine how they might be used.

The Engagement Geologist now addresses these barriers by a reaching out to Indigenous groups with invitations to participate in knowledge sharing activities and by preparing compilations highlighting the most important pieces of information with explanations of how the material might be used in their decision-making processes.

4. The language of geoscience

Like most specialized disciplines, geoscience has its own language. For example, the current Glossary of Geology published by the American Geological Institute (Neuendorf et al., 2005) is almost 800 pages long; many of the terms are arcane and obscure or have different meanings in simple English. Most of the geoscience literature is written using this technical language and most contain concepts that are likely to be foreign to many readers. Thus, anyone without significant training can easily be intimidated when confronted with deciphering the significance of a given publication. To overcome this barrier and ensure that Indigenous groups can fully absorb and then use the information contained in geoscience reports, the Engagement Geologist takes three approaches. First, they serve as a dedicated a point of contact who can be called upon to discuss technical aspects. Second, they prepare short courses, hands-on workshops and, most importantly, field trips where individuals can be active participants and gain first-hand geoscience experience to better understand written documents. Third, they prepare summaries that render terminology-filled documents containing foreign concepts into language that can be readily understood by anyone without losing the meaning of the original.

Creating easily understandable products from recent mineral potential modelling work is an example. The Survey is meeting a heightened demand for geoscience information needed to guide land-use decisions and co-management of mineral resources by increased delivery of Mineral Lands Assessment reports that evaluate the significance of mineral resources in an area and the likelihood of mineral exploration and mining continuing in the future. These reports are aided by new mineral potential modelling, which the Survey revitalized after a period of relative inactivity lasting about 30 years (Wearmouth et al., 2024a, b). Mineral potential modelling is a tool that supports informed land-use decisions by integrating current geological knowledge of mineral systems with data such as geological maps, geophysical and geochemical surveys, and known mineral occurrences to identify areas more likely and less likely to have mineral resource potential. Developments in programming languages and exponential increases in computing power have led to significant advances in applying geographic information system (GIS) platforms and using computerized statistical methods to model mineral potential and create maps that portray the relative ranking of mineral potential. However, these maps can easily be misunderstood because they have inherent uncertainties and limitations. So, in addition to highly technical documents, which detail how the maps are created and the statistical methods used (Wearmouth et al., 2024a, b), the Survey has created more accessible Informational Circulars (British Columbia Geological Survey 2025a, b, c, d) that explain the limitations of the maps and how they can be best used.

5. New projects

British Columbia Geological Survey field geologists typically undertake their research by living and traveling on the lands of Indigenous Peoples. Given that Indigenous Nations must be meaningfully engaged in scholarship that concerns them and may be relied upon for decision making (e.g., Smylie et al., 2020), the Survey works to foster stronger relationships with Indigenous communities as an integral part of fieldwork programs. Influenced strongly by the work of Bharadwaj (2014), who described how past health research projects were too often carried out with little or no community interaction, which led to disenchantment in the communities, the Survey has taken a collaborative approach in which new projects go through multiple engagement sessions before, during, and after studies on Indigenous lands are carried out. Through its Indigenous Peoples Engagement Policy, which was created with input from various Indigenous groups, the Survey adopts a predictable path for engaging with Indigenous communities and leadership in areas where a project is proposed (Fig. 2). The Engagement Geologist gathers all the project information and prepares a package that is then submitted to the Indigenous group of concern. If needed, meetings are scheduled to discuss the project and data sovereignty and implement accommodations. After the project is concluded, the Engagement Geologist continues to be available to share the results of a project and address questions. Because of the time required to adequately engage with all affected rights holders, the cycle (Fig. 2) may take longer than a year to complete.

During the normal course of conducting fieldwork, BCGS geologists may inadvertently encounter sites of Indigenous historical value. Recognizing that respect for the history of First Nations preserved at archeological sites is an essential part of reconciliation efforts, the BCGS has introduced a protocol that Survey personnel must follow when finding unreported archaeological materials, commonly referred to as 'chance finds', that emphasizes informing local Indigenous communities of finds. The primary BCGS goal is not to search for but to document and report inadvertently found previously undiscovered cultural sites to help preserve Indigenous heritage.

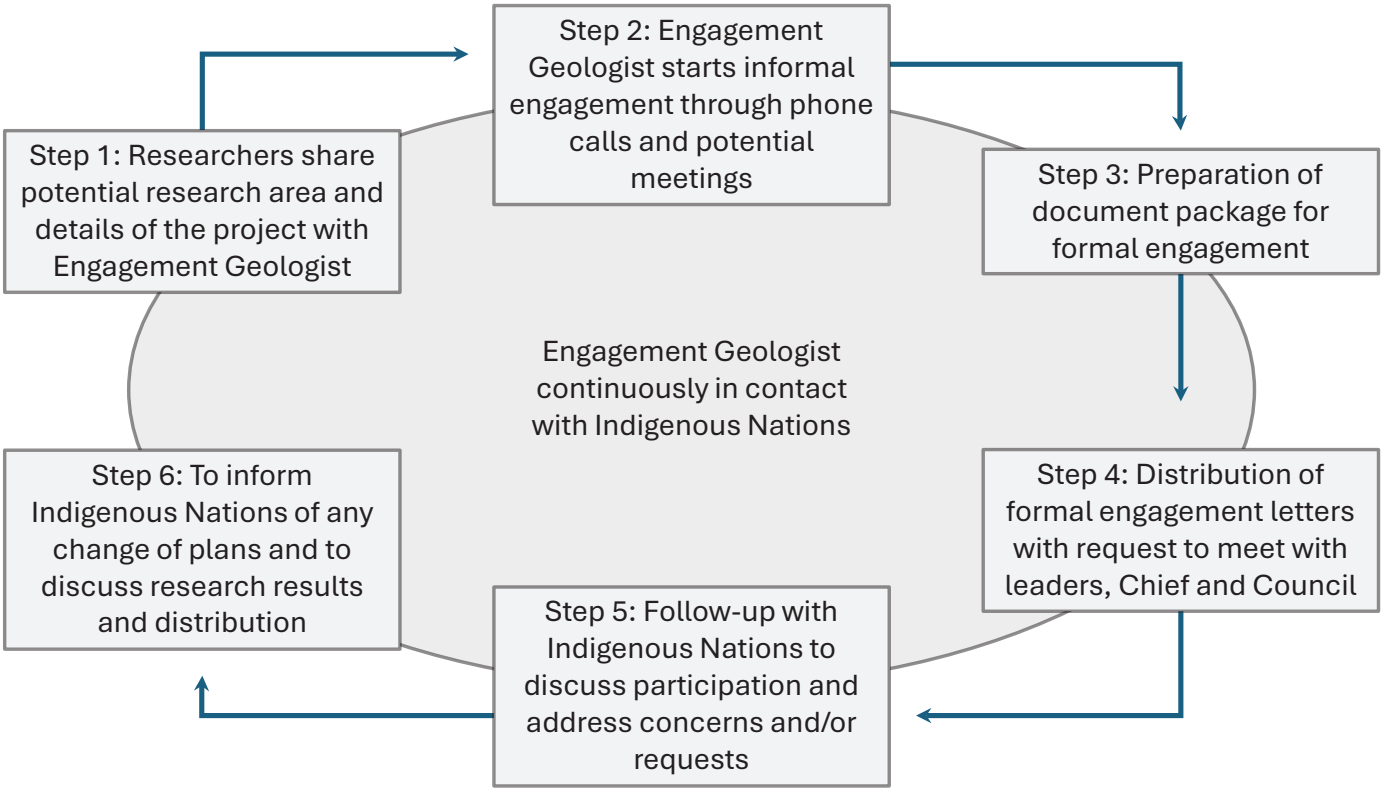


Fig. 2. Diagram depicting engagement workflow cycle for BCGS projects.

6. Traditional Knowledge and Western science

Traditional Knowledge, which is acquired from living on the land and passed down from generation to generation, and Western science are not mutually exclusive and "… with good will and open-mindedness, can complement one another." (White, 2006, p. 401). By adopting a 'two eyes one vision' (Urquhart, 2001) or 'two-eyed seeing' (e.g., Bartlett et al., 2012) approach, which integrates Indigenous perspectives and Western science in our understanding of how the land has evolved, both researchers and traditional knowledge keepers can learn from each other in meaningful ways. This integration has been important in fields such as wildlife management and conservation, land management, and biodiversity (Moller et al., 2004; Schuster et al., 2019; O'Bryan et al., 2020) and public health (Bharadwaj, 2014; Tonkin et al., 2018; Tagalik, 2009; Smylie et al., 2020; Caron et al., 2023).

In the geosciences, Fidler (2010) showed the value of having Indigenous perspectives of mine development incorporated into environmental assessments at the Galore Creek project in northwestern British Columbia, and Allard and Curran (2023) described how Indigenous-led assessments can influence the mine permitting system in the province. Traditional Knowledge with a rich tradition of storytelling and artwork has been of particular importance in documenting historical seismic and tsunami events related to the Cascadia subduction zone along the west coast of North America on Vancouver Island and in Washington State, Oregon, and northern California. Ludwin et al. (2005) and McAdoo et al. (2008) demonstrated that traditional knowledge saved lives during the 2007 Solomon Islands tsunami.

For engagement by the BCGS, opportunities exist in using geology as a neutral and constructive entry point in land-use discussions because Traditional Knowledge and Western science intersections can serve as a foundation for dialogue to build a common understanding of the natural history and geological resources in the province.

7. A positive example: Citxw Nlaka'pamux Assembly (CNA) field trip and geology short course

The simple joy of being on the land is something that most geologists and Indigenous Peoples have in common. Furthermore, learning from first-hand experience or 'learning by doing' is generally accepted as the key to fully absorbing abstract concepts discussed in a classroom setting. Thus, geological field trips provide valuable opportunities for Indigenous Peoples and geoscientists to come together in the setting they prefer to build a common understanding of natural history and mineral resources. In addition, Tonkin et al. (2018) have shown that community activities such as field trips are appreciated by Elders because they provide opportunities in which cultural knowledge and traditional teachings can be passed on to youth. Furthermore, Onstad and van der Flier-Keller (2025) have documented a marked deficiency in participatory activities for geoscience communication in British Columbia.

In a recent field trip with the Citxw Nlaka'pamux Assembly (CNA), parties shared stories, knowledge, worldviews, and concerns such as abandoned mines. The CNA represents eight participating groups: Ashcroft Indian Band, Boston Bar First Nation, Cook's Ferry Indian Band, Coldwater Indian Band, Shackan Indian Band, Siska Indian Band, Nooaitch Indian Band, and Nicomen Indian Band. Within CNA, the Territorial Stewardship Department work is "rooted in ensuring nłeʔképmx people have a say in decisions that matter for our people, in accordance with our values and knowledge. Together we will determine how to protect our culture and care for our lands, water, fish, and wildlife" (Citxw Nlaka'pamux Assembly, 2026).

The interaction between BCGS and CNA initiated in June 2024 when representatives from the Territorial Stewardship Department contacted BCGS to request more information about mineral exploration and mining cycles. Following several months of meetings and discussions, both parties agreed that it would be beneficial to co-develop a geology short course and a field trip for CNA staff, which took place in August 2025 near Merritt (Bacha, 2025). CNA participants experienced first-hand how geological research is carried out and visited current exploration sites (MPD project, Kodiak Copper Corp.; New Craigmont project, Nicola Mining Inc.). In exchange, BCGS and industry geologists learned about CNA cultural values, worldviews, and understandings of nature.

Feedback from participants was unanimously positive, both for the short course (Fig. 3; e.g., "amazing, extremely helpful and packed with knowledge… thorough but not overwhelming") and the field trip (Figs. 4, 5; e.g., "I loved the days in the field and getting to see the different outcrops…



Fig. 4. CNA staff becoming familiar with a Brunton compass.



Fig. 5. Ethan di Marco and Logan di Marco, CNA Land Guardians, investigating an outcrop.



Fig. 3. Classroom geology with CNA staff.

it was really helpful to be in the field and apply what we had learned in class"), and all considered that the activities would help them in performing their jobs.

8. Conclusion

Through its Engagement Program, the Survey works with Indigenous Nations to raise awareness of research projects on their lands, identify opportunities and challenges, and explore partnerships. The program has worked together with about 50 of more than 200 Indigenous Nations in British Columbia through multiple degrees of interactions, from addressing simple requests to accessing information to year-long partnerships with long-term mutually beneficial activities. Core to the Program is that geoscience data are generated in harmonious ways in partnership with Indigenous Nations and that both parties benefit from the production of new geoscience knowledge. Capacity building activities such as short courses and field trips should increase the capacity of Indigenous Nations to the point that they can independently assess and use the data in their decision-making processes.

Acknowledgments

It is an immense honour to work with and write about Indigenous Peoples. The lessons learned come from time spent from 2023 to 2025 with the Carcross/Tagish First Nation, Citxw Nlaka'pamux Assembly, Gitanyow Hereditary Chiefs, K'ómoks First Nation, Nisga'a Nation, Taku River Tlingit First Nation, Tl'azt'en Nation, Tsay Keh Dene Nation, and T̂silhqot'in National Government. I appreciate the critical reviews by Trina Setah from the Xeni Gwet'in (Nemiah) community of the T̂silhqot'in National Government (The People of the River), Roger McMillan, and Marc-André Brideau, which substantially improved the quality of this paper.

References cited

Allard, C., and Curran, D., 2023. Indigenous influence and engagement in mining permitting in British Columbia, Canada: Lessons for Sweden and Norway? Environmental Management, 72. <https://doi.org/10.1007/s00267-021-01536-0>

Bacha, R.R.B., 2025. Field trip guidebook to the geology near Merritt, south-central British Columbia, for the Citxw Nlaka'pamux Assembly. British Columbia Ministry of Mining and Critical Minerals, British Columbia Geological Survey GeoFile 2025-22, 14 p.

Bartlett, C., Marshall, M., and Marshall, A., 2012. Two-Eyed Seeing and other lessons learned within a co-learning journey of bringing together indigenous and mainstream knowledges and ways of knowing. Journal of Environmental Studies and Sciences, 2, 331-340.

Berger, T.R., 1977. Northern frontier, northern homeland. The report of the Mackenzie Valley Pipeline Inquiry, Volume 1. Ministry of Supply and Services Canada, 246 p.

Bharadwaj, L., 2014. A framework for building research partnerships with First Nations communities. Environmental Health Insights, 8, 15-25.

Booth, A.L., and Skelton, N.W., 2011. Improving First Nations' participation in environmental assessment processes: Recommendations from the field. Impact Assessment and Project Appraisal, 29, 49-58.

British Columbia Geological Survey, 2026. Publication catalogue. <https://www2.gov.bc.ca/gov/content/industry/mineral-exploration-mining/british-columbia-geological-survey/publications>

British Columbia Geological Survey, 2025a. Tahltan Land Use Planning area mineral potential map for porphyry, volcanogenic massive sulphide (VMS), and magmatic mafic-ultramafic deposits. British Columbia Ministry of Mining and Critical Minerals, British Columbia Geological Survey Information Circular 2025-10, 2 p.

British Columbia Geological Survey, 2025b. Kaska Land Use Planning area mineral potential map for porphyry, volcanogenic massive sulphide (VMS), magmatic mafic-ultramafic, sedimentary exhalative (SEDEX) and Mississippi Valley Type (MVT) deposits. British Columbia Ministry of Mining and Critical Minerals, British Columbia Geological Survey Information Circular 2025-11, 2 p.

British Columbia Geological Survey, 2025c. Meziadin Land Use Planning area mineral potential map for porphyry, volcanogenic massive sulphide (VMS), and magmatic mafic-ultramafic deposits. British Columbia Ministry of Mining and Critical Minerals, British Columbia Geological Survey Information Circular 2025-12, 2 p.

British Columbia Geological Survey, 2025d. TRT Land Use Planning area mineral potential map for porphyry, volcanogenic massive sulphide (VMS), and magmatic mafic-ultramafic deposits. British Columbia Ministry of Mining and Critical Minerals, British Columbia Geological Survey Information Circular 2025-13, 2 p.

Caron, N.R., Adam, W., Anderson, K., Boswell, B.T., Chongo, M., Deineko, V., Dick, A., Hall, S.E., Hatcher, J.T., Howard, P., Hunt, M., Linn, K., and O'Neill, A., 2023. Partnering with First Nations in northern British Columbia Canada to reduce inequity in access to genomic research. International Journal of Environmental Research and Public Health, 20, article 5783. <https://doi.org/10.3390/>

Citxw Nlaka'pamux Assembly (2026). Territorial stewardship. <https://www.cna-trust.ca/territorial-stewardship.htm> (last accessed March 2026).

Fidler, C., 2010. Increasing the sustainability of a resource development: Aboriginal engagement and negotiated agreements. Environment, Development and Sustainability, 12, 233-244.

Ludwin, R.S., Dennis, R., Carver, D., McMillan, A.D., Losey, R., Clague, J., Jonientz-Trisler, C., Bowechop, J., Wray, J., and James, K., 2005. Dating the 1700 Cascadia earthquake: Great coastal earthquakes in Native stories. Seismological Research Letters, 76, 140-148.

McAdoo, B.G., Moore, A., and Jennifer Baumwoll, J., 2008. Indigenous knowledge and the near field population response during the 2007 Solomon Islands tsunami. Natural Hazards, 48, 73-82.

Moller, H., Berkes, F., Lyver, P.O., and Kislalioglu, M., 2004. Combining science and traditional ecological knowledge: Monitoring populations for co-management. Ecology and Society, 9. <http://www.ecologyandsociety.org/vol9/iss3/art2/>

Neuendorf, K.K.E, Mehl Jr., J.P., and Jackson, J.A., (Editors), 2005. Glossary of geology, fifth edition. American Geological Institute, 779 p.

O'Bryan, C.J., Garnett, S.T., Fa, J.E., Leiper, I., Rehbein, J.A., Fernández-Llamazares, A., Jackson, M.V., Jonas, H.D., Brondizio, E.S., Burgess, N.D., Robinson, C.J., Zander, K.K., Molnár, Z., Venter, O., and Watson, J.E.M., 2020. The importance of Indigenous Peoples' lands for the conservation of terrestrial mammals. Conservation Biology, 35, 1002-1008.

Onstad, C.C., and van der Flier-Keller, E., 2025. Geoscience communication: A content analysis of practice in British Columbia, Canada, using science communication models. Geoscience Communication, 8, 125-149. <https://doi.org/10.5194/gc-8-125-2025>

Schuster, R., Germain, R.R., Bennett, J.R., Reo, N.J., and Arcese, P., 2019. Vertebrate biodiversity on indigenous-managed lands in Australia, Brazil, and Canada equals that in protected areas. Environmental Science and Policy, 101, 1-6.

Smylie, J., Marsden, N., Star, L., Gahagan, J., Zarowsky, C., Mykhalovskiy, E., Masuda, J., and Potvin, L., 2020. Requirement for meaningful engagement of First Nations, Inuit, Métis, and Indigenous Peoples in publications about them. Canadian Journal of Public Health, 111, 826-830.

Tagalik, S., 2009. Inuit Quujimajatuqangit: The role of Indigenous knowledge in supporting wellness in Inuit communities in Nunavut. National Collaborating Centre for Aboriginal Health. <https://www.ccnsa-nccah.ca/docs/health/FS-InuitQaujimajatuqangitWellnessNunavut-Tagalik-EN.pdf>

Tonkin, R., Freeman, S., Martin, J., Ward, V., and Skinner, K., 2018, First Nation Elders' perspectives of engagement in community programs in Nak'azdli Whut'en, British Columbia, Canada. Canadian Journal of Public Health, 109, 717-725.

Urquhart, D., (Ed.), 2001. Two eyes: One vision, conference summary. Yukon Fish and Wildlife Management Board, 76 p.

White, G., 2006. Cultures in collision: Traditional Knowledge and Euro-Canadian governance processes in northern land-claim boards. Arctic, 59, 401-414.

Wearmouth, C.D., Peters, K.J., Czertowicz, T.A., and Orovan, E.A., 2024a. Mineral potential modelling results for northwestern British Columbia, a comparison between past and current work at the British Columbia Geological Survey. In: Geological Fieldwork 2023, British Columbia Ministry of Energy, Mines and Low Carbon Innovation, British Columbia Geological Survey Paper 2024-01, pp. 79-95.

Wearmouth, C., Czertowicz, T., Peters, K.J., and Orovan, E., 2024b. Mineral potential modelling at the British Columbia Geological Survey: Renewed methods with application to northwestern British Columbia. British Columbia Ministry of Energy, Mines and Low Carbon Innovation, British Columbia Geological Survey Paper 2024-02, 28 p.

Mineralogical control on critical companion metal distribution: Expanded workflow, with examples from the Sullivan Pb-Zn-Ag deposit

Luke Ootes[1, a], Audrey C. Graham[1], Keani Whitmore[1, 2], Dylan Goudie[3], Stephen J. Piercey[4], Shaun Barker[5], Sarah Milne[5], and Chris McFarlane[6]

[1] British Columbia Geological Survey, Ministry of Mining and Critical Minerals, Victoria, BC, V8W 9N3
[2] School of Earth and Ocean Sciences, University of Victoria, Victoria, BC, V8W 3P6
[3] Core Research Equipment and Instrument Training (CREAIT) Network, Memorial University of Newfoundland, St. John's, NL, A1C 5S7
[4] Department of Earth Sciences, Memorial University of Newfoundland, St. John's, NL, A1B 1N3
[5] Mineral Deposit Research Unit, University of British Columbia, Vancouver, BC, V8W 3P6
[6] Department of Earth Sciences, University of New Brunswick, Fredericton, NB, E3B 5A3
[a] corresponding author: Luke.Ootes@gov.bc.ca

Recommended citation: Ootes, L., Graham, A.C., Whitmore, K., Goudie, D., Piercey, S.J., Barker, S., Milne, S., and McFarlane, C., 2026. Mineralogical control on critical companion metal distribution: Expanded workflow, with examples from the Sullivan Pb-Zn-Ag deposit. In: Geological Fieldwork 2025, British Columbia Ministry of Mining and Critical Minerals, British Columbia Geological Survey Paper 2026-01, pp. 45-52.

Abstract

Relative to primary ore metals (e.g., Cu, Zn) critical companion metals (e.g., In, Sn, PGEs, Te) generally occur in low concentrations and, although typically not exploration targets, they can represent significant by- or co-product opportunities during mining. Understanding the distribution and coupling or decoupling of these companion metals with primary ore metals will help further understand their distribution in deposits and their potential economic viability. We use samples from the past-producing Sullivan Pb-Zn-Ag mine to illustrate an expanded workflow for critical mineral projects at the British Columbia Geological Survey. Geochemical analyses, thin section petrography, and quantitative mineralogy by scanning electron microscope-mineral liberation analysis (SEM-MLA) are successful in identifying major and trace minerals. However, some minerals contain minor elements in solid solution that SEM-MLA is unable to identify. For these elements the workflow required expansion and micro x-ray fluorescence (μXRF) analysis was added as an element mapping tool. Whole rock geochemical analyses from some samples of Sullivan mineralization yielded >100 ppm In, but neither the SEM-MLA nor μXRF work resolved the mineralogical host. Thus, we also employed elemental mapping by laser ablation-inductively coupled-plasma mass spectrometry (LA-ICP-MS). This mapping revealed that even though the minor phase cassiterite (SnO_2) contains the highest In concentrations, In is predominantly hosted in solid solution in sphalerite. Cassiterite is uncommon in the samples investigated and Sn is predominantly in boulangerite ($Pb_5Sb_4S_{11}$). These results indicate that Sn and In are coupled in cassiterite but decoupled and in solid solution in boulangerite (Sn) and sphalerite (In), an observation significant for the exploration and production of these metals. The expanded workflow and tool combination provide quantitative insights into metal coupling and decoupling in mineralization and can be applied in cases where mineralogical control on elemental distribution is elusive.

Keywords: Critical companion metals, LA-ICP-MS, SEM-MLA, μXRF, Sullivan

1. Introduction

Relative to primary ore metals (e.g., Cu, Zn) critical companion metals (e.g., Sn, PGEs, Te) generally occur in low concentrations and, although typically not exploration targets, they can represent significant by- or co-product opportunities during mining (e.g., Holley et al., 2025). For example, sedimentary exhalative (SEDEX) and related deposits in predominantly siliciclastic successions contain primary commodities Pb, Zn, and Ag and can contain recoverable concentrations of companion metals (e.g., Ge, Sn, In). These companion metals can occur either as discrete mineralogical phases (e.g., cassiterite, SnO_2) or as solid solution substitutions in the crystal lattice of other minerals, such as trace metals in sphalerite (e.g., Bonnet et al., 2016), or in sulphosalts (e.g., Moëlo et al., 2008). Understanding the distribution and coupling or decoupling of these companion metals with primary ore metals will help further understand their distribution in deposits and their potential economic viability. To resolve this in British Columbia mineral deposits, the application of modern analytical techniques is required to quantify mineralogical control on critical companion metals (e.g., Wei et al., 2026).

Using quantitative geochemical analysis, Graham et al. (2025) demonstrated abundances of Sn and In at the past-producing Sullivan Pb-Zn-Ag deposit. However, the mineralogical relationship of these companion metals to the primary ore metals remains unresolved. In this study, we use the same samples as Graham et al. (2025) to identify the host

minerals at Sullivan and to detail a modified version of the project workflow for critical minerals (Piercey et al., 2025), which combines Zeiss Axioscan petrographic images with scanning electron microscope-mineral liberation analysis (SEM-MLA) expanded to include micro x-ray fluorescence analysis (μXRF). This combined approach determined the host mineralogical phase of most metals (e.g., Sb, As) but was only partially successful for some metals (e.g., Sn) and failed for others (e.g., In). To further constrain the mineralogical control on elemental distribution we also conducted elemental mapping by laser ablation-inductively coupled plasma-mass spectrometry (LA-ICP-MS).

2. Methods and workflow

The ten samples used in this study come from the past-producing Sullivan mine (Fig. 1) and represent a range of mineralization styles from the deposit including massive sulphide from the 'Main ore band' and 'Bedded ore bands'. These samples were previously collected and stored in the British Columbia Geological Survey (BCGS) rock archive (Rukhlov et al., 2023). Geochemical results from these rocks are presented in Graham et al. (2025) and Graham and Ootes (2025). Sample offcuts were prepared as polished thin sections.

The BCGS has adopted the mineral systems approach to its critical minerals projects (e.g., Hickin et al., 2024). Analytical work prioritizes: 1) producing mines; 2) past-producing mines; 3) advanced exploration projects; and 4) showings and prospects. Geochemical analysis is the first step in quantifying metal contents of samples (Fig. 2; e.g., Graham et al., 2025; Piercey et al., 2025). Samples that contain critical companion metals are followed up with petrographic analysis and mineralogical quantification using scanning electron microscope-mineral liberation analysis (SEM-MLA). This study also conducted micro x-ray fluorescence (μXRF) analysis to determine elemental distributions (Fig. 2). For elemental distribution (e.g., Sn, In) that could not be resolved by these methods, laser ablation-inductively coupled plasma-mass spectrometry (LA-ICP-MS) analysis was employed. This geochemical and micro-analytical workflow provides quantification of mineralogical control on critical companion metals (Figs. 2-5; Tables 1, 2).

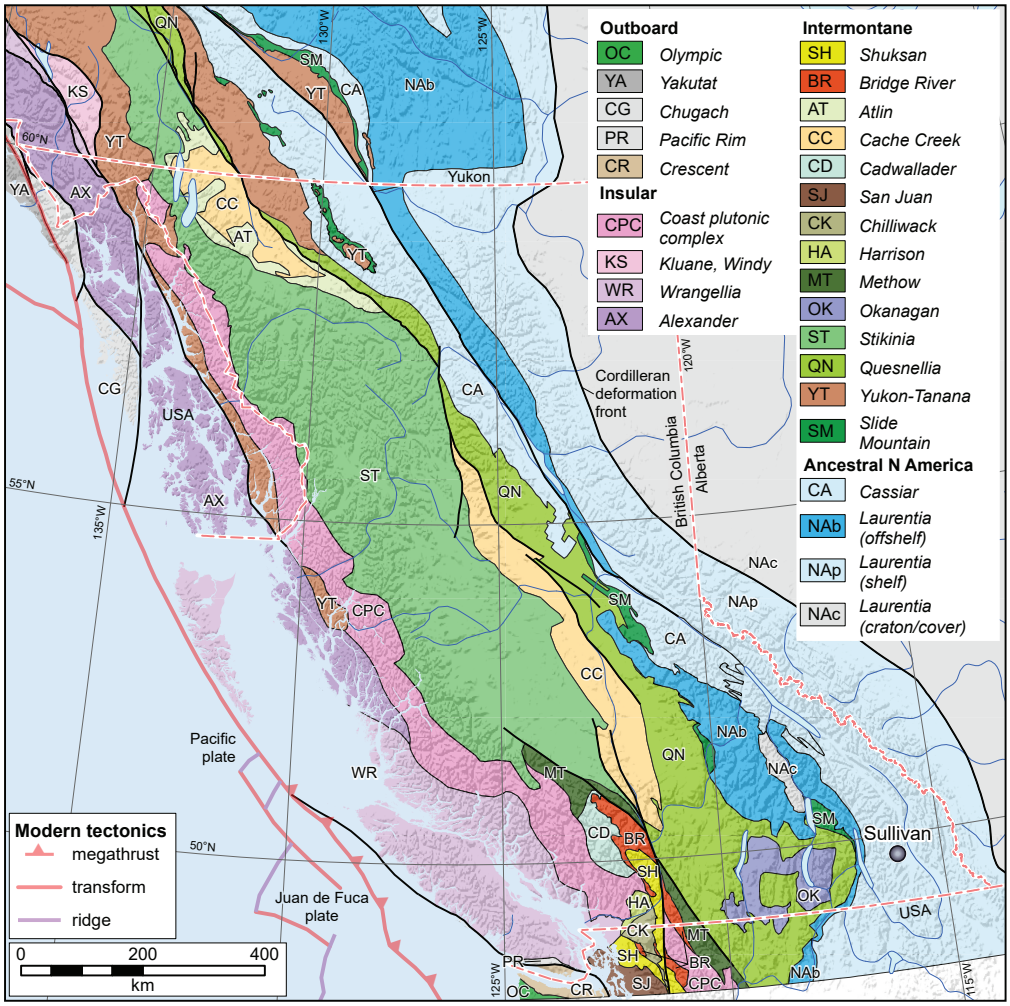


Fig. 1. Location of the Sullivan deposit. Terranes after Colpron (2020).

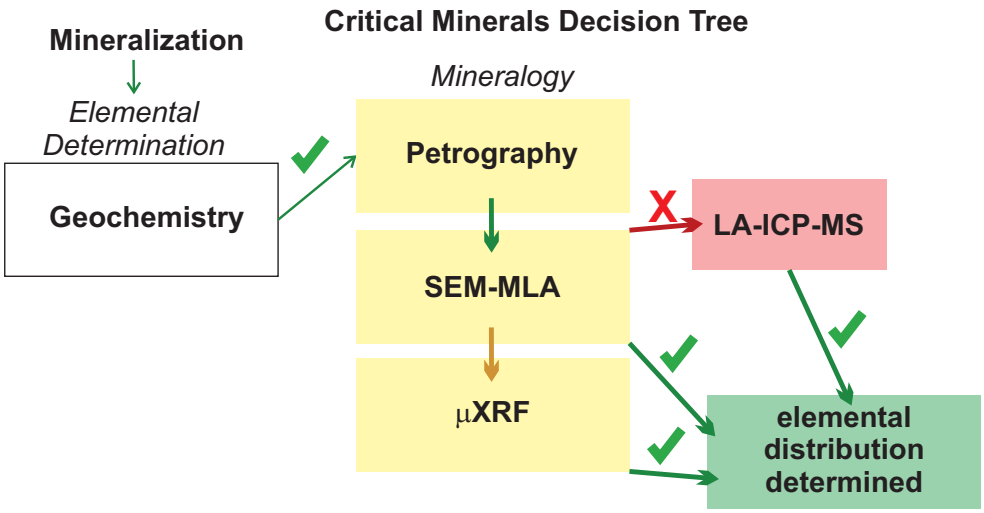


Fig. 2. Decision tree and workflow for critical companion metals projects at the British Columbia Geological Survey, expanded after Piercey et al. (2025). Green check marks and arrows indicate positive determination of mineral host to metals. Orange arrow indicates that only a subset of samples are investigated with μXRF. Red X and arrow indicate that LA-ICP-MS analysis is required for determination.

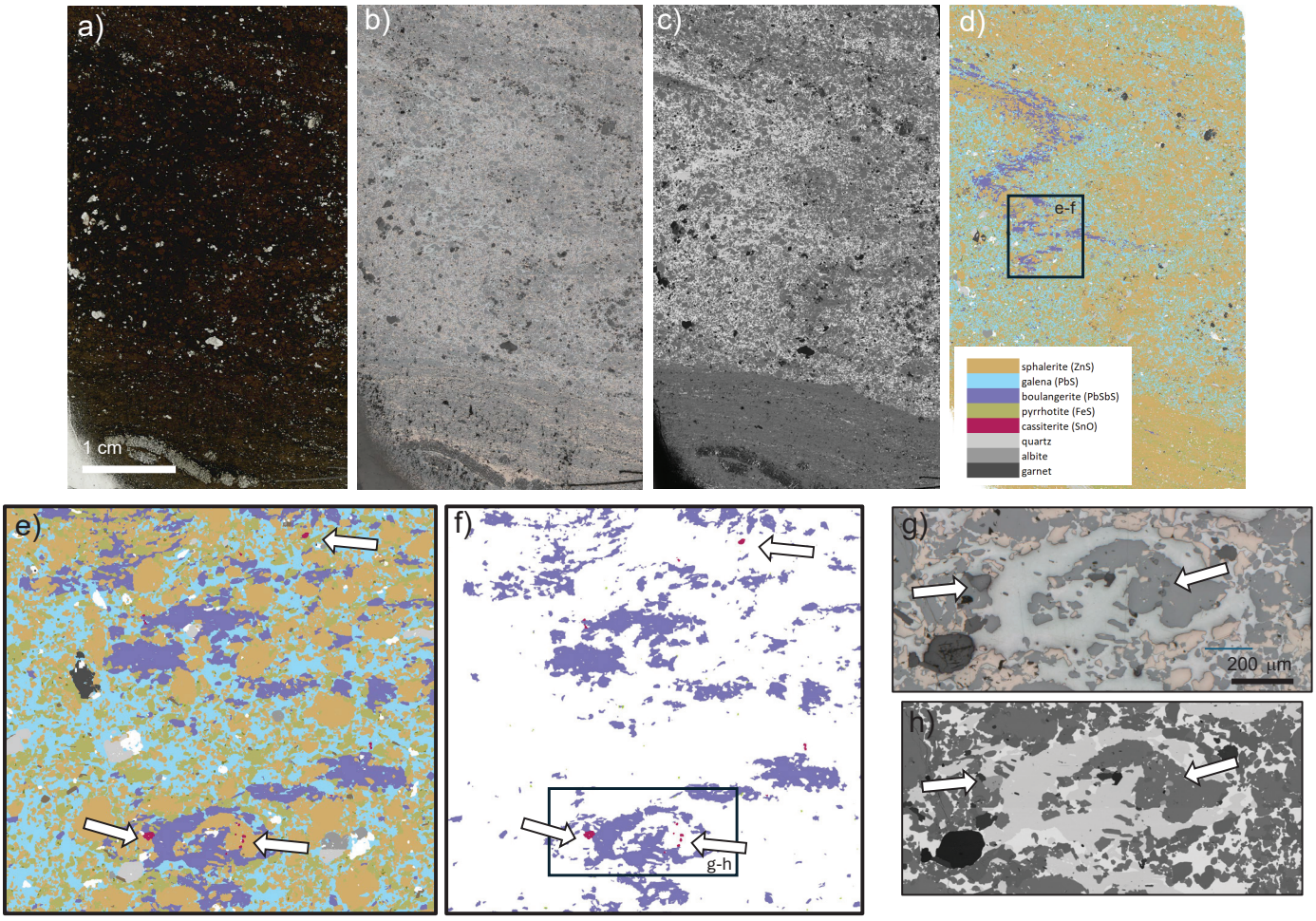


Fig. 3. Thin section images of a Sullivan Main band sample. **a)** Photomicrograph, plane polarized light. **b)** Photomicrograph, reflected light. **c)** Backscattered electron (BSE) image. **d)** False colour MLA image; legend applies to images d-f. **e-f)** Examples using false colour MLA, including resampling colours, to find trace minerals in samples using cassiterite (SnO_2; arrows) as an example. **g)** Reflected light and **h)** BSE images that highlight the difficulty of finding cassiterite without the use of MLA.

2.1. Petrography

Polished thin sections were prepared and automated petrographic images were created using Zeiss Axioscan Geo7 at the University of British Columbia, Mineral Deposits Research Unit. These images include plane, polarized, circular polarized, and reflected light photomicrographs that are hosted online and have real-time pan and zoom functionality (Figs. 3a, b). This system allows the petrographer the ability to conduct thin-section-scale to micron-scale mineralogical and textural evaluation of samples and allows heads-up comparison with other datasets.

2.2. Scanning electron microscope-mineral liberation analysis

To assist in the mineralogical and elemental assessment, automated mineralogical mapping using SEM-MLA was conducted at CREAIT Microanalysis Facility (MAF), Memorial University of Newfoundland. Polished thin sections were mapped using a scanning electron microscope with derived backscatter electron (BSE) images and quantitative mineral abundance maps by mineral liberation analysis. The SEM work used a FEI MLA 650 field emission gun SEM equipped with two Brucker silicon drift EDS detectors. Operating conditions included 25 kV accelerating voltage for BSE images. Operating conditions for MLA included a 25 kV accelerating voltage, 10 nA current, and a 5.85 electron beam spot size. Thin sections were measured in GXMAP (grain-based x-ray mapping) mode where x-ray analyses were triggered for a BSE range of 40 to 255. Each x-ray measurement was acquired for 12 ms on a 1.5 by 1.5 mm frame with a resolution of 500 pixels per frame and an imaging scan speed of 16 µsec. Data reduction was performed on MLA Data View (FEI) software version 3.1.4.683.

The SEM-MLA provides full thin-section data as BSE images and false colour mineralogical maps (Figs. 3c, d). In-house Python™ coding enables rapid colour changes to MLA images, highlighting different mineral phases and allowing comparison to photomicrographs and BSE images (Figs. 3e-h). Each false-colour MLA image is accompanied by a quantitative

Table 1. Selected results of SEM-MLA quantitative mineralogy from a Main band sample, Sullivan deposit (see Figure 3).

Mineral	Wt.%	Area%	Area (micron)	Particle Count	Grain Count
Total	100.00	100.00	732005342.97	1698	267375
Sphalerite	41.29	48.71	356544422.34	1033	51383
Galena	35.64	22.73	166385090.57	770	121430
Pyrrhotite	19.15	19.58	143328920.14	649	59969
Quartz	1.55	2.79	20454776.04	422	5709
Boulangerite	0.57	2.68	19596283.07	345	4047
Albite	0.45	0.82	5987058.75	369	1399
Fe-Ca Rhodocrosite	0.13	0.64	4652136.87	404	3103
Chlorite	0.36	0.57	4154413.57	391	3999
Biotite	0.33	0.51	3711215.97	397	3837
Mn-Fe-Ca Garnet	0.09	0.42	3065875.40	227	1032
Pyrite	0.25	0.24	1738439.48	411	6021
Muscovite	0.06	0.10	758617.92	268	1384
Mn Siderite	0.02	0.10	720595.37	272	903
Fe Mg Al silicate	0.01	0.03	214244.55	201	450
Apatite	0.01	0.02	159740.81	193	567
Tetrahedrite	0.02	0.02	152710.37	286	739
Chalcopyrite	0.02	0.02	132941.72	223	422
Ilmenite	0.01	0.01	64393.56	150	273
Cassiterite	0.01	0.01	63504.46	76	113

Table 2. Selected elemental concentrations of sulphide minerals from LA-ICP-MS mapping (see Figure 5).

Mineral	S^{34}	±2s	Fe^{56}	±2s	Zn^{66}	±2s	Pb^{208}	±2s	Sn^{118}	±2s	Sb^{121}	±2s	Ag^{107}	±2s	Cd^{111}	±2s	Bi^{209}	±2s	In^{115}	±2s
	ppm		ppm		ppm		ppm		ppm		ppm		ppm		ppm		ppm		ppm	
Pyrrhotite	524572.9	31452.0	467533.2	15885.9	1539.4	791.7	36504.2	47308.0	3.1	4.0	63.3	63.5	4.6	1.7	11.4	7.9	2.5	2.6	0.2	0.3
Pyrrhotite	507374.0	20327.4	439852.3	37386.1	6778.0	7866.3	11884.9	10424.8	2.3	2.0	387.6	142.9	13.1	10.2	79.0	87.5	0.5	0.4	4.7	5.7
Pyrrhotite	494821.7	19443.5	432786.5	36634.6	9234.7	6979.6	62382.6	49823.5	8.0	6.5	409.7	264.7	69.5	54.9	91.6	91.2	4.1	3.2	11.7	10.6
Sphalerite	387786.7	8980.3	44968.2	1205.3	564239.6	9156.7	172.8	27.6	0.1	0.0	11.3	5.7	3.3	0.4	1739.6	26.3	0.0	0.0	149.4	5.3
Sphalerite	394380.3	8468.6	47534.5	955.2	554846.5	8004.2	383.4	66.9	0.1	0.0	13.0	4.2	3.7	0.5	1812.2	63.2	0.0	0.0	144.8	3.7
Sphalerite	386068.3	3497.1	48790.0	961.7	561909.0	3152.1	190.7	18.8	0.4	0.1	18.7	3.8	6.7	2.1	2007.5	61.2	0.0	0.0	148.1	3.5
Cassiterite	32258.0	20948.0	9176.8	6742.1	28451.9	30026.4	9043.7	3948.0	852277.5	126511.0	1853.2	811.6	2.8	3.0	97.9	92.1	0.8	0.6	2731.5	390.2
Boulangerite	216566.2	4804.8	56.2	14.3	306.4	191.4	618679.6	8086.2	121.3	3.6	164088.2	4672.0	55.0	23.7	21.7	41.0	49.5	0.9	0.5	0.0
Boulangerite	220102.8	2944.5	367.7	568.5	419.7	256.3	615125.6	5485.7	139.0	4.7	163966.4	4996.3	24.2	4.2	1.4	0.5	49.8	1.4	0.6	0.0
Boulangerite	221223.1	5516.2	50.0	8.6	127.3	23.8	613742.6	7113.5	135.0	3.5	164576.0	3069.5	25.4	2.0	0.8	0.1	53.1	1.0	0.6	0.0
Galena	109358.7	6675.0	50.6	17.3	112.9	25.9	889886.0	6760.4	37.6	2.0	764.7	57.4	698.8	61.7	8.4	0.9	19.5	0.5	0.2	0.0
Galena	122687.3	5615.9	228.8	90.7	254.7	99.1	876202.4	5641.9	43.6	2.4	822.9	38.8	732.4	34.5	9.7	2.6	20.8	0.4	0.2	0.1
Galena	130036.5	5893.6	218.4	192.5	187.9	91.6	868667.4	5776.0	35.4	1.1	1096.3	629.0	705.3	36.6	7.8	0.8	28.8	0.5	0.2	0.0

±2s refers to the internal standard error

mineralogical table that specifies the mineral species in the sample and the spatial distribution and number of crystals in the sample (Table 1).

2.3. μXRF

A Bruker TornadoPlus μXRF instrument fitted with two 60 mm^2 detectors, housed in the Mineral Deposit Research Unit, University of British Columbia, was used for analysis. An Rh x-ray tube, excited to 50 kV and 600 nA current generated x-rays, which are focused through a polycapillary x-ray optic on the sample. The x-ray spot generated has a diameter of ~19 mm. Data were collected with a spatial resolution of 50 mm (generating images with a pixel resolution of 50 by 50 mm), with a counting time of 10 ms per pixel, typically generating several thousand x-ray counts per pixel. Sampling occurs as a sequential line scan, whereby the 19 mm spot moves along the sample as the instrument stage travels from left to right, the stage then steps back to its starting point, travels 100 mm down, and then travels left to right again. Data were processed in Bruker ESPRIT® software. In the software, a colour stretch is applied to count data so that higher counts appear as brighter colours producing intensity maps. Finally, a fundamental parameter (FP) method in Bruker ESPRIT® software was applied to each map to quantify results, which accounts for peak overlaps and background corrections. Because no standards were analyzed with unknown samples, the results should be treated as semi-quantitative, with significant uncertainties on any individual pixel. However, the FP method has the advantage that it helps the viewer to determine likely 'true' variations in element intensities in a sample by removing variations in count rates caused by sample geometry and colour stretches, which are applied across very low count rate elements. Colours that occur outside the edge of the sample represent artefacts introduced by the background substrate of the samples and should be taken as being inaccurate.

2.4. Laser ablation-inductively coupled plasma-mass spectrometry

To support the SEM-MLA and μXRF results, the metal distribution was mapped by LA-ICP-MS analysis in the Department of Earth Sciences, University of New Brunswick (Table 2). Two samples with high In were targeted, and in each thin section four sub-areas were chosen based on textural and mineralogical diversity (Fig. 5). Trace-element raster maps were acquired using an Applied Spectra Inc. ASI RESOlution 193 nm laser ablation system connected to an Agilent 8900 QQQ-ICP-MS. A Norris Scientific 'fast-funnel' and Quadlock™ device were used to achieve fast washout and eliminate spectra skew. Rectangular areas of interest were ablated using a series of raster lines space at 25 mm and using a laser beam diameter of 26 mm, a pulse rate set by the Quadlock system (18-19 Hz), and a stage scan speed of 60 mm/s. The ICP-MS was set to collect a suite of 24 elements (^{24}Mg, ^{27}Al, ^{29}Si, ^{31}P, ^{34}S, ^{39}K,^{44}Ca, ^{47}Ti, ^{55}Mn, ^{56}Fe, ^{63}Cu, ^{66}Zn, ^{71}Ga, ^{73}Ge, ^{75}As, ^{107}Ag, ^{111}Cd, ^{115}In, ^{118}Sn, ^{121}Sb, ^{125}Te, ^{208}Pb, and ^{209}Bi) with a total quadrupole sweep

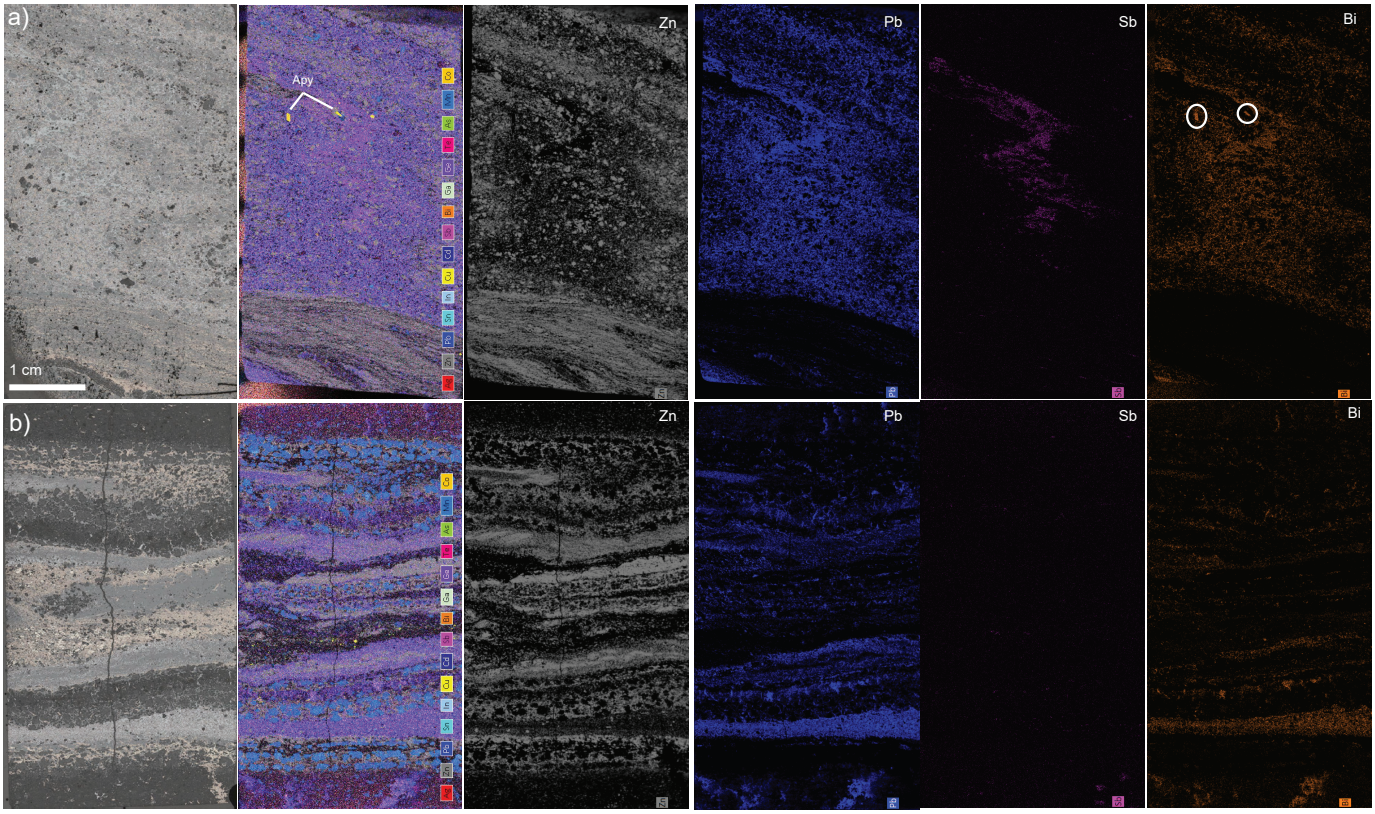


Fig. 4. Results of µXRF scans. Samples from **a)** Sullivan Main band. **b)** Sullivan C band. Left to right: photomicrograph (reflected light); full colour µXRF; results for Pb, Zn, Sb, and Bi. Because µXRF was conducted on thin section cutoffs, the photomicrograph and µXRF images do not exactly match.

time <0.25 s. The instrumentation was tuned on NIST610 glass to obtain oxide production (^{248}ThO/^{232}Th) <0.2%, doubly charged production (22 M/^{44}Ca) <0.2%, and ^{238}U/^{232}Th of 1.02. Standards USGS BCR2-G and MASS-1 were also measured throughout the run to act as primary and secondary standards.

Trace-element maps were produced offline using Iolite4 and the 3D Trace-element Data Reduction Scheme that includes a normalization to 100% calculation approach obviating the need for internal standardization. The 3D Trace-element DRS also includes a criteria function to parse mineral phases based on major-element compositions (e.g., Pb for galena; Zn for sphalerite; Fe for pyrite and pyrrhotite; Sb for boulangerite; Si for silicates; Sn for cassiterite). This allows full quantification of trace-element maps (e.g., Fig. 5) on the basis of observed mineralogy. Mean concentrations are derived from circular regions of interest selected on several examples of each mineral in the laser map.

3. Discussion

Petrographic and SEM-MLA quantitative mineralogy (Fig. 3; Table 1) demonstrates the ability to identify various mineralogical phases. For example, a boulangerite ($Pb_5Sb_4S_{11}$) band (Fig. 3d) is segregated from galena (PbS) indicating that Sb is localized and concentrated in Sullivan ore, rather than being uniformly distributed throughout, consistent with mine-scale metal distribution (Freeze, 1966). Rare and tiny (<100 mm) cassiterite crystals (SnO_2) only occur locally in this sample (Table 1), and these were only found through interrogation of the false-colour MLA image (Figs. 3e-f); these crystals would be difficult to find and identify using reflected light petrography or BSE images alone (Figs. 3g, h). However, unlike Sb-in-boulangerite and Sn-in-cassiterite, some minerals contain minor elements in solid solution that SEM-MLA was unable to identify.

The application of µXRF to thin section offcuts provides maps of elemental distribution (Fig. 4). Zinc and Pb do not form solid-solution minerals together, and their decoupling as sphalerite and galena-boulangerite is clear on the µXRF images. The µXRF results agree with the MLA observations that Sb is segregated (Fig. 4a). Bismuth minerals (e.g., bismuthinite; Bi_2S_3) are uncommon in the Sullivan samples. However, µXRF shows that Bi is distributed within galena-boulangerite and trace arsenopyrite crystals (Fig. 4). The same is true for Sn (not shown). This indicates solid solution within boulangerite and galena (Pb and Sb) and decoupling from sphalerite (Zn; Fig. 4).

The Sullivan Main band sample (Figs. 3, 4a, 5) contains >100 ppm In (Graham et al., 2025; Graham and Ootes, 2025), but neither the SEM-MLA nor µXRF could resolve the In distribution, and LA-ICP-MS analysis was employed. Those results, along with all other resultant data maps, were

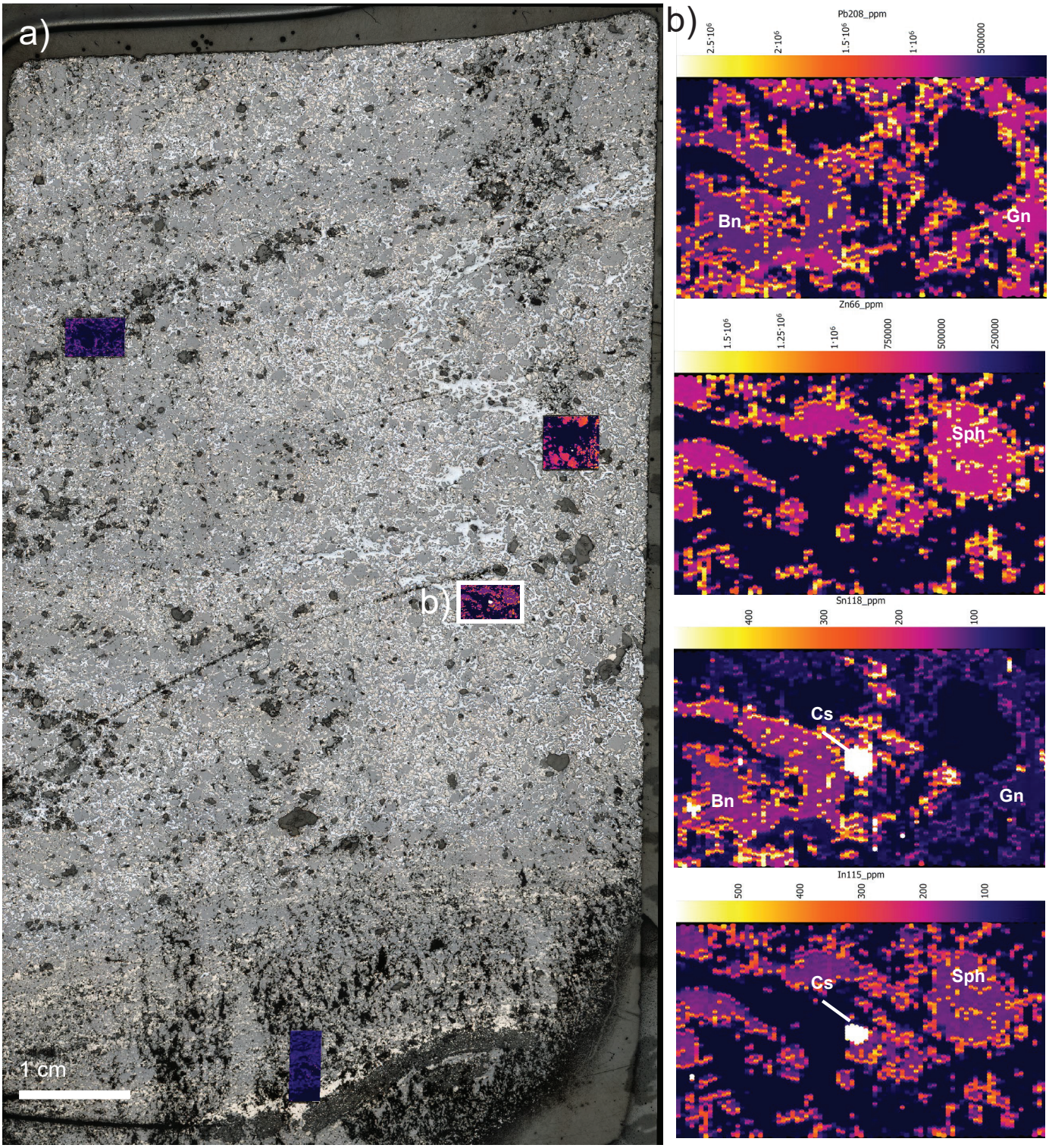


Fig. 5. a) Thin section photomicrograph of the Sullivan Main band (reflected light). The four coloured boxes are the locations of LA-ICP-MS elemental maps, all showing the distribution ^{115}In. **b)** Examples of elemental distribution of one of the mapped areas. From top to bottom are elemental distributions on ^{208}Pb, ^{66}Zn, ^{118}Sn, and ^{115}In. The circular white mineral in the Sn and In maps is cassiterite (see Figure 3). Colour ramps are in parts per million (ppm).

georeferenced (Fig. 5); for simplicity here we use the reflected light photomicrograph of Sullivan Main band sample as a base. Each coloured box on Figure 5a are the In distribution maps from LA-ICP-MS. Elemental comparison (Fig. 5b) highlights the distribution of Pb, Zn, Sn, and In in the mapped area. An isolated cassiterite crystal contains the highest concentration of In in the sample (~2700 ppm; Table 2), indicating In is preferentially hosted in cassiterite (Fig. 5b). Additional In is hosted in sphalerite (~150 ppm; Table 2). In both cases, the In is in solid solution within these minerals.

As outlined below, these data offer a tentative interpretation that envisages coupling of Sn-In-in-cassiterite and decoupling of Sn-in-boulangerite and In-in-sphalerite, which has significant exploration and production implications. Because cassiterite is an oxide, the massive sulphide zone of the Sullivan main band would have been oxygen deficient. Thus, once oxygen in the system was exhausted, the Sn could no longer form as cassiterite and needed an alternative mineral host. The LA-ICP-MS maps and data show secondary abundance of Sn-in-boulangerite, but not in galena or sphalerite (Table 2; Figs. 3, 5). The maps and data also show secondary abundance of In-in-sphalerite, but not in boulangerite or galena. It may have been that excess Sn moved into solid solution in boulangerite and that the remaining In, which also required a mineralogical home, was accommodated by sphalerite (Fig. 5b). Acknowledging that this is a preliminary interpretation and limited LA-ICP-MS mapping, if elemental coupling and decoupling occurs at a deposit-scale, understanding and quantifying this distribution and mineralogical control would be paramount in the exploration for and production of these metals.

4. Conclusion

The expanded workflow for critical minerals projects at the BCGS allows the identification and quantification of the mineralogical control and distribution of critical companion metals in mineral systems. The combination of petrography, SEM-MLA, and μXRF is sufficient to identify mineralogical phases and elemental distribution. In some cases, the resolving power of LA-ICP-MS is required to identify elemental phases and their mineralogical control. The benefit of SEM-MLA is thin section-scale analysis that can be combined with whole rock geochemical results, whereas the μXRF provides fine-scale, high-spatial resolution results that quantify the distribution of otherwise unfindable trace metals.

Acknowledgment

We thank Brian McNulty for comments to an early draft that improved this contribution.

References cited

Bonnet, J., Mosser-Ruck, R., Caumon, M-C., Rouer, O., Andre-Myer, A-S., Cauzid, J., and Peiffert, C., 2016. Trace element distribution (Cu, Ga, Ge, Cd, and Fe) in sphalerite from the Tennessee MVT deposits, USA, by combined EMPA, LA-ICP-MS, Raman spectroscopy, and crystallography. The Canadian Mineralogist, 54, 1261-1284. <https://doi.org/10.3749/canmin.1500104>

Colpron, M., 2020. Yukon terranes-A digital atlas of terranes for the northern Cordillera. Yukon Geological Survey. <https://data.geology.gov.yk.ca/Compilation/2#InfoTab>

Freeze, A.C., 1966. On the origin of the Sullivan orebody, Kimberley, BC. British Columbia Geological Survey, Property File 680182, 194 p.

Graham, A.C., and Ootes, L., 2025. Geochemical analyses of SEDEX deposits in eastern British Columbia. British Columbia Ministry of Mining and Critical Minerals, British Columbia Geological Survey GeoFile 2025-13, 9 p.

Graham, A.C., Wearmouth, C.D., Northcote, B., and Ootes, L., 2025. A preliminary assessment of critical companion elements in SEDEX deposits of eastern British Columbia: Examples from the historic Sullivan mine and the Cirque project. In: Geological Fieldwork 2024, British Columbia Ministry of Mining and Critical Minerals, British Columbia Geological Survey Paper 2025-01, pp. 141-152.

Holley, E.A., Hadden, K.M., Hammerling, D., Eggert, R., Spiller, D.E., and Nelson, P.P., 2025. By-product recovery from US metal mines could reduce import reliance for critical minerals, Science, 389, 1325-1331. <https://doi.org/10.1126/science.adw8997>

Hickin, A.S., Ootes, L., Orovan, E.A., Brzozowski, M.J., Northcote, B.K., Rukhlov, A.S., and Bain, W.M., 2024. Critical minerals and mineral systems in British Columbia. In: Geological Fieldwork 2023, British Columbia Ministry of Energy, Mines and Low Carbon Innovation, British Columbia Geological Survey Paper 2024-01, pp. 13-51.

Moëlo, Y., Makovicky, E., Mozgova, N.N., Jambor, J.L., Cook, N., Pring, A., Paar, W., Nickel, E.H., Graeser, S., Karup-Møller, S., Balic-Žunic, T., Mumme, W.G., Vurro, F., Topa, D., Bindi, L., Bente, K., and Shimizu, M., 2008. Sulfosalt systematics: a review. Report of the sulfosalt sub-committee of the IMA Commission on Ore Mineralogy. European Journal of Mineralogy, 20, 7-46. <https://doi.org/10.1127/0935-1221/2008/0020-1778>

Piercey, S.J., Pietruszka, D., and Goudie, D., 2025. Critical metals in volcanogenic massive sulphide (VMS) deposits in British Columbia: A progress report. In: Geological Fieldwork 2024, British Columbia Ministry of Mining and Critical Minerals, British Columbia Geological Survey Paper 2025-01, pp. 189-201.

Rukhlov, A.S., Coats, B., Van der Vlugt, J., Beaupre-Olsen, I.J., and Zaborniak, K., 2023. British Columbia Geological Survey sample archive: An emerging resource for public geoscience. In: Geological Fieldwork 2022, British Columbia Ministry of Energy, Mines and Low Carbon Innovation, British Columbia Geological Survey Paper 2023-1, pp. 85-90.

Wei, C., Pietruszka, D.K., Piercey, S.J., Aylward, W., Kommescher, S., Scanlan, E., and Layton-Matthews, D., 2026. Critical metal distributions in volcanogenic massive sulphide (VMS) deposits in British Columbia: A progress report. In: Geological Fieldwork 2025, British Columbia Ministry of Mining and Critical Minerals, British Columbia Geological Survey Paper 2026-01, pp. 53-67.

Critical metal distributions in volcanogenic massive sulphide (VMS) deposits in British Columbia: A progress report

Chen Wei[1], Dorota K. Pietruszka[1], Stephen J. Piercey[1], Wanda Aylward[2], Sebastian Kommescher[2], Emma Scanlan[3], and Daniel Layton-Matthews[3]

[1] Department of Earth Sciences, Memorial University of Newfoundland, 9 Arctic Avenue, St. John's, NL, A1B 1N3
[2] Core Research Equipment and Instrument Training (CREAIT) Network, Memorial University of Newfoundland, 230 Elizabeth Avenue, St. John's, NL, A1C 5S7
[3] Department of Geological Sciences and Geological Engineering, Queen's University, Kingston, ON, K7L 3N6
[a] corresponding author: c.wei@mun.ca

Recommended citation: Wei, C., Pietruszka, D.K., Piercey, S.J., Aylward, W., Kommescher, S., Scanlan, E., and Layton-Matthews, D., 2026. Critical metal distributions in volcanogenic massive sulphide (VMS) deposits in British Columbia: A progress report. In: Geological Fieldwork 2025, British Columbia Ministry of Mining and Critical Minerals, British Columbia Geological Survey Paper 2026-01, pp. 53-67.

Abstract

Quantitative analysis of major and minor elements using electron probe microanalyzer (EPMA) and determination of trace elements using laser ablation-inductively coupled plasma-mass spectrometry (LA-ICP-MS) of samples from the Granduc, Anyox/Hidden Creek, and Goldstream volcanogenic massive sulphide deposits reveal critical metal distributions and elemental partitioning behaviors between various mineral phases. Most of the critical metals, such as Co, are hosted in multiple mineral phases with highly variable concentrations. Cobalt enrichment follows the sequence: $Co_{cobaltite}$>$Co_{willyamite}$>Co_{pyrite}>$Co_{pyrrhotite}$>$Co_{sphalerite}$> $Co_{magnetite}$. LA-ICP-MS imaging shows that individual mineral phases can simultaneously accommodate several critical metals. For the magnetite-pyrrhotite-chalcopyrite assemblage: magnetite is enriched in Mg, Al, V, Mn, and Ga; pyrrhotite preferentially hosts Co and Ni; and chalcopyrite concentrates Zn, Se, In, Ag, and Cd. In addition, trace elements in sphalerite, particularly critical metals Co, Ga, In, and Sn, display remarkable variations across the VMS deposits studied. These differences appear to be mainly controlled by geological setting and ore-forming processes, with limited influence from variations in inferred hydrothermal fluid temperature and sulphur fugacity (fS_2) The next phase of work will include developing quantitative models for critical metal deportment, demonstrating how systematic regularities in the partitioning of specific critical metals among coexisting minerals can be used to predict their mineralogical distribution in VMS systems.

Keywords: Volcanogenic massive sulphide, critical metal abundance, elemental partitioning behavior, electron probe, LA-ICP-MS

1. Introduction

The low-carbon, green energy transition is driving unprecedented demand for critical metals, such as copper (Cu), cobalt (Co), and nickel (Ni), which are vital for technologies such as electric vehicles, batteries, and wind turbines (e.g., Jowitt et al., 2018; Reich and Simon, 2024). Volcanogenic massive sulphide (VMS) deposits are important Canadian and global suppliers of base and precious metals, including Cu, Zn, Pb, Au, and Ag (e.g., Franklin et al., 2005; Galley et al., 2007; Piercey, 2011; Hannington, 2013) and can also be economically significant sources of metals such as Co, Ga, Se, Cd, In, Sn, Sb, Tl, and Bi (e.g., Layton-Matthews et al., 2008; Monecke et al., 2016; Piercey et al., 2025).

The VMS deposits in British Columbia represent an important past and potentially future economic contributor to the provincial mining sector (e.g., Hickin et al., 2024). Recent work has shown that VMS deposits in British Columbia contain a variety of critical metals currently on the national critical minerals list (NRCan, 2024), such as Co, In, Sn, Sb, Te, and Bi (e.g., Piercey et al., 2025; Cawood et al., 2025). Although many of these commodities are present as trace elements within mineral phases, their absolute abundance, distribution, and mineral-scale partitioning are not well resolved.

In-situ microanalytical techniques such as electron probe microanalyzer (EPMA) and laser ablation-inductively coupled plasma-mass spectrometry (LA-ICP-MS) provide micron-scale spatial resolution for mineral chemistry. EPMA has high spatial resolution (down to 1 μm) but is constrained by relatively high detection limits (commonly >100 ppm), limiting its utility for accurately measuring many elements at trace levels (Zhao et al., 2015). In contrast, LA-ICP-MS allows for the simultaneous analysis and characterization of multiple elements within a single mineral grain down to sub-ppm levels (e.g., Sylvester, 2006; Cook et al., 2016; Danyushevsky and Thompson, 2025).

Together, EPMA and LA-ICP-MS provide complementary constraints on mineral chemistry. This paper establishes an integrated analytical approach to evaluate critical element distributions and partitioning between different mineral phases in British Columbia VMS deposits. Here, we summarize progress and present representative examples of quantitative EPMA analysis of major and minor elements and LA-ICP-MS spot and mapping analyses of trace elements in mineral phases

from the Granduc, Anyox/Hidden Creek, and Goldstream mafic-siliciclastic (or Besshi) VMS deposits (Fig. 1). These results are used to: 1) evaluate critical-metal distributions across different mineral assemblages using Co as a case study; 2) investigate elemental partitioning among coexisting, spatially associated minerals; and 3) use sphalerite as an example to evaluate the trace element distributions and the factors controlling their variations. The full results of our analytical work can be found in a supplementary publication (Pietruszka et al., 2026).

2. Samples and mineralogy

Samples used in this study were previously reported by Piercey et al. (2025). These samples were obtained from the archives of the British Columbia Geological Survey and the Mineral Deposit Research Unit at the University of British Columbia. Here, we focus on three mafic-siliciclastic VMS deposits: Goldstream (n=2), Anyox (Hidden Creek) (n=3), and Granduc (n=4). Past producers and resources of Cu, these deposits contain byproduct critical metals, including Co (e.g., Peter and Scott, 1999).

The samples were analyzed by bulk assays (see Piercey et al., 2025 for details), and most were subjected to detailed mineral chemical investigations. The main ore and gangue mineral assemblages for the studied samples in these three deposits are summarized in Table 1. Overall, the three deposits share broadly similar major mineral phases, but differ in their minor and trace mineral phases. Specifically, the mineral assemblage from the Anyox (Hidden Creek) deposit consists of pyrite, pyrrhotite, chalcopyrite, and minor sphalerite and hematite (Table 1; Figs. 2a-b). Associated gangue minerals are amphibole, chlorite, quartz, plagioclase, and calcite, and minor apatite and dolomite. The predominant sulphide phases in the Goldstream deposit are pyrrhotite, chalcopyrite, and minor sphalerite, with minor galena (Table 1; Figs. 2e-f). The gangue minerals include amphibole, chlorite, quartz, calcite, muscovite, biotite, and minor plagioclase and apatite. The Granduc deposit has a more complex mineral assemblage, including magnetite, pyrite, pyrrhotite, chalcopyrite, and minor sphalerite, galena, cobaltite, and willyamite, with trace molybdenite (Table 1; Figs. 2c-d). The gangue minerals are predominantly amphibole, chlorite, quartz, calcite, epidote, muscovite, apatite, and minor dolomite.

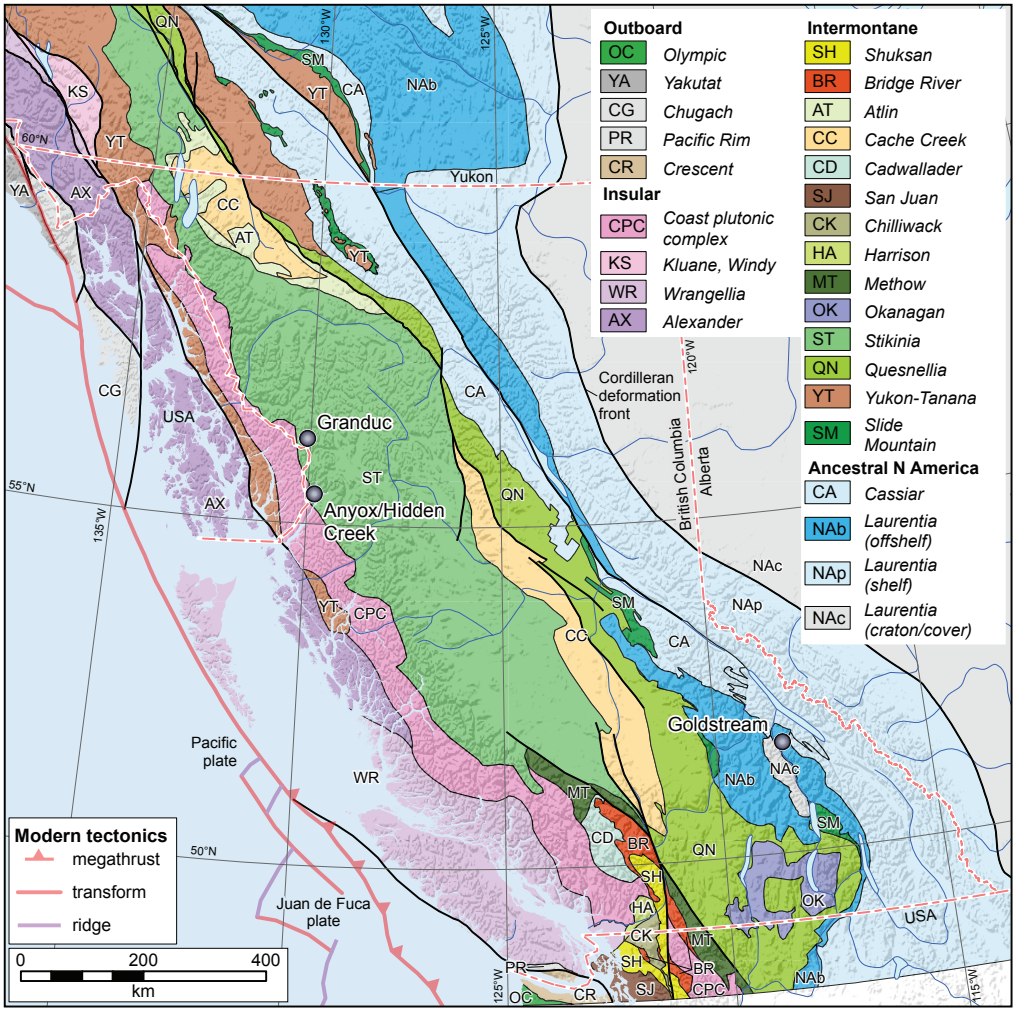


Fig. 1. Location of volcanogenic massive sulphide deposits sampled for this study. Terrane boundaries after Colpron (2020).

Table 1. Summary of mineral phases identified in selected samples from the Granduc, Anyox/Hidden Creek, and Goldstream deposits.

Deposits	Sample ID	Oxides			Sulphides								Main gangue mineral association												Accessory minerals
		Mt	Hem	Ilm	Cob	Wly	Py	Po	Ccp	Sph	Mo	Gn	Px	Chl	Qz	Am	Cal	Ep	Sd	Msc	Bt	Ap	Dol	Pl	Ilt	
Anyox	An-1		xx				xxx	xxx	xxx	xx				xx	x	xxx	xxx					x	x			Talc, Tit, Mrc
	Anyox-1-1						xxx	xx	xx	x				x	xxx		xxx	x		x				xx		Tit, Grh
	Anyox-2						xxx	xxx	xxx	x		x		x		x	xxx					x	x			
Goldstream	HW-2v						x	xxx	xxx	x			x	xxx	xxx	x	xxx	x		xxx	xxx	xxx		xx	xx	Tit, Rut, All
	TS2302						x	xxx	xxx	xxx		x	x	xx	xxx	x	xxx	x	x	xxx	x	x			x	Tit, All
Granduc	GD-9	xxx			x	x		xxx	xxx	x	x	x	xx	xx	xxx	xxx	xxx	xxx	x	xx		xx				Tit, All
	GD-9-02	xxx			x	x		xxx	xxx	x	x	x	x	xxx	xxx	xxx	xxx	xxx	x	x			x			Tit, All
	GR01-112	xxx		x			xxx	xxx	xxx	xx			xx	xxx	xxx	xxx	xxx	xx		xxx		xxx	x			Tit, All
	GRANDUC	xxx			x		x		xxx	xx	x		x	x	x	xxx	x		x	x		xx				

Note: Mineral phases were identified using MLA and verified by SEM and optical microscopy. The Fe-oxides and sulphides are considered reliable, and all major phases are included. Some gangue minerals, particularly silicates, may be present but were not accurately quantified.

x=trace (<1 wt.%); xx=minor (1-5 wt.%); xxx=major (>5 wt.%). Mineral abbreviations: All-allanite; Am-Amphibole; Ap-Apatite; Bt-Biotite; Cal-Calcite; Ccp-Chalcopyrite; Chl-Chlorite; Cth-Clausthalite; Cob-Cobaltite; Dol-Dolomite; Ep-Epidote; Gn-Galena; Graphite-Grh; Hem-Hematite; Ilt-Illite; Ilm-Ilmenite; Marcasite-Mrc; Mt-Magnetite; Mo-Molybdenite; Msc-Muscovite; Pl-Plagioclase; Py-Pyrite; Px-Pyroxene; Po-Pyrrhotite; Qtz-Quartz; Rut-Rutile; Sd-Siderite; Sp-Sphalerite; Tit-Titanite; Wly-Willyamite.

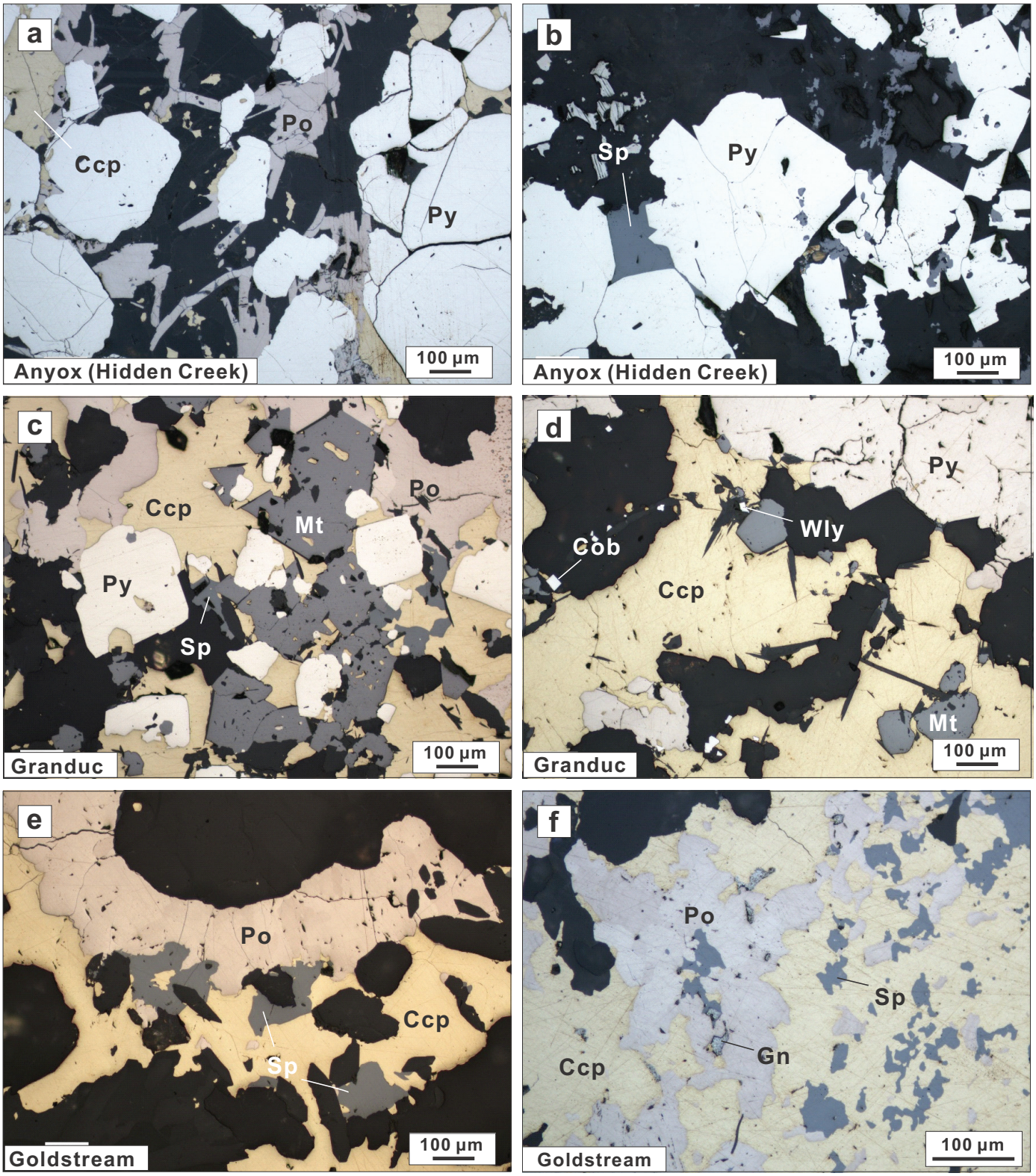


Fig. 2. Reflected light photomicrographs of samples from the Anyox/Hidden Creek, Granduc, and Goldstream deposits. **a)** Pyrrhotite and chalcopyrite along the margins of euhedral pyrite, infilling interstitial voids. **b)** Sphalerite fills vugs within euhedral pyrite crystals. **c)** Euhedral magnetite and pyrite overgrown or enclosed by later-formed chalcopyrite and pyrrhotite. **d)** Fine-grained euhedral willyamite and cobaltite in vugs of chalcopyrite. **e)** Typical association of pyrrhotite, chalcopyrite, and sphalerite. **f)** Pyrrhotite partially replaced by chalcopyrite, which also hosts minor interstitial sphalerite. Abbreviations: Ccp-Chalcopyrite; Cob-Cobaltite; Gn-Galena; Mt-Magnetite; Py-Pyrite; Po-Pyrrhotite; Sp-Sphalerite; Wly-Willyamite.

Given that ore minerals likely host most of the critical elements, we analyzed sulphide minerals, including pyrite, pyrrhotite, chalcopyrite, sphalerite, locally cobaltite, and willyamite, together with coexisting Fe-oxides such as magnetite, across different mineral assemblages (Pietruszka et al., 2026).

3. Analytical methods

Mineral chemistry of these mineral phases was quantified by EPMA and LA-ICP-MS. EPMA was used for phase identification and to provide major- and minor-element data. LA-ICP-MS mapping was used to evaluate grain-scale spatial variability and to constrain elemental partitioning among coexisting phases, whereas LA-ICP-MS spot analyses were used to quantify trace-element concentrations.

3.1. Electron probe microanalysis

The chemical compositions of sulphides and Fe-oxides were determined at the Hibernia Electron Beam Facility at the Core Research Equipment and Instrument Training (CREAIT) Network in the Department of Earth Sciences, Memorial University of Newfoundland. We used a JEOL JXA-8230 SuperProbe EPMA equipped with five wavelength-dispersive spectrometers (WDS) and a tungsten filament electron gun. The analyses were performed using an accelerating voltage of 20 kV, a 20-nA beam current, and the beam focused to 1 µm. Elemental counting times ranged from 5 to 30 s, including 5 to 15 s for background measurements and 10 to 30 s on peak signals for calibration. The full list of analyzed elements for each mineral, together with primary and interference standards, is provided in Pietruszka et al. (2026). Both natural and synthetic standards were used to calibrate the instrument. Additional secondary standards were measured periodically (i.e., for each mineral phase at the start of each run, after 20-25 unknown analyses, and at the end of each run) to demonstrate their reproducibility. Sulphide analyses with totals falling outside the 100 ±2 wt.% range were rejected.

3.2. LA-ICP-MS elemental imaging

LA-ICP-MS elemental maps were carried out by an ESI-NWR 193 nm ArF Eximer laser ablation system coupled with iCAP TQs ICP-MS (Thermo Scientific) at the Queen's Facility for Isotope Research, Queen's University. Element compositional maps were constructed by scanning the target area with a series of parallel laser lines. The ablation was performed at a fluence of 3 J/cm^2 with a constant pulse frequency of 10 Hz. The laser operated with a beam diameter ranging from 5 to 10 µm and a scan speed between 2.5 and 5 µm/s. At the beginning of each raster, a 5-second background measurement was recorded, and a 30-second delay was applied after each line to allow for cell wash-out.

The following isotopes were monitored: ^{23}Na, ^{24}Mg, ^{27}Al, ^{29}Si, ^{32}S, ^{44}Ca, ^{47}Ti, ^{51}V, ^{52}Cr, ^{55}Mn, ^{57}Fe, ^{59}Co, ^{60}Ni, ^{65}Cu, ^{66}Zn, ^{69}Ga, ^{71}Ga, ^{72}Ge, ^{74}Ge, ^{75}As, ^{77}Se, ^{90}Zr, ^{93}Nb, ^{95}Mo, ^{107}Ag, ^{109}Ag, ^{111}Cd, ^{113}In, ^{115}In, ^{118}Sn, ^{121}Sb, ^{125}Te, ^{133}Cs, ^{137}Ba, ^{157}Gd, ^{178}Hf, ^{181}Ta, ^{182}W, ^{185}Re, ^{197}Au, ^{202}Hg, ^{205}Tl, ^{206}Pb, ^{207}Pb, ^{208}Pb, ^{209}Bi, ^{232}Th, and ^{238}U. Two isotopes each for Ag, Ga, Ge, and In were included in the element suite to monitor potential interferences. Rasters were done on reference materials STDGL3 (Belousov et al., 2023), MASS-1 (Wilson et al., 2002), and GSE-1G (Jochum et al., 2005) at the start and end of a mapping run to correct for instrumental drift. Images were compiled and processed using Iolite 4 (Paton et al., 2011). Unlike the quantitative data, element maps cannot be corrected for potential interference for Ga, Ge, and In isotopes. All LA-ICP-MS maps were produced for each element using the same logarithmic colour scale.

3.3. LA-ICP-MS spot analysis

Spot analysis of minor and trace elements in sulphides was performed by LA-ICP-MS using a GeoLasPro 193 nm ArF Excimer laser ablation system (Coherent) coupled to an Element XR HR-ICP-MS instrument (Thermo Scientific) at the Microanalysis Facility at the Core Research and Equipment Training (CREAIT) Network, Memorial University of Newfoundland. Laser ablation was carried out in a pure He atmosphere, with the aerosol mixed with Ar before entering the ICP torch. Spot ablation was carried out using a 30 µm spot size, with an energy density of 5 J/cm^2 and a pulse frequency of 5 Hz. Each analysis consisted of 30 s background acquisition, followed by 40 s ablation, and 30 s washout. Washout time was increased after, for example, high-Pb abundance phases such as galena were analyzed. The ICP-MS was tuned for high sensitivity while maintaining a ThO/Th ratio of $<0.3\%$; all analyses were performed in low-resolution mode. The following isotopes were monitored: ^{24}Mg, ^{27}Al, ^{29}Si, ^{34}S, ^{43}Ca, ^{49}Ti, ^{232}Th, and ^{238}U (dwell time 5 ms); ^{51}V, ^{53}Cr, ^{90}Zr, ^{93}Nb, ^{157}Gd, ^{178}Hf, and ^{181}Ta (dwell time 10 ms); ^{55}Mn, ^{57}Fe, ^{59}Co, ^{60}Ni, ^{65}Cu, ^{66}Zn, ^{69}Ga,^{71}Ga, ^{72}Ge, ^{74}Ge, ^{75}As, ^{77}Se, ^{95}Mo,^{107}Ag, ^{109}Ag, ^{111}Cd, ^{113}In,^{115}In, ^{118}Sn, ^{121}Sb, ^{125}Te, ^{182}W, ^{185}Re, ^{197}Au, ^{202}Hg, ^{205}Tl, ^{206}Pb, ^{207}Pb, ^{208}Pb, and ^{209}Bi (dwell time 20 ms). Reference materials MASS-1 (Wilson et al., 2002) and NIST SRM 610 (Jochum et al., 2011) were used for external calibration. MASS-1 was used for chalcophile and siderophile elements, and NIST SRM610 for lithophile elements. Duplicate analyses of both reference materials were performed at the start of the session and after every 10 to 16 sample analyses to monitor instrument stability and data quality.

Data reduction was done using the LADR software package (Norris and Danyushevsky, 2018). Quantification in both instances was performed using ^{57}Fe as the internal standard for Fe-bearing sulphides including pyrite, pyrrhotite, chalcopyrite, sphalerite, tennantite-tetrahedrite, with all concentrations normalized to 100 wt.%. Significant elemental fractionations relative to Fe were corrected following the method of Danyushevsky et al. (2011). The contents of S and O were estimated based on mono-sulphide and oxide stoichiometry. Isobaric interferences of ^{74}Se on ^{74}Ge, ^{113}Cd on ^{113}In, and ^{115}Sn on ^{115}In were corrected using known isotopic proportions of Cd, Sn, and Se. Interferences of ZrO and NbO on Ag were found to be insignificant due to the low contents of Zr and Nb in the samples.

4. Results

Below, we summarize representative mineral compositions and trace-element distributions among coexisting phases. We first present EPMA data using Co as an example, then present a representative LA-ICP-MS map that illustrates element partitioning, and finally show LA-ICP-MS sphalerite chemistry across the three deposits.

4.1. EPMA mineral compositions

Cobalt concentrations determined by EPMA are reported here for minerals in which Co is detectable. Concentrations vary widely among different minerals, ranging from per cent levels in discrete Co-bearing phases to ppm levels in common sulphides and Fe-oxides (Table 2). Common sulphides such as pyrite, pyrrhotite, sphalerite, and chalcopyrite within the VMS deposits contain minor to trace Co (Fig. 3). In addition to these sulphides, discrete Co-bearing minerals, including cobaltite and willyamite, have been identified in the Granduc deposit (Fig. 2d). Magnetite also hosts trace amounts of Co. Cobaltite and willyamite have the highest Co concentrations, with cobaltite containing 16.9-32.8 wt.% (mean $\pm 2\sigma$: 27.6 ±7.8 wt.%) and willyamite ranging from 14.9-25.5 wt.% (22.7 ±6.0 wt.%). The higher average Co content in cobaltite compared to willyamite indicates a $Co_{Cobaltite} > Co_{willyamite}$ enrichment trend among discrete Co-bearing minerals.

For common sulphide phases, comparisons of Co among these phases are made using the geometric mean, which better represents the central tendency for skewed (≈log-normal) data than the arithmetic mean, given the high variability of Co within individual phases (cf., Wei et al., 2024). Among the major sulphide phases, pyrite is the most Co-rich mineral where present, with the concentrations reaching up to 2.26 wt.% (Table 2). The second Co-rich mineral is pyrrhotite (Fig. 3), which typically contains Co in the range of <0.01 to 0.23 wt.% (Table 2). In sphalerite, more than two-thirds of the analytical spots for all studied deposits are above the detection limits, with the concentrations from <0.01 to 0.14 wt.% (Table 2). Cobalt was only detected in about half (or fewer) of the chalcopyrite analytical spots. Where present, concentrations are generally lower than in sphalerite for Granduc and Goldstream, ranging from <0.01 to 0.05 wt.%. Surprisingly, a spot in chalcopyrite from Granduc has up to 1.56 wt.% Co (Table 2). In addition, magnetite from Granduc generally contains detectable Co, with concentrations from <0.01 to 0.11 wt.% (Table 2).

4.2. LA-ICP-MS elemental mapping

LA-ICP-MS mapping of a magnetite-pyrrhotite-chalcopyrite assemblage from Granduc reveals distinct mineral preferences for certain trace elements (Fig. 4). Magnesium, Al, V, Mn, and Ga are concentrated in magnetite, whereas Co and Ni, and Se are mainly enriched in pyrrhotite. Zinc, Ag, In, Se, and possibly Cd and Te are preferentially enriched in chalcopyrite. Chalcopyrite contains trace amounts of Co and Ni, although their concentrations are lower than those observed in pyrrhotite. The distributions of trace elements such as Mg, Al, Ni, Zn, and possibly Co within the individual mineral phase show considerable heterogeneity. In chalcopyrite, speckled textures marked by patchy enrichment of Co, Ni, and Zn are observed. In magnetite, intersecting stripe-like fabrics enriched in Mg and Al are also present. In addition, grain boundaries of these minerals (possibly galena) show low levels of Sb and Pb.

4.3. LA-ICP-MS trace-element chemistry

In sphalerite, LA-ICP-MS ablation profiles were generally flat and smooth (Fig. 5), suggesting internally consistent concentrations within individual spots; however, element concentrations show considerable variation across spots (Table 3; Fig. 6). The full dataset of minor and trace elements of sphalerite is summarized in Table 3 and can be found in Pietruszka et al. (2026).

Iron is the most common lattice-bound element in sphalerite, typically ranging from 8-12 wt.%. Manganese, Cu, and Cd are also incorporated into the sphalerite lattice, generally at hundreds to tens of thousands of ppm. Trace elements, including Co, Se, Ag, and In, are commonly present at tens to hundreds of ppm. Most of these elements are not unexpected because they are interpreted to substitute for Zn in the sphalerite lattice, either directly or through coupled substitution (e.g., Cook et al., 2009; Ye et al., 2011). Trace elements such as Sn, Sb, and Te occur at around or below 10 ppm, but are detected in more than two-thirds of the analyses. In addition, As, Ge, Ni, Tl, and Bi were predominantly at or below detection limits (Pietruszka et al., 2026).

From a comparison of the three deposits, sphalerite from Anyox is systematically enriched in most trace elements, including Cu (186-9542 ppm; mean=1534 ppm), Ga (9.15-37.4 ppm; mean=17.0 ppm), Ag (7.95-77.5 ppm; mean=23.7 ppm), Cd (3799-5473 ppm; mean=4516 ppm), In (85.8-251 ppm; mean=140 ppm), and Sn (0.79-14.7 ppm; mean=3.39 ppm). In contrast, Goldstream sphalerite has the highest Mn (5839-9957 ppm; mean=7901 ppm) and Te (0.04-6.36 ppm; mean=0.39 ppm), whereas Granduc sphalerite contains the greatest Fe (8.29-17.6 wt.%; mean=10.5 wt.%) and Co (500-1074 ppm; mean=839 ppm). Goldstream sphalerite also exhibits the lowest Cu (17.9-1987 ppm; mean=224 ppm), Ag (0.97-12.8 ppm; mean=4.59 ppm), In (0.33-1.05 ppm; mean=0.57 ppm), and possibly Cd (2453-3879 ppm; mean=3048 ppm). In comparison, Granduc sphalerite exhibits the lowest Ga (<0.07-0.43 ppm) and Sn (<0.21-1.19 ppm), whereas all spots for Co in Anyox sphalerite are below detection limits. In addition, Se concentrations are broadly similar in Goldstream and Granduc sphalerite, whereas Anyox shows a wider range but a lower mean Se content (Fig. 6).

5. Interpretations and discussion

Below, we examine the critical metal distributions among different mineral phases, consider element partitioning among coexisting phases, and evaluate the controls on trace-element variations.

Table 2. Summary of cobalt concentrations in mineral phases determined by EPMA from the Granduc, Anyox/Hidden Creek, and Goldstream deposits.

Deposits	Samples	Statistical Parameter	Cobaltite	Willyamite	Magnetite	Pyrite	Pyrrhotite	Chalcopyrite	Sphalerite
Anyox/Hidden Creek (n = 3)	AN-1	m				15	12	16	9
		% of #DL				47%	92%	63%	67%
		Max				0.06	0.07	0.05	0.05
		Median				0.01	0.03	0.02	0.02
		Mean				0.02	0.03	0.02	0.02
		Min				<0.01	<0.01	<0.01	<0.01
	ANYOX-2	m				11	9	8	
		% of #DL				100%	89%	38%	
		Max				0.45	0.10	0.05	
		Median				0.23	0.04	0.01	
		Mean				0.18	0.04	0.02	
		Min				0.03	<0.01	<0.01	
	ANYOX-1-1	m				19	3	13	5
		% of #DL				42%	67%	62%	0%
		Max				0.04	0.03	0.05	<0.01
		Median				0.01	0.01	0.02	
		Mean				0.02	0.02	0.02	
		Min				<0.01	<0.01	<0.01	
Goldstream (n=2)	HW-2v	m					12	9	1
		% of #DL					92%	44%	0%
		Max					0.08	0.05	<0.01
		Median					0.05	0.01	
		Mean					0.04	0.02	
		Min					<0.01	<0.01	
	TS2303-02	m					6	13	8
		% of #DL					50%	38%	75%
		Max					0.06	0.03	0.05
		Median					0.02	0.01	0.02
		Mean					0.02	0.01	0.02
		Min					<0.01	<0.01	<0.01
Granduc (n= 4)	GR01-112	m	1		23	9	10	18	11
		% of #DL	100%		91%	82%	100%	56%	100%
		Max	16.9		0.11	2.26	0.23	0.05	0.14
		Median			0.05	0.86	0.19	0.02	0.10
		Mean			0.05	0.67	0.19	0.02	0.10
		Min			<0.01	0.16	0.14	<0.01	0.05
	Granduc	m	21		9	2	8	14	3
		% of #DL	100%		78%	100%	100%	36%	100%
		Max	30.0		0.06	0.17	0.16	1.56	0.10
		Median	27.7		0.02	0.13	0.13	0.01	0.08
		Mean	26.4		0.03	0.13	0.12	0.02	0.07
		Min	18.8		<0.01	0.10	0.09	<0.01	0.04
	GD-09	m	12	15	12		7	8	
		% of #DL	100%	100%	67%		100%	50%	
		Max	32.8	25.5	0.05		0.22	0.05	
		Median	31.2	24.2	0.03		0.17	0.02	
		Mean	31.0	22.7	0.03		0.17	0.02	
		Min	29.0	14.9	<0.01		0.14	<0.01	
	GD-09-2	m			20			8	
		% of #DL			100%			63%	
		Max			0.10			0.05	
		Median			0.07			0.03	
		Mean			0.06			0.02	
		Min			0.01			<0.01	

n, the numbers of analyzed samples. Mean, geometric mean; m, the number of measurements; % of #DL**,** the percentage of analyzed values above the detection limit. If <50% of data were below the detection limit, those values were set to the detection limit for the calculations of the medians and means (cf., van den Boogaart and Tolosana-Delgado, 2013).

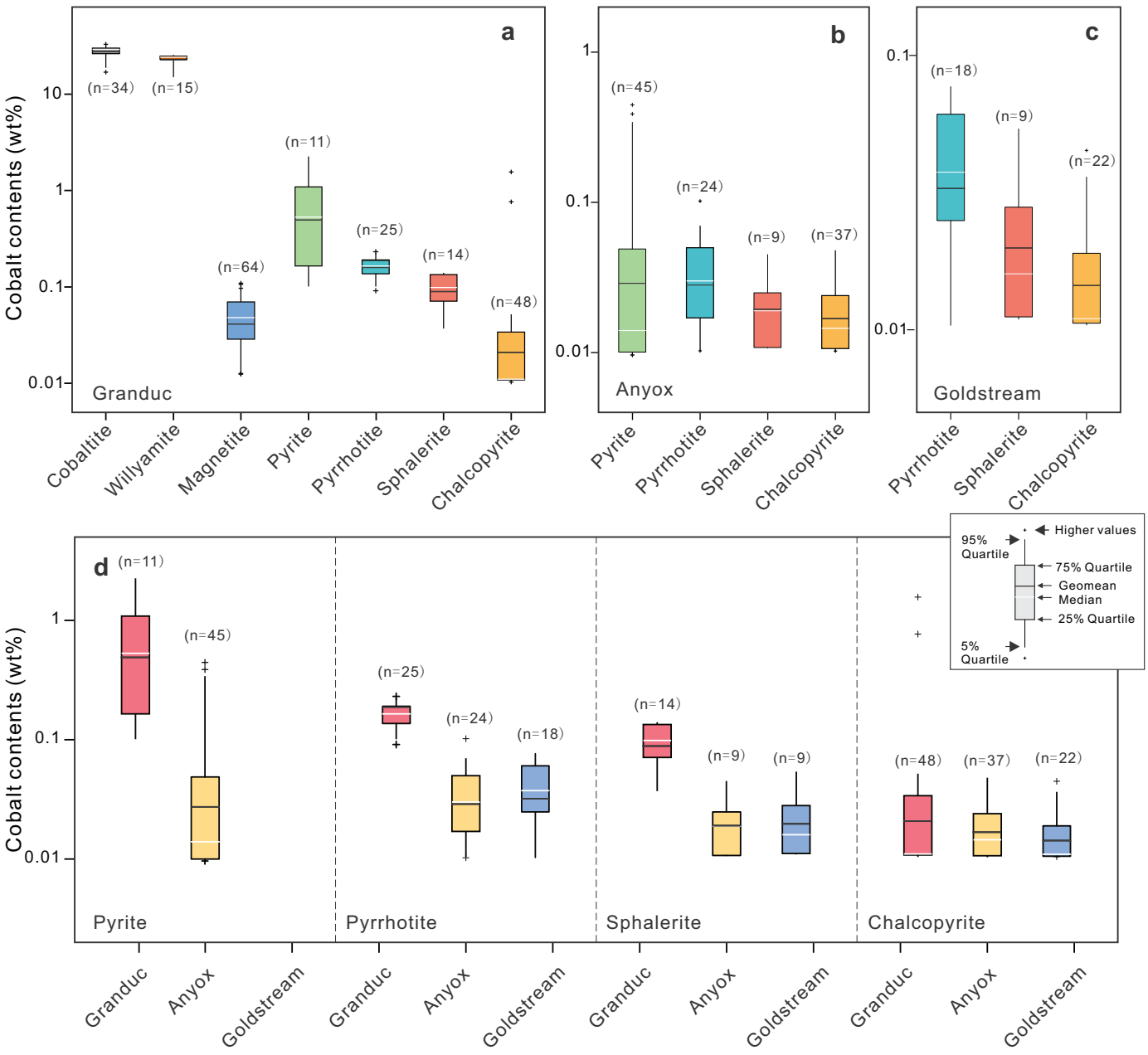


Fig. 3. Box-and-whisker plots displaying Co concentrations in different mineral phases. **a)** Granduc deposit. **b)** Anyox/Hidden Creek deposit. **c)** Goldstream deposit. **d)** Co concentrations in common sulphide minerals across all three deposits. Data below the detection limits are replaced by their detection limits included in the plots.

5.1. Critical-metal distribution among mineral phases

Bulk rock assays demonstrated that mafic-siliciclastic VMS deposits in British Columbia contain higher levels of Co, Cu, In, Mn, Se, Sn, and Te relative to felsic-hosted deposits (Piercey et al., 2025). However, the specific minerals bearing these critical metals remain unclear because most are present only as minor or trace components within mineral phases (Piercey et al., 2025), except for the primary commodities of Cu and Zn. We use the distribution of Co as an illustrative example.

Cobalt concentrations determined by EPMA are used here for comparison because Co in the most Co-bearing minerals previously recognized is well above the EPMA detection limits (Table 2) and the fine grain size of some Co-bearing minerals precludes reliable LA-ICP-MS spot analyses due to signal mixing with adjacent phases. Overall, for each mineral phase, Co concentrations vary significantly among the three deposits (Fig. 3). This deposit-level pattern is similar across all analyzed sulphides: Granduc has the highest Co concentrations in pyrite, pyrrhotite, and sphalerite, followed by Goldstream and Anyox. In chalcopyrite, however, Co concentrations do not show the same systematic difference between Goldstream and Anyox (Fig. 3d).

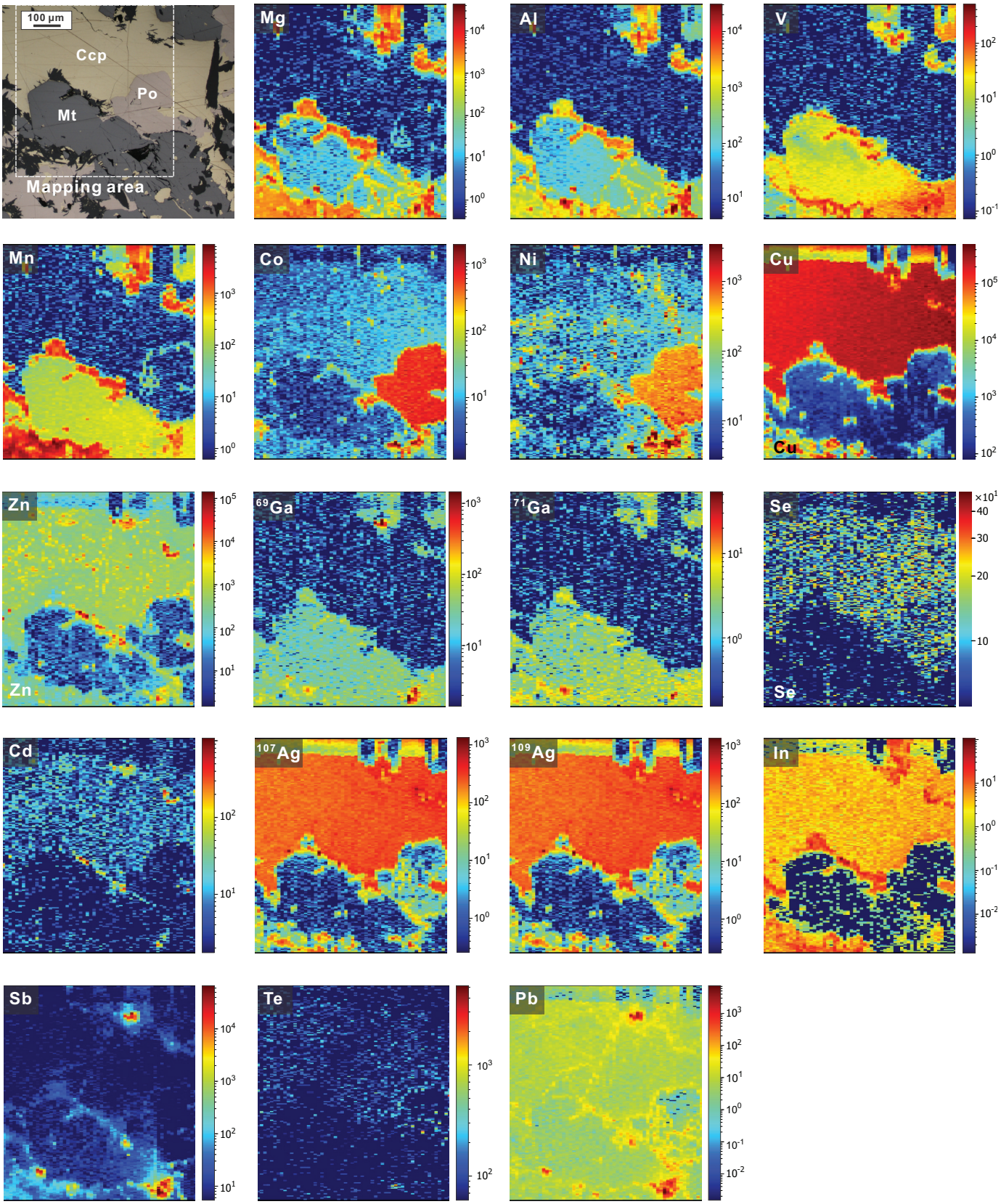


Fig. 4. LA-ICP-MS element maps of the magnetite-pyrrhotite-chalcopyrite assemblage; top left is a reflected light image. Elemental maps illustrate mineral-specific enrichment and partitioning among magnetite, pyrrhotite, and chalcopyrite. Scales in counts-per-second (cps). Sample from the Granduc deposit.

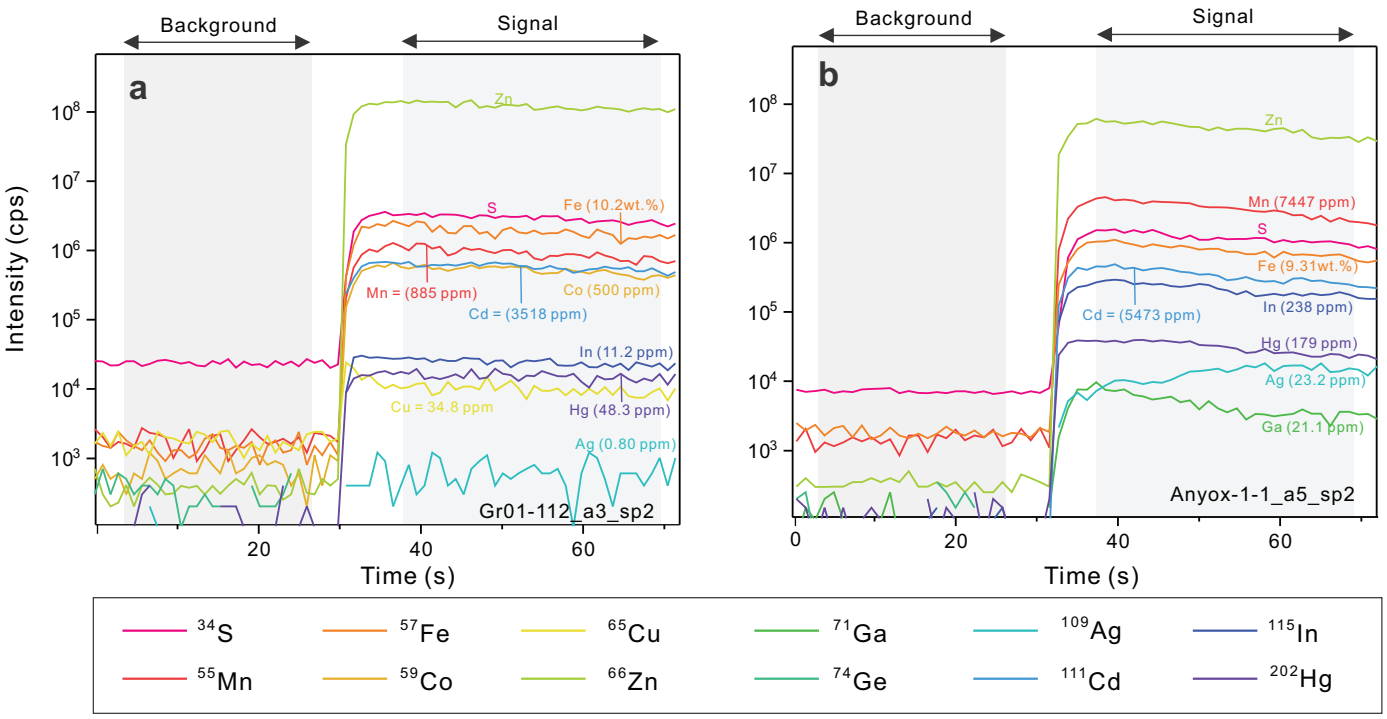


Fig. 5. Typical single-spot LA-ICP-MS spectra for selected elements in sphalerite. **a)** Time-resolved depth profile of Co-rich sphalerite from Granduc deposit. **b)** Smooth signals for all elements in In-rich sphalerite from Anyox/Hidden Creek deposit. Numbers in brackets are concentrations.

Despite these inter-deposit differences in absolute Co concentrations, the relative enrichment sequence among mineral phases is consistent across the studied samples: $Co_{cobaltite}$>$Co_{willyamite}$>Co_{pyrite}>$Co_{pyrrhotite}$>$Co_{sphalerite}$>$Co_{magnetite}$. This mineral-specific sequence is also broadly consistent across the different mineral assemblages examined (Fig. 3a), suggesting a consistent mineralogical control on Co partitioning across assemblage types. Similar Co partitioning among pyrite-pyrrhotite-sphalerite-magnetite associations has been reported in other types of deposits, including skarn Fe deposits and magmatic Fe-Ti oxide deposits (e.g., Liang et al., 2023; Zhang et al., 2025). However, Co in chalcopyrite commonly approaches EPMA detection limits, which rules out a quantitative assessment of Co partitioning between magnetite and chalcopyrite based on EPMA spot data alone. We further use LA-ICP-MS mapping in the following section to assess the relative Co enrichment between these two minerals in a textural context.

5.2. Partitioning and enrichment among coexisting phases

Except for Cu and Zn, most critical metals occur in trace levels in host minerals (e.g., Reich and Simon, 2024). The LA-ICP-MS element imaging technique enables visualizing the spatial distribution of elements of interest at scales from µm to cm, providing direct insight into how these metals are distributed and partitioned among various minerals (Chew et al., 2021). To quantify partitioning behaviors of critical metals, we use a sample with magnetite-pyrrhotite-chalcopyrite mineral assemblage to illustrate elemental partitioning behaviors and to evaluate the reliability of identifying Co-host phases through EPMA.

The partitioning of critical metals, such as Co, Ga, Ge, Se, In, Sb, Te, and Bi in base metal sulphides, seems to be relatively well-constrained (George et al., 2016; Xu et al., 2021; Wei et al., 2024; Cawood et al., 2025, and references therein). However, it remains unclear how these elements are partitioned between Fe-oxide and sulphide phases, especially because magnetite can host critical metals such as Co, Ga, and Ge (e.g., Dare et al., 2014; Nadoll et al., 2014; Zhang et al., 2025).

In the Granduc sample, the LA-ICP-MS maps show that the highest levels of Co and Ni are in pyrrhotite, followed by chalcopyrite, and the lowest in magnetite (Fig. 4). This suggests a partitioning trend for both elements: $Co_{pyrrhotite}$> $Co_{chalcopyrite}$>$Co_{magnetite}$ and $Ni_{pyrrhotite}$>$Ni_{chalcopyrite}$>$Ni_{magnetite}$. The pattern is consistent with our EPMA results for the relative enrichment of Co in pyrrhotite over magnetite. Similar trends for Co and Ni have also been reported for the ABM (Yukon) and Windy Craggy (British Columbia) VMS deposits, where pyrrhotite has higher Co and Ni concentrations than chalcopyrite (Denisová et al., 2024; Cawood et al., 2025).

Cobalt partitioning can differ among ore systems and some studies considered that magnetite is enriched in Co relative to chalcopyrite in Fe-skarns (e.g., Liang et al., 2023; Liu et al., 2024). For example, in the Galinge deposits of China, magnetite contains higher Co contents than coexisting chalcopyrite (~7 ppm vs. ~2 ppm; Liu et al., 2024). Such differences likely

Table 3. Summary of sphalerite chemistry as determined by LA-ICP-MS, and estimated crystallization temperatures and $\log_{10}(fS_2)$ values (arithmetic means ±2σ) from the Granduc, Anyox/Hidden Creek, and Goldstream deposits.

Deposits	Sample	Statistical Parameter	Mn (ppm)	Fe (wt.%)	Co (ppm)	Cu (ppm)	Zn (wt.%)	Ga (ppm)	Se (ppm)	Ag (ppm)	Cd (ppm)	In (ppm)	Sn (ppm)	Sb (ppm)	Te (ppm)	$T_{GGIMFis}$ (°C)	$2\sigma_{ext}$ (°C)	$\log_{10}(fS_2)$	$2\sigma_{ext}$ (fS_2)
Anyox (n=2)	An-1 (m=8)	% of #DL	100%	100%	0%	100%	100%	100%	100%	100%	100%	100%	100%	100%	63%				
		Max	4744	10.8	<0.66	9542	57.9	37.4	25.9	77.5	5155	142	12.8	35.3	0.48				
		Median	3834	9.35	-	2144	56.2	10.7	10.4	22.5	4233	111	2.13	10.5	0.13	354 ±8	±76	−8.6 ±0.3	±2.5
		Mean	3822	9.32	-	1707	56.0	14.1	11.7	25.2	4268	109	2.25	10.6	0.16				
		Min	3040	7.77	-	186	53.9	9.15	7.21	7.95	3799	85.8	0.79	3.04	<0.09				
	Anyox-1-1 (m=4)	% of #DL	100%	100%	0%	100%	100%	100%	100%	100%	100%	100%	100%	100%	75%				
		Max	7932	9.74	<0.67	3194	56.3	29.7	272	35.9	5473	251	14.7	17.1	0.74				
		Median	7520	9.40		1051	55.7	24.9	254	20.4	4988	231	8.03	13.2	0.49	354 ±7	±76	−8.6 ±0.3	±2.5
		Mean	7602	9.35		1238	55.7	24.7	257	21.0	5057	231	7.67	9.70	0.45				
		Min	7447	8.87		709	55.1	20.5	251	13.3	4806	212	3.71	3.14	<0.24				
Goldstream (n=1)	TS2303-02 (m=20)	% of #DL	100%	100%	100%	100%	100%	100%	100%	100%	100%	100%	95%	95%	80%				
		Max	9957	11.2	257	1987	57.6	11.6	126	12.8	3879	1.05	2.03	2.15	6.36				
		Median	7952	10.1	185	251	55.2	6.23	93.6	5.94	3057	0.63	0.61	0.69	0.47	340 ±4	±73	−9.2 ±0.2	±2.4
		Mean	7901	10.0	184	224	55.3	5.87	91.8	4.59	3048	0.57	0.74	0.52	0.39				
		Min	5839	8.13	129	17.9	53.8	2.88	54.2	0.97	2453	0.33	0.38	0.06	<0.08				
Granduc (n=2)	GR01-112 (m=8)	% of #DL	100%	100%	100%	100%	100%	73%	100%	100%	100%	100%	91%	91%	73%				
		Max	885	17.6	1074	29681	57.7	0.24	133	26.7	4611	23.4	1.19	11.8	1.84				
		Median	311	9.84	926	579	56.1	0.15	109	9.84	4117	18.8	0.31	2.46	0.26	374 ±5	±78	−7.9 ±0.2	±2.3
		Mean	342	10.2	857	639	55.1	0.14	111	7.07	4098	16.3	0.33	1.48	0.26				
		Min	183	8.29	500	34.8	44.9	<0.07	97.4	0.80	3217	11.2	<0.21	<0.05	<0.08				
	GRANDUC (m=4)	% of #DL	100%	100%	100%	100%	100%	100%	100%	100%	100%	100%	100%	100%	100%				
		Max	190	12.3	1070	7251	55.4	0.43	95.3	45.2	2610	21.8	0.38	5.79	1.13				
		Median	98.5	11.4	730	3607	53.7	0.17	73.5	21.6	2406	9.86	0.32	0.89	0.15	361 ±5	±77	8.5 ±0.1	±2.6
		Mean	111	11.4	790	3377	53.9	0.19	76.6	21.1	2426	11.9	0.28	1.19	0.20				
		Min	82.7	10.6	684	1720	53.0	0.11	67.2	11.3	2294	9.34	0.15	0.48	0.07				

n, Mean, m, % of #DL and median/mean calculation methods are defined as in Table 2. $T_{GGIMFis}$, and $\log_{10}(fS_2)$ are internal uncertainties only, resulting from compositional variations in sphalerite. External uncertainties shown as $2\sigma_{extl}$ in separate columns contain all sources of error, including the calibration of the GGIMFis geothermometer (Frenzel et al., 2016) and the model for $\log_{10}(fS_2)$ based on sphalerite composition (cf. Frenzel et al., 2016). All uncertainty estimates correspond to ±2 standard errors. For $\log_{10}(fS_2)$, most external uncertainty arises from the uncertainty in the absolute GGIMFis temperature.

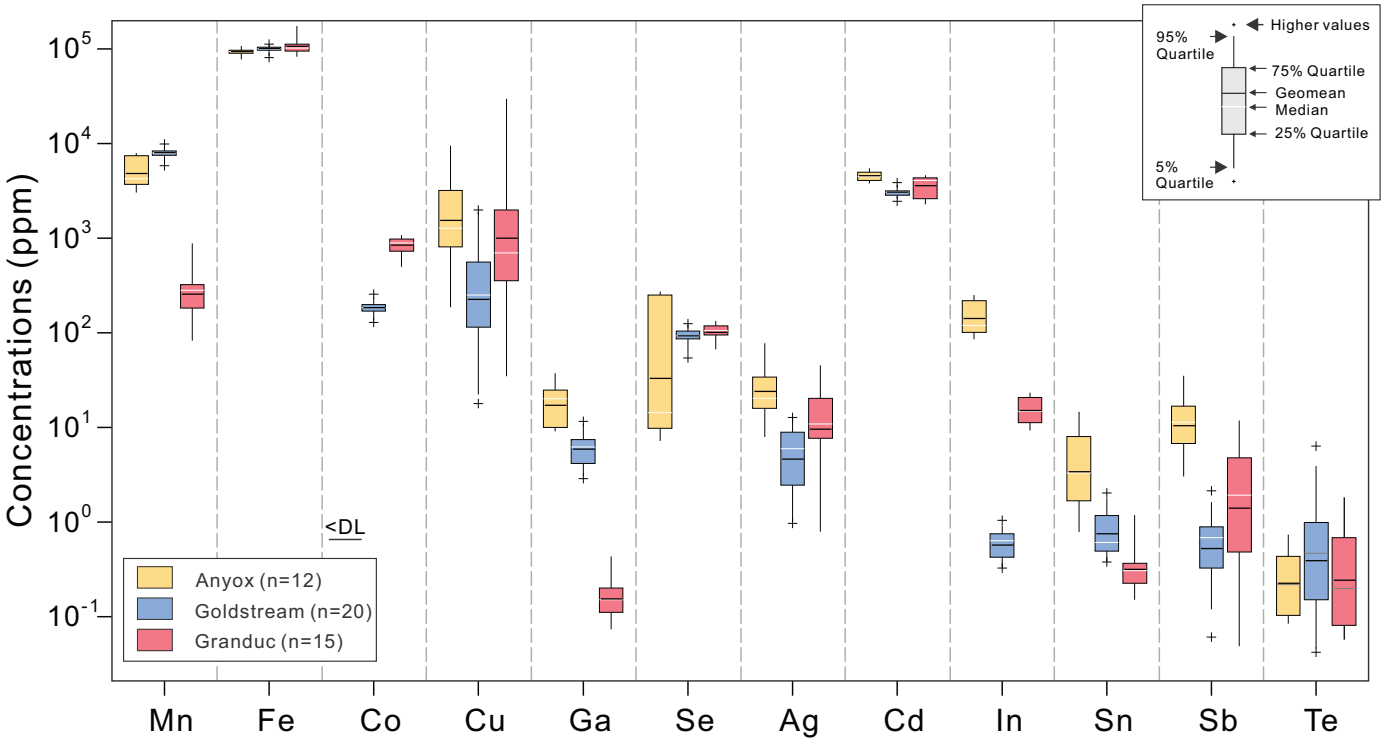


Fig. 6. Box-and-whisker plots of trace element concentrations in sphalerite from the Granduc, Anyox/Hidden Creek, and Goldstream deposits. More than half of the data above detection limits are included in the plots.

reflect variation in ore-forming processes or local geology. In our Granduc samples, LA-ICP-MS spot data indicate low Co concentrations in chalcopyrite (mean ±2δ: 19 ±3 ppm) and in magnetite (less than 10 ppm). Together with the mapping results, these data suggest that chalcopyrite and magnetite are unlikely to be the predominant hosts for Co unless they constitute a large proportion of the ore.

Magnetite also has the highest Ga concentrations in the magnetite-pyrrhotite-chalcopyrite assemblage, exceeding those in pyrrhotite and chalcopyrite (Fig. 4). Detectable Ga in magnetite (20 ppm) has been reported from other VMS deposits (Makvandi et al., 2016). Because Ga is compatible with magnetite via direct substitution into the magnetite lattice ($Ga^{3+} \leftrightarrow Fe^{3+}$; Nadoll et al., 2014), it is readily incorporated into the mineral phase as it precipitates from hydrothermal fluids. If a large amount of magnetite is present in the VMS deposit, it could thus be the main host for Ga.

In addition, chalcopyrite has the highest levels of Zn, Ag, In, Cd, and possibly Te relative to pyrrhotite and magnetite. In our samples, the concentrations of these elements in magnetite are below detection limits, consistent with data from other VMS deposits (Makvandi et al., 2016). Pyrrhotite may contain trace amounts of Zn and Ag, but at levels lower than those determined in chalcopyrite. Thus, for these elements, including Zn, Ag, In, and Cd, their concentrations follow the order: chalcopyrite> pyrrhotite>magnetite. A similar pattern of relative enrichment between chalcopyrite and pyrrhotite was observed for Ag and Zn in the Windy Craggy VMS deposit (Cawood et al., 2025), and for In in the Dulong Sn-Zn(-In) deposit (Xu et al., 2021). Both chalcopyrite and pyrrhotite are enriched in Se, but their relative Se enrichments cannot be determined in this study nor in Cawood et al. (2025). Further investigation is warranted. The lithophile elements such as Mg, Al, V, and Mn are commonly found as minor or trace elements in magnetite (e.g., Dare et al., 2014; Nadoll et al., 2014; Makvandi et al., 2016). Thus, it is not surprising that these elements are preferentially incorporated into magnetite relative to chalcopyrite and pyrrhotite.

5.3. Controls on trace-element variations

In VMS hydrothermal systems, sphalerite is a common sulphide that precipitates across wide physicochemical conditions and accommodates a broad range of minor and trace elements (e.g., Cook et al., 2009; Ye et al., 2011). Consequently, variations in sphalerite trace-element chemistry can record changes in ore-forming conditions (cf., Frenzel et al., 2022; Wei et al., 2025). Here, we use sphalerite as an example to evaluate the controls on trace-element variations. Key factors that may affect the trace element variations in sphalerite include physicochemical conditions (e.g., temperature, pressure, sulphur fugacity [fS_2]), fluid composition, and the competition of other crystallizing mineral phases (e.g., Wei et al., 2021; Frenzel, 2023). To evaluate the effect of temperature and fS_2, we estimated sphalerite crystallization temperatures and fS_2 using the GGIMFis geothermometer and Fe contents in

sphalerite (Table 3; see Frenzel et al., 2016, 2022). Because the temperature and fS_2 ranges overlap among the three deposits within uncertainty, the observed elemental variations appear to show no clear systematic relationship with either temperature or fS_2 change in the current dataset. This suggests that other factors, such as fluid composition and evolution, the source metal endowment, and the competition of co-crystallized mineral phases (cf., Huston et al., 1996), are significant. These potential causes will be evaluated in future work.

Sphalerite is a significant critical mineral host for In, Ga, and Ge in hydrothermal mineral systems (e.g., Frenzel et al., 2017), and the economic recovery of these metals alongside primary commodity Zn has become increasingly important. However, the distribution of these elements varies markedly among deposits and may even vary markedly at the hand-specimen scale. For example, the In and Ga concentrations of sphalerite in the deposits we studied vary by more than three orders of magnitude (Fig. 6; Table 3). It is therefore essential to quantify their concentrations and to resolve their spatial and temporal distributions across deposit-scale and regional-scale frameworks.

In addition to concentration, modal abundance should also be considered. Although chalcopyrite can host minor In, its contents are commonly less than those of co-crystallized sphalerite (e.g., Xu et al., 2021). However, where chalcopyrite is the predominant sulphide in Cu-rich VMS ore and sphalerite occurs only in trace amounts, even very high In concentrations in sphalerite (up to wt.%) may contribute little to the bulk In budget. In such systems, chalcopyrite could be the main In host by virtue of its greater modal abundance. Consequently, assessing the recovery potential of these critical metals must account for both the concentrations of the metals of interest and the modal abundance of their host minerals.

Such mineralogical deportment studies have focused chiefly on precious metals such as Au and Ag (e.g., Chryssoulis and Cabri, 1990; Gregory et al., 2013; Nourizenouz et al., 2025), and PGE (e.g., Cabri et al., 2002; Barnes et al., 2008; Osbahr et al., 2013). However, critical metals have received comparatively little attention (e.g., Frenzel et al., 2019). The next step of our work is to undertake a quantitative mineralogical deportment study to: 1) determine the phase-specific hosts of critical metals in VMS deposits; 2) evaluate how mineral proportions, textures, and liberation characteristics influence mineral deportment and metal distribution; and 3) test if these relationships exhibit predictable regularities across VMS systems. This information is necessary to identify practical options for increasing recoveries and to guide processing strategies in VMS-related mineralization.

6. Summary

The mineral chemistry across various mineral phases from the Granduc, Anyox/Hidden Creek, and Goldstream VMS deposits indicates that critical metals are partitioned among several hosts with markedly different concentrations. For Co, our dataset indicates the following enrichment sequence among analyzed minerals: cobaltite (CoAsS)>willyamite (Co,Ni)SbS >pyrite>pyrrhotite>sphalerite>magnetite. Although not all deposits contain the full suite of these phases, this general trend is broadly consistent across the samples examined. Furthermore, elemental partitioning behavior results show that individual mineral phases can host several different metals of interest. In a magnetite-pyrrhotite-chalcopyrite assemblage, magnetite concentrates Mg, Al, V, Mn, and Ga; pyrrhotite is mainly enriched in Co and Ni; and chalcopyrite preferentially hosts Zn, Ag, Se, In, and Cd. Moreover, trace elements in sphalerite, especially Co, Ga, and In, show considerable variations. This appears to be related to the geological setting of specific deposits and/or ore-forming process rather than variations in temperature and fS_2.

Considering the complex mineral assemblages and multi-host behavior of many critical metals, identifying their mineralogical hosts should consider not only absolute concentrations but also the modal abundance of the host phases. The continued work in this project aims to develop a quantitative model framework for critical metal deportment, demonstrating how systematic regularities in the partitioning of specific critical metals among coexisting minerals can be used to predict their mineralogical distribution in VMS systems.

Acknowledgments

This work was financially and logistically supported by the British Columbia Geological Survey and an NSERC Alliance Missions Critical Minerals grant. Assistance from and discussions with Audrey Graham, Adrian Hickin, Luke Ootes, Alexei Rukhlov, Freia de Waal from the BCGS, and Shaun Barker, Nikola Denisová, and Brian McNulty with MDRU are greatly appreciated. We are also indebted to Colin Aldis at Queen's Facility for Isotope Research for their assistance during LA-ICP-MS elemental imaging. Thanks to Brian McNulty and an anonymous reviewer for constructive comments and suggestions.

References cited

Barnes, S.J., Prichard, H.M., Cox, R.A., Fisher, P.C., and Godel, B., 2008. The location of the chalcophile and siderophile elements in platinum-group element ore deposits (a textural, microbeam and whole rock geochemical study): Implications for the formation of the deposits. Chemical Geology, 248, 295-317.

Belousov, I., Danyushevsky, L., Goemann, K., Gilbert, S., Olin, P., Thompson, J., Lounejeva, E., and Garbe-Schönberg, D., 2023. STDGL3, a reference material for analysis of sulfide minerals by laser ablation ICP-MS: An assessment of matrix effects and the impact of laser wavelengths and pulse widths. Geostandards and Geoanalytical Research, 47, 493-508.

Cabri, L.J., Wilson, J.M.D., Distler, V.V., Kingston, D., Nejedlý, Z., and Sluzheniken, S.F., 2002. Mineralogical distribution of trace platinum-group elements in the disseminated sulphide ores of Noril'sk 1 layered intrusion. Applied Earth Science, 111, 15-22.

Cawood, T.K., Peter, J.M., Petts, D.C., and Polivchuk, M.J., 2025. Syn-and postdepositional controls on the composition of pyrite and pyrrhotite in the Windy Craggy Cu-Co volcanogenic massive sulfide deposit, British Columbia, Canada. Economic Geology, 120.
<https://doi.org/10.5382/econgeo.5181>

Chew, D., Drost, K., Marsh, J.H., and Petrus, J.A., 2021. LA-ICP-MS imaging in the geosciences and its applications to geochronology. Chemical Geology, 559, article 119917. <https://doi.org/10.1016/j.chemgeo.2020.119917>

Chryssoulis, S.L., and Cabri, L.J., 1990. Significance of gold mineralogical balances in mineral processing. Transactions of the Institutions of Mining and Metallurgy. Section C, Mineral processing and extractive metallurgy, 99, C1-C10.

Colpron, M., 2020. Yukon terranes-A digital atlas of terranes for the northern Cordillera. Yukon Geological Survey. <https://data.geology.gov.yk.ca/Compilation/2#InfoTab>

Cook, N.J., Ciobanu, C.L., Pring, A., Skinner, W., Shimizu, M., Danyushevsky, L., Saini-Eidukat, B., and Melcher, F., 2009. Trace and minor elements in sphalerite: A LA-ICP-MS study. Geochimica et Cosmochimica Acta, 73, 4761-4791.

Cook, N., Ciobanu, C.L., George, L., Zhu, Z.Y., Wade, B., and Ehrig, K., 2016. Trace element analysis of minerals in magmatic-hydrothermal ores by laser ablation inductively-coupled plasma mass spectrometry: Approaches and opportunities. Minerals, article 111. <https://doi.org/10.3390/min6040111>

Danyushevsky, L., Robinson, P., Gilbert, S., Norman, M., Large, R., McGoldrick, P., and Shelley, M., 2011. Routine quantitative multi-element analysis of sulphide minerals by laser ablation ICP-MS: Standard development and consideration of matrix effects: Geochemistry: Exploration Environment Analysis, 11, 51-60.

Danyushevsky, L.V., and Thompson, J.M., 2025. Laser Ablation-ICP-MS for the In Situ Analysis of Geological Samples. In: Philip, J.P., Kathryn, L.L., Garbe-Schönberg, D., Philip, R., and Matthew S.A., (Eds.), Horstwood GGR Handbook of Rock and Mineral Analysis. Geostandards and Geoanalytical Research, 49, pp.457-493.

Dare, S.A., Barnes, S.J., Beaudoin, G., Méric, J., Boutroy, E., and Potvin-Doucet, C., 2014. Trace elements in magnetite as petrogenetic indicators. Mineralium Deposita, 49, 785-796.

Denisová, N., Piercey, S.J., and Wälle, M., 2024. Mineralogy and mineral chemistry of the ABM replacement-style volcanogenic massive sulfide deposit, Finlayson Lake district, Yukon, Canada. Mineralium Deposita, 59, 473-503.

Franklin, J.M., Gibson, H.L., Jonasson, I.R., and Galley, A., 2005. Volcanogenic massive sulfide deposits. In: Hedenquist, J.W., Thompson, J.F.H., Goldfarb, R.J., Richards, J.P. (Eds.), Economic Geology 100th Anniversary Volume, pp. 523-560.

Frenzel, M., Hirsch, T., and Gutzmer, J., 2016. Gallium, germanium, indium, and other trace and minor elements in sphalerite as a function of deposit type-A meta-analysis. Ore Geology Reviews, 76, 52-78.

Frenzel, M., Mikolajczak, C., Reuter, M.A., and Gutzmer, J., 2017. Quantifying the relative availability of high-tech by-product metals-the cases of gallium, germanium and indium. Resources Policy, 52, 327-335.

Frenzel, M., Bachmann, K., Carvalho, J.R., Relvas, J.M., Pacheco, N., and Gutzmer, J., 2019. The geometallurgical assessment of by-products-geochemical proxies for the complex mineralogical deportment of indium at Neves-Corvo, Portugal. Mineralium Deposita, 54, 959-982.

Frenzel, M., Voudouris, P., Cook, N.J., Ciobanu, C.L., Gilbert, S., and Wade, B.P., 2022. Evolution of a hydrothermal ore-forming system recorded by sulfide mineral chemistry: a case study from the Plaka Pb-Zn-Ag Deposit, Lavrion, Greece. Mineralium Deposita, 57, 417-438.

Frenzel, M., 2023. Making sense of mineral trace-element data-How to avoid common pitfalls in statistical analysis and interpretation. Ore Geology Reviews, 159, article 105566. <https://doi.org/10.1016/j.oregeorev.2023.105566>

Galley, A., Hannington, M., and Jonasson, I., 2007. Volcanogenic massive sulfide deposits. In: Goodfellow, W.D., (Ed.), Mineral Deposits of Canada: A Synthesis of Major Deposit Types, District Metallogeny, the Evolution of Geological Provinces and Exploration Methods. Geological Association of Canada, Mineral Deposits Division, Special Publication 5, pp. 141-161.

George, L.L., Cook, N.J., and Ciobanu, C.L., 2016. Partitioning of trace elements in co-crystallized sphalerite-galena-chalcopyrite hydrothermal ores. Ore Geology Reviews, 77, 97-116.

Gregory, M.J., Lang, J.R., Gilbert, S. and Hoal, K.O., 2013. Geometallurgy of the Pebble porphyry copper-gold-molybdenum deposit, Alaska: Implications for gold distribution and paragenesis. Economic Geology, 108, 463-482.

Hannington, M.D., 2013. Volcanogenic massive sulfide deposits. In: Holland H.D., and Turekian, K.K., (Eds.), Treatise on Geochemistry, Second Edition. Elsevier, pp. 463-488.

Hickin, A.S., Ootes, L., Orovan, E.A., Brzozowski, M.J., Northcote, B.K., Rukhlov, A.S., and Bain, W.M., 2024. Critical minerals and mineral systems in British Columbia. In: Geological Fieldwork 2005, British Columbia Ministry of Mining and Critical Minerals, British Columbia Geological Survey Paper 2025-01, pp.13-51.

Huston, D.L., Jablonski, W., and Sie, S.H., 1996. The distribution and mineral hosts of silver in eastern Australian volcanogenic massive sulfide deposits. The Canadian Mineralogist, 34, 529-546.

Jochum, K.P., Willbold, M., Raczek, I., Stoll, B., and Herwig, K., 2005. Chemical characterisation of the USGS reference glasses GSA-1G, GSC-1G, GSD-1G, GSE-1G, BCR-2G, BHVO-2G and BIR-1G Using EPMA, ID-TIMS, ID-ICP-MS and LA-ICP-MS. Geostandards and Geoanalytical Research, 29, 285-302.

Jochum, K.P., Weis, U., Stoll, B., Kuzmin, D., Yang, Q., Raczek, I., Jacob, D.E., Stracke, A., Birbaum, K., Frick, D.A., and Günther, D., 2011. Determination of reference values for NIST SRM 610-617 glasses following ISO guidelines. Geostandards and Geoanalytical Research, 35, 397-429.

Jowitt, S.M., Mudd, G.M., Werner, T.T., Weng, Z., Barkoff, D.W., and McCaffrey, D., 2018. The critical metals: An overview and opportunities and concerns for the future. In: Antonio, M.R.A., and Mauk, L.J., (Eds.), Metals, Minerals, and Society. Society of Economic Geologists Special Publication, 21, pp. 25-38. <https://doi.org/10.5382/SP.21.02>

Layton-Matthews, D., Peter, J.M., Scott, S.D., and Leybourne, M.I., 2008. Distribution, mineralogy, and geochemistry of selenium in felsic volcanic-hosted massive sulfide deposits of the Finlayson Lake District, Yukon Territory, Canada. Economic Geology, 103, 61-88. <https://doi.org/10.2113/gsecongeo.103.1.61>

Liang, X., Wang, F.Y., Zhang, L., Zhang, J.W., Wei, C.S., Fan, Y., Guo, X.Z., Zhou, T.F., Zhang, J.Q., and Lü, Q.T., 2023. Cobalt distribution and enrichment in skarn iron deposits: A case study of the Zhuchong skarn iron deposit, Eastern China. Ore Geology Reviews, 163, article 105778. <https://doi.org/10.1016/j.oregeorev.2023.105778>

Liu, T., Jiang, S.Y., Cao, S., Wang, W., Su, H.M., Yang, D., Li, H., and He, S., 2024. Cobalt enrichment and metallogenic mechanism of the Galinge skarn iron deposit in the Eastern Kunlun metallogenic belt, western China. Ore Geology Reviews, 170, article 106147. <https://doi.org/10.1016/j.oregeorev.2024.106147>

Makvandi, S., Ghasemzadeh-Barvarz, M., Beaudoin, G., Grunsky, E.C., McClenaghan, M.B., Duchesne, C., and Boutroy, E., 2016. Partial least squares-discriminant analysis of trace element compositions of magnetite from various VMS deposit subtypes: Application to mineral exploration. Ore Geology Reviews, 78, 388-408.

Monecke, T., Petersen, S., Hannington, M.D., Grant, H., and Samson, I.M., 2016. The minor element endowment of modern sea-floor massive sulfides and comparison with deposits hosted in ancient volcanic successions. In: Verplanck, P.L., and Hitzman, W.M., (Eds.), Rare Earth and Critical Elements in Ore

Deposits. Society of Economic Geologists Special Publication, 18, pp. 115-136. <https://doi.org/10.5382/Rev.18.06>

Nadoll, P., Angerer, T., Mauk, J.L., French, D., and Walshe, J., 2014. The chemistry of hydrothermal magnetite: A review. Ore Geology Reviews, 61, 1-32.

Norris, A., and Danyushevsky, L., 2018, Towards estimating the complete uncertainty budget of quantified results measured by LA-ICP-MS: Goldschmidt conference, 28th, Boston, USA, 2008, Extended Abstracts, p. 1894

Nourizenouz, Z., Guy, B.M., Gutzmer, J., Ebert, D., Braumann, R., and Frenzel, M., 2025. The deportment of silver in Kupferschiefer ores at the Spremberg-Graustein-Schleife deposit, Germany. Mineralium Deposita. <https://doi.org/10.1007/s00126-025-01377-5>

NRCan (Natural Resources Canada), 2024. Critical Minerals List. Government of Canada. <https://www.canada.ca/en/campaign/critical-minerals-in-canada/critical-minerals-an-opportunity-for-canada.html>

Osbahr, I., Klemd, R., Oberthür, T., Brätz, H., and Schouwstra, R., 2013. Platinum-group element distribution in base-metal sulfides of the Merensky Reef from the eastern and western Bushveld Complex, South Africa. Mineralium Deposita, 48, 211-232.

Paton, C., Hellstrom, J., Paul, B., Woodhead, J., and Hergt, J., 2011. Iolite: Freeware for the visualisation and processing of mass spectrometric data. Journal of Analytical Atomic Spectrometry, 26, 2508-2518.

Peter, J.M., and Scott, S.D., 1999. Windy Craggy, northwestern British Columbia; The world's largest Besshi-type deposit. Reviews in Economic Geology, 8, 261-295.

Piercey, S.J., 2011. The setting, style, and role of magmatism in the formation of volcanogenic massive sulfide deposits. Mineralium Deposita, 46, 449-471.

Piercey, S.J., Pietruszka, D., and Goudie, D., 2025. Critical metals in volcanogenic massive sulphide (VMS) deposits in British Columbia: A progress report. In: Geological Fieldwork 2025, British Columbia Ministry of Mining and Critical Minerals, British Columbia Geological Survey Paper 2025-01, pp. 189-201.

Pietruszka, D.K., Wei, C., Piercey, S.J., Aylward, W., and Kommescher, K., 2026. Supplementary data for: Critical metal distributions in volcanogenic massive sulphide (VMS) deposits in British Columbia: A progress report. British Columbia Ministry of Mining and Critical Minerals, British Columbia Geological Survey GeoFile 2026-01, 3 p.

Reich, M., and Simon, A.C., 2024. Critical minerals. Annual Review of Earth and Planetary Sciences, 53, 141-168.

Sylvester, P.J., 2006. Trends in analytical developments and earth science applications in LA-ICP-MS and LA-MC-ICP-MS for 2004 and 2005. Geostandards and Geoanalytical Research, 30(3), 197-207.

Van den Boogaart, K.G., and Tolosana-Delgado, R., 2013. Analyzing compositional data with R: Berlin, Springer, 200 p.

Wei, C., Ye, L., Hu, Y., Huang, Z., Danyushevsky, L., and Wang, H., 2021. LA-ICP-MS analyses of trace elements in base metal sulfides from carbonate-hosted Zn-Pb deposits, South China: A case study of the Maoping deposit. Ore Geology Reviews, 130, article 103945. <https://doi.org/10.1016/j.oregeorev.2020.103945>

Wei, C., Frenzel, M., Ye, L., Huang, Z., and Danyushevsky, L., 2024. Germanium distribution in Mississippi Valley-Type systems from sulfide deposition to oxidative weathering: A perspective from Fule Pb-Zn (-Ge) deposit, South China. American Mineralogist, 109, 1481-1498.

Wei, C., Frenzel, M., Ye, L., de Oliveira, S.B., Danyushevsky, L., Huang, Z.L., and Gutzmer, J., 2025. Sphalerite Chemistry and Carbonate (C, O) Isotope Zonation in the Nayongzhi Mississippi Valley-Type Deposit, Southwest China. Economic Geology, 120, 1751-1776.

Wilson, S.A., Ridley, W.I., and Koenig, A.E., 2002. Development of sulfide calibration standards for the laser ablation inductively-coupled plasma mass spectrometry technique. Journal of Analytical Atomic Spectrometry, 17, 406-409.

Xu, J., Cook, N.J., Ciobanu, C.L., Li, X., Kontonikas-Charos, A., Gilbert, S., and Lv, Y., 2021. Indium distribution in sphalerite from sulfide-oxide-silicate skarn assemblages: A case study of the Dulong Zn-Sn-In deposit, Southwest China. Mineralium Deposita, 56, 307-324.

Ye, L., Cook, N.J., Ciobanu, C.L., Liu, Y.L., Zhang, Q., Liu, T.G., Gao, W., Yang, Y.L., and Danyushevsky, L., 2011. Trace and minor elements in sphalerite from base metal deposits in South China: A LA-ICP-MS study. Ore Geology Reviews, 39, 188-217.

Zhang, Z., Hu, X., Ruan, B., Lv, X., and Liu, R., 2025. Distribution, occurrence and enrichment mechanism of Co in Fe-Ti oxide deposits: An example from the giant Hongge deposit, SW China. Ore Geology Reviews, 177, article 106465. <https://doi.org/10.1016/j.oregeorev.2025.106465>

Zhao, D., Zhang, Y., and Essene, E.J., 2015. Electron probe microanalysis and microscopy: Principles and applications in characterization of mineral inclusions in chromite from diamond deposit. Ore Geology Reviews, 65, 733-748.

Critical companion metals in porphyry deposits in British Columbia: Lithogeochemistry and scanning electron microscopy-mineral liberation analysis (SEM-MLA) from the Schaft Creek, Mount Polley, and New Afton deposits

Audrey C. Graham[1, a], Keanna Vaughan Forrester[1], Luke Ootes[1], Wyatt Bain[2], Roddy W. Campbell[1], and Dylan Goudie[3]

[1] British Columbia Geological Survey, Ministry of Mining and Critical Minerals, Victoria, BC, V8W 9N3
[2] Department of Earth Sciences, University of Western Ontario, London, ON, N6A 3K7
[3] Core Research Equipment and Training (CREAIT) Network, Memorial University of Newfoundland, St. John's, NL, A1C 5S7
[a] corresponding author: Audrey.Graham@gov.bc.ca

Recommended citation: Graham, A.C., Vaughan Forrester, K., Ootes, L., Bain, W., Campbell, R.W., and Goudie, D., 2026. Critical companion metals in porphyry deposits in British Columbia: Lithogeochemistry and scanning electron microscopy-mineral liberation analysis (SEM-MLA) from the Schaft Creek, Mount Polley, and New Afton deposits. In: Geological Fieldwork 2025, British Columbia Ministry of Mining and Critical Minerals, British Columbia Geological Survey Paper 2026-01, pp. 69-83.

Abstract

Porphyry deposits are major sources of Cu, Au, Ag, and Mo and provide many critical metals as byproducts (e.g., Sb, Bi, Te). British Columbia is Canada's largest producer of Cu and only producer of Mo, which occur in porphyry Cu ±Mo ±Au, alkalic Cu-Au, and low-F type Mo ±Cu porphyry deposits. However, the potential for production of critical companion metals from these deposits is poorly understood. Here we present new lithogeochemistry and scanning electron microscopy-mineral liberation analysis (SEM-MLA) results from three Late Triassic porphyry Cu-Au-Ag ±Mo deposits: Schaft Creek, Mount Polley, and New Afton. At Schaft Creek, geochemical data and mineralogy reveal enrichments in Bi and Te that correlate with observed Bi-Te tellurides, native alloys, sulphosalts, and sulphides. The New Afton and Mount Polley alkalic Cu-Au deposits exhibit enrichment of platinum-group elements (PGE), Re, and Te. Enrichment of PGE, particularly Pd, is highest at New Afton, where platinum group minerals (PGM) are identified by quantitative mineralogy. A comparison of geochemical data with similar data from five additional deposits demonstrates variations in critical metal assemblages between subtypes of porphyry deposits in British Columbia.

Keywords: Au-rich porphyry, New Afton, Schaft Creek, Mount Polley, critical minerals, companion metals

1. Introduction

British Columbia is Canada's largest producer of Cu and only producer of Mo, both of which are currently mined exclusively from porphyry deposits (Hickin et al., 2024). Metals that are produced as byproducts are considered 'companion metals' and many are on the critical minerals lists of Canada and allied jurisdictions (Mudd et al., 2014, 2017; Nassar et al., 2015; Hickin et al., 2024; NRCan, 2024). Globally, critical companion metals in porphyry deposits can include Re, Te, W, Sn, Sb, Bi, In, Nb, PGE, and rare earth elements (REE; John and Taylor, 2016; Hofstra and Kreiner, 2020). Although critical companion metals typically occur in relatively low concentrations in mined ore, their production can be feasible due to the large volumes extracted from porphyry deposits (John and Taylor, 2016; Lawley et al., 2025). Positive spatial and mineralogical correlations of potential byproduct metals with primary commodities (Cu, Au, Ag, Mo) increases the likelihood of economically feasible recovery (Mudd et al., 2014). Currently, the potential for production of critical companion metals from porphyry deposits in British Columbia is not well understood, in part due to a lack of information on the concentrations and deportment of these metals (e.g., Lawley et al., 2025).

This study presents new lithogeochemistry and scanning electron microscopy-mineral liberation analysis (SEM-MLA) results from the Schaft Creek Cu-Au-Mo-Ag deposit, and the Mount Polley and New Afton Cu-Au-Ag deposits (Late Triassic; Fig. 1). We compare the geochemical results to data from the Galore Creek (Lawley et al., 2025), Huckleberry and Berg (Orovan et al., 2025), and Kitsault (Orovan et al., 2024) porphyry deposits, and the E&L mafic magmatic Ni-Cu-PGE deposit (Fig. 2; Brzozowski and Zaborniak, 2024; Lawley et al., 2025). This comparison demonstrates variations in critical metal contents between deposit subtypes, which can be used to inform where opportunities may exist for economically viable companion metal production.

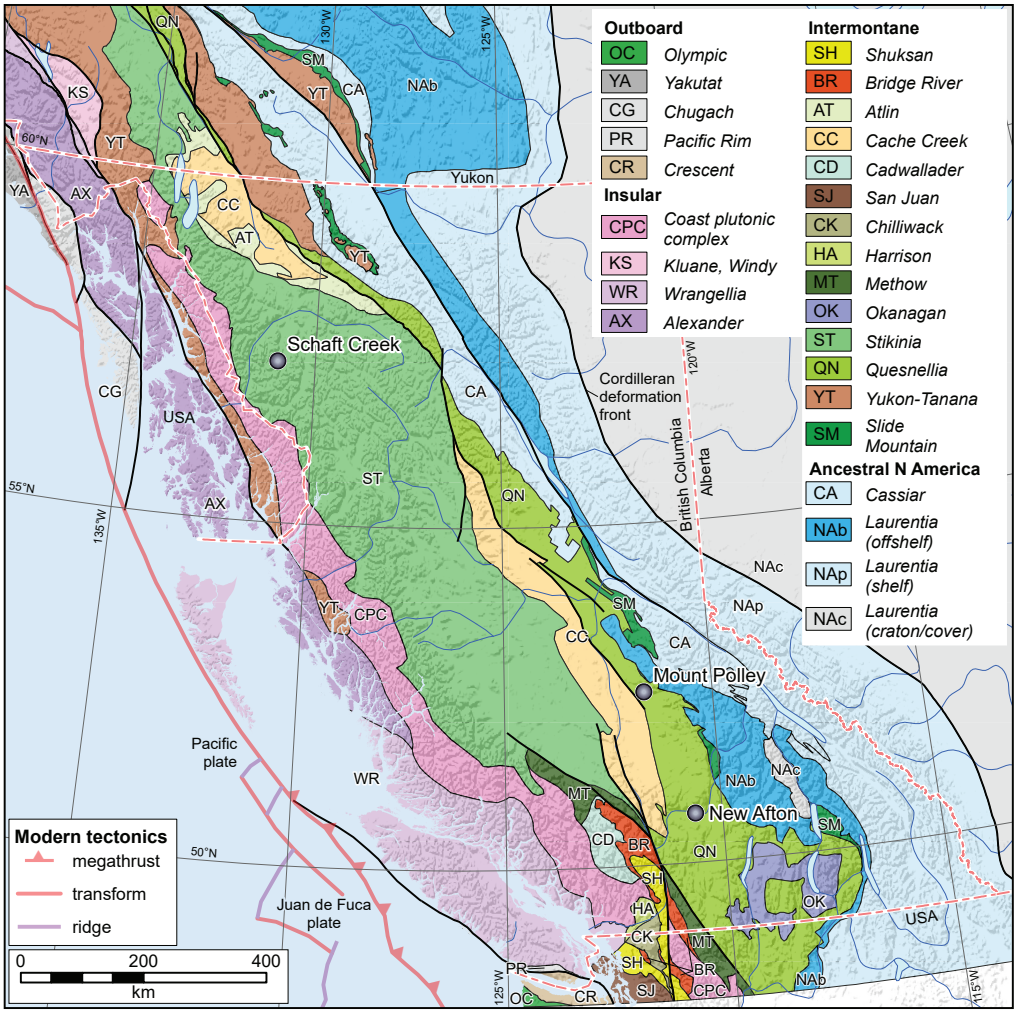


Fig. 1. Locations of Mount Polley, New Afton, and Schaft Creek deposits. Terranes after Colpron (2020).

2. Metal enrichments in magmatic and magmatic-hydrothermal environments

Mineral deposits formed in magmatic and magmatic-hydrothermal environments can be classified into mineral systems and deposit types with distinct metal assemblages (Fig. 3; e.g., Hofstra and Kreiner, 2020; Hofstra et al., 2021). Mafic magmatic mineral systems host various types of mafic-ultramafic intrusion-hosted deposits (Fig. 3). These deposits typically form at continental rifts where minerals containing Ni, Cu, Fe, Ti, Cr, and PGE crystallize from immiscible liquids in layered intrusions and conduits (Hofstra and Kreiner, 2020; Hofstra et al., 2021). Less commonly, magmatic Ni-Cu-PGE deposits form at convergent margins or supra-subduction/post-subduction settings (Manor et al., 2016; Nixon et al., 2020). Orthomagmatic Ni-Cu-PGE mineralization in Alaskan-type (i.e., devoid of orthopyroxene) mafic-ultramafic intrusive complexes form an important subclass of arc-related magmatic deposits in British Columbia (Nixon et al., 2019, 2020). Other arc-related magmatic Ni-Cu deposits (e.g., Manor et al., 2016) are classified as tholeiitic-related Ni-Cu-Co (e.g., E&L deposit; Brzozowski and Zaborniak, 2024; British Columbia Geological Survey, 2026).

Porphyry mineral systems typically form in upper crustal magmatic-hydrothermal environments and include porphyry, skarn, epithermal, and replacement deposits (e.g., Hofstra and Kreiner, 2020; Fig. 3). The peripheral deposits (e.g., skarn) can vary widely in metal content and may include critical metals (e.g., Co, Te, W, Sn, In, Ge) in potentially economic concentrations (e.g., Hofstra and Kreiner, 2020; Hickin et al., 2024).

2.1. Metal enrichments in porphyry deposits

Porphyry deposits have been classified according to magmatic affinity (i.e., alkaline or calc-alkaline; Lang et al., 1995; Logan and Mihalynuk, 2014) and by the assemblages of primary commodities Cu, Au, Mo, and Sn (Fig. 3; McMillan et al., 1996; Seedorf et al., 2005; Osatenko et al., 2020). Herein we distinguish between porphyry Mo (±Cu), porphyry Cu ±Mo ±Au, and alkalic Cu-Au deposits, for consistency with some current critical minerals research and MINFILE, the provincial

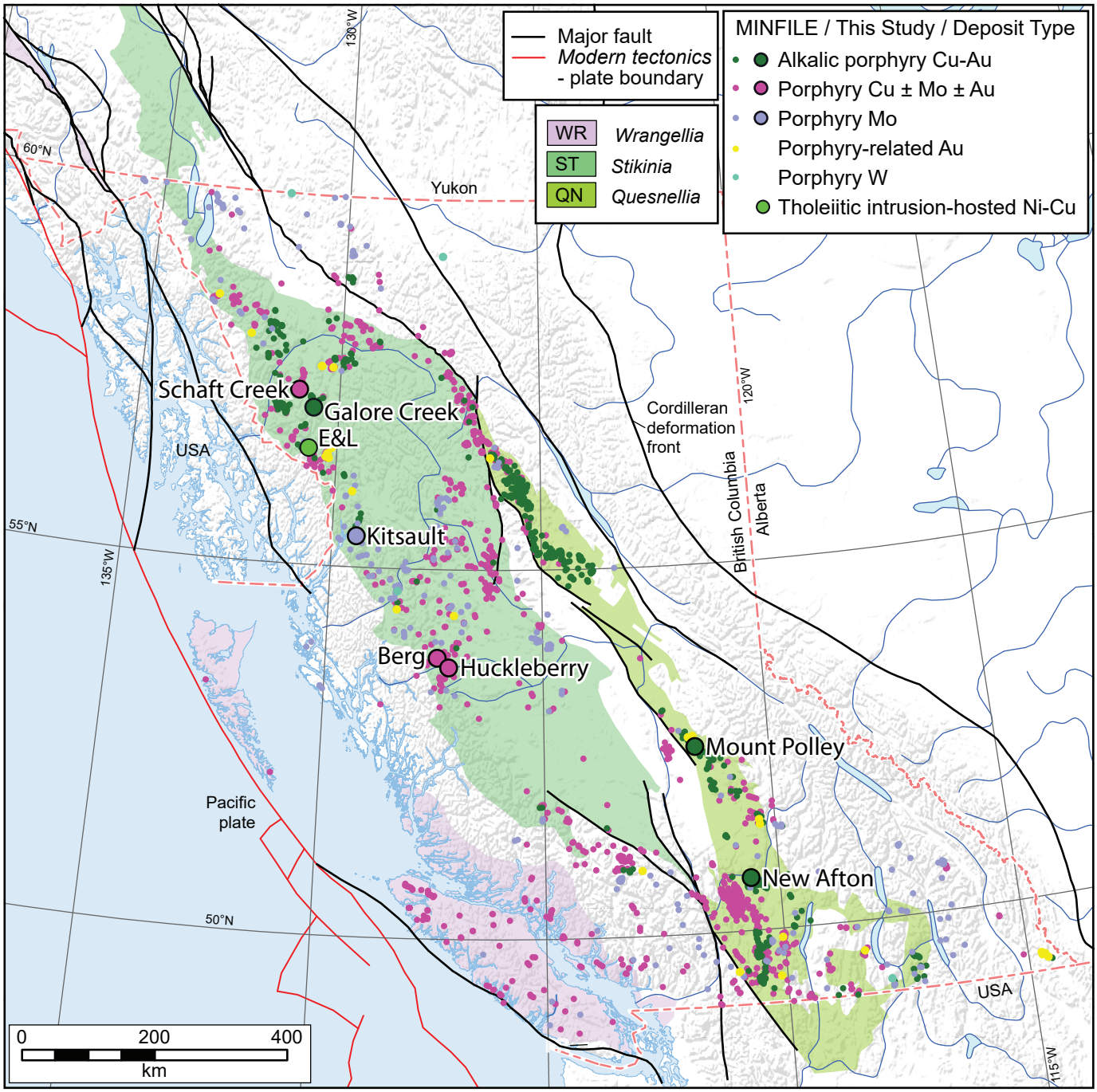


Fig. 2. Locations of deposits discussed herein and porphyry-type occurrences of different deposit sub-types in Quesnel, Stikine, and Wrangell terranes from MINFILE database (British Columbia Geological Survey, 2026). Terranes after Colpron (2020).

mineral occurrence inventory (British Columbia Geological Survey, 2026).

Globally, porphyry Cu ±Mo ±Au deposits are commonly enriched in Te, Re, U, PGE, Sc, Co, and Bi; alkalic porphyry Au ±Cu deposits can contain Bi, Te, and PGE (John and Taylor, 2016; Hofstra and Kreiner, 2020). Porphyry Mo deposits are commonly enriched in Sn, Re, REE, Sc, and W (Sinclair, 2007; Singer et al., 2008; Hofstra and Kreiner, 2020).

Silver is a common co-product of all types of porphyry Cu deposits, where it typically resides in solid solution in chalcopyrite and bornite (John and Taylor, 2016). Rhenium typically occurs as a solid solution in molybdenite and is concentrated in the upper portions of some continental arc deposits (John and Taylor, 2016). Where concentrations of Zn are present, they typically occur in argillic alteration zones at upper and outer parts of deposits and in late-stage veins (John and Taylor, 2016;

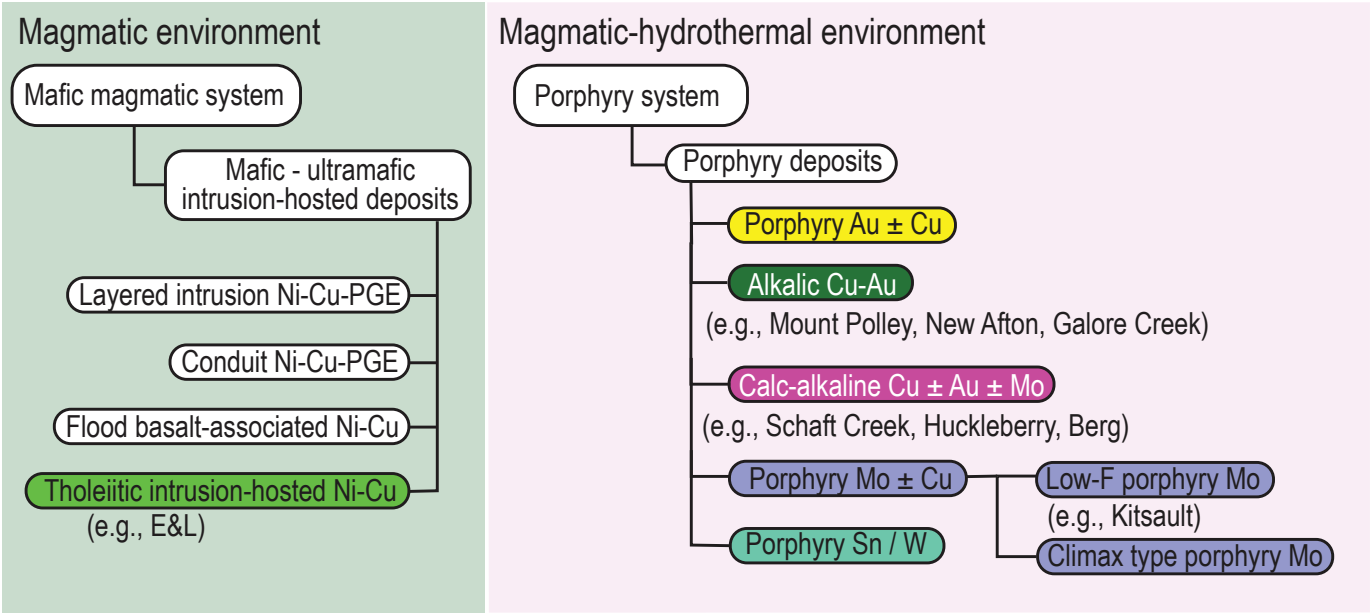


Fig. 3. Selected mineral systems and deposit types in the magmatic and magmatic-hydrothermal mineralizing environments. Deposit types discussed herein are coloured as in Figure 2. Simplified after Hofstra and Kreiner (2020), Hofstra et al. (2021), and British Columbia Geological Survey (2026).

Halley, 2020). Platinum group elements can form potentially economic byproduct concentrations in solid solution in hypogene bornite (Thompson et al., 2001), Ni-Co-rich pyrite (Boucher et al., 2023; Robb et al., 2023), or as discrete platinum group minerals (PGM) in late-stage hydrothermal veins (LeFort et al., 2011; Eliopoulos et al., 2014). Enrichment of PGE is commonly paragenetically associated with a complex semi-metal assemblage and is more common in porphyry deposits formed in island arc environments associated with alkaline magmas (Eliopoulos et al., 2014; McFall et al., 2021; Karatas Ahmadli, 2025).

3. British Columbia porphyry deposits

3.1. Geologic setting

Most porphyry deposits in British Columbia were formed either: 1) in the Late Triassic through Middle Jurassic in Stikine terrane (Stikinia), Quesnel terrane (Quesnellia), and Wrangell terrane (Wrangellia) island arcs before or during their accretion to Ancestral North America; or 2) in the Cretaceous through Eocene, after accretion of the Insular superterrane to the Intermontane superterrane (Figs. 1, 2; Nelson and Colpron, 2007; Nelson et al., 2013; Logan and Mihalynuk, 2014; Colpron et al., 2022).

The Stikine and Quesnel island arc terranes are thought to share similar Devonian through Early Jurassic histories (Nelson and Colpron, 2007; Nelson et al., 2013; Logan and Mihalynuk, 2014). The oldest island arc volcanic and coeval intrusive rocks are Devonian to Permian and are now preserved as the stratigraphic basement to Stikinia (Stikine assemblage, e.g., Logan and Koyanagi, 1994) and Quesnellia (e.g., Lay Range assemblage, Asitka Group; Ootes et al., 2022a, b). The second major episode of arc magmatism was during the Late Triassic, forming the mafic to intermediate volcanosedimentary (e.g., Stuhini Group in Stikinia; Takla Group and Nicola Group in Quesnellia) and allied plutonic rocks that commonly host porphyry deposits (Logan and Mihalynuk, 2014). Late Triassic to Early Jurassic magmatism followed, resulting in deposition of Hazelton Group volcanosedimentary rocks in Stikine terrane (e.g., Nelson and Colpron, 2007; Nelson et al., 2018).

During the Cretaceous, the orogen was subjected to crustal shortening and transpression, and intrusions with local porphyry Cu ±Mo mineralization were emplaced in deformation zones (Nelson et al., 2013). Porphyry Mo (±Cu) deposits associated with crustal extension-driven magmatism formed during the Eocene (e.g., Gehrels et al., 2009).

3.2. Mineralization characteristics and metal enrichments

Most porphyry deposits in British Columbia have been classified based on magmatic affinity and metal contents as porphyry Cu ±Mo ±Au, alkalic Cu-Au, or low-F Mo deposits (Osatenko et al., 2020; British Columbia Geological Survey, 2026). Herein we refer to deposits as 'pre-accretionary' (formed in an island arc setting) and 'post-accretionary' (formed in a continental setting).

During the Late Triassic through Early Jurassic, both alkalic Cu-Au and Cu ±Mo ±Au deposits formed in Quesnel and Stikine terranes (Figs. 1-3). A particularly prolific epoch of porphyry deposit formation was during an approximately 15-million-year period spanning the Triassic-Jurassic boundary (Logan and Mihalynuk, 2014). Porphyry Cu ±Mo ±Au deposits that formed during this time are typically associated with calc-alkaline magmatism, exhibit potassic, phyllic, and

propylitic alteration assemblages and mineralization styles including hypogene quartz-sulphide vein stockwork (Logan and Mihalynuk, 2014; Lawley et al., 2025). They commonly host Ag and Mo coproducts, but little is known about potential critical mineral byproducts (e.g., Lawley et al., 2025).

The alkalic Cu-Au porphyry deposits typically display early, predominantly magnetite alteration near a potassic (K-feldspar-biotite-magnetite) core, and peripheral calc-potassic (garnet-diopside-biotite-K-feldspar) and calc-sodic (albite-diopside) alteration. These deposits contain Au-rich metal assemblages, and geologic features (e.g., hydrothermal breccias and dike swarms) implying relatively shallow (i.e., subvolcanic) formation (Tosdal et al., 2009; Murakami et al., 2010; Osatenko et al., 2020; Chiaradia, 2021; Thompson et al., 2021). A subset of these deposits is associated with silica-undersaturated magma series (e.g., Galore Creek; Lang et al., 1995; Thompson et al., 2001). Previous workers identified significant enrichment of PGE (100s of ppb to 10s of ppm locally), particularly Pd, in many of British Columbia's Cu-Au porphyry deposits (Thompson et al., 2001; Nixon, 2004; LeFort et al., 2011; Hanley et al., 2020; Boucher et al., 2023; Robb et al., 2023; Karatas Ahmadli, 2025).

Post-accretionary porphyry deposits include Cretaceous Cu-Mo ±Au (e.g., Huckleberry) and Eocene porphyry Mo-rich deposits (i.e., Mo ±Cu). These Eocene Mo-bearing mineralized systems are classified as both low-F Mo porphyry deposits (e.g., Kitsault), and calc-alkalic Cu-Mo (e.g., Berg; Figs. 2, 3). The Kitsault and Berg deposits host elevated Ag, Te, Bi, Sn, Zn, and In predominantly in late-stage transitional veins (Orovan et al., 2024, 2025).

4. Overview of the Shaft Creek, Mount Polly, and New Afton deposits

4.1. Schaft Creek porphyry Cu-Mo-Au-Ag deposit

The Schaft Creek deposit is in Stikine terrane, northwest British Columbia (Figs. 1, 2). The mineralization is on the eastern margin of the Hickman batholith where quartz monzodiorite to quartz monzonite dikes (225 to 219 Ma) intrude and locally brecciate Stuhini Group mafic volcanic rocks (Table 1; Jutras and Bailey, 2016; Erbalaban, 2023; Campbell and van Straaten, 2025). Two 'syn-mineral' porphyritic intrusions yielded U-Pb zircon dates of 219.27 ±0.26 and 219.43 ±0.18 Ma (Bailey et al., 2025). The intrusions and mineralization may be related to slight east-west extension across the Hickman batholith during the Late Triassic (Nelson and van Straaten, 2020). Scott et al. (2008) considered that significant syn- and post-mineralization deformation indicates that the deposit may have formed in a crustal-scale shear zone that facilitated multiple pulses of magmatic fluids.

Mineralization comprises bornite, chalcopyrite, and molybdenite as disseminations in intrusions and volcanic wall rock, and within veins and breccias of predominantly quartz and carbonate, veins of predominantly sulphide, and tourmaline veins and breccias (Scott et al., 2008). A secondary phase comprising molybdenite and specular hematite-bearing veins and late quartz-chalcopyrite-galena-sphalerite±pyrite veins has been recognized (Scott et al., 2008).

4.2. Mount Polley alkalic Cu-Au porphyry deposit

Mount Polley is in Quesnel terrane of south-central British Columbia (Figs. 1, 2). Mineralization formed ca. 205 Ma (Table 1) and is associated with diorite, monzonite, plagioclase porphyry, and syenite dikes that were emplaced into mafic volcanic and volcanosedimentary rocks of the Nicola Group (Logan and Mihalynuk, 2005, 2014). The intrusions vary from silica saturated to silica undersaturated; hydrothermal alteration and veining lack quartz (Lang et al., 1995; Rees et al., 2020).

The deposit comprises several mineralized zones and breccia complexes within a north-northwest-trending corridor (Rees et al., 2020). Although no significant faults are recognized, syn-magmatic fabrics localized at vertical contacts between intrusive rocks, dikes, and breccia bodies suggest a structural control and a possible deep feeder structure (Brown et al., 2016). Mineralization comprises chalcopyrite and locally bornite-rich veins and matrix material to hydrothermal and intrusive breccias, and is associated with magnetite (Rees et al., 2020). Native gold is present as inclusions in chalcopyrite and rare tetrahedrite, galena, sphalerite, and molybdenite are present (Rees et al., 2020).

4.3. New Afton alkalic Cu-Au porphyry deposit

New Afton is in Quesnel terrane of south-central British Columbia (Figs. 1, 2) and is related to intrusions of the Iron Mask batholith (ca. 205 Ma; Table 1; Logan and Mihalynuk, 2014). At New Afton, mineralization is associated with silica-saturated porphyritic monzonites that intrude mafic volcanic rocks of the Nicola Group (Hall and May, 2013; Lipske et al., 2020; Mihalynuk and Diakow, 2020). Relatively small volumes of picrite occur and may be associated with metal enrichment, representing a mantle-derived magma within the mineralized system (Logan and Mihalynuk, 2014; Milidragovic and Spence, 2026). A complex structural framework for New Afton includes northwest- and east-trending faults that may have focussed ore-forming fluids and controlled Cu-Au distribution along the north margin of the Iron Mask intrusions (Hall and May, 2013; Lipske et al., 2020). In contrast to Mount Polley and Schaft Creek, magmatic-hydrothermal breccia bodies are not a significant component of the New Afton mineralization (Osatenko et al., 2020).

Mineralization comprises bornite-chalcopyrite with lesser chalcocite-covellite and accessory sulphosalts, and occurs as veins and vein breccias, densely concentrated as replacements of mafic phenocrysts, and as disseminations in intrusions (Hanley et al., 2020). Secondary (Late Jurassic) hypogene mineralization, defined by tennantite-tetrahedrite associated with argillic alteration, overprints primary Cu-Au mineralization (Robb et al., 2023). In the upper portion of the deposit, supergene enrichment consists of chalcocite, native copper, and minor copper oxides (Hanley et al., 2020).

Table 1. Deposits discussed herein with MINFILE database classification (British Columbia Geological Survey, 2026).

Deposit/ MINFILE No.	Deposit type[1]	Primary commodities	Secondary metals	Mineralization age (Ma)	Tectonic setting	Terrane
Schaft Creek 104G 015	Porphyry Cu ±Mo ±Au	Cu, Mo, Au, Ag[2]	Bi, Re, Te, W, Sb[3]	221.2 ±0.3 and 222.4 ±1 Re-Os Mo[4] Late Triassic	Pre-accretionary volcanic arc[2]	Stikine
Galore Creek 104G 090	Alkalic porphyry Cu-Au	Cu, Au, Ag	Bi, Te, Pt, Pd[5]	210-204.5 U-Pb zircon and titanite[4, 6, 7] Late Triassic	Pre-accretionary island arc[2]	Stikine
Mount Polley 093A 008	Alkalic porphyry Cu-Au	Cu, Au, Ag	Mn,[9] Pt, Re, Bi, Te, Pd (Up to 0.32 ppm[10])	205[9] Late Triassic	Pre-accretionary island arc	Quesnel
New Afton 092INE023	Alkalic porphyry Cu-Au	Cu, Au, Ag	Pt, Te, Bi, Pd (Up to 3.8 ppm[11]), Co, Ni, Se, As[12]	204.5 ±0.6 to 201.39 ±0.75[6,8] U-Pb zircon Late Triassic	Pre-accretionary island arc	Quesnel
E&L 104B 006	Tholeiitic intrusion-hosted Ni-Cu	Ni, Cu	Pt, Pd, Au, Ag, Te[5]	180-186[5] Early Jurassic	Island arc	Stikine
Huckleberry 093E 037	Porphyry Cu ±Mo ±Au	Cu, Mo, Au, Ag[13]	Pd, Bi, Te, W, Zn, Sb[13]	85.66 ±0.35[14] Re-Os in Mo Late Cretaceous	Post-accretionary continental arc	Stikine
Kitsault 103P 120	Porphyry Mo (low-F type)	Mo, Ag, Cu	Pb, Zn, Bi, Sb, W, Cd, In, Te, Re[2, 3, 14]	55.84 ±0.23 Re-Os in Mo[14] Eocene	Post-accretionary[14] continental arc	Stikine
Berg 093E 046	Porphyry Cu ±Mo ±Au	Cu, Mo, Ag[13]	Bi, Re, Te, Sb, Pb, Zn, In, As, W[13]	53.16 ±0.21 Re-Os in Mo[14] Eocene	Post-accretionary continental arc	Stikine

1: British Columbia Geological Survey (2026); 2: Osatenko et al. (2020); 3: this study; 4: Bailey et al. (2025); 5: Lawley et al. (2025); 6: Mortensen et al. (1995); 7: van Straaten et al. (2023); 8: Logan and Mihalynuk (2005); 9: Logan and Mihalynuk (2014); 10: Thompson et al. (2001); 11: Nixon (2003); 12: Boucher et al. (2023); 13: Orovan et al. (2025); 14: Graham et al. (2025).

The New Afton deposit is enriched in Co, Ni, and PGE, the transport and deposition of which are distinct from Cu-Au deposition (Boucher et al., 2023). Early hypogene pyrite is enriched in Co-Ni-Pd-Pt-Se-As, with Co and Ni concentrations similar to those in mafic-ultramafic PGE, iron-oxide apatite (IOA), and iron-oxide-Cu-Au (IOCG) deposits (Boucher et al., 2023). According to Robb et al. (2023), secondary hydrothermal alteration remobilized PGE from the early pyrite and re-deposited them as PGM in late-stage polymetallic and carbonate-bearing veins.

5. Methods

Lithogeochemical samples from Schaft Creek (n=24), Mount Polley (n=36), and New Afton (n=102) were collected from drill core during site visits in 2024. Samples are representative across multiple ore zones and mineralization facies at each deposit. Samples were split, crushed, and pulverized at the BCGS and sent to ALS Canada Ltd. in North Vancouver for geochemical analysis (for method details see Graham et al., 2025). Polished thin sections were examined using scanning electron microscopy-mineral liberation analysis (SEM-MLA) at the CREAIT Microanalysis Facility, Memorial University of Newfoundland, following methods in Graham et al. (2025).

6. Results

Summarized below are geochemical and SEM-MLA results; the complete datasets will be presented elsewhere.

6.1. Metal assemblages in Schaft Creek, Mount Polley, and New Afton deposits

We evaluate the geochemical results from this study by normalizing to average continental crust trace metal values (Fig. 4; Rudnick and Gao, 2014). Only samples with >500 ppm Cu are included. Samples from New Afton (n=79) are very strongly enriched in Cu (interquartile range: 0.53-3.77%).

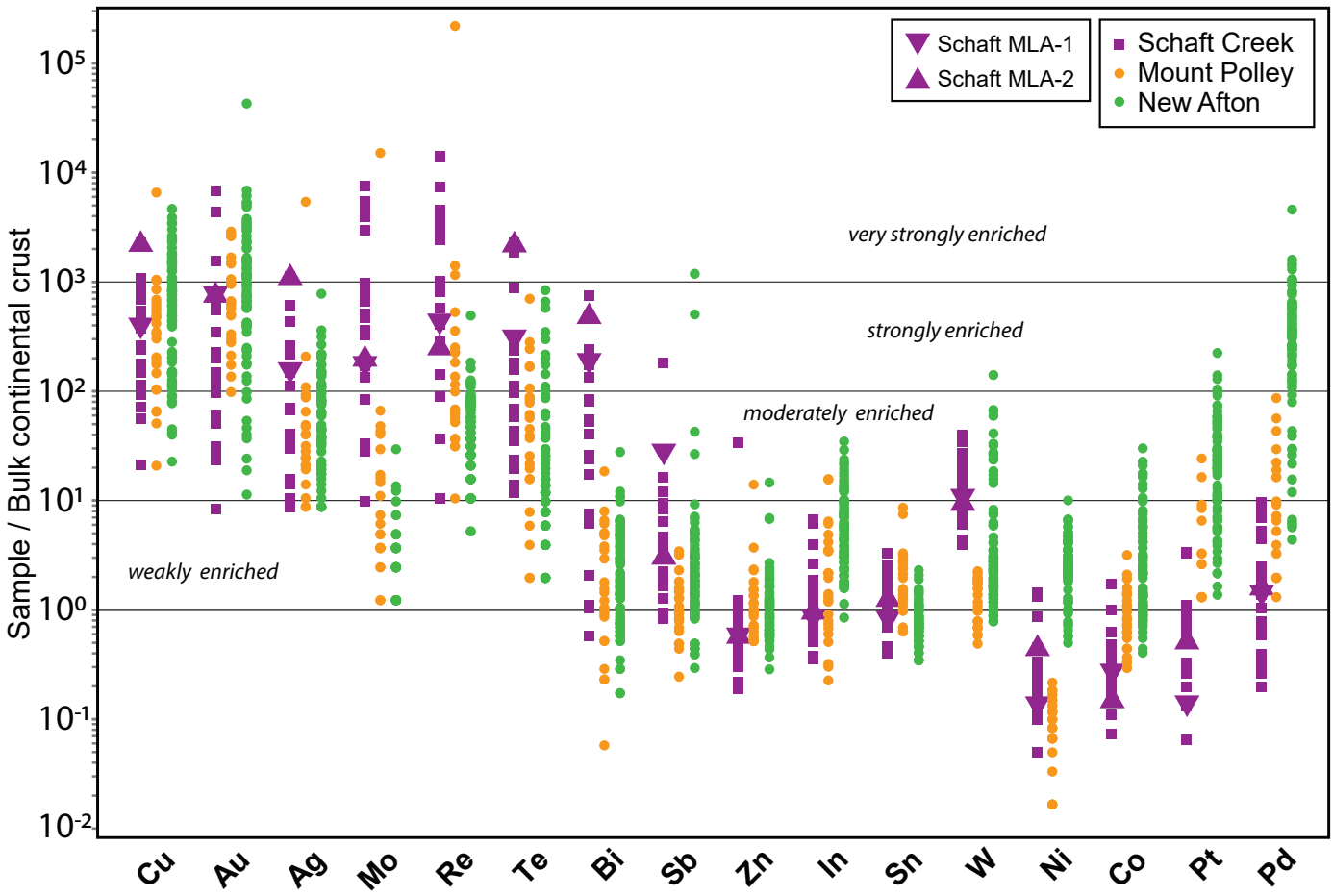


Fig. 4. Lithogeochemical results from Schaft Creek (n=23), Mount Polley (n=25), and New Afton (n=79) samples, filtered by Cu >0.05%. Trace element diagram of primary commodity and potential companion metals normalized to bulk continental crust of Rudnick and Gao (2014). Enrichment levels are defined as weak (1-10x average crust); moderate (10-100x bulk crust); strong (100-1000x bulk crust); very strong (>1000x bulk crust). Selected samples refer to those in Figure 5.

Samples from Mount Polley (n=25) and Schaft Creek (n=23) are similarly strongly enriched in Cu (interquartile ranges: 0.40-1.62% and 0.44-1.93%, respectively).

Samples from all three deposits are moderately to strongly enriched in Au and Ag (Fig. 4). Schaft Creek samples generally have the highest Ag concentrations with a mean of 10.0 and interquartile range of 1.3-13.1 ppm Ag; Ag is positively correlated with Cu in these samples (r=+0.87). Mount Polley samples yielded a mean of 15.6 and interquartile range of 0.6-2.8 ppm Ag, with one sample of massive sulphide breccia yielding 18% Cu, 307 ppm Ag, and 3.56 ppm Te. At New Afton, Ag values are similar (interquartile range: 1.0-6.2 ppm) despite stronger Cu grades (r=+0.65).

Gold values are highest at New Afton (mean: 2624 ppb; interquartile range: 520-2420 ppb), comparable at Mount Polley (mean: 1333 ppb; interquartile range: 430-1953 ppb), and slightly lower at Schaft Creek (mean: 1049 ppb; interquartile range: 72-864 ppb). One sample of iron oxide-clay altered breccia crosscut by a sulphide-bearing quartz-calcite vein at New Afton yielded 56.4 ppm Au and 6.98 ppm Pd.

At Schaft Creek, both Mo (mean: 1133 ppm; interquartile range: 147-759 ppm) and Re (mean: 401 ppb; interquartile range: 49-595 ppb) are strongly to very strongly enriched. Samples from Mount Polley are typically only weakly to moderately enriched in Mo (interquartile range: 3-14 ppm) and moderately to strongly enriched in Re (interquartile range: 10-44 ppb). However, one molybdenite vein sample from Mount Polley yielded 12,250 ppm Mo and 41.7 ppm Re (Fig. 4). Although Mo is only weakly enriched in New Afton samples, Re is moderately to strongly enriched (interquartile range: 4-14 ppb).

Samples from all three deposits are moderately to strongly enriched in Te; Schaft Creek samples tend slightly higher (≤11.55 ppm; Fig. 4). Schaft Creek samples are also weakly to strongly enriched in Bi (mean:19.44 ppm; interquartile range: 1.19-26.70 ppm; ≤130 ppm), whereas Mount Polley and New Afton are weakly enriched (mean values of <0.6 ppm Bi). Schaft Creek has higher concentrations of Sb (interquartile range: 0.4-1.5 ppm) and W (interquartile range: 7.4-20.7 ppm) and lower concentrations of Zn, In, and Sn than Mount Polley; New Afton samples span a larger range, up to strong enrichment of W and Sb (≤143 ppm W; ≤241 ppm Sb; Fig. 4).

New Afton is more enriched in Ni, Co, Pt, and Pd than Schaft Creek and Mount Polley, where Ni is depleted relative to bulk crust (Fig. 4). New Afton is strongly enriched in Pd (mean: 681 ppb; interquartile range: 197-877 ppb; ≤6980 ppb) and Pd is positively correlated with Au (r=+0.84) and As (r=+0.66). Mount Polley is weakly to moderately enriched in Pt and Pd (≤37 ppb Pt and ≤132 ppb Pd) and Schaft Creek is not. Collectively there is a pattern of Co, Pt, and Pd, where New Afton>Mount Polley>Schaft Creek (Fig. 4).

6.2. SEM-MLA

SEM-MLA quantitative mineralogy indicate that all three deposits contain electrum, Cu (±Fe) sulphides (chalcopyrite, bornite, chalcocite), Fe (±Ni) sulphides (pyrite, pyrrhotite, pentlandite), sphalerite, galena, and tetrahedrite-tennantite (Table 2). Mount Polley has the simplest mineralogy. For example, electrum is the only discrete Ag mineral and cosalite is the only discrete Bi mineral (Table 2). Mount Polley has minor amounts of native Au, enargite, sulphosalts, and scheelite.

Schaft Creek and New Afton contain diverse Ag, Bi, and Te-bearing minerals, where they occur as native metals, tellurides (hessite, tellurobismuthite), sulphides (acanthite, bismuthinite), and sulphosalts (wittichenite). At Schaft Creek, electrum and wittichenite are associated with fine-grained bornite at the margins of chalcopyrite masses (Figs. 5a-d). In another example, a bornite-rich vein (Fig. 5e) contains fine-grained Cu-sulphosalts (bournonite and tetrahedrite), galena, and molybdenite (Fig. 5f). Uniquely, New Afton samples contain platinum group minerals froodite and Pd-Sb alloys (Table 2; Bain et al., 2026).

At Mount Polley, the lack of discrete Te and Ag minerals (excluding electrum) implies they may occur in solid solution in sulphides and/or tetrahedrite (Fig. 4; Table 2). The SEM-MLA method does not resolve trace metals in solid solution; other methods such as µXRF or LA-ICP-MS are required to map elemental distribution of trace metals within minerals (e.g., Ootes et al., 2026).

7. Discussion

7.1. Variations in metal assemblages across deposits

Comparison of geochemical results presented in this study (Fig. 4) with previously published results (Brzozowski and Zaborniak, 2024; Graham et al., 2025; Lawley et al., 2025) shows that different porphyry deposit types in British Columbia contain distinct trends in precious and critical companion metal assemblages (Fig. 6; Table 1). The Eocene Mo-bearing Berg and Kitsault deposits contain the highest concentrations of Ag, Te, Bi, Sb, Zn, and In (Fig. 6a). Among pre-accretionary deposits, Schaft Creek contains higher concentrations of Te and Bi and lower Ni, Co, and PGE than the Mount Polley, New Afton, and Galore Creek Cu-Au deposits (Figs. 4, 6). Nickel, Co, and PGE are highest in the E&L mafic magmatic deposit. The New Afton metal assemblage differs from other porphyry mineralization but is similar to the E&L mafic magmatic deposit with enriched Ni, Co, Pt, and Pd and low Mo, although with an order of magnitude less Ni and higher normalized Pd/Pt (Fig. 6). Platinum group elements, particularly Pd, are more enriched in alkalic Cu-Au than Cu ±Mo ±Au porphyry deposits (Figs. 3, 4, 6). All deposits studied have Pd>Pt, and Pd is positively correlated with Au. Mount Polley and Galore Creek exhibit similar normalized Pd/Pt patterns as New Afton but at lower concentrations.

Positive spatial correlations of potential byproducts with primary commodities improve the potential for their economic extraction. All samples studied have positive correlations of Cu with Au, Ag, Bi, and Te, whereas Mo and Sb are largely decoupled from Cu (Figs. 7a-f). Rhenium is strongly correlated with Mo in all deposits except E&L and New Afton (Fig. 7g). Typically, Re is in solid solution within molybdenite (John and Taylor, 2016; McFall et al., 2021), which is more prevalent in porphyry Cu ±Mo ±Au deposits (Fig. 6). The data in this study show that alkalic Cu-Au deposits contain higher proportions of Re relative to Mo (Fig. 7g) and both E&L and New Afton have moderately enriched Re without the presence of molybdenite (Figs. 6, 7g), implying that Re resides in another mineral (Lawley et al., 2025).

7.2. Sub-epithermal enrichment of precious metals, post-transition metals, and metalloids

Late-stage transitional (post-porphyry, pre-epithermal) veins with high concentrations of critical companion metals have been recognized in several porphyry deposits in British Columbia (LeFort et al., 2011; Robb et al., 2023; Lawley et al., 2025; Orovan et al., 2024, 2025). For example, the high concentrations of semi-metals (Ag, Te, Bi, Sb, Zn, In) identified in the Eocene Berg and Kitsault Cu-Mo deposits are hosted predominantly within sub-epithermal (transitional) veins, as inferred on the basis of spatial and crosscutting relationships, the prevalence of sulphosalts, and carbonate gangue typically associated with low-temperature alteration at relatively shallow depths (Orovan et al., 2024, 2025).

At Schaft Creek, critical companion metals are hosted by sulphosalts (e.g., Bi in wittichenite and Sb in bournonite; Table 2), tellurides (Bi and Te in tellurobismuthite), and spatially associated with carbonate and secondary Cu minerals (e.g., chalcocite; Fig. 5), implying that Bi and Te may be concentrated or upgraded by late-stage mineralizing processes or subsequent hydrothermal activity during repeated deformation (Scott et al., 2008). The presence of fine grains of Bi ±Cu-sulphides, tellurides, and native metals at the margins of chalcopyrite and bornite suggests post-magmatic exsolution from original solid solution in the Cu-Fe sulphides. Alternatively, Bi and Te may have precipitated from the same fluids as the Cu-sulphides during slow cooling of the magmatic-hydrothermal system but formed discrete minerals after saturation of the sulphides (McFall et al., 2021; Karatas Ahmadli, 2025).

Analogous veins in alkalic igneous environments host PGM, deposited from Au-PGE-As-Sb-Bi-Te-B-rich fluids in late (post-porphyry, pre-epithermal) stages of the magmatic-

Table 2. Minerals identified by SEM-MLA.

Mineral group	Mineral	Chemical formula	Schaft Creek	Mount Polley	New Afton
Native element and alloy	Native gold	Au		x	
	Electrum	(Ag, Au)	x	x	x
	Native silver	Ag	x		
	Native bismuth	Bi	x		
Telluride	Hessite	Ag_2Te	x		
	AgTe	AgTe			x
	Tellurobismuthite	Bi_2Te	x		
Oxide	Gossanized chalcopyrite				x
	Cuprite	Cu_2O	x		x
Sulpharsenide	Cobaltite	CoAsS	x		x
	Enargite	Cu_3AsS_4	x	x	
Sulphide	Acanthite (argentite)	Ag_2S	x		
	Bismuthinite	Bi_2S_3	x		
	Molybdenite	MoS_2	x	x	
	Bornite	Cu_5FeS_4	x	x	x
	Chalcopyrite	$CuFeS_2$	x	x	x
	Chalcocite	Cu_2S	x	x	x
	Covellite	CuS	x		
	Sphalerite	ZnS	x	x	x
	Galena	PbS	x	x	x
	Pentlandite	$(Fe,Ni)_9S_8$	x	x	x
	Pyrite	FeS_2	x	x	x
	Pyrrhotite	FeS	x	x	x
	Arsenopyrite	FeAsS			x
Sulphosalt	Wittichenite	Cu_3BiS_3	x		
	Cosalite	$Pb_2Bi_2S_5$		x	
	Tetrahedrite-tennantite	$(Cu,Fe)_{12}(Sb, As)_4S_{13}$	x	x	x
	Bournonite	$PbCuSbS_3$	x		
	Cd-Cu-Fe-S				x
Tungstate	Scheelite	$CaWO_4$		x	
Platinum group mineral	Froodite	$PdBi_2$			x
	Pd Sb	Alloys			x

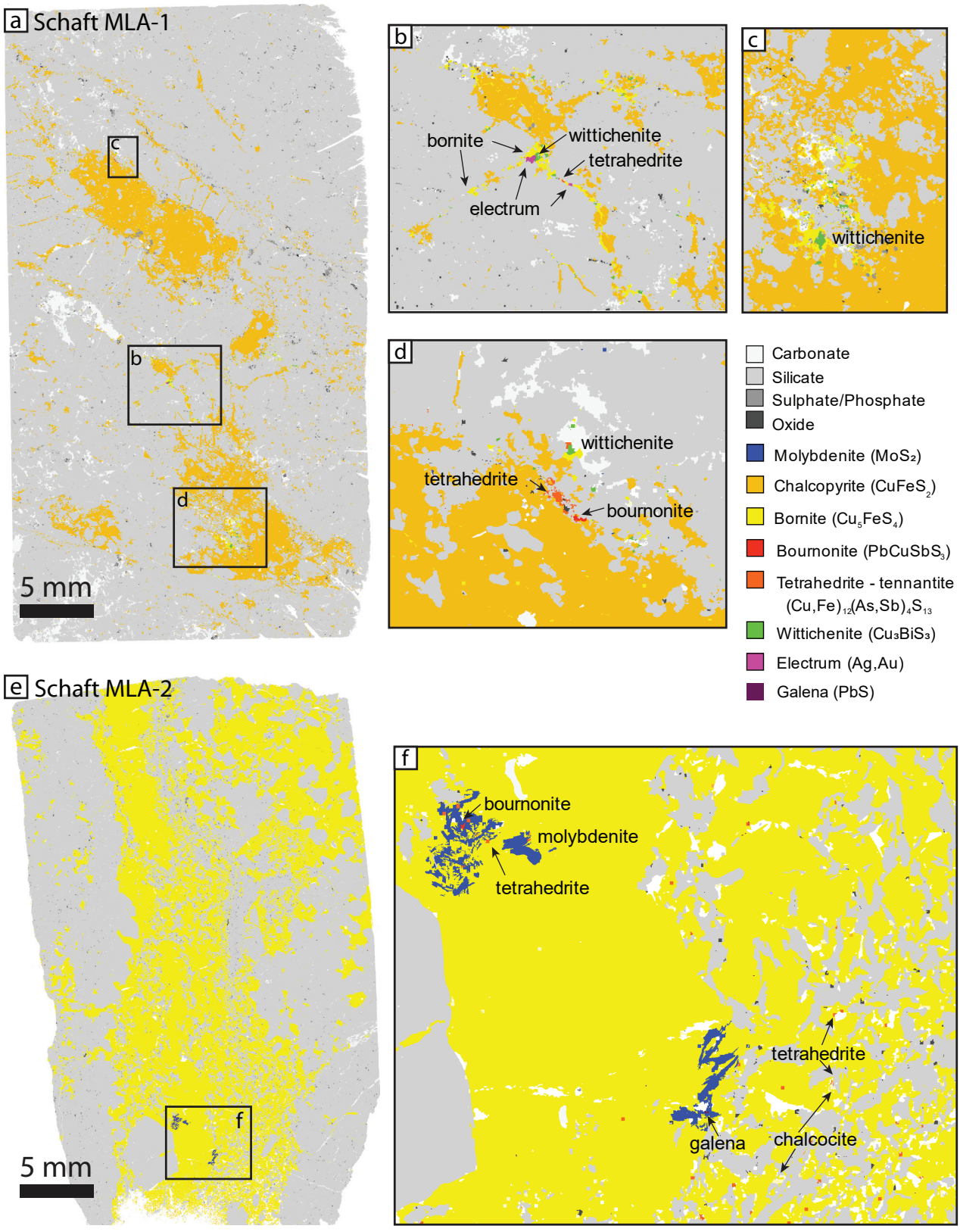


Fig. 5. SEM-MLA images from two Schaft Creek sample thin sections. **a)** False-colour mineralogy of Schaft MLA-1 (sample 24RCA-197-73a) showing locations of insets b-d. **b)** Wittichenite, electrum, and tetrahedrite in bornite veinlet at margin of chalcopyrite. **c)** Wittichenite in bornite with carbonate at margins of chalcopyrite clot. **d)** Wittichenite, tetrahedrite, and bournonite at margins of chalcopyrite vein. **e)** False-colour mineralogy of Schaft MLA-2 (sample 24RCA-195-55b) showing location of inset f. **f)** Bournonite, tetrahedrite, and galena as fine grains within and at margins of molybdenite clusters in bornite vein and tetrahedrite-chalcocite with carbonate at bornite margins.

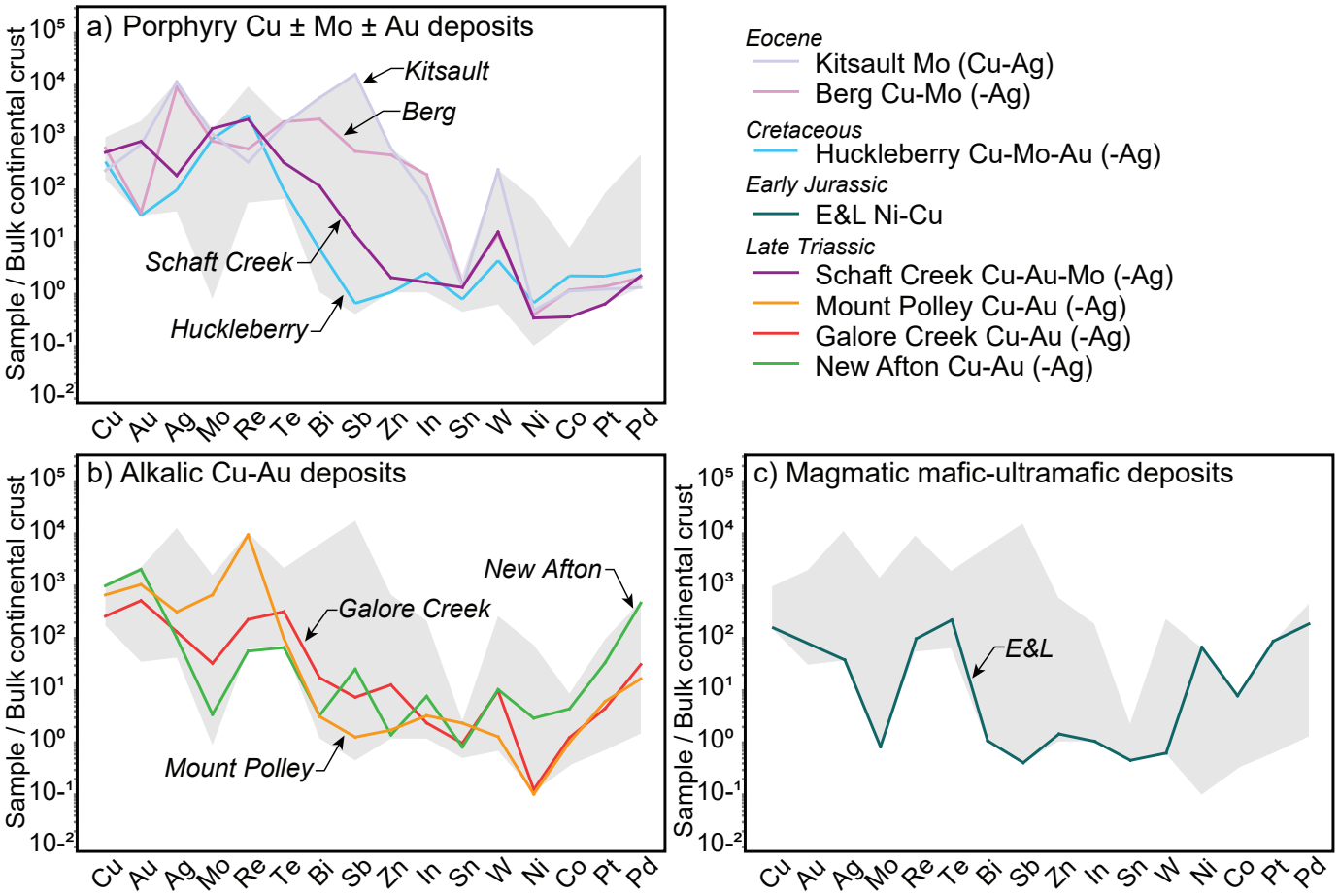


Fig. 6. Bulk continental crust-normalized mean commodity and potential companion metals. **a)** Porphyry Cu ±Mo ±Au deposits, including pre- and post-accretionary examples. **b)** Alkalic porphyry Cu-Au deposits. **c)** Mafic magmatic E&L deposit. Light grey shaded background represents the range of results for all data. Galore Creek data from Lawley et al. (2025), E&L data from Brzozowski and Zaborniak (2024).

hydrothermal system (LeFort et al., 2011; Robb et al., 2023). This results in a low- to intermediate-sulfidation epithermal-like style of mineralization of complex polymetallic but Cu-poor mineralization adjacent to Cu-Au ore (LeFort et al., 2011).

8. Conclusion

Bulk rock geochemical data and automated SEM-MLA mineralogy have revealed critical metal enrichment in mineralized rock samples from the Schaft Creek, Mount Polley, and New Afton porphyry deposits. The Schaft Creek Cu-Au-Mo-Ag deposit is enriched in Bi and Te, which is confirmed by the presence of Bi and Te within tellurides, native alloys, sulphosalts, and sulphides. The New Afton and Mount Polley Cu-Au deposits have PGE enrichment, and concentrations of Co and Pd at New Afton are similar to those at the E&L mafic magmatic deposit. Comparison with other British Columbia deposits highlights a variety of metal assemblages and critical companion metals.

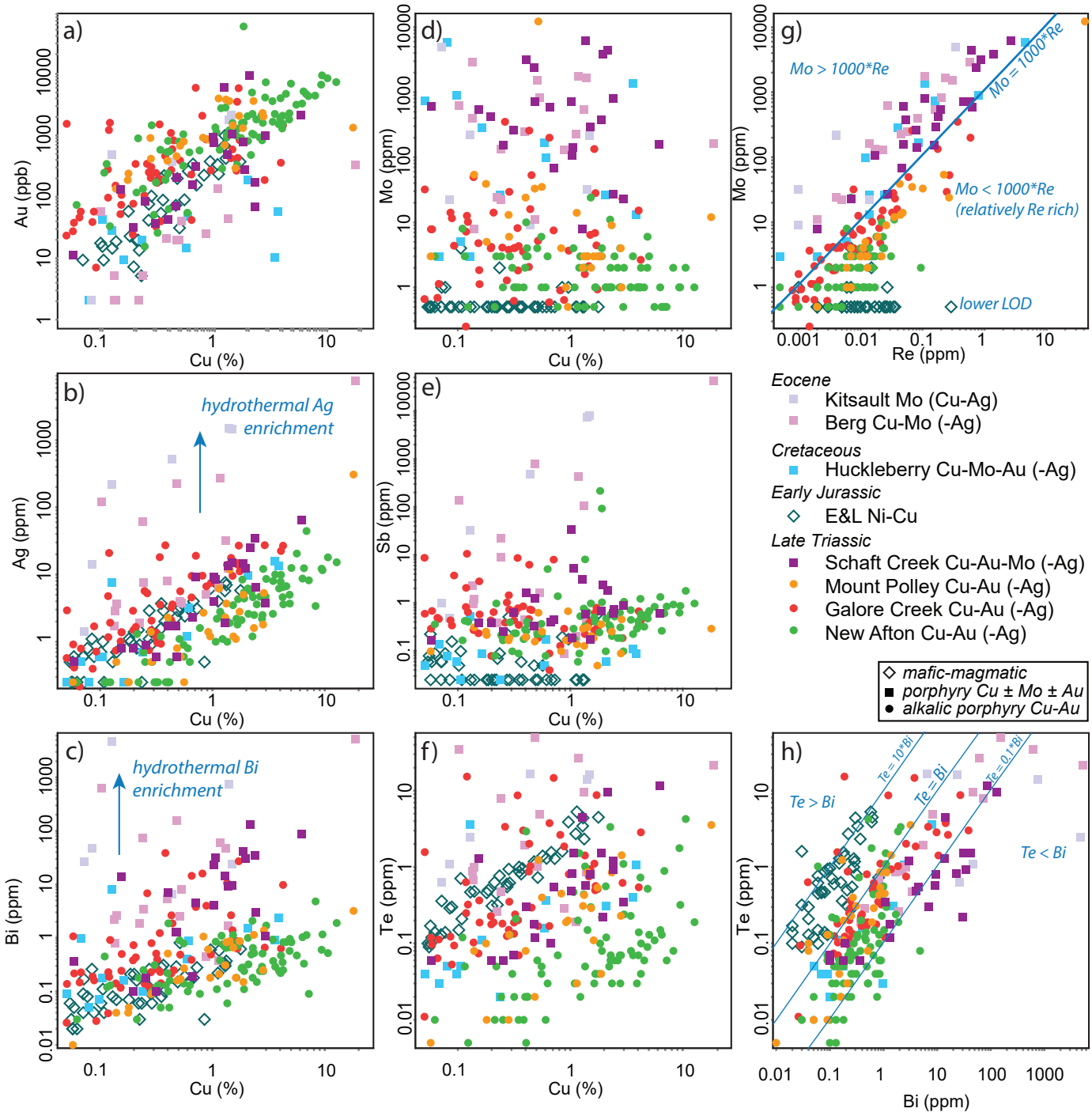


Fig. 7. Co-variation between Cu (wt.%) and **a)** Au (ppb), **b)** Ag (ppm), **c)** Bi (ppm), **d)** Mo (ppm), **e)** Sb (ppm), and **f)** Te (ppm). **g)** Co-variation between Re (ppm) and Mo (ppm). **h)** Co-variation between Bi (ppm) and Te (ppm). Galore Creek data from Lawley et al. (2025), E&L data from Brzozowski and Zaborniak (2024).

Acknowledgments

We thank Matthew Manor for a very thoughtful and constructive review. Chris Herron (Teck Resources) is thanked for discussion on critical metal zonation at Schaft Creek. Samples from Mount Polley were collected by Evan Orovan.

References cited

Bailey, L., Kim, R., Takaichi, M., Logan, J., Crowley, J., Friedman, R., Wall, C., van Straaten, B.I., and Campbell, R., 2025. U-Pb geochronological data for intrusive rocks near the Schaft Creek and Galore Creek deposits (southern Telegraph Creek area, NTS 104G), northwestern British Columbia. British Columbia Ministry of Mining and Critical Minerals, British Columbia Geological Survey GeoFile 2025-14, 16 p.

Bain, W., Joudrie, R., Mihalynuk, M.G., de Waal, F., and Goudie, D., 2026. Distribution and texture of platinum group minerals in the C and West Cave zones of the New Afton Cu-Au deposit, British Columbia. In: Geological Fieldwork 2025, British Columbia Ministry of Mining and Critical Minerals, British Columbia Geological Survey Paper 2026-01, pp. 85-95.

Boucher, B.M., Robb, S.J., Hanley, J.J., Kerr, M.J., and Mungall, J.E., 2023. Platinum-group elements (PGE) in the New Afton alkalic Cu-Au porphyry deposit, Canadian Cordillera, I: relationships between PGE, accessory metals and sulfur isotopes in pyrite. Frontiers in Earth Science, 11, article 819129. <https://doi.org/10.3389/feart.2023.819129>

British Columbia Geological Survey, 2026. MINFILE database. British Columbia Ministry of Energy, Mines and Low Carbon Innovation, British Columbia Geological Survey. <https://www2.gov.bc.ca/gov/content/industry/mineral-exploration-mining/british-columbia-geological-survey/mineralinventory>

Brown, R., Roste, G., Baron, J., and Rees, C., 2016. Mount Polley mine technical report, Cariboo Mining Division, British Columbia, Canada. NI 43-101 Technical Report prepared for Imperial Metals Corporation, 226 p. <https://www.sedarplus.ca/>

Brzozowski, M.J., and Zaborniak, K., 2024. Sulphide mineralization at the E&L magmatic Ni-Cu-PGE deposit: Textural evidence for contamination, vapour saturation, fluid immiscibility, and metal remobilization. In: Geological Fieldwork 2023, British Columbia Ministry of Energy, Mines and Low Carbon Innovation, British Columbia Geological Survey Paper 2024-01, pp. 65-78.

Campbell, R.W., and van Straaten, B.I., 2025. New data on Late Triassic to late Early Jurassic plutonic suites in the northern Golden Triangle region of northwest British Columbia. In: Geological Fieldwork 2024, British Columbia Ministry of Mining and Critical Minerals, British Columbia Geological Survey Paper 2025-01, pp. 49-72.

Chiaradia, M., 2021. Magmatic controls on metal endowments of porphyry Cu-Au deposits. In: Sholeh, A., and Wang, R., (Eds.), Tectonomagmatic Influences on Metallogeny and Hydrothermal Ore Deposits: A Tribute to Jeremy P. Richards (Volume I). Society of Economic Geologists Special Publication 24, pp. 1-16. <https://doi.org/10.5382/SP.24.01>

Colpron, M., 2020. Yukon terranes-A digital atlas of terranes for the northern Cordillera. Yukon Geological Survey. <https://data.geology.gov.yk.ca/Compilation/2#InfoTab>

Colpron, M., Sack, P.J., Crowley, J.L., Beranek, L.P., and Allan, M., 2022. Late Triassic to Jurassic magmatic and tectonic evolution of the Intermontane terranes in Yukon, northern Canadian Cordillera: transition from arc to syn-collisional magmatism and post-collisional lithospheric delamination. Tectonics, 41, article e2021TC007060. <https://doi.org/10.1029/2021TC007060>

Eliopoulos, D.G., Economou-Eliopoulos, M., and Zelyaskova-Panayiotova, M., 2014. Critical factors controlling Pd and Pt potential in porphyry Cu-Au deposits: Evidence from the Balkan Peninsula. Geosciences, 4, 31-49. <https://doi.org/10.3390/geosciences4010031>

Erbalaban, G., 2023. 2022 Assessment report on the Schaft Creek porphyry-copper-gold-molybdenum-silver deposit. British Columbia Ministry of Energy, Mines and Low Carbon Innovation, British Columbia Geological Survey Assessment Report 40875, 1132 p.

Gehrels, G., Rusmore, M., Woodsworth, G., Crawford, M., Andronicos, C., Hollister, L., Patchett, J., Ducea, M., Butler, M., Klepeis, K., Davidson, C., Friedman, R., Haggart, J., Mahoney, B., Crawford, W., Pearson, D., and Girardi, J., 2009. U-Th-Pb geochronology of the Coast Mountains batholith in north-coastal British Columbia: Constraints on age and tectonic evolution. Geological Society of America Bulletin, 121, 1341-1361. <https://doi.org/10.1130/b26404.1>

Graham, A.C., Orovan, E., Wall, C., Goudie, D., Creaser, R., Layton-Matthews, D., and Ootes, L., 2025. Data release from critical mineral studies of the Kitsault, Huckleberry, and Berg porphyry deposits. British Columbia Ministry of Mining and Critical Minerals, British Columbia Geological Survey GeoFile 2025-23, 7 p.

Hall, R.D., and May, B., 2013. Geology of the New Afton porphyry copper-gold deposit, Kamloops, British Columbia, Canada. In: Logan, J., and Schroeter, T., (Eds.), Porphyry Systems of Central and Southern BC: Prince George to Princeton. Society of Economic Geologists Field Trip Guidebook 44, pp. 117-128.

Halley, S., 2020. Mapping magmatic and hydrothermal processes from routine exploration geochemical analyses. Economic Geology, 115, 489-503. <https://doi.org/10.5382/econgeo.4722>

Hanley, J., Kerr, M., LeFord, D., Warren, M., MacKenzie, M., and Sedge, C., 2020. Enrichment of platinum-group elements (PGE) in alkalic porphyry Cu-Au deposits in the Canadian Cordillera: New insights from mineralogical and fluid inclusion studies. In: Lang, J.R., Sharman, E.R., and Chapman, J.B., (Eds.), Porphyry deposits of the Northwestern Cordillera of North America: A 25-year update. Canadian Institute of Mining, Metallurgy and Petroleum, Special Volume 57, pp. 88-109.

Hickin, A.S., Ootes, L., Orovan, E.A., Brzozowski, M.J., Northcote, B.K., Rukhlov, A.S., and Bain, W.M., 2024. Critical minerals and mineral systems in British Columbia. In: Geological Fieldwork 2023, British Columbia Ministry of Energy, Mines and Low Carbon Innovation, British Columbia Geological Survey Paper 2024-01, pp. 13-51.

Hofstra, A.H., and Kreiner, D.C., 2020. Systems-deposits-commodities-critical minerals table for the Earth Mapping Resources Initiative (ver. 1.1, May 2021): U.S. Geological Survey Open-File Report 2020-1042, 26 p. <https://doi.org/10.3133/ofr20201042>

Hofstra, A., Lisitsin, V., Corriveau, L., Paradis, S., Peter, J., Lauzière, K., Lawley, C., Gadd, M., Pilote, J., Honsberger, I., Bastrakov, E., Champion, D., Czarnota, K., Doublier, M., Huston, D., Raymond, O., VanDerWielen, S., Emsbo, P., Granitto, M., and Kreiner, D., 2021. Deposit classification scheme for the Critical Minerals Mapping Initiative Global Geochemical Database. U.S. Geological Survey Open-File Report 2021-1049, 60 p. <https://doi.org/10.3133/ofr20211049>

John, D.A., and Taylor, R.D., 2016. By-products of porphyry copper and molybdenum deposits. In: Verplanck, P.L., and Hitzman, M.W., (Eds.), Rare Earth and Critical Elements in Ore Deposits. Reviews in Economic Geology, Society of Economic Geologists, 18, pp. 137-164. <https://doi.org/10.5382/Rev.18.07>

Jutras, G., and Bailey, L., 2016. Drilling geological geochemical geophysical report on the Schaft Creek property. British Columbia Ministry of Energy and Mines, British Columbia Geological Survey Assessment Report 35967, 1345 p.

Karatas Ahmadli, C., 2025. Platinum Group Elements and gold deportment in the Kwanika copper-gold ±molybdenum porphyry system, British Columbia, Canada. Unpublished M.Sc. thesis, The University of British Columbia, Vancouver, Canada, 298 p.

Lang, J.R., Lueck, B., Mortensen, J.K., Russell, J.K., Stanley, C.F., and Thompson, J.F.H., 1995. Triassic-Jurassic silica-undersaturated and silica-saturated alkalic intrusions in the Cordillera of British Columbia: Implications for arc magmatism. Geology, 23, 5, 451-454.

Lawley, C.J.M., Petts, D.C., Lee, W.-S., Cajal, Y., Carrasco-Godoy, C., Campbell, I.H., Dlugosz, J., Larson, K.P., Savard, D., Kjarsgaard, I., and van Straaten, B.I., 2025. Critical raw material

potential of porphyry copper-gold deposits in the Golden Triangle, northwest British Columbia, Canada. Ore Geology Reviews, 178, article 106463.
<https://doi.org/10.1016/j.oregeorev.2025.106463>

LeFort, D., Hanley, J., and Guillong, M., 2011. Subepithermal Au-Pd mineralization associated with an alkalic porphyry Cu-Au deposit, Mount Milligan, Quesnel Terrane, British Columbia, Canada. Economic Geology, 106, 781-808.
<https://doi.org/10.2113/econgeo.106.5.781>

Lipske, J.L., Wade, D., Hall, R.D., and Petersen, M.A., 2020. Geology and mineralization of the New Afton Cu-Au alkalic porphyry deposit, Kamloops, British Columbia. In: Lang, J.R., Sharman, E.R., and Chapman, J.B., (Eds.), Porphyry deposits of the Northwestern Cordillera of North America: A 25-year update. Canadian Institute of Mining, Metallurgy and Petroleum, Special Volume 57, pp. 648-667.

Logan, J.M., and Koyanagi, V.M., 1994. Geology and mineral deposits of the Galore Creek area (104G/3, 4). British Columbia Ministry of Energy, Mines and Petroleum Resources, British Columbia Geological Survey Bulletin 92, 103 p.

Logan, J.M., and Mihalynuk, M.G., 2005. Regional geology and setting of the Cariboo, Bell, Springer and Northeast porphyry Cu-Au zones at Mount Polley, south-central British Columbia. In: Geological Fieldwork 2004, British Columbia Ministry of Energy and Mines, British Columbia Geological Survey Paper 2005-1, pp. 249-268.

Logan, J.M., and Mihalynuk, M.G., 2014. Tectonic controls on Early Mesozoic paired alkaline porphyry deposit belts (Cu-Au Ag-Pt-Pd-Mo) within the Canadian Cordillera. Economic Geology, 109, 827-858.
<https://doi.org/10.2113/econgeo.109.4.827>

Manor, M.J., Scoates, J.S., Nixon, G.T., and Ames, D.E., 2016. The Giant Mascot Ni-Cu-PGE deposit, British Columbia: mineralized conduits in a convergent margin tectonic setting. Economic Geology, 111, 57-87.

McFall, K., McDonald, I., and Wilkinson, J.J., 2021. Assessing the role of tectono-magmatic setting in the precious metal (Au, Ag, PGE) and critical metal (Te, Se, Bi) endowment of porphyry Cu deposits. In: Sholeh, A., and Wang, R., (Eds.), Tectonomagmatic Influences on Metallogeny and Hydrothermal Ore Deposits: A Tribute to Jeremy P. Richards, Volume II. Society of Economic Geologists, Special Publication 24, pp. 277-295.
<https://doi.org/10.5382/SP.24.15>

McMillan, W.J., Thompson, J.F.H., Hart, C.J.R., and Johnston, S.T., 1996. Porphyry deposits of the Canadian Cordillera. Geoscience Canada, 23, 125-134.

Mihalynuk, M.G., and Diakow, L.J., 2020. Southern Nicola Arc geology (NTS 092H/7NE, 8NW, 9W, 10E, 15E, 16W; 092I/1SW, 2SE). British Columbia Ministry of Energy, Mines and Low Carbon Innovation, British Columbia Geological Survey Geoscience Map 2020-01, scale 1:50,000.

Milidragovic, D., and Spence, D.W., 2026. Degassing-driven ascent and explosive eruption of picritic slurries in arc settings. Contributions to Mineralogy and Petrology, 181, 10.
<https://doi.org/10.1007/s00410-025-02292-8>

Mortensen, J.K., Ghosh, D., and Ferri, F., 1995. U-Pb age constraints of intrusive rocks associated with copper-gold porphyry deposits in the Canadian Cordillera. In: Schroeter, T.G., (Ed.), Canadian Institute of Mining, Metallurgy, and Petroleum, Special Volume 46, pp. 142-158.

Mudd, G.M., Yellishetty, M., Reck, B.K., and Graedel, T.E., 2014. Quantifying the recoverable resources of companion metals: A preliminary study of Australian mineral resources. Resources, 3, 657-671.
<https://doi.org/10.3390/resources3040657>

Mudd, G.M., Jowitt, S.M., and Werner, T.T., 2017. The world's byproduct and critical metal resources part I: Uncertainties, current reporting practices, implications and grounds for optimism. Ore Geology Reviews, 86, 924-938.

Murakami, H., Seo, J.H., and Heinrich, C.A., 2010. The relation between Cu/Au ratio and formation depth of porphyry-style Cu-Au ±Mo deposits. Mineralium Deposita, 45, 11-21.
<https://doi.org/10.1007/s00126-009-0255-1>

Nassar, N.T., Graedel T.E., and Harper, E.M., 2015. By-product metals are technologically essential but have problematic supply. Science Advances, article 1400180.
<https://doi.org/10.1126/sciadv.1400180>

Nelson, J.L., and Colpron, M., 2007. Tectonics and metallogeny of the British Columbia, Yukon and Alaskan Cordillera, 1.8 Ga to the present. In: Goodfellow, W.D., (Ed.), Mineral Deposits of Canada: A Synthesis of Major Deposit-Types, District Metallogeny, the Evolution of Geological Provinces, and Exploration Methods. Geological Association of Canada Mineral Deposits Division Special Publication 5, pp. 755-791.

Nelson, J.L., and van Straaten, B.I., 2020. Recurrent syn- to post subduction mineralization along deep crustal corridors in the Iskut Stewart-Kitsault region of western Stikinia, northwestern British Columbia. In: Sharman, E.R., Lang, J.R., and Chapman, J.B., (Eds.), Porphyry Deposits of the Northwestern Cordillera of North America: A 25-Year Update. Canadian Institute of Mining, Metallurgy and Petroleum Special Volume 57, pp. 149-211.

Nelson, J.L., Colpron, M., and Israel, S., 2013. The Cordillera of British Columbia, Yukon, and Alaska: tectonics and metallogeny. In: Colpron, M., Bissig, T., Rusk, B., and Thompson, J.F.H., (Eds.), Tectonics, Metallogeny, and Discovery-the North American Cordillera and Similar Accretionary Settings. Society of Economic Geologists Special Publication 17, pp. 53-109.

Nelson, J., Waldron, J., van Straaten, B., Zagorevski, A., and Rees, C., 2018. Revised stratigraphy of the Hazelton Group in the Iskut River region, northwestern British Columbia. In: Geological Fieldwork 2017, British Columbia Ministry of Energy, Mines and Petroleum Resources, British Columbia Geological Survey Paper 2018-1, pp. 15-38.

Nixon, G.T., 2004. Platinum-group elements in the Afton Cu-Au porphyry deposit, southern British Columbia. In: Geological Fieldwork 2003, British Columbia Ministry of Energy and Mines, British Columbia Geological Survey Paper 2004-1, pp. 263-290.

Nixon, G.T., Scheel, J.E., Scoates, J.S., Friedman, R.M., Wall, C.J., Gabites, J., and Jackson-Brown, S., 2019. Syn-accretionary multistage assembly of an Early Jurassic Alaskan-type intrusion in the Canadian Cordillera: U-Pb and $^{40}Ar/^{39}Ar$ geochronology of the Turnagain ultramafic-mafic intrusive complex, Yukon-Tanana terrane. Canadian Journal of Earth Sciences, 57, 575-600.

Nixon, G.T., Scoates, J.S., Milidragovic, D., Nott, J., Moerhuis, N., Ver Hoeve, T.J., Manor, M.J., and Kjarsgaard, I.M., 2020. Convergent margin Ni-Cu-PGE-Cr ore systems: U-Pb petrochronology and environments of Cu-PGE versus Cr-PGE mineralization in Alaskan-type intrusions. In: Bleeker, W., and Houle, M.G., (Eds.), Targeted Geoscience Initiative 5: Advances in the understanding of Canadian Ni Cu-PGE and Cr ore systems-Examples from the Midcontinent Rift, the Circum-Superior Belt, the Archean Superior Province, and Cordilleran Alaskan-type intrusions. Geological Survey of Canada Open File 8722, pp. 197-218.
<https://doi.org/10.4095/326897>

NRCan (Natural Resources Canada), 2024. Critical Minerals List. Government of Canada.
<https://www.canada.ca/en/campaign/critical-minerals-in-canada/critical-minerals-an-opportunity-for-canada.html>

Ootes, L., Ferri, F., Milidragovic, D., and Wall, C., 2022a. The age and provenance of the Lay Range assemblage provides an indirect record of basement to north-central Quesnellia, British Columbia. In: Geological Fieldwork 2021, British Columbia Ministry of

Energy, Mines and Low Carbon Innovation, British Columbia Geological Survey Paper 2022-01, pp. 31-44.

Ootes, L., Milidragovic, D., Friedman, R., Wall, C., Cordey, F., Luo, Y., Jones, G., Pearson, D.G., and Bergen, A., 2022b. A juvenile Paleozoic ocean floor origin for eastern Stikinia, Canadian Cordillera. Geosphere, 18. <https://doi.org/10.1130/GES02459.1>

Ootes, L., Graham, A.C., Whitmore, K., Goudie, D., Piercey, S.J., Barker, S., Milne, S., and McFarlane, C., 2026. Mineralogical control on critical companion metal distribution: Expanded workflow, with examples from the Sullivan Pb-Zn-Ag deposit. In: Geological Fieldwork 2025, British Columbia Ministry of Mining and Critical Minerals, British Columbia Geological Survey Paper 2026-01, pp. 45-52.

Orovan, E.A., Zaborniak, K., and Hooker, K., 2024. Textural evidence for ore fluid transport and the magmatic to hydrothermal transition at the past-producing Kitsault Mo-Ag mine. In: Geological Fieldwork 2023, British Columbia Ministry of Energy, Mines and Low Carbon Innovation, British Columbia Geological Survey Paper 2024-01, pp. 53-64.

Orovan, E.A., Ebert, S., Baldazzi, P., Saxton, D., and Goudie, D.J., 2025. Critical minerals at the Berg and Huckleberry porphyry deposits, British Columbia, using scanning electron microscropy-mineral liberation analysis (SEM-MLA). In: Geological Fieldwork 2024, British Columbia Ministry of Mining and Critical Minerals, British Columbia Geological Survey Paper 2025-01, pp. 73-84.

Osatenko, M., Riedell, K. B., and Lang, J. R., 2020. Characteristics of porphyry copper and porphyry molybdenum deposits in the northwestern Cordillera: A comprehensive compilation. In: Lang, J.R., Sharman, E.R., and Chapman, J.B., (Eds.), Porphyry Deposits of the Northwestern Cordillera of North America: A 25-Year Update. Canadian Institute of Mining, Metallurgy and Petroleum, Special Volume 57, pp. 27-67.

Rees, C.J., Gillstrom, G., and Riedell, K.B., 2020. The Mount Polley porphyry copper deposit, south-central British Columbia. In: Lang, J.R., Sharman, E.R., and Chapman, J.B., (Eds.), Porphyry Deposits of the Northwestern Cordillera of North America: A 25-Year Update. Canadian Institute of Mining, Metallurgy and Petroleum, Special Volume 57, pp. 567-600.

Robb, S.J., Boucher, B.M., Mungall, J.E., and Hanley, J.J., 2023. Platinum-group elements (PGE) in the New Afton alkalic Cu-Au porphyry deposit, Canadian Cordillera, II: PGE distribution and models for the hydrothermal coprecipitation of Co-Ni-Pd-Pt in pyrite. Frontiers in Earth Science, 11, 819109. <https://doi.org/10.3389/feart.2023.819109>

Rudnick, R.L., and Gao, S., 2014. Chapter 4.1-Composition of the continental crust. In: Treatise on Geochemistry (Second Edition), revision to v. 3, pp. 1-64. <https://doi.org/10.1016/B978-0-08-095975-7.00301-6>

Scott, J.E., Richards, J.P., Heaman, L.M., Creaser, R.A., and Salazar, G.S., 2008. The Schaft Creek porphyry Cu-Mo-(Au) deposit, northwestern British Columbia. Exploration and Mining Geology, 17, 163-196. <https://doi.org/10.2113/gsemg.17.3-4.163>

Seedorf, E., Dilles, J.H., Proffett, J.M., Einaudi, M.T. Jr., Zurcher, L., Stavast, W.J.A., Johnson, D.A., and Barton, M.D., 2005. Porphyry deposits: Characteristics and origin of hypogene features. In: Hedenquist, J.W., Thompson, J.F.H., Goldfarb, R.J., and Richards, J.P. (Eds.), Society of Economic Geologists One Hundredth Anniversary Volume, pp. 251-298.

Sinclair, W.D., 2007. Porphyry deposits. In: Goodfellow, W.D., (Ed.), Mineral Deposits of Canada: A Synthesis of Major Deposit Types, District Metallogeny, the Evolution of Geological Provinces, and Exploration Methods. Geological Association of Canada, Mineral Deposits Division Special Publication 5, pp. 223-243.

Singer, D.A., Berger, V.I., and Moring, B.C., 2008. Porphyry copper deposits of the world-database and grade and tonnage models. U.S. Geological Survey Open-File Report 2008-1155, 45 p. <http://pubs.usgs.gov/of/2008/1155/>

Thompson, J., Lang, J., and Stanley, C., 2001. Platinum group elements in alkaline porphyry deposits, British Columbia. In: Exploration and Mining in British Columbia 2001 Part B, British Columbia Ministry of Energy and Mines, British Columbia Geological Survey, pp. 57-64.

Tosdal, R.M., Dilles, J.H., and Cooke, D.R., 2009. From source to sinks in auriferous magmatic-hydrothermal porphyry and epithermal deposits. Elements, 5, 289-295. <https://doi.org/10.2113/gselements.5.5.289>

Distribution and texture of platinum group minerals in the C and West Cave zones of the New Afton Cu-Au deposit, British Columbia

Wyatt Bain[1, a], Robin Joudrie[1], Freia de Waal[2], Mitchell G. Mihalynuk[3], and Dylan Goudie[4]

[1] Department of Earth Sciences, University of Western Ontario, London, ON, N6A 3K7
[2] University of Victoria, Victoria, BC, V8P 5C2
[3] British Columbia Geological Survey, Ministry of Mining and Critical Minerals, Victoria, BC, V8W 9N3
[4] Core Research Equipment and Instrument Training (CREAIT) Network, Memorial University of Newfoundland, St. John's, NL, A1C 5S7
[a] corresponding author: wbain2@uwo.ca

Recommended citation: Bain, W., Joudrie, R., de Waal, F., Mihalynuk, M.G., and Goudie, D., 2026. Distribution and texture of platinum group minerals in the C and West Cave zones of the New Afton Cu-Au deposit, British Columbia. In: Geological Fieldwork 2025, British Columbia Ministry of Mining and Critical Minerals, British Columbia Geological Survey Paper 2026-01, pp. 85-95.

Abstract

Alkalic Cu-Au porphyry deposits in the Quesnel terrane of British Columbia represent an important source of Cu-Au and commonly contain byproduct platinum group elements (PGE) and discrete platinum group minerals (PGM). Several studies have evaluated the occurrence of PGM in alkalic porphyries in British Columbia, but the occurrence of PGM and the processes that drive PGE enrichment in this setting remain incompletely understood. This study evaluates the paragenesis and mineral associations of PGM in the C and West Cave zones of the New Afton deposit, using quantitative scanning electron microscopy-mineral liberation analysis (SEM-MLA). PGM occur in ore-stage mineralization from most underground zones (e.g., C, West Cave, and East Extension) with the C and West Cave zones having the highest relative abundances identified to date. The textures and mineral association of PGM of the C and West Cave zones indicate that they crystallized throughout the paragenesis of these areas and are intergrown with the primary mineralogy of Fe oxide-apatite veins, Fe oxide-sulphide veins, sulphide veins, zones of disseminated sulphides, and late-stage carbonate veins. Occurrences of PGM grains suggest contemporaneity with intense potassic and sodic-potassic alteration, and PGM grains commonly co-occur with grains of electrum, tetrahedrite, and Ag-Hg tellurides. The distribution of PGM in hypogene Cu-Au mineralization and late carbonate-bearing veins suggests the New Afton deposit had multi-stage PGE enrichment and mobilization in the presence of magmatic fluids.

Keywords: Alkalic porphyry Cu-Au, New Afton, critical minerals, platinum group elements, cobalt, nickel

1. Introduction

Canada (NRCan, 2024) and many of its trading partners identify platinum group elements (PGEs) as critical minerals (e.g., Table 1 in Hickin et al., 2024). PGEs are among the rarest elements in the Earth's crust, typically having concentrations of <0.6 ppb (Rudnick and Gao, 2014). Deposits featuring high concentrations of these metals are relatively rare. Most of the world's PGE supply is produced as a byproduct or co-product of Ni and Cu refining outside of North America (Gunn, 2014). As the need for PGEs grows, so too will the need for secure supply chains, including potential domestic PGE sources (NRCan, 2024).

With the closure of Canada's only primary PGE-producing mine (Lac-des-Iles, Ontario) in 2026, domestic PGE production in Canada will be primarily as a byproduct of nickel production from magmatic sulphide deposits in eastern Canada. However, ore concentrates from several 'alkalic' porphyry Cu-Au-Ag±Mo deposits (Barr et al., 1976) in British Columbia contain significant concentrations of PGEs (Nixon and Laflamme, 2002) that might support additional domestic PGE production.

Quesnel and Stikine terranes (Fig. 1) contain one of the largest concentrations of alkalic porphyry Cu-Au-Ag±Mo deposits in the world (Logan and Mihalynuk, 2014). In addition to primary Cu-Au±Ag production, these deposits contain significant PGE, Te, Re, Co, and Bi (Hofstra and Kreiner, 2020). Recent work on alkalic porphyry deposits such as New Afton and Kwanika (Fig. 2a) shows that PGEs commonly occur in high abundances with primary Cu-Au minerals, and in some cases are concentrated in PGE-rich minerals (Hofstra and Kreiner, 2020; Boucher et al., 2023; Robb et al., 2023; Karatas Ahmadli, 2025; Polar, 2025). Reliable prediction of PGE grade and production requires detailed knowledge of PGE mineralogy (Bissig and Cooke, 2014).

The New Afton alkalic deposit in south-central British Columbia is primarily a Cu-Au-Ag porphyry. However, ore from this deposit commonly has elevated concentrations of PGEs (Pd >1 ppm) and hosts platinum group minerals (PGMs; discrete Pd-Pt-Sb-As-Te-Hg-Bi mineral phases in which PGEs are a major constituent by weight; Boucher et al., 2023; Robb et al., 2023). Limited metallurgical testing

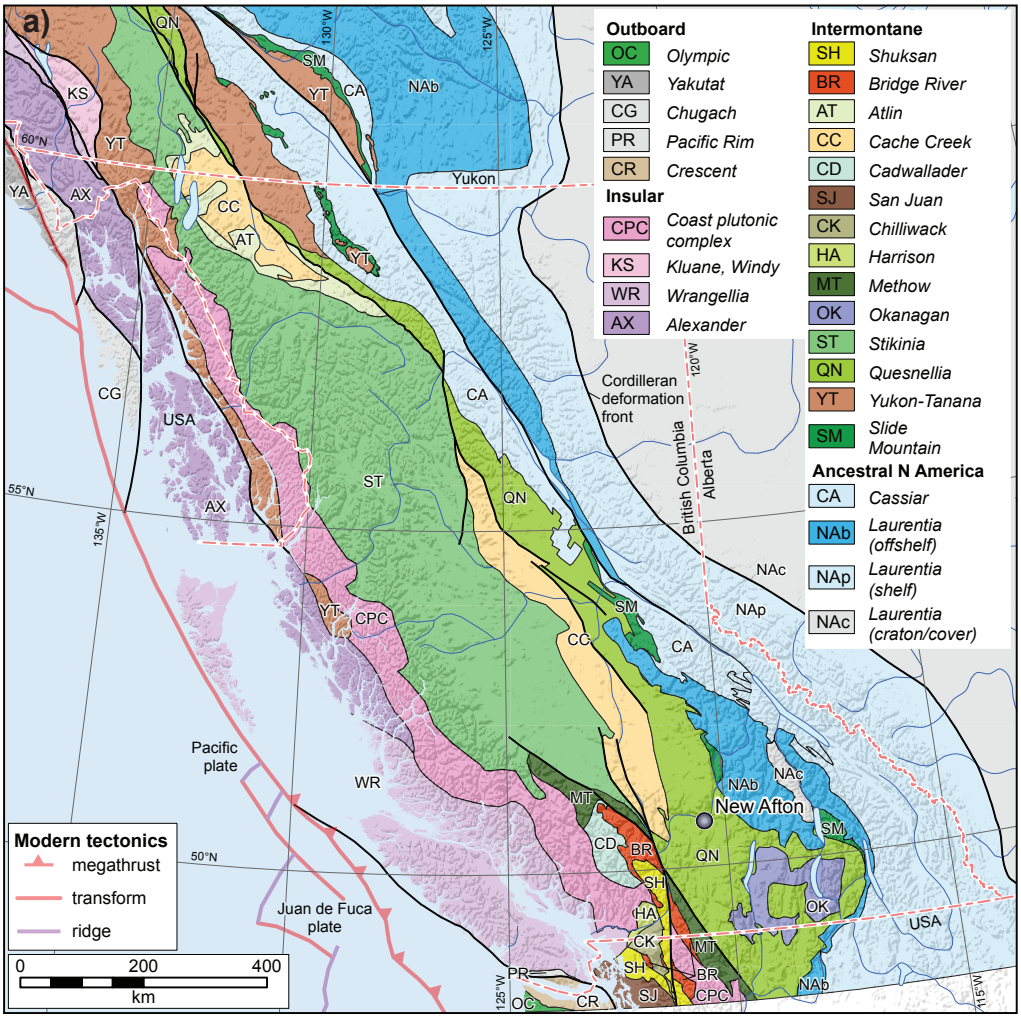


Fig. 1. a) Location of the New Afton deposit in British Columbia. Terranes modified from Colpron (2020). **b)** Locations of alkalic porphyry deposits in Quesnel and Stikine terranes and the location of the Iron Mask batholith; modified after Logan and Mihalynuk (2014).

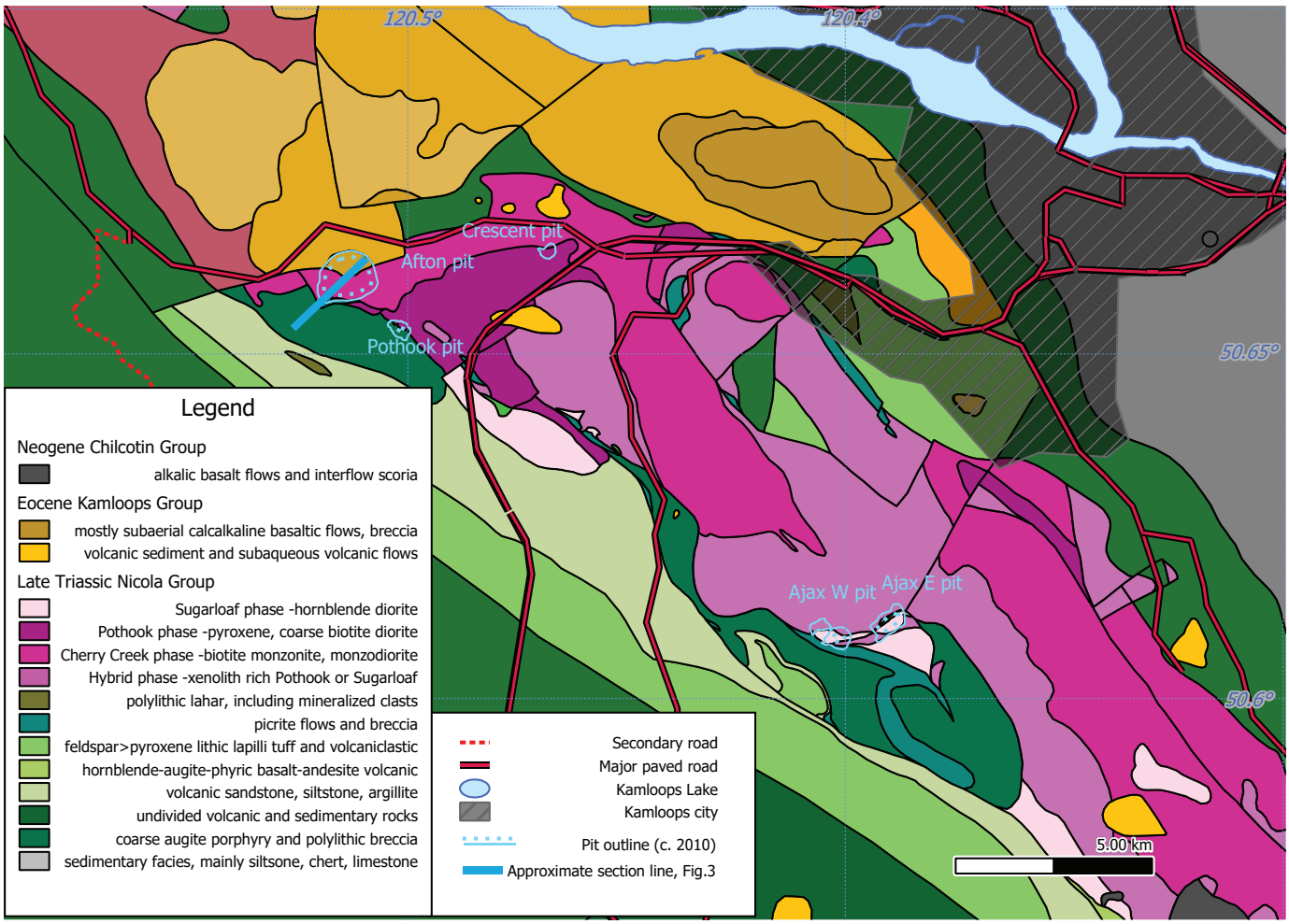


Fig. 2. Geologic map showing the location of the New Afton deposit and other porphyry deposits in the Iron Mask batholith. Modified after Logan et al. (2006) and Diakow and Mihalynuk (unpublished).

in 2024 produced an ore concentrate containing 62% copper with 2.95 g/t of recoverable Pd (Parson et al., 2024). In this paper, we report on the mineralogical and textural features of rock types with anomalous PGE contents, and on microscale mineral affinities and distributions of PGM in the New Afton underground deposit. We highlight the occurrence of PGM throughout the paragenesis of mineralization and importantly, in secondary mineralization not typically targeted for production at New Afton, such as Fe oxide veins, Fe oxide-apatite veins, and late-stage carbonate veins.

2. Alkalic porphyry deposits

Porphyry deposits are low-grade high tonnage magmatic-hydrothermal deposits that can be subdivided into calc-alkalic and alkalic varieties based on the composition of causative intrusions (Cooke et al., 2005; Sillitoe, 2010). In British Columbia, alkalic Cu-Au porphyry deposits occur mainly in arc settings (e.g., Logan and Mihalynuk, 2014) and are classically associated with silica-undersaturated to saturated intrusive rocks (Barr et al., 1976; Sillitoe, 2010). A distinctive feature of alkalic porphyries is their discrete, magnetite-rich alteration footprints. These footprints commonly comprise a high-temperature potassic (biotite-K-feldspar-magnetite), calc-potassic (epidote-magnetite-actinolite-K-feldspar±garnet-apatite), or calc-sodic (albite-epidote±diopside) cores surrounded by zones of sericite-anhydrite-carbonate and propylitic alteration (Lang et al., 1995a, b; Polar, 2025). High-grade mineralization in alkalic porphyry deposits is most commonly associated with potassic and calc-potassic alteration (Cooke et al., 2007; Polar, 2025).

A number of studies have highlighted elevated PGE concentrations in alkalic porphyry deposits and alkaline igneous complexes in British Columbia (Fig. 1b), including Mt. Polley (Pass et al., 2009; Pass, 2010), Galore Creek (Lang et al., 1995b; Thompson et al., 2002), Lorraine (Nixon, 2003a; Nixon and Peatfield, 2003), Mt. Milligan (LeFort et al., 2011), Kwanika (Karatas Ahmadli, 2025), Ajax East, New Afton (Nixon, 2003b; Hanley et al., 2020; Robb et al., 2023; Boucher et al., 2023), and the Whiterocks Mountain and Sappho alkaline complex (Nixon, 2001, 2002; Nixon and Carbno, 2001; Nixon and Archibald, 2002). Thompson et al. (2002) examined heavy mineral concentrates from Galore Creek, Lorraine, Mt. Milligan, Mt. Polley, and Ajax East and noted that high PGE values were associated

with a mixture of sulphides (bornite, chalcopyrite, and pyrite) and oxides (magnetite and hematite), suggesting that the PGE-bearing mineral phases were part of ore-stage sulphide-oxide mineralization. Additional work by Robb et al. (2023), Boucher et al. (2023), and Karatas Ahmadli (2025) examined the distribution of PGEs in the New Afton and Kwanika deposits and further showed that high PGE values correlate with PGE-bearing mineral phases.

3. The New Afton deposit

The New Afton deposit (Late Triassic; 204.5 ±0.6 to 201.39 ±0.75 Ma; U-Pb zircon; Logan et al., 2007; Logan and Mihalynuk, 2014) is one of several centres of alkalic porphyry mineralization in the southern Quesnel terrane related to the Iron Mask batholith (Logan and Mihalynuk, 2005; Logan et al., 2006, 2007; Lipske et al., 2020, 2021). The southern portion of the Quesnel terrane is predominantly a Late Triassic volcanic arc, comprising volcanic and volcanosedimentary rocks (Nicola Group) and allied plutonic rocks (Logan et al., 2007; Mihalynuk et al., 2016; Mihalynuk and Diakow, 2020).

At the New Afton deposit (Figs. 2, 3) mineralization is spatially associated with porphyritic monzonite rocks that intrude Nicola Group, andesitic to picritic basalt flows, breccias, and tuffs (Hall and May, 2013; Lipske et al., 2020). The Cu-Au mineralization comprises chalcopyrite±bornite, lesser chalcocite-covellite, and sulphosalts that occur in veinlets, breccias, and disseminated sulphides within potassic, calc-potassic, and calc-sodic alteration zones, primarily in Nicola Group volcanic rocks, monzodiorite and, to a lesser extent, diorite intrusions (e.g., Polar, 2025). The mineralization is structurally controlled, with steep north-trending extensional structures interpreted as the principal conduits for emplacement of both magmas and magmatic-hydrothermal fluids (e.g., Hall and May, 2013; Polar, 2025).

Mineralized zones in the New Afton deposit contain elevated Pd and variably elevated Pt; Pd-Pt occurs in association with pyrite and chalcopyrite and with Pd-Pt-Sb-As-Te-Hg ±Bi PGM (temagamite, isomertieite, mertieite, cooperite, naldrettite, sperrylite, moncheite, and kotulskite). Boucher et al. (2023) showed that high PGE concentrations are associated with Co-Ni-bearing pyrite having growth zones defined by variations in PGE concentrations. Similarly, Robb et al. (2023) noted that PGM are most common in areas where whole-rock assays for Pd+Pt are >1 ppm and typically with elevated Au grades.

Although magnetite enrichment is common in alkalic deposits, Fe oxide-apatite veins are not. At the New Afton deposit, Fe oxide-apatite veins are a characteristic feature (Polar, 2025 and referenced therein) and appear to have an association with Cu-Au and PGE-enrichment that is not well understood.

4. Methods

4.1. Sample selection

Samples used in this study were collected during the summer of 2024, targeting high-PGE grade intersections in drill core cut between 2006 and 2022. Sample selection focused on

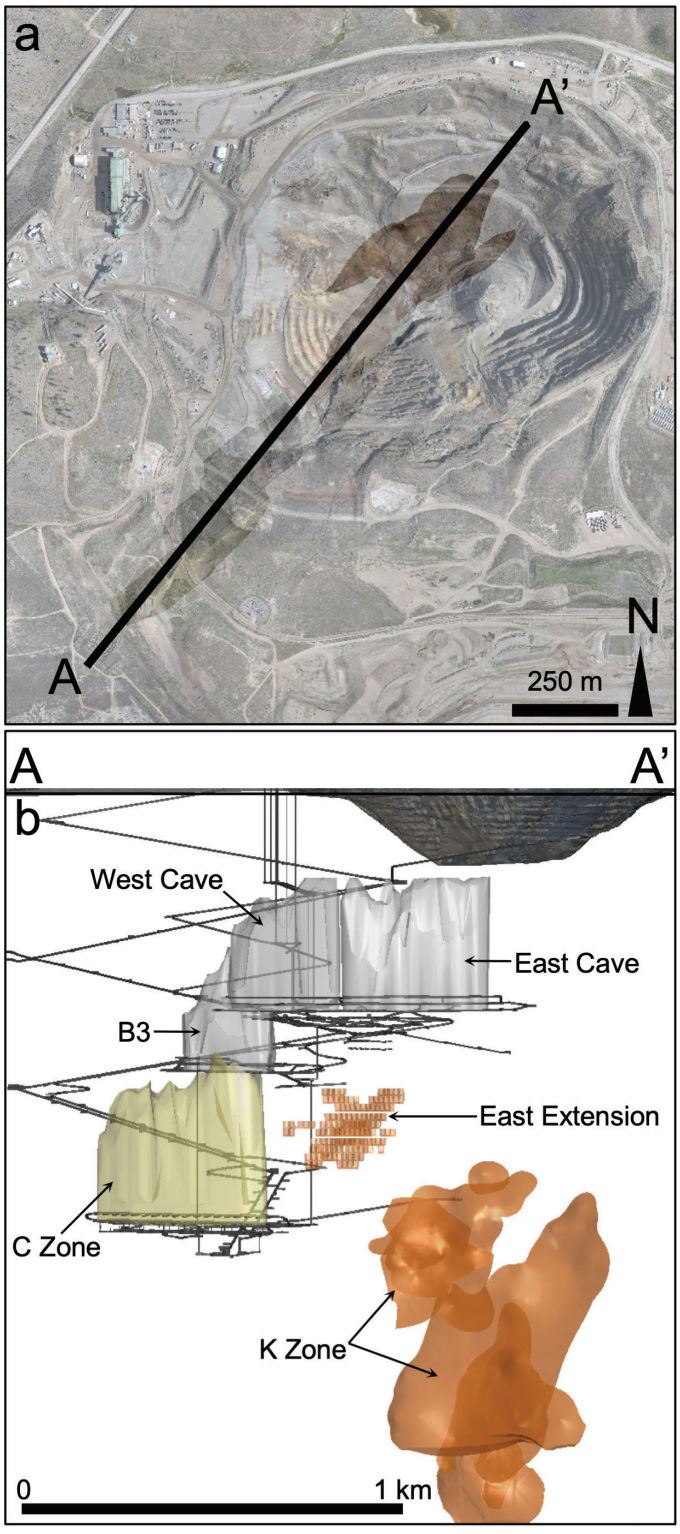


Fig. 3. a) Satellite image of the New Afton open pit showing the section line for b). **b)** Schematic 3D cross-section of the New Afton open pit showing the location of ore zones. Grey shapes (East Cave, West Cave, B3) denote volumes that have already been mined. The gold shape (C zone) denotes a volume currently under production. The orange shapes denote unmined parts of the deposit. No vertical exaggeration. Images courtesy of New Gold Inc.

zones with correlated elevations of Co, Ni, and PGE contents, typically where 2 m assay intervals returned >100 ppm Co, >100 ppm Ni, or >0.1 ppm PGE_{tot}, or on intervals displaying characteristic alteration and mineralization styles. Core samples were typically 10-20 cm long intervals halved into subsamples for analysis and archiving. A total of 38 samples were selected from the C, West Cave, East Cave, East Extension, B3, and K zones (Fig. 3b) for SEM-MLA analysis. We focus here on samples from the West Cave and C zones.

4.2. Scanning electron microscopy-mineral liberation analysis (SEM-MLA)

Quantitative mineral studies were conducted at Memorial University of Newfoundland's CREAIT Microanalysis Facility using a FEI Quanta field emission gun 650 scanning electron microscope (SEM) equipped with mineral liberation analysis (MLA) software version 3.14 (Sylvester, 2012; Grant et al., 2018; Beranek et al., 2023). Instrument conditions included a 25 kV accelerating voltage, 13.5 mm working distance, and 10 nA beam current. The MLA frames were 1.5 by 1.5 mm with a resolution of 500 by 500 pixels. Backscatter electron (BSE) images of each frame were used to identify features based on the contrast in the BSE signal across mineral grain boundaries. Features were identified at a baseline resolution of 30 µm, or less in cases where adjacent mineral grains had dramatically different contrast in BSE images. MLA maps were created using GXMAP mode by acquiring energy-dispersive X-ray spectra at a grid spacing of 10 pixels, with a spectral dwell time of 12 ms, and comparing them against an in-house library of mineral reference spectra. The accuracy of mineral identification was verified using in situ imaging and point analysis in the CREAIT Microanalysis Facility during SEM-MLA data collection. MLA images were then processed in Adobe® Photoshop® to highlight various features, such as mineralogical contrast, crosscutting relationships, and key mineral phases.

5. Results

Platinum group minerals were detected in samples from the C (n=7), West Cave (n=4), and East Extension (n=3) zones and comprise discrete Pd-Pt-Sb-As-Bi mineral phases. In all cases, PGM are closely associated with electrum and tetrahedrite (Fig. 4; Figs. 5a, d), and in most cases, Ag-Hg tellurides. Samples lacking PGM, including those from the B3, East Cave, and K zones, typically contained abundant electrum and tetrahedrite, with variable Ag-Hg tellurides, but were not evaluated further in this study. The highest PGM abundances (on the basis of particle count and area % per sample) are in samples from the West Cave and C zones.

5.1. PGE minerals in C zone samples

PGM in the C zone are associated with disseminated sulphides, sulphide-carbonate±quartz veins, Fe oxide-sulphide veins, and Fe oxide-apatite veins. PGM are most abundant in samples of specular hematite-rich Fe oxide-sulphide veins (Fig. 5) and Fe oxide-apatite veins (Fig. 6).

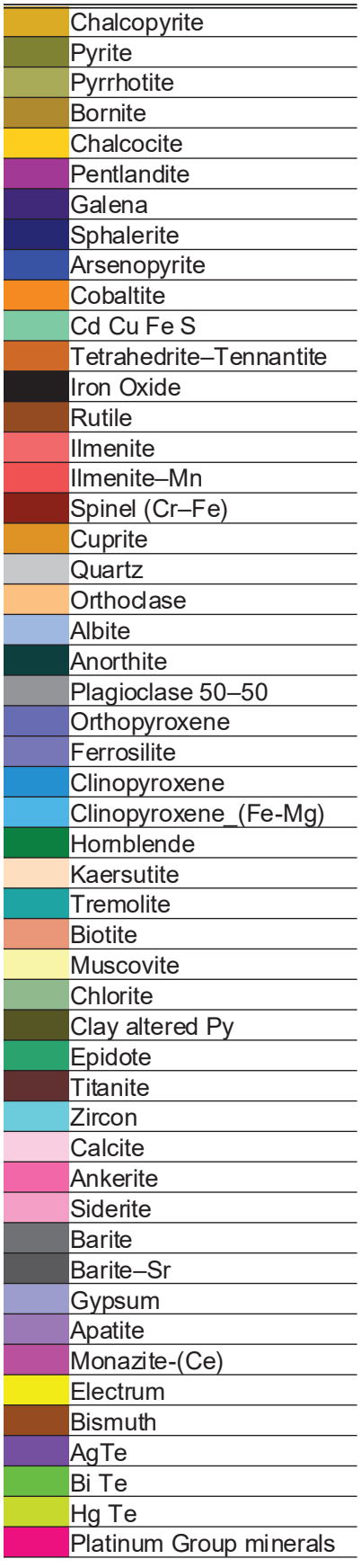
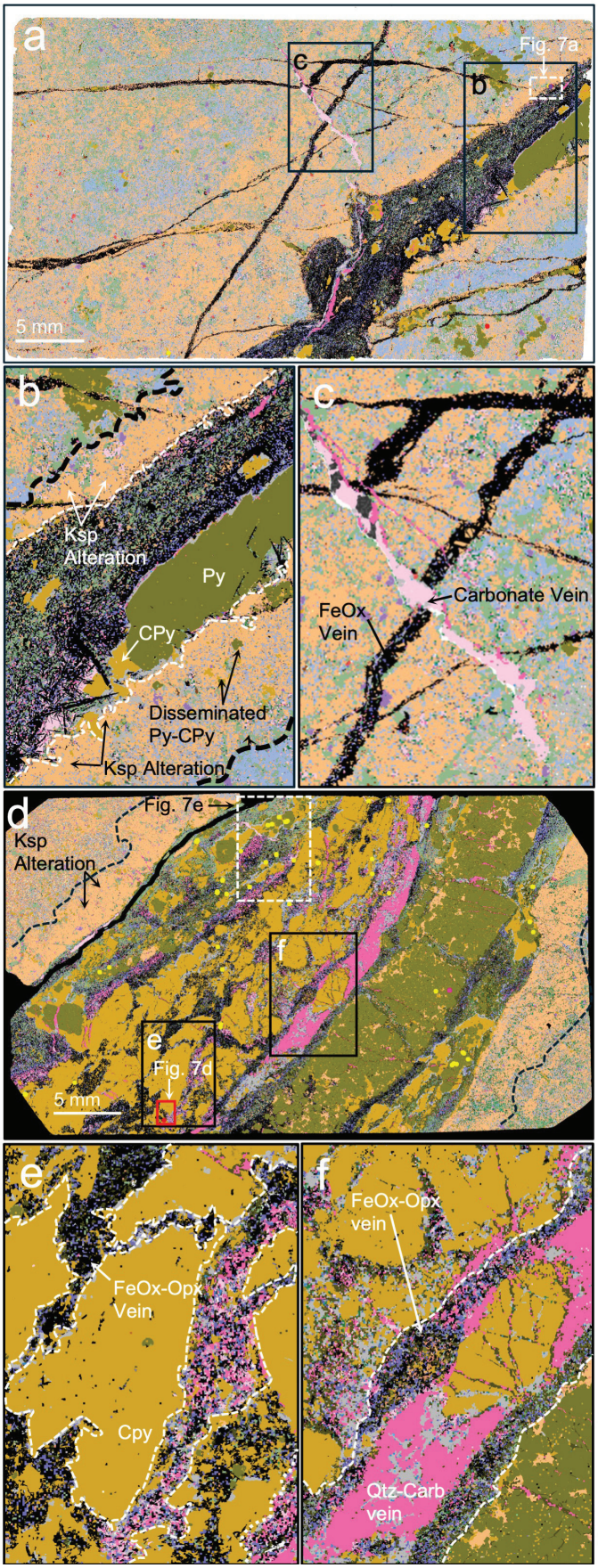


Fig. 4. Legend for the colour SEM-MLA maps in Figures 5-10.



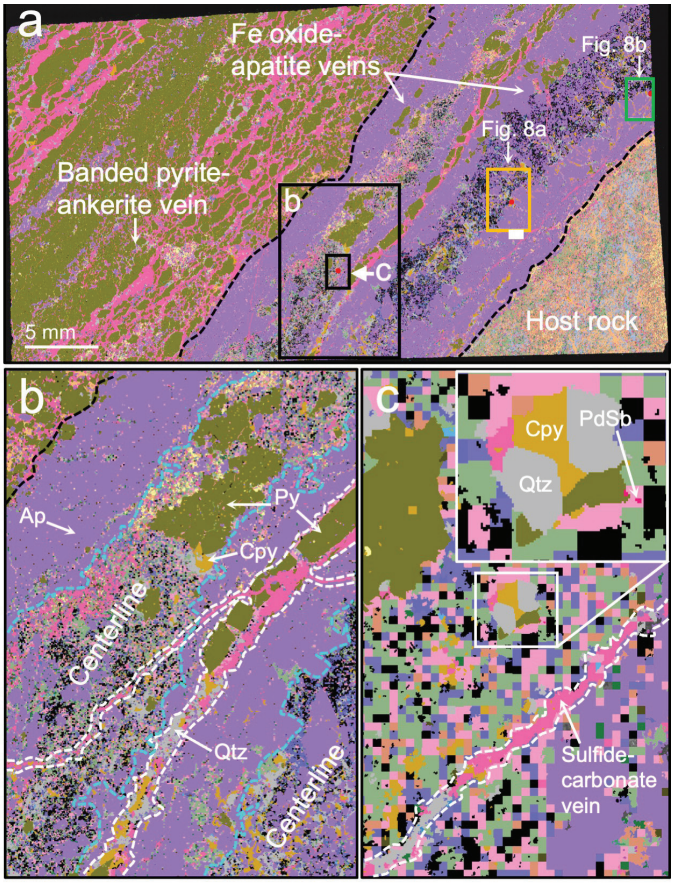


Fig. 6. a) Colour maps of sample 206-18G showing an Fe oxide-apatite vein from the C zone. The inset image in Figure 8a is outlined in orange. The inset image shown in Figure 8b is outlined in green. Red dots denote the location of PGM grains. **b)** Inset image showing the centreline of an Fe oxide-apatite vein and a subparallel, crosscutting sulphide-carbonate vein. **c)** Inset image showing the location of intergrown calcite, quartz (Qtz), pyrite (Py), and chalcopyrite (CPy) hosting a grain of PdSb in the centreline mineralogy.

Fig. 5. Colour maps of selected samples from the C zone. **a)** Colour map of sample 206-18M showing a sulphide-poor Fe oxide-sulphide vein. The area shown in Figure 7a is outlined with a white dashed line. **b)** Inset image showing the edges of the Fe oxide-sulphide vein (outlined with a dashed white line), the outer edge of the potassic (Ksp) alteration halo (outlined with a black dashed line) and disseminated pyrite (Py) and chalcopyrite (CPy). **c)** Secondary carbonate veins crosscutting earlier Fe-oxide veins. **d)** Colour maps of sample 206-18N showing a sulphide-rich Fe oxide-sulphide vein. Red dot denotes the location of PGM grains. Yellow dots denote the location of electrum grains. The area shown in Figure 7d, is outlined in red. The area shown in Figure 7e, is outlined with a white dashed line. **e, f)** Inset images showing banding of coarse sulphides and the fine-grained intergranular gauge mineralogy. Note the later-stage carbonate-sulphide vein (outlined with a white dashed line) crosscutting the earlier sulphides in f).

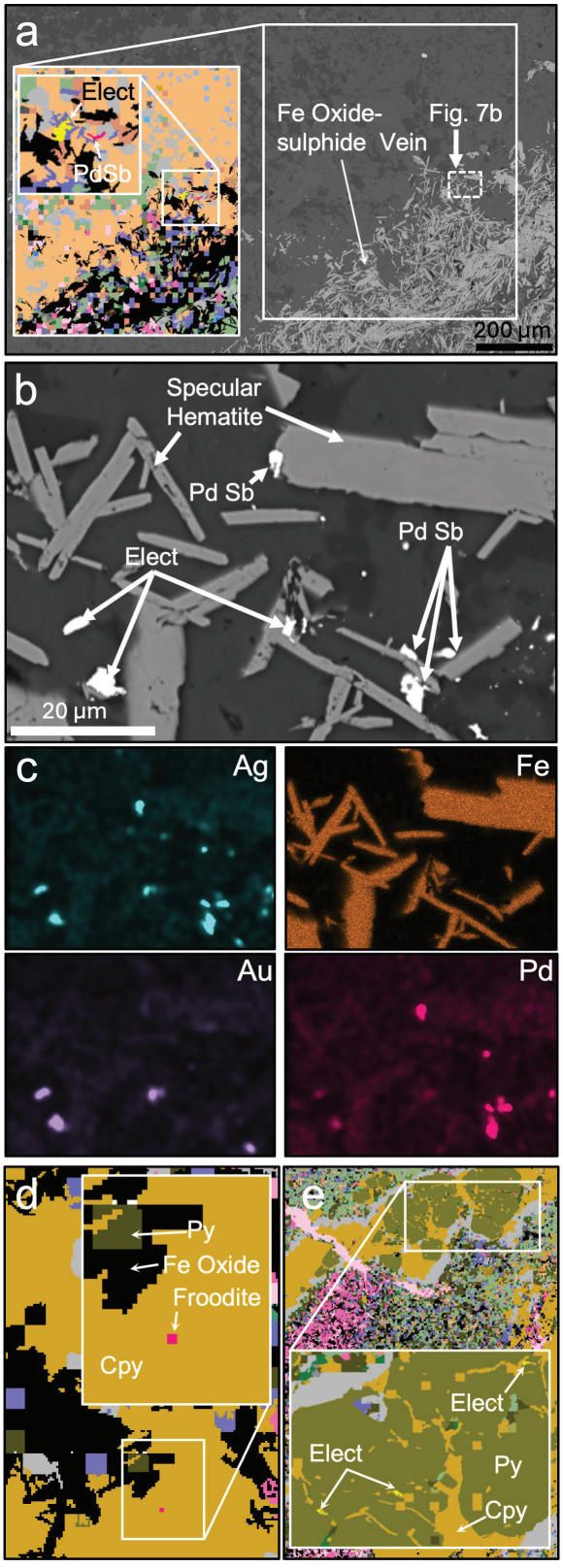


Fig. 7. a) BSE image with MLA inset image showing electrum and PdSb along the edge of the sulphide-poor Fe oxide (FeOx)-sulphide vein shown in Figure 5a. **b, c)** Close-up BSE image and corresponding EDS maps showing intergrown PdSb, electrum (Elect), and specular hematite. **d, e)** Inset images outlined on Figure 5d showing a froodite grain and electrum hosted in chalcopyrite.

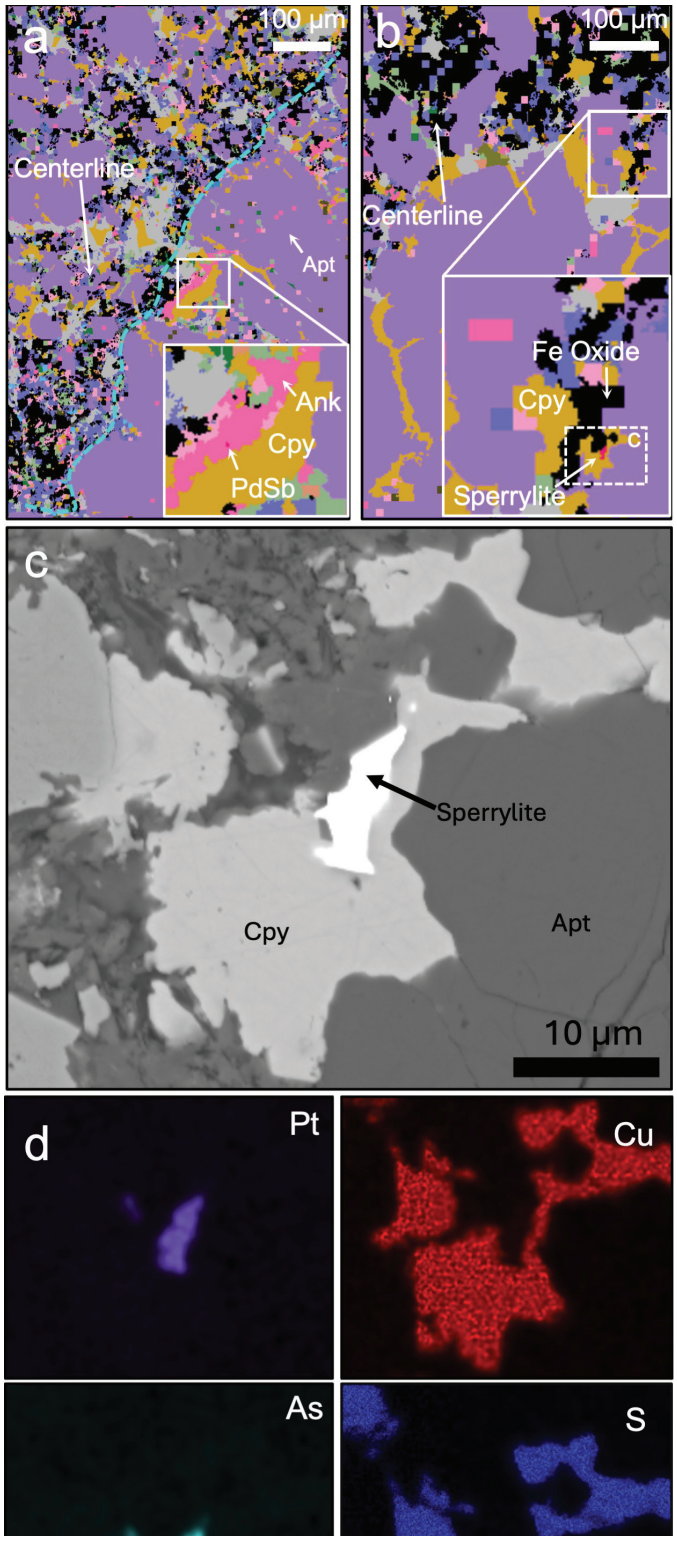


Fig. 8. Images of outlined areas shown in Figure 6a. **a)** Carbonate- and **b)** Chalcopyrite-hosted PdSb and sperrylite in the centreline of a comb-textured Fe oxide-apatite vein. **c)** Close-up BSE image and **d)** Corresponding EDS maps of the chalcopyrite-hosted sperrylite grain shown in b). Area of panels in d) is the same as that shown in c). Ap=apatite; Ank=ankerite.

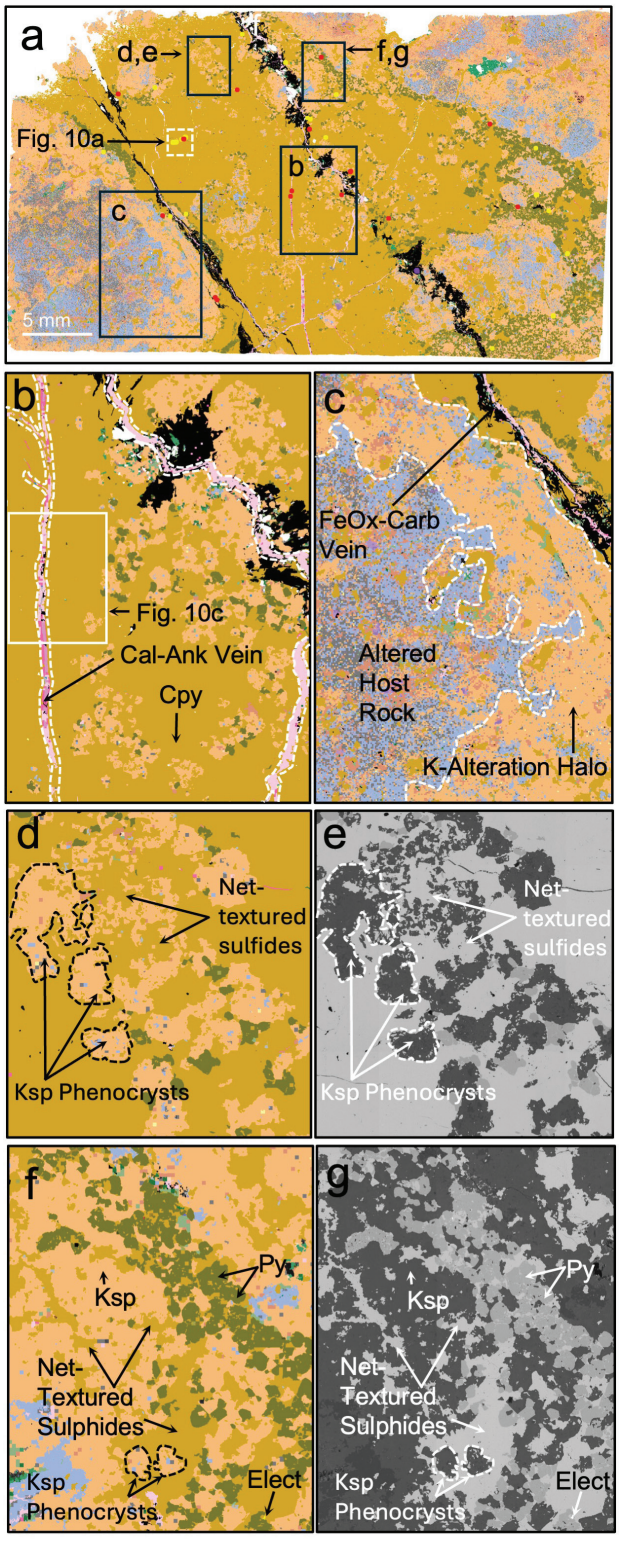


Fig. 9. a) Colour maps of a sulphide vein from the West Cave zone (Sample 210-34J). Red dots denote the location of PGM grains. Yellow dots denote the location of electrum grains. The white dashed square indicates the location of Figure 10a. **b)** Inset image showing calcite-ankerite (Cal-Ank) veins crosscutting primary chalcopyrite. White rectangle indicates location of Figure 10c. **c)** Inset image showing the intense potassic (K) alteration halo along the edges of the sulphide vein. **d, f)** Colour maps and corresponding BSE images **e, g)** of net-textured chalcopyrite surrounding euhedral orthoclase crystals.

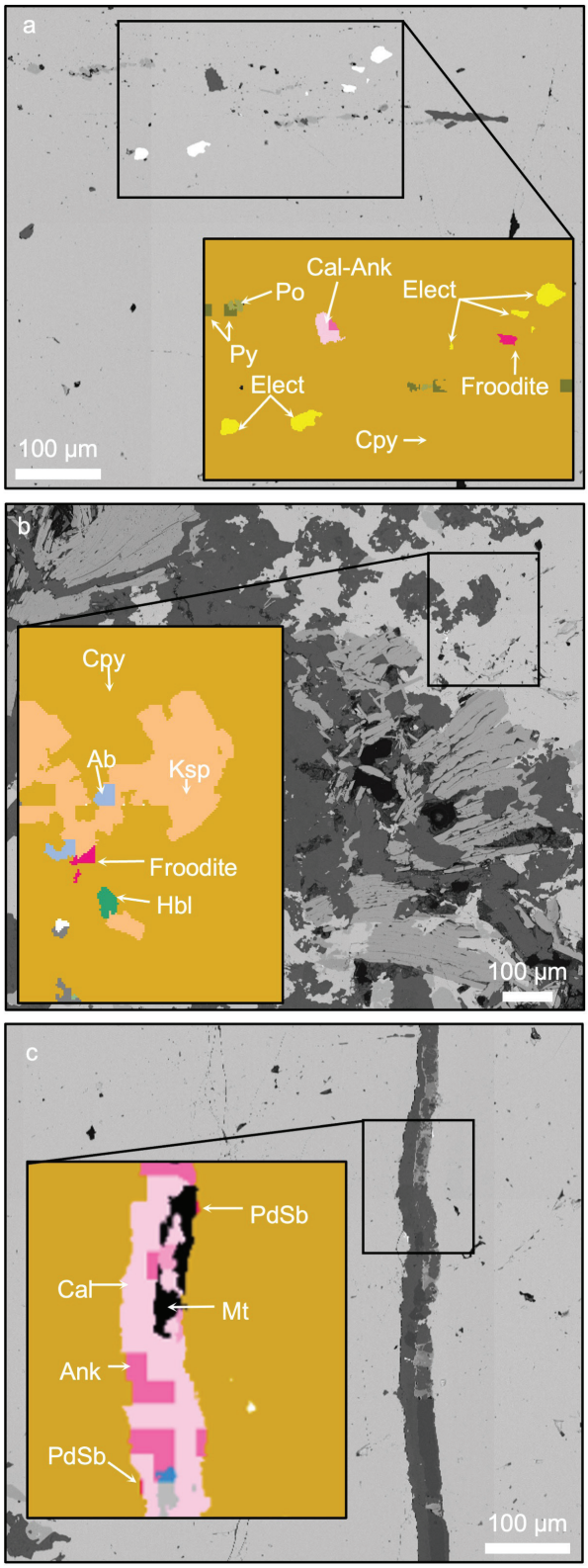


Fig. 10. a) BSE image with MLA inset image showing electrum and froodite grains in chalcopyrite. See Figure 9a for context. **b)** BSE image with MLA inset image showing a froodite grain associated with net-textured chalcopyrite. See Figure 9c for context **c)** Secondary calcite-ankerite (Cal-Ank) vein with PbSb grains along its margins. See Figure 9b for context. Mt=Magnetite; Ab=Albite; Hbl=hornblende; Ksp=orthoclase.

5.1.1. Specular hematite-rich Fe oxide-sulphide veins

In the C zone, PGM-bearing specular hematite-rich Fe oxide-sulphide veins commonly crosscut sodic-potassic-altered host rock and are surrounded by halos of intense potassic alteration with variable concentrations of disseminated pyrite and chalcopyrite (Figs. 5b, c, d). The veins range in composition and texture from predominantly specular hematite with subordinate pyrite-chalcopyrite and intergranular carbonate-magnetite-epidote-feldspar-quartz-pyroxene (i.e., sulphide-poor; Figs. 5a, c), to predominantly pyrite-chalcopyrite surrounded by fine-grained Fe oxide-carbonate-epidote-feldspar-quartz-pyroxene (i.e., sulphide-rich; Figs. 5d-f). In both cases, the sulphide minerals are typically concentrated along vein margins (Fig. 5b) or cores (Figs. 5d-f). Commonly, the most sulphide-rich veins have a banded appearance and are composed of multiple, parallel sets of veins (Figs. 5d, 6). Both the sulphide-poor and sulphide-rich veins are crosscut by carbonate-quartz-sulphide veins (Figs. 5c, 6b).

PGE minerals in sulphide-poor veins include PdSb alloy and froodite ($PdBi_2$). Pb-Sb alloy is commonly found together with electrum and intergrown with specular hematite and fine-grained silicates along vein margins (Fig. 7) or in the disseminated pyrite. Froodite is accompanied by electrum and occurs as crystals intergrown with chalcopyrite in sulphide-rich veins (Figs. 7d, e). PGM in sulphide-poor and sulphide-rich Fe oxide-sulphide veins from the East Extension zone display similar textures and mineral associations but are hosted in veins with more intense sodic-calcic alteration.

5.1.2. Fe oxide-apatite veins

PGM-bearing Fe oxide-apatite veins sampled from the C zone contain comb-textured apatite at vein margins with vein centrelines composed of fine-grained Fe oxide-carbonate-quartz-pyroxene-epidote-chlorite-sulphide (Fig. 6). Sulphide in this setting ranges in texture and composition from pyrite to fine-grained intergranular chalcopyrite (Figs. 6b, c). The Fe oxide-apatite veins are commonly part of larger banded sulphide veins, as seen in Figure 6a where two parallel Fe oxide-apatite veins are bound on one side by sodic-potassic altered host rock and on the other by a parallel banded pyrite-ankerite vein (Fig. 6b). The two Fe oxide-apatite veins in this instance are separated by and crosscut by a parallel pyrite-ankerite veinlet of ankerite.

PGM associated with Fe oxide-apatite veins include PdSb alloy and sperrylite ($PtAs_2$; Figs. 8c, d) intergrown with chalcopyrite, carbonate, and Fe oxide along the centrelines of the veins (e.g., Fig. 6c; Figs. 8a, b). PGM in this setting. PGE minerals in Fe oxide-apatite veins from the East Extension zone display similar textures and mineral associations.

5.2. PGE minerals in West Cave zone samples

PGM are present in four samples from the West Cave zone. In this zone, they are predominantly hosted in sulphide veins (e.g., Figs. 9, 10) and in disseminated sulphides within host rocks, which are overprinted by intense sodic-potassic and potassic alteration. Sparse PGM are also present in Fe oxide-sulphide and Fe oxide-apatite veins.

5.2.1. Sulphide veins

PGM-bearing sulphide veins display intense halos of potassic alteration where they crosscut sodic-potassic altered host rocks. They are, in turn, cut by carbonate and carbonate-Fe oxide-filled fractures (Figs. 9a-c). Sulphide veins contain massive chalcopyrite with abundant pyrite along the vein margins. In the veins, chalcopyrite surrounds K-feldspar crystals and exhibits a net-textured appearance (Figs. 9d-g). Chalcopyrite veins in the C zone have a similar net-textured appearance and contain electrum.

PGM observed in sulphide veins include PdSb alloy and froodite (Fig. 10). Froodite most commonly occurs with chalcopyrite, electrum, and orthoclase displaying net-textured sulphides (Figs. 10a, b). PdSb alloy most commonly occurs along the margins of carbonate-Fe oxide-filled fractures where they crosscut earlier chalcopyrite veins (Fig. 10c).

6. Discussion

PGM in the C and West Cave zones are hosted by early Fe oxide-apatite veins, ore-stage Fe oxide-sulphide veins, and late-stage carbonate veins. This suggests PGE mobilization, enrichment, and deposition under variable oxidation and sulfidation conditions at multiple times during the formation of the New Afton deposit.

The mineralogic and textural associations of PGM described in this paper are consistent with those presented by Robb et al. (2023) and Boucher et al. (2023) and with observations of PGE mineralization in other alkalic porphyry deposits in British Columbia (Pass, 2010; LeFort et al., 2011), including nearby deposits also within the Iron Mask batholith (Nixon and Leflamme, 2002; Nixon, 2003b; MacKenzie, 2009). In their study of PGE mineralization in the New Afton deposit, Robb et al. (2023) and Boucher et al. (2023) concluded that PGE enrichment in sulphides occurred during the formation of early- and main-stage hypogene mineralization via discrete pulses of high-temperature magmatic fluids and under conditions of fluctuating temperature, fO_2, and fS_2. PGM abundances increased during remobilization of PGEs from hypogene sulphides during secondary hydrothermal processes involving the formation of carbonate-rich, oxidized alteration assemblages (Robb et al., 2023; Boucher et al., 2023). Observations presented here, including PGM in hypogene Cu-Au mineralization and late-stage carbonate veins, are consistent with those presented by Robb et al. (2023) and Boucher et al. (2023) and likely reflect a similar model of fluid evolution and deposit formation.

7. Conclusion

This study and previous studies examining PGE enrichment in deposits like New Afton highlight that critical metals such as PGEs, Co, and Te, can occur as potentially economic byproducts on the deposit scale but be overlooked during exploration and

processing. Our study demonstrates the utility of quantitative SEM-MLA in rapidly recognizing and characterizing subtle mineralogic features associated with enrichment of PGEs.

Acknowledgments

We thank Dr. Evan Orovan (Thesis Gold), Dr. Stephen Piercey (Memorial University), Sean Tombe and Devin Wade (New Gold) for their reviews, which substantially improved this paper. We also thank Sean Tombe and Devin Wade for their help with accessing the drill core and arranging fieldwork at the New Afton deposit. Kaitlyn McLaren (BCGS) provided geographic information system support.

References cited

Bain, W.M., de Waal, F., and Goudie, D.J., 2025. Co-Te mineralization in iron skarns on Vancouver Island and Texada Island. In: Geological Fieldwork 2024, British Columbia Ministry of Mining and Critical Minerals, British Columbia Geological Survey Paper 2025-01, pp. 153-175.

Barr, D.A., Fox, P.E., Northcote, K.E., and Preto, V.A., 1976. The alkaline suite porphyry deposits: A summary. In: Sutherland Brown, A., (Ed.), Porphyry Deposits of the Canadian Cordillera. Canadian Institute of Mining and Metallurgy, Special Volume 15, pp. 359-367.

Beranek, L.P., Hutter, A.D., Pearcey, S., James, C., Langor, V., Pike, C., Goudie, D., and Oldham, L., 2023. New evidence for the Baltican cratonic affinity and Tonian to Ediacaran tectonic evolution of West Avalonia in the Avalon Peninsula, Newfoundland, Canada. Precambrian Research, 390. <https://doi.org/10.1016/j.precamres.2023.107046>

Bissig, T., and Cooke, D.R., 2014. Introduction to the Special Issue devoted to alkalic porphyry Cu-Au and epithermal Au deposits. Economic Geology, 109, 819-825. <https://doi.org/10.2113/econgeo.109.4.819>

Boucher, B.M., Robb, S.J., Hanley, J.J., Kerr, M.J., and Mungall, J.E., 2023. Platinum-group elements (PGE) in the New Afton alkalic Cu-Au porphyry deposit, Canadian Cordillera, I: Relationships between PGE, accessory metals and sulfur isotopes in pyrite. Frontiers in Earth Science, 11. <https://www.frontiersin.org/journals/earth-science/articles/10.3389/feart.2023.819129/full>

Colpron, M., 2020. Yukon terranes-A digital atlas of terranes for the northern Cordillera. Yukon Geological Survey. <https://data.geology.gov.yk.ca/Compilation/2#InfoTab>

Cooke, D.R., Hollings, P., and Walshe, J.L., 2005. Giant porphyry deposits: Characteristics, distribution, and tectonic controls. Economic Geology, 100, 801-818.

Cooke, D.R., Wilson, A.J., House, M.J., Wolfe, R.C., Walshe, J.L., Lickfold, V., and Crawford, A.J., 2007. Alkalic porphyry Au-Cu and associated mineral deposits of the Ordovician to Early Silurian Macquarie Arc, New South Wales. Australian Journal of Earth Sciences, 54, 445-463. <https://doi.org/10.1080/08120090601146771>

Grant, D.C., Goudie, D.J., Voisey, C., Shaffer, M., and Sylvester, P., 2018. Discriminating hematite and magnetite via Scanning Electron Microscope-Mineral Liberation Analyzer in the -200 mesh size fraction of iron ores. Applied Earth Science, 127, 30-37. <https://doi.org/10.1080/03717453.2017.1422334>

Gunn, G., 2014. Platinum-group metals. In: Gunn, G., (Ed.), Critical Metals Handbook. John Wiley & Sons, pp. 284-311.

Hall, R.D., and May, B.B., 2013. Geology of the New Afton porphyry copper-gold deposit, Kamloops, British Columbia, Canada. In: Logan, J., and Schroeter, T., (Eds.), Porphyry Systems of Central and Southern BC: Prince George to Princeton. Society of Economic Geologists Field Trip Guidebook 44, pp. 117-128.

Hanley, J., Kerr, M., LeFort, D., Warren, M., MacKenzie, M., and Sedge, C., 2020. Enrichment of platinum-group elements (PGE) in alkalic porphyry Cu-Au deposits in the Canadian Cordillera: New insights from mineralogical and fluid inclusion studies. In: Lang, J.R., Sharman, E.R., and Chapman, J.B., (Eds.), Porphyry Deposits of the Northwestern Cordillera of North America: A 25-Year Update. Canadian Institute of Mining, Metallurgy and Petroleum, Special Volume 57, pp. 88-109.

Hickin, A.S., Ootes, L., Orovan, E.A., Brzozowski, M.J., Northcote, B.K., Rukhlov, A.S., and Bain, W.M., 2024. Critical minerals and mineral systems in British Columbia. In: Geological Fieldwork 2023, British Columbia Ministry of Energy, Mines and Low Carbon Innovation, British Columbia Geological Survey Paper 2024-01, pp. 13-51.

Hofstra, A.H., and Kreiner, D.C., 2020. Systems-deposits-commodities-critical minerals table for the Earth Mapping Resources Initiative (ver. 1.1). U.S. Geological Survey Open File Report 2020-1042, 26 p. <https://doi.org/10.3133/ofr20201042>

Karatas Ahmadli, C., 2025. Platinum-group elements and gold deportment in the Kwanika copper-gold±molybdenum porphyry system, British Columbia, Canada. Unpublished M.Sc. thesis, The University of British Columbia, Vancouver, Canada, 298 p.

Lang, J.R., and Stanley, C.R., 1995a. Contrasting styles of alkalic porphyry Cu-Au deposits in the northern part of the Iron Mask batholith, Kamloops, British Columbia. Canadian Institute of Mining and Metallurgy, Special Volume 46, pp. 581-592.

Lang, J.R., Stanley, C.R., Thompson, J.F.H., and Dunne, K.P., 1995b. Na-K-Ca magmatic-hydrothermal alteration in alkalic porphyry Cu-Au deposits, British Columbia. Mineralogical Association of Canada Short Course 23, pp. 339-366.

LeFort, D., Hanley, J., and Guillong, M., 2011. Subepithermal Au-Pd mineralization associated with an alkalic porphyry Cu-Au deposit, Mount Milligan, Quesnel terrane, British Columbia, Canada. Economic Geology, 106, 781-808. <https://doi.org/10.2113/econgeo.106.5.781>

Lipske, J.L., Wade, D., Hall, R.D., and Petersen, M.A., 2020. Geology and mineralization of the New Afton Cu-Au alkalic porphyry deposit, Kamloops, British Columbia. In: Lang, J.R., Sharman, E.R., and Chapman, J.B., (Eds.), Porphyry Deposits of the Northwestern Cordillera of North America: A 25-Year Update. Canadian Institute of Mining, Metallurgy and Petroleum, Special Volume 57, pp. 648-667.

Lipske, J.L., Wade, D., Hall, R.D., and Petersen, M.A., 2021. Geology and mineralization of the new Afton Cu-Au alkalic porphyry deposits, Kamloops, British Columbia. In: Lang, J.R., Sharman, E.R., and Chapman, J.B., (Eds.), Porphyry Deposits of the Northwestern Cordillera of North America: A 25-Year Update. Canadian Institute of Mining, Metallurgy and Petroleum, Special Volume 57, pp. 648-667.

Logan, J.M., and Mihalynuk, M.G., 2005. Porphyry Cu-Au deposits of the Iron Mask Batholith, southeastern British Columbia. In: Geological Fieldwork 2004, British Columbia Ministry of Energy, Mines and Petroleum Resources, British Columbia Geological Survey Paper 2005-01, pp. 271-290.

Logan, J.M., and Mihalynuk, M.G., 2014. Tectonic Controls on Early Mesozoic Paired Alkaline Porphyry Deposit Belts (Cu-Au Ag-Pt-Pd-Mo) Within the Canadian Cordillera. Economic Geology, 109, 827-858. <https://doi.org/10.2113/econgeo.109.4.827>

Logan, J.M., Mihalynuk, M.G., Ullrich, T.D., and Friedman, R.M., 2006. Geology of the Iron Mask batholith. British Columbia Ministry of Energy, Mines and Petroleum Resources, British Columbia Geological Survey Open File 2006-11, 1:25,000 scale.

Logan, J.M., Mihalynuk, M.G., Ullrich, T., and Friedman, R.M., 2007. U-Pb ages of intrusive rocks and $^{40}Ar/^{39}Ar$ plateau ages of copper-gold-silver mineralization associated with alkaline intrusive centres at Mount Polley and the Iron Mask batholith, southern and central British Columbia. In: Geological Fieldwork 2006, British Columbia Ministry of Energy and Mines, British Columbia Geological Survey Paper 2007-01, pp. 93-116.

MacKenzie, M.K., 2009. Mineralogical controls on the distribution of platinum-group elements and gold in the Afton porphyry deposits, Kamloops, British Columbia. Unpublished B.Sc. thesis, Saint Mary's University, Halifax, Canada, 144 p.

Mihalynuk, M.G., and Diakow, L.J., 2020. Southern Nicola Arc geology (NTS 092H/7NE, 8NW, 9W, 10E, 15E, 16W; 092I/1SW, 2SE). British Columbia Ministry of Energy, Mines and Low Carbon Innovation, British Columbia Geological Survey Geoscience Map 2020-01, 1:50,000 scale.

Mihalynuk, M.G., Diakow, L.J., Friedman, R.M., and Logan, J.M., 2016. Chronology of southern Nicola Arc stratigraphy and deformation. In: Geological Fieldwork 2015, British Columbia Ministry of Energy and Mines, British Columbia Geological Survey Paper 2016-01, pp. 31-63.

Nixon, G.T., 2001. Alkaline-hosted Cu-PGE mineralization in British Columbia: The Whiterocks Mountain plutonic complex, south-central B.C. British Columbia Ministry of Energy and Mines, British Columbia Geological Survey Open File 2001-14, 1:20,000 scale.

Nixon, G.T., 2002. Alkaline hosted Cu-PGE mineralization: The Sappho alkaline plutonic complex, south-central B.C. British Columbia Ministry of Energy and Mines, British Columbia Geological Survey Open File 2002-07, 1:5000 scale.

Nixon, G.T., 2003a. Geological setting of the Lorraine Cu-Au porphyry deposit: New concepts. British Columbia Ministry of Energy and Mines, British Columbia Geological Survey GeoFile 2003-05 (poster).

Nixon, G.T., 2003b. Platinum-group elements in the Afton Cu-Au porphyry deposit, southern British Columbia. In: Geological Fieldwork 2003, British Columbia Ministry of Energy and Mines, British Columbia Geological Survey Paper 2004-01, pp. 263-290.

Nixon, G.T., and Archibald, D.A., 2002. Age of platinum group-element mineralization in the Sappho alkaline complex, south-central British Columbia. In: Geological Fieldwork 2001, British Columbia Ministry of Energy and Mines, British Columbia Geological Survey Paper 2002-01, pp. 171-176.

Nixon, G.T., and Carbono, B., 2001. Whiterocks Mountain alkaline complex, south-central British Columbia: Geology and PGE mineralization. In: Geological Fieldwork 2000, British Columbia Ministry of Energy and Mines, British Columbia Geological Survey Paper 2001-01, pp. 191-222.

Nixon, G.T., and Laflamme, J.H.G., 2002. Cu-PGE mineralization in alkaline plutonic complexes. British Columbia Ministry of Energy and Mines, British Columbia Geological Survey GeoFile 2002-02 (poster).

Nixon, G.T., and Peatfield, G.R., 2003. Geological setting of the Lorraine Cu-Au porphyry deposit, Duckling Creek Syenite Complex, north-central British Columbia. British Columbia Ministry of Energy and Mines, British Columbia Geological Survey Open File 2003-04, 24 p.

Nixon, G.T., Scheel, J.E., Scoates, J.S., Friedman, R.M., Wall, C.J., Gabites, J., and Jackson-Brown, S., 2020. Syn-accretionary multistage assembly of an Early Jurassic Alaskan-type intrusion in the Canadian Cordillera: U-Pb and $^{40}Ar/^{39}Ar$ geochronology of the Turnagain ultramafic-mafic intrusive complex, Yukon-Tanana terrane. Canadian Journal of Earth Sciences, 57, 464-480.

NRCan (Natural Resources Canada), 2024. Canada's critical minerals. <https://www.canada.ca/en/campaign/critical-minerals-in-canada/critical-minerals-an-opportunity-for-canada.html> (last accessed March 2026).

Parsons, J., Wade, D., Katchen, J., and Nadeau-Benoit, V., 2024. NI 43-101 Technical Report on the New Afton Mine, British Columbia, Canada. New Gold Inc., Technical Report, effective date December 31, 2024, 174 p. Available from: <http://sedar.com/>

Pass, H.E., 2010. Breccia-hosted chemical and mineralogical zonation patterns of the northeast zone, Mt. Polley Cu-Ag-Au alkalic porphyry deposit, British Columbia, Canada. Unpublished Ph.D. thesis, University of Tasmania, Hobart, Australia, 286 p. <https://doi.org/10.25959/23210969.v1>

Pass, H.E., Danyushevsky, L., Gilbert, S., Cooke, D.R., and Williams, P.J., 2009. LA-ICP-MS analyses of PGE in pyrite and Cu-sulfides from the Mount Polley alkalic porphyry Cu-Au deposit. In: Smart Science for Exploration and Mining, Proceedings of the 10th Biennial SGA Meeting, Townsville, Australia, pp. 738-740.

Polar, F.A.H.G., 2025. Geology and footprints of porphyry deposits in the Iron Mask District, British Columbia. Unpublished MSc. thesis, University of British Columbia, Vancouver, Canada, 618 p.

Robb, S.J., Boucher, B.M., Mungall, J.E., and Hanley, J.J., 2023. Platinum-group elements (PGE) in the New Afton alkalic Cu-Au porphyry deposit, Canadian Cordillera, II: PGE distribution and models for the hydrothermal coprecipitation of Co-Ni-Pd-Pt in pyrite. Frontiers in Earth Science, 11. <https://doi.org/10.3389/feart.2023.819109>

Rudnick, R.L., and Gao, S., 2014. Composition of the continental crust. In: Treatise on Geochemistry (2nd ed.), Elsevier, pp. 1-64. <https://doi.org/10.1016/B978-0-08-095975-7.00301-6>

Sillitoe, R.H., 2010. Porphyry copper systems. Economic Geology, 105, 3-41.

Sylvester, P.J., 2012. Use of the mineral liberation analyzer (MLA) for mineralogical studies of sediments and sedimentary rocks. In: Sylvester, P., (Ed.), Quantitative Mineralogy and Microanalysis of Sediments and Sedimentary Rocks: Mineralogical Association of Canada Short Course 4, pp. 1-16.

Thompson, J.F.H., Lang, J.R., and Stanley, C.R., 2002. Platinum group elements in alkaline porphyry deposits, British Columbia. In: Exploration and Mining in British Columbia 2001, British Columbia Ministry of Energy and Mines, British Columbia Geological Survey, pp. 57-64.

A multi-analytical approach to stream-sediment samples from modern drainages enhances the search for REE and rare metals

Alexei S. Rukhlov[1, a], Luke Ootes[1], Quinn F. Cunningham[1], Dylan Goudie[2], Anette von der Handt[3], Jody Spence[4], Corey Wall[5], and Shaun Barker[6]

[1] British Columbia Geological Survey, Ministry of Mining and Critical Minerals, Victoria, BC, V8W 9N3
[2] Core Research Equipment and Instrument Training (CREAIT) Network, Memorial University of Newfoundland, 45 Arctic Avenue, St. John's, NL, A1C 5S7
[3] Electron Microbeam & X-Ray Diffraction Facility, Department of Earth, Ocean and Atmospheric Sciences, The University of British Columbia, Vancouver, BC, V6T 2B4
[4] School of Earth and Ocean Sciences, University of Victoria, Victoria, BC, V8P 5C2
[5] Pacific Centre for Isotopic and Geochemical Research, Department of Earth, Ocean and Atmospheric Sciences, The University of British Columbia, Vancouver, BC, V6T 1Z4
[6] Mineral Deposits Research Unit, Department of Earth, Ocean and Atmospheric Sciences, The University of British Columbia, Vancouver, BC, V6T 2B4
[a] corresponding author: Alexei.Rukhlov@gov.bc.ca

Recommended citation: Rukhlov, A.S., Ootes, L., Cunningham, Q.F., Goudie, D., von der Handt, A., Spence, J., Wall, C., and Barker, S., 2026. A multi-analytical approach to stream-sediment samples from modern drainages enhances the search for REE and rare metals. In: Geological Fieldwork 2025, British Columbia Ministry of Mining and Critical Minerals, British Columbia Geological Survey Paper 2026-01, pp. 97-117.

Abstract

Mineralogical assessment of stream-sediment samples downstream of known carbonatite and related-rock occurrences confirms the occurrence of such rocks in the catchment basin upstream. Application of qualitative X-ray diffraction, quantitative evaluation of minerals by scanning electron microscopy (QEMSCAN®), scanning electron microscopy-mineral liberation analysis (SEM-MLA) and micro-X-ray fluorescence (μXRF) identify minerals such as columbite, pyrochlore supergroup, other Nb-Ta oxides, and REE carbonate contained in stream sediments. Chemistry of detrital minerals such as zircon and apatite and application of discrimination diagrams are further indicators of enhanced prospectivity of the drainages. These preliminary results suggest that micro-analysis (SEM-MLA, μXRF) on stream-sediment samples, in conjunction with detrital mineral chemistry, can enhance the interpretation of multivariate Regional Geochemical Survey (RGS) lithogeochemical anomalies of modern drainages and help identify prospective catchment basins for REE, Nb, Ta, and other commodities. The indicator-mineral approach applied to archived RGS samples informs prospectivity for critical minerals at a regional scale.

Keywords: Scanning electron microscopy-mineral liberation analysis (SEM-MLA), carbonatite, alkaline rock, stream sediment, heavy mineral concentrate (HMC), rare metals, rare earth elements (REE), zircon, apatite

1. Introduction

Niobium and rare earth elements (REE) are mainly produced from carbonatites and related silica-undersaturated and alkaline silicate rocks. British Columbia hosts numerous occurrences of these rocks along the western flank of Ancestral North America (Fig. 1), some of which contain REE and Nb-Ta mineralization (e.g., Mäder, 1987; Pell, 1994; Dalsin et al., 2015; Kulla and Hardy, 2015; Rukhlov et al., 2018). Based on Regional Geochemical Survey (RGS) data and machine learning, Rukhlov et al. (2024) evaluated the prospectivity of modern drainage catchments in terms of a multivariate critical mineral index. Samples with high scores of this index have a lithogeochemical response that suggests the occurrence of carbonatite- or related rock-hosted rare metals and REE in the catchment basin upstream.

This study continues the drainage prospectivity assessment (Rukhlov et al., 2025a). We consider previously reported lithogeochemical and new grain count data from two of our nine sampling sites (downstream of the Switch Creek and Ren (Ratchford Creek) carbonatites; Fig. 1) and provide new data from qualitative X-ray diffraction analysis, quantitative evaluation of minerals by scanning electron microscopy (QEMSCAN®), scanning electron microscopy-mineral liberation analysis (SEM-MLA), micro-X-ray fluorescence (μXRF), detrital zircon and apatite trace-element analysis, and U-Pb detrital zircon geochronology. Indicator minerals identified confirm the occurrence of carbonatites in the catchment basins upstream.

2. Sampling

We collected a total of 36 stream-sediment samples from nine drainage sites downstream of carbonatite and related-rock occurrences, or related RGS anomalies (Fig. 1; Table 1). To inform the optimal medium, we examined both panned,

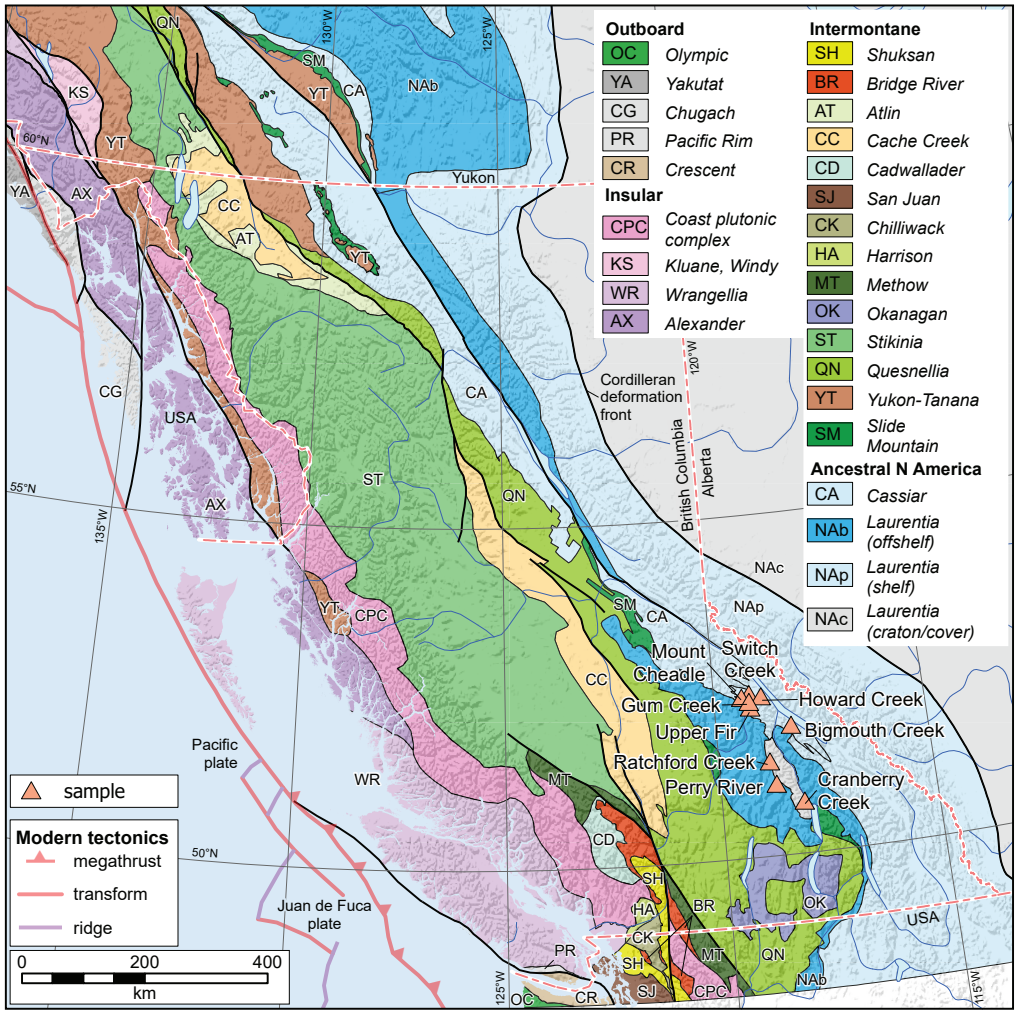


Fig. 1. Sampling sites, southeastern British Columbia. Terranes modified from Colpron (2020).

heavy-mineral concentrate (HMC) and bulk stream-sediment samples, both fine (<0.18 mm) and coarse (0.18-1.0 mm) fractions. Below we focus on samples collected downstream of the Switch Creek (Fig. 2) and Ren (Ratchford Creek; Fig. 3) carbonatites.

3. Qualitative X-ray diffraction analysis

A representative portion of each sample was split using micro-riffle splitter at Activation Laboratories Ltd. (Ancaster, Ontario). A qualitative X-ray diffraction analysis was performed on a Bruker D8 Endeavour diffractometer equipped with Cu X-ray source and operating at the following conditions: 40 kV and 40 mA; range 4-70° 2Θ; step size 0.02° 2Θ; time per step 0.5 seconds; fixed divergence slit, angle 0.30°; sample rotation 15 rpm. The PDF4/Minerals ICDD database was used for mineral identification. Minerals that were identified include: quartz, plagioclase, K-feldspar, Ca-Na amphibole, diopside/augite, almandine, kyanite, muscovite, biotite, chlorite, smectite, apatite, magnetite, and dolomite.

4. Scanning electron microscopy

4.1. Quantitative evaluation of minerals by scanning electron microscopy (QEMSCAN®)

Quantitative mineralogical analysis was carried out using a FEI QEMSCAN® field emission gun scanning electron microscope (SEM) at Activation Laboratories Ltd. (Ancaster, Ontario). Approximately 2 g of material was embedded in epoxy resin for preparing round polished grain mounts (30 mm diameter). Two grain mounts were made per sample: normal and transverse (cross-section). Transverse sections were used for bulk modal mineralogy and normal sections for trace mineral search. Minerals are identified using energy dispersive X-ray spectroscopy (EDS) spectra, which are indicative of mineral chemistry. Therefore, minerals with similar chemical composition (e.g., kyanite and sillimanite) cannot be resolved. Additionally, elements with atomic number (Z) of <11 (Na) cannot be detected. Particles <10 µm (i.e., close to the beam spot spacing) may not be detected.

Table 1. Stream-sediment samples. For full details see Rukhlov et al. (2025b).

Id	Site Id	Locality	Latitude	Longitude	Fraction
1	24ARU-2001	Bigmouth Creek	51.904038	-118.222807	<0.18 mm; BSS
2					0.18 to 1.0 mm; BSS
3					<0.18 mm; HMC
4					0.18 to 1.0 mm; HMC
5	24ARU-2002	Switch Creek	52.413113	-119.149492	<0.18 mm; BSS
6					0.18 to 1.0 mm; BSS
7					<0.18 mm; HMC
8					0.18 to 1.0 mm; HMC
9	24ARU-2003a	Howard Creek	52.363868	-118.868337	<0.18 mm; BSS
10					0.18 to 1.0 mm; BSS
11					<0.18 mm; HMC
12					0.18 to 1.0 mm; HMC
13	24ARU-2003b	Mount Cheadle	52.326285	-119.164279	<0.18 mm; BSS
14					0.18 to 1.0 mm; BSS
15					<0.18 mm; HMC
16					0.18 to 1.0 mm; HMC
17	24ARU-2004	Gum Creek	52.313559	-119.161888	<0.18 mm; BSS
18					0.18 to 1.0 mm; BSS
19					<0.18 mm; HMC
20					0.18 to 1.0 mm; HMC
21	24ARU-2005	Upper Fir	52.299607	-119.164953	<0.18 mm; BSS
22					0.18 to 1.0 mm; BSS
23					<0.18 mm; HMC
24					0.18 to 1.0 mm; HMC
25	24ARU-2006	Perry River	51.068451	-118.700786	<0.18 mm; BSS
26					0.18 to 1.0 mm; BSS
27					<0.18 mm; HMC
28					0.18 to 1.0 mm; HMC
29	24ARU-2007	Ratchford Creek	51.365787	-118.754744	<0.18 mm; BSS
30					0.18 to 1.0 mm; BSS
31					<0.18 mm; HMC
32					0.18 to 1.0 mm; HMC
33	24ARU-2008	Cranberry Creek	50.779047	-118.097014	<0.18 mm; BSS
34					0.18 to 1.0 mm; BSS
35					<0.18 mm; HMC
36					0.18 to 1.0 mm; HMC

BSS – bulk stream sediment; HMC – panned heavy mineral concentrate.

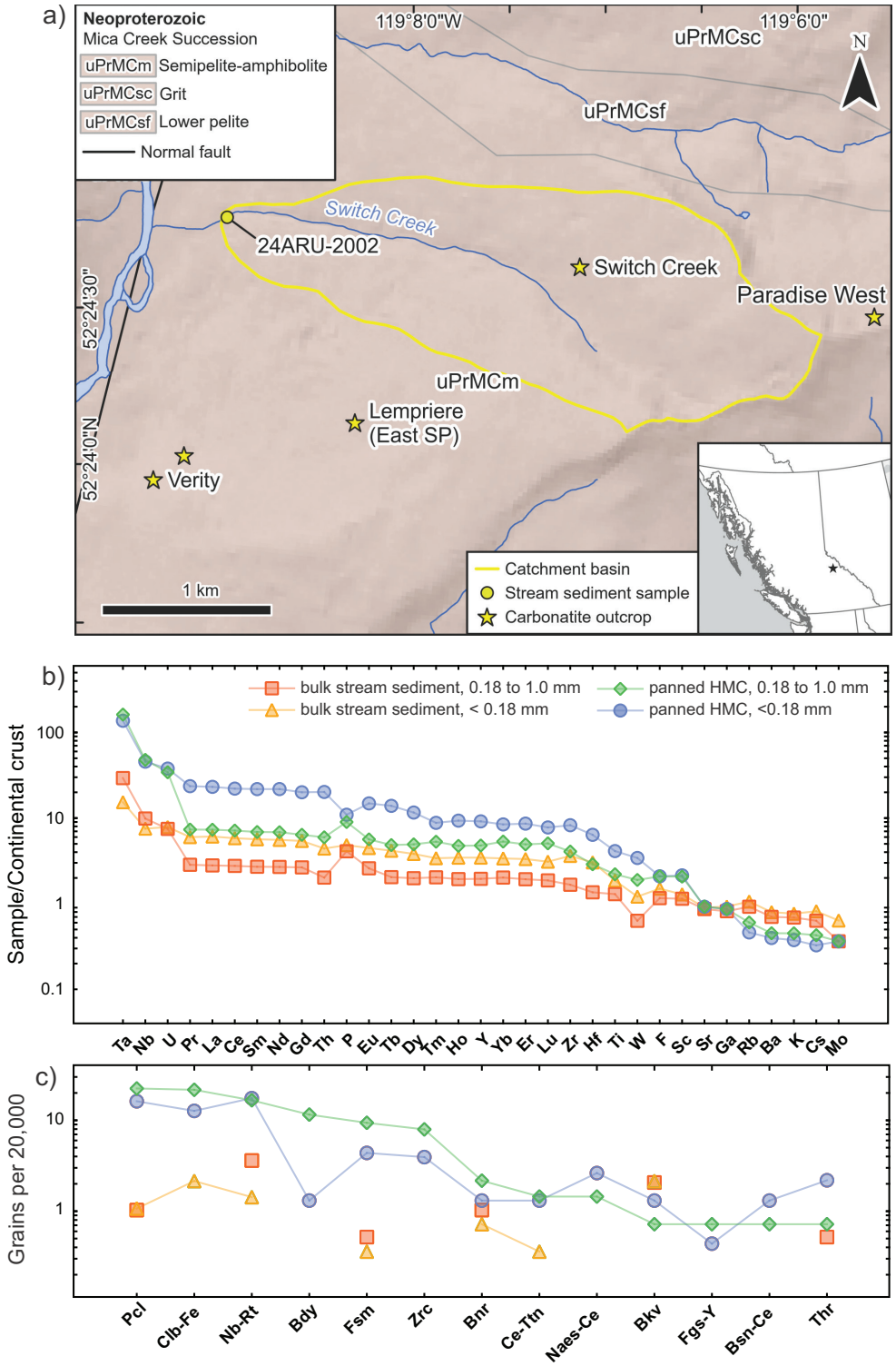


Fig. 2. a) Sampling site and catchment basin (area=3.17 km^2) at Switch Creek, downstream of Switch Creek carbonatite, Blue River area (83D/06). Carbonatite occurrences after Rukhlov et al. (2018). Geology after Campbell (1968), Simony et al. (1980), Raeside and Simony (1983), Pell and Simony (1987), McDonough et al. (1991, 1992), Murphy (2007), and British Columbia Geological Survey (2019). **b)** Bulk stream sediment and panned, heavy mineral concentrate (HMC) lithogeochemical data (Rukhlov et al., 2025b) normalized to bulk continental crust values of Rudnick and Gao (2014). **c)** Grain counts of indicator minerals in bulk stream sediment and panned, heavy mineral concentrate (HMC) per 20,000 total grains by scanning electron microscopy-mineral liberation analysis (SEM-MLA; Table 2); Mineral abbreviations (Warr, 2021): Bdy – baddeleyite, Bkv – belkovite, Bnr – brannerite, Bsn-Ce – bastnaesite-(Ce), Ce-Ttn – REE-titanite, Clb-Fe – columbite-(Fe), Fgs-Y – fergusonite-(Y), Fsm – fersmite, Naes-Ce – nioboaeschynite-(Ce), Nb-Rt – Nb-rutile, Pcl – pyrochlore supergroup, Thr – thorite, Zrc – zirconolite.

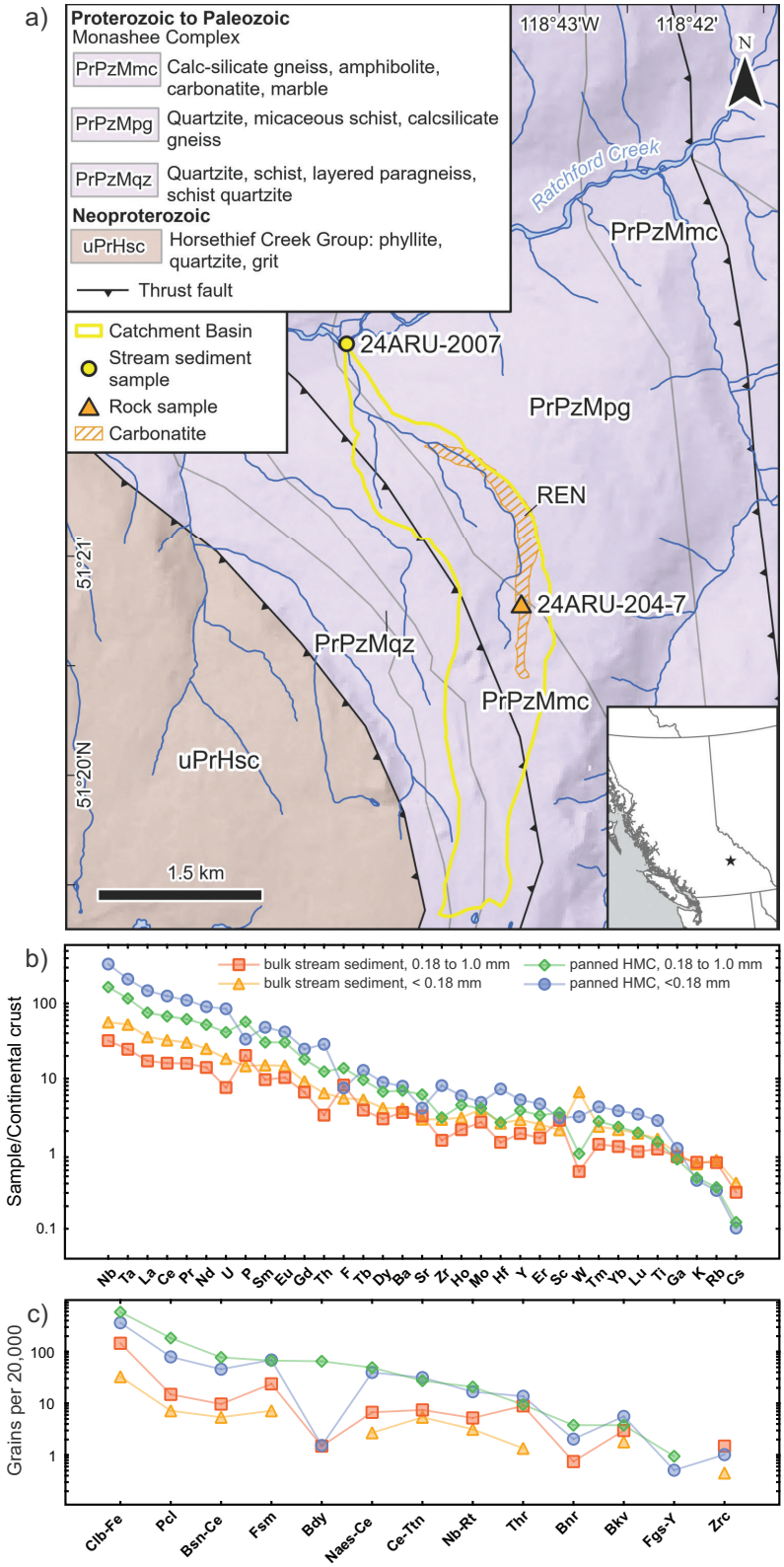


Fig. 3. a) Sampling sites and catchment basin (area=3.85 km^2) downstream of Ren (Ratchford Creek) carbonatite, Ratchford Creek valley (82M/07). Carbonatite footprint after Ya'acoby (2014). Geology after Wheeler and Fox (1964), Höy and Brown (1980), Logan (2002), and British Columbia Geological Survey (2019). **b)** Bulk stream sediment and panned, heavy mineral concentrate (HMC) lithogeochemical data (Rukhlov et al., 2025b) normalized to bulk continental crust values of Rudnick and Gao (2014). **c)** Grain counts of indicator minerals in bulk stream sediment and panned, heavy mineral concentrate (HMC) per 20,000 total grains by scanning electron microscopy-mineral liberation analysis (SEM-MLA; Table 2); Mineral abbreviations as in Figure 2c.

4.2. Mineral liberation analysis (MLA)

To generate mineral abundance maps and quantitative determinations, MLA was carried out using a FEI MLA 650 field emission gun SEM equipped with two Brucker silicon drift EDS detectors on the same grain mounts (normal sections) at the Core Research Equipment and Instrument Training (CREAIT) Microanalysis Facility (MAF), Memorial University of Newfoundland. Operating conditions for MLA included a 25 kV accelerating voltage and 10 nA current. Grain mounts were measured in XBSE (eXtended BackScattered Electron) mode where X-ray analyses were triggered for a backscattered electrons (BSE) range of 40 to 255. Each X-ray measurement was acquired for 0.012 seconds on a 1.5 by 1.5 mm or 2 by 2 mm frame, depending on the grain size (2 by 2 mm frame used for coarse-grained samples), with a resolution of 1000 pixels per frame and an imaging scan speed of 16 µs. Data reduction was performed on MLA Data View (FEI) software version 3.1.4.683.

Figure 4 shows typical EDS spectra for detrital rare-metal and REE minerals encountered in this study. Both QEMSCAN® and MLA scans produced consistent quantitative mineral abundances (Fig. 5). The value of MLA is the output of high-resolution, BSE and false-colour mineral maps, which were re-coloured using a Python™ script to highlight the minerals of interest (Fig. 6).

5. Micro X-ray fluorescence (µXRF) spectrometry

Elemental maps (Figs. 7, 8) were acquired using a Bruker TornadoPlus micro X-ray fluorescence (µXRF) instrument fitted with two 60 mm^2 detectors, housed in the Mineral Deposit Research Unit, University of British Columbia. Data were collected with a spatial resolution of 20 µm (generating images with a pixel resolution of 20 by 20 µm), with a counting time of 0.010 seconds per pixel, typically generating several thousand X-ray counts per pixel. Data were processed in Bruker ESPRIT® software. In the software, a colour stretch was applied to count data so that higher counts appear as brighter colors producing intensity maps. Interference and background corrections were applied, and concentrations calculated using a fundamental parameter (FP) method in Bruker ESPRIT® software. Because no standards were analyzed with our unknown samples, the results should be treated as semi-quantitative, with significant uncertainties at the level of individual pixels.

6. Detrital zircon analysis

Analytical details follow those documented in Ootes et al. (2022). Detrital zircons (Fig. 9) were separated from stream-sediment samples at the Pacific Centre for Isotopic and Geochemical Research at The University of British Columbia. Zircon crystals (>75 µm) were selected using conventional density and magnetic mineral-separation methods. The entire zircon separate was annealed at 900°C for 60 hours, then individual grains were hand-picked and mounted, polished, and imaged by cathodoluminescence (CL; Fig. 9b). From these images, grains were selected for isotopic analysis using a Resonetics RESOlution M-50-LR, connected via a Teflon squid to an Agilent 7700x quadrupole inductively coupled plasma mass spectrometer (ICP-MS). Pb/U and Pb/Pb ratios were determined on the same spots, along with trace-element concentration determinations (Fig. 9c). After data reduction, data were further screened using trace elements and concordance, and analytical results >6% discordant were removed (Fig. 9a).

7. Detrital apatite analysis

Apatite grains were recovered from bedrock carbonatite and stream-sediment samples (Rukhlov et al., 2025a) using conventional density and magnetic mineral-separation methods at the British Columbia Geological Survey. Modified analytical procedure generally follows that outlined in Mao et al. (2016, 2017). Individual grains were hand-picked, mounted, polished, and imaged by CL (Fig. 10a), BSE, and secondary electrons (SE) on a Hitachi SU3900 SEM equipped with dual Bruker XFlash7 30 mm^2 SDD energy-dispersive X-ray microanalysis system at the Electron Microbeam/Xray Diffraction Facility (EMXDF) at The University of British Columbia. A single electron probe micro-analysis (EPMA) was performed on each grain using a fully automated JEOL JXA-iHP200F field emission electron microprobe, equipped with five wavelength-dispersive spectrometers (WDS) at EMXDF. EPMA was performed using the WDS mode, accelerating voltage of 15 kV, beam current of 15 nA, and beam diameter of 10 µm.

Following the SEM and EPMA, apatite grains (n=436) were analyzed for 39 isotopes (Z=5 to 92) on an Agilent 8800 Triple Quadrupole ICP-MS/MS equipped with a Teledyne LSX-213 $G2^+$ laser ablation system at the School of Earth and Ocean Sciences, University of Victoria.

8. Discussion

8.1. Scanning electron microscopy

Samples downstream of both the Switch Creek and Ren (Ratchford Creek) carbonatites display significant enrichments in Ta, Nb, and REE relative to crust (Figs. 2b, 3b; Rukhlov et al., 2025a), reflecting the presence of detrital pyrochlore supergroup, columbite-(Fe), Nb-rutile, fersmite, nioboaeschynite-(Ce), bastnaesite-(Ce), zirconolite, and other carbonatite indicators (Fig. 6). These are relatively high-density minerals and thus are more abundant in panned HMC relative to bulk stream sediment (Figs. 2c, 3c). Both the <0.18 mm and 0.18 to 1.0 mm fractions show generally similar abundances of rare-metal and REE indicator minerals, except for baddeleyite (ZrO_2), which appears to concentrate in the coarse panned fraction. Although panned HMC is a preferred sample medium for rare-metal and REE (Rukhlov et al., 2024, 2025a), carbonatite indicator minerals were also detected in bulk stream-sediment samples (Tables 2, 3), suggesting the utility of automated mineralogy when applied to conventional RGS samples (<0.18 mm fraction of bulk stream sediment).

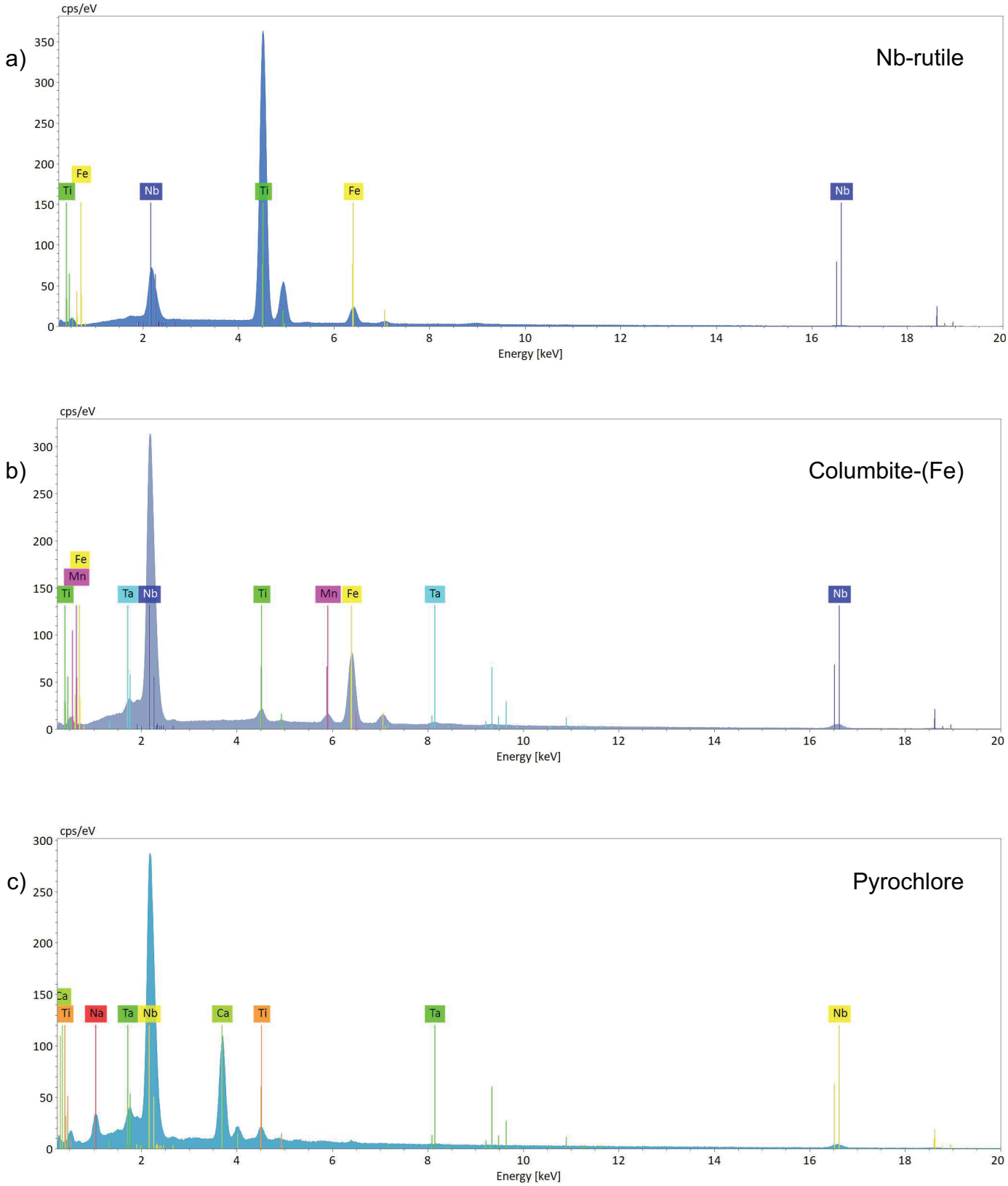


Fig. 4. Examples randomly picked from 36 sample set of X-ray energy dispersive spectra (EDS) for rare earth element (REE) and rare-metal minerals identified in stream-sediment samples. **a)** Nb-rutile. **b)** Columbite-(Fe). **c)** Pyrochlore.

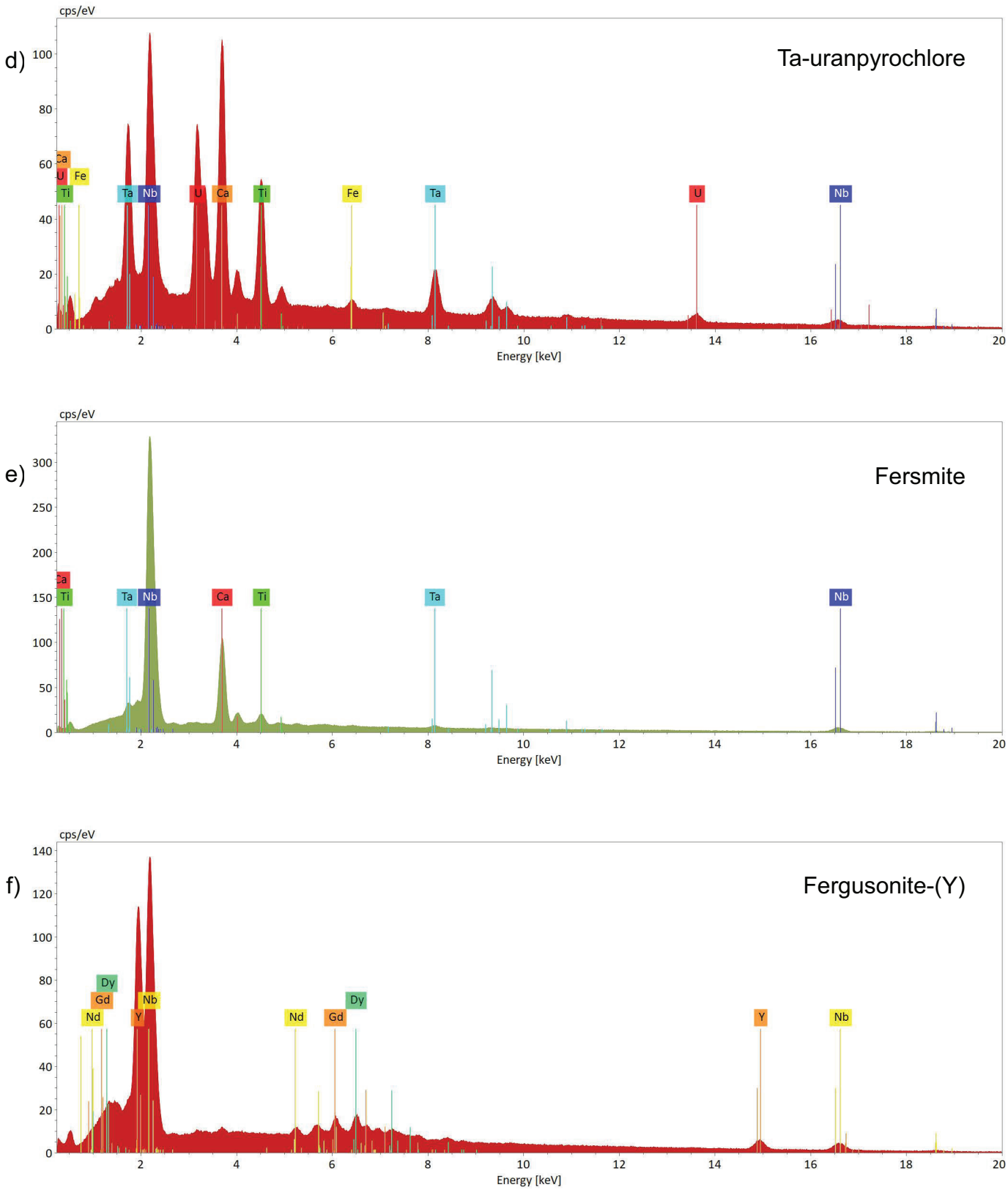


Fig. 4. Continued. **d)** Ta-uranpyrochlore. **e)** Fersmite. **f)** Fergusonite-(Y).

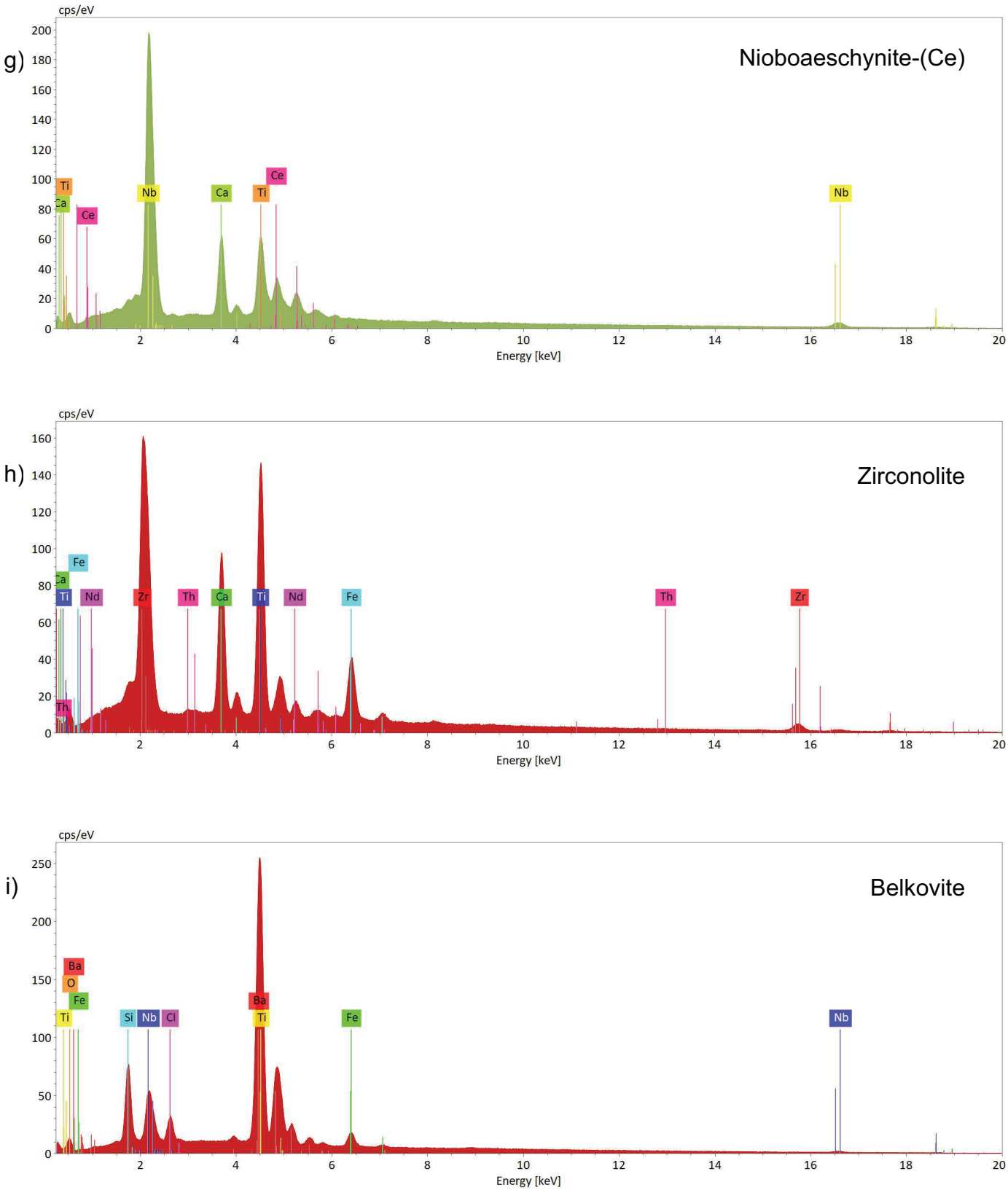


Fig. 4. Continued. **g)** Nioboaeschynite-(Ce). **h)** Zirconolite. **i)** Belkovite.

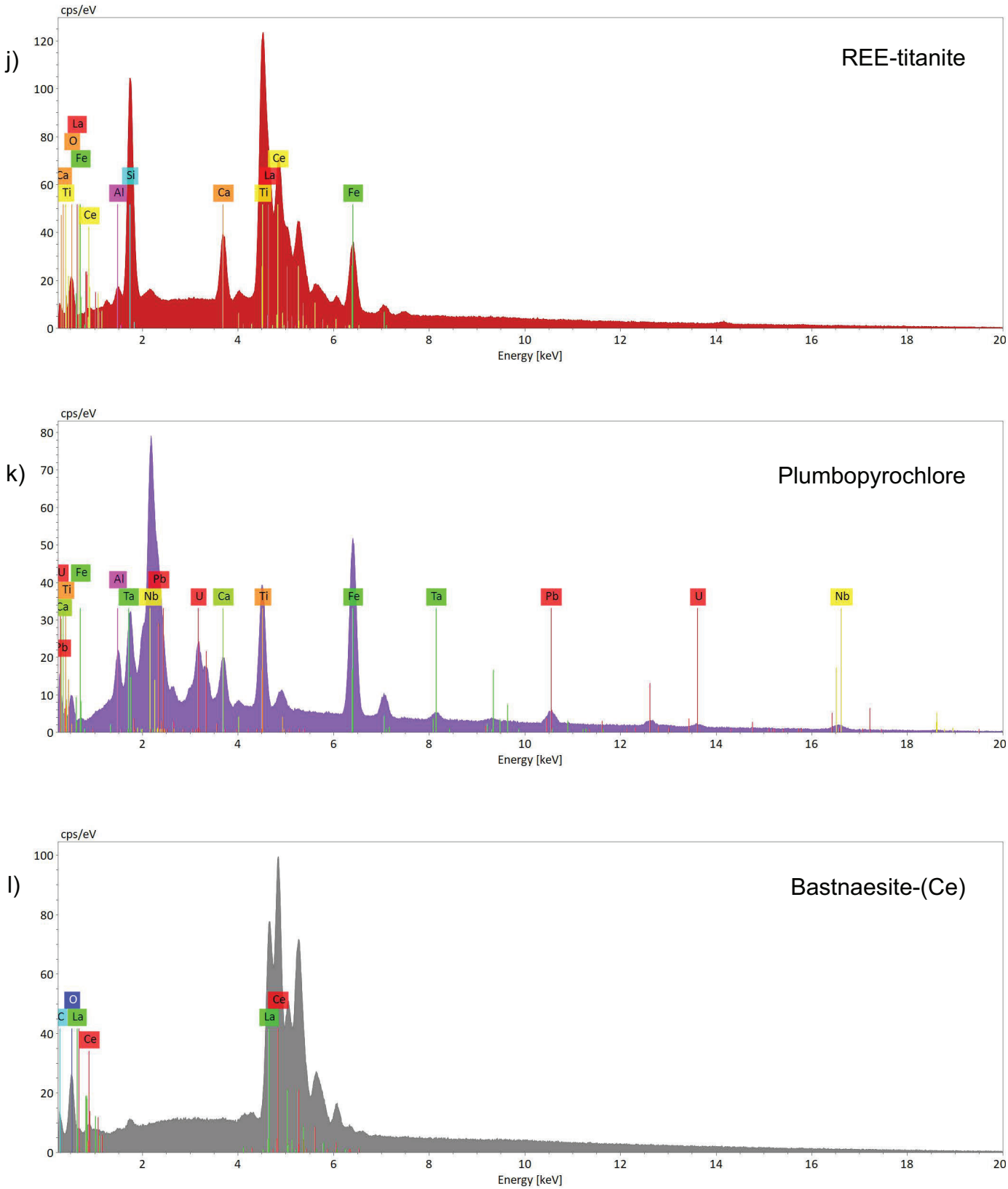


Fig. 4. Continued. **j)** REE-titanite. **k)** Plumbopyrochlore. **l)** Bastnaesite-(Ce).

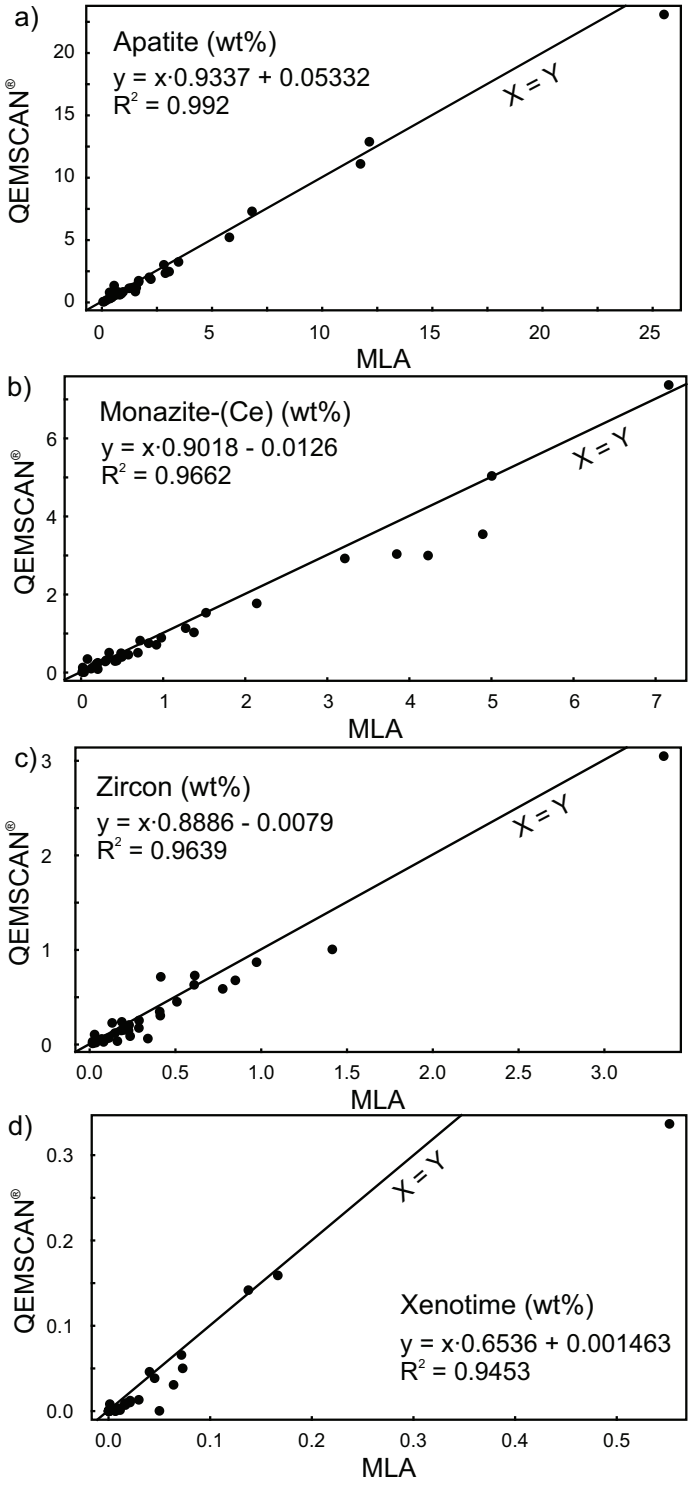


Fig. 5. Indicator mineral abundances in all 36 stream-sediment samples determined by mineral liberation analysis (MLA) vs. QEMSCAN®, ordinary least square regression equations, and correlation coefficients (R^2). **a)** Apatite (wt.%) by MLA vs. apatite (wt.%) by QEMSCAN®. **b)** Monazite-(Ce) (wt.%) by MLA vs. monazite-(Ce) (wt.%) by QEMSCAN®. **c)** Zircon (wt.%) by MLA vs. zircon (wt.%) by QEMSCAN®. **d)** Xenotime (wt.%) by MLA vs. xenotime (wt.%) by QEMSCAN®.

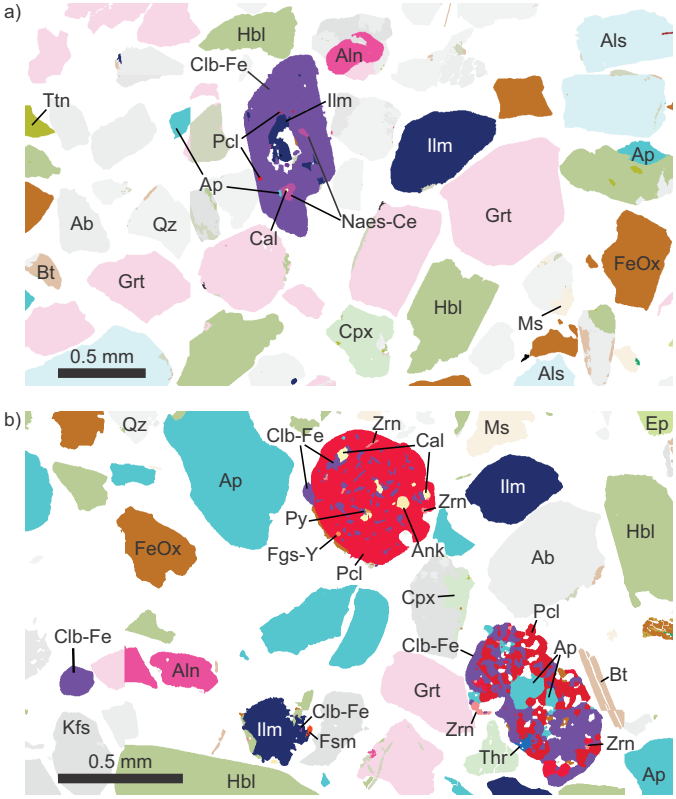


Fig. 6. Examples of false-colour, SEM-MLA maps of panned, heavy mineral concentrate (HMC) of stream sediment (0.18-1.0 mm fraction) in polished, 30 mm-diameter mounts. **a)** Sample 24ARU-2002; Switch Creek, downstream of Switch Creek carbonatite (Figure 2). **b)** Sample 24ARU-2007; tributary of Ratchford Creek, downstream of Ren (Ratchford Creek) carbonatite (Figure 3). Mineral abbreviations (Warr, 2021): Ab – albite, Aln – allanite, Als – aluminosilicate, Ank – ankerite, Ap – apatite, Bt – biotite, Cal – calcite, Clb-Fe – columbite-(Fe), Cpx – clinopyroxene, Ep – epidote, FeOx – iron oxide, Fgs-Y – fergusonite-(Y), Fsm – fersmite, Grt – garnet, Hbl – hornblende, Ilm – ilmenite, Kfs – K-feldspar, Ms – muscovite, Naes-Ce – nioboaeschynite-(Ce), Pcl – pyrochlore supergroup, Py – pyrite, Qz – quartz, Thr – thorite, Ttn – titanite, Zrn – zircon.

Detrital columbite, pyrochlore, and aeschynite could also be derived from pegmatites, syenites, and granites (e.g., Černý and Ercit, 2005; Dixon et al., 2014), which are more widespread than carbonatites in the study area, which is mostly underlain by high-grade metamorphic rocks. However, we consider that the presence of composite detrital particles such as columbite-pyrochlore-nioboaeschynite-ilmenite-apatite-calcite (Fig. 6a) or pyrochlore-columbite-zircon-fergusonite-ankerite-calcite-pyrite (Fig. 6b) parageneses unequivocally indicates the occurrence of carbonatites in the catchment basin upstream. Chemical compositions of detrital pyrochlore supergroup and other rare metal and REE minerals 'fingerprint' their host rocks (e.g., Mackay and Simandl, 2015; Simandl et al., 2017).

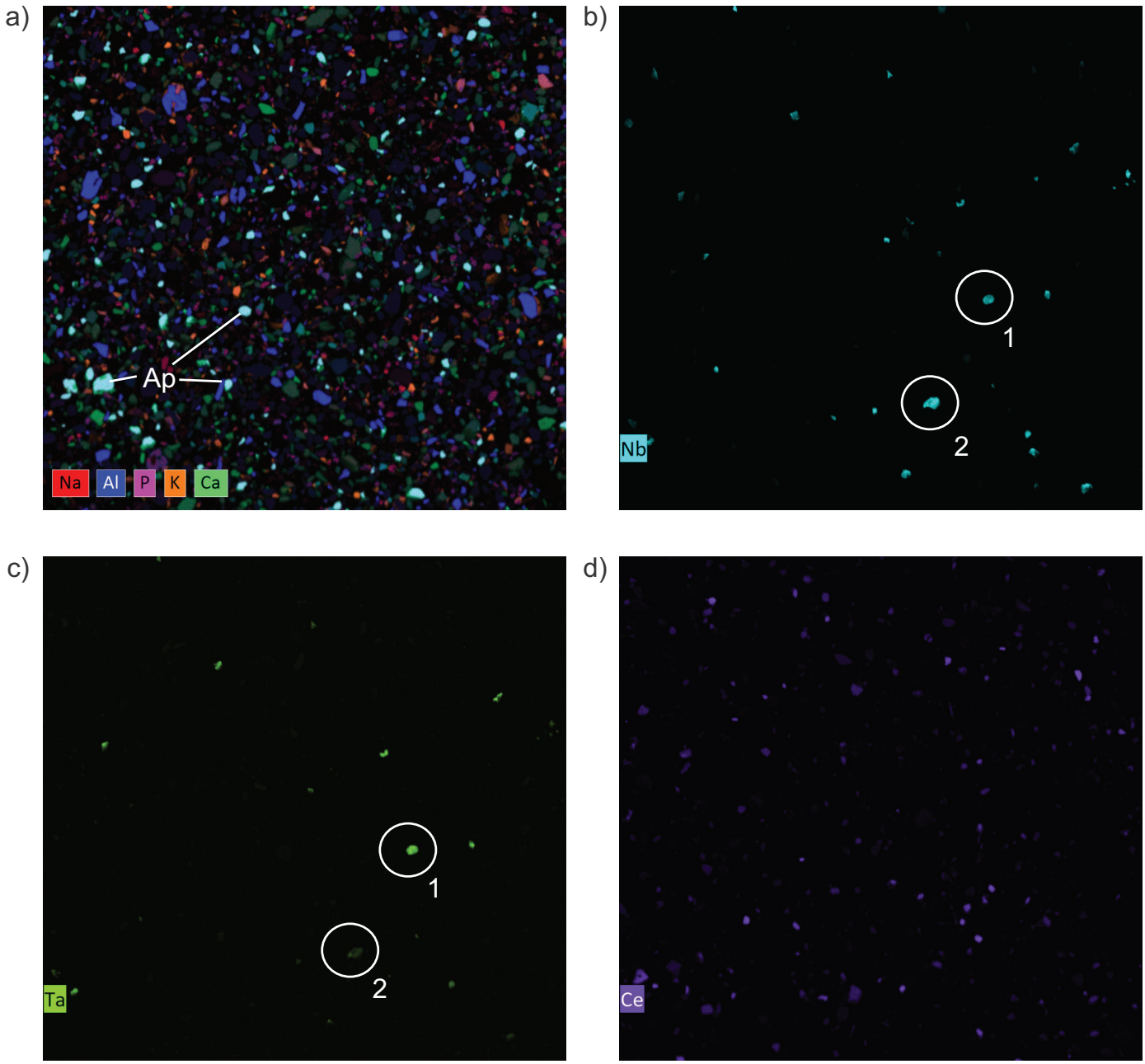


Fig. 7. Element intensity maps (21 by 21 mm area; count data) on polished, 30 mm-diameter mount of sample 24ARU-2002 collected downstream of Switch Creek carbonatite (Figure 2) by µXRF; brighter colours correspond to higher element intensity. **a)** Mixed Na-Kα, Al-Kα, P-Kα, K-Kα, and Ca-Kα; Ap - apatite. **b)** Nb-Kα. **c)** Ta-Lα. **d)** Ce-Lα. Note Ta-rich (circle 1) and Ta-poor (circle 2) Nb phases.

8.2. µXRF

Elemental maps derived from µXRF analysis highlight rare-metal and REE minerals and reveal compositional variations that are not apparent in MLA maps (Figs. 7, 8). For example, Ca and P highlight apatite, and variable Ta intensity differentiates Nb-Ta minerals downstream of Switch Creek and Ren carbonatites. High Ce counts highlight mainly detrital monazite-(Ce). Overall, µXRF is not an alternative to a much more powerful SEM-MLA approach but is a useful add-on to reveal compositional variations between indicator minerals.

8.3. Detrital zircon

The detrital zircons (Fig. 9a) reveal several distinct age populations ranging from Neoarchean to Eocene, including the 720, 530, and 330 Ma events marked by carbonatitic, alkaline, and mafic magmatism related to mantle-plume and rift activity (e.g., Heaman et al., 1992; Colpron et al., 2002; Lund et al., 2003; Millonig et al., 2012).

The trace-element compositions of zircons are sensitive to the petrogenesis and equilibrium mineral assemblage of their parental rock (e.g., Heaman et al., 1990; Grimes et al., 2007). These attributes make zircon a powerful indicator mineral for

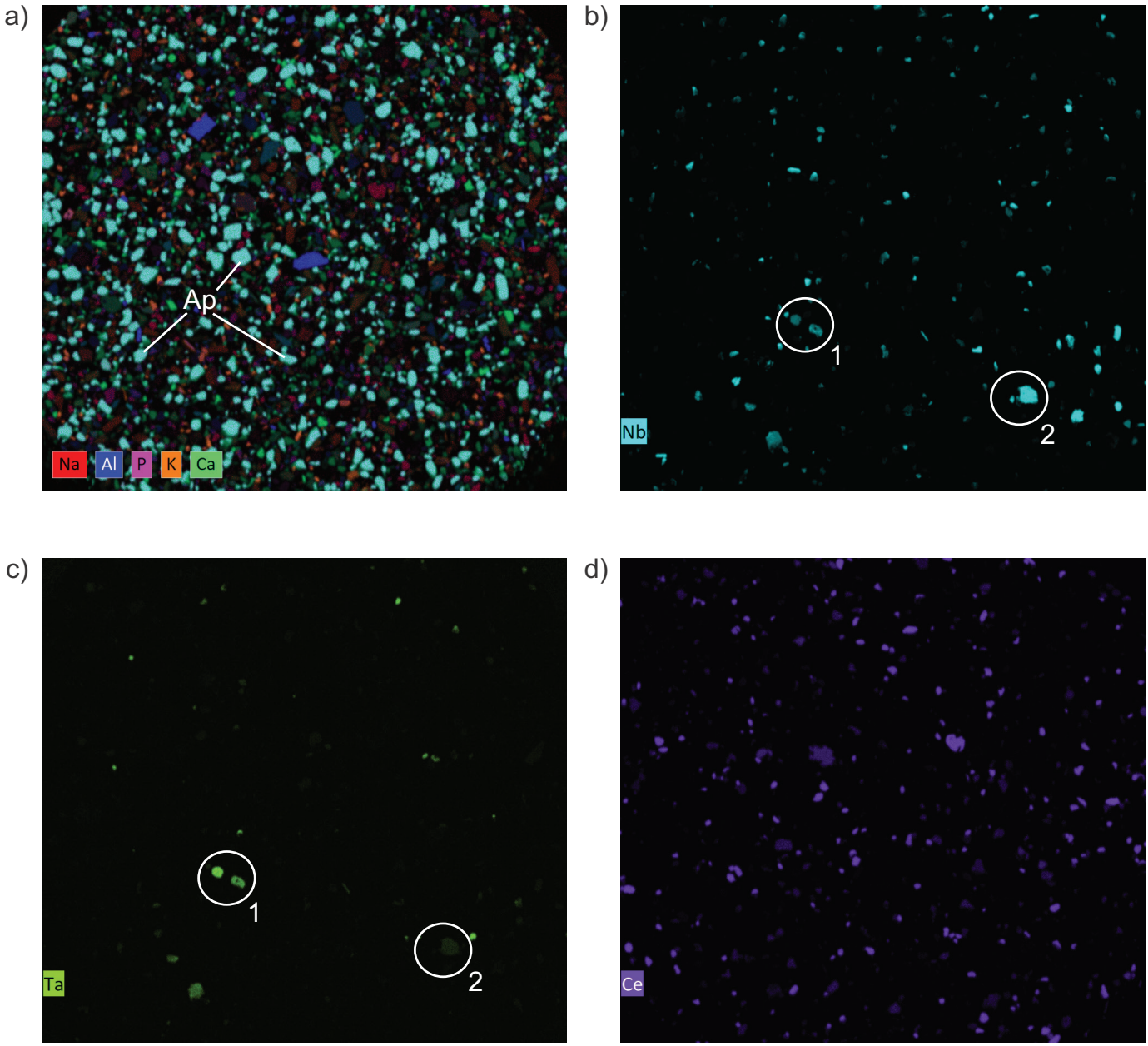


Fig. 8. Element intensity maps (21 by 21 mm area; count data) on polished, 30 mm-diameter mount of sample 24ARU-2007 collected downstream from Ren (Ratchford Creek) carbonatite (Figure 3) by µXRF; brighter colours correspond to higher element intensity. **a)** Mixed Na-Kα, Al-Kα, P-Kα, K-Kα, and Ca-Kα; Ap - apatite. **b)** Nb-Kα. **c)** Ta-Lα. **d)** Ce-Lα. Note Ta-rich (circle 1) and Ta-poor (circle 2) Nb phases.

identifying igneous source rocks, including kimberlites and carbonatites (Hardman et al., 2025). However, zircon is very rare in some carbonatites hosting REE and Nb (e.g., Dalsin et al., 2015; Gammons et al., 2024; Gary and Gammons, 2024), which limits its utility as an indicator mineral for carbonatite-hosted critical minerals.

Projected into the DPA discrimination diagram of Hardman et al. (2025), the trace-element compositions of the detrital zircon show most scatter defined by the <300 Ma population (Fig. 9c). A few Neoproterozoic to Carboniferous zircons plot within the field of carbonatites and related silica-undersaturated and alkaline rocks, and some 450 to 300 Ma zircons plot within the field of kimberlite and other low-volume 'kimberlite-like' rocks such as ultramafic lamprophyres.

8.4. Apatite

Apatite is ubiquitous in carbonatites and silica-undersaturated and alkaline silicate rocks (Kukharenko et al., 1965; Chakhmouradian et al., 2017; Rukhlov et al., 2018). Projected into the DPA discrimination diagram of Mao et al. (2016), the trace-element compositions of detrital apatite downstream from the Switch Creek (n=17) and Ren (n=21) carbonatites as well as those of apatite from other carbonatites in our total sample set (from Little Chicago, Felix, Ren, Three Valley Gap, and

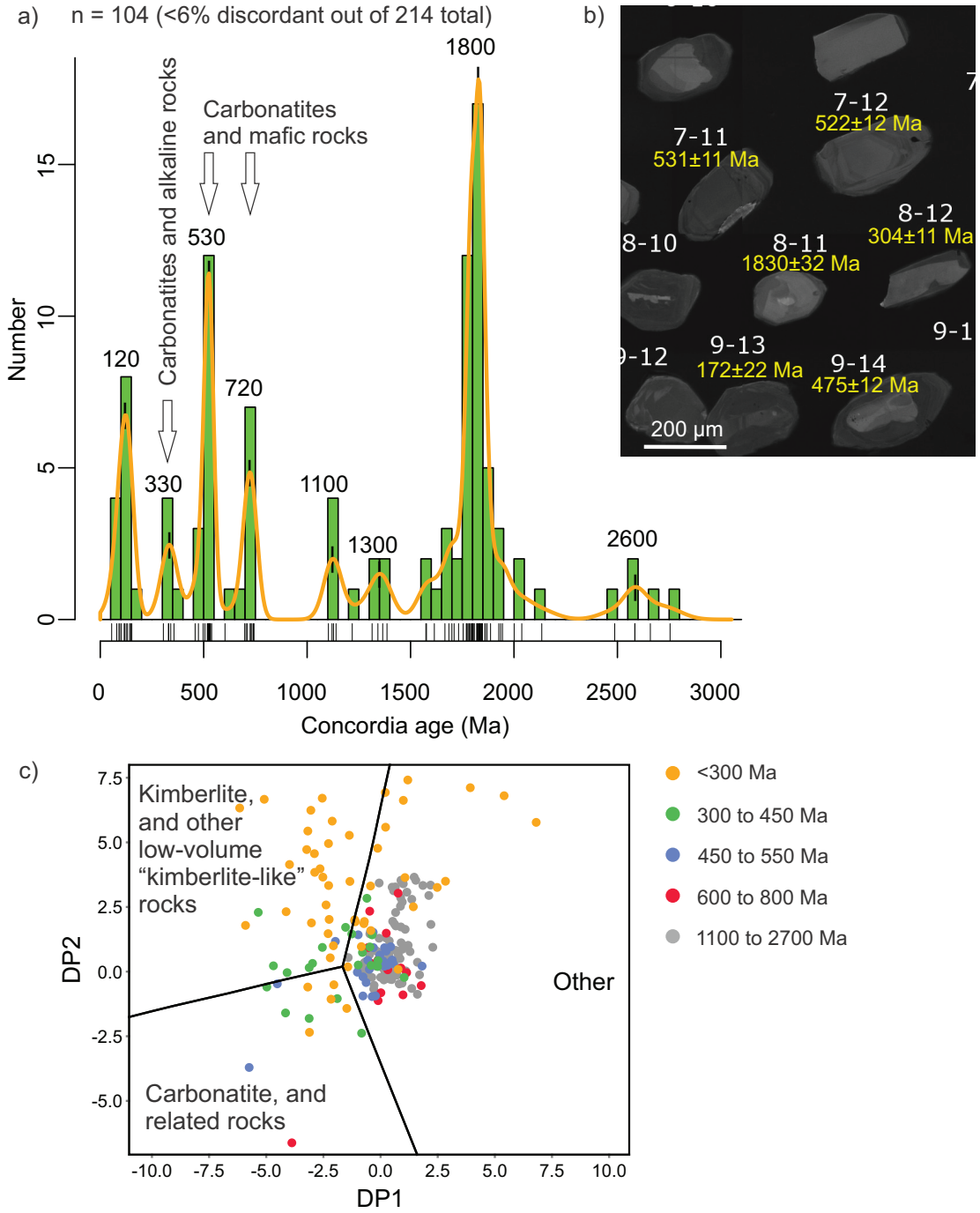


Fig. 9. LA-ICP-MS analyses of detrital zircons from stream sediment downstream of Switch Creek carbonatite, sample 24ARU-2002 (Figure 2). **a)** U-Pb concordia age (Ma) probability density plot showing the main probability age peaks. **b)** Examples of cathodoluminescence images of detrital zircons, showing their internal structures, and U-Pb concordia ages. **c)** Trace-element compositions of detrital zircons projected into DPA plot (after Hardman et al., 2025) based on 20 elemental variables.

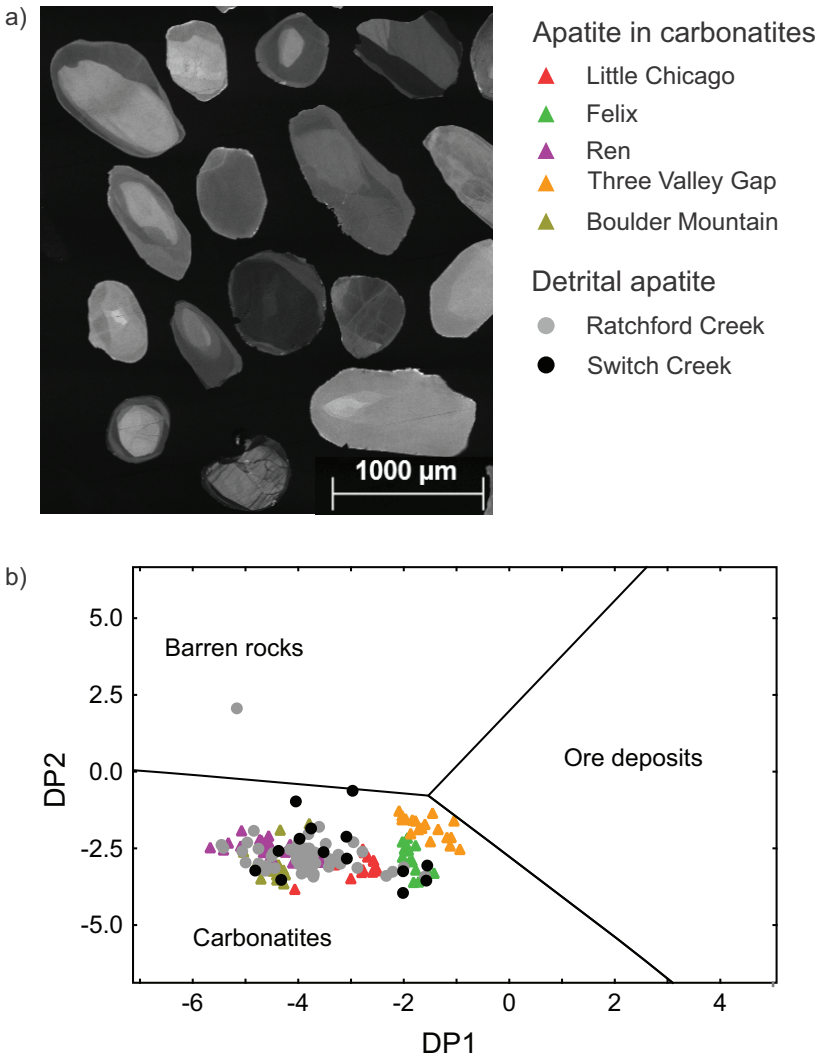


Fig. 10. a) Cathodoluminescence images of detrital apatite from stream sediment downstream of Ren (Ratchford Creek) carbonatite, sample 24ARU-2007 (Figure 3), showing their internal structures. **b)** LA-ICP-MS analyses of detrital apatite from stream sediments downstream of Switch Creek and Ren carbonatites, and apatite in some British Columbia carbonatites (see Rukhlov et al., 2025a for details) projected into DPA plot (after Mao et al., 2016) based on 11 elemental variables.

Boulder Mountain; see Rukhlov et al., 2025a) fall within the field of apatite compositions from global carbonatites (Fig. 10b). Considering that apatite is a common accessory mineral in most igneous and metamorphic rock, it is surprising that all detrital data points except one plot in the carbonatite field. This might reflect finer grain sizes (<0.18 mm) of non-carbonatitic apatite (cf., we used the 0.18 to 1.0 mm fraction for mineral separation), or a very low proportion of detrital apatite derived from local metamorphic rocks relative to ubiquitous, coarse-grained apatite sourced from the carbonatites (Rukhlov et al., 2018, 2025a).

Although we might have missed detrital apatite from other host rocks, the results downstream of both Switch Creek and Ren carbonatites are striking, because identifying even a single carbonatitic apatite grain in a stream sediment would render the catchment basin upstream prospective for carbonatites. It is interesting to note the clustering of data from individual carbonatite occurrences (Fig. 10b), reflecting compositional differences between the parental magmas. Our data confirm the utility of the approach used by Mao et al. (2016) in drainage prospecting for carbonatite-hosted critical minerals.

9. Conclusion

An indicator mineral approach using automated SEM mineralogy (QEMSCAN®, MLA), µXRF, and trace-element compositions of detrital zircon and apatite enhance the interpretation of multi-element lithogeochemical dispersal in modern drainages. Rare-metal and REE minerals concentrate in panned HMC, which display up to 100 times background (average continental crust) contrast, and is thus the preferred sample medium for ongoing REE, Nb, Ta, and other critical minerals prospecting. Our findings suggest that the approach

Table 2. Counts of mineral grains identified by scanning electron microscopy-mineral liberation analysis (SEM-MLA) in stream-sediment samples.

id	Total	Naes-Ce	Bdy	Aln	Bkv	Bnr	Clb-Fe	Fgs-Y	Fsm	Mnz-Ce	Pcl	Bsn-Ce	Nb-Rt	Thr	Ce-Ttn	Xtm
1	38040	nd	nd	167	7	3	6	nd	1	85	2	1	4	1	1	7
2	25075	3	nd	120	2	nd	4	nd	nd	42	3	nd	2	2	1	13
3	32707	nd	nd	168	3	nd	8	nd	2	197	12	1	3	2	nd	12
4	18496	nd	nd	89	9	1	6	nd	1	73	nd	nd	11	1	nd	16
5	55827	nd	nd	488	6	2	6	nd	1	34	3	nd	4	nd	1	7
6	38736	nd	nd	201	4	2	nd	nd	1	23	2	nd	7	1	nd	3
7	45661	6	3	414	3	3	29	1	10	149	37	3	40	5	3	13
8	27679	2	16	224	1	3	30	1	13	54	31	1	23	1	2	25
9	38018	nd	nd	196	nd	7	8	nd	nd	40	5	1	3	2	1	7
10	16319	nd	nd	84	4	2	3	nd	nd	21	nd	nd	3	1	nd	7
11	31577	nd	5	461	7	2	8	nd	2	179	10	nd	14	1	4	14
12	13863	nd	11	126	5	2	3	1	nd	42	2	nd	11	1	1	28
13	49938	1	nd	325	16	4	16	nd	nd	81	9	2	20	1	4	14
14	28946	nd	nd	221	4	2	11	nd	nd	19	2	nd	7	2	nd	3
15	33897	2	nd	318	14	4	16	1	nd	111	7	nd	23	3	9	15
16	21432	9	nd	279	30	3	255	nd	35	52	38	5	30	1	3	15
17	45791	2	nd	307	9	4	7	nd	2	151	6	3	11	nd	2	8
18	19308	nd	nd	98	1	3	2	nd	nd	30	3	2	8	nd	2	7
19	28392	10	nd	216	6	3	32	1	8	414	9	11	20	7	9	23
20	19618	10	nd	164	5	1	68	nd	6	123	9	8	38	1	11	34
21	58226	nd	nd	456	5	4	1	nd	nd	38	nd	nd	1	3	3	6
22	42190	nd	nd	271	8	1	4	1	nd	9	6	nd	4	1	1	5
23	43327	1	nd	513	5	4	24	1	nd	112	8	nd	8	1	7	17
24	31759	nd	nd	334	4	3	5	2	nd	19	2	nd	5	nd	1	6
25	43736	nd	nd	253	15	2	6	nd	nd	108	7	5	2	4	nd	2
26	19206	nd	nd	119	14	1	1	nd	nd	21	1	6	2	1	3	nd
27	31556	nd	2	392	9	1	4	nd	nd	422	8	8	4	2	5	9
28	17407	nd	nd	163	23	nd	nd	nd	nd	98	3	9	5	1	5	4
29	44465	6	nd	501	4	nd	73	nd	16	180	16	12	7	3	12	1
30	26774	9	2	292	4	1	195	nd	32	96	20	13	7	12	10	nd
31	39268	78	3	707	11	4	713	1	136	1101	156	90	33	27	62	7
32	21123	52	69	272	4	4	618	1	71	409	194	82	22	10	29	2
33	42762	nd	nd	137	10	1	1	nd	nd	61	1	1	8	nd	1	11
34	20967	nd	2	84	6	2	nd	nd	nd	21	nd	nd	8	nd	nd	4
35	31274	nd	nd	138	8	2	nd	nd	nd	845	nd	20	22	9	1	74
36	14925	nd	nd	75	6	nd	nd	nd	nd	44	1	2	8	2	nd	4

Table 2. Continued.

id	Zrc	Ap	Zrn	Cal	Ank	Ilm	Ti-Mag	Ttn	Ol	Cpx	Brt	Ab	Als	Apy	Bt	Ccp	Chl	Chr
1	nd	253	142	4	17	72	11	338	90	316	1	7790	576	nd	3448	nd	3812	8
2	nd	106	153	5	9	54	15	228	24	88	2	3414	232	nd	2566	nd	4494	8
3	nd	317	228	4	11	222	17	623	100	501	3	4621	941	nd	899	2	2295	16
4	nd	85	358	3	22	111	7	212	17	126	1	1480	384	nd	872	1	2794	63
5	nd	409	120	4	16	311	42	947	24	358	nd	6499	299	nd	6901	nd	7675	8
6	nd	284	152	nd	10	519	69	959	10	139	7	3021	218	nd	7091	1	7288	7
7	9	716	345	4	12	1098	186	1424	31	505	1	3347	735	nd	3837	nd	5116	16
8	11	306	326	3	22	845	144	615	36	200	nd	1487	333	nd	3451	3	5408	22
9	nd	348	131	1	16	245	3	341	13	125	nd	5089	446	nd	6458	14	2036	4
10	nd	100	210	4	12	108	3	243	12	42	1	1703	241	nd	2738	3	1561	7
11	4	709	440	4	27	713	55	837	39	180	nd	3021	1109	nd	1186	18	1307	15
12	2	116	494	6	8	410	54	269	21	39	nd	490	430	nd	737	7	1556	40
13	nd	122	113	nd	15	407	90	567	144	319	nd	8062	410	nd	4886	nd	8165	10
14	nd	76	125	1	8	142	19	566	7	82	1	3438	104	nd	4277	nd	5713	9
15	nd	138	163	nd	25	604	104	709	146	306	nd	4722	592	nd	2525	nd	4006	42
16	nd	56	207	1	22	353	70	346	30	160	2	1841	399	1	2350	nd	4197	44
17	nd	257	115	3	19	273	15	295	27	207	5	6176	536	nd	8743	1	5259	37
18	nd	49	105	4	9	169	10	125	3	95	1	1662	183	nd	4351	1	3655	29
19	nd	263	260	3	26	577	56	321	23	211	37	2844	1178	nd	2547	nd	3042	79
20	nd	63	379	4	26	391	45	158	12	102	53	949	592	nd	2657	nd	4257	200
21	nd	59	70	nd	24	163	42	440	331	257	2	7654	141	nd	4852	nd	14031	36
22	1	51	105	nd	21	101	13	484	558	156	nd	4543	99	nd	3943	nd	10668	65
23	nd	110	159	1	34	556	97	873	803	620	nd	5116	425	nd	2132	nd	6905	118
24	nd	75	111	1	19	180	64	424	585	264	1	2827	164	nd	2040	nd	7484	109
25	nd	650	121	3	13	141	58	305	51	612	nd	9186	172	nd	2790	nd	5212	6
26	nd	220	69	5	20	93	144	260	9	146	nd	3325	40	nd	1232	1	2837	17
27	1	1208	455	5	24	462	123	514	76	945	5	5253	123	nd	935	4	2389	7
28	nd	255	130	5	46	211	80	220	19	270	nd	2311	113	nd	1105	2	2517	24
29	1	1095	77	24	1041	236	58	326	73	1599	61	5984	105	nd	5365	2	5390	30
30	2	655	115	27	248	239	27	384	58	870	19	3618	16	nd	3559	1	3075	17
31	2	2602	359	51	957	1226	240	657	108	2596	323	3469	195	nd	2036	6	2285	48
32	nd	1337	190	50	297	571	84	288	36	820	84	1746	53	nd	1770	5	1873	60
33	nd	170	136	2	18	111	25	236	278	780	1	6667	357	1	3497	2	2744	5
34	nd	84	101	1	5	55	9	116	27	105	nd	3424	137	nd	2172	3	1673	9
35	1	365	426	5	29	575	92	441	592	1508	4	3517	289	1	1153	5	1173	33
36	nd	68	124	3	21	126	23	196	112	398	nd	1677	225	1	1102	5	1135	19

Table 2. Continued.

id	Ep	Gn	Grt	Hbl	FeOx	Ms	Kfs	Pl	Py	Qz	Rsv	Rt	Sch	Sp	St	Crn	X
1	385	3	1932	3691	450	2834	2543	1086	10	7652	38	86	nd	1	166	nd	nd
2	276	1	1022	2031	442	2490	2315	425	13	4127	57	82	nd	2	199	nd	3
3	383	nd	4113	4094	190	603	1692	712	20	9300	16	150	2	2	221	nd	1
4	143	nd	2324	1540	316	523	703	228	54	5639	16	120	nd	nd	145	nd	2
5	572	nd	1849	6286	398	4646	3436	1376	8	12294	101	120	nd	nd	569	nd	7
6	370	2	2009	2810	692	2784	2920	545	27	5718	182	164	nd	nd	491	nd	3
7	764	2	4893	4555	1628	1389	2197	613	22	10389	96	449	nd	nd	546	nd	17
8	403	nd	3346	1553	1477	1331	1592	231	12	3234	50	244	nd	nd	553	nd	14
9	675	nd	1514	2972	549	3541	1024	2030	199	9407	270	146	nd	1	150	nd	nd
10	257	1	874	1194	232	1094	659	611	84	3669	166	219	nd	nd	143	nd	3
11	801	1	5540	4089	689	424	514	1320	231	6540	174	674	nd	1	207	nd	1
12	143	nd	2322	833	484	282	168	231	84	3726	53	471	nd	nd	150	nd	4
13	315	nd	1550	5795	485	3622	3141	1130	7	9249	120	118	1	nd	600	nd	2
14	150	nd	1292	2489	421	2124	3956	362	3	2618	167	50	nd	nd	473	nd	2
15	257	nd	1854	4694	555	1244	2141	594	28	7273	88	170	nd	nd	390	1	4
16	198	2	1231	2118	458	1191	1515	274	12	2893	77	131	nd	nd	491	nd	7
17	324	nd	1355	4159	287	4699	1552	1040	28	9028	144	93	nd	nd	599	nd	3
18	187	nd	1329	1025	291	1557	765	346	10	2560	114	54	nd	nd	462	nd	1
19	257	nd	3638	1944	468	848	407	704	26	6834	155	312	3	nd	551	nd	9
20	69	nd	1932	891	482	893	291	230	29	3393	151	263	nd	1	623	nd	4
21	426	1	2493	8723	413	3830	3280	1318	10	7642	126	45	nd	nd	1300	nd	nd
22	319	1	1634	5957	715	2358	4432	762	4	3808	128	78	nd	nd	872	nd	3
23	378	nd	2618	7736	612	1447	2535	838	5	7588	84	152	nd	nd	680	1	4
24	318	nd	1707	5342	508	1537	2702	365	3	3673	125	72	nd	1	670	nd	5
25	427	nd	801	3369	434	2201	6285	1867	14	7363	14	104	nd	nd	1132	2	1
26	253	nd	389	1416	263	1883	3020	490	15	2164	6	132	nd	1	586	nd	1
27	415	nd	1445	2811	1199	1428	3588	1173	53	5333	12	106	4	nd	594	13	nd
28	215	nd	683	1295	619	1404	2144	410	32	2024	38	151	nd	nd	768	3	5
29	446	nd	1890	7135	1543	1244	3417	1471	142	4333	91	61	nd	3	389	nd	2
30	276	nd	847	3802	911	924	3870	680	54	1508	32	38	nd	nd	207	nd	2
31	353	1	2142	4889	3898	628	2396	878	254	3195	100	104	1	2	132	1	6
32	125	5	992	2675	1637	683	1897	362	77	1343	39	71	nd	4	100	nd	10
33	421	nd	389	2391	436	3200	7095	866	40	11778	12	137	nd	2	722	nd	11
34	244	nd	193	719	323	2670	3888	312	14	4024	9	99	nd	nd	419	nd	5
35	313	1	2166	2270	744	1543	3569	509	56	8169	10	244	1	1	341	nd	9
36	177	1	524	728	195	1541	2051	242	16	3568	5	127	nd	nd	353	nd	20

Total – total count of grains; 'nd' – not detected; X – unknown phase. Mineral abbreviations (Warr, 2021): Ab – albite, Aln – allanite, Als – aluminosilicate, Ank – ankerite, Ap – apatite, Apy – arsenopyrite, Bdy – baddeleyite, Bkv – belkovite, Bnr – brannerite, Bsn Ce – bastnaesite-(Ce), Brt – baryte, Bt – biotite, Cal – calcite, Ccp – chalcopyrite, Ce-Ttn – REE-titanite, Chl – chlorite, Chr – chromite, Clb-Fe – columbite-(Fe), Cpx – clinopyroxene, Crn – corundum, Ep – epidote, FeOx – iron oxide, Fgs-Y – fergusonite-(Y), Fsm – fersmite, Gn – galena, Grt – garnet, Hbl – hornblende, Ilm – ilmenite, Kfs – K-feldspar, Mnz-Ce – monazite-(Ce), Ms – muscovite, Naes Ce – nioboaeschynite-(Ce), Nb-Rt – Nb-rutile, Ol – olivine, Pcl – pyrochlore supergroup, Pl – plagioclase, Py – pyrite, Qz – quartz, Rsv – rasvumite, Rt – rutile, Sch – scheelite, Sp – sphalerite, St – staurolite, Thr – thorite, Ti-Mag – Ti-magnetite, Ttn – titanite, Zrc – zirconolite, Zrn – zircon, Xtm – xenotime.

Table 3. Detrital indicator minerals identified in stream sediments by scanning electron microscopy-mineral liberation analysis (SEM-MLA).

Mineral	General formula	Significance
Bastnaesite-(Ce)	$(Ce,La)(CO_3)(F)$	REE
Nioboaeschynite-(Ce)	$(Ce,Ca)(Nb,Ti)_2(O,OH)_6$	REE, Nb
Baddeleyite	ZrO_2	Carbonatites, undersaturated and alkaline silicate rocks
Brannerite	$(U,Ce,Th,Ca)(Ti,Fe^{3+},Nb)_2(O,OH)_6$	REE, Nb
Columbite-(Fe)	$(Fe^{2+},Mn)(Nb,Ta)_2O_6$	Nb ±Ta
Fergusonite-(Y)	$YNbO_4$	REE, Nb
Fersmite	$(Ca,Ce,Na)(Nb,Ta,Ti)_2(O,OH,F)_6$	REE, Nb ±Ta
Nb-rutile	$(Ti,Nb)O_2$	Nb
Thorite	$Th(SiO_4)$	Alkaline rocks, pegmatites
Pyrochlore	$(Ca,Na,U,Fe,Pb)_2(Nb,Ta,Ti)_2O_6(F,OH,O)$	Nb ±Ta
Zirconolite	$(Ca,Nd)Zr(Ti,Fe,Th)_2O_7$	REE
Apatite	$Ca_5(PO_4)_3(F,Cl,OH)$	Abundant in carbonatites; indicator chemistry[1]
Monazite-(Ce)	$Ce(PO_4)$	REE
Xenotime	$Y(PO_4)$	REE
Allanite-(Ce)	$(Ca,Ce)_2(Al,Fe)_3(Si_2O_7)(SiO_4)O(OH)$	REE
Belkovite	$Ba_3(Nb,Ti,Fe)_6(Si_2O_7)_2O_{12}$	Nb
REE-titanite	$(Ca,Ce,La)(Ti,Al)(SiO_4)O$	REE
Zircon	$Zr(SiO_4)$	Occurs in carbonatites; indicator chemistry[2]

[1] Mao et al. (2016). [2] Hardman et al. (2025). REE - rare earth elements.

also suits small volume (~2 g), bulk stream-sediment samples in the RGS archive. In addition to identifying new critical mineral targets, data from indicator minerals inform tectonic evolution, geology, and metallogeny of the catchment basins.

Acknowledgments

We are grateful to K. Whitmore (BC Geological Survey) for building a script for re-processing MLA images. We thank E. Hrischeva (Activation Laboratories Ltd.) for analytical services and Christopher H. Gammons (Montana Technological University) and Lawrence B. Aspler (BC Geological Survey) for thorough reviews and helpful comments.

References cited

British Columbia Geological Survey, 2019. British Columbia Digital Geology. British Columbia Ministry of Mining and Critical Minerals, British Columbia Geological Survey. Data version 2019-12-19. <https://www2.gov.bc.ca/gov/content/industry/mineral-exploration-mining/british-columbia-geological-survey/geology/bcdigitalgeology>

Campbell, R.B., 1968. Geology, Canoe River, British Columbia. Geological Survey of Canada Preliminary Map 15-1967, 1:253,400 scale.

Černý P., and Ercit, T.S., 2005. The classification of granitic pegmatites revisited. The Canadian Mineralogist, 43, 2005-2026.

Chakhmouradian, A.R., Reguir, E.P., Zaitsev, A.N., Couëslan, C., Xu, C., Kynický, J., Mumin, A.H., and Yang, P., 2017. Apatite in carbonatitic rocks: Compositional variation, zoning, element partitioning and petrogenetic significance. Lithos, 274-275, 188-213.

Colpron, M., 2020. Yukon terranes-A digital atlas of terranes for the northern Cordillera. Yukon Geological Survey. <https://data.geology.gov.yk.ca/Compilation/2#InfoTab>

Colpron, M., Logan, J.M., and Mortensen, J.K., 2002. U-Pb zircon age constraint for late Neoproterozoic rifting and initiation of the lower Paleozoic passive margin of western Laurentia. Canadian Journal of Earth Sciences, 39, 133-143.

Dalsin, M.L., Groat, L.A., Creighton, S., and Evans, R.J., 2015. The mineralogy and geochemistry of the Wicheeda carbonatite complex, British Columbia, Canada. Ore Geology Reviews, 64, 523-542.

Dixon, A., Cempírek, J., and Groat, L.A., 2014. Mineralogy and geochemistry of pegmatites on Mount Begbie, British Columbia. The Canadian Mineralogist, 52, 129-164.

Gammons, C.H., Risedorf, S., Wyss, G., and Lowers, H., 2024. Occurrences of the rare, REE minerals daqingshanite, törnebohmite, biraite, sahamalite, and ferriperbøeite from the Sheep Creek area, Montana, USA. Minerals 14, article1047. <https://doi.org/10.3390/min14101047>

Gary, M.A., 2024. Using indicator minerals from stream sediment samples to detect rare earth element deposits. Unpublished M.Sc. thesis, Montana Technological University, Butte, MT, USA, 80 p. <https://digitalcommons.mtech.edu/grad_rsch/321>

Gary, M.A., and Gammons, C.H., 2024. Using indicator minerals from stream sediment samples to detect rare earth element deposits. In: Van Rythoven, A., and Barth, S., (Eds.), Proceedings of the Montana Mining and Mineral Symposium 2023, September 27-30, 2023, Butte, Montana, Montana Bureau of Mines and Geology, Special Publication 124, pp. 53-58. <https://mbmg.mtech.edu/pdf-publications/SP124.pdf>

Grimes, C.B., John, B.E., Kelemen, P.B., Mazdab, F.K., Wooden, J.L., Cheadle, M.J., Hanghoj. K., and Schwartz, J.J., 2007. Trace element chemistry of zircons from oceanic crust: a method for distinguishing detrital zircon provenance. Geology, 35, 643-646. <https://doi.org/10.1130/G23603A.1>

Hardman, M.F., Pearson, D.G., DuFrane, S.A., Cabral Neto, I., Azzone, R.G., Shu, Q., Hinde, J., and Rukhlov, A.S., 2025. Improved trace element discrimination of kimberlitic and carbonatitic zircon: implications for zircon origin in kimberlite and the search for superdeep diamonds. Mineralogy and Petrology, 119, 583-605. <https://doi.org/10.1007/s00710-025-00916-2>

Heaman, L.M., Bowins, R., and Crocket, J., 1990. The chemical composition of igneous zircon suites: implications for geochemical tracer studies. Geochimica et Cosmochimica Acta, 54, 1597-1607.

Heaman, L., LeCheminant, A., and Rainbird, R.H., 1992. Nature and timing of Franklin igneous events, Canada: implications for a late Proterozoic mantle plume and the break–up of Laurentia. Earth and Planetary Science Letters, 109, 117-131.

Höy, T., and Brown, R.L., 1980. Geology of the eastern margin of Shuswap Complex, Frenchman Cap area. British Columbia Ministry of Energy, Mines and Petroleum Resources, British Columbia Geological Survey Preliminary Map 43, 1:100,000 scale.

Kukharenko, A.A., Orlova, M.P., Bulakh, A.G., Bagdasarov, E.A., Rimskaya-Korsakova, O.M., Nefedov, E.I., Ilynsky, G.A., Sergeev, A.S., and Abakumova, N.B., 1965. Caledonian complex of ultrabasic, alkaline rocks, and carbonatites of the Kola Peninsula and Northern Karelia (Geology, Petrology, Mineralogy, and Geochemistry). Nedra, Moscow, 772 p.

Kulla, G., and Hardy, J., 2015. Commerce Resources Corp. Blue River tantalum-niobium project, British Columbia, Canada, project update report. NI 43-101 Technical Report, 138 p. <https://www.sedarplus.ca/csfsprod/data151/filings/02317786/00000003/C%3A%5CFILINGS%5CSEDAR%5CCommerce%5CCCE_tech_rpt_031815.pdf>

Logan, J.M., (compiler), 2002. Intrusion-related mineral occurrences of the Cretaceous Bayonne magmatic belt, southeast British Columbia. British Columbia Ministry of Energy and Mines, British Columbia Geological Survey Geoscience Map 2002-01, 1:500,000 scale.

Lund, K., Aleinikoff, J.N., Evans, K.V., and Fanning, C.M., 2003. SHRIMP U-Pb geochronology of Neoproterozoic Windermere Supergroup, central Idaho: Implications for rifting of western Laurentia and synchroneity of Sturtian glacial deposits. Geological Society of America Bulletin, 115, 349-372.

Mackay, D.A.R., and Simandl, G.J., 2015. Pyrochlore and columbite-tantalite as indicator minerals for specialty metal deposits. Geochemistry: Exploration, Environment, Analysis, 15, 167-178.

Mäder, U.K., 1987. The Aley carbonatite complex, northern Rocky Mountains, British Columbia (94B/5). In: Geological Fieldwork 1986, British Columbia Ministry of Energy, Mines and Petroleum Resources, British Columbia Geological Survey Paper 1987-1, pp. 283-288.

Mao, M., Rukhlov, A.S., Rowins, S.M., Spence, J., and Coogan, L.A., 2016. Apatite trace element compositions: A robust new tool for mineral exploration. Economic Geology, 111, 1187-1222.

Mao, M., Rukhlov, A.S., Rowins, S.M., Hickin, A.S., Ferbey, T., Bustard, A., Spence, J., and Coogan, L.A., 2017. A novel approach using detrital apatite and till geochemistry to identify covered mineralization in the TREK area of the Nechako Plateau, British Columbia. In: Ferbey, T., Plouffe, A., and Hickin, A.S., (Eds.), Indicator Minerals in Till and Stream Sediments of the Canadian Cordillera. Geological Association of Canada Special Paper Volume 50, and Mineralogical Association of Canada Topics in Mineral Sciences Volume 47, pp. 191-243.

McDonough, M.R., Simony, P.S., Morrison, M.L., Oke, C., Sevigny, J.H., Robbins, D.B., Seigel, S.G., and Grasby, S.E., 1991. Howard Creek, British Columbia. Geological Survey of Canada Open File 2411, 1:50,000 scale.

McDonough, M.R., Simony, P.S., Sevigny, J.H., Robbins, D.B., Raeside, R., Doucet, P., Pell, J., and Dechesne, R.G., 1992. Geology of Nagle Creek and Blue River, British Columbia (83D/2 and 83D/3). Geological Survey of Canada Open File 2512, 1:50,000 scale.

Millonig, L.J., Gerdes, A., and Groat, L.A., 2012. U-Th-Pb geochronology of meta-carbonatites and meta-alkaline rocks in the southern Canadian Cordillera: A geodynamic perspective. Lithos, 152, 202-217.

Murphy, D.C., (compiler), 2007. Geology, Canoe River, British Columbia-Alberta. Geological Survey of Canada Map 2110A, 1:250,000 scale.

Ootes, L., Ferri, F., Milidragovic, D., and Wall, C., 2022. The age and provenance of the Lay Range assemblage provides an indirect record of basement to north-central Quesnellia, British Columbia. In: Geological Fieldwork 2021, British Columbia Ministry of Energy, Mines and Low Carbon Innovation, British Columbia Geological Survey Paper 2022-01, pp. 31-44.

Pell, J., 1994. Carbonatites, nepheline syenites, kimberlites and related rocks in B.C. British Columbia Ministry of Energy, Mines and Petroleum Resources, British Columbia Geological Survey Bulletin 88, 136 p.

Pell, J., and Simony, P.S., 1987. New correlations of Hadrynian strata, south-central British Columbia. Canadian Journal of Earth Sciences, 24, 302-313.

Raeside, R.P., and Simony, P.S., 1983. Stratigraphy and deformational history of the Scrip Nappe, Monashee Mountains, British Columbia. Canadian Journal of Earth Sciences, 20, 639-650.

Rudnick, R.L., and Gao, S., 2014. Composition of the continental crust. In: Holland, H.D., Turekian, K.K., and Rudnick, R.L., (Eds.), The Crust, Treatise on Geochemistry, 2nd Edition, Volume 4, Elsevier, Amsterdam, pp. 1-51. <http://dx.doi.org/10.1016/B978-0-08-095975-7.00301-6>

Rukhlov, A.S., Chudy, T.C., Arnold, H., and Miller, D., 2018. Field trip guidebook to the Upper Fir carbonatite-hosted Ta-Nb deposit, Blue River area, east-central British Columbia. British Columbia Ministry of Energy, Mines and Petroleum Resources, British Columbia Geological Survey GeoFile 2018-6, 67 p.

Rukhlov, A.S., Cui, Y., Cunningham, Q., Fortin, G., and Anderson, C., 2024. Geochemical signals of carbonatite-related critical metals in provincial stream sediments. In: Geological Fieldwork 2023, British Columbia Ministry of Energy, Mines and Low Carbon Innovation, British Columbia Geological Survey Paper 2024-01, pp. 97-122.

Rukhlov, A.S., Ootes, L., Creaser, R.A., Cunningham, Q.F., de Waal, F.S., and Wenger, D.K., 2025a. British Columbia carbonatites revisited: New whole rock Sr-Pb-Nd isotopic insights and drainage prospectivity trends. In: Geological Fieldwork 2024, British Columbia Ministry of Mining and Critical Minerals, British Columbia Geological Survey Paper 2025-01, pp. 119-139.

Rukhlov, A.S., Ootes, L., Creaser, R.A., Cunningham, F.Q., de Waal, S.F., and Wenger, D.K., 2025b. Supplementary data for British Columbia carbonatites revisited: New whole rock Sr-Pb-Nd isotopic insights and drainage prospectivity trends. British Columbia Ministry of Mining and Critical Minerals, British Columbia Geological Survey GeoFile 2025-09, 4 p.

Simandl, G.J., Mackay, D.A.R., Ma, X., Luck, P., Gravel, J., and Akam, C., 2017. The direct indicator mineral concept and QEMSCAN® applied to exploration for carbonatite and carbonatite-related ore deposits. In: Indicator Minerals in Till and Stream Sediments of the Canadian Cordillera, Ferbey, T., Plouffe, A. and Hickin, A.S., (Eds.), Geological Association of Canada, Special Paper Volume 50 and Mineralogical Association of Canada, Topics in Mineral Sciences Volume 47, pp. 175-190.

Simony, P.S., Ghent, E.D., Craw, D., and Mitchell, W., 1980. Structural and metamorphic evolution of the northeast flank of the Shuswap complex, southern Canoe River area, British Columbia. In: Crittenden, M.D., Coney, P.J., and Davis, G.H., (Eds.), Cordilleran Metamorphic Core Complexes. Geological Society of America, Memoir 153, pp. 445-461.

Warr, L.N., 2021. IMA-CNMNC approved mineral symbols. Mineralogical Magazine, 85, 291-320. <https://doi.org/10.1180/mgm.2021.43>

Wheeler, J.O., and Fox, P.E., 1964. Geology, Big Bend, Seymour Arm, east half, British Columbia. Geological Survey of Canada Preliminary Map, 12-1964, 1:253,440 scale.

Ya'acoby, A., 2014. The petrology and petrogenesis of the Ren carbonatite sill and fenites, southeastern British Columbia, Canada. Unpublished M.Sc. thesis, The University of British Columbia, Canada, 463 p.

Rossland Group extends north: Detrital zircon U-Pb ages allow supracrustal unit reassignments in southern British Columbia and have tectonic implications

Luke Ootes[1], Corey Wall[2], and Mitchell G. Mihalynuk[1]

[1] British Columbia Geological Survey, Ministry of Mining and Critical Minerals, Victoria, BC, V8W 9N3
[2] Pacific Centre for Isotopic and Geochemical Research, Earth and Ocean Sciences, The Univesity of British Columbia, Vancouver, BC, V6T 1Z4
[a] corresponding author: Luke.Ootes@gov.bc.ca

Recommended citation: Ootes, L., Wall, C., and Mihalynuk, M.G., 2026. Rossland Group extends north: Detrital zircon U-Pb ages allow supracrustal unit reassignments in southern British Columbia and have tectonic implications. In: Geological Fieldwork 2025, British Columbia Ministry of Mining and Critical Minerals, British Columbia Geological Survey Paper 2026-01, pp. 119-130.

Abstract

Sedimentary rocks preserved in a series of outliers in southeast British Columbia and considered part of Quesnel terrane were variously assigned by previous workers to the Nicola Group, the Slocan Group, and the Harper Ranch Group. New detrital zircon U-Pb results indicate that rocks at two locations previously thought to be Harper Ranch Group (Carboniferous-Devonian) are Late Triassic. Exclusively Triassic zircon in these two samples points to provenance from weathering, erosion, and deposition close to the Nicola Group and its intrusive equivalents (Late Triassic). Samples from two other locations have mostly Late Triassic to Jurassic detrital zircons, and Jurassic maximum depositional ages (ca. 200 Ma and ca. 183 Ma). These samples also contain zircon populations spreading from the Mesoproterozoic, indicating exposure to diverse older erosional sources during sedimentation. However, these ages are incompatible with derivation from currently nearby Archean and Paleoproterozoic Ancestral North America and may indicate sources now in southwestern USA or Mexico or a cryptic crustal block. The age of the ca. 200 Ma sample and its position beneath pyroxene-phyric basalts suggest a stratigraphic relationship and correlation to the Archibald and Elise formations of the Rossland Group. The younger sample has the same maximum depositional age as the recently identified Salmon River succession and Lions Head succession. This younger unit can be correlated to the Hall Formation of the Rossland Group. A fifth sample, collected from the Slocan Group, contains Triassic zircon and has a Late Triassic maximum depositional age. It also contains a spread of Mesoproterozoic (Ecclassian), Neoproterozoic (Ediacaran and Tonian), and Paleozoic (Carboniferous-Devonian and Cambrian) zircon, and currently nearby Ancestral North America-aged zircon populations appear to be lacking, again suggesting derivation from exotic sources and opening the possibility of significant orogen-parallel terrane displacements.

Beneath the Rossland Group and Triassic sedimentary units are ‘quartzites’ of the Chase Formation. However, North American detrital zircon from the Chase Formation are not recycled into the Rossland Group and the quartzites display mylonitic fabrics. We tentatively conclude that the Chase Formation records a previously unrecognized shear zone and that the juxtaposition preserved today is structural, not stratigraphic. Age-cumulative probability modelling support that the units in this study were deposited at a convergent margin, likely in a forearc or trench basin at the leading edge of Quesnellia as it approached the North American margin. However, where on the North American margin remains to be demonstrated. Based on detrital zircon data presented herein, we put forward a speculative yet testable alternative to current tectonic models that envisage eastward subduction during evolution of the Nicola arc by postulating westward subduction and an east-facing oceanic arc. Accordingly, we explain the exclusively Triassic zircon populations in older (Triassic) rocks to have been derived from local, roughly coeval sources, and mixed detrital zircon populations in younger (Jurassic) rocks to indicate arrival of older crust (Paleozoic to Precambrian) of uncertain origin.

Keywords: Quesnel terrane, Rossland Group, Slocan Group, Nicola Group, Harper Ranch Group, Chase Formation, detrital zircon, mylonite

1. Introduction

The transition between Quesnel terrane and Ancestral North America (Fig. 1) remains enigmatic, partly because of limited exposures and partly because of different geologists working over a span of decades making observations at isolated outcrops. Most of the rocks that form a series of hills east and west of Vernon (Fig. 2) are poorly exposed grey graphitic phyllite with only rare visible contacts (Okulitch, 1979). Thompson et al. (2006) provided the most up-to-date bedrock mapping and map compilation in the area and assigned some of the rocks that underly the hills as outliers of the Slocan Group (also see Okulitch, 1979) that were thought to be the lateral facies equivalents of Nicola Group volcanic rocks (Late Triassic; e.g., Untershutz et al., 2002; Mihalynuk and Diakow, 2020). Before this, these rocks were variously assigned to the Cache Creek Group (Jones, 1959) and the Nicola, Slocan, and Harper Ranch groups (Okulitch, 1979; Schiarizza and Church, 1996). In tectonostratigraphic terms, these rocks represent the suprastructure to an infrastructure represented by Precambrian and Paleozoic orthogneiss and paragneiss of the Shuswap metamorphic core complex (Fig. 2; e.g., Parrish et al., 1988; Glombick et al., 2006; Brown et al., 2017).

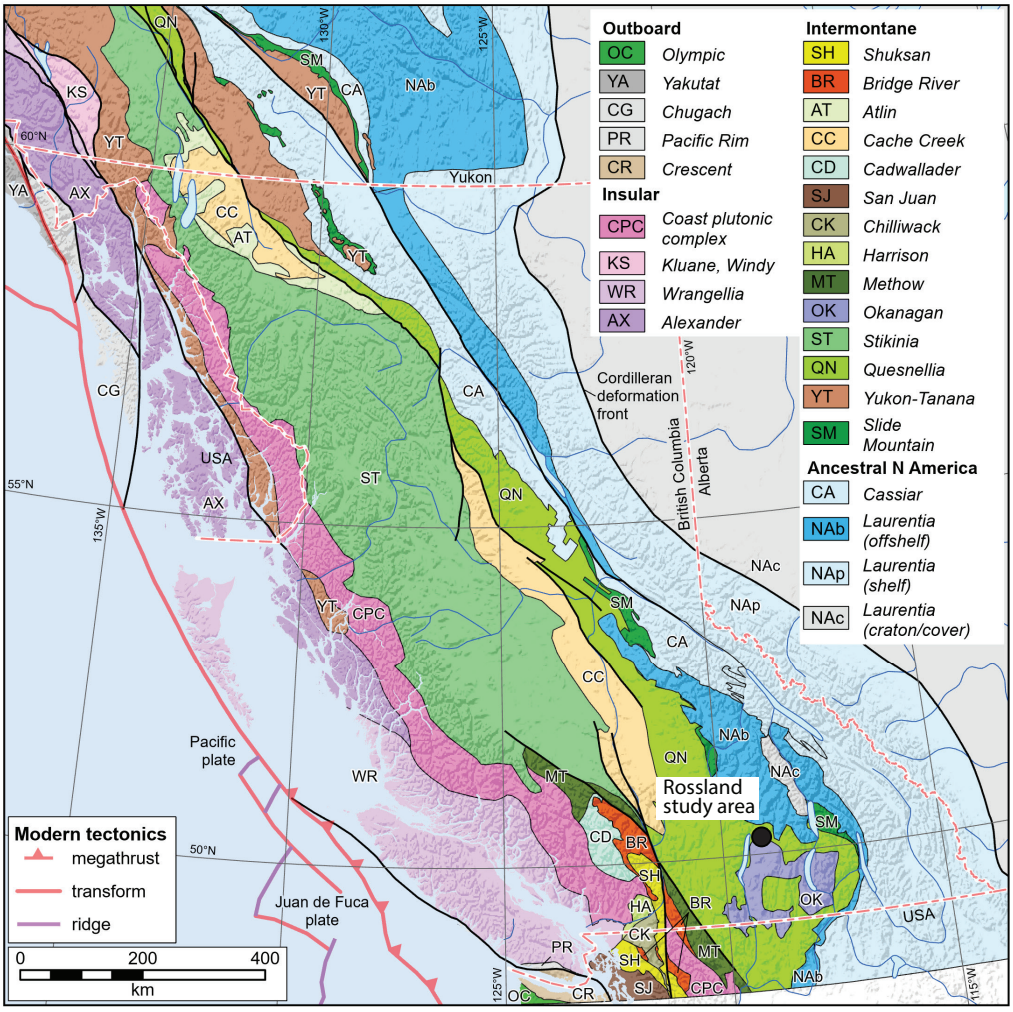


Fig. 1. Location of the study area. Terranes after Colpron (2020).

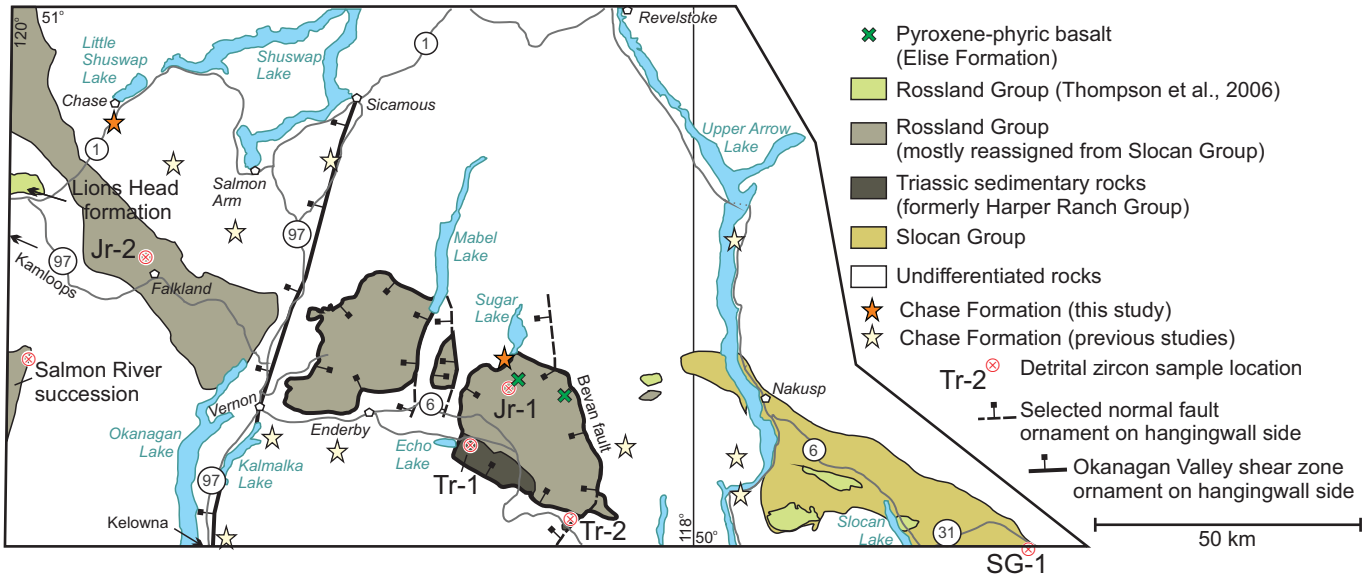


Fig. 2. Simplified geological map highlighting units that were previously assigned to the Nicola and Slocan groups. Based on the results in this study, these units may be best included in the Rossland Group. The distribution of Harper Ranch Group rocks is also in question. Undifferentiated units range from Paleoproterozoic gneissic rocks to Miocene basalt. Geology is simplified after Thompson et al. (2006); known exposures of the Chase Formation from Thompson et al. (2006); Glombick et al. (2006), and Lemieux et al. (2007). The Okanagan Valley shear zone is from Parrish et al. (1988) and Brown et al. (2017).

Unterschutz et al. (2002) provided radiogenic isotopic data for these supracrustal rocks and, because they were considered as stratigraphic equivalents to Nicola Group volcanic rocks, these data were interpreted to represent the isotopic signature of the Late Triassic volcanic arc component of Quesnel terrane. Accordingly, these data were thought to indicate that Ancestral North American basement was present during the development of the Nicola arc (Unterschutz et al., 2002; Thompson et al., 2006). New detrital zircon and field data presented herein address unit assignments in the area and open the possibility of a speculative but testable model for the nature of the transition between Quesnel terrane and Ancestral North America.

This study was initiated to field check the available bedrock geology of the Vernon area before updating the BC Digital Geology database (British Columbia Geological Survey, 2019). We collected samples to establish detrital zircon U-Pb provenance and maximum depositional ages of units in the area. This paper provides an overview of five new detrital zircon U-Pb results from: 1) a turbiditic unit with graded sandstone-mudstone beds that outcrops west of Arrow Lake, previously considered as Harper Ranch Group (Thompson et al., 2006); 2) an isolated sandstone-bearing outcrop from east of Echo Lake, previously assigned to the Harper Ranch Group (Thompson et al., 2006); 3) a rare, strongly deformed sandstone bed within graphitic phyllite southeast of Sugar Lake, previously assigned to the Slocan Group (Thompson et al., 2006); 4) a turbiditic unit with graded sandstone-mudstone beds that outcrops north of Falkland, previously assigned to the Slocan Group (Thompson et al., 2006); and 5) for comparison, a rare sandstone sample from the Slocan Group east of Slocan Lake.

2. Past unit assignments and reassignments

Bedrock mapping of the Vernon NTS sheet in the 1950s (Jones, 1959) identified a mixed unit of orthogneiss and paragneiss that was called the Monashee Group and a northwest-trending belt of supracrustal rocks that were assigned to the Cache Creek Group. Okulitch (1979) updated this geology, reassigning Cache Creek rocks to other units, including the Harper Ranch, Nicola, and Slocan groups (Quesnel terrane) and was later updated for BC Digital Geology by Schiarizza and Church (1996). Currently, the Nicola Group is reserved for Late Triassic volcanic and volcanosedimentary rocks in Quesnel terrane, sensu stricto (e.g., Mihalynuk and Diakow, 2020; Schiarizza, 2024). Sedimentary rocks that are considered equivalent to the Nicola Group are commonly referred to as Slocan Group (e.g., Schiarizza, 2024) but nowhere have stratigraphic or chronological links been clearly demonstrated and the relationship remains conjectural. Thompson et al. (2006) referred to most of the rocks in the Vernon area as Slocan Group because they almost entirely appear to be of sedimentary origin.

East of Kamloops, sedimentary rocks that unconformably overly the Harper Ranch Group (Devonian) were assigned to the Nicola Group (Okulitch, 1979). Using fossil assemblages, Beatty et al. (2006) recognized these rocks were deposited in the Jurassic and referred to them as the Lions Head succession. To the south near Salmon River, Schiarizza et al. (2022) used detrital zircons to demonstrate that some sedimentary units that had been assigned to the Nicola Group were deposited after ca. 183 Ma (Jurassic) and they referred to these rocks as the Salmon River succession (Fig. 2). They suggested that these rocks may correlate to the Lions Head succesion and the Hall Formation of the Rossland Group to the south (Höy and Dunne, 1997).

3. Sampling

The area investigated (Fig. 2) is commonly covered by vegetation, and Quaternary cover is extensive; the best exposures are typically in roadcuts along highways, resource roads, and logging slashes. Most of the Mesozoic supracrustal rocks are fine-grained strongly deformed graphitic phyllite and slate or calcareous sandstones and mudstones (Fig. 3) that are less than ideal candidates for undertaking detrital zircon provenance and maximum depositional age work. Fortunately, we were able to find rare sandstone beds more suitable for sampling (Fig. 3; Table 1) but mostly from isolated outcrops. Because stratigraphic relationships are not typically preserved, regional correlations from the results we present below are interpretations constrained by the available data. For regional comparison, we include a sample from an exposure east of Slocan Lake that is typical of the Slocan Group in its eponymous area.

4. Detrital zircon analysis

4.1. Methods

Analytical details follow those in Ootes et al. (2022). Detrital zircon were separated from rock samples at the Pacific Centre for Isotopic and Geochemical Research at the University of British Columbia. Zircon crystals (>75 mm) were selected from conventional density and magnetic mineral separation methods. The entire zircon separate was annealed at 900°C for 60 hours, then individual grains were hand-picked and mounted, polished, and imaged by cathodoluminescence (CL) on a scanning electron microscope. From these images, grains were selected for U-Pb isotopic analysis, conducted using a Resonetics RESOlution M-50-LR, connected via a Teflon squid to an Agilent 7700x quadrupole ICP-MS. After data reduction, data were further screened using trace elements and analytical results >10% discordant were removed. To test the maximum deposition age of some samples, the youngest zircon grains were plucked from the grain mount and analyzed by chemical abrasion-thermal ionization mass spectrometry (CA-TIMS) following the methods in Ootes and Wall (2024).

4.2. Results

4.2.1. Tr-1; 22lo5-30

Sample Tr-1 (Triassic 1) was collected along the southern leg of the Creighton Valley road, southeast of Echo Lake (Fig. 2; Table 1). The sample is from an isolated outcrop of sandstone and carbonate (Fig. 3a), previously assigned as

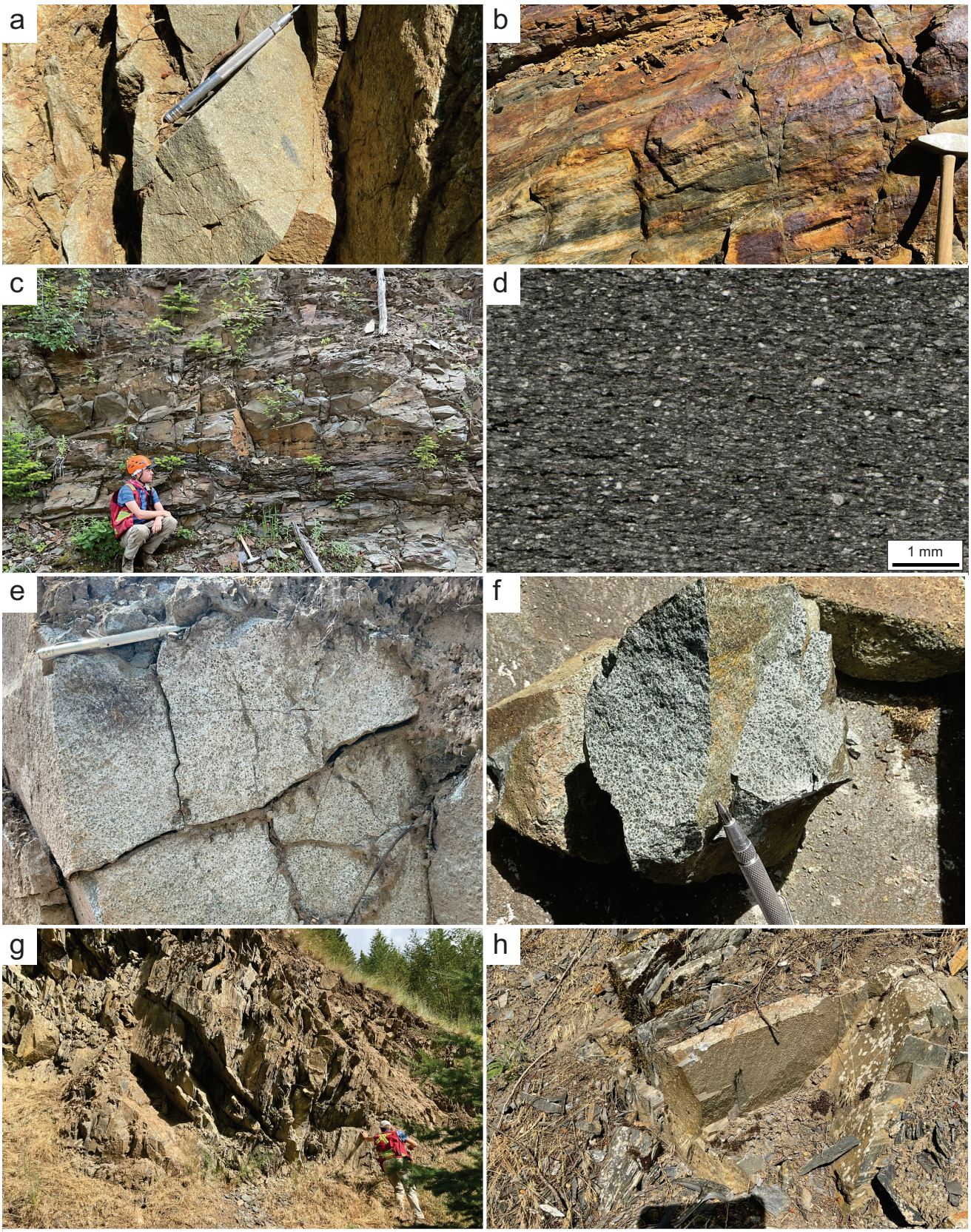


Fig. 3. Outcrop photographs of sample locations in this study. **a)** Sandstone, sample Tr-1, **b)** Rusty sandstone-mudstone beds at sample location Tr-2. **c)** Deformed phyllitic rocks with a rare sandstone bed at sample location Jr-1. **d)** Thin section photomicrograph of fine-grained and strongly deformed sample Jr-1; plane polarized light. **e-f)** Massive pyroxene-phyric basalt outcrops topographically above Jr-1 sample location. **g)** Steeply dipping sandstone to mudstone fining-upward sequences at sample location Jr-2. **h)** Rare, ~20 cm thick beige sandstone bed; sample Jr-2.

Table 1. New U-Pb zircon samples, unit reassignments, and maximum depositional ages.

Sample	Station ID	New^	Previous Group*	Maximum depositional age (Ma)*	Lat.	Long.
Jr-2	22lo18-93	Rossland Group	Slocan	182.73 ±0.05	50.542508	119.600851
Jr-1	22lo6-38	Rossland Group	Slocan	199.914 ±0.036	50.29986	118.541245
Tr-2	22lo4-23	Triassic sedimentary unit	Harper Ranch	ca. 220	50.03599	118.363879
Tr-1	22lo5-30	Triassic sedimentary unit	Harper Ranch	ca. 230	50.19397	118.655057
SG-1	MMI21-12-01	Slocan Group	Slocan	ca. 210	49.9795	117.0116

^New assignments are from detrital zircon results in this study and Schiarizza et al. (2022) and previous Group assignments are from Okulitch (1979) and Thompson et al. (2006 and references therein).

*Estimated maximum depositional age from LA-ICP-MS is given as circa (ca.).

Harper Ranch Group (Thompson et al., 2006). Sixty-seven concordant zircons (of 85 analyses) have a unimodal age population between 250 and 225 Ma (Fig. 4a). Using the 'minimum' option in a radial plot (Vermeesch, 2021), a maximum depositional age is estimated at ca. 230 Ma (Fig. 4a).

4.2.2. Tr-2; 22lo4-23

Sample Tr-2 was collected from a resource roadcut north of Highway 6, west of Arrow Lake (Fig. 2; Table 1). At this location, a switchback road provides outcrops of rusty turbiditic sandstone-mudstone beds with preserved primary and locally graded bedding (Fig. 3b). Previously, this was assigned as Harper Ranch Group (Thompson et al., 2006). A sample was collected from a fine-grained sandstone bed, but only a modest number of zircon was retrieved (n=9). Uranium-lead results (n=7) have a narrow range of unimodal ages between 225 to 215 Ma (Fig. 4b). The limited number of zircon allows a weighted mean calculation of ca. 220 Ma, interpreted as the maximum depositional age (Fig. 4b).

4.2.3. Jr-1; 22lo6-38

This sample (Jurassic 1) was collected from a rare arenaceous bed in otherwise strongly deformed phyllitic rocks along a resource road southeast of Sugar Lake (Fig. 2; Table 1). Primary sedimentary structures are not preserved because of the strong deformation (Figs. 3c, d) indicating the layering may be compositional and structurally transposed rather than bedding. From the sample location, the resource road climbs to higher elevations where exposures of fine-grained mafic rock with pyroxene phenocrysts (basalt) occur (Figs. 3e, f). These rocks appear less deformed than the underlying phyllitic rocks but no primary volcanic features were observed (Figs. 3e, f). The strongly deformed fine-grained arenaceous sample yielded 121 detrital zircons. Concordant U-Pb ages (n=107) are predominantly ca. 200 Ma (n=75), with minor Paleozoic (n=12) and Precambrian (n=20) populations (Fig. 5a). To test the maximum depositional age, six zircon grains were removed from the laser ablation mount, dissolved and analyzed by CA-TIMS, yielding a weighted mean U-Pb age of 199.914 ±0.036 Ma (n=5/6), interpreted as the maximum time of deposition (Fig. 5a; Table 1).

4.2.4. Jr-2; 22lo18-93

This sample was collected from northwest of Falkland, where the Chase-Falkland road intersects the Six Mile Creek road (Fig. 2; Table 1). The creek-side outcrop consists of 2 to 3 m cliff faces of vertically dipping thin (~5 cm) sandstone-mudstone beds. A well-preserved foliation is clockwise to bedding and an intersection lineation on the bedding planes has a shallow plunge to the southeast. The outcrop was thoroughly searched for sandstone layer coarse grained enough for detrital zircon work, and a bed ~20 cm thick was sampled. Concordant U-Pb results (n=116) have a tight range from Late Triassic to Early Jurassic (n=114). In addition, one zircon yielded an age of ca. 280 Ma, and another zircon yielded an age of ca. 1030 Ma (Fig. 5b). Six single zircon grains were analyzed by CA-TIMS and yielded three populations younger than ca. 186 Ma, with the two overlapping results providing a maximum depositional age of 182.73 ±0.05 Ma (Fig. 5b; Table 1).

4.2.5. SG-1; MMI21-12-01

This sample was collected south of Highway 31A near a bridge crossing the Kaslo River (Figs. 2, 6a; Table 1). A single fine to medium-grained, 1.5 cm thick sandstone layer within dark grey to black argillite (Fig. 6b) was sampled for detrital zircon analysis. One-hundred and twenty-two zircon grains were analyzed by LA-ICP-MS, of which 84 passed further filtering and are <10% discordant. Multiple age populations are in the sample including a minor Mesoproterozoic mode (ca. 1300 Ma; Eclassian), a Neoproterozoic (Tonian) mode, and significant Neoproterozoic (Ediacaran) to Cambrian (580 to 500 Ma), Devonian through Carboniferous (400 to 300 Ma), and Late Triassic (240 to 220 Ma) modes (Fig. 6). Using the 'minimum'

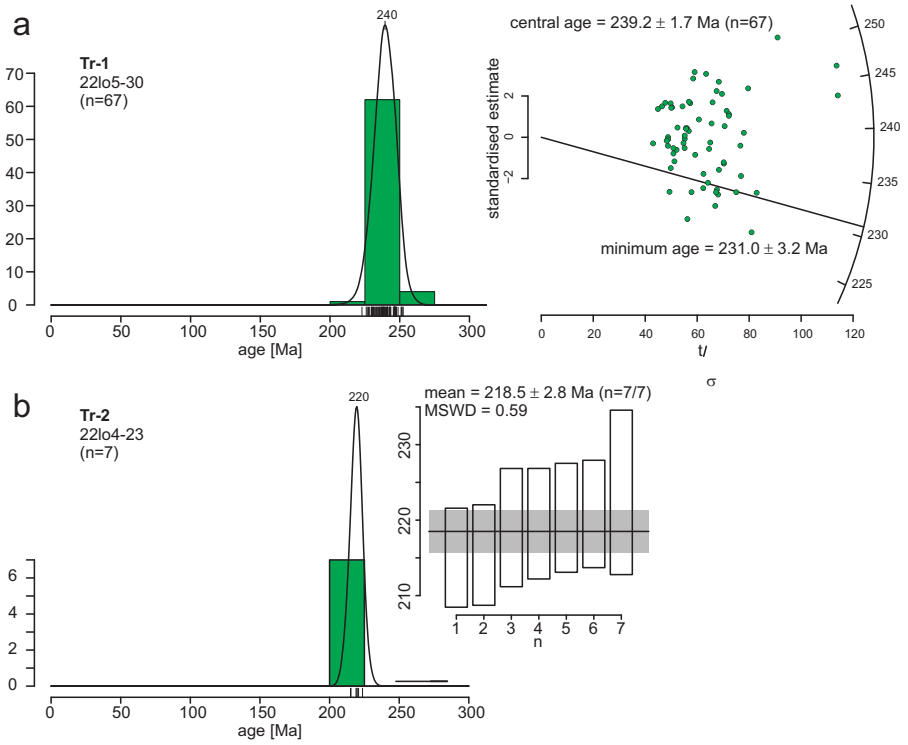


Fig. 4. Detrital zircon geochronology of Triassic samples. **a)** Kernel density estimate (KDE) with rug plot and radial plot of concordant zircon U-Pb ages of sample Tr-1, with an estimated maximum depositional age of ca. 230 Ma and a single population at ca. 240 Ma. **b)** Sample Tr-2 KDE and weighted mean age of ca. 220 Ma from concordant zircons in the sample, interpreted as the maximum depositional age of the sample. All plots generated using IsoplotR (Vermeesch, 2018) and maximum depositional ages are derived following Vermeesch (2021).

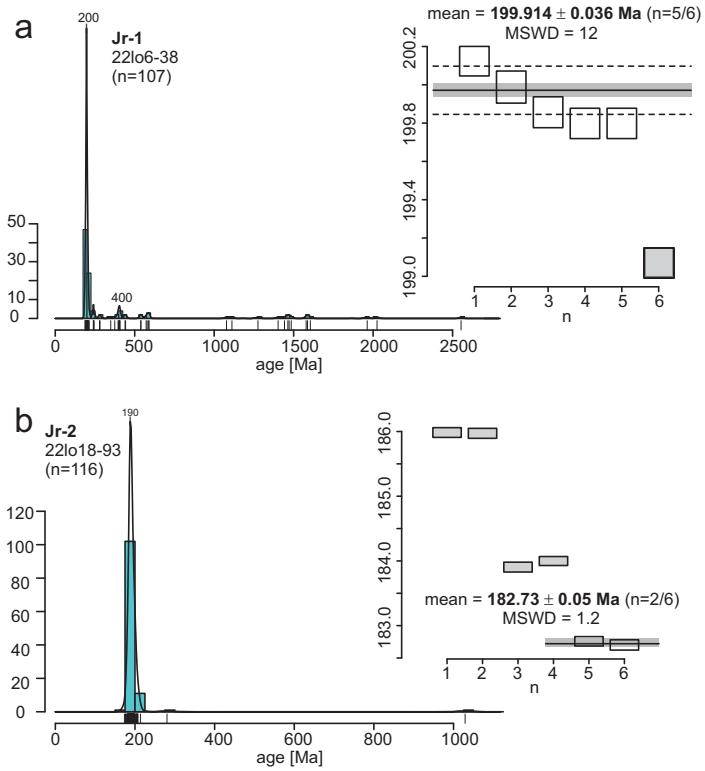


Fig. 5. Detrital zircon geochronology of Jurassic samples. **a)** Sample Jr-2 KDE plot and weighted mean of concordant zircon from CA-TIMS, yielded a maximum depositional age of 199.914 ±0.036 Ma. One younger zircon at 199 Ma was excluded from the weighted mean. **b)** Sample Jr-2 KDE and weighted mean ages from concordant zircon from CA-TIMS. The two youngest overlapping zircon grains yield a weighted mean age of 182.73 ±0.05 Ma, interpreted as the maximum depositional age of the sample.

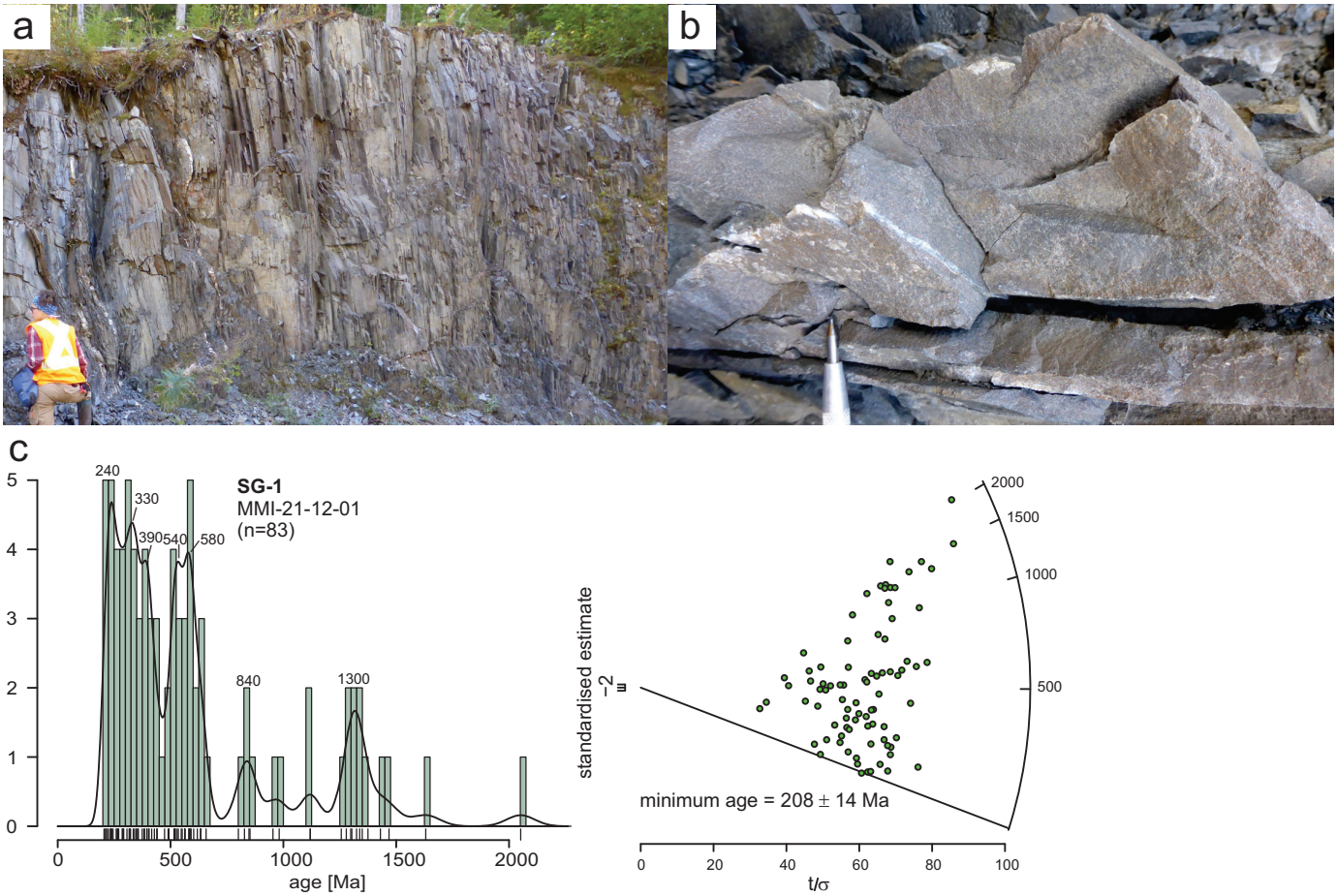


Fig. 6. a-b) Outcrop photographs of the Slocan Group sample location in a roadside quarry and photograph of the rare sandstone sampled for this study. **c)** Sample SG-1 KDE plot showing a range of <10% discordant zircon ages with age modes labelled. Radial plot with estimated maximum depositional age of the sample at ca. 210 Ma. All plots generated using IsoplotR (Vermeesch, 2018).

option in a radial plot (Vermeesch, 2021), a maximum depositional age is estimated at ca. 210 Ma (Fig. 6) that is consistent with Carnian to Norian conodont ages reported from the same area by Orchard (1985).

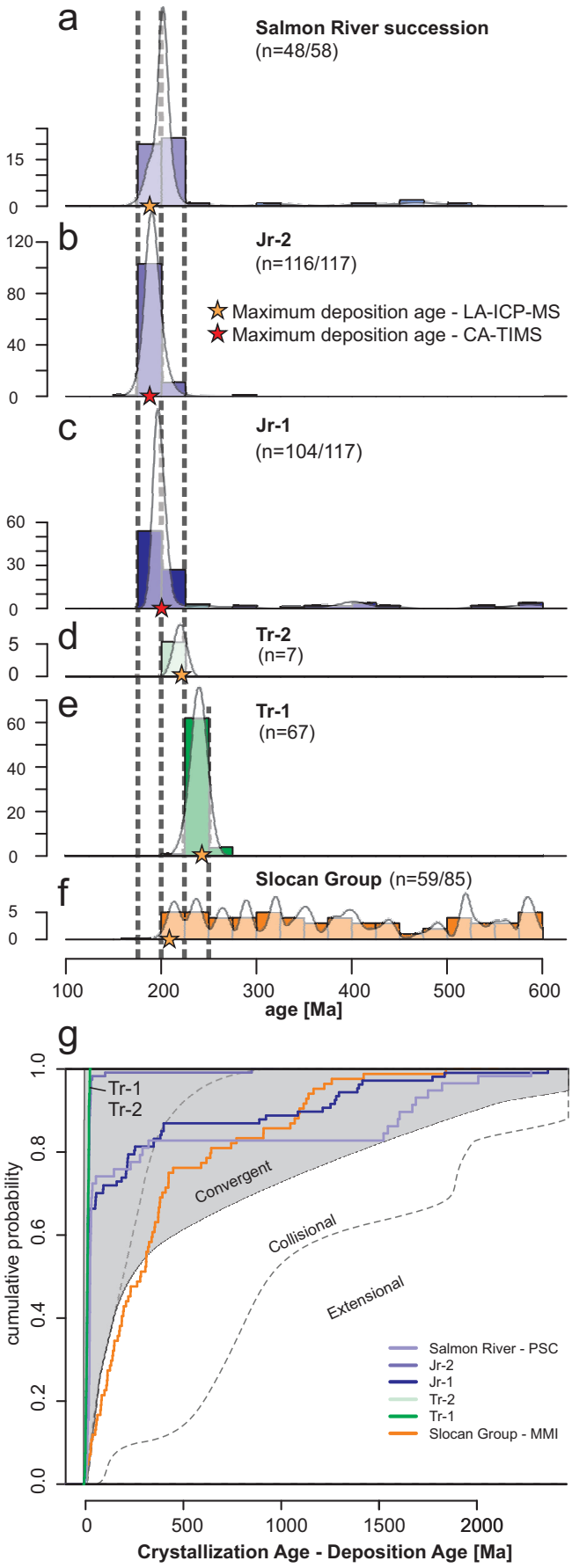
5. Discussion

5.1. Triassic sedimentary rocks

Both Tr-1 and Tr-2 contain Late Triassic zircon populations and maximum depositional ages. Sample Tr-1 has a relatively older population (ca. 240 Ma) compared with a slightly younger population in Tr-2 (ca. 220 Ma), although this sample has a low number of age results (Figs. 4, 7). Both are consistent with detritus derived from the Nicola Group, or intrusive equivalents, and do not include zircon from any other sources. Both samples are from isolated enclaves and the ability to correlate them to localities elsewhere is difficult without other supporting information. Rocks at the Tr-2 sample location were previously assigned to the Harper Ranch Group (Thompson et al., 2006) probably because of resemblance to turbiditic sandstone-mudstone beds at the type locality near Kamloops (Fig. 2) as described by Beatty et al. (2006). However, the detrital zircon results indicate that sample Tr-2 is ~150 million years younger than the Harper Ranch Group (Devonian to Carboniferous; Beatty et al., 2006). These results call into question the true distribution of the Harper Ranch Group away from its type locality.

The Slocan Group sample has Triassic U-Pb zircon ages but also contains abundant older populations (SG-1; Figs. 6, 7). The Triassic ages are similar to Tr-1 and Tr-2 (Fig. 7). The Devonian to Carboniferous zircon populations could record derivation from the oldest units in Quesnel terrane such as the Lay Range assemblage in northern Quesnellia (Ootes et al., 2022), but the older Paleozoic and Precambrian populations (Fig. 6) are unlike the ages of Quesnel terrane rocks, currently nearby Archean and Paleoproterozoic Ancestral North America, or of second-cycle zircons that may have been reworked from passive margin sedimentary rocks deposited on nearby Ancestral North American basement. However, these older zircon ages are similar to the ages of rocks now exposed in the southwestern USA and Mexico (e.g., Matthews et al., 2018).

In summary, samples Tr-1 and Tr-2 indicate that a single source was exposed to erosional levels during sedimentation: the



Nicola Group and allied intrusions (Figs. 4, 7). In contrast, the Slocan sample indicates erosion of both significantly older and diverse sources and Triassic sources (Fig. 7). What these older sources may have been remains unclear; further detrital zircon, trace element, and eHf^{T} isotopic work may help resolve the question.

5.2. Jurassic sedimentary rocks: Rossland Group?

The sandstones represented by sample Jr-1 were deposited after ca. 200 Ma (Figs. 5, 7). Because of the pyroxene-phyric basalts exposed at higher elevation (Figs. 2, 3e, f), these rocks may best be correlated to the Rossland Group (Höy and Dunne, 1997). The phyllites may be equivalent to the Archibald Formation (Sinemurian; 199.5 to 192.9 Ma) and the basalts equivalent to the Elise Formation (Sinemurian to Pliensbachian; Höy and Dunne, 1997). It remains unclear where the ca. 400 Ma zircon population in Jr-1 may have been derived from. East of the sample location and west of Arrow Lake (Fig. 2), Okulitch (1979) and Thompson et al. (2006) identified an outlier of Rossland Group volcanic rocks (unit lJR). An adjacent outlier was re-assigned to Slocan Group by Thompson et al. (2006). Given the evidence in this study this outlier is likely also part of the Rossland Group (Fig. 2).

The sandstone represented by sample Jr-2 was deposited close to or after ca. 183 Ma (Toarcian; Figs. 5, 7). This is the same maximum depositional age determined by Schiarizza et al. (2022) for the Salmon River succession to the southwest (Figs. 2, 7), which they correlated to the Lions Head succession above the Harper Ranch Group east of Kamloops (Beatty et al., 2006) and, potentially, to the Hall Formation of the Rossland Group (Höy and Dunne, 1997). The Hall Formation has never been tested with detrital zircon geochronology, but its depositional age is constrained by Toarcian fossil assemblages (184.2 to 174.7 Ma; Höy and Dunne, 1997), supporting that these units are equivalent to the Hall Formation.

Fig. 7. a-f) Kernel density estimate plots (600-100 Ma) showing a stepwise variation in zircon provenance and maximum depositional age of each sample. Concordant (<10% discordant) ages used for the plot. Maximum depositional ages from LA-ICP-MS and CA-TIMS are differentiated by coloured stars. Salmon River succession sample is from Schiarizza et al. (2022). **g)** Zircon crystallization (Crystallization Age) minus the time of deposition (Deposition Age) versus cumulative probability plot. The steep trends of all samples show that >75% of the detrital zircons in the samples are near the depositional age, consistent with sedimentation in a trench or forearc at a convergent margin, rather than in a back-arc or foreland basin (collisional field), or continental rift to passive margin basins. Samples Tr-1 and Tr-2 contain only zircon populations that are close to when source rocks crystallized. Samples Jr-1 and Slocan Group contain zircon populations that record derivation from older sources. Diagram and fields modified from Cawood et al. (2012).

We interpret that the Jurassic depositional ages determined in this study represent all similar rocks (mostly grey graphitic phyllite) in the outliers that form the hills east of Vernon and continue to the west, past Falkland to the Kamloops area (Fig. 2). Most of the rocks in this area were assigned to the Slocan Group and interpreted to be equivalent to the Nicola Group to the west (Okulitch, 1979; Untershutz et al., 2002; Thompson et al., 2006). Reassignment to the Rossland Group is more consistent with depositional ages <200 Ma (Figs. 5, 7; Höy and Dunne, 1997; Beatty et al., 2006; Schiarizza et al., 2022). In contrast to Unterschutz et al. (2002), we consider that their whole-rock radiogenic isotope (eNd^T) data represent rocks that are younger than 200 Ma and do not represent the relationship between Nicola Group (Late Triassic) and Ancestral North America. These data likely indicate mixing of juvenile and more evolved sources or reflect minor input of older detritus as recorded by older zircon in the samples (Figs. 5, 7). Detrital zircon eHf^T data should help clarify this.

5.3. Comparison of detrital sources

Each of the samples in this study has a different provenance (Fig. 7). The Jurassic samples have similar ca. 200 Ma zircon populations, but they differ slightly in detail. Sample Jr-1 has a zircon population (ca. 200 Ma) that is older than sample Jr-2 and the sample from the Salmon River succession, which contain predominantly 190 Ma zircon (Fig. 7; Schiarizza et al., 2022). The Triassic samples have older populations, and each sample locality has different populations (Fig. 7). The Slocan Group sample contains equal amounts of both Triassic zircon and older Neoproterozoic to Paleozoic populations (Fig. 7f).

The steep trends on cumulative probability plots (Fig. 7g) indicate most of the detrital zircon ages (i.e., crystallization age of the zircon) are close to the maximum depositional age of the rocks, consistent with sedimentation at a convergent margin. Given unimodal ages from the Triassic samples we would interpret deposition in a trench or forearc basin (Fig. 8). There is little evidence for detritus from nearby Archean and Paleoproterozoic Ancestral North America (Figs. 4-8). Based on these data, we introduce a speculative westward subduction tectonic model as an alternative interpretation. This alternative differs from conventionally held views (e.g., Nelson et al., 2013) that envisage the Nicola arc as having been generated by eastward subduction beneath North America. Instead, we explain exclusively Triassic zircon populations to have been derived from roughly coeval local sources, and mixed populations in younger (Jurassic) rocks to indicate arrival of evolved crust of uncertain origin. This alternative interpretation corroborates results from northern Quesnel terrane (Jones et al., 2022; Ootes et al., 2022), where the influence of Ancestral North American rocks on the magmatic evolution of Quesnel terrane, even to Early Cretaceous, is absent.

5.4. Chase Formation mylonite

The Chase Formation (Jones, 1959) is a white to grey weathered calcareous quartzite with a diagnostic pitted appearance, traced from Chase to east of Arrow Lake and south to the Kelowna area (Figs. 2 and 8; Okulitch, 1979; Glombick et al., 2006; Thompson et al., 2006; Lemieux et al., 2007). The unit was thought to be overlain by Slocan Group rocks, considered as lateral facies equivalent of the Nicola Group volcanic

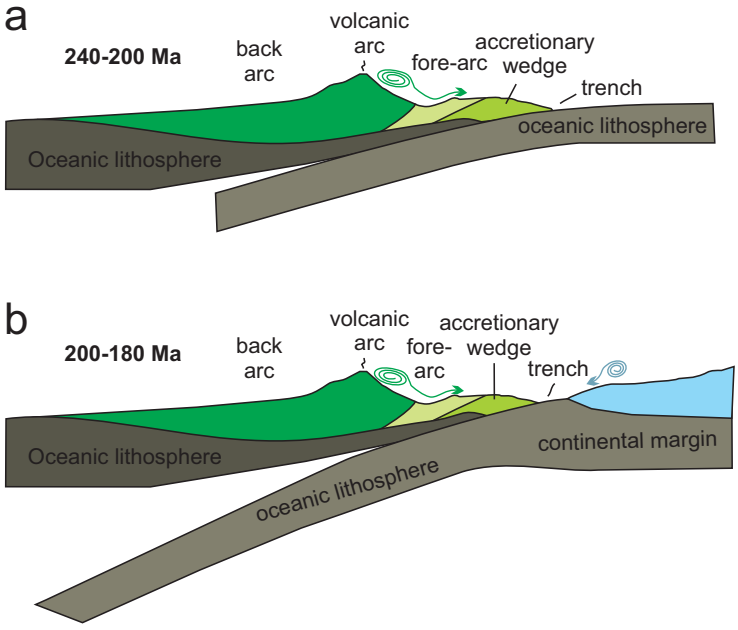


Fig. 8. Schematic diagram of westward subduction and an east-facing oceanic arc in the Triassic, with sedimentation in a forearc or trench; erosion and transport detrital zircon indicated by swirls and arrows. **a)** 240 to 200 Ma with unimodal zircon derived from arc. **b)** 200-180 Ma, the arrival of evolved crust of uncertain origin accounts for the appearance of older (pre-Triassic) zircon populations that are not typical of northern Ancestral North America.

rocks, and therefore it was regarded to link North America passive margin stratigraphy to Quesnel terrane (Unterschutz et al., 2002; Thompson et al., 2006; Lemieux et al., 2007).

Although there are different views on correlating these distinctive rocks across a wide area (cf. Lemieux et al., 2007 with Colpron and Nelson, 2009), the unit displays high-strain features. For rocks west and away from Arrow Lake, Thompson et al. (2006) referred to both primary bedding and structurally transposed compositional layering, and Glombick et al. (2006) described exposures at Kalamalka Lake and Kelowna airport as mylonites. We examined the Chase Formation at a new highway exposure along Highway 1 southwest of the town of Chase, and at a new resource roadcut southwest of Sugar Lake (Figs. 2 and 9a). No primary depositional features are preserved in these rocks, but the rocks display a prominent compositional layering (Fig. 9a), and petrographic examination reveals a lineation suggestive of dynamic recrystallization (Fig. 9b; see also Glombick et al., 2006). In short, we consider that the Chase Formation may represent a mylonitic shear zone.

A separate question is if the outlier phyllites (now Rossland Group) were deposited on the Chase Formation (Fig. 10a) or if the superposition is structural (Fig. 10b). Although we cannot negate stratigraphic interpretations (cf. Okulitch, 1979; Thompson et al., 2006), we favour a structural interpretation. Rossland Group rocks are topographically above the Chase Formation at Sugar Lake (sample Jr-1; also see figure 5a of Glombick et al., 2006) but no contacts have been observed in the field. We consider that this relationship represents a relatively flat lying shear zone that continues for the extent of the Chase Formation (>80 km) from the town of Chase in the northwest to Sugar Lake in the southeast and as far south as Kelowna (Fig. 2). Highly strained Chase Formation rocks occur both north and south of and at lower elevations than phyllitic rocks of the Rossland Group that constitute the hills east and west of Vernon and we consider that the Rossland Group is preserved in a nappe that overrides the Chase Formation (Fig. 10b). Glombick et al. (2006) present U-Pb zircon and titanite geochronology from Chase Formation mylonitic quartzite that indicates a long and complex structural and metamorphic history from Late Jurassic to Eocene. Parrish et al. (1988) included the Sugar Lake location as part of the Okanagan Valley shear zone (Eocene; Brown et al., 2017), but the Chase location is too far to the west to be part of this deformation zone (Fig. 2). It is possible that the deformation in each Chase Formation location: 1) developed before the Okanagan Valley shear zone; 2) is diachronous; or 3) the Okanagan Valley shear zone, or equivalent structure, needs to be extended to the area near the town of Chase.

A structural relationship between Quesnel terrane and nearby Ancestral North America is likely because northern Quesnel magmatic rocks lack evidence of contributions from continental basement (Jones et al., 2022; Ootes et al., 2022) and similar structural relationships between southern Quesnel rocks and Ancestral North America has been inferred by Acton et al. (2002). A potential test of the stratigraphic link between the Chase Formation mylonite and the Rossland Group rocks could be through the detrital zircon record. If there was a stratigraphic relationship, there should be recycling of zircons from the Chase quartzites (North American detritus; Lemieux et al., 2007) into the younger Rossland Group rocks. However, except for minor amounts of ca. 430 Ma zircon, evidence that would indicate recycling of nearby material with North American affinity (particularly Archean and Paleoproterozoic

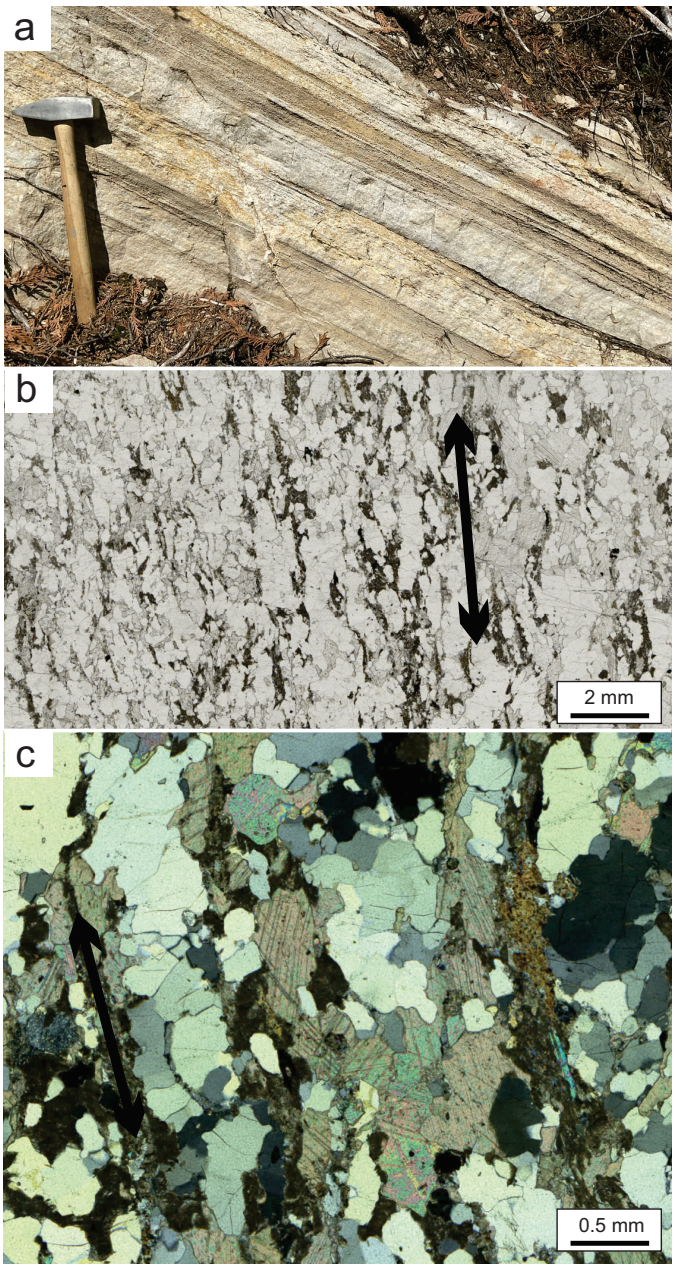


Fig. 9. a) Outcrop of the Chase Formation pitted quartzite southwest of Sugar Lake (Figure 2). No primary depositional features are preserved. **b)** Plane-polarized and **c)** Cross-polarized light photomicrographs of Chase Formation quartzite from south of the town of Chase. Recrystallized quartz ribbons define a lineation (arrow) supporting that this rock unit is a mylonite and that the layering in a) is compositional from transposition during ductile strain and not primary.

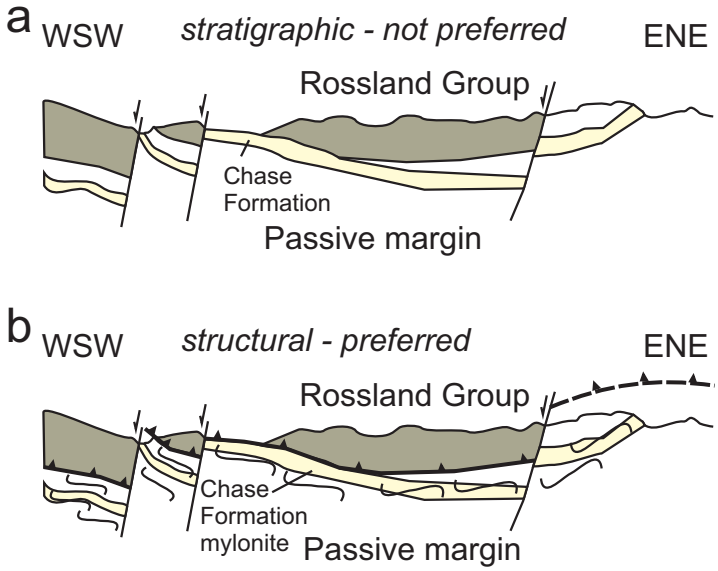


Fig. 10. Schematic cross-sections depicting two possible models for the relationship between the Rossland Group (this study) and underlying units that include the Chase Formation. **a)** The relationship is stratigraphic and later deformed. **b)** The relationship is structural and Rossland Group is preserved as a thrust nappe (teeth on hangingwall side of thrust line). This is the preferred interpretation because it accounts for the deformation of the Chase Formation mylonite, the deformation of the Rossland Group rocks close to the Chase Formation and the lack of recycled detrital zircon from the underlying stratigraphy into this part of the Rossland Group. Sugar Lake area (Figure 2) and simplified after Glombick et al. (2006, their Figure 3). The Okanagan Valley shear zone (Eocene; Parrish et al., 1988; Brown et al., 2017) is not depicted in this figure.

rocks; see Matthews et al., 2018) is absent in this study (Fig. 7), which would favour a structural imbrication model where the Rossland Group is the hangingwall of a shear zone (Fig. 10b). Given the zircon populations (Fig. 7f), the Vernon area may represent part of the Nicola arc as it evolved from initiation in the oceanic realm to arrival with North America (Fig. 8). Where it arrived adjacent to North America remains ambiguous, but given the lack of currently nearby North America detrital zircons in these rocks, the location was probably not at present latitudes.

6. Conclusion

New detrital zircon and field data presented herein lead to stratigraphic unit reassignments in the Vernon area. Some of the rocks in the area are likely part of the Rossland Group, expanding the unit's areal extent. The results also open the possibility of a speculative but testable model for the nature of the transition between Quesnel terrane and Ancestral North America as preserved in the Canadian Cordillera. Key interpretations and tests are as follows.

First, we interpret that rocks in this area now assigned to the Rossland Group lie structurally on rocks of possible North American affinity. A possible test of this interpretation is the comparison of detrital zircon U/Pb-Hf data between these rocks and the underlying rocks.

Second, we consider that this area of the Cordilleran orogen preserves a forearc or trench basin that evolved from the Late Triassic through Early Jurassic. This is counter to established models for the evolution of the Quesnel terrane but can be tested by tracer isotope studies of Quesnel terrane rocks and those of Ancestral North American affinity.

Third, the Chase Formation is laterally extensive. Detrital zircon U/Pb-Hf data from the Chase Formation rocks may help influence regional correlations and provide a provenance record of this unit.

Finally, the Chase Formation represents a deformation zone that: 1) developed before the Okanagan Valley shear zone; 2) is diachronous; or 3) the Okanagan Valley shear zone, or equivalent structure, needs to be extended to the area near the town of Chase. If stratigraphic correlations can be proved through U/Pb-Hf studies, a directed structural and a strategic geochronological approach is required to resolve the regional tectonic relationships.

Acknowledgments

This study benefited from the competent assistance of A. West during the summer of 2022, and we thank the PCIGR team for assistance with mineral separation and zircon mounting. We appreciate the thoughtful and constructive reviews provided by T. Höy, P. Schiarizza, and H.D. Gibson who disagree, in some cases strongly, with some of our interpretations, which should be viewed as alternatives to be tested. The challenges posed by these reviewers helped improve this contribution.

References cited

Acton, S.L., Simony, P.S., and Heaman, L.M., 2002. Nature of the basement to Quesnel Terrane near Christina Lake, southeastern British Columbia. Canadian Journal of Earth Sciences, 39, 66-78. <https://doi.org/10.1139/e01-056>

Beatty, T.W., Orchard, M.J., and Mustard, P.S., 2006. Geology and tectonic history of the Quesnel terrane in the area of Kamloops, British Columbia. In: Colpron, M., and Nelson, J.L., (Eds.), Paleozoic Evolution and Metallogeny of Pericratonic Terranes at the Ancient Pacific Margin of North America, Canadian and Alaskan cordillera. Geological Association of Canada, Special Paper 45, pp. 483-504.

British Columbia Geological Survey, 2019. British Columbia Digital Geology. British Columbia Ministry of Mining and Critical Minerals, British Columbia Geological Survey. Data version 2019-12-19.

Brown, S.R., Andrews, G.D.M., and Gibson, H.D., 2017. Corrugated architecture of the Okanagan Valley shear zone and the Shuswap metamorphic complex, Canadian Cordillera. Lithosphere, 8, 412-421.

Cawood, P.A., Hawkesworth, C.J., and Dhuime, B., 2012. Detrital zircon record and tectonic setting. Geology, 40, 875-878.

Colpron, M., 2020. Yukon Terranes-A digital atlas of terranes for the northern Cordillera. Yukon Geological Survey. <data.geology.gov.yk.ca/Compilation/2#InfoTab>

Colpron, M., and Nelson, J.L., 2009. A Palaeozoic Northwest Passage: incursion of Caledonian, Baltican and Siberian terranes into eastern Panthalassa, and the early evolution of the North American Cordillera. In: Cawood, P.A., and Kröner, A., (Eds.), Earth Accretionary Systems in Space and Time. The Geological Society, London, Special Publications, 318, pp. 273-307. <https://doi:10.1144/SP318.10>

Glombick, P., Thompson, R., Erdmer, P., Heaman, L., Friedman, M., Villeneuve, M., and Daughtry, K., 2006. U-Pb constraints on the thermotectonic evolution of the Vernon antiform and the age of the Aberdeen gneiss complex, southeastern Canadian Cordillera. Canadian Journal of Earth Sciences, 43, 213-244. <https://doi:10.1139/e05-096>

Höy, T., and Dunne, K.P.E., 1997. Early Jurassic Rossland Group, southern British Columbia: Part I-stratigraphy and tectonics. British Columbia Ministry of Employment and Investment, British Columbia Geological Survey Bulletin 102, 123 p.

Jones, A.G., 1959. Vernon map area, British Columbia. Geological Survey of Canada, Memoir 296, 186 p.

Jones, G., Ootes, L., Luo, Y., Vezinet, A., Stern, R., Milidragovic, D., and Pearson, D.G., 2023. The relative roles of ancient and juvenile crust in building accretionary orogens-Minimal ancient crust involved in the magmatic evolution of a North American Cordillera accreted terrane indicated by igneous zircon Hf-O. Lithos, 452-453, article 107213. <https://doi.org/10.1016/j.lithos.2023.107213>

Lemieux, Y., Thompson, R.I., Erdmer, P., Simonetti, A., and Creaser, R.A., 2007. Detrital zircon geochronology and provenance of Late Proterozoic and mid-Paleozoic successions outboard of the miogeosyncline, southeastern Canadian Cordillera. Canadian Journal of Earth Sciences, 44, 1675-1693. <https://cdnsciencepub.com/doi/10.1139/e07-048>

Matthews, W., Guest, B., and Madronich, L., 2018. Latest Neoproterozoic to Cambrian detrital zircon facies of western Laurentia. Geosphere, 14, 243-264. <https://doi.org/10.1130/GES01544.1>

Mihalynuk, M.G., and Diakow, L.J., 2020. Southern Nicola arc geology. British Columbia Ministry of Energy, Mines and Low Carbon Innovation, British Columbia Geological Survey Geoscience Map 2020-01, 2 sheets, 1:50,000 scale.

Nelson, J.L., Colpron, M., and Israel, S., 2013. The Cordillera of British Columbia, Yukon and Alaska: Tectonics and metallogeny. In: Colpron, M., Bissig, T., Rusk, B.G., and Thompson, F.H., (Eds.), Tectonics, Metallogeny, and Discovery: The North American Cordillera and Similar Accretionary Settings. Society of Economic Geologists, Special Publication 17, pp. 53-109.

Okulitch, A.V.,1979. Geology and mineral occurrences of the Thompson-Shuswap-Okanagan Region, south-central British Columbia. Geological Survey of Canada Open File 637. <https://doi.org/10.4095/129552>

Ootes, L., and Wall, C., 2024. High-precision U-Pb zircon igneous crystallization and detrital zircon maximum depositional ages from the Toodoggone region, north-central British Columbia. British Columbia Ministry of Energy, Mines and Low Carbon Innovation, British Columbia Geological Survey Open File 2024-06, 10 p.

Ootes, L., Ferri, F., Milidragovic, D., and Wall, C., 2022. The age and provenance of the Lay Range assemblage provides an indirect record of basement to north-central Quesnellia, British Columbia. In: Geological Fieldwork 2021, British Columbia Ministry of Energy, Mines and Low Carbon Innovation, British Columbia Geological Survey Paper 2022-01, pp. 31-44.

Orchard, M.J., 1985. Carboniferous, Permian and Triassic conodonts from the central Kootenay arc, British Columbia: constraints on the age of the Milford, Kaslo and Slocan groups. In: Current Research Part A, Geological Survey of Canada Paper 85-1A, pp. 287-300. <https://doi.org/10.4095/120054>

Parrish, R., Carr, S.D., and Parkinson, D.L., 1988. Eocene extensional tectonics and geochronology of the southern Omineca belt, British Columbia and Washington. Tectonics, 7, 181-212.

Schiarizza, P., 2024. Bedrock geology, Bonaparte Lake-Quesnel River, parts of NTS 92P, 93A, 93B. British Columbia Ministry of Energy, Mines and Low Carbon Innovation, British Columbia Geological Survey Geoscience Map 2024-01, 1:125,000 scale.

Schiarizza, P.A., and Church, B.N., 1996. The Geology of the Thompson-Okanagan Mineral Assessment Region (East Part). British Columbia Ministry of Energy, Mines and Petroleum Resources, British Columbia Geological Survey Open File 1996-20, digital files.

Schiarizza, P., Orchard, M.J., and Friedman, R.M., 2022. Conodonts and detrital zircons from Triassic and Jurassic rocks above the Salmon River unconformity, Thompson Plateau, south-central British Columbia. In: Geological Fieldwork 2021, British Columbia Ministry of Energy, Mines and Low Carbon Innovation, British Columbia Geological Survey Paper 2022-01, pp. 17-30.

Thompson, R.I., Glombick, P., Erdmer, P., Heaman, L.M., Lemieux, Y., and Daughtry, K.L., 2006. Evolution of the ancestral Pacific margin, southern Canadian Cordillera: Insights from new geologic maps. In: Colpron, M., and Nelson, J.L., (Eds.), Paleozoic Evolution and Metallogeny of Pericratonic Terranes at the ancient Pacific Margin of North America, Canadian and Alaskan cordillera. Geological Association of Canada, Special Paper 45, pp. 433-482.

Unterschutz, J.L.E., Creaser, R.A., Erdmer, P., Thompson, R.I., and Daughtry, K.L., 2002. North American margin origin of Quesnel terrane strata in the southern Canadian cordillera: Inferences from geochemical and Nd isotopic characteristics of Triassic metasedimentary rocks. Geological Society of America Bulletin, 114, 462-475.

Vermeesch, P., 2018. IsoplotR: A free and open toolbox for geochronology. Geoscience Frontiers, 9, 1479-1493. <https://doi:10.1016/j.gsf.2018.04.001>

Vermeesch, P., 2021. Maximum depositional age estimation revisited. Geoscience Frontiers, 12, 843-850.

Paleozoic to Eocene intrusions in the Golden Triangle, northwestern British Columbia: A project update

Roddy W. Campbell[1, a], Kaitlyn Gibson[1], and Bram I. van Straaten[1]

[1] British Columbia Geological Survey, Ministry of Mining and Critical Minerals, Victoria, BC, V8W 9N3
[a] corresponding author: Roddy.Campbell@gov.bc.ca

Recommended citation: Campbell, R.W., Gibson, K., and van Straaten, B.I., 2026. Paleozoic to Eocene intrusions in the Golden Triangle, northwestern British Columbia: A project update. In: Geological Fieldwork 2025, British Columbia Ministry of Mining and Critical Minerals, British Columbia Geological Survey Paper 2026-01, pp. 131-142.

Abstract

New fieldwork as part of an ongoing study to develop a plutonic framework for the Golden Triangle included examining rocks of the Texas Creek plutonic suite (Early Jurassic) in the Bronson corridor near Iskut River and in the Salmon Glacier area. The areally extensive Texas Creek batholith, Summit Lake stock, and Iskut River/Bronson stocks (ca. 197-193 Ma) range in composition from hornblende granodiorite to quartz monzonite and are coeval with distinctive K-feldspar porphyritic to megacrystic marginal phases, stocks, dikes, and related flows including the Red Bluff stock, Premier porphyry, and intrusions in the Kyber pass area. Several Au-rich (±Ag) mineral systems are on the periphery of the areally extensive granodiorite-quartz monzonite intrusions including the Scottie gold camp. K-feldspar porphyritic to megacrystic phases are spatially associated with, and locally host, porphyry Au-Cu mineralization including intrusions genetically related to the Bronson slope deposit.

Keywords: Plutonic rocks, Stikinia, Golden Triangle, porphyry Cu-Au-Mo, Jurassic, Texas Creek plutonic suite, Snip North, Bronson Slope, Scottie Gold, Red Bluff stock, Iskut River stock, Summit Lake stock, Texas Creek batholith

1. Introduction

This paper provides a progress update on an ongoing multi-year study of plutonic rocks in the 'Golden Triangle' of northwestern British Columbia, an area with numerous porphyry, epithermal, and VMS mineral deposits (Fig. 1; e.g., Nelson and van Straaten, 2020) on the traditional lands of the Tahltan Nation, Gitanyow Hereditary Chiefs, Metlakatla First Nation, Tsetsaut Skii Km Lax Ha, and Nisga'a Nation. The project is aimed at developing a framework for Paleozoic to Eocene intrusions in the region, which host numerous porphyry, epithermal, and VMS systems and is a companion to a project focused on developing a framework for Triassic-Jurassic supracrustal rocks (van Straaten, 2026). Through detailed field and drill core studies of areally extensive plutons and intrusions associated with significant mineralization, complemented by geochronological, petrographic, lithogeochemical, radiogenic isotope, physical property, and mineral chemistry analyses, the project will provide improved constraints on the magmatic and metallogenic evolution of the region. By providing a consistent characterization and framework for regionally significant intrusions, including known mineralizing phases, this project aims to assist mineral exploration companies in targeting prospective intrusions.

The project is in its second year. Preliminary results from the first year of fieldwork in the Telegraph Creek area (Fig. 2) are reported in Campbell and van Straaten (2025), complemented by geochronological studies reported in Bailey et al. (2025). In this paper, we provide an interim progress report on the project and provide examples from studies of the Texas Creek plutonic suite in the Bronson corridor and Salmon Glacier areas (Fig. 2).

2. Geological setting

The Golden Triangle is underlain by rocks of Stikine terrane (Stikinia), a Paleozoic to Mesozoic island arc terrane which, along with the Quesnel island arc terrane, hosts most of the porphyry deposits in the Canadian Cordillera (e.g., Logan and Mihalynuk, 2014). The stratigraphic architecture and plutonic framework of Stikinia was strongly influenced by a series of collisional processes that began during the Late Triassic and ended with the Middle Jurassic accretion of Stikinia and other Intermontane terranes to Ancestral North America (e.g., Mihalynuk et al., 2004; Nelson et al., 2013; Nelson and van Straaten, 2020).

The Late Triassic to Early Jurassic stratigraphy of the Golden Triangle includes Stuhini Group (Upper Triassic) mafic to intermediate volcanic, volcaniclastic and sedimentary rocks and lower Hazelton Group (uppermost Triassic-Lower Jurassic) intermediate, lesser felsic and mafic volcanic, volcaniclastic, and sedimentary rocks (Fig. 3; e.g., Nelson et al., 2018, 2022). The Texas Creek plutonic suite (ca. 204-185 Ma, latest Triassic-Early Jurassic) is comagmatic and coeval with lower Hazelton Group volcanic rocks (Kaip, 1997; Lewis et al., 2001; Nelson et al., 2018, 2022; Febbo et al., 2019; Campbell, 2021), and genetically related to most porphyry Cu-Au and epithermal Au-Ag deposits in the region (e.g., Britton et al., 1989; Alldrick, 1993; Kyba and Nelson, 2015; Nelson and van Straaten, 2020). The Texas Creek plutonic suite includes small volume, hypabyssal diorite to monzonite to quartz monzonite intrusions (ca. 204-185 Ma; Febbo, 2016; Febbo et al., 2019; Campbell, 2021) that are in many cases genetically linked to porphyry and epithermal

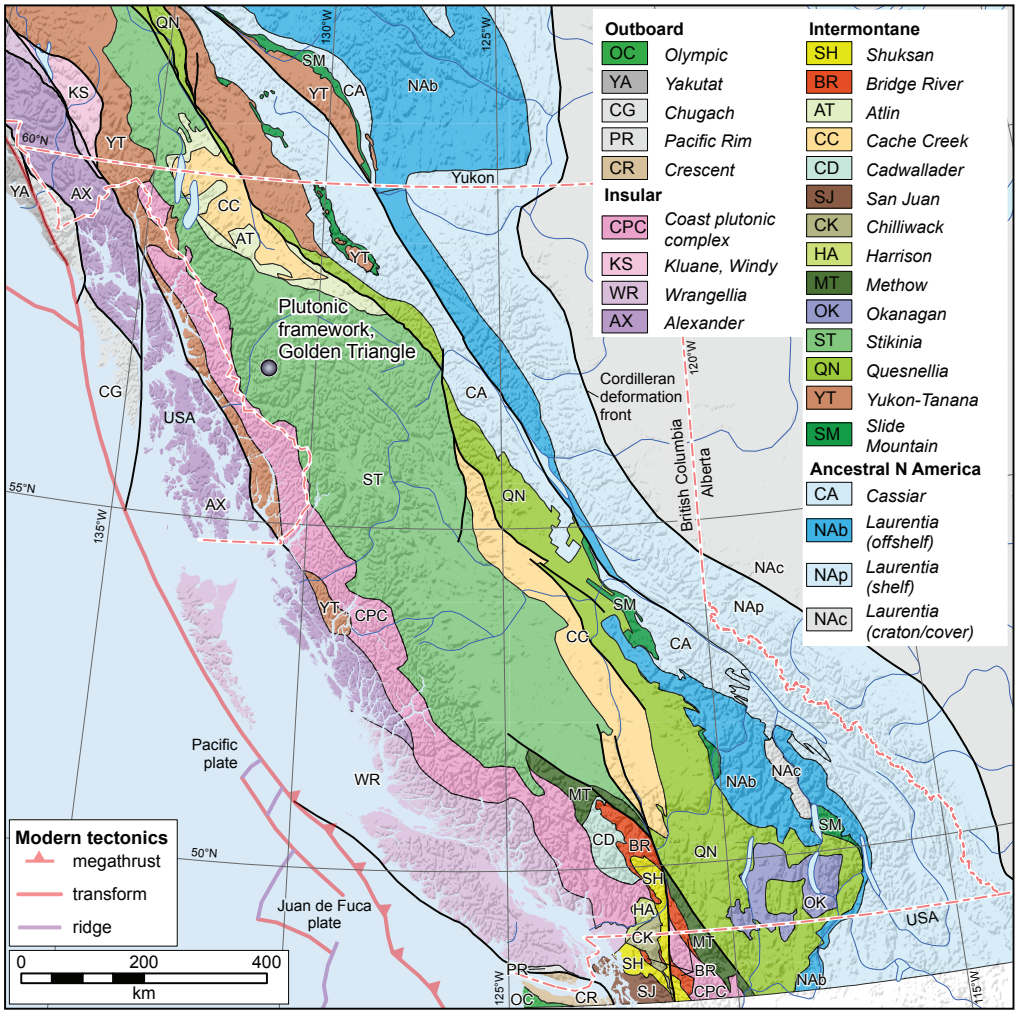


Fig. 1. Location of the Golden Triangle plutonic framework project. Terranes after Colpron (2020).

deposits. The suite also includes a series of areally extensive granodiorite to quartz monzonite plutons (ca. 195-193 Ma; Alldrick, 1993; Lewis et al., 2001; Evenchick et al., 2004; Miller et al., 2025a, b) that outcrop from Kitsault to the lower Iskut River (e.g., Bulldog Creek pluton, Texas Creek batholith, Summit Lake stock, and Lehto pluton; Fig. 2).

3. Fieldwork carried out to date

In 2024, we carried out eight weeks of fieldwork in the northern portion of the Golden Triangle (Fig. 2). Preliminary results on Late Triassic to Early Jurassic intrusions are reported in Campbell and van Straaten (2025), and additional fieldwork focused on the Forrest Kerr and More Creek plutonic suites (Late Devonian-Mississippian), Gnat Lakes plutonic suite (Late Triassic), Three Sisters plutonic suite (Middle Jurassic), and younger intrusions. In 2024, we also carried out one week of field studies in the southwestern portion of the Golden Triangle including the Texas Creek and Melville plutonic suites (Early Jurassic), and Hyder and Alice Arm plutonic suites (Eocene; Fig. 2).

In 2025, we carried out eight weeks of fieldwork between Galore Creek and Stewart (Fig. 2). At each location, we studied areally extensive plutons and intrusions associated with mineralization and took samples for further analytical studies. To date we have submitted 671 samples for lithogeochemistry and 57 samples for geochronology.

4. Bronson corridor and Salmon Glacier

Below we present observations from two of our ten 2025 field sites, the Bronson corridor and Salmon Glacier area (Fig. 2).

4.1. Bronson corridor

The Bronson corridor (Metcalfe and Moors, 1993) is a belt of mineral occurrences between the Iskut-Verrett and Sky faults (Fig. 4), which includes (from northwest to southeast): the Snip North porphyry Cu-Au occurrence (Adam, 2023; MINFILE 104B 312); the past-producing Snip and Johnny Mountain gold veins (Rhys, 1993; MINFILE 104B 250, 107); the Bronson Slope porphyry Cu-Au deposit (Rhys, 1995; MINFILE 104B 077); the Khyber Pass,

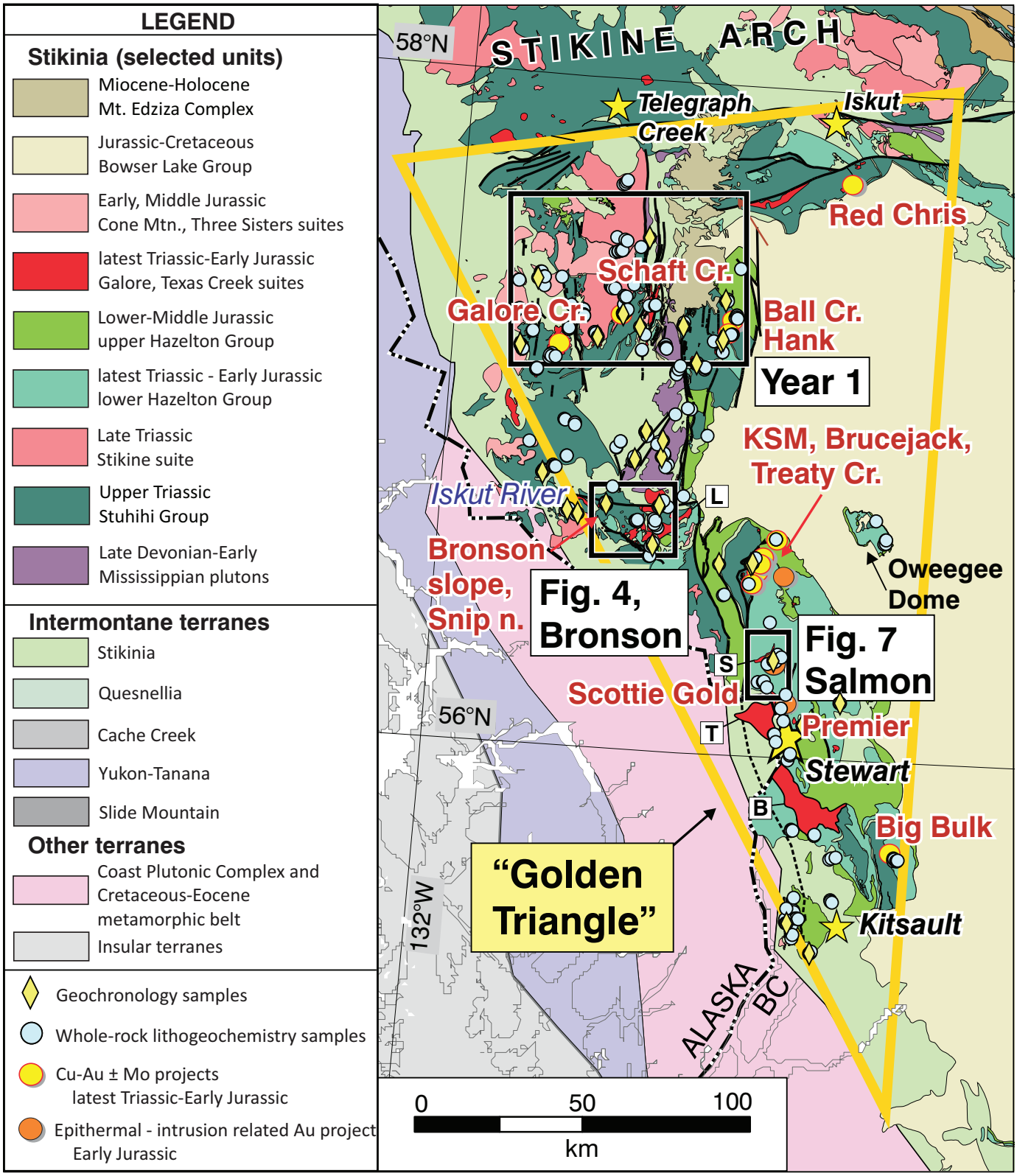


Fig. 2. Late Triassic to Middle Jurassic stratigraphy, plutonic suites, and structural setting of northwestern British Columbia. The Golden Triangle hosts numerous porphyry, epithermal, and volcanogenic massive sulphide deposits. Year 1 refers to work in Campbell and van Straaten (2025); insets for geology of the Bronson corridor (Figure 4) and Salmon Glacier (Figure 7) areas. Abbreviations: L – Lehto pluton, I – Inel stock, S – Summit Lake stock, T – Texas Creek batholith, and B – Bulldog Creek pluton. Geochronology and whole-rock lithogeochemistry samples include all samples submitted following the 2024 and 2025 field seasons. After Nelson and van Straaten (2020).

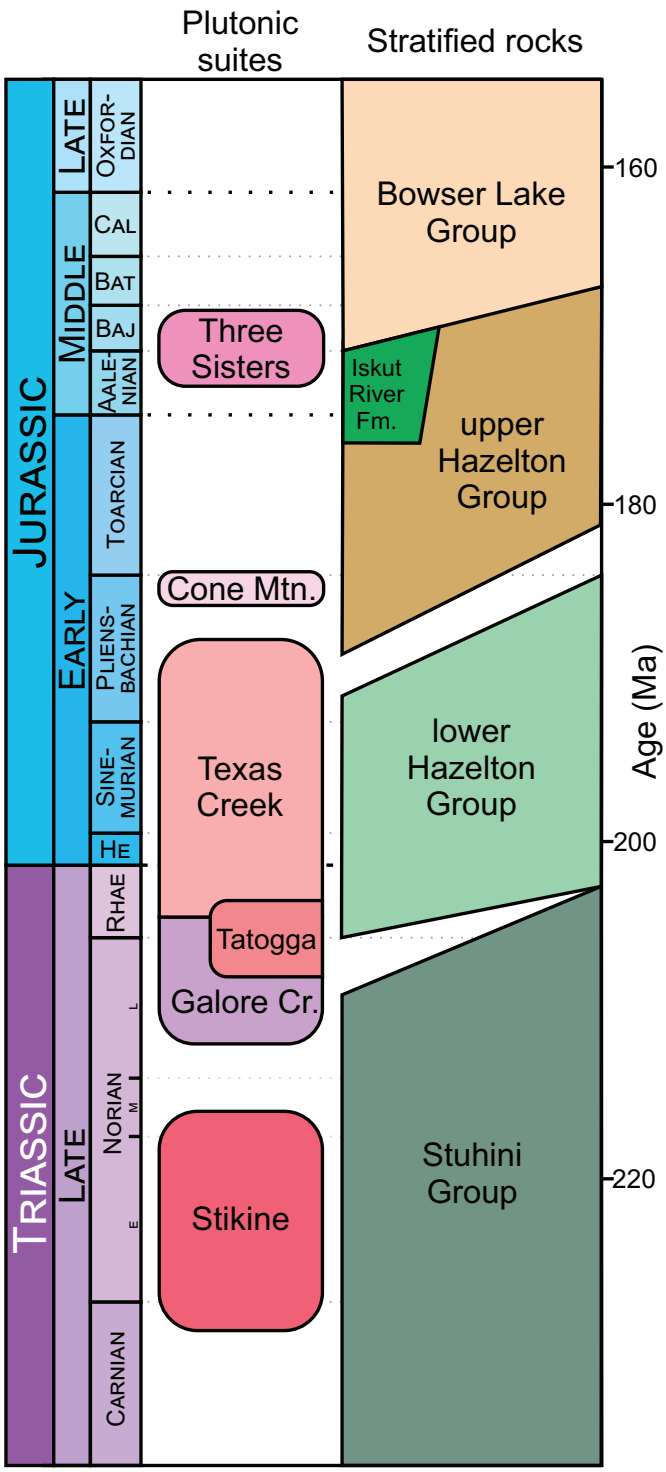


Fig. 3. Schematic Triassic-Jurassic stratigraphic and intrusive framework of the Golden Triangle. Geological timescale after Cohen et al. (2025).

Inel, and Camp porphyry occurrences (MINFILE 104B 113, 138, 697); broad sericite-quartz-pyrite alteration at Sericite Ridge (MINFILE 104B 116); and the Pins and Pins Bowl occurrences (MINFILE 104B 111, 115, 636). Many of these mineral occurrences are spatially associated with, and locally hosted by, Early Jurassic plutons, stocks, and dikes that we assign to the Texas Creek plutonic suite, and include (from northwest to southeast) the Iskut River/Bronson stock (9 km^2); Red Bluff stock (0.75 km^2); the Inel stock (3 km^2; Lefebure and Gunning, 1989; Britton et al., 1990; Rhys and Lewis, 1993; Rhys et al., 1995; Lewis, 2013; Oliver, 2018); small intrusions in the Kyber pass area (0.1 km^2; Kyba and Nelson, 2015; Oliver, 2018; Nelson and van Straaten, 2020); and the areally extensive Lehto pluton (at least 83 km^2; Britton et al., 1989; Lewis, 2013; Kyba and Nelson, 2015; Oliver, 2018). Based on 2025 fieldwork, we distinguish two Texas Creek plutonic suite (Early Jurassic) units in the northwestern and central parts of the Bronson corridor (Fig. 4), one a hornblende quartz monzodiorite unit (EJTdqmd) the other a K-feldspar megacrystic quartz monzonite unit (EJTdqm.tm).

4.1.1. Hornblende quartz monzodiorite unit (EJTdqmd)

The Iskut River/Bronson stock outcrops on either side of the Iskut River (Fig. 4). The poorly exposed southeastern portion of the stock consists of an equigranular to weakly K-feldspar porphyritic, hornblende quartz monzodiorite to monzodiorite (Fig. 5a; Table 1).

4.1.2. K-feldspar megacrystic quartz monzonite unit (EJTdqmz.tm)

A K-feldspar porphyritic to megacrystic, biotite-bearing to hornblende-bearing quartz monzonite unit is exposed in the northwestern and western parts of the Iskut River/Bronson stock, in the Red Bluff stock, and at the Khyber Pass occurrence (Fig. 4; Table 1). Relative to the hornblende quartz monzodiorite unit (EJTdqmd), the rocks are more feldspar porphyritic, with large (>10-45 mm) K-feldspar phenocrysts, have no or minor hornblende, and an aphanitic to fine-grained groundmass. At Snip North, drilling intersected quartz monzonite to monzonite, interpreted as the western margin of the Iskut River/Bronson stock, and related m-scale dikes hosted by Stuhini Group sedimentary rocks (Fig. 5b; Adam, 2023). This is broadly consistent with previous descriptions by Lefebure and Gunning (1989), Britton et al. (1990) and Mihalynuk et al. (2011). The Red Bluff stock is a tabular body consisting of hornblende-bearing(?) K-feldspar porphyritic monzonite to quartz monzonite(?). The stock is comparable to quartz monzodiorite to quartz diorite compositions reported by Rhys (1995) and a pre-mineral monzonite stock cut by early- to syn-mineral quartz monzonite dikes and a late-mineral quartz monzonite plug reported by Nevarez (2025).

4.1.3. Relationship of intrusions and mineralization

Gold and copper mineralization at Bronson slope is in quartz-magnetite (±chalcopyrite, pyrite) veins and breccia zones partially hosted by the margin of the potassically altered Red Bluff stock (Rhys, 1995; Adam, 2023; Nevarez, 2025). At the Khyber Pass occurrence, drilling intersected m- to 10s of m-wide hornblende-bearing quartz monzonite to monzonite dikes, similar to monzonite intrusions identified in surface

Table 1. Lithology of major intrusions in the western and central portions of the Bronson corridor and the Salmon Glacier area. Abbreviations: d = diorite, gd = granodiorite, qmd = quartz monzodiorite, md = monzodiorite, qmz = quartz monzonite, mz = monzonite, eq = equigranular, wpo = weakly porphyritic (1-20% porphyritic phenocrysts), po =porphyritic (20-50% porphyritic phenocrysts), cpo = crowded porphyritic (>50% phenocrysts), mx = megacrystic (phenocrysts >20 mm), aph = aphanitic (not visible with the naked eye), f = fine grained (<1 mm), m = medium grained (1-5 mm), c = coarse grained (5- 30 mm), vc = very coarse grained (>30 mm), Kfs = K-feldspar, Pl = plagioclase, Fsp = feldspar, Hbl = hornblende, and Bt = biotite. Source: [1] Brown (1987), [2] Alldrick (1993), [3] Macdonald et al. (1992), [4] Lewis et al. (2001), [5] A. Zagorevski (pers. comm., 2026).

Unit	Name	Composition	Texture	Kfs and mafic mineral abundance and size	Groundmass grain size	U-Pb zircon age (Ma)
EJT dqmd	Bronson/Iskut River stock (SE)	qmd-md	eq-wpo	15-20% Kfs (2-8 mm incl. sparse 1-2% 15-20 mm), 10-20% Hbl (1-8 mm)	f-c	
EJTdqmz.tm	Bronson/Iskut River stock (W, NW)	qmz-mz(?)	po-cpo-mx	5-15% Kfs (10-45+ mm), <25-40% Fsp (Pl>Kfs; 1-4 mm), <3% Bt(?) (<1 mm)	aph-f	195.98 ±0.79[5], 193.9 +6.0/-0.6[4]
	Red Bluff stock	qmz-mz(?)	po-mx	0.5-15% Kfs (2-20+ mm), <5-8% Hbl(?)	aph-f	195 ±1[3]
	Khyber pass	qmz-mz(?)	po-mx	5-10% Kfs (5-20 mm), 0-5% Hbl (1-3 mm)	aph-f	
EJTgd	Texas Creek batholith 'main phase'	gd, gd-qmd	eq-wpo	5-10% Kfs (3-5 mm incl. 0-2% 10-15 mm), 10-20% Hbl (3-15 mm), 0-5% Bt (2-3 mm)	m, m-c	
	Summit Lake stock	gd-qmd	eq-wpo	5-10% Kfs (2-6 mm incl. 0-2% >10 mm), 15-20% Hbl (4-20 mm), 5-8% Bt (2-4 mm)	m-c	192.8 ±2[2]
EJT gd.tm	Texas Creek batholith 'porphyry phase'	gd-qmd(?)	po-mx	10-15% Kfs (3-33 mm), 8-20% Hbl (3-10 mm)	f, aph-f	195 ±2[2]
	Premier porphyry dikes[1, 2]	gd-d(?)	po-mx	<0.1-10% Kfs (<10-50 mm), 2-8% Hbl (<10 mm)	aph-f	194.8 ±2[2]

mapping by Oliver (2018). In the Khyber Pass and Snip North areas, Au-Cu mineralization is hosted by quartz-sericite-pyrite and biotite ±magnetite-K-feldspar altered Stuhini Group rocks rather than intrusive rocks (Oliver, 2018; Adam, 2023; Nevarez, 2025). At both Khyber Pass and Snip North, intrusive rocks are locally hydrothermally altered and veined. Available geochronological data indicates that intrusions are broadly contemporaneous with mineralization. A Re-Os molybdenite age of 196.5 ±0.8 Ma (Dawson, 2015, 2016) was obtained from a silica-sericite-pyrite altered and quartz veined granodiorite intrusion adjacent to weakly Cu-Au mineralized Stuhini Group sedimentary rocks (drill hole KSP14-002, 490 metres west of the Khyber Pass occurrence; Fig. 4).

Within the Bronson corridor, overlapping 197.4 ±1.0, 196.5 ±1.0, and 196.5 ±0.8 Ma Re-Os ages were obtained from the Red Bluff porphyry by Nevarez (2025) and the Kyber Pass occurrence by Dawson (2015, 2016; Fig. 6). These ages of mineralization overlap within error a 195.98 ±0.79 Ma U-Pb zircon age from the Iskut River/Bronson stock (A. Zagorevski, pers. comm., 2026), and a 193.9 +6.0/-0.6 Ma U-Pb zircon age obtained from the Iskut River stock (Lewis et al., 2001), although a location, lithology description, and analytical data have not been reported for the latter. A 195 ±1 Ma U-Pb zircon minimum age was reported from the Red Bluff stock (Macdonald et al., 1992; Fig. 6). The apparent 195 ±1 Ma U-Pb age is affected by lead loss and may be too young, based on new Re-Os molybdenite ages of mineralization cutting the pre-mineral stock (Nevarez, 2025). Further high-precision geochronological work is required to determine exact temporal relationships between local intrusive phases and metallogenetic events.

4.2. Salmon Glacier area

The Salmon Glacier area includes the past-producing Scottie gold mine and the Blueberry gold deposit (Fig. 7; MINFILE 104B 034, 133; Bird, 2025). Gold mineralization is generally described as intrusion-related shear vein-hosted, generally within 1 km of the southeastern to southern margin of the Summit Lake stock. We studied the 205 km^2 Texas Creek batholith and the 13 km^2 elongate northeast

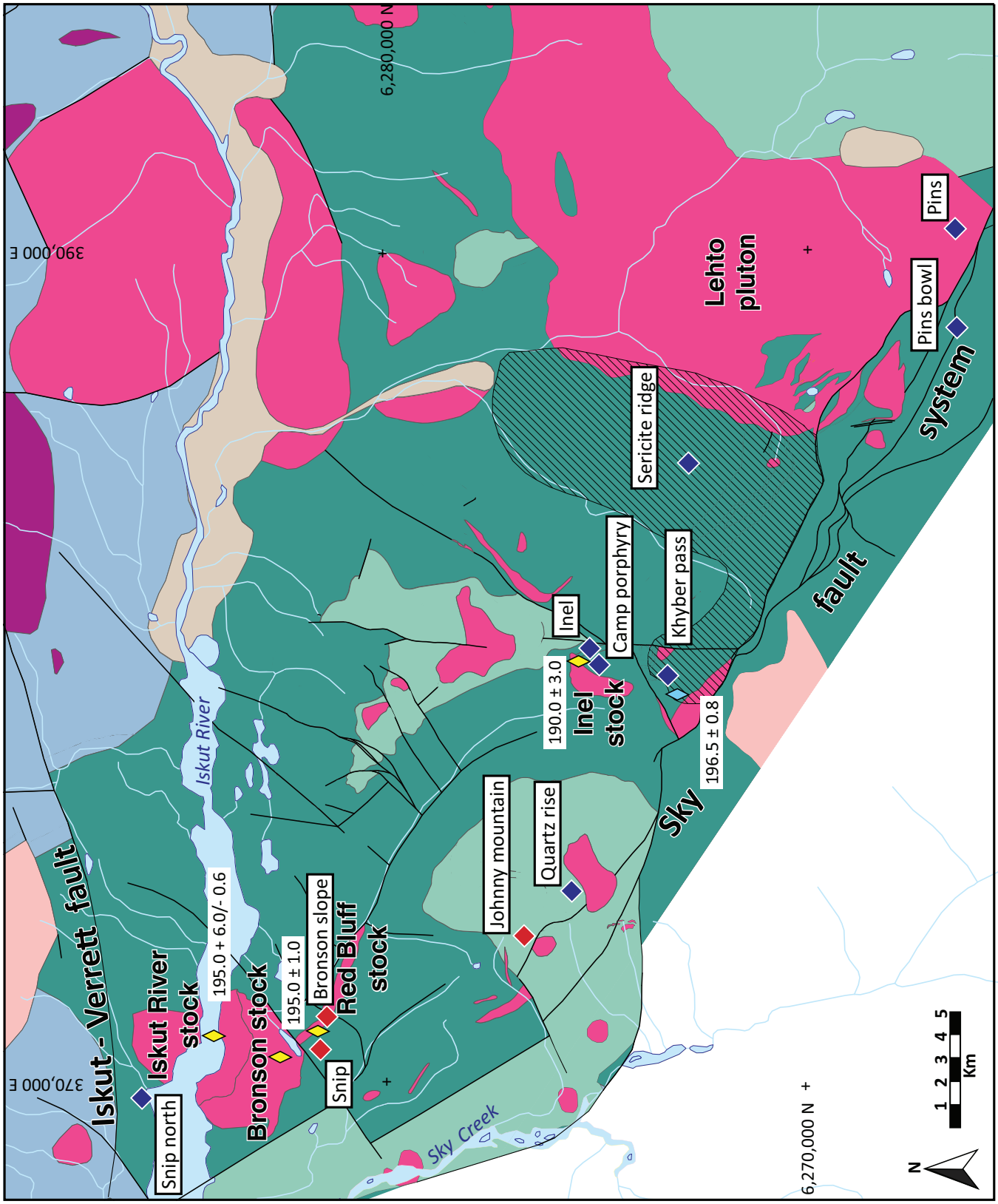


Fig. 4. a) Geology of the Bronson corridor after Lewis (2013), Kyba and Nelson (2015), and British Columbia Geological Survey (2019). UTM Zone 9 north, NAD 83. **b)** Legend.

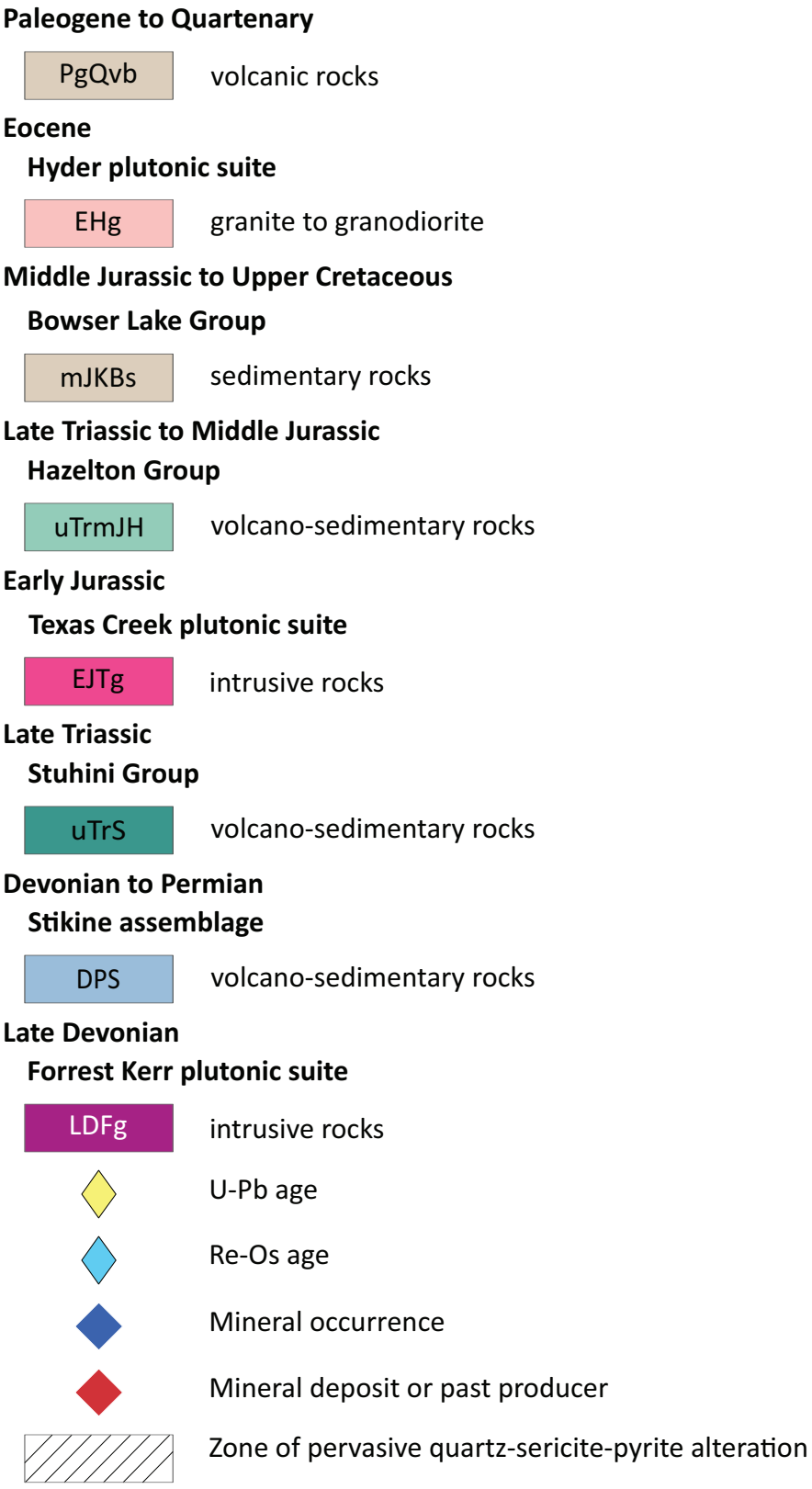


Fig. 4. b) Legend.

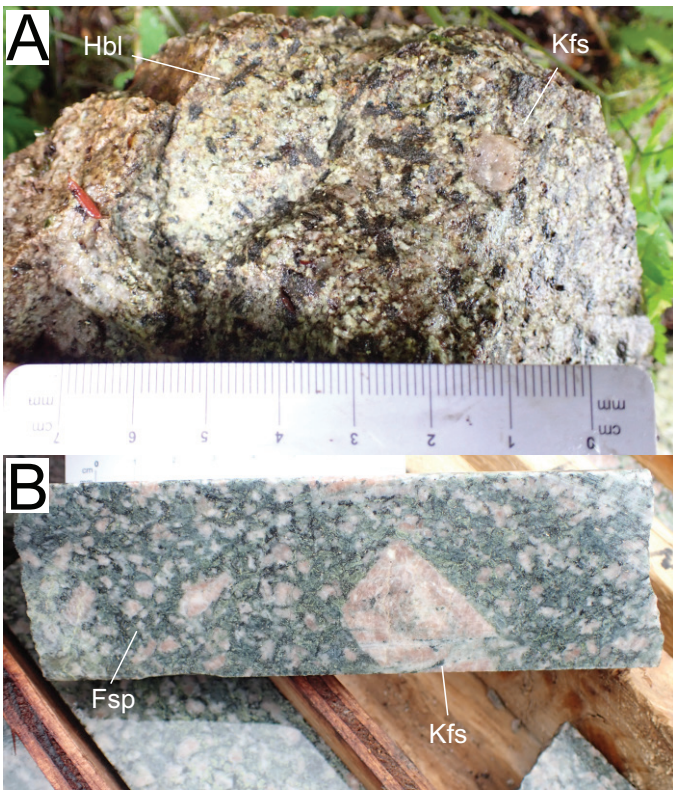


Fig. 5. Texas Creek plutonic suite intrusions from the Bronson corridor. **a)** Medium-grained, weakly K-feldspar porphyritic, hornblende quartz monzodiorite (unit EJTdmzd) from the southeastern Iskut River/Bronson stock. 56.686218°N, 131.086597°W. **b)** Porphyritic to K-feldspar megacrystic quartz monzonite to monzonite(?) (unit EJTdqmz.tm) with 5 to 25% salmon pink, zoned K-feldspar (10-40+ mm), and 20% feldspar (1-4 mm) from the Snip north project (northwestern Iskut River/Bronson stock). Drill hole SN-24-22 collared at 56.691331°N, 131.128932°W.

trending Summit Lake stock (Alldrick, 1993), both part of the Texas Creek plutonic suite (Fig. 7), distinguishing a hornblende granodiorite unit (EJTgd) and a K-feldspar megacrystic hornblende granodiorite unit (EJTgd.tm).

4.2.1. Hornblende granodiorite unit (EJTgd)

The hornblende granodiorite unit is the main phase of the Texas Creek batholith, and the sole phase of the Summit Lake stock. We observed the Texas Creek batholith along the Granduc mine road (Alaska) as a weakly K-feldspar porphyritic hornblende granodiorite. Northwest and northeast of Mount Lindeborg, close to the northern contact of the Texas Creek batholith, it consists of an equigranular biotite-bearing hornblende granodiorite to quartz monzodiorite. Our observations corroborate descriptions of the 'main phase' of the batholith by Alldrick (1993). The Summit Lake stock consists of biotite hornblende granodiorite to quartz monzodiorite with a slightly higher biotite abundance than the northern Texas Creek batholith (Fig. 8a), consistent with the description of Alldrick (1993). The core of the Summit Lake stock is weakly K-feldspar porphyritic.

4.2.2. K-feldspar megacrystic hornblende granodiorite (EJTgd.tm)

Near the northern margin of the Texas Creek batholith, is an estimated 600 m-wide, weakly K-feldspar megacrystic hornblende granodiorite to quartz monzodiorite (Fig. 8b). Alldrick (1993) mapped a comparable 'porphyry phase' (up to several 100 m wide) along the eastern margin of the Texas Creek batholith. The 'porphyry phase' cuts the 'main phase' hornblende granodiorite, and Alldrick (1993) considered the 'porphyry phase' to be texturally and compositionally similar to a series of K-feldspar megacrystic to porphyritic dikes and coeval flows in the lower Hazelton Group (termed 'Premier porphyry' in Brown, 1987).

4.2.3. Relationship to mineralization

U-Pb zircon geochronological data from the porphyry phase of the Texas Creek batholith (195.0 ±2.0 Ma; Alldrick, 1993) overlaps with K-feldspar porphyritic 'Premier porphyry' dikes collected near the Premier mine (194.8 ±2 Ma; Alldrick, 1993). Both ages are older than or overlap determinations from the Summit Lake stock (192.8 ±2.0 Ma U-Pb zircon; Alldrick, 1993). The ca. 193 Ma age for the Summit Lake stock is also supported by a 192.6 ±0.8 Ma Re-Os molybdenite age collected from a quartz-molybdenite veined, sericite altered, porphyritic granodiorite on the northern margin of the stock (van Straaten et al., 2014). An unpublished 192.55 ±1.0 Ma Re-Os molybdenite age from the Blueberry zone (T. Mumford, pers. comm., 2026) overlaps with the age of the Summit Lake stock and provides further indications that mineralization at Scottie Gold and Blueberry may be genetically related to the intrusion. Work is ongoing to better constrain the timing of these intrusive phases, and the Texas Creek plutonic suite more regionally, through high precision CA-TIMS geochronology.

5. Conclusion

New field studies in the central portion of the Golden Triangle region, from Galore Creek south to Stewart include a subset of field observations from the Texas Creek plutonic suite in the Bronson corridor and Salmon Glacier areas. In both areas, Early Jurassic Au-Cu and Au-Ag mineralization is in Stuhini Group and/or lower Hazelton Group rocks at the periphery of areally extensive Texas Creek plutonic suite hornblende granodiorite to quartz monzodiorite plutons and stocks (including the Scottie gold mine and the Summit Lake stock), or associated with and locally hosted by a distinctive suite of coeval K-feldspar porphyritic to megacrystic intrusions (including the Bronson slope porphyry deposit partially hosted by the Red Bluff stock). Existing Re-Os dates indicate the episodic nature of mineralization in the Bronson corridor to Salmon Glacier areas. Further analytical work will seek to better distinguish the age and character of these intrusions through high-precision geochronologic, lithogeochemical, isotopic, and mineral chemistry studies.

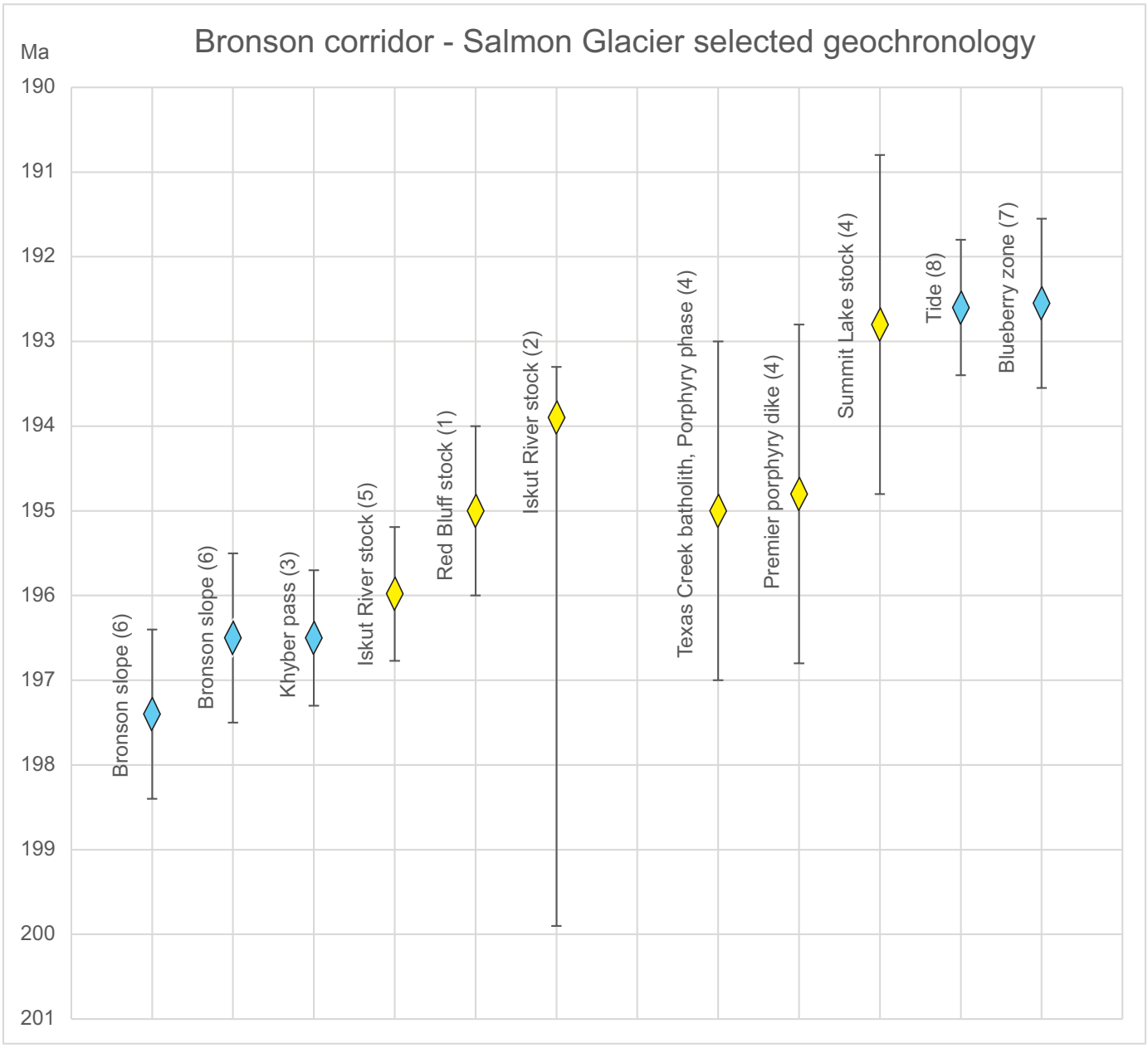


Fig. 6. Selected geochronological data from Bronson corridor and Salmon Glacier area. Ages from [1] Macdonald et al. (1992), [2] Lewis, et al. (2001), [3] Dawson (2015), [4] Alldrick (1993), [5] A. Zagorevski (pers. comm., 2026), [6] Yagual Nevarez (2025), [7] T. Mumford (pers. comm., 2026), and [8] van Straaten et al. (2014). Yellow diamonds indicate Re-Os from molybdenite and blue diamonds indicate U-Pb from zircon.

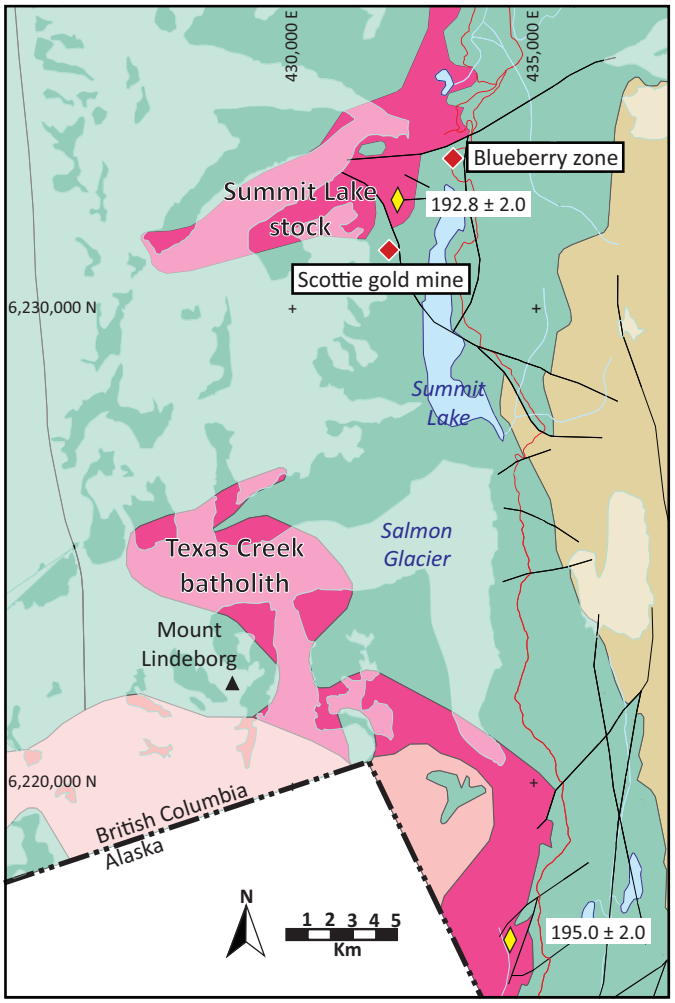


Fig. 7. Geology of the Salmon Glacier area after Alldrick (1993) and British Columbia Geological Survey (2019).

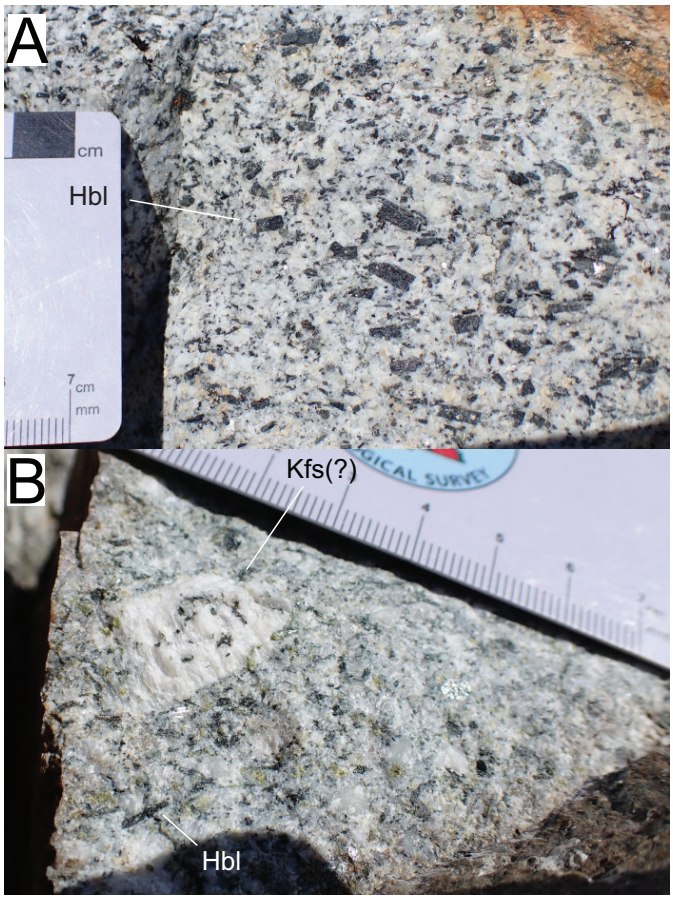


Fig. 8. Texas Creek plutonic suite intrusions from the Salmon Glacier area. **a)** Medium-grained, equigranular to weakly hornblende porphyritic, biotite-bearing hornblende granodiorite (unit EJTgd) from the Summit Lake stock. 56.231810°N, 130.098072°W. **b)** Medium-grained, K-feldspar megacrystic hornblende granodiorite (unit EJTgd. tm) from north of Mount Lindeborg. 56.169897°N, 130.151777°W.

Acknowledgments

Fieldwork in 2025 was made possible through the generous logistical assistance from Seabridge Gold Inc., Scottie Resources Corp., Ascot Resources Ltd., Metallis Resources Inc., Etruscus Resources Corp., Tudor Gold Corp., Goldstorm Metals Corp., Skeena Resources Limited, Enduro Metals Corporation, MTB Metals, Romios Gold Resources Inc., and Kingfisher Metals. For support, discussions and camp hospitality we thank: Kate Gleadow, Ryan Friesen, Jesse Baldwin, Daniel Madrigal, Alex Munro, Colin Langford and team (Seabridge Gold), Thomas Mumford, Dave Nuttall, Katarina Horvat and crew (Scottie Resources), Martin Kral (Premier), Adrian Newton, Crystal Chung, John Tyler, Cole Spence, Regan Markel and company (Skeena Resources), Carl Ryan, Vince Cappa and Dave Dupre (Etruscus-Metallis), and Stephen Wetherup (Enduro), Lucia Theny (MTB), Dustin Perry, Gayle Febbo, Paul Stewart, Olly May, Stephanie Sykora and group (Kingfisher), Jeff Auston (Goldstorm), Kevin Bosse, Ken Konkin (Tudor Gold), and John Biszok (Romios). Thanks also to the numerous helicopter and camp crews. Expert figure drafting was by Oceane Horvath and David Zhang, with field assistance from Oceane Horvath, Leigh Phillips, and Nate Corcoran. Emily Miller, Matteo Ferri, Leonie Ebert, and Gabi Rubinoff contributed to sample collection in the southeastern portion of the Golden Triangle. Reviews by JoAnne Nelson improved this paper significantly.

References cited

Adam, M., 2023. 2022 and 2023 Assessment report on the Iskut property, British Columbia for Seabridge Gold PLC. British Columbia Ministry of Mining and Critical Minerals, British Columbia Geological Survey Assessment Report 41979, 4836 p. <https://apps.nrs.gov.bc.ca/pub/aris/Detail/41979>

Alldrick, D.J., 1993. Geology and metallogeny of the Stewart mining camp, northwestern British Columbia. British Columbia Ministry of Energy, Mines and Petroleum Resources, British Columbia Geological Survey Bulletin 85, 105 p.

Bailey, L., Kim, R., Takaichi, M., Logan, J., Crowley, J., Friedman, R., Wall, C., van Straaten, B.I., and Campbell, R.W., 2025. U-Pb geochronological data for intrusive rocks near the Schaft Creek and Galore Creek deposits (southern Telegraph

Creek area, NTS 104G), northwestern British Columbia. British Columbia Ministry of Mining and Critical Minerals, British Columbia Geological Survey GeoFile 2025-14, 16 p.
Bird, S., 2025. NI 43-101 2025 Mineral resource estimate for the Scottie gold mine project, B.C. NI 43-101 Technical Report prepared for Scottie Resources Corporation, 137 p. <https://www.sedarplus.ca/>
British Columbia Geological Survey, 2019. British Columbia Digital Geology. British Columbia Ministry of Mining and Critical Minerals, British Columbia Geological Survey. Data version 2019-12-19. <https://www2.gov.bc.ca/gov/content/industry/mineralexploration-mining/british-columbia-geological-survey/geology/bcdigitalgeology>
Britton, J.M., Fletcher, B.A., and Alldrick, D.J., 1990. Snippaker map area (104B/6E, 7W, 10W, 11E). In: Geological Fieldwork 1989, British Columbia Ministry of Energy, Mines and Petroleum Resources, British Columbia Geological Survey Paper 1990-1, pp. 115-125.
Britton, J.M., Webster, I.C.L., and Alldrick, D.J., 1989. Unuk map area (104B/7E, 8W, 9W, 10E). In: Geological Fieldwork 1988, British Columbia Ministry of Energy, Mines and Petroleum Resources, British Columbia Geological Survey Paper 1990-1, pp. 241-250.
Brown, D.A., 1987. Geological setting of the volcanic-hosted Silbak Premier mine, northwestern British Columbia, (104 A/4, B/1). M.Sc. thesis, The University of British Columbia, Vancouver, B.C., Canada, 216 p. <https://circle.ubc.ca/handle/2429/26174> (last accessed April 12, 2012).
Buddington, A.F., 1929. Geology of Hyder and vicinity, southeastern Alaska. United States Geological Survey Bulletin 807, 124 p.
Campbell, M.E., 2021. The geology and geochemistry of the Sulphurets district porphyry Au-Cu-Mo deposits, British Columbia, Canada: Insights from a long-lived, gold-enriched porphyry district. Ph.D. thesis, Oregon State University, Corvallis, Oregon, U.S.A., 238 p.
Campbell, R.W., and van Straaten, B.I., 2025. New data on Late Triassic to late Early Jurassic plutonic suites in the northern Golden Triangle region of northwest British Columbia. In: Geological Fieldwork 2024, British Columbia Ministry of Mining and Critical Minerals, British Columbia Geological Survey Paper 2025-01, pp. 49-72.
Dawson, J.G., 2015. Geological, geochemical, prospecting and diamond drilling report on the KSP Property, Liard Mining Division, British Columbia, Canada. British Columbia Ministry of Energy and Mines, British Columbia Geological Survey Assessment Report 35184, 1025 p. <https://apps.nrs.gov.bc.ca/pub/aris/Report/35184.pdf/>
Dawson, J.G., 2016. Geological, geochemical, prospecting and geophysical report on the KSP Property, Liard Mining Division, British Columbia, Canada. British Columbia Ministry of Energy and Mines, British Columbia Geological Survey Assessment Report 35943, 1203 p. <https://apps.nrs.gov.bc.ca/pub/aris/Report/35943.pdf/>
Evenchick, C.A., McNicoll, V.J., and Snyder, L.D., 2004. Stratigraphy, geochronology, and geochemistry of the Georgie River area, northwest British Columbia, and implications for mineral exploration. Canadian Journal of Earth Sciences, 41, pp. 199-216.
Febbo, G.E., 2016. Structural evolution of the Mitchell Au-Cu-Ag-Mo porphyry deposit, northwestern British Columbia. M.Sc. thesis, University of British Columbia, Vancouver, British Columbia, Canada, 98 p.
Febbo, G.E., Friedman, R.M., Kennedy, L.A., and Nelson, J.L., 2019. U-Pb geochronology of the Mitchell deposit, northwestern British Columbia. British Columbia Ministry of Energy, Mines and Petroleum Resources, British Columbia Geological Survey GeoFile 2019-03, 8 p.
Kaip, A., 1997. Geology, alteration and mineralization on the Hank property, northwestern British Columbia: A near-surface, low-sulphidation epithermal system. M.Sc. thesis, University of British Columbia, Vancouver, British Columbia, Canada, 147 p.
Kyba, J., and Nelson, J., 2015. Stratigraphic and tectonic framework of the Khyber-Sericite-Pins mineralized trend, lower Iskut River, northwest British Columbia. In: Geological Fieldwork 2014, British Columbia Ministry of Energy and Mines, British Columbia Geological Survey Paper 2015-01, pp. 41-58.
Lefebure, D.V., and Gunning, M.H., 1989. Geology of the Bronson Creek area (NTS 104B/10W, 11E), British Columbia Ministry of Energy, Mines and Petroleum Resources, British Columbia Geological Survey Open File 1989-28, 1:25,000 scale.
Lewis, P.D., 2013. Iskut River area geology, Northwest British Columbia (104B/08, 09, 10 & part of 104B/01, 07, 11). Geoscience BC Report 2013-05; 3 1:50,000-scale maps, legend and notes; .shp files.
Lewis, P.D., Mortensen, J.K., Childe, F., Friedman, R.M., Gabites, J.M., Ghosh, D., and Bevier, M.L., 2001. Geochronology data set, Chapter 9. In: Lewis, P.D., Toma, A., Tosdal, R.M., (Eds.), Metallogenesis of the Iskut River Area, Northwestern British Columbia. Mineral Deposit Research Unit, Special Publication Number 1, pp. 89-96.
Logan, J.M., and Mihalynuk, M.G., 2014. Tectonic controls on Early Mesozoic paired alkaline porphyry deposit belts (Cu-Au±Ag-Pt-Pd-Mo) within the Canadian Cordillera. Economic Geology, 109, 827-858.
Macdonald, A.J., van der Heyden, P., Lefebure, D.V., and Alldrick, D.J., 1992. Geochronometry of the Iskut River area-an update (104A and B). In: Geological Fieldwork 1991, British Columbia Ministry of Energy, Mines and Petroleum Resources, British Columbia Geological Survey Paper 1992-1, pp. 495-501.
Metcalfe, P., and Moors, J.G., 1993. Refinement and local correlation of the upper Snippaker ridge section, Iskut River area, B.C. (104B/10W and 11E). In: Geological Fieldwork 1992, British Columbia Ministry of Energy, Mines and Petroleum Resources, British Columbia Geological Survey Paper 1993-1, pp. 335-340.
Mihalynuk, M.G., Erdmer, P., Ghent, E.D., Cordey, F., Archibald, D.A., Friedman, R.M., and Johannson, G.G., 2004. Coherent French Range blueschist: Subduction to exhumation in <2.5 m.y.? Geological Society of America Bulletin, 116, 910-922.
Mihalynuk, M.G., Logan, J.M., and Zagorevski, A., 2011. East Hoodoo Mountain-Iskut River geology (NTS 104B/14E and 11NE). British Columbia Ministry of Energy and Mines, British Columbia Geological Survey Open File 2011-4, 1:50,000 scale.
Miller, E.A., Ferri, M.D., van Straaten, B.I., and Wall, C., 2025a. Stratigraphic framework, structural setting, and timing of VMS, epithermal, and porphyry mineralization in the Kitsault River area, northwest British Columbia. In: Geological Fieldwork 2024, British Columbia Ministry of Mining and Critical Minerals, British Columbia Geological Survey Paper 2025-01, pp. 17-47.
Miller, E.A., Ferri, M.D., Wall, C., Creaser, R.A., van Straaten, B.I., and Graham, A.C., 2025b. New geochronologic data, Kitsault River area, northwestern British Columbia: Igneous zircons (high-precision CA-TIMS), detrital zircons (LA-ICP-MS), and molybdenite (Re-Os). British Columbia Ministry of Mining and Critical Minerals, British Columbia Geological Survey GeoFile 2025-21, 6 p.
Nelson, J.L., and van Straaten, B.I., 2020. Recurrent syn- to post-subduction mineralization along deep crustal corridors in the Iskut-Stewart-Kitsault region of western Stikinia,

northwestern British Columbia. In: Sharman, E.R., Lang, J.R., and Chapman, J.B., (Eds.), Porphyry Deposits of the Northwestern Cordillera of North America: A 25-Year Update, CIM Special Volume 57, pp. 149-211.

Nelson, J.L., Colpron, M., and Israel, S., 2013. The Cordillera of British Columbia, Yukon, and Alaska: Tectonics and metallogeny. In: Colpron, M., Bissig, T., Rusk, B.G., and Thompson, J.F.H., (Eds.), Tectonics, Metallogeny and Discovery: The North American Cordillera and Similar Accretionary Settings, Society of Economic Geologists Special Publication 17, pp. 53-110.

Nelson, J.L., Waldron, J., van Straaten, B.I., Zagorevski, A., and Rees, C., 2018. Revised stratigraphy and regional digital map representation of the Hazelton Group in the Iskut River region, northwestern British Columbia. In: Geological Fieldwork 2017, British Columbia Ministry of Energy, Mines and Petroleum Resources, British Columbia Geological Survey Paper 2018-1, pp. 15-38.

Nelson, J.L., van Straaten, B., and Friedman, R., 2022. Latest Triassic-Early Jurassic Stikine-Yukon-Tanana terrane collision and the onset of accretion in the Canadian Cordillera: Insights from Hazelton Group detrital zircon provenance and arc-back-arc configuration. Geosphere, 18, pp. 670-696. <https://doi.org/10.1130/GES02444.1>

Nevarez, L.J.Y., 2025. Metal zonation and evolution of the Bronson slope porphyry Cu-Au-Mo deposit in the Iskut region of British Columbia, Canada. M.Sc. thesis, The University of Texas at El Paso, El Paso, Texas, U.S.A., 92 p.

Oliver, J., 2018. Drilling, on the KSP, Liard, British Columbia, Canada. British Columbia Ministry of Mining and Critical Minerals, British Columbia Geological Survey Assessment Report 37604, 2690 p. <https://apps.nrs.gov.bc.ca/pub/aris/Report/37604.pdf>

Rhys, D.A., 1993. Geology of the Snip mine, and its relationship to the magmatic and deformational history of the Johnny Mountain area, northwestern British Columbia. M.Sc. thesis, The University of British Columbia, Vancouver, B.C., Canada, 275 p.

Rhys, D.A., 1995. The Red Bluff gold-copper porphyry and associated precious and base metal veins, northwestern British Columbia. In: Porphyry Deposits of the Northwestern Cordillera of North America, Schroeter, T.G., (Ed.), Canadian Institute of Mining and Metallurgy Special Volume 46, pp. 838-850.

Rhys, D.A., and Lewis, P.D., 1993. Geology of the Inel deposit, Iskut River, northwestern British Columbia (104B/11). In: Geological Fieldwork 1992, British Columbia Ministry of Energy, Mines and Petroleum Resources, British Columbia Geological Survey Paper 1993-1, pp. 341-347.

van Straaten, B.I., 2026. A Triassic-Jurassic stratigraphic framework for the Golden Triangle, northwestern British Columbia: A project update. In: Geological Fieldwork 2025, British Columbia Ministry of Mining and Critical Minerals, British Columbia Geological Survey Paper 2026-01, this volume.

van Straaten, B.I., McLeish, D.F., and Harding, B.E., 2014. Diamond drilling, geological, geochemical, and geophysical work on the Tennyson property. British Columbia Ministry of Energy, Mines and Petroleum Resources Assessment Report 34816, 1105 p. <https://apps.nrs.gov.bc.ca/pub/aris/Detail/34816>

A Triassic-Jurassic stratigraphic framework for the Golden Triangle, northwestern British Columbia: A project update

Bram I. van Straaten[1, a]

[1] British Columbia Geological Survey, Ministry of Mining and Critical Minerals, Victoria, BC, V8W 9N3
[a] corresponding author: Bram.vanStraaten@gov.bc.ca

Recommended citation: van Straaten, B.I., 2026. A Triassic-Jurassic stratigraphic framework for the Golden Triangle, northwestern British Columbia: A project update. In: Geological Fieldwork 2025, British Columbia Ministry of Mining and Critical Minerals, British Columbia Geological Survey Paper 2026-01, pp. 143-151.

Abstract

This paper provides an interim report on development of a Triassic-Jurassic stratigraphic framework for the Golden Triangle region in northwestern British Columbia. The project is aimed at providing improved constraints on the tectono-magmatic and metallogenic evolution of the region, which hosts numerous Triassic-Jurassic porphyry, epithermal, and VMS deposits. In 2022-2025, stratigraphic field studies were carried out at Red Chris, GJ, Galore Creek, Eskay Creek, Red Mountain, Johnny Mountain, and Bruce Glacier, which complement previously published British Columbia Geological Survey studies in the Galore Creek, Stikine arch, and Kitsault River areas. Further analytical work will include geochronological, paleontological, petrographic, lithogeochemical, and radiogenic isotope analyses.

Keywords: Stratigraphy, metallogeny, Golden Triangle, Triassic, Jurassic, Stuhini Group, Hazelton Group, exhalite, VMS

1. Introduction

Globally, significant magmatic-hydrothermal mineralizing events are broadly coeval with major tectonic events, commonly coinciding with the start and end of major magmatic cycles (e.g., Richards, 2009; Sillitoe, 2010). Establishing the record preserved in stratigraphic units is key for constraining the tectono-magmatic evolution of such metallotects. The British Columbia Geological Survey is continuing a multi-year project to establish a stratigraphic framework for Triassic to Jurassic strata in the 'Golden Triangle', which hosts broadly coeval porphyry, epithermal, and VMS systems (Figs. 1, 2). This work, on the traditional lands of the Tahltan Nation, Gitanyow Hereditary Chiefs, Metlakatla First Nation, Tsetsaut Skii Km Lax Ha, and Nisga'a Nation, complements ongoing investigations to establish the framework of plutonic rocks in the region (Bailey et al., 2025; Campbell and van Straaten, 2025; Campbell et al., 2026). Through detailed field studies of representative stratigraphic sections and magmatic-hydrothermal mineral deposits, supported by geochronological, paleontological, petrographic, lithogeochemical, and radiogenic isotope analyses, the project will provide improved constraints on the tectono-magmatic and metallogenic evolution of the region. It will shed light on major erosional events, the duration of major volcano-magmatic pulses, the timing of mineralization, the nature of pre-, syn-, and post-mineral strata, and regional prospectivity for magmatic-hydrothermal mineral systems. The project builds on previously reported fieldwork carried out in the Galore Creek area (van Straaten et al., 2023; Johnston, 2025), Stikine arch (van Straaten, 2024), and Kitsault River area (Miller et al., 2025a, 2025b; Fig. 2).

2. Geological setting

The Golden Triangle is a loosely defined region in northwestern British Columbia that includes numerous porphyry, epithermal, and VMS mineral deposits (Fig. 2). It is in Stikine terrane (Stikinia), which comprises a series of Paleozoic to Mesozoic arc-related successions and allied plutonic rocks. Most of the mineral systems in the Golden Triangle are Late Triassic to Middle Jurassic and are broadly coeval with three unconformity-bounded volcano-sedimentary successions: the Stuhini Group (Upper Triassic), lower Hazelton Group (uppermost Triassic to Lower Jurassic), and upper Hazelton Group (Lower to Middle Jurassic; Fig. 3).

The main axis of Late Triassic magmatism in Stikinia is defined by thick accumulations of predominantly mafic volcanic strata of the Stuhini Group and accompanying ca. 229-216 Ma Stikine plutonic suite intrusions. These volcanic and intrusive units extend for at least 1300 km along the eastern margin and northern part of Stikinia and have been interpreted to have formed as an east-facing magmatic arc (Nelson and van Straaten, 2020; van Straaten et al., 2023). Stuhini arc activity terminated in latest Triassic by a collision between northern Stikinia and the Yukon-Tanana terrane. This collision is expressed by deformation, localized small-volume alkalic magmatism, and a regional-scale unconformity between the Stuhini and Hazelton groups (Nelson et al., 2018, 2022; van Straaten et al., 2023). The lower Hazelton Group includes local basal conglomerate and sandstone of the Jack Formation and its correlatives (Rhaetian to Hettangian), succeeded by widespread intermediate and rare felsic volcanic rocks of the Betty Creek Formation (Rhaetian to Pliensbachian; Nelson et al., 2018). The Tatogga and

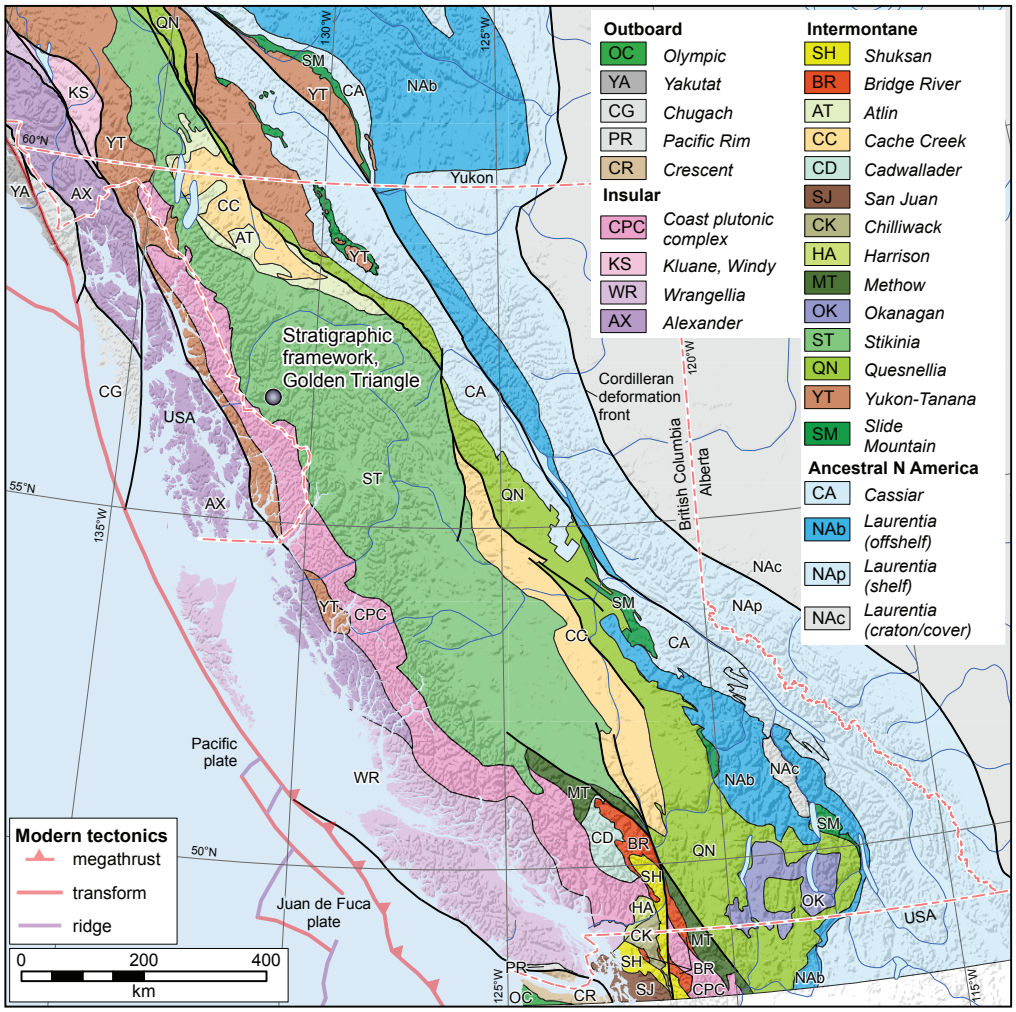


Fig. 1. Location of study area in Stikine terrane. Modified from Colpron (2020).

Texas Creek plutonic suites (latest Triassic to Early Jurassic) are coeval and comagmatic with lower Hazelton Group volcanic units and are responsible for the formation of numerous porphyry Cu-Au and epithermal Au-Ag deposits (Nelson and van Straaten, 2020). The upper Hazelton Group in the Golden Triangle comprises sedimentary rocks of the Spatsizi and Quock formations (Gagnon et al., 2012), local rift-related bimodal volcanic and sedimentary rocks of the Iskut River Formation that host the Eskay Creek VMS deposit (Nelson et al., 2018), and arc-like volcanic rocks (e.g., Kitsault unit and Horn Mountain Formation; van Straaten et al., 2022b; van Straaten, 2024; Miller et al., 2025a). Accretion of Stikinia to inboard terranes and the Ancestral North American margin is recorded by deposition of Bowser Lake Group siliciclastic rocks (Middle Jurassic to mid-Cretaceous) in a foreland basin atop Stikinia (Evenchick et al., 2007). Bowser Lake Group and older rocks are deformed by Cretaceous Skeena fold-and-thrust belt deformation, linked to continued convergence between accreted terranes and Ancestral North America (Evenchick et al., 2007).

3. Field stratigraphic studies

Development and refinement of Stuhini Group and Hazelton Group stratigraphy has guided field studies at the Red Chris porphyry Cu-Au mine, GJ porphyry Cu-Au deposit, Galore Creek porphyry Cu-Au deposit, Eskay Creek VMS Au-Ag deposit, past-producing Johnny Mountain gold mine, Red Mountain Au-Ag deposit, Treaty Creek porphyry Au-Cu deposit, VMS prospects near the Bruce Glacier, and the past-producing Scottie gold mine (Fig. 2). Work was largely carried out in 2022-2025, complemented by earlier work completed in 2015-2017. At each location studied, structural studies were used to reconstruct stratigraphic superposition, with unit thicknesses calculated by measuring the distance perpendicular to strike between stations and correcting for bedding dip, elevation change, and the presence of folds. Stratigraphic sections were constructed from detailed lithostratigraphic descriptions, the relationship between stratigraphy and mineralization was investigated, and samples were collected for further analytical studies.

Two examples illustrate the importance of detailed field observations and strategic sampling for constructing composite

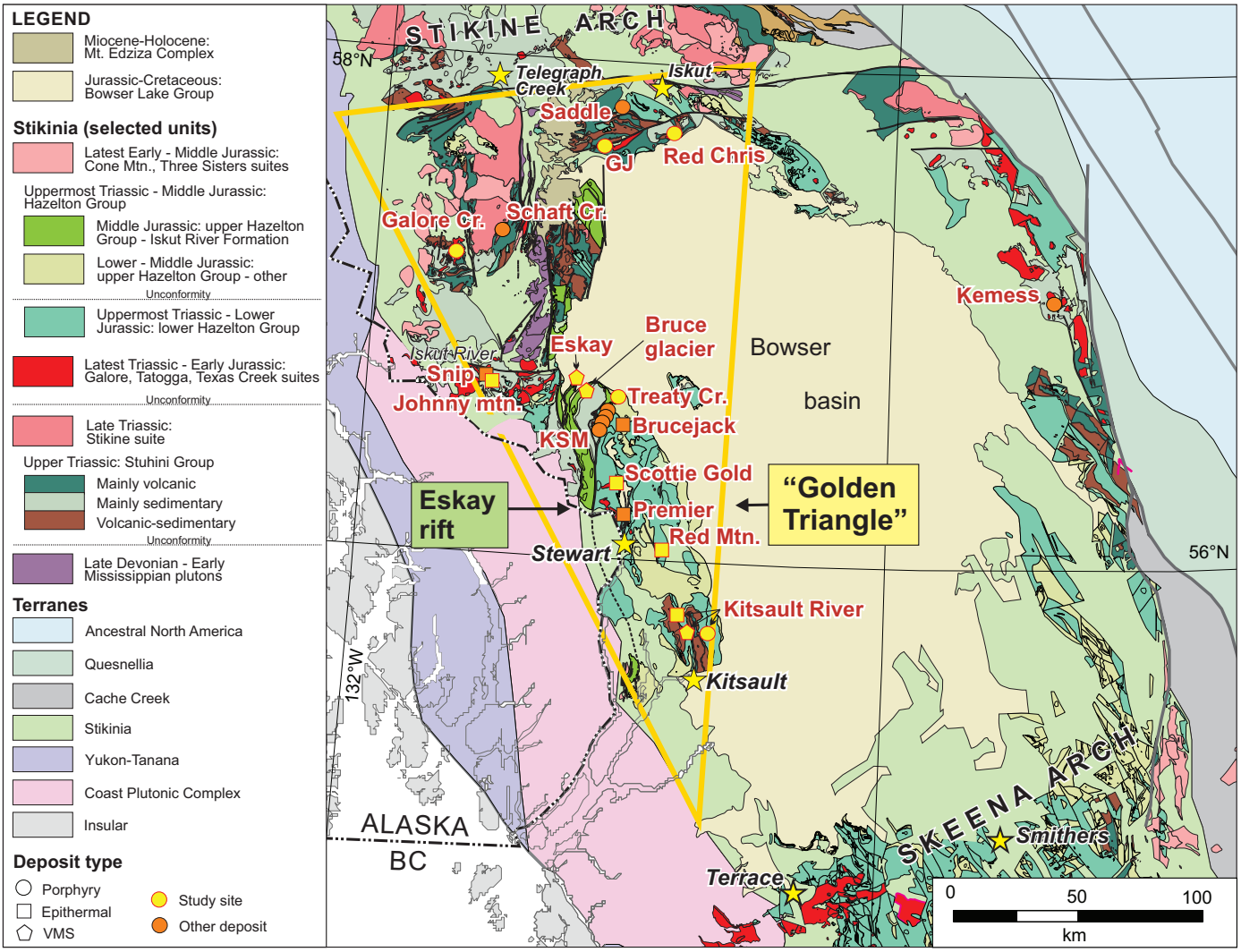


Fig. 2. Simplified geological map with Late Triassic to Middle Jurassic stratified rocks and intrusions of northwestern British Columbia. The Golden Triangle hosts numerous porphyry, epithermal, and volcanogenic massive sulphide deposits. After Nelson and van Straaten (2020).

stratigraphic columns. Near the toe of the Jack Glacier (~3.5 km east-northeast of the Bruce Glacier; Fig. 2) we studied a well-exposed angular unconformity (Fig. 4a) between sedimentary rocks of the Stuhini Group (Upper Triassic) and overlying sedimentary rocks of the Jack Formation (part of the lower Hazelton Group, Lower Jurassic) as previously documented by Henderson et al. (1992). The Stuhini Group includes laminated to thinly bedded black mudstone, siltstone, and grey to orange fine-grained to rare medium-grained sandstone arranged in sharp-based fining-upward sequences (Fig. 4b). A rare very thick bed of very coarse-grained sandstone to granule conglomerate with ~10% quartz grains was sampled for U-Pb detrital zircon geochronology. The overlying Jack Formation includes interbedded siltstone, black mudstone, lime mudstone to wackestone, sandstone with ~10% quartz grains, and minor pebble conglomerate with stratified mud/siltstone, volcanic, and chert clasts. A lime mudstone bed was sampled for microfossil processing. Sampling was aimed at better constraining the timing of deformation. Although the unconformity is widespread throughout the region (e.g., Nelson et al., 2018), detailed studies on the time span contained within the hiatus are limited. The unconformity marks the end of Stuhini Group arc volcanism, collision between Stikine and Yukon-Tanana terranes, and the onset of Hazelton Group, Tatogga plutonic suite, and Texas Creek plutonic suite magmatism which coincides with prolific porphyry- and epithermal-style mineralization in the region.

At Treaty Creek, strongly quartz-clay (advanced) argillic altered rocks interpreted as part of the Betty Creek Formation (lower Hazelton Group, uppermost Triassic to Lower Jurassic) are unconformably overlain by sedimentary rocks of the Spatsizi Formation (upper Hazelton Group, Lower to Middle Jurassic) and succeeded by bimodal volcanic rocks of the Iskut River Formation (upper Hazelton Group; Fig. 5). The upper Hazelton Group represents a post-mineral succession that partially covers a north-northeasterly trend of lithocap-style

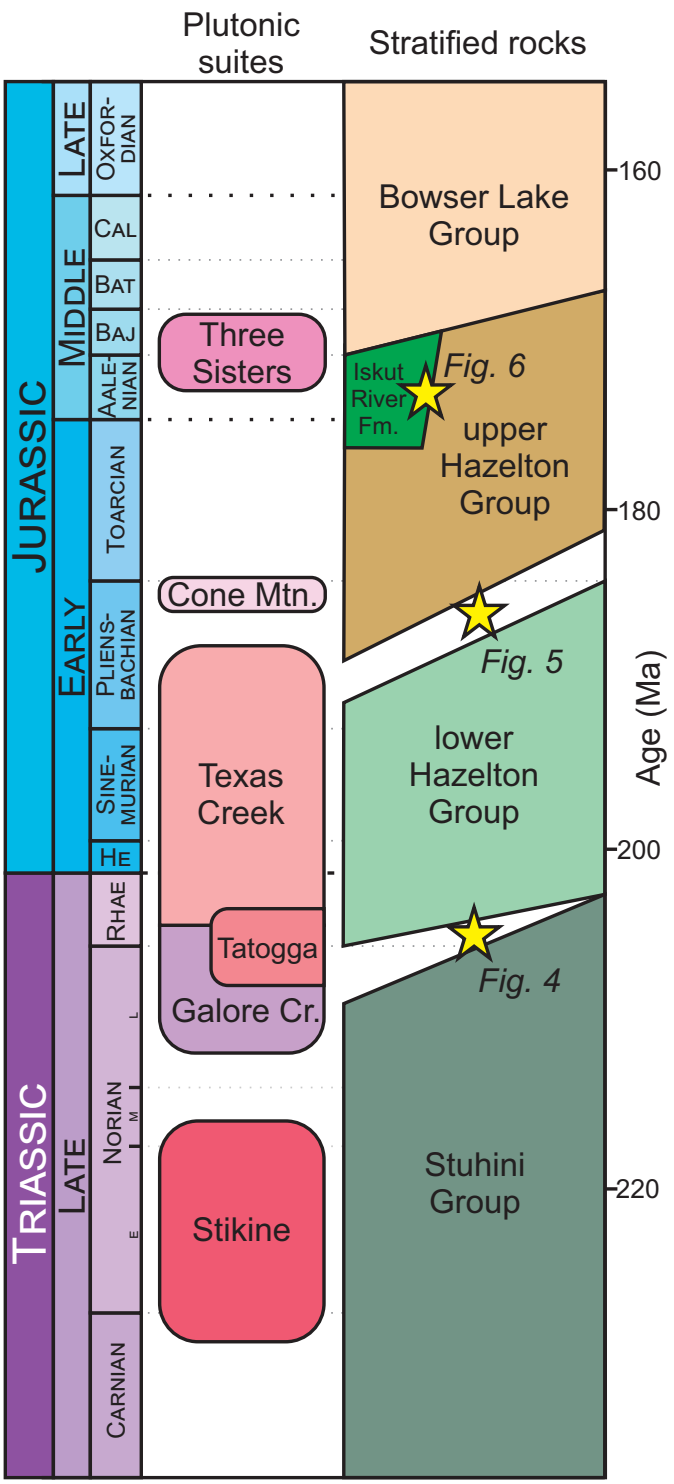


Fig. 3. Schematic Mesozoic stratigraphic and intrusive framework of the Golden Triangle. Approximate stratigraphic position of Figures 4, 5, and 6 shown for reference. Geological timescale after Cohen et al. (2025), Norian substages after Ogg et al. (2020). Modified after van Straaten (2024).

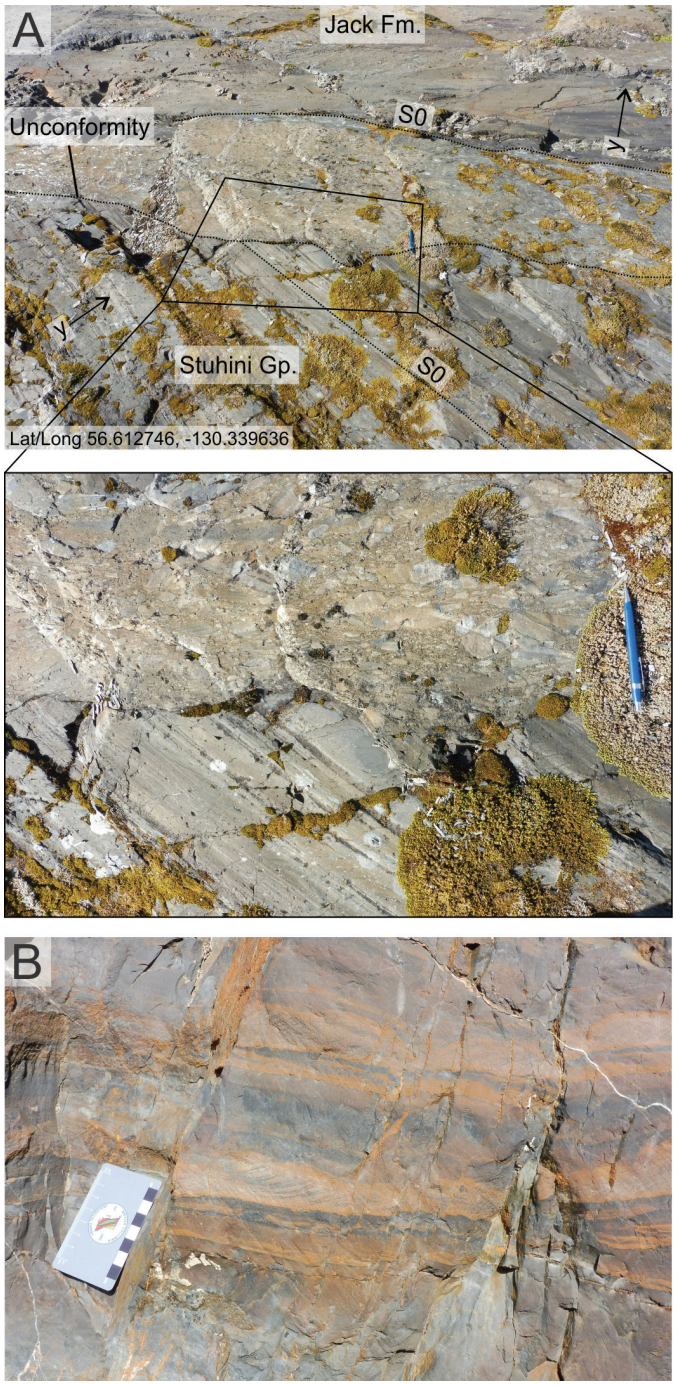


Fig. 4. a) Angular unconformity between Stuhini Group sedimentary rocks (Upper Triassic) and Jack Formation of the lower Hazelton Group (uppermost Triassic to Lower Jurassic) near the toe of the Jack Glacier (east of the Bruce Glacier). View towards the west. y= younging direction. **b)** Stuhini Group sedimentary unit with sharp-based sandstone (with small-scale cross-stratification) to mudstone fining upward sequences. Latitude/longitude here and elsewhere in this paper in WGS84 Web Mercator Auxiliary Sphere (EPSG 3857).

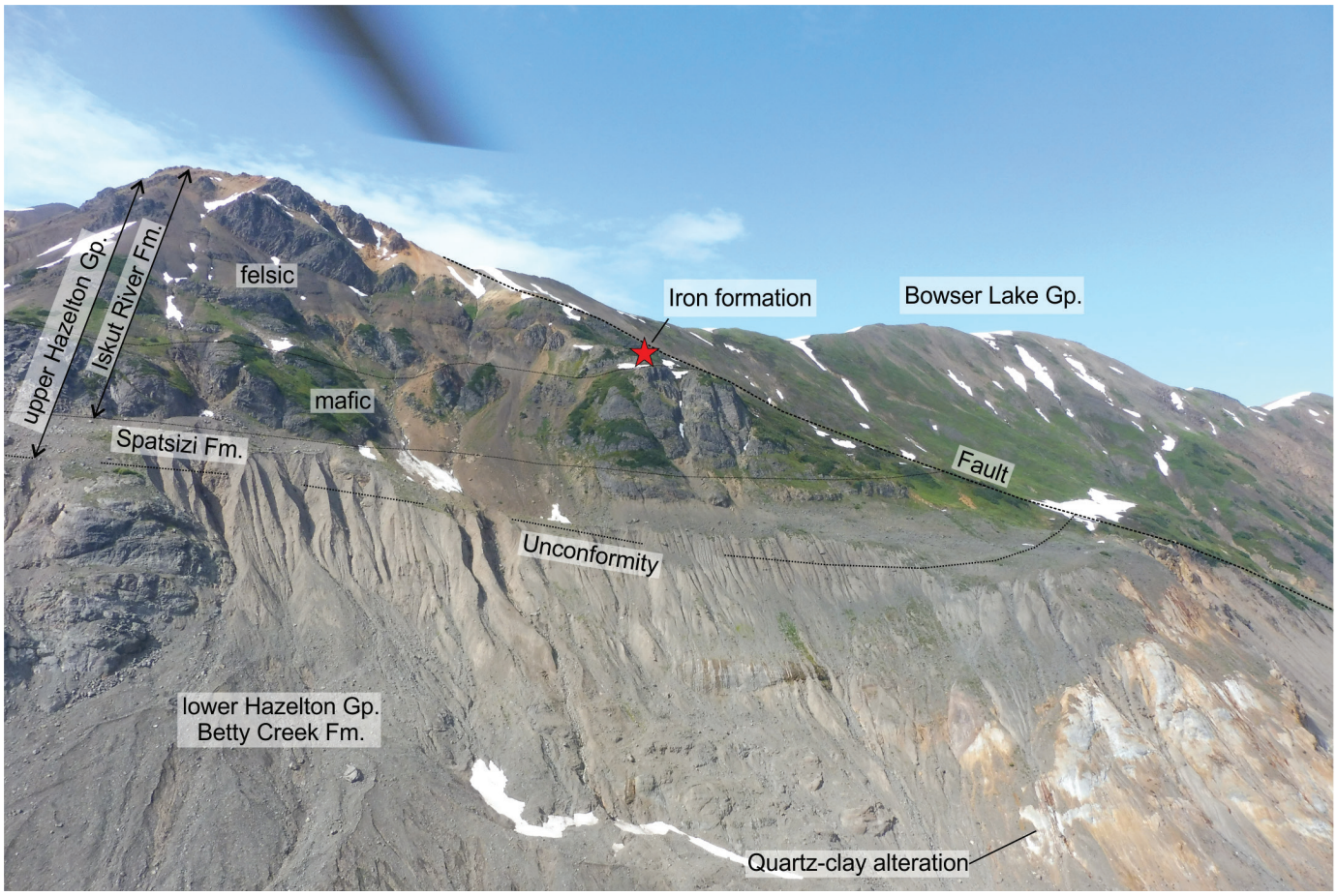


Fig. 5. Unconformity between strong quartz-clay lithocap-style alteration of the Orpiment showing (MINFILE 104B 590) in the Betty Creek Formation of the lower Hazelton Group (Lower Jurassic) and Spatsizi Formation sedimentary rocks succeeded by Iskut River Formation mafic and felsic volcanic rocks (both upper Hazelton Group, Lower to Middle Jurassic) at Treaty Creek. View towards the north.

alteration developed in lower Hazelton Group rocks that extends for at least 6 km from the Treaty Gossan (MINFILE 104B 078) to the Orpiment showing (MINFILE 104B 590) above Treaty camp. The lithocap may represent the dismembered upper portion of the nearby Goldstorm porphyry Cu-Au-Ag deposit (MINFILE 104B 704), or the upper expression of a previously unrecognized porphyry system.

The overlying upper Hazelton Group includes a lower sedimentary unit (Spatsizi Formation), overlain by a mafic volcanic succession, and succeeded by an upper felsic volcanic succession (Fig. 5; both volcanic successions part of the Iskut River Formation). The sedimentary unit includes interbedded mudstone, siltstone, sandstone, pebbly sandstone, and lesser reworked felsic lapilli-tuff to tuff and reworked mafic lapilli-tuff. Locally, fine-grained siliciclastic sedimentary strata contain ammonoid and shell fossils. The overlying mafic volcanic succession includes mafic tuff breccia containing amygdaloidal aphyric volcanic clasts. It is overlain by an upper succession of felsic lapilli-tuff, felsic crystal tuff, felsic lapillistone, lesser volcanic siltstone, mudstone, siltstone, volcanic sandstone, felsic tuff breccia, and a rare, disrupted limestone bed; clasts include white to medium grey to green-grey aphanitic to rarely flow-banded felsic volcanic clasts, and locally subordinate limestone clasts. The upper succession is locally cut by aphanitic felsic subvolcanic intrusions. Ammonoids and rare limestone indicate that the bimodal succession was emplaced in a submarine environment. Field studies in 2025 documented a new mineral occurrence (‘Red brick’, MINFILE 104B 768) comprising a bed of iron formation (~0.8 m thick) intercalated with fragmental felsic volcanic to reworked felsic volcanic rocks (Figs. 5, 6a). Transmitted and reflected light microscopy show that the iron formation consists of hematite, minor magnetite, trace pyrite, and irregular blebs and veinlets of prehnite(?) and quartz (Fig. 6b). Newly acquired lithogeochemical data from the iron formation show high Fe and low Ti, Mn, and Al concentrations (Table 1; Fig. 7), and supports classification as an Algoma-type iron formation precipitated from venting of hydrothermal fluids such as in a submarine volcanic arc, back arc, spreading ridge, or rift (see Peter, 2003; Piercey, 2005). Lithogeochemistry data show moderately enriched Sb and As concentrations (Table 1), with values greater than ten times average upper continental crustal abundance (Rudnick and Gao, 2014). Its geochemical signature is similar to VMS-associated iron formations

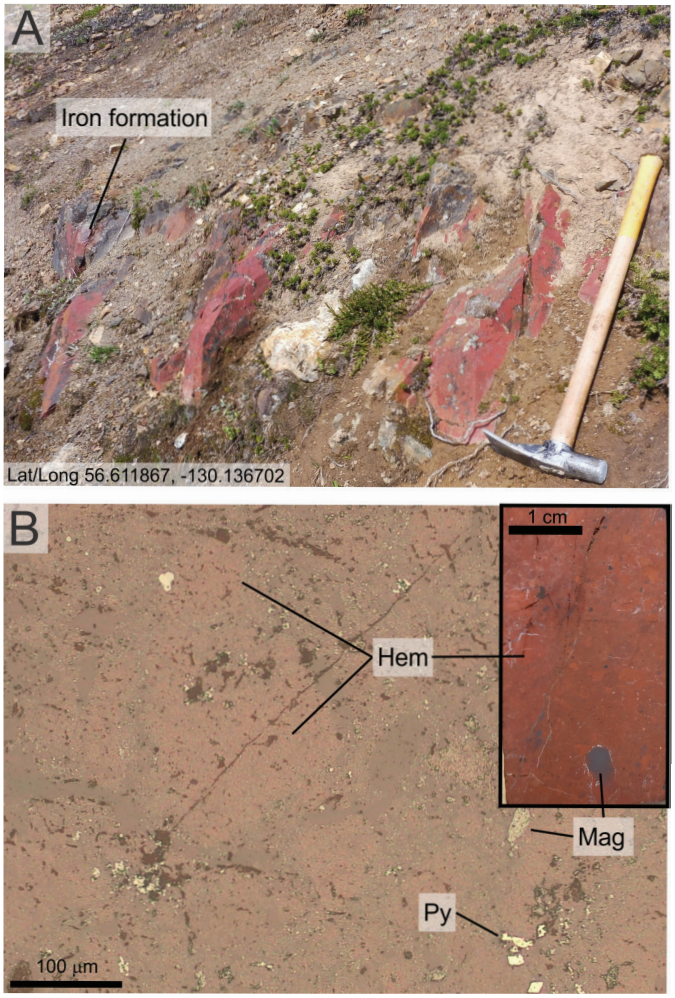


Fig. 6. a) Outcrop of iron formation bed at the new 'Red brick' occurrence near Treaty Creek. **b)** Reflected light microscope photograph of iron formation with hematite (Hem), minor magnetite (Mag), and rare pyrite (Py); inset shows thin section offcut.

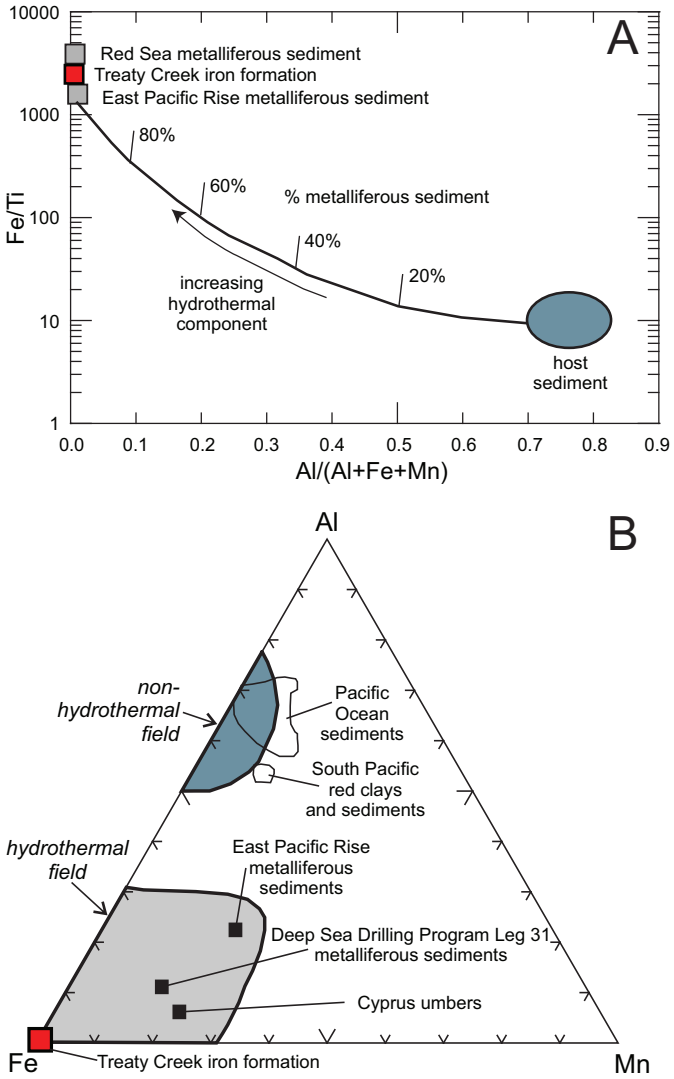


Fig. 7. Geochemistry of iron formation at the new 'Red brick' occurrence near Treaty Creek. **a)** Al/(Al+Fe+Mn) vs. Fe/Ti plot and **b)** Al-Fe-Mn ternary diagram showing that the iron formation has a composition similar to modern seafloor hydrothermal vent sediments. Figures modified from Peter (2003) and Piercey (2005).

globally and suggests potential for the broader area to host VMS mineralization. In known VMS camps such as Bathurst (New Brunswick, Canada), iron formation extends laterally from massive sulphide mineralization for distances up to 12 km (Peter, 2003 and references therein). Further interpretation of the stratigraphy using lithogeochemical and geochronological data is aimed at better understanding prospectivity for VMS mineralization.

Conclusion

As part of an ongoing project examining the Triassic-Jurassic stratigraphy and metallogeny of the Golden Triangle, new stratigraphic field studies have been carried out at Red Chris, GJ, Galore Creek, Eskay Creek, Red Mountain, Johnny Mountain, and Bruce Glacier and will refine the tectono-magmatic and metallogenic evolution of the region. Further analytical work will include geochronological, paleontological, petrographic, lithogeochemical, and radiogenic isotope analyses. Geochronological studies will include U-Pb LA-ICP-MS and high-precision CA-TIMS detrital and igneous zircon analyses. Lithogeochemical analyses of igneous rocks will expand an existing dataset of fusion and four acid digestion data with ultra-low minimum detection limits (van Straaten et al., 2022a; Van der Vlugt et al., 2022).

Table 1. Lithogeochemical data for iron formation at the new 'Red brick' occurrence near Treaty Creek. The sample was coarse crushed at the BCGS laboratory in Victoria, followed by pulverization in a mild steel mill at ALS Global, and analyses at ALS Global using lithium borate fusion, four acid, and aqua regia digestion methods.
Sample 25BvS-113a (geochem ID 67803); lat/long 56.611867, -130.136702.

%	Fusion	Four acid	Aqua regia
Si	36.2		
Al	0.08	0.08	
Fe	15.1	15.15	
Ca	0.39	0.38	
Mg	0.012	0.01	
Na	0.015	0.017	
K	0.017	0.01	
Cr	0.003	0.0041	
Ti	0.006	0.004	
Mn	0.046	0.0467	
P	0.14	0.141	
Sr	<0.008	0.0016	
Ba	0.009	0.0048	
LOI	0.6		
Total	100.77		
C	0.05		
S	0.01	0.01	

ppm	Fusion	Four acid	Aqua regia
Ag	<1	0.006	
As		74.9	81.4
Au		0.0013	
B		30	
Be	7	8.52	
Bi		0.003	<0.01
Cd		0.145	
Ce	1.6	1.64	
Co	0.5	0.425	
Cs	0.76	0.56	
Cu	<5	3	
Dy	0.58	0.493	
Er	0.44	0.351	
Eu	0.09	0.079	
Ga	0.2	0.31	
Gd	0.59	0.446	
Ge	6.3	<0.05	

ppm	Fusion	Four acid	Aqua regia
Hf	<0.05	0.04	
Hg			0.008
Ho	0.11	0.112	
In	<0.05	<0.005	<0.005
La	1.7	1.625	
Li		0.8	
Lu	0.06	0.061	
Mo	4	3.88	
Nb	0.16	0.134	
Nd	1.3	1.235	
Ni	5	1.23	
Pb	<5	1	
Pd		<0.002	
Pr	0.27	0.265	
Pt		<0.004	
Rb	0.3	0.31	
Re		<0.0004	<0.001
Sb		22.9	17.75
Sc	<0.5	0.22	
Se		0.016	<0.2
Sm	0.37	0.302	
Sn	<0.5	0.07	
Ta	<0.1	0.005	
Tb	0.07	0.066	
Te		<0.005	<0.01
Th	0.05	0.048	
Tl	0.08	0.016	0.02
Tm	0.07	0.053	
U	1	0.944	
V	249	244	
W	11.4	12.25	
Y	7.4	6.59	
Yb	0.32	0.368	
Zn	19	18	
Zr	2	1.5	

Acknowledgments

This project would not have been possible without the logistical support from Galore Creek Mining Corporation, Imperial Metals Corporation, Newcrest Mining Limited (now Newmont Corporation), Skeena Resources Limited, Seabridge Gold Inc., IDM Mining Ltd. (acquired by Ascot Resources Ltd., now Cambria Gold Mines Inc.), Tudor Gold Corp., Scottie Resources Corp., Eskay Mining Corp., and Goldstorm Metals Corp. I would like to acknowledge the exploration and mining company geologists and staff for their support, discussions, and warm welcome in their camps. Thanks to Emily Miller, Bruce Guo, Raf Bacha, and Nate Corcoran who assisted with fieldwork in 2022-2025. A constructive review by JoAnne Nelson helped improve the paper.

References cited

Bailey, L., Kim, R., Takaichi, M., Logan, J., Crowley, J., Friedman, R., Wall, C., van Straaten, B.I., and Campbell, R.W., 2025. U-Pb geochronological data for intrusive rocks near the Schaft Creek and Galore Creek deposits (southern Telegraph Creek area, NTS 104G), northwestern British Columbia. British Columbia Ministry of Mining and Critical Minerals, British Columbia Geological Survey GeoFile 2025-14, 16 p.

Campbell, R.W., and van Straaten, B.I., 2025. New data on Late Triassic to late Early Jurassic plutonic suites in the northern Golden Triangle region of northwest British Columbia. In: Geological Fieldwork 2024, British Columbia Ministry of Mining and Critical Minerals, British Columbia Geological Survey Paper 2025-01, pp. 49-72.

Campbell, R.W., Gibson, K., and van Straaten, B.I., 2026. Paleozoic to Eocene intrusions in the Golden Triangle, northwestern British Columbia: A project update. In: Geological Fieldwork 2025, British Columbia Ministry of Mining and Critical Minerals, British Columbia Geological Survey Paper 2026-01, this volume.

Cohen, K., Harper, D., Gibbard, P., and Car, N., 2025. The ICS international chronostratigraphic chart this decade. Episodes, 48, 105-115. <https://doi.org/10.18814/epiiugs/2025/025001>

Colpron, M., 2020. A digital atlas of terranes for the northern Cordillera. Yukon Geological Survey. <https://data.geology.gov.yk.ca/Compilation/2>

Evenchick, C.A., McMechan, M.E., McNicoll, V.J., and Carr, S.D., 2007. A synthesis of the Jurassic-Cretaceous tectonic evolution of the central and southeastern Canadian Cordillera: Exploring links across the orogen. In: Sears, J.W., Harms, T.A., and Evenchick, C.A., (Eds.), Whence the Mountains? Inquiries into the Evolution of Orogenic Systems: A Volume in Honor of Raymond A. Price. Geological Society of America Special Paper, 433, pp. 117-145.

Gagnon, J-F., Barresi, T., Waldron, J.W.F., Nelson, J.L., Poulton, T.P., and Cordey, F., 2012. Stratigraphy of the upper Hazelton Group and the Jurassic evolution of the Stikine terrane, British Columbia. Canadian Journal of Earth Sciences, 49, 1027-1052. <https://doi.org/10.1139/e2012-042>

Henderson, J.R., Kirkham, R.V., Henderson, M.N., Payne, J.G., Wright, T.O., and Wright, R.L., 1992. Stratigraphy and structure of the Sulphurets area, British Columbia. In: Current Research, Part A, Cordillera and Pacific Margin. Geological Survey of Canada, Paper 92-1A, pp. 323-332.

Johnston, R.J., 2025. Anomalous deformation corridors and the structural evolution of the Galore Creek district, northwestern British Columbia. M.Sc. thesis, University of British Columbia, Vancouver, B.C., Canada, 111 p.

Miller, E.A., Ferri, M.D., van Straaten, B.I., and Wall, C., 2025a. Stratigraphic framework, structural setting, and timing of VMS, epithermal, and porphyry mineralization in the Kitsault River area, northwest British Columbia. In: Geological Fieldwork 2024, British Columbia Ministry of Mining and Critical Minerals, British Columbia Geological Survey Paper 2025-01, pp. 17-47.

Miller, E.A., van Straaten, B.I., Ferri, M.D., and Hunter, R., 2025b. Preliminary bedrock geology of the Kitsault River area, northwestern British Columbia: GIS data. British Columbia Ministry of Mining and Critical Minerals, British Columbia Geological Survey GeoFile 2025-20, 3 p.

Nelson, J.L., and van Straaten, B.I., 2020. Recurrent syn- to post-subduction mineralization along deep crustal corridors in the Iskut-Stewart-Kitsault region of western Stikinia, northwestern British Columbia. In: Sharman, E.R., Lang, J.R., and Chapman, J.B., (Eds.), Porphyry Deposits of the Northwestern Cordillera of North America: A 25-Year Update, CIM Special Volume 57, pp. 149-211.

Nelson, J.L., Waldron, J., van Straaten, B.I., Zagorevski, A., and Rees, C., 2018. Revised stratigraphy and regional digital map representation of the Hazelton Group in the Iskut River region, northwestern British Columbia. In: Geological Fieldwork 2017, British Columbia Ministry of Energy, Mines and Petroleum Resources, British Columbia Geological Survey Paper 2018-1, pp. 15-38.

Nelson, J.L., van Straaten, B., and Friedman, R., 2022. Latest Triassic-Early Jurassic Stikine-Yukon-Tanana terrane collision and the onset of accretion in the Canadian Cordillera: Insights from Hazelton Group detrital zircon provenance and arc-back-arc configuration. Geosphere, 18, 670-696.

Ogg, J.G., Chen, Z-Q., Orchard, M.J., and Jiang, H.S., 2020. Chapter 25-The Triassic period. In: Gradstein, F.M., Ogg, James, G., Schmitz, M.D., and Ogg, G.M., (Eds.), Geologic Time Scale 2020, pp. 903-953.

Piercey, S.J., 2005. Reconnaissance geological and geochemical studies of the Joe Mountain Formation, Joe Mountain region (NTS 105D/15), Yukon. In: Yukon Exploration and Geology 2004, Yukon Geological Survey, pp. 213-226.

Peter, J.M., 2003. Ancient iron formations: Their genesis and use in the exploration for stratiform base metal sulphide deposits, with examples from the Bathurst mining camp. In: Lentz, D.R., (Ed.), Geochemistry of Sediments and Sedimentary Rocks: Evolutionary Considerations to Mineral Deposit-Forming Environments, Geological Association of Canada, GeoText 4, pp. 145-176.

Richards, J.P., 2009. Postsubduction porphyry Cu-Au and epithermal Au deposits: Products of remelting of subduction-modified lithosphere. Geology, 37, 247-250.

Rudnick, R.L., and Gao, S., 2014. Chapter 4.1-Composition of the continental crust. In: Treatise on Geochemistry, Second Edition, pp. 1-64. <https://doi.org/10.1016/B978-0-08-095975-7.00301-6>

Sillitoe, R.H., 2010. Porphyry copper systems. Economic Geology, 105, 3-41.

van Straaten, B.I., 2024. Upper Hazelton Group stratigraphy along the Stikine arch, northwestern British Columbia. In: Geological Fieldwork 2023, British Columbia Ministry of Energy, Mines and Low Carbon Innovation, British Columbia Geological Survey Paper 2024-01, pp. 149-177.

van Straaten, B.I., Logan, J.M., Hunter, R.C., Nelson, J.L., and Miller, E.A., 2022a. Igneous lithogeochemistry data for the Dease Lake, Kitsault River, Galore Creek, Telegraph Creek, Foremore, and other areas in northwestern British Columbia. British Columbia Ministry of Energy, Mines and Low Carbon Innovation, British Columbia Geological Survey GeoFile 2022-12, 14 p.

van Straaten, B.I., Logan, J.M., Nelson, J.L., Moynihan, D.P., Diakow, L.J., Gibson, R., Bichlmaier, S.J., Wearmouth, C.D.,

Friedman, R.M., Golding, M.L., Miller, E.A., and Poulton, T.P., 2022b. Bedrock geology of the Dease Lake area. British Columbia Ministry of Energy, Mines and Low Carbon Innovation, British Columbia Geological Survey Geoscience Map 2022-01, 1:100,000 scale.

van Straaten, B.I., Friedman, R.M., and Camacho, A., 2023. Stratigraphy of the Stuhini Group (Upper Triassic) in the Galore Creek area, northwestern British Columbia. In: Geological Fieldwork 2023, British Columbia Ministry of Energy, Mines and Low Carbon Innovation, British Columbia Geological Survey Paper 2023-01, pp. 33-49.

Van der Vlugt, J., Rukhlov, A.S., and van Straaten, B.I., 2022. Lithogeochemical re-analysis of British Columbia Geological Survey archived rock samples from northwestern British Columbia. British Columbia Ministry of Energy, Mines and Low Carbon Innovation, British Columbia Geological Survey GeoFile 2022-14, 15 p.

Application of radiolarian biostratigraphy in constraining the geology of the northern Canadian Cordillera, British Columbia and Yukon

Alex Zagorevski[1, a], Fabrice Cordey[2], Mitchell G. Mihalynuk[3], and Aeron Vaillancourt[1]

[1] Geological Survey of Canada, 601 Booth Street, Ottawa, ON, K1A 0E8
[2] Laboratoire de Géologie de Lyon, Terre, Planètes, Environnement, CNRS-UMR 5276 Université Claude Bernard Lyon 1, France
[3] British Columbia Geological Survey, Ministry of Mining and Critical Minerals, Victoria, BC, V8W 9N3
[a] corresponding author: Alex.Zagorevski@nrcan-rncan.gc.ca

Recommended citation: Zagorevski, A., Cordey, F., Mihalynuk, M.G., and Vaillancourt, A., 2026. Application of radiolarian biostratigraphy in constraining the geology of the northern Canadian Cordillera, British Columbia and Yukon. In: Geological Fieldwork 2025, British Columbia Ministry of Mining and Critical Minerals, British Columbia Geological Survey Paper 2026-1, pp. 153-162.

Abstract

Pelagic sedimentation of radiolarian tests in deep-water oceanic settings leads to accumulations of oozes that become lithified as chert. The biostratigraphy of radiolaria preserved in such cherts is an important tool for establishing the geological history of oceanic crustal fragments. Deep-water oceanic rocks in the northern Cordillera have historically been considered ophiolitic terranes. However, radiolarian biostratigraphy from nearly four decades of sampling in the Atlin, British Columbia-Teslin, Yukon Territory area, demonstrates that most pelagic strata comprise disrupted Middle Triassic to Early Jurassic overlap successions, predominantly the Kedahda Formation. Older, late Paleozoic chert is either interbedded with carbonate platform deposits such as the Horsefeed Formation or occurs as slivers in accretionary complexes such as the Lincoln complex.

Keywords: Radiolaria, fossil age, geochronology, ribbon chert, Atlin terrane, Cache Creek terrane, Sentinel complex, Lincoln complex, Kedahda Formation, Shonektaw Formation, Nakina suite, Jurassic, Triassic, Permian, ophiolite, tectonic accretion, Cordilleran geoscience

1. Introduction

Crustal fragments that comprise much of the Cordillera (Fig. 1) have historically been classified with a focus on the principal tectonic setting in which they were formed. Fragments that have been significantly displaced with respect to the North American continent to which they are now attached are called terranes, which are classified as peri-continental margin, back-arc basin, volcanic arc, or offshore 'oceanic' derivation. 'Oceanic' terranes are made of chert, limestone, within-plate volcanic rocks, siliciclastic rocks, and ocean crust sequences (ophiolites) on which the others were interpreted to have formed (e.g., Coney et al., 1980; Silberling et al., 1992).

In the few decades following the birth of the new plate tectonic hypothesis in the late 1960s, ophiolites were generally accepted to represent mid-oceanic or back-arc ridges. Grouping all apparently related 'oceanic' rocks of the Canadian Cordillera into a few terranes made sense in this historical context. As such, it was natural to assume that oceanic plateau-like sequences were built on top of older ophiolitic ocean floor. Biogenic chert deposition was expected on the ocean floor below and adjacent to the volcanic plateau (Monger et al., 1991), and chert deposition was expected above carbonate that capped plateaus as they thermally subsided.

Further work revealed two serious problems with this view of the general geological evolution of the former Cache Creek oceanic terrane. First, the widespread mafic sequences assumed to be plateau substrate for carbonate bank successions were found to lack geochemical characteristics of ocean island basalts (OIB) but were instead mostly characterized by primitive island arc tholeiite geochemistry (IAT; English et al., 2002, 2010; English and Johnston, 2005; Zagorevski et al., 2021). Perhaps the more serious problem is that the isotopic age of this IAT ocean crust is now known to be mostly younger (ca. 264-245 Ma) than the carbonate banks (ca. 359-254 Ma) that were thought to be built atop the plateaux (Mihalynuk et al., 2003a, b; Zagorevski et al., 2021). Cherts were deposited throughout the lifetime of both the carbonate bank and IAT crust formation (though mostly coeval with the IATs) allowing the evaluation of the link between various environments and deformational events that juxtapose them. Evaluation of the relationship between the carbonate bank and ophiolites was made possible through the use of isotope and macrofossil geochronology, but, critically, depended on identification of widespread radiolaria, the primary component of biogenic chert.

In this paper, we explore the utility of radiolarian cherts and other radiolarian-bearing rocks found in oceanic sequences of the Cache Creek and ophiolitic Atlin terranes of northern British Columbia, near Atlin, and southern Yukon, near Teslin (Fig. 1; e.g., Aitken, 1959; Gabrielse, 1969, 1998; Monger, 1975; Cordey et al., 1991; Monger et al., 1991; Mihalynuk et al., 1999, 2003a, 2004a, b; Cordey, 2020; Zagorevski et al., 2021) in the traditional territories of the Taku River Tlingit First Nation,

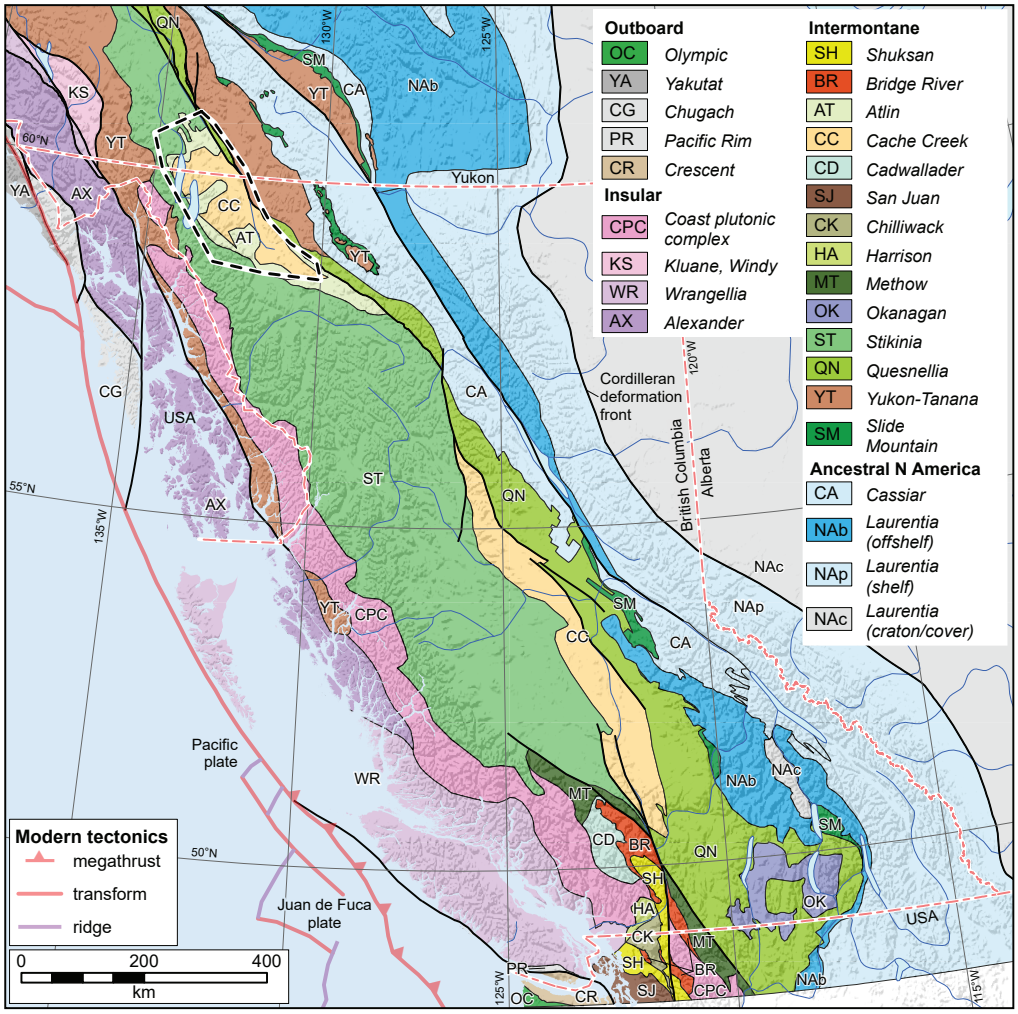


Fig. 1. Location of study area. Terranes after Colpron (2020) and Zagorevski et al. (2021).

Carcross-Tagish First Nation, Teslin Tlingit Council and Tahltan First Nation. We also present new biochronological age data from radiolarian chert samples collected in the 2024 field season (Table 1). In a companion publication (Zagorevski et al., 2026), we compile these biostratigraphic data together with other unpublished and published sources (Figs. 2, 3). We demonstrate that these data facilitate tectonic analysis by constraining the ages of ophiolites, mélanges, and other oceanic sequences, as well as widespread marine sedimentation that accompanied and postdated initial terrane amalgamation.

2. Methods

Radiolaria are unicellular marine protists, generally less than 1 mm in diameter, that first appeared in the Early Cambrian fossil record (Chang et al., 2018) and have rapidly evolved into a diverse array of forms since then. An even older origin in the Neoproterozoic is suggested by fossil-calibrated molecular clocks (760 Ma; Sandin et al., 2025). Approximately 15,000 species of radiolaria are known, with ~90% found only in the fossil record (Bánki et al., 2025, and references therein). Intricate opaline silica skeletal remains of radiolaria were the principal contributor to biogenic silica production in ocean basins (pelagic 'silica ooze') in the Paleozoic and Mesozoic. Largely due to their adaptability and entirely planktonic lifestyle, they were carried by currents to every part of the marine environment. This ubiquity, together with their rapid and diverse morphological evolution, underpins their usefulness as a biochronometer. Radiolarians are still present in modern oceans but have been partly replaced by diatoms as primary pelagic silica producers since the Cenozoic (Westacott et al., 2021).

Chert biochronology is a relatively simple, inexpensive, and effective method for determining the age of pelagic strata that may otherwise be difficult to date, even when applying costly isotopic techniques. Radiolaria can commonly be seen with the unaided eye in chert bands (Fig. 4) but may require the use of a hand lens. The general rule is that unless radiolaria can be seen, collection and submission for the purpose of radiolarian dating is not done. However, sampling of key undated intervals of pelagic strata that lack visible radiolaria, especially where

Table 1. New radiolarian sample collection.

SAMPLE	Lat	Long	Unit	Lithology and field notes	Lab observations/ Preservation	Radiolarian/conodont taxa or features	Age	Comments (biochronology)
24ZE1602A01	59.1041	-132.4983	Lincoln	Grey chert with ghostly rads	radiolarians/ poor	internal moulds of ***Parafollicucullus*** sp. or ***Follicucullus*** sp.	**Permian**	preservation insufficient to establish a more precise age
24ZE1613A01	59.1074	-132.4887	Lincoln	Bedded grey chert, well preserved radiolaria apparent in	abundant radiolarians including internal moulds/ moderate	***Haploaxon*** sp., ***Latentifistula*** sp., ***Parafollicucullus scalpratus*** ,	**Early Permian, Cisuralian**	age based on occurrence of *P. scalpratus* (Aitchison et al., 2017)
24ZE1619A01	59.1069	-132.5076	-	dark grey chert	recrystallization	-	-	-
24ZE1651A01	59.4523	-133.4378	Sentinel	Basalt with interpillow limestone and blocks of dark grey chert	radiolarians, recrystallized matrix/ poor	***Latentifistula*** sp., internal moulds of ***Parafollicucullus*** sp. or ***Follicucullus*** sp.	**Permian**	preservation insufficient to establish a more precise age within the Permian
24ZE1669A01	59.4242	-133.4299	-	White chert	recrystallized matrix, silica fragments	-	-	-
24ZE1669A02	59.4242	-133.4299	-	Large >20m pod of laminated grey to beige chert; very similar to Horsefeed Fm. in the Nakina	silica fragments, clays	-	-	-
24ZE1674A01	59.4284	-133.4315	-	Laminated grey green chert	silica fragments, clays	-	-	-
24ZE1690B01	59.4352	-133.4682	Sentinel	Finely to medium bedded cherty tuff, and locally graded turbidite beds overlain by light grey chert. Looks like a large block within basalt breccia.	radiolarians, silica fragments, clays/ poor	internal mould of ***Parafollicucullus*** sp. or ***Follicucullus*** sp., ***Pseudotormentus*** sp.	**Permian**	preservation insufficient to establish a more precise age within the Permian
24ZE1691A01	59.4358	-133.4689	-	Immediately above gabbro sill, beautifully bedded and laminated light gray chert	recrystallized matrix, silica fragments	-	-	-
24ZE1699A01	59.4359	-133.4823	Sentinel	Well bedded haematitic / dark gray chert with radiolaria	abundant radiolarians recrystallized matrix/ moderate	***Hegleria*** sp., ***Latentifistula*** sp., ***Follicucullus monacanthus***	**Late Permian, Wordian-Capitanian**	age based on occurrence of *F. monacanthus* (UA 9-12; Xiao et al., 2018)
24ZE1702B01	59.4371	-133.4897	-	Haematitic basalt overlain by red shale to cherty shale	abundant red clays, radiolaria, matrix fragments/ moderate	***Albaillella*** sp., ***Ishigaum*** sp., ***Latentifistula*** sp., ***Latentibifistula*** sp., ***Murcheyella triporosa*** , ***M*** . sp. aff. ***triporosa*** (Murchey, 1990), ***Parafollicucullus*** sp. ***G*** (Ishiga, 1982)	**Pennsylvanian, Moscovian-Gzhelian**	correlation with assemblage 6 and part of assemblage 7 of Murchey (1990)
24ZE1707A01	59.4440	-133.4941	-	White weathering chert, black on fresh surfaces	siliceous matrix fragments, clays		-	-
24ZE1709A01	59.4455	-133.5010	Sentinel	Folded dark grey cherts	recrystallized matrix, abundant spheres	***Latentifistula*** sp., ***Parafollicucullus scalpratus***	**Early Permian, Cisuralian**	age based on occurrence of *P. scalpratus* (Aitchison et al., 2017)
24ZE1710A01	59.4461	-133.5012	-	Red, green, and dark gray chert	spheres and rods, but no clear morphologies	-	-	-
24ZE1720A01	59.4826	-133.4484	-	Black chert to black argillite, seems to be most of the cliff face	siliceous matrix fragments, clays	-	-	-
24ZEAV237A01	59.8311	-133.1313	-	Light gray chert	silica spheres, clays	-	-	-
MMI24-06-04	59.8449	-133.0830	-	Dark gray chert	abundant silica spheres, unfortunately undiagnostic	-	-	too recrystallized
MMI24-06-05	59.8445	-133.0831	-	Dark gray chert	silica spheres, clays, silica fragments	-	-	-

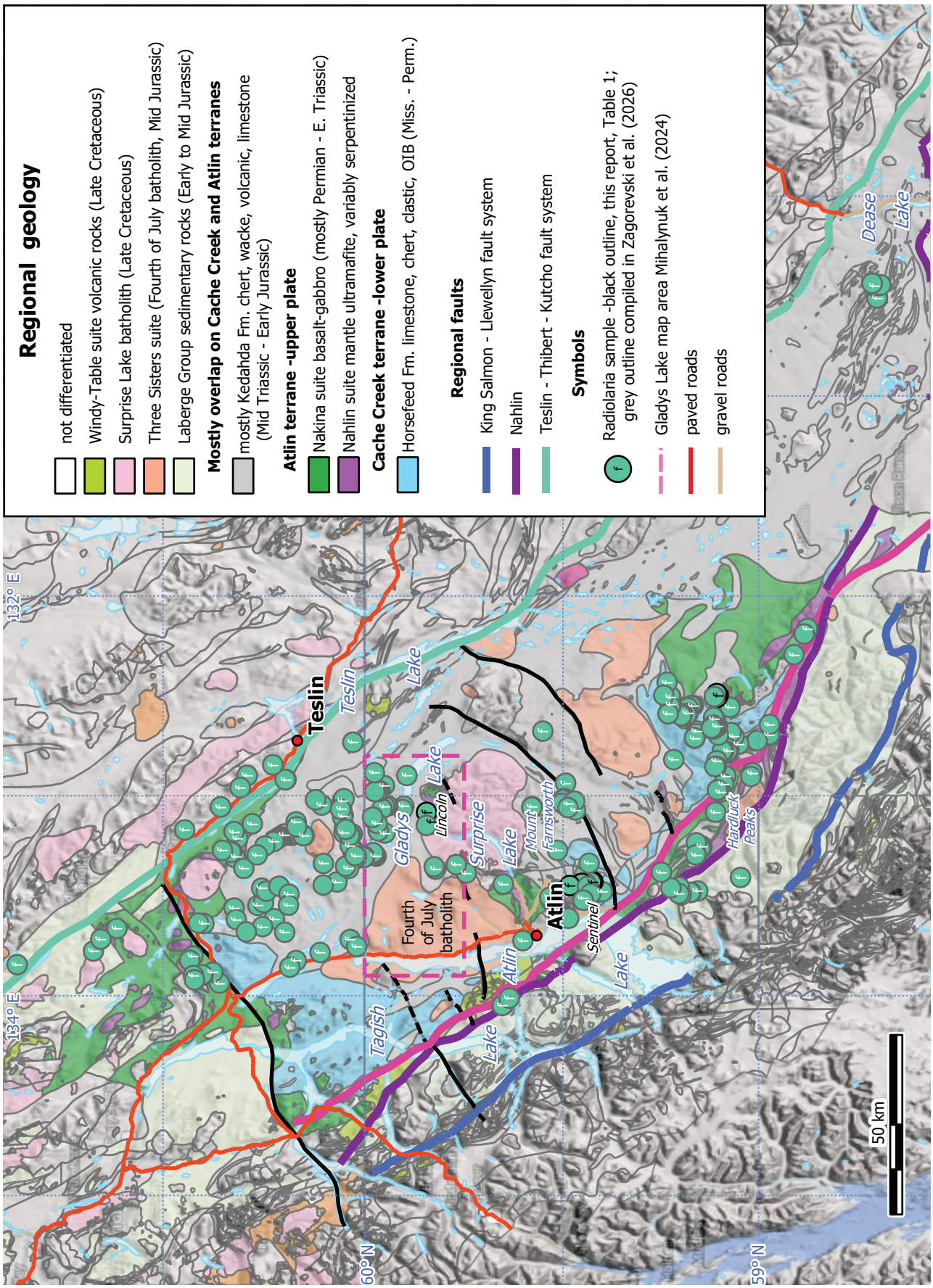


Fig. 2. Geological setting of radiolarian samples in the Atlin-Teslin area. Samples reported here for the first time (Table 1) are shown with a black outline, and those are compiled together with samples from previous studies (shown with grey outlines in Zagorevski et al., 2026). Bedrock geology in Yukon derived mostly from Yukon Geological Survey (2019).

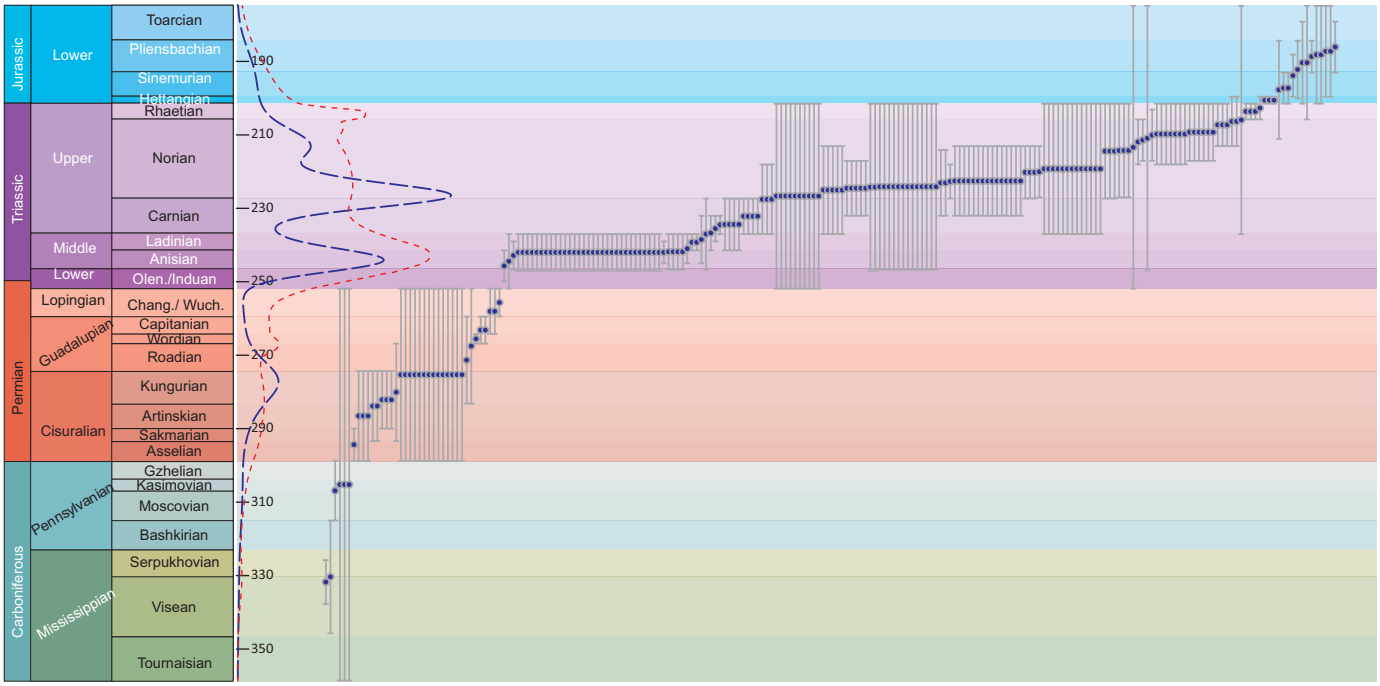


Fig. 3. Summary of biostratigraphic data from radiolaria-bearing samples in this study and in previous work (Zagorevski et al., 2026). Absolute age calibration of time period boundaries is from the International Chronostratigraphic Chart (Cohen et al., 2025). Red dashed line: Probability Density Plot derived from conversion of biostratigraphic data into numerical scale and treating the age range as a 2σ error (see methods in Zagorevski et al., 2026). Blue Dashed line: Kernel Density Plot from conversion of biostratigraphic data into numerical scale and using the median biostratigraphic age and kernel density of 4 (Vermeesch, 2018).



Fig. 4. Radiolarian chert in outcrop. Dark grey to almost black, spherical radiolaria (~0.2 mm) visible on a weathered surface of light grey and rusty chert outcrop north of Gladys Lake (site of sample RCA23-19-26). Samples collected nearby returned Late Triassic ages. Scale divisions are in mm.

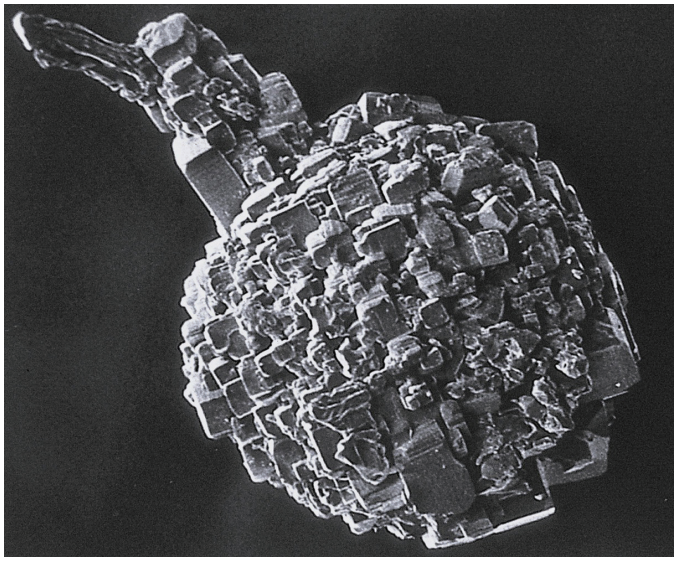


Fig. 5. SEM photomicrograph of a pyritized radiolarian test from the Stuhini Group south of Atlin (diameter of the sphere is 0.3 mm).

unmetamorphosed, may be worthwhile, and lead to unexpected results. For example, sampling of the Stuhini Group, south of Atlin yielded radiolaria delicately replaced by pyrite, and identifiable to the species level (Fig. 5).

Extraction of radiolaria generally relies on collection of residues following serial dissolution of the samples in hydrofluoric acid (HF). Rinsed residues are dried and microfossils are separated with the aid of a binocular microscope. Radiolaria are mounted and examined with the use of a scanning electron microscope (SEM) as required.

2.1. Sampling of cherts

Many cherts containing diagnostic radiolaria are shades of grey (ranging from black to almost white). However, beige to tan, green and red chert varieties, as well as argillites, can also yield diagnostic radiolaria. Depending on the sample, radiolarian tests may be best observed on fresh surfaces, weathered surfaces, and are commonly accentuated in glossless, weathered outcrop rinds. Radiolaria preservation can be limited to only specific beds within an outcrop, or even to certain parts of beds, or individual boudins. Chert and argillite samples collected for radiolarian analysis can typically be small, with ~20 cm^3 being sufficient.

Recrystallization of chert leads to degradation of fossil

radiolaria and is a common problem. Collectors should attempt to screen samples in the field, rejecting sucrosic (granular) samples. Whitening and deformation of radiolarian tests into ovoids generally indicate extensive recrystallization. So too, is extensive veining and patchy discolouration of chert. At a finer scale, diffuse margins of radiolaria can be a sign of recrystallization; radiolaria with sharp margins are most likely to yield high quality determinations. Screening using thin sections may also be useful (Figs. 6, 7, 8).

Although proximity to intrusions generally correlates with recrystallization, it does not necessarily rule out preservation of radiolaria. For example, some samples in Zagorevski et al. (2026) were collected from enclaves in the mafic dike zone of an ophiolite, and others were from within the thermal-metamorphic halo of the Surprise Lake batholith. In both cases, the material sampled included radiolaria that were visible to the unaided eye.

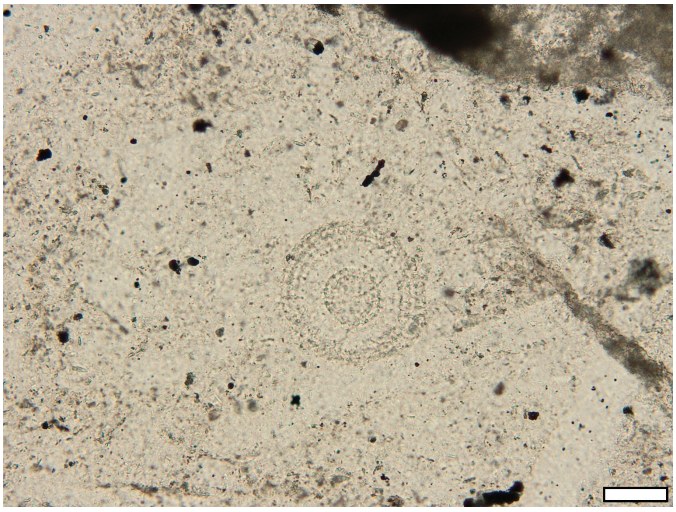


Fig. 6. Photomicrograph of a well-preserved test in a chert clast in a pebble conglomerate north of Sterlin Lake, southern Yukon. Internal structure of the radiolarian test is clearly visible, and the outer margin is sharp, both excellent indications of a sample that will yield identifiable microfossils. Nearby chert samples yielded a Late Triassic radiolarian age determination. Scale bar is 50 μm.

3. Stratigraphic overview of northern Cache Creek and Atlin terranes

Radiolarian biostratigraphic age control has provided critical constraints on the definition of key stratigraphic units in the Atlin BC-Teslin YT area. The stratigraphic nomenclature summarized herein follows Zagorevski et al. (2021) who suggested revisions consistent with modern tectonic environments, with updates from Mihalynuk et al. (2024). Due to radiolaria age data, we now know that the most widespread chert unit in the Atlin-Teslin area, the Kedahda Formation, is Mesozoic and largely an overlap on older conjoined terranes (together with the more restricted Shonektaw Formation) and have been since deformed. Paleozoic chert, in part comprising

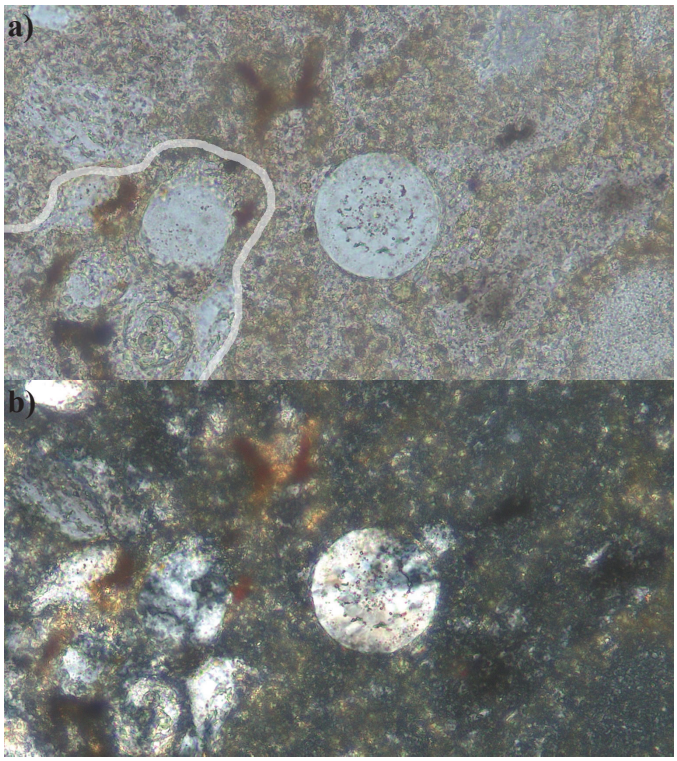


Fig. 7. Photomicrographs of radiolaria in siltstone-argillite beds of probable Carnian age, southern Atlin Lake area. **a)** Partly recrystallized radiolaria with a quartz overgrowth in a fine-grained wacke grain (translucent white outline), versus a sharply defined and larger specimen at right displaying relict interior structure (field of view is ~2 mm). **b)** Same view as a) but in cross-polarized light, which reveals feathery quartz in recrystallized and overgrown radiolarian test versus incipient recrystallization of the sharply defined test at right.

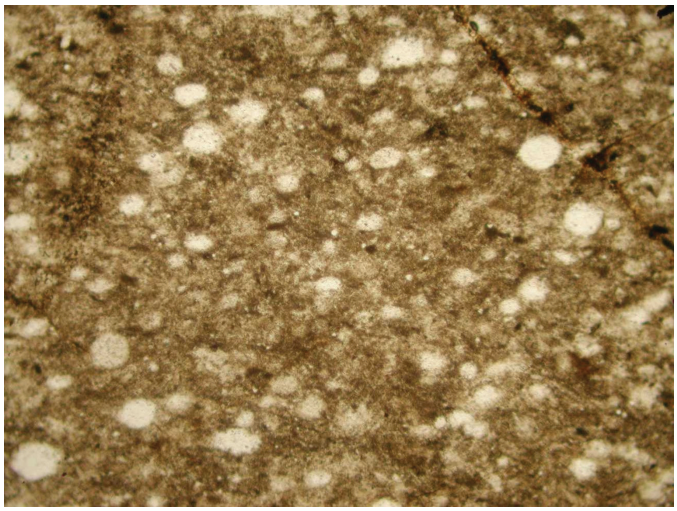


Fig. 8. Photomicrograph of an argillaceous chert sample from near Hardluck Peaks, ~75 km south of Atlin, that contains abundant radiolaria tests (field of view ~4 mm), but with diffuse margins indicating that they are too recrystallized to be reliably identified which, together with deformation of the rock, makes it difficult to distinguish radiolarian tests from mineral grains (from Mihalynuk et al., 2004b).

accretionary complexes and/or mélange (Lincoln complex and Sentinel complex) but also deposited on ocean crust and mantle of the Nakina suite, are a relatively minor component of the northern Cache Creek and Atlin terranes. However, the term 'mélange' has historically been widely applied to the northern Cache Creek terrane as well as a variety of structurally or stratigraphically complex regions of other 'oceanic' terranes in the Cordillera where it has become a prominent defining feature. Yet in many cases the use of 'mélange' as a genetic descriptor inferring subduction zone processes is unwarranted. For example, competent chert beds in otherwise incompetent chert-argillite sequences are commonly pervasively boudinaged and dismembered in a scaly, ductile argillite matrix, resulting in a sedimentary 'mélange'. Similarly, deformation and serpentinization of peridotite intruded by gabbro results in gabbro knockers in a fault zone of scaly serpentinite 'mélange'. Sedimentary and fault zone mélanges are characterized by local rock types, they lack exotic clasts, and they are better described as 'broken formation' (Raymond, 1984) and igneous equivalents.

3.1. Cache Creek terrane

In the northern Canadian Cordillera, the Cache Creek terrane is typified by thick accumulations of late Paleozoic carbonate rocks named the Horsefeed Formation by Monger (1975). Relatively thin mafic volcanic layers interbedded with these carbonate rocks generally have geochemical signatures consistent with OIB (Zagorevski et al., 2021) or enriched mid-ocean ridge basalt (enriched MORB; English et al., 2010; Mihalynuk et al., 2018). In contrast, large tracts of basalt in adjacent areas (Nakina Formation of Monger, 1975) are IAT (Zagorevski et al., 2021), and these are juxtaposed with the Horsefeed Formation across crustal-scale faults interpreted as reworked subduction zone structures. Thus, an upper plate (Nakina arc)-lower plate (Horsefeed ocean island/plateau) relationship is preserved. At the interface is accretionary complex represented by true mélange as preserved, for example, in the Lincoln and Sentinal complexes, derived mostly from the subducting plate, and are therefore included with the Cache Creek terrane.

3.1.1. Lincoln complex

Recent mapping near Lincoln Lake (Gladys Lake area of northern British Columbia), demonstrated a tectonic mélange origin for structurally interleaved peridotite, serpentinite, gabbro, basalt, argillite and other siliciclastic rocks, limestone/marble, and chert, and comprises the type locality of the Lincoln complex (Mihalynuk et al., 2024). This is one of several areas that demonstrably contain interleaving of a variety of crustal and mantle rock types, indicating a tectonic mélange origin (e.g., Mihalynuk et al., 2003a, 2024; Zagorevski et al., 2021). Targeted sampling of chert in the Lincoln complex yielded Paleozoic radiolaria (Table 1).

3.1.2. Sentinel complex

The Sentinel Range south of Atlin exposes a section of Paleozoic basalt, limestone, chert, and diabase (e.g., Monger, 1975; Bloodgood et al., 1990). These rocks are in fault contact with Paleozoic limestones of the Horsefeed Formation (Cache Creek terrane) and Middle Permian to Middle Triassic Atlin terrane ophiolitic rocks and are unconformably overlain by the Late Triassic rocks of the Kedahda Formation. Mafic rocks display a variety of geochemical signatures including MORB, OIB, and back-arc tholeiite. Chert and lesser limestone occur between clasts and basalt flows and also appear to stratigraphically overlie the basalts. These cherts are also intruded by mafic sills with contact zones locally displaying peperite-like and fluidal textures suggesting wet sediment-magma interaction, and range in age from Carboniferous to Permian (Table 1), although field relationships suggest that most of the chert accumulated in the Permian. Several distinct chert-bearing imbricated thrust panels are inferred. Some of these thrust panels may correlate with less coherent slices within the Lincoln complex. Similar rocks may occur elsewhere in northern British Columbia and Yukon, such as on the western shores of Teslin Lake and in the Nakina Lake area.

3.2. Atlin terrane

The Nakina Formation was originally defined by Monger (1975) and its rank was changed to Nakina suite (Zagorevski et al., 2021; Mihalynuk et al., 2024) to be more consistent with the traditionally included rock types and the stratigraphic code (North American Commission on Stratigraphic Nomenclature, 2021). The Nakina suite, as originally defined, is generally a massive and structureless, or laminated to "flow banded", commonly rubbly-weathering IAT basalt. Detailed investigations indicate that many localities of the Nakina suite include a significant proportion of deformed and mylonitized hypabyssal rocks (basaltic, diabase, micro-gabbro dikes or sills). In some places (e.g., Hardluck Peaks south of Atlin, or King Mountain east of Dease Lake), the Nakina suite forms the upper crustal portion of the Atlin terrane ophiolites. However, the general paucity of middle to lower crustal rocks at most localities suggests that spreading was tectonically accommodated, similar to modern ocean core complexes (Zagorevski et al., 2021; Bogatu et al., 2023; Mihalynuk et al., 2024). Permian chert is locally present as screens within hypabyssal rocks or is intruded by sparse mafic sills within these core complexes, demonstrating that these old chert units form part of the Atlin terrane ophiolites. Broad tracts of the Atlin terrane are primitive IAT, including the ophiolite basalt as well as poorly developed volcanic edifices constructed atop them that are dated by U-Pb isotopic techniques and radiolaria as ranging from Late Permian to early Middle Triassic (Zagorevski, 2021 and sources therein).

3.3. Shonektaw Formation

The Upper Triassic Shonektaw Formation is exposed on the

east side of Teslin Lake (e.g., Gordey and Stevens, 1994a, b). This unit comprises fine-grained siliciclastic rocks, augite and/or hornblende porphyritic volcanic and volcaniclastic rocks, chert, and minor limestone. Gordey and Stevens (1994b) identified several bodies of harzburgite, pyroxenite, dunite, and gabbro within the Shonektaw Formation. Contained volcaniclastic units locally include altered ultramafic clasts and are characterized by anomalously high Cr concentrations (Zagorevski et al., 2018). This suggests that the Shonektaw Formation unconformably overlies and is partly derived from the mafic-ultramafic plutonic rocks and mantle rocks (Nakina suite, see above) and incorporated clasts derived through either volcanic or sedimentary processes (Zagorevski et al., 2018).

3.4. Kedahda Formation, disrupted overlap

The widespread Kedahda Formation (Watson and Mathews, 1944; Gabrielse, 1969; Monger, 1975) is generally characterized by variably, but generally highly folded chert, argillite, wacke, and minor limestone. Locally, siliciclastic rocks and epiclastic rocks containing fresh hornblende, feldspar, clinopyroxene, quartz, epidote, and biotite are abundant (Aitken, 1959; Gabrielse, 1969; Monger, 1975). Numerous collections of Kedahda Formation chert and limestone have yielded Middle to Late Triassic, as well as some Early Jurassic, radiolaria and conodonts (Cordey et al., 1991, 2024, 2025; Golding et al., 2016; Mihalynuk et al., 2002, 2003a). Zagorevski et al. (2021) suggested that the Kedahda Formation should be restricted to Middle Triassic to Early Jurassic chert, argillite, wacke, and minor limestone. This restriction does not change the current distribution of the Kedahda Formation, except in Yukon, where Middle Triassic to Early Jurassic rocks have been previously excluded from the Kedahda Formation (Cordey et al., 1991; Yukon Geological Survey, 2019). Monger et al. (1991) inferred that parts of the Kedahda Formation may be correlative with the Laberge Group (Early Jurassic, Sinemurian). This is consistent with the Early Jurassic radiolaria in cherts and siltstones that are interbedded with siliciclastic rocks (e.g., Cordey, 2020) and presence of Mesozoic radiolarian chert clasts in the Laberge Group (e.g., Mihalynuk et al., 2004a).

Previous inferences that the Kedahda Formation either underlies or is interbedded/interfingered with the Paleozoic limestone have created significant confusion for deciphering regional stratigraphic relationships. Although Paleozoic radiolaria have been recovered from some chert in northern British Columbia and southern Yukon, notably from interbeds in Paleozoic carbonate successions, almost all of the Kedahda Formation is Mesozoic. Hence, Paleozoic stratigraphic relationships are largely incorrect. The base of the Kedahda Formation is poorly exposed but an angular unconformity has been inferred at several localities (e.g., Monger, 1975; Zagorevski et al., 2021; Mihalynuk et al., 2024). At least some of the Paleozoic chert localities appear to occur along or below this unconformity. These unconformable relationships, as well as detrital evidence of derivation from underlying and adjacent terranes, suggest that the Kedahda Formation is a regional marine overlap assemblage that, at least in part, postdates terrane amalgamation (e.g., Zagorevski et al., 2021; Mihalynuk et al., 2024; Milidragovic et al., 2024). Constraining the paleogeographic evolution, including the amount of syn- and post-depositional deformation, will require much more work.

3.4.1. Farnsworth wacke, volcanic sandstone, and volcaniclastic units

The Farnsworth volcanic-sourced clastic beds are considered a subunit of the Kedahda Formation. Mapping near Gladys Lake (Mihalynuk et al., 2024) and, to the south, in the Mount Farnsworth area, identified these clastic units with interbedded chert and chert reworked as sharpstone conglomerate pebbles and coarse sand grains. Volcanic grains and clasts are locally predominant; they are typically plagioclase porphyry ±hornblende/pyroxene/biotite/titanite. Occurrence of detrital grains of secondary minerals such as epidote and pumpellyite indicates erosion of hydrothermally altered volcanic rocks or those subjected to regional low-grade metamorphism. Coarse-grained strata are interbedded with silty and argillaceous beds in turbiditic successions, locally affected by soft-sediment deformation and incised by coarse mass flow deposits. In rare instances, they can be observed resting on mantle peridotite. They contain radiolaria and detrital zircon populations as young as Early Jurassic (Zagorevski et al., 2025).

4. Summary of data and implications

Radiolarian chert and pelagic argillite are a very common but underused components of oceanic terranes in the northern Canadian Cordillera. Out of 342 radiolaria-bearing chert, siltstone, or limestone localities (Fig. 2) compiled by Zagorevski et al. (2026), 220 yielded radiolarian and/or conodont fossils that are diagnostic enough to make an age determination (Fig. 3). Of these, 182 yielded Triassic to Early Jurassic fauna and form part of a disrupted overlap assemblage, comprising the Kedahda Formation and its equivalents. An additional 38 localities yielded Paleozoic radiolaria. Although the tectono-stratigraphic position of some Paleozoic samples is unknown, Lincoln complex and Sentinel complex yielded exclusively Paleozoic ages. These Paleozoic cherts may be diagnostic of the oceanic basement of the Atlin terrane. Eleven localities yielded very imprecise determinations, but they are still useful for separating overlap from oceanic basement terranes.

Consideration of global events is important when interpreting radiolarian biochronology. The scarcity of latest Permian and Early Triassic radiolaria (Fig. 3; Zagorevski et al., 2026) demonstrates changes in radiolaria productivity across the Permo-Triassic boundary, with a massive increase of productive chert samples in the Mesozoic. Although effects of sampling bias on this age distribution cannot be ruled out, the difference in radiolarian productivity is likely a result of the

Permo-Triassic mass extinction and related ocean conditions, and to tectonic factors influencing radiolarian abundance globally. Such inferences can be tested through complementary siliciclastic provenance or sedimentary geochemistry studies.

Use of chert and radiolaria in mapping and tectonic reconstructions is currently limited by several factors, including availability of comparative data, skill of the collector, calibration of the radiolarian (and conodont) time scales and, most critically, availability of paleontological expertise. This paper, in conjunction with the companion compilation of Zagorevski et al. (2026) addresses some aspects of data availability, albeit for only a small part of the Canadian Cordillera. We highlight the importance of radiolaria as an affordable chronostratigraphic tool in regional mapping, especially in regions where U-Pb zircon and other isotopic dating cannot be applied. In terranes containing pelagic strata, radiolarian biochronology can be applied by any informed individual with a hand lens and access to a willing paleontologist with expertise in radiolaria identification.

Acknowledgments

This is a contribution to the GEM-GeoNorth Program (Geological Survey of Canada-British Columbia Geological Survey). It sources regional work that was completed under several programs including GeoMapping for Energy and Minerals 1 and 2 (GSC-BCGS, 2009-current), Targeted Geoscience Initiative (GSC-BCGS, 2000-2004) and others. We are thankful to all contributors, mappers and paleontologists, and to the pilots and helicopter base managers that got us in and out of the field safely, including Discovery (Atlin) and Capital (Whitehorse) Helicopters. Roddy Campbell helped with photographing sample RCA23-19-26.

References cited

Aitken, J.D., 1959. Atlin map-area, British Columbia. Geological Survey of Canada, Memoir 307, 89 p.

Bánki, O., Roskov, Y., Döring, M., Ower, G., Hernández Robles, D.R., Plata Corredor, C.A., Stjernegaard Jeppesen, T., Örn, A., Pape, T., Hobern, D., Garnett, S., Little, H., DeWalt, R.E., Ma, K., Miller, J., Orrell, T., Aalbu, R., Abbott, J., Adlard, R. et al., 2025. Catalogue of Life. (Version 2025-02-13), Amsterdam, Netherlands. <https://doi.org/10.48580/dgnfb>

Bloodgood, M.A., Bellefontaine, K.A., Maddison, L., and Gertz, I.C., 1990. Geology of the Dixie Lake and Teresa Island map area; NTS 104N/5, 6. British Columbia Ministry of Energy, Mines and Petroleum Resources, British Columbia Geological Survey Branch, Open File 1990-06, 1:50,000 scale.

Bogatu, A., Bédard, J.H., Labrousse, L., Zagorevski, A., and Tremblay, A., 2023. An oceanic core complex preserved in the Squanga Lake ophiolite, northern Atlin terrane, Yukon. Lithos, 454, article107269. <https://doi.org/10.1016/j.lithos.2023.107269>

Chang, S., Feng, Q., and Zhang, L., 2018. New siliceous microfossils from the Terreneuvian Yanjiahe Formation, South China: The possible earliest radiolarian fossil record. Journal of Earth Science, 29, 912-919.

Cohen, K., Harper, D., Gibbard, P., and Car, N., 2025. The ICS international chronostratigraphic chart this decade. Episodes, 48, 105-114. <https://doi.org/10.18814/epiiugs/2025/025001>

Colpron, M., 2020. Yukon terranes-A digital atlas of terranes for the northern Cordillera. Yukon Geological Survey. <https://data.geology.gov.yk.ca/Compilation/2#InfoTab>

Coney, P.J., Jones, D.L., and Monger, J.W.H., 1980. Cordilleran suspect terranes. Nature, 288, 329-333.

Cordey, F., 2020. Timing of Cache Creek Ocean closure; insights from new Jurassic radiolarian ages in British Columbia and Yukon and their significance for Canadian Cordillera tectonics. Canadian Journal of Earth Sciences, 57, 1167-1179.

Cordey, F., Gordey, S.P., and Orchard, M.J., 1991. New biostratigraphic data for the northern Cache Creek Terrane, Teslin map area, southern Yukon. In: Current Research, Part E, Geological Survey of Canada, Paper 91-1E, pp. 67-76.

Cordey, F., Zagorevski, A., Mihalynuk, M.G., and Campbell, R.W., 2024. Report on samples collected for radiolaria identification in the Gladys Lake-Mount Bryde area, near Atlin, British Columbia. British Columbia Ministry of Energy, Mines and Low Carbon Innovation, British Columbia Geological Survey GeoFile 2024-13, 2 p.

Cordey, F., Zagorevski, A., and Mihalynuk, M.G., 2025. Report on samples collected for radiolaria identification, Atlin area, northwest British Columbia. British Columbia Ministry of Mining and Critical Minerals, British Columbia Geological Survey GeoFile 2025-17, 3 p.

English, J.M., Mihalynuk, M.G., Johnston, S.T., and Devine, F.A., 2002. Atlin TGI Part III: Geology and Petrochemistry of Mafic Rocks within the Northern Cache Creek Terrane and Tectonic Implications. In: Geological Fieldwork 2001, British Columbia Ministry of Energy and Mines, British Columbia Geological Survey Paper 2002-01, pp. 19-30.

English, J.M., and Johnston, S.T., 2005. Collisional orogenesis in the northern Canadian Cordillera: Implications for Cordilleran crustal structure, ophiolite emplacement, continental growth, and the terrane hypothesis. Earth and Planetary Science Letters, 232, 333-344.

English, J.M., Mihalynuk, M.G., and Johnston, S.T., 2010. Geochemistry of the northern Cache Creek terrane and implications for accretionary processes in the Canadian Cordillera. Canadian Journal of Earth Sciences, 47, 13-34.

Gabrielse, H., 1969. Geology of Jennings River map-area, British Columbia (104-0). Geological Survey of Canada Paper 68-55, 37 p.

Gabrielse, H., 1998. Geology of the Cry Lake and Dease Lake map areas, north-central British Columbia. Geological Survey of Canada Bulletin 504, 147 p.

Golding, M.L., Orchard, M.J., and Zagorevski, A., 2016. Microfossils from the Cache Creek Complex in northern British Columbia and southern Yukon. Geological Survey of Canada, Open File 8033, 25 p.

Gordey, S.P., and Stevens, R.A., 1994a. Preliminary interpretation of bedrock geology of the Teslin area (105C), southern Yukon. Geological Survey of Canada Open-File 2886. <https://doi.org/10.4095/205239>

Gordey, S.P., and Stevens, R.A., 1994b. Tectonic framework of the Teslin region, southern Yukon Territory. In: Current Research, Geological Survey of Canada Paper 1999-A, pp. 11-18.

Mihalynuk, M.G., Mountjoy, K.J., Smith, M.T., Currie, L.D., Gabites, J.E., Tipper, H.W., Orchard, M.J., Poulton, T.P., and Cordey, F., 1999. Geology and mineral resources of the Tagish Lake area (NTS 104M/8, 9, 10E, 15 and 104N/12W), northwestern British Columbia. British Columbia Ministry of Energy and Mines, British Columbia Geological Survey Bulletin 105, 235 p.

Mihalynuk, M.G., Johnston, S.T., Lowe, C., Cordey, F., English, J.M., Devine, F.A.M., Larson, K., and Merran, Y., 2002. Atlin TGI; Part II, Preliminary results from the Atlin Targeted

Geoscience Initiative, Nakina area, Northwest British Columbia. In: Geological Fieldwork 2001, British Columbia Ministry of Energy and Mines, British Columbia Geological Survey Paper 2002-1, pp. 5-18.

Mihalynuk, M.G., Johnston, S.T., English, J.M., Cordey, F., Villeneuve, M.E., Rui, L., and Orchard, M.J., 2003a. Atlin TGI, Part II, Regional geology and mineralization of the Nakina area (NTS 104N/2W and 3). In: Geological Fieldwork 2002, British Columbia Ministry of Energy and Mines, British Columbia Geological Survey Paper 2003-1, pp. 9-37.

Mihalynuk, M.G., Villeneuve, M.E., and Cordey, F., 2003b. Atlin TGI, Part III, Geological setting and style of mineralization at the Joss'alun occurrence, Atlin area (NTS 104N/2SW). In: Geological Fieldwork 2002, British Columbia Ministry of Energy and Mines, British Columbia Geological Survey Paper 2003-1, pp. 39-50.

Mihalynuk, M.G., Erdmer, P., Ghent, E.D., Cordey, F., Archibald, D.A., Friedman, R.M., and Johannson, G.G., 2004a. Coherent French Range blueschist; subduction to exhumation in <2.5 m.y.? Geological Society of America Bulletin, 116, 910-922.

Mihalynuk, M.G., Ferreira, L., Robertson, S., Devine, F.A.M., and Cordey, F., 2004b. Geology and New Mineralization in the Joss'alun Belt, Atlin Area. In: Geological Fieldwork 2003, British Columbia Ministry of Energy and Mines, British Columbia Geological Survey Paper 2004-01, pp. 61-82.

Mihalynuk, M.G., Zagorevski, A., Milidragovic, D., Tsekhmistrenko, M., Friedman, R.M., Joyce, N., Camacho, A., and Golding, M., 2018. Geologic and geochronologic update of the Turtle Lake area, NTS 104M/16, northwest British Columbia. In: Geological Fieldwork 2017, British Columbia Ministry of Energy, Mines and Petroleum Resources, British Columbia Geological Survey Paper 2018-1, pp. 83-128.

Mihalynuk, M.G., Zagorevski, A., Campbell, R., Haji Egeh, A., and Vaillancourt, A., 2024. Preliminary results from revision mapping of the Gladys Lake area, near Atlin, northwest British Columbia. In: Geological Fieldwork 2023, British Columbia Ministry of Energy, Mines and Low Carbon Innovation, British Columbia Geological Survey Paper 2024-01, pp. 131-148.

Milidragovic, D., Ootes, L., Zagorevski, A., Cleven, N., Wall, C.J., Luo, Y., and Friedman, R.M., 2024. Detrital geochronology of the Cunningham Lake formation: an overlap succession linking Cache Creek terrane to Stikinia at ~205 Ma. Canadian Journal of Earth Sciences, 61, 39-57.

Monger, J.W.H., 1975. Upper Paleozoic rocks of the Atlin Terrane, northwestern British Columbia and south-central Yukon. Geological Survey of Canada Paper 74-47, 63 p. <https://doi.org/10.4095/102554>

Monger, J.W.H., Wheeler, J.O., Tipper, H.W., Gabrielse, H., Harms, T., Struik, L.C., Campbell, R.B., Dodds, C.J., Gehrels, G.E., and O'Brien, J., 1991. Part B, Cordilleran terranes in Upper Devonian to Middle Jurassic assemblages. In: Gabrielse, H., and Yorath, C.J., (Eds.), Geology of the Cordilleran Orogen in Canada, Geological Survey of Canada, Geology of Canada Volume 4, pp. 281-327.

North American Commission on Stratigraphic Nomenclature, 2021. North American Stratigraphic Code., North American Commission on Stratigraphic Nomenclature. Stratigraphy, 18, 153-204.

Raymond, L.A., 1984. Classification of mélanges. In: Raymond, L.A., (Ed.), Mélanges: Their Nature, Origin, and Significance. Geological Society of America Special Paper 198, pp. 7-20.

Sandin, M.M., Renaudie, J., Suzuki, N., and Not, F., 2025. Extant diversity, biogeography, and evolutionary history of Radiolaria. Current Biology, 35, 2524-2538.

Silberling, N.J., Jones, D.L., Monger, J.W.H., and Coney, P.J., 1992. Lithotectonic terrane map of the North American Cordillera. United States Geological Survey Miscellaneous Investigations Series Map 2176, 2 sheets, 1:5,000,000 scale.

Vermeesch, P., 2018. IsoplotR, a free and open toolbox for geochronology. Geoscience Frontiers, 9, 1479-1493.

Watson, K.D., and Mathews, W.H., 1944. The Tuya-Teslin area, Northern British Columbia. Bulletin-British Columbia Department of Mines, 17, p. 11.

Westacott, S., Planavsky, N.J., Zhao, M.Y., and Hull, P.M., 2021. Revisiting the sedimentary record of the rise of diatoms. Proceedings of the National Academy of Sciences, 118, article e2103517118. <https://doi.org/10.1073/pnas.2103517118>

Wheeler, J.O., Brookfield, A.J., Gabrielse, H., Monger, J.W.H., Tipper, H.W., and Woodsworth, G.J., 1991. Terrane map of the Canadian Cordillera. Geological Survey of Canada, Map 1713A, 2 sheets, 1:2,000,000 scale.

Yukon Geological Survey, 2019. Yukon Digital Bedrock Geology. <http://www.geology.gov.yk.ca/update_yukon_bedrock_geology_map.html>

Zagorevski, A., Soucy La Roche, R., Golding, M., Joyce, N., Regis, D., and Coleman, M., 2018. Stikinia bedrock, British Columbia and Yukon; GEM-2 Cordillera Project, Report of Activities 2018. Geological Survey of Canada, Open File 8485, 12 p.

Zagorevski, A., Staal, C.R.V., Bédard, J.H., Bogatu, A., Canil, D., Coleman, M., Golding, M., Joyce, N., Lawley, C., McGoldrick, S., Mihalynuk, M.G., Milidragovic, D., Parsons, A., and Schiarizza, P., 2021. Overview of Cordilleran oceanic terranes and their significance for the tectonic evolution of the northern Cordillera. In: Geological Survey of Canada Bulletin 610, pp. 21-66.

Zagorevski, A., Mihalynuk, M.G., and Vaillancourt, A., 2025. Reimagining the terrane framework of the Intermontane Superterrane of the Northern Canadian Cordillera. GAC-MAC-IAH-CNC 2025 Ottawa Meeting: Abstracts, Volume 48. Geoscience Canada, 52, 81-267. <https://doi.org/10.12789/geocanj.2025.52.223>

Zagorevski, A., Cordey, F., Mihalynuk, M.G., and Vaillancourt, A., 2026. Compilation of micropaleontological data from the northern Canadian Cordillera, British Columbia and Yukon. British Columbia Ministry of Mining and Critical Minerals, British Columbia Geological Survey GeoFile 2026-02.

24 Ma Giant Copper polymetallic porphyry-related breccia of the ancestral Cascades, southwest British Columbia

Mitchell G. Mihalynuk[1, a], and Janet E. Gabites[2, *]

[1] British Columbia Geological Survey, Ministry of Mining and Critical Minerals, Victoria, BC, V8W 9N3
[2] Pacific Centre for Isotopic and Geochemical Research, Department of Earth, Ocean and Atmospheric Sciences, The University of British Columbia, Vancouver, BC, V6T 1Z4
* retired
[a] corresponding author: Mitch.Mihalynuk@gov.bc.ca

Recommended citation: Mihalynuk, M.G., and Gabites, J.E., 2026. 24 Ma Giant Copper polymetallic porphyry-related breccia of the ancestral Cascades, southwest British Columbia. In: Geological Fieldwork 2025, British Columbia Ministry of Mining and Critical Minerals, British Columbia Geological Survey Paper 2026-01, pp. 163-174.

Abstract

A recent metallogenic study of mineralized breccias at Giant Copper in southwestern British Columbia suggested that the Invermay magmatic suite (24.9 ±0.2 Ma, late Oligocene) is responsible for mineralization. We corroborate this inference by $^{40}Ar/^{39}Ar$ (biotite) geochronology on both the Invermay magmatic suite and the mineralization. Ar release spectra from the intrusion and two from mineralized samples yield ages of 24.22 ±0.15 Ma, 24.87 ±0.33 Ma, and 24.08 ±0.19 Ma. Copper-silver-gold-bearing breccias of Giant Copper are the northernmost known (49.16°N) part of the ancestral Cascade belt of porphyry-related deposits defined in Washington state. However, Oligocene magmatic rocks, some with past-producing mineral deposits, span the length of western British Columbia.

Keywords: Giant Copper, porphyry copper, copper-silver-gold tourmaline breccia, $^{40}Ar/^{39}Ar$ geochronology, Oligocene, thermochronology, Invermay magmatic suite, ancestral Cascade porphyry belt, Hozameen terrane, Bridge River terrane, Methow basin, Ladner Group, Dewdney Creek Formation

1. Introduction

Giant Copper is a tourmaline-magnetite breccia-hosted deposit in southwest British Columbia, 37 km southeast of Hope and 20 km north of the US border (Figs. 1, 2) in an area that includes the lands and traditional territories of many Indigenous rights holders. The deposit has an indicated resource of 45.37 million tonnes grading 0.47% copper, 11.19 g/t silver, and 0.38 g/t gold (Pinsent, 1998). In addition, zinc (in sphalerite) is commonly found in the breccia pipes, and some zones contain molybdenite (±associated uraninite) and galena. At the time of our sampling (2006), the mineral tenures were surrounded by parkland (Skagit River Park to the west and Manning Park on all other sides). However, the claims have since been surrendered to the Province of British Columbia (Imperial Metals Corporation, 2022).

Mineralization at Giant Copper is concentrated in a cluster of seven breccia bodies (Fig. 3). The first was discovered in 1930, the AM breccia (MINFILE 092HSW001), followed by the Invermay breccia in 1933 (MINFILE 092HSW002). Mineral production has only been recorded from the Invermay body, which generated 94 metric tonnes of ore between 1936 and 1947, from which 10.6 tonnes of zinc, 9.65 tonnes of lead, 313 kg of silver and 0.7 kg of gold were recovered (copper production is not reported, MINFILE 092HSW002). Since 1947, mineral exploration at Giant Copper has been intermittent (Robertson, 2006), with the last major effort including drilling and production of a digital map, conducted in 1996 by Imperial Minerals Corp., followed by geochemical surveys in 2015 (Miller-Tait, 2016). Recent metallogenic study of the Giant Copper tourmaline breccia pipes (Fischer, 2022; Fischer et al., 2023, 2024) focused primarily on the AM body, which is analogous to other porphyry-related pipes globally, such as those at the world's third largest porphyry copper deposit, Rio Blanco-Los Bronces, in Chile (Frikken et al., 2005).

Laser ablation ICP-MS dating of the Invermay intrusive suite at Giant Copper by Fischer (2022) produced a weighted mean U-Pb age of 24.9 ±0.2 Ma (from 99 zircon grains). Such a young age was unexpected because previous work inferred a Cretaceous age (e.g., Robertson, 2006; Miller-Tait, 2016). Based on the assumption that the intrusive suite dated was the source of mineralization, this Oligocene date (time scale of Cohen et al., 2025) was taken to be the maximum limit on mineralized breccia pipe formation (Fischer, 2022). Herein we present $^{40}Ar/^{39}Ar$ (biotite) geochronologic data from three Invermay magmatic suite samples including two that provide estimates for the time of mineralization. Our results confirm the previous U-Pb dates for the intrusion (Fischer, 2022) and indicate that mineralization was penecontemporaneous with emplacement of the Invermay body.

2. Regional geologic setting

Following early transect and 4-mile mapping by Cairnes (1924, 1944), many workers have contributed to understanding

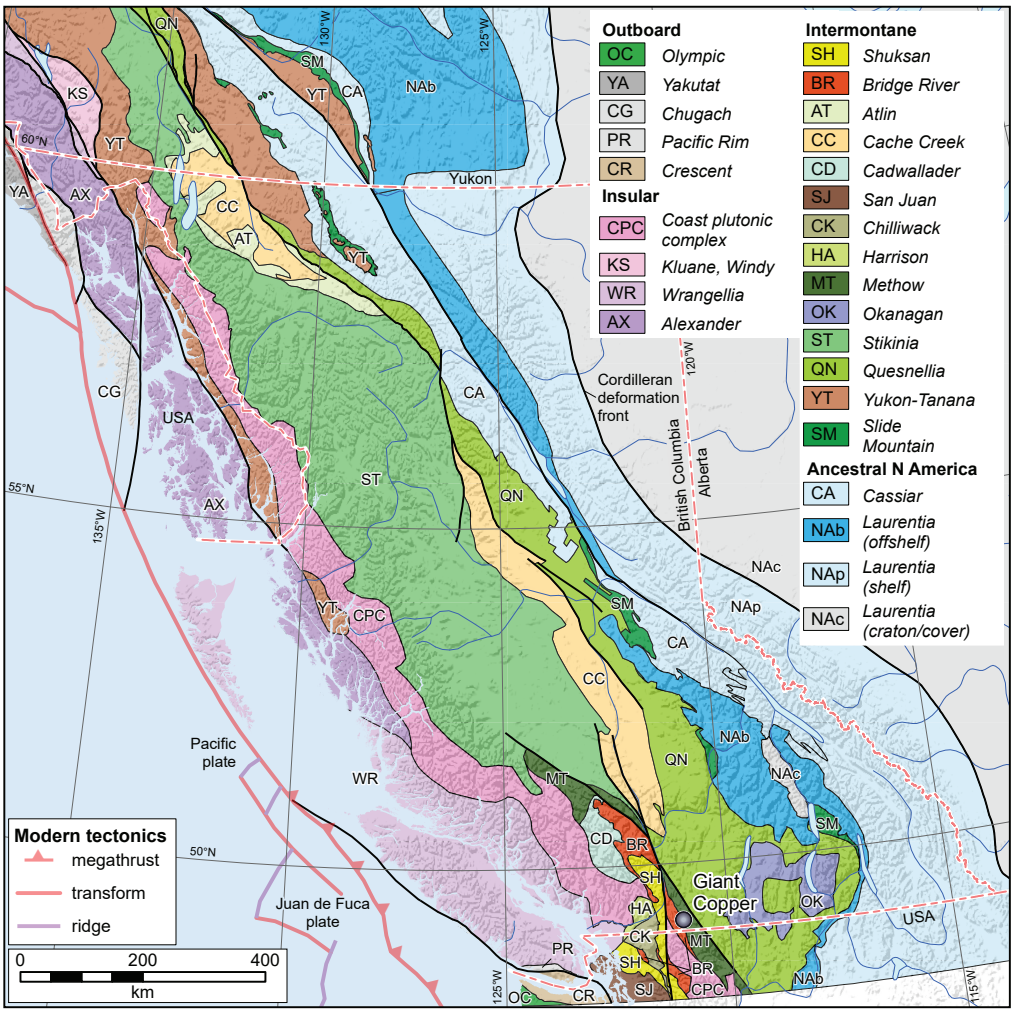


Fig. 1. Location of study area. Terranes (modified from Colpron, 2020; after Wheeler et al., 1991; Zagorevski et al., 2021).

the regional geology of Giant Copper including: 1:50,000-scale mapping of Manning Park by Coates (1974); 1:250,000-scale mapping of the Hope map sheet by Monger (1989); and 1:20,000-scale mapping of the Cascade Recreational area by Schmitt and Koyanagi (1992). Property-scale mapping (e.g., Miller-Tait 2016) added significant details.

Three main rock packages form basement across the area (Fig. 3). The oldest of these is in the west, the Hozameen Group (commonly spelled Hozomeen in US), which includes deep-marine sedimentary rocks and ophiolitic rocks having ocean island to island arc tholeiite chemistry (Ray, 1990). These rocks represent the Hozameen terrane which is interpreted as equivalent to the Bridge River terrane from which it has been offset by the Fraser-Straight Creek fault (Umhoefer and Miller, 1996; Umhoefer and Schiarizza, 1996; Fig. 3). Fossils in chert and sparse limestone beds are Pennsylvanian to Late Jurassic (Haugerud and Tabor, 2009).

Bounding Hozameen terrane on its east is the Hozameen fault, delineated by a belt of serpentinite bodies (Ray, 1986) and separating it from the Jura-Cretaceous strata of the Methow terrane. At the latitude of Figure 3, Methow basin is equivalent to the Methow terrane. The basin may have been floored by Triassic mid-ocean ridge basalts (Spider Peak Formation; Ray, 1990) and was filled in the Early Jurassic by lower Ladner Group turbiditic marine siliciclastic deposits, followed by volcaniclastic-rich strata of the Dewdney Creek Formation (Middle to Late Jurassic; cf. O'Brien, 1987; O'Brien et al., 1992). Wacke and coarse polymictic conglomerate of the Jackass Mountain Group (Early Cretaceous) overlie the Methow terrane and are interpreted to have been derived from proximal eastern sources that were isolated from the craton (Surpless et al., 2014).

The eastern limits of the Methow terrane are mostly defined by the Pasayten fault which separates the terrane from the highly attenuated composite plutons of the Eagle plutonic complex that young to the south (Late Jurassic to Early Cretaceous; Greig et al., 1992; Hurlow and Nelson, 1993). The Eagle complex was underthrust by the western edge of Quesnel terrane, which was subjected to medium-pressure amphibolite-grade metamorphism (Oliver, 2011).

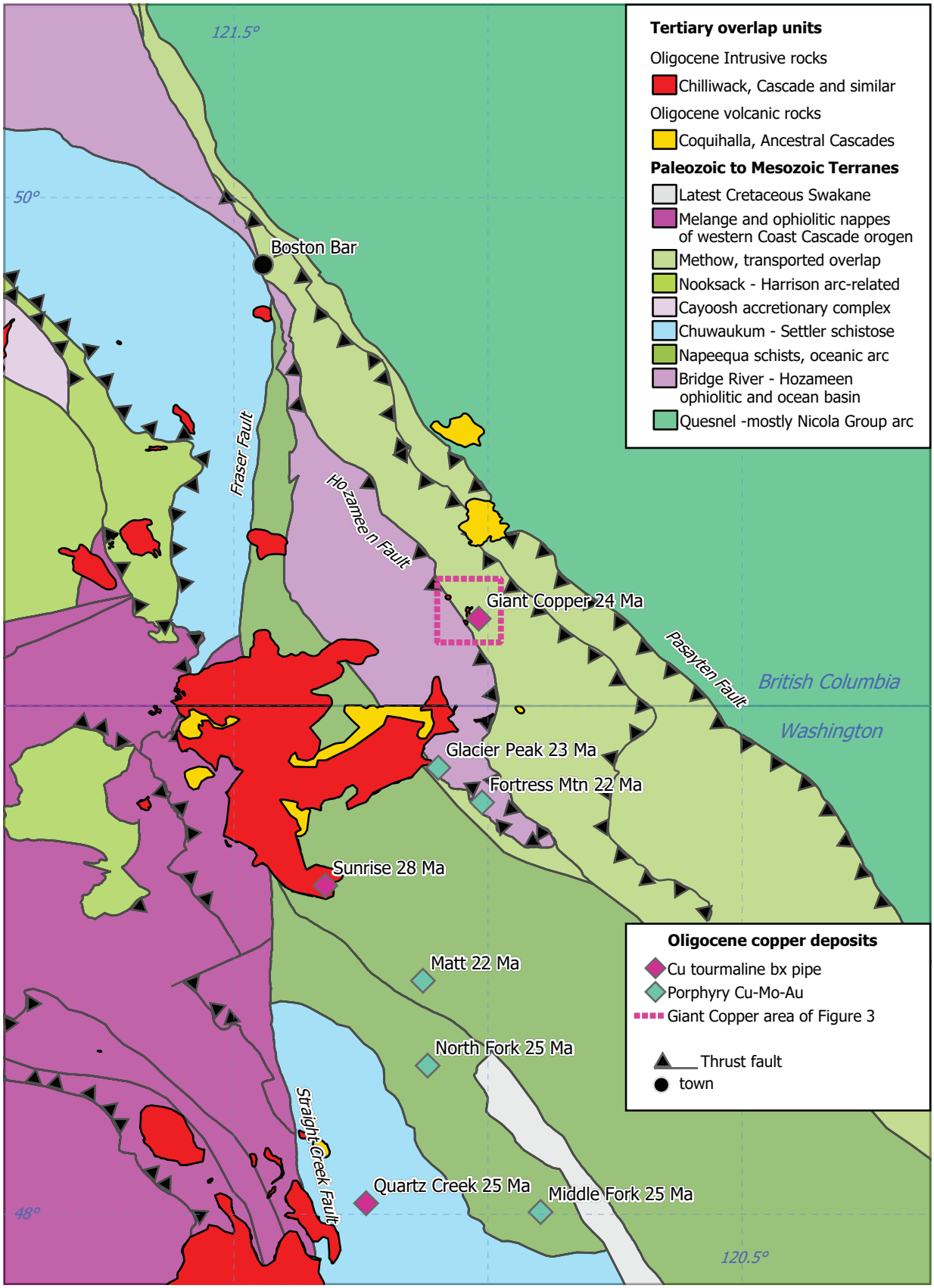


Fig. 2. Regional geological setting of the Giant Copper deposit based on work by Cairnes (1920, 1924, 1929, 1944), Tabor et al. (2003), Haugerud and Tabor (2009), Monger and Brown (2016), and Tabor and Haugerud (2016).

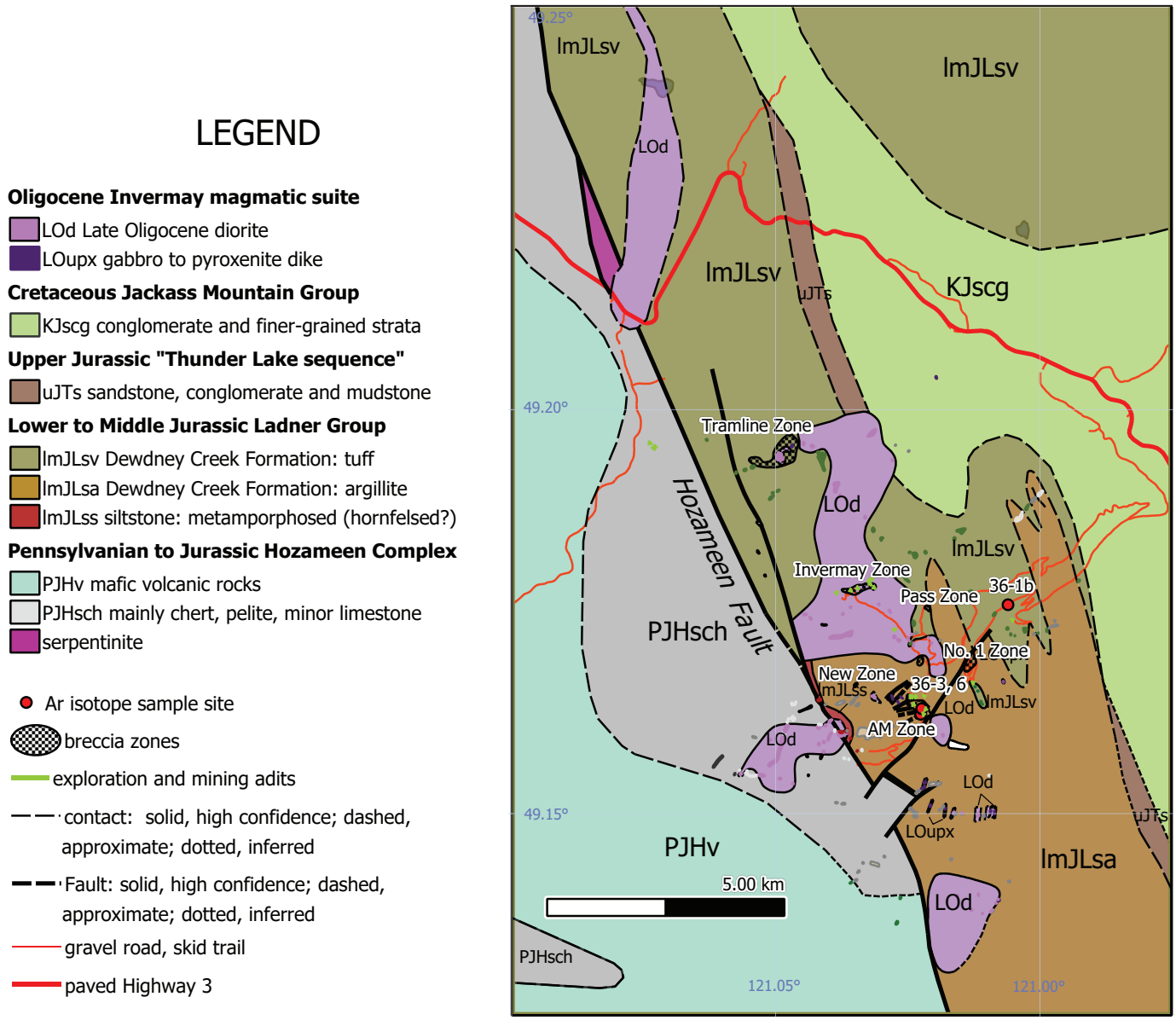


Fig. 3. Geologic setting of breccia zones at Giant Copper principally based on the distribution of rock units exposed in outcrops shown on property maps (and shown here) by Imperial Metals Corporation (e.g., Miller-Tait, 2016). Correlation with regional geological units is constrained by regional mapping by Cairnes (1924, 1944), Monger et al. (1989), and local property-scale observations.

In the Giant Copper area, both Hozameen and Methow terranes are intruded by the Invermay suite of plutons that have irregular outlines and are up to about 3 km long. If the main Hozameen fault trace has been mapped correctly, Invermay intrusions cut across the fault (Fig. 3).

3. $^{40}Ar/^{39}Ar$ analysis

3.1. $^{40}Ar/^{39}Ar$ analytical methods

Clean and fresh samples for $^{40}Ar/^{39}Ar$ analysis were crushed and sieved to 0.2-0.4 mm size fraction. Mineral separates were hand-picked, washed in acetone, dried, wrapped in aluminum foil and stacked in an irradiation capsule with similar-aged samples and neutron flux monitors (Fish Canyon Tuff sanidine; 28.02 Ma, (Renne et al., 1998).

The samples were irradiated in March 2007 at the McMaster Nuclear Reactor in Hamilton, Ontario, for 90 MWH, with a neutron flux of approximately $3x10^{16}$ neutrons/cm^2. Analyses (n=60) of 20 neutron flux monitor positions produced errors of <0.5% in the J value.

The samples were analyzed at the Noble Gas Laboratory, Pacific Centre for Isotopic and Geochemical Research, The University of British Columbia, Vancouver, BC, Canada. The mineral separates were step-heated at incrementally higher powers in the defocused beam of a 10W CO_2 laser (New Wave Research

MIR10) until fused. The gas evolved from each step was analyzed by a VG5400 mass spectrometer equipped with an ion-counting electron multiplier. All measurements were corrected for total system blank, mass spectrometer sensitivity, mass discrimination, radioactive decay during and subsequent to irradiation, as well as interfering Ar from atmospheric contamination and the irradiation of Ca, Cl and K (Isotope production ratios: $(^{40}Ar/^{39}Ar)_K$=0.0302 ±0.00006, $(^{37}Ar/^{39}Ar)_{Ca}$=1416.4 ±0.5, $(^{36}Ar/^{39}Ar)_{Ca}$=0.3952 ±0.0004, Ca/K=1.83 ±0.01 ($^{37}Ar_{Ca}/^{39}Ar_K$)).

Ages of heating steps were calculated using ArArCalc (Koppers, 2002). Release spectrum plateaus and correlation ages were calculated using Isoplot ver. 3.09 (Ludwig, 2003). Errors are quoted at the 2σ (95% confidence) level and are propagated from all sources except mass spectrometer sensitivity and age of the flux monitor. The most justifiable plateau and plateau age were picked based on the following criteria: three of more contiguous steps comprising more than 50% of the ^{39}Ar; the probability of fit of the weighted mean age greater than 5%; the slope of the error-weighted line through the plateau ages equals zero at 5% confidence; the ages of the two outermost steps on a plateau are not significantly different from the weighted-mean plateau age (at 1.8σ, six or more steps only); and the outermost two steps on either side of a plateau must not have nonzero slopes with the same sign (at 1.8σ, nine or more steps only).

3.2. $^{40}Ar/^{39}Ar$ geochronologic results

Complete details of the analyses, including inverse correlation plots, are presented in Gabites and Mihalynuk (2026). Plateau and correlation ages were calculated using Isoplot ver. 3.09 (Ludwig, 2003). Errors are quoted at the 2-sigma (95% confidence) level and are propagated from all sources except mass spectrometer sensitivity and age of the flux monitor.

3.2.1. Sample MMI06-36-1b Location, -121.00600°E, 49.17585°N; UTM zone 10, NAD 83: 645412 mE, 5448708 mN

Sample MMI06-36-1b is representative of the Invermay suite of hornblende and biotite porphyry intrusions. A biotite porphyritic intrusive sample was collected from the 1500-level dump for analysis. It is quartz->plagioclase->orthoclase->biotite-porphyritic and contains 1-2% chalcopyrite in tourmaline veinlets. Step heating results from sample MMI06-36-1b (Table 1; Fig. 4) give an age of 24.22 ±0.13 Ma from a 5-step plateau produced by 79.1% of the ^{39}Ar released.

3.2.2. Sample MMI06-36-3 Location, -121.02254°E, 49.16230°N; UTM zone 10, NAD 83: 644245 mE, 5447171 mN

Sample MMI06-36-3 is a rusty-weathering, dark grey-brown, medium-grained biotite hornfels (Fig. 5), part of the alteration assemblage related to intrusion and mineralization at the AM zone. Step heating results of biotite from sample MMI06-36-3 (Table 2; Fig. 6) indicate an undisturbed 6-step plateau

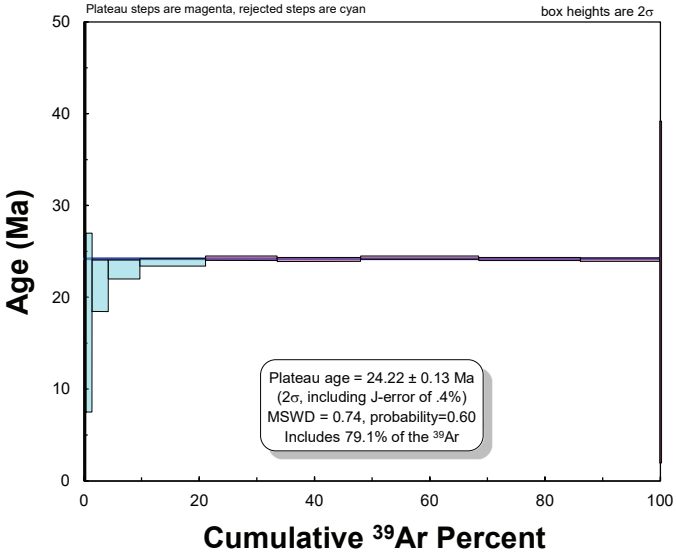


Fig. 4. Argon release spectrum from biotite phenocrysts of sample MMI06-36-1b. Low temperature steps trimmed to chart area. See Gabites and Mihalynuk (2026) for unmodified plot.



Fig. 5. Cut sample MMI06-36-3 biotite hornfels showing rusty weathering exterior and dark brown-grey interior. Biotite was extracted from this sample for $^{40}Ar/^{39}Ar$ analysis.

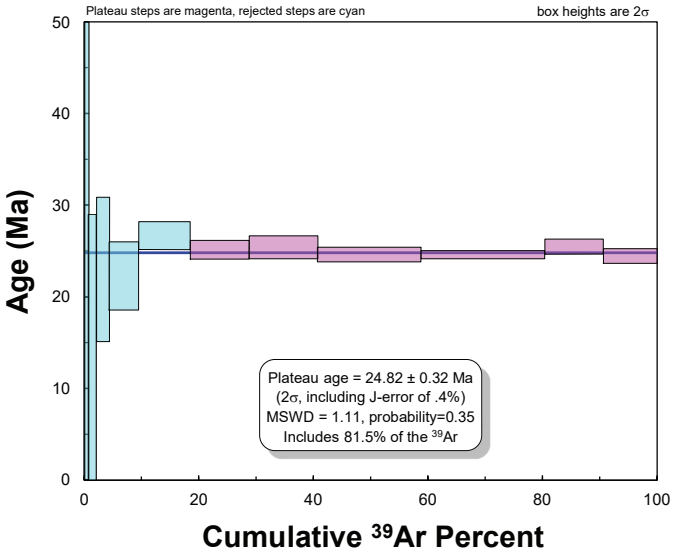


Fig. 6. Argon release spectrum from sample MMI06-36-1b. Low temperature steps trimmed to chart area. See Gabites and Mihalynuk (2026) for unmodified plot.

Table 1. $^{40}Ar/^{39}Ar$ analytical results from step heating of sample MMI06-36-1b. Analysis by Tom Ullrich, revised by Janet Gabites, Pacific Centre for Isotopic and Geochemical Research, The University of British Columbia.

MMI06-36-1b Biotite

Laser			Isotope Ratios												
Power(%)	40Ar/39Ar	2σ	36Ar/39Ar	2σ	39Ar/40Ar	2σ	36Ar/40Ar	2σ	Rho	K/Ca	%40Ar rad	f 39Ar	40Ar*/39ArK	Age	2σ
2.0	245.66	0.02	0.83100	0.04600	0.0041	0.0001	0.00338	0.00007	0.26	1.58	1.00	0.07	0.43	8.01	± 92.49
2.2	60.50	0.02	0.20500	0.09000	0.0168	0.0002	0.00336	0.00015	0.06	1.16	1.01	0.10	0.47	8.71	± 49.32
2.4	27.69	0.01	0.09100	0.04000	0.0363	0.0003	0.00327	0.00006	0.09	0.68	1.04	1.11	0.93	17.29	± 9.76
2.6	7.68	0.01	0.02200	0.04600	0.1318	0.0007	0.00288	0.00007	0.05	3.98	1.18	2.80	1.15	21.27	± 2.81
2.8	3.36	0.01	0.00700	0.05200	0.3031	0.0014	0.00212	0.00006	0.03	14.93	1.62	5.43	1.25	23.07	± 1.02
3.0	2.22	0.01	0.00300	0.04600	0.4592	0.0019	0.00141	0.00003	0.01	34.48	2.48	11.40	1.29	23.81	± 0.40
3.2	1.68	0.01	0.00100	0.06400	0.6108	0.0026	0.00071	0.00002	0.01	37.04	5.17	12.47	1.31	24.28	± 0.24
3.4	1.54	0.01	0.00100	0.08400	0.6697	0.0028	0.00047	0.00002	0.00	33.33	8.18	14.43	1.31	24.15	± 0.20
3.6	1.50	0.01	0.00100	0.09000	0.6847	0.0029	0.00038	0.00002	0.01	29.41	10.42	20.55	1.32	24.34	± 0.18
3.8	1.50	0.01	0.00100	0.08000	0.6837	0.0028	0.00040	0.00002	0.00	35.71	9.73	17.56	1.31	24.19	± 0.17
4.0	1.50	0.01	0.00100	0.09400	0.6867	0.0028	0.00039	0.00002	0.00	32.26	9.89	13.84	1.31	24.13	± 0.19
4.2	35.06	0.02	0.11500	0.06000	0.0290	0.0002	0.00328	0.00010	0.07	1.19	1.03	0.25	1.11	20.60	± 18.61

J = 0.010311 ± 0.000012; Volume 39ArK = 2583.76 x E-13 cm3 NPT

Integrated Date = 24.19 ± 0.08 Ma

Plateau age = 24.22 ± 0.13 Ma; (2σ, including J-error of .2%), MSWD = 0.74, probability = 0.60, Includes 79.1% of the 39Ar, steps 7 through 12

Inverse isochron (correlation age) results: Model 1 Solution (±95%-conf.) on 12 points

Age = 23.91 ± 0.10 Ma Initial 40Ar/36Ar = 290.8 ± 2.8; MSWD = 0.91, Probability = 0.52

Table 2. $^{40}Ar/^{39}Ar$ analytical results from step heating of sample MMI06-36-3. Analysis by Tom Ullrich, revised by Janet Gabites, Pacific Centre for Isotopic and Geochemical Research, The University of British Columbia.

MMI06-36-3 Biotite

Laser			Isotope Ratios												
Power(%)	40Ar/39Ar	2σ	36Ar/39Ar	2σ	39Ar/40Ar	2σ	36Ar/40Ar	2σ	Rho	K/Ca	%40Ar rad	f 39Ar	40Ar*/39ArK	Age	2σ
2.0	104.48	0.02	0.35400	0.04200	0.0095	0.0001	0.00338	0.00007	0.07	0.92	1.00	0.79	0.19	3.57	± 38.34
2.2	49.94	0.01	0.16800	0.04200	0.0201	0.0001	0.00335	0.00007	0.06	0.93	1.01	1.33	0.50	9.34	± 19.58
2.4	22.75	0.02	0.07300	0.04200	0.0444	0.0004	0.00320	0.00006	0.10	1.09	1.06	2.29	1.24	23.01	± 7.89
2.6	11.28	0.01	0.03400	0.04000	0.0898	0.0006	0.00303	0.00006	0.07	1.59	1.12	5.15	1.21	22.31	± 3.75
2.8	4.28	0.01	0.01000	0.05800	0.2393	0.0014	0.00224	0.00007	0.04	1.11	1.54	8.96	1.45	26.72	± 1.54
3.0	3.30	0.03	0.00700	0.05200	0.3116	0.0052	0.00199	0.00005	0.20	0.88	1.75	10.39	1.36	25.17	± 1.04
3.2	3.47	0.01	0.00700	0.06200	0.2949	0.0019	0.00205	0.00007	0.03	0.55	1.70	11.87	1.38	25.41	± 1.25
3.4	2.66	0.01	0.00500	0.05600	0.3851	0.0024	0.00173	0.00006	0.07	0.27	2.08	18.04	1.33	24.63	± 0.82
3.7	1.77	0.02	0.00200	0.09000	0.5850	0.0050	0.00081	0.00004	0.06	0.96	4.61	21.59	1.33	24.63	± 0.47
4.0	1.83	0.03	0.00200	0.14200	0.5736	0.0103	0.00077	0.00007	0.08	1.07	4.88	10.21	1.38	25.51	± 0.85
4.4	1.70	0.01	0.00100	0.20200	0.6251	0.0031	0.00064	0.00009	0.01	2.23	5.92	9.38	1.32	24.49	± 0.80

J = 0.010318 ± 0.00001; Volume 39ArK = 822.79 x E-13 cm3 NPT

Integrated Date = 24.87 ± 0.30 Ma

Plateau age = 24.82 ± 0.32 Ma; (2σ, including J-error of .2%), MSWD = 1.11, probability = 0.35, Includes 81.5% of the 39Ar, steps 6 through 11

Inverse isochron (correlation age) results: Model 1 Solution (±95%-conf.) on 11 points

Age = 24.30 ± 0.54 Ma Initial 40Ar/36Ar = 293.7 ± 4.4; MSWD = 1.9, Probability = 0.045

produced by 81.5% of the ^{39}Ar released. The plateau provides an age of 24.82 ±0.32 Ma. This age is very close to the age of the causative intrusion, (sample MMI06-36-1b), confirming the consanguinity interpreted from field relationships where the intrusion and coarse sulphides are intermingled (Fig. 7).

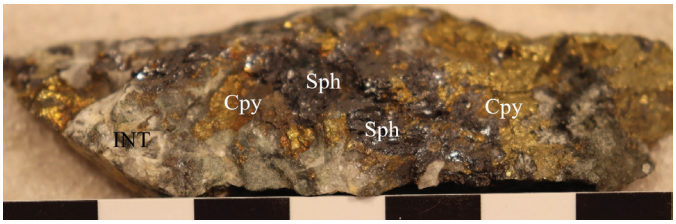


Fig. 7. Sample MMI06-36-2, showing coarse chalcopyrite (Cpy) and sphalerite (Sph) intergrown with Invermay intrusion (INT) shows consanguinity of mineralization and intrusion. Scale divisions are in cm.

3.2.3. Sample MMI06-36-6 Location, -121.02235°E, 49.16298°N; UTM zone 10, NAD 83: 644256 mE, 5447248 mN

This sample was obtained from diamond-drill hole DDH GCS06-02 at a recorded depth of 620 feet (189 m) in the AM zone. It is a sample of sedimentary host rock overprinted by pre- to syn-mineralization biotite hornfels. Textural relations show that biotite crystallization immediately preceded and accompanied mineralization and constrains the age of mineralization. Step heating results of biotite from sample MMI06-36-2 (Table 3; Fig. 8) show an 11-step plateau produced by 99.02% of the ^{39}Ar released. The plateau provides an age of 24.08 ±0.17 Ma. This age overlaps within errors the age of the Invermay suite intrusion, (sample MMI06-36-1b), again confirming the consanguinity interpreted from field relationships.

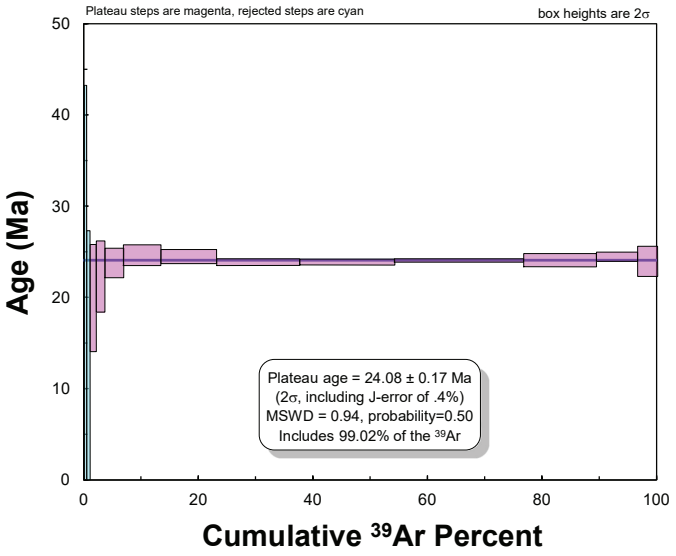


Fig. 8. Argon release spectrum from sample MMI06-36-6. Low temperature steps trimmed to chart area. See Gabites and Mihalynuk (2026) for unmodified plot.

Table 3. ^{40}Ar/^{39}Ar analytical results from step heating of sample MMI06-36-6. Analysis by Tom Ullrich, revised by Janet Gabites, Pacific Centre for Isotopic and Geochemical Research, The University of British Columbia.

MMI06-36-6 Biotite

Laser	*Isotope Ratios*														
Power(%)	*40Ar/39Ar*	*2 σ*	*36Ar/39Ar*	*2 σ*	*39Ar/40Ar*	*2 σ*	*36Ar/40Ar*	*2 σ*	*Rho*	*K/Ca*	*%40Ar rad*	*f 39Ar*	*40Ar*/39ArK*	*Age*	*2σ*
2.0	77.43	0.01	0.26400	0.04000	0.0131	0.0001	0.00339	0.00007	0.13	0.41	1.00	0.39	-0.19	-3.53	± 27.72
2.2	33.59	0.01	0.11200	0.04600	0.0305	0.0002	0.00331	0.00008	0.03	0.25	1.02	0.59	0.73	13.60	± 13.73
2.4	12.76	0.01	0.04100	0.05200	0.0817	0.0006	0.00309	0.00009	0.11	0.22	1.10	1.07	1.08	19.95	± 5.86
2.6	6.28	0.02	0.01800	0.08000	0.1698	0.0014	0.00271	0.00012	0.06	0.43	1.26	1.56	1.21	22.32	± 3.89
2.8	3.97	0.03	0.00900	0.06000	0.2657	0.0035	0.00225	0.00007	0.20	0.94	1.53	3.23	1.29	23.81	± 1.61
3.0	2.58	0.02	0.00400	0.08800	0.4069	0.0048	0.00159	0.00008	0.10	0.94	2.21	6.60	1.33	24.65	± 1.13
3.2	2.27	0.02	0.00400	0.07600	0.4593	0.0042	0.00138	0.00006	0.09	0.48	2.59	9.61	1.33	24.49	± 0.78
3.4	1.90	0.02	0.00200	0.04800	0.5481	0.0044	0.00105	0.00003	0.10	0.50	3.50	14.53	1.29	23.92	± 0.38
3.6	1.63	0.01	0.00100	0.06600	0.6408	0.0047	0.00065	0.00003	0.07	0.78	5.96	16.55	1.29	23.91	± 0.31
3.8	1.48	0.01	0.00100	0.08200	0.7023	0.0041	0.00036	0.00002	0.03	2.44	12.09	22.52	1.30	24.10	± 0.21
4.0	1.47	0.05	0.00100	0.24600	0.7203	0.0171	0.00027	0.00005	0.10	3.58	17.04	12.67	1.31	24.12	± 0.73
4.2	1.52	0.02	0.00100	0.21600	0.7108	0.0068	0.00027	0.00006	0.01	2.78	17.33	7.20	1.32	24.47	± 0.51
4.7	1.72	0.01	0.18000	0.36000	0.6578	0.0455	0.00056	0.00020	0.00	1.18	6.97	3.48	1.30	23.99	± 1.65

J = 0.010315±0.000012; Volume 39ArK = 1453.83 x E-13 cm3 NPT

Integrated Date = 24.08 ± 0.14 Ma

Plateau age = 24.08 ± 0.17 Ma; (2σ, including J-error of .2%), MSWD = 0.94, probability = 0.50, Includes 99.02% of the 39Ar, steps 3 through 13

Inverse isochron (correlation age) results: Model 1 Solution (±95%-conf.) on 13 points

Age = 23.59 ± 0.16 Ma Initial 40Ar/36Ar = 290.6 ± 14; MSWD = 0.91, Probability = 0.53

4. Discussion

4.1. Breccia pipe relation to porphyry copper systems

Porphyry deposits typically form within a subduction-related volcanic arc, or continentward of the arc, where they are attributed to a shallowly dipping or flat subducted slab segment, but uncertainties persist in flat-slab models that project porphyry deposit formation far inland of the active margin (e.g., Glazner, 2022). Classical calc-alkalic porphyry deposits formed in a normal volcanic arc setting are enriched in one or more of copper, molybdenum, gold, and silver. Other base metals (e.g., lead and zinc) may occur in these porphyry deposits, mainly as sulphides, but they rarely constitute a substantial byproduct, except where distal veins and replacement zones are well-developed (e.g., Bisbee and Cochise, Warren district, Stegen et al., 2005); typical of carbonate replacement-style mineralization in mantos and chimneys distal to copper porphyry deposits (Lefebure and Jones, 2020). More evolved granitoids, especially those having a continental crustal component and historically attributed to flat-slab subduction, may comprise tin, tungsten, and molybdenum porphyry deposits, in which silver, copper, lead, and zinc sulphides can be important ore constituents (e.g., Climax, Colorado, White et al., 1981; Potosi, Bolivia, Lehman, 1994; Mount Pleasant, New Brunswick, Sinclair, 1994). Polymetallic porphyry-related tourmaline breccia pipe deposits are intermediate in ore metal diversity and tectonic setting between these two major classes of porphyry deposits and share common characteristics (Sillitoe and Sawkins, 1974; Sillitoe, 1985). These breccia pipe deposits can have distinctive geochemical footprints and occur within well-defined belts superimposed on older arc strata, such as in the ancestral Cascades of southern British Columbia and Washington state (Fig. 9) and other arcs globally.

4.2. Syn-kinematic intrusion and faulting

The age data presented here are consistent with the LA-ICP-MS U-Pb age from the Invermay intrusive suite presented by Fischer (2022), ending speculation that mineralization is related to Late Cretaceous intrusions (e.g., Robertson, 2006), which was based on a K-Ar biotite age of 85.7 ±6 Ma by Wanless et al. (1967) from a body 6 km to the northwest.

Regionally, the small Invermay suite intrusive bodies in the Giant Copper area are dwarfed by the well-known, coeval Chilliwack batholith extending across the international border 15 to 45 km to the southwest, and apparently stitching together Hozameen (Bridge River), Shuksan, and Chilliwack terranes (Fig. 1) by Oligocene. Co-magmatic volcanic rocks (22-21 Ma) are felsic to intermediate pyroclastics and flows of the Coquihalla Formation. To the north, these rocks rest atop Methow terrane and the Eagle Plutonic complex (Monger, 1989). To the south in Washington state, Haugerud and Tabor, 2009, mapped the equivalent Ohanapecosh volcanic rocks east of the Hozameen terrane, where they rest on Methow terrane. The southern extents of the Hozameen terrane are mapped as a thrust sheet underlain by Methow basin and metamorphosed equivalents (Fig. 2). Where metamorphosed Methow extends beneath and west of the Hozameen thrust sheet, it is extensively overlain by Ohanapecosh volcanic strata and is also cut by co-magmatic Snoqualmie intrusions. At Giant Copper, the Invermay intrusions cut the western terrane-bounding Hozameen fault but are also cut by a splay of the fault that extends into the Methow terrane (Fig. 3). Thus, a late syn-kinematic relationship between intrusion and faulting is suggested.

4.3. Oligocene magmatism and mineralization in the Cordillera

Oligocene porphyry deposits are not well known in the Canadian Cordillera. In British Columbia, they are overshadowed by the prolific Late Triassic-Early Jurassic porphyry epoch (Logan and Mihalynuk, 2014). However, in the US Cordillera, Bingham (Utah), the world's seventh largest copper deposit (Cooke et al., 2005; second in terms of contained gold), is also Oligocene to Late Eocene, with mineralization dated at 37.0 ±0.27 Ma, and the host intrusions having formed in less than a third of a million years, between 38.10 and 37.78 Ma (von Quadt et al., 2011). Closer to Giant Copper, Oligocene Coquihalla volcanic units and co-magmatic Chilliwack intrusions are part of the ancestral Cascade arc, best known in the Pacific northwest USA (Fig. 9). The arc has traditionally been divided into the Eocene to Miocene western Cascades or 'Ancestral Cascades arc' (Stern and Dumitru, 2019) , and the Pliocene to Holocene High Cascades (Tepper and Clark, 2024).

In Washington state, rocks coeval with the Invermay suite include the 'Snoqualmie family' of intrusive rocks (Oligocene-Miocene; Haugerud and Tabor, 2009) which cut Hozameen Group rocks. Coeval volcanic strata of the 'Ohanapecosh episode' (Oligocene) are considered the oldest volcanic rocks of the Cascade magmatic arc and may have been cannibalized by co-magmatic Snoqualmie intrusions (28-22 Ma, Haugerud and Tabor, 2009). The oldest part of the ancestral Cascade arc are 35-29 Ma plutons of the "Index family" (Haugerud and Tabor, 2009), but coeval volcanic rocks have apparently all been removed by erosion. Both Index and Snoqualmie intrusions are responsible for several other examples of mineralized tourmaline breccias as compiled by Singer et al. (2008) and Fischer (2022) from Black Jack (19.6 Ma, near Portland, 45.5°N) to Sunrise (28.2 Ma, 48.2°N), and porphyry copper deposits, from Margaret (21 Ma, 46.4°N) to North Fork (25 Ma, 47.7°N), and Glacier Peak (23.3 Ma, 48.2°N).

Attempts to address the plate tectonic setting of the ancestral Cascades commonly do not consider the old arc units as extending into northernmost Washington State and southern British Columbia (e.g., Madsen et al., 2006; Stern and Dumitru, 2019; Humphreys and Grunder, 2022). In contrast, regional mapping and isotopic age compilations by Haugerud and Tabor (2009) and Monger (1989) show Oligocene extrusive and intrusive rocks that are a northern extension of the ancestral Cascade belt. In particular, intrusive rocks thought to be the comagmatic with Coquihalla Formation extend as far north as Hells Gate on the Fraser River (~10 km south of Boston Bar, Fig. 9).

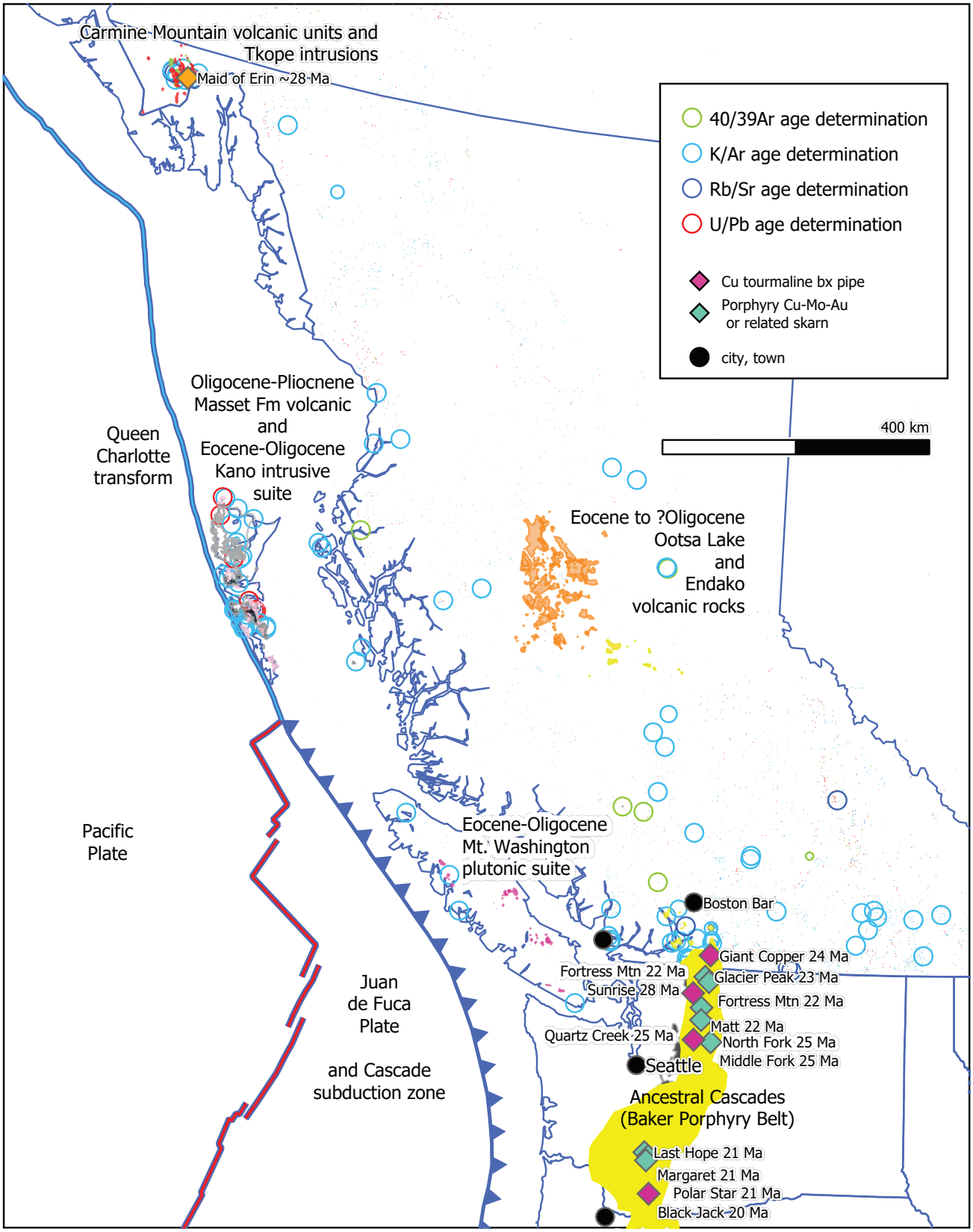


Fig. 9. Distribution of the ancestral Cascade belt magmatic rocks in British Columbia, Washington State, and Oregon (45-5 Ma volcanic and intrusive rocks combined, after Stern and Dumitru, 2019); age data from Engels et al. (1976), Mullen et al. (2018). Distribution of Oligocene ages in British Columbia are from Han et al. (2020). Copper porphyry and breccia deposits in Washington and Oregon from Singer et al. (2008), Lasmanis (1995), and Iveson et al. (2016).

What the true northern extent of the ancestral Cascade arc in British Columbia actually is, and what the plate tectonic explanation for the paleogeographic limit of Cascade subduction is, are unanswered questions and beyond the scope of this paper. However, Oligocene magmatism and mineralization span the length of western British Columbia (Fig. 9), and at several localities Oligocene intrusions are related to mineralization with past production.

4.3.1. Tkope suite and Carmine Mountain volcanic feeders

In the far northwest part of the province, Tkope suite tonalite and quartz monzonite intrusions are associated with skarn mineralization; some zones have small tonnage past production (Fig. 9). Examples include the Maid of Erin (or Carmichael, Rainy Hollow) and State of Montana (or Arizona, Montana, Rainy Hollow). Sulphide minerals in garnet-epidote skarn are bornite, chalcopyrite, sphalerite, and in some instances, argentiferous wittichenite (Cu_3BiS_3) and gold (cf. MINFILE 114P 007 and 008). Breccia is noted at the Maid of Erin (Wilson, 1983, Figure 015-83-17) and, at the Bornite prospect (or Cat, Horrible; MINFILE 114P 019), extensive intrusive breccias and skarn contain copper, molybdenum, lead, zinc, silver, and gold mineralization interpreted as related to a porphyry system.

Co-magmatic volcanic rocks found in the same region are named after a prominent massif, Carmine Mountain. Porphyry dikes, feeders to the volcanic rocks that underlie Carmine Mountain, are associated with silver- and gold-enriched epidote-diopside skarn containing pods of galena, sphalerite and chalcopyrite (Fair prospect, MINFILE 114P 070), but with no record of past production.

4.3.2. Nechako suite

Perhaps the most extensive Oligocene rocks are those of the Nechako suite in central British Columbia. However, most related mineralization is precious metal, low sulphidation epithermal in nature. Porphyry copper prospects in the area have no clear association with this Oligocene suite.

5. Summary

Geochronological data presented here confirm the Oligocene age of the Invermay intrusive suite at the past-producing Giant Copper deposit and show that the breccia pipe mineralization has the same age. The Invermay suite is part of ancestral Cascade arc volcanic rocks, intrusions, and related breccia and porphyry mineralization that extend into Washington and Oregon. The northern limits of the ancestral Cascade arc probably stretch at least to Hell's Gate (49.8°N). Oligocene magmatic rocks are known to extend the length of western British Columbia, and Oligocene intrusive-related polymetallic deposits with past production are known from both ends of the province.

Acknowledgments

The lead author thanks Imperial Metals Corporation for the invitation to visit the Giant Copper deposit and the willingness of their geological team to share technical information. The field program was facilitated by David Lefebure who also contributed to field discussions and aided in the collection of samples at Giant Copper. Tom Ullrich conducted the $^{40}Ar/^{39}Ar$ analysis of the samples reported here.

References cited

Cairnes, C.E., 1920. Coquihalla Area, British Columbia. In: Geological Survey of Canada, Summary Report, 1920, Part A, pp. 24-42.

Cairnes, C.E., 1924. Coquihalla Area, British Columbia. Geological Survey of Canada, Memoir 139, 187 p.

Cairnes, C.E., 1929. The Serpentine Belt of Coquihalla Region, Yale District, British Columbia. In: Geological Survey of Canada, Summary Report, Part A; pp. 144-197.

Cairnes, C.E., 1944. Hope, Yale and New Westminster Districts, British Columbia. Geological Survey of Canada, Map 737A.

Coates, J.A., 1974. Geology of the Manning Park area, British Columbia. Geological Survey of Canada, Bulletin 238, 177 p.

Cohen, K., Harper, D., Gibbard, P., and Car, N., 2025. The ICS international chronostratigraphic chart this decade. Episodes, 48, 105-114. <https://doi.org/10.18814/epiiugs/2025/025001>

Colpron, M., 2020. Yukon terranes-A digital atlas of terranes for the northern Cordillera. Yukon Geological Survey. <https://data.geology.gov.yk.ca/Compilation/2#InfoTab>

Cooke, D.R., Hollings, P., and Walshe, J.L., 2005. Giant porphyry deposits: Characteristics, distribution, and tectonic controls. Economic Geology, 100, 801-818.

Engels, J.C., Tabor, R.W., Miller, F.K., and Obradovich, J.D., 1976. Summary of K-Ar, Rb-Sr, U-Pb, and fission-track ages of rocks from Washington State prior to 1975 (exclusive of Columbia Plateau Basalts); U.S. Geological Survey Miscellaneous Field Studies Map MF-710, 1:500,000 scale.

Fischer, W.T., 2022. Tourmaline breccia pipes of the giant copper property, Southern British Columbia: Understanding the significance of tourmaline and breccia pipes as vectoring tools in porphyry copper deposits. Ph.D. thesis, Simon Fraser University, Burnaby, British Columbia, Canada, 318 p.

Fischer, W.T., Marshall, D.D., Hanchar, J.M., Riley, D. and Hiebert, S., 2023. Differentiating tourmaline species via chemistry and reflectance spectroscopy at the Giant Copper porphyry deposit and associated tourmaline breccia pipes: Testing tourmaline as a mineral vector. Economic Geology, 118, 883-902.

Fischer, W.T., Marshall, D.D., and Miller-Tait, J., 2024. Tourmaline breccia pipes of the Giant Copper porphyry system: Extending the Cascadia porphyry district into southern British Columbia, Canada. CIM Journal, 15, 136-157.

Frikken, P.H., Cooke, D.R., Walshe, J.L., Archibald, D., Skarmeta, J., Serrano, L., and Vargas, R., 2005. Mineralogical and isotopic zonation in the Sur-Sur tourmaline breccia, Río Blanco-Los Bronces Cu-Mo deposit, Chile: Implications for ore genesis. Economic Geology, 100, 935-961.

Gabites, J.E., and Mihalynuk, M.G., 2026. $^{40}Ar/^{39}Ar$ geochronologic data from samples collected at Giant Copper. British Columbia Ministry of Mining and Critical Minerals, British Columbia Geological Survey GeoFile 2026-in press.

Glazner, A.F., 2022, Cenozoic magmatism and plate tectonics in western North America: Have we got it wrong? In: Foulger, G.R., Hamilton, L.C., Jurdy, D.M., Stein, C.A., Howard, K.A., and Stein, S., (Eds.), In the Footsteps of Warren B. Hamilton: New Ideas in Earth Science. Geological Society of America Special

Paper 553, pp. 1-14. <https://doi.org/10.1130/2021.2553(09)>
Greig, C.J., Armstrong, R.L., Harakal, J.E., Runkle, D., and der Heyden, P.V., 1992. Geochronometry of the Eagle plutonic complex and the Coquihalla area, southwestern British Columbia. Canadian Journal of Earth Sciences, 29, 812-829.
Han, T., Ootes, L., and Yun, K., 2020. The British Columbia Geological Survey geochronologic database: Preliminary release of ages. British Columbia Ministry of Energy, Mines and Low Carbon Innovation, British Columbia Geological Survey GeoFile 2020-10, 4 p.
Haugerud, R.A., and Tabor, R.W., 2009. Geologic map of the north Cascade Range, Washington. US Department of the Interior, US Geological Survey, Scientific Investigations, Map 2940, 29 p.
Humphreys, E.D., and Grunder, A.L., 2022. Tectonic controls on the origin and segmentation of the Cascade Arc, USA. Bulletin of Volcanology, 84, 102. <https://doi.org/10.1007/s00445-022-01611-2>
Hurlow, H.A., and Nelson, B.K., 1993. U-Pb zircon and monazite ages for the Okanogan Range batholith, Washington: Implications for the magmatic and tectonic evolution of the southern Canadian and northern United States Cordillera. Geological Society of America Bulletin, 105, 231-240.
Imperial Metals Corporation, 2022. News Release: 2022.01.19 Imperial to Surrender Giant Copper Property. <https://imperialmetals.com/assets/docs/2022.01.19%20Imperial%20to%20Surrender%20Giant%20Copper%20Property.pdf>
Iveson, A.A., Webster, J.D., Rowe, M.C., and Neill, O.K., 2016. Magmatic-hydrothermal fluids and volatile metals in the Spirit Lake pluton and Margaret Cu-Mo porphyry system, SW Washington, USA. Contributions to Mineralogy and Petrology, 171, 20 p. <https://doi.org/10.1007/s00410-015-1224-6>
Koppers, A.A.P., 2002, ArArCALC-software for $^{40}Ar/^{39}Ar$ age calculations. Computers and Geosciences, 28, 605-619.
Lasmanis, R., 1995. Regional geological and tectonic setting of porphyry deposits in Washington State. In: Schroeter, T.G., (Ed.), Porphyry deposits of the northwestern Cordillera of North America: Canadian Institute of Mining, Metallurgy and Petroleum Special Volume, 46, pp. 77-102.
Lefebure, D.V., and Jones, L.D., (compilers), 2022. British Columbia Geological Survey mineral deposit profiles, 1995 to 2012; updated with new profiles for VMS, porphyry, and mafic-ultramafic deposits. British Columbia Ministry of Energy, Mines and Low Carbon Innovation, British Columbia Geological Survey GeoFile 2020-11, 652 p.
Lehmann, B., 1994. Petrochemical factors governing the metallogeny of the Bolivian tin belt. In: Reutter, K-J., Scheuber, E., and Wigger, P.J., (Eds.), Tectonics of the Southern Central Andes. Structure and Evolution of an Active Continental Margin. Springer-Verlag, Berlin and Heidelberg, pp. 317-326.
Logan, J.M., and Mihalynuk, M.G., 2014. Tectonic controls on early Mesozoic paired alkaline porphyry deposit belts (Cu-Au ±Ag-Pt-Pd-Mo) within the Canadian Cordillera. Economic Geology, 109, 827-858.
Ludwig, K.R., 2003. Isoplot 3.09 A Geochronological Toolkit for Microsoft Excel. Berkeley Geochronology Center, Special Publication No. 4.
Madsen, J.K., Thorkelson, D.J., Friedman, R.M., and Marshall, D.D., 2006. Cenozoic to Recent plate configurations in the Pacific Basin: Ridge subduction and slab window magmatism in western North America. Geosphere, 2, 11-34.
Miller-Tait, J., 2016, Geochemical Assessment Report (2015 Soil Sampling Program) on the Giant Copper Property. British Columbia Ministry of Mining and Critical Minerals, Assessment Report 36083, 74 p.
MINFILE. Mineral Inventory. British Columbia Ministry of Mining and Critical Minerals, British Columbia Geological Survey. <https://www2.gov.bc.ca/gov/content/industry/mineral-exploration-mining/british-columbia-geological-survey/mineralinventory> (last accessed July 2025).
Monger, J.W.H., and Brown, W.H., 2016. Tectonic Evolution of the Southern Coast-Cascade Orogen, Northwestern Washington and Southwestern British Columbia. The Geology of Washington and Beyond: From Laurentia to Cascadia, University of Washington Press, Volume 10, pp. 101-130.
Monger, J.W.H., 1989. Hope map area. Geological Survey of Canada, Open File Map 41-1989, 1:250,000 scale.
Mullen, E.K., Paquette, J.L., Tepper, J.H., and McCallum, I.S., 2018. Temporal and spatial evolution of Northern Cascade Arc magmatism revealed by LA-ICP-MS U-Pb zircon dating. Canadian Journal of Earth Sciences, 55, 443-462.
O'Brien, J.A., 1987. Jurassic biostratigraphy and evolution of the Methow Trough, southwestern British Columbia. M.Sc. thesis, The University of Arizona, Tucson, 170 p.
O'Brien, J.A., Gehrels, G.E., and Monger, J.W.H., 1992. U-Pb geochronology of plutonic clasts from conglomerates in the Ladner and Jackass Mountain groups and the Peninsula Formation, southwestern British Columbia. In: Current Research, Part A, Geological Survey of Canada Paper 92-1A, pp. 209-214.
Oliver, S.L., 2011. The Eastgate-Whipsaw metamorphic belt as Paleozoic underpinnings to the Nicola Group. M.Sc. thesis, The University of British Columbia, Vancouver, 109 p.
Pinsent, R.H., 1998. Exploration and development highlights southwestern British Columbia, 1997. In: Exploration in British Columbia 1997, British Columbia Ministry of Energy and Mines, British Columbia Geological Survey, pp. 53-64.
Ray, G.E., 1986. The Hozameen fault system and related Coquihalla serpentine belt of southwestern British Columbia. Canadian Journal of Earth Science, 23, 1022-1041.
Ray, G.E., 1990. The geology and mineralization of the Coquihalla gold belt and Hozameen fault system, southwestern British Columbia. British Columbia Ministry of Energy, Mines and Petroleum Resources, British Columbia Geological Survey Bulletin 79, 109 p.
Renne, P.R., Swisher, C.C., III, Deino, A.L., Karner, D.B., Owens, T., and DePaolo, D.J., 1998. Intercalibration of standards, absolute ages and uncertainties in $^{40}Ar/^{39}Ar$ dating. Chemical Geology, 145, 117-152.
Robertson, S., 2006. Giant Copper Property, Southern British Columbia: Imperial Metals Corporation, 43-101 Technical Report, 47 p.
Schmitt, H.R., and Koyanagi, V.M., 1992. Cascade Recreation Area, preliminary geology and mineral potential. In: Geological Fieldwork 1991. British Columbia Ministry of Energy, Mines and Petroleum Resources, British Columbia Geological Survey Paper 1992-01, pp. 47-64.
Sillitoe, R.H., and Sawkins, F.J., 1974. Geologic, mineralogic, and fluid inclusion studies relating to the origin of copper-bearing tourmaline breccia pipes, Chile. Economic Geology, 66, 1028-1041.
Sillitoe, R.H., 1985. Ore-related breccias in volcanoplutonic arcs. Economic Geology, 80, 1467-1514.
Sinclair, W.D., 1994. Tungsten-molybdenum and tin deposits at Mount Pleasant, New Brunswick, Canada: Products of ore-fluid evolution in a highly fractionated granitic system. In: Seltmann, Käampf, and Möller, (Eds.), Metallogeny of Collisional Orogens, Czech Geological Survey, Prague, pp. 410-417.
Singer, D.A., Berger, V.I., and Moring, B.C., 2008. Porphyry copper deposits of the world: Database and grade and tonnage models, 2008. US Geological Survey Open File Report 2008-1155, 45 p., and digital files.

Stegen, R.J., Wright, E., and Bryant, D.G., 2005. Field guide to the Warren (Bisbee) Mining District, Cochise County, Arizona. Guidebook for the Arizona Geological Society, Spring Field Trip, April 30, 2005, 41 p.

Stern, R.J., and Dumitru, T.A., 2019. Eocene initiation of the Cascadia subduction zone: A second example of plume-induced subduction initiation? Geosphere, 15, 659-681.

Surpless, K.D., Sickmann, Z.T., and Koplitz, T.A., 2014. East-derived strata in the Methow basin record rapid mid-Cretaceous uplift of the southern Coast Mountains batholith. Canadian Journal of Earth Science, 51, 339-357.

Tabor, R.W., and Haugerud, R.A., 2016. Geology of the North Cascades-summary and enigmas. In: Cheney, E., (Ed.), Geology of Washington, University of Washington Press, Seattle, pp. 131-155.

Tabor, R.W., Haugerud, R.A., Hildreth, W., and Brown, E.H., 2003. Geologic Map of the Mount Baker 30′ × 60′ Quadrangle, Washington. U.S. Geological Survey Geologic Investigations Series I-2660, 1:100,000 scale, 2 sheets, 73 p.

Tepper, J.H., and Clark, K.P., 2024. Initiation of the Cascade arc. Geology, 52, 297-301. <https://doi.org/10.1130/G51888.1>

Umhoefer, P.J., and Miller, R.B., 1996. Mid-Cretaceous thrusting in the southern Coast Belt, British Columbia and Washington, after strike-slip fault reconstruction. Tectonics, 15, 545-565.

Umhoefer, P.J., and Schiarizza, P., 1996. Latest Cretaceous to early Tertiary dextral strike-slip faulting on the southeastern Yalakom fault system, southeastern Coast Belt, British Columbia. Geological Society of America Bulletin, 108, 768-785.

von Quadt, A., Erni, M., Martinek, K., Moll, M., Peytcheva, I., and Heinrich, C.A., 2011. Zircon crystallization and the lifetimes of ore-forming magmatic-hydrothermal systems. Geology, 39, 731-734.

Wanless, R.K., Stevens, R.D., Lachance, G.R., and Edmonds, C.M., 1967. Age determinations and geological studies K-Ar Isotopic ages, Report 7. Geological Survey of Canada, Paper, 66-17, 120 p. <https://doi.org/10.4095/100968>

Wheeler, J.O., Brookfield, A.J., Gabrielse, H., Monger, J.W.H., Tipper, H.W., and Woodsworth, G.J., 1991. Terrane map of the Canadian Cordillera, Geological Survey of Canada, “A” Series Map 1713A, 1:2,000,000 scale, 2 sheets.

White, W.H., Bookstrom, A.A., Kamilli, R.J., Ganster, M.W., Smith, R.P., Ranta, D.E., and Steininger, R.C., 1981. Character and origin of Climax-type molybdenum deposits. Economic Geology, 75th anniversary volume, 270-316.

Wilson, J.R., 1983. Diamond Drilling Assessment Report on (a) ME 2 Group Mineral Claims (b) ME 7 Group Mineral Claims. British Columbia Ministry of Mining and Critical Minerals, British Columbia Geological Survey, Assessment Report 11835, 15 p.

Zagorevski, A., van Staal, C.R., Bédard, J.H., Bogatu, A., Canil, D., Coleman, M., Golding, M., Joyce, N.L., Lawley, C., McGoldrick, S., Mihalynuk, M.G., Milidragovic, D., Parsons, A., and Schiarizza, P., 2021. Overview of Cordilleran oceanic terranes and their significance for the tectonic evolution of the northern Cordillera. In: Ryan, J.J., and Zagorevski, A., (Eds.), Northern Cordillera geology: A Synthesis of Research from the Geo-mapping for Energy and Minerals program, British Columbia and Yukon. Geological Survey of Canada, Bulletin 610, pp. 21-65.

Early Jurassic intrusion and deformation in the Wark-Colquitz complex, Victoria, British Columbia

JoAnne Nelson[1, a]

[1] Emeritus Scientist, British Columbia Geological Survey, Ministry of Mining and Critical Minerals, Victoria, BC, V8W 9N3
[a] corresponding author: JoAnne.Nelson@gov.bc.ca

Recommended citation: Nelson, J., 2026. Early Jurassic intrusion and deformation in the Wark-Colquitz complex, Victoria, British Columbia. In: Geological Fieldwork 2025, British Columbia Ministry of Mining and Critical Minerals, British Columbia Geological Survey Paper 2026-01, pp. 175-181.

Abstract

Precise U-Pb zircon ages from deformed and crosscutting, post-kinematic intrusive phases of the Wark-Colquitz plutonic-metamorphic complex in downtown Victoria are ca. 193 Ma and agree within error, indicating a short-lived episode of intrusion accompanied by ductile deformation. This age coincides with Early Jurassic volcanism in the Bonanza Group (LeMare Lake volcanic unit) and emplacement of the oldest intrusions of the Island Plutonic Suite, considered to have fed the Bonanza arc. In agreement with previous workers, we consider the Wark-Colquitz complex to be an exhumed deep-crustal portion of Wrangellia that exposes the roots of the Triassic-Jurassic Bonanza magmatic arc. Episodic syn-plutonic ductile deformation may be the result of subduction-related strain due to coupling with the down-going plate.

Keywords: Wark-Colquitz, Bonanza arc, Island Plutonic Suite, Wrangellia, Westcoast complex, Victoria

1. Introduction

The Wark-Colquitz plutonic-metamorphic complex is exposed on southernmost Vancouver Island (Fig. 1), in the traditional territory of the lək̓ʷəŋən-speaking (Lekwungen; Songhees and Xʷsepsəm (Ko-sap-sum)/Esquimalt) peoples. It forms an isolated, west-northwesterly trending, fault-bounded belt that extends westward from Victoria (Fig. 2). It represents the southernmost extent of Wrangellia and is distinct from the Paleozoic to Jurassic supracrustal section that characterizes most of this accreted terrane. On its southwest border, the complex lies in the hanging wall of the Survey Mountain thrust fault, above metamorphosed siliciclastic rocks of the Leech River complex, which forms part of the subduction-related Pacific Rim terrane. Its northeastern limit is an unnamed, steeply dipping fault that juxtaposes the complex with Mesozoic Wrangellia supracrustal strata, cut by Jurassic plutons of the Island Plutonic Suite. All of these units and structures are truncated by the northeast-striking San Juan fault (Fig. 2). Restoration of 25 kilometres of sinistral displacement on this fault aligns the Wark-Colquitz complex with the equivalent Westcoast complex farther west near Port Renfrew, which forms the outermost unit of Wrangellia along the west coast of Vancouver Island (Isachsen, 1984; Canil et al., 2010).

Original work on the Wark-Colquitz complex subdivided it into mafic and felsic units: Wark gneiss, consisting of massive to gneissic metadiorite, metagabbro, and amphibolite; and Colquitz quartz-feldspar gneiss, both considered to be Paleozoic (Muller, 1983). More recent studies have shown that the Wark-Colquitz and Westcoast complexes (193-174 Ma) represent a single highly variable, syntectonic intrusive entity containing minor remnant pre-plutonic protoliths (Isachsen, 1984; Canil et al., 2010, 2013). On outcrop scale, unfoliated, generally more felsic phases intrude older mafic and felsic phases that have undergone ductile strain, locally forming protomylonites. These rocks are considered to represent the deep-crustal infrastructure of the Jurassic Bonanza magmatic arc (deBari et al., 1999; Larocque, 2008), which elsewhere on Vancouver Island includes the predominantly volcanic Bonanza Group and Island Plutonic Suite. The Bonanza arc was active between 202 and 169 Ma, based on U-Pb zircon dating of volcanic rocks (Nixon and Orr, 2007).

Given its urban location, remarkably little is known about the Wark-Colquitz complex. Prior to this study, very few reliable U-Pb zircon dates were available. In particular, ages of coexisting foliated and unfoliated phases were not known, which left unconstrained the timing and duration of high strain in the complex. In 2007-2008, excavation for a building foundation adjacent to the Jack Davis Building on Blanshard Street offered a unique opportunity to study and sample freshly blasted outcrops of Wark-Colquitz intrusive bodies. This paper presents field and U-Pb zircon geochronology results from these outcrops.

2. Local geology

The Wark-Colquitz complex, well-exposed on rocky hilltops and beaches in the Victoria area, shows great variety of intrusive phases that range in composition from mafic to felsic. In a given outcrop, the degree of deformation varies markedly between and, in some cases, within intrusive phases. In some areas, remnants of pre-intrusive metamorphosed supracrustal units – meta-tuffs, metaclastics, and calc-silicates – are preserved; notably at Cattle Point (Fig. 2). The age and affinity

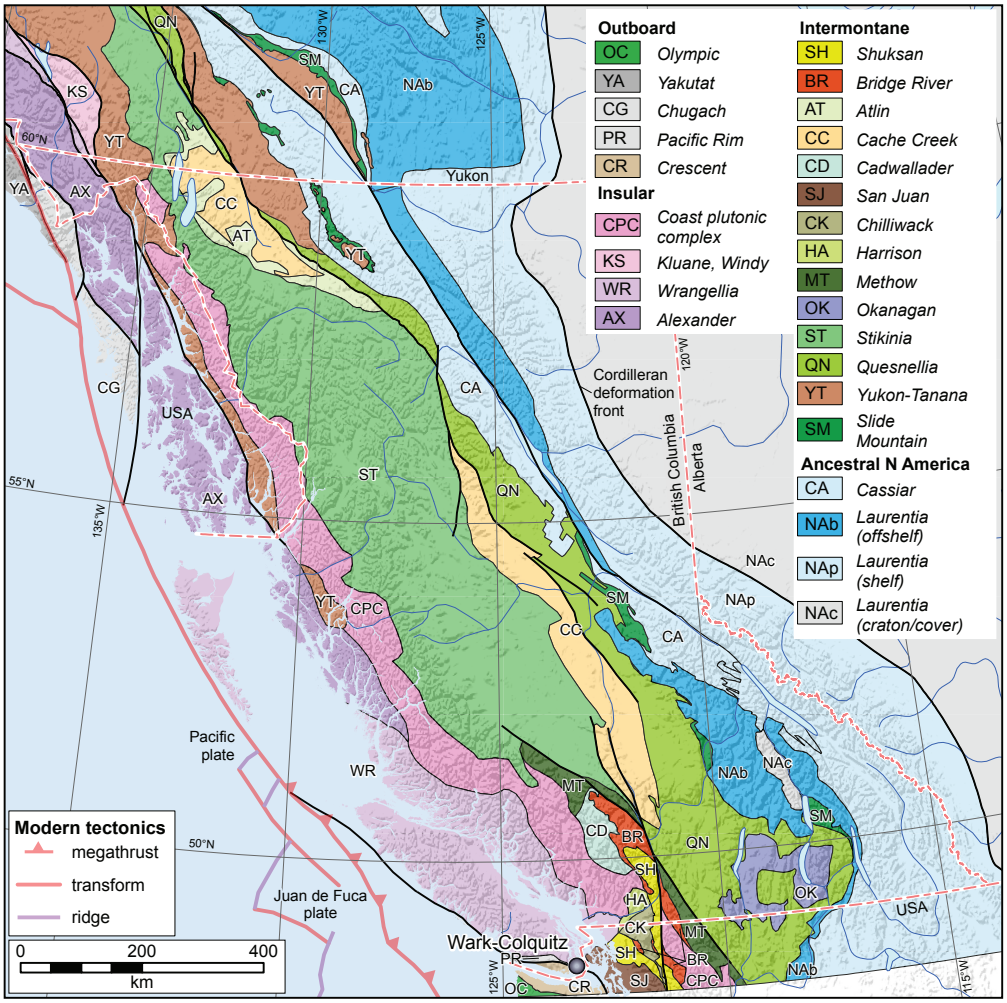


Fig. 1. Tectonic elements of the Canadian Cordillera in British Columbia and location of study site in Victoria. Terrane boundaries after Colpron (2020).

of their protoliths are unknown. Muller (1983) suggested they are correlative with the Sicker Group, but supporting geochronological data are currently lacking; conceivably, they could be derived from pre-Sicker units in the basement of Wrangellia.

The faulted northern margin of the Wark-Colquitz complex demarcates different depths of crustal exposure. To the south, Al-in-hornblende barometry indicates that Wark-Colquitz complex plutons were emplaced in the middle to lower crust, at depths of 10-18 km (Canil et al., 2010). North of the fault, weakly metamorphosed upper crustal strata of the Karmutsen and Bonanza groups are intruded by unfoliated plutons of the Island Plutonic Suite, which have yielded local U-Pb dates of 167-173 Ma (Fig. 2; Breitsprecher and Mortensen, 2004). The current trace of the fault is consistent with a near-vertical dip (Fig. 2; Harrichhausen et al., 2023). A trench excavated in 2023 on the eastern shore of Elk Lake exposed a fault-propagation fold within deformed Quaternary sediments above the southwest-dipping fault. Using the WSÁNEĆ peoples' name for Elk Lake in the SENĆOTEN language (pronounced hul-lakl-lik), Harrichhausen et al. (2023) applied the local name XEOLXELEK-Elk Lake fault. The fold indicates reverse motion of the southern (Wark-Colquitz) block on top of the upper crustal strata to the north. The larger-scale structural relationship between mid-crustal rocks of the Wark-Colquitz complex and Mesozoic strata to the north is unknown. Was the original intervening fault a top-to-the-north reverse fault, or is recent motion superimposed on a north-dipping denudation fault?

The intricate geology of the Wark-Colquitz complex is evident in its many outcrops. Instead of true orthogneisses, the complex consists of a wide range of plutonic and meta-plutonic bodies. Degree of deformation varies widely, from large areas of weakly deformed diorite to local zones of protomylonite. Multiple crosscutting phases are common at outcrop scale. Foliations are folded, and in general ductile deformation was succeeded by ductile-brittle shearing.

3. This study

In 2008, two samples were collected from a pit being blasted

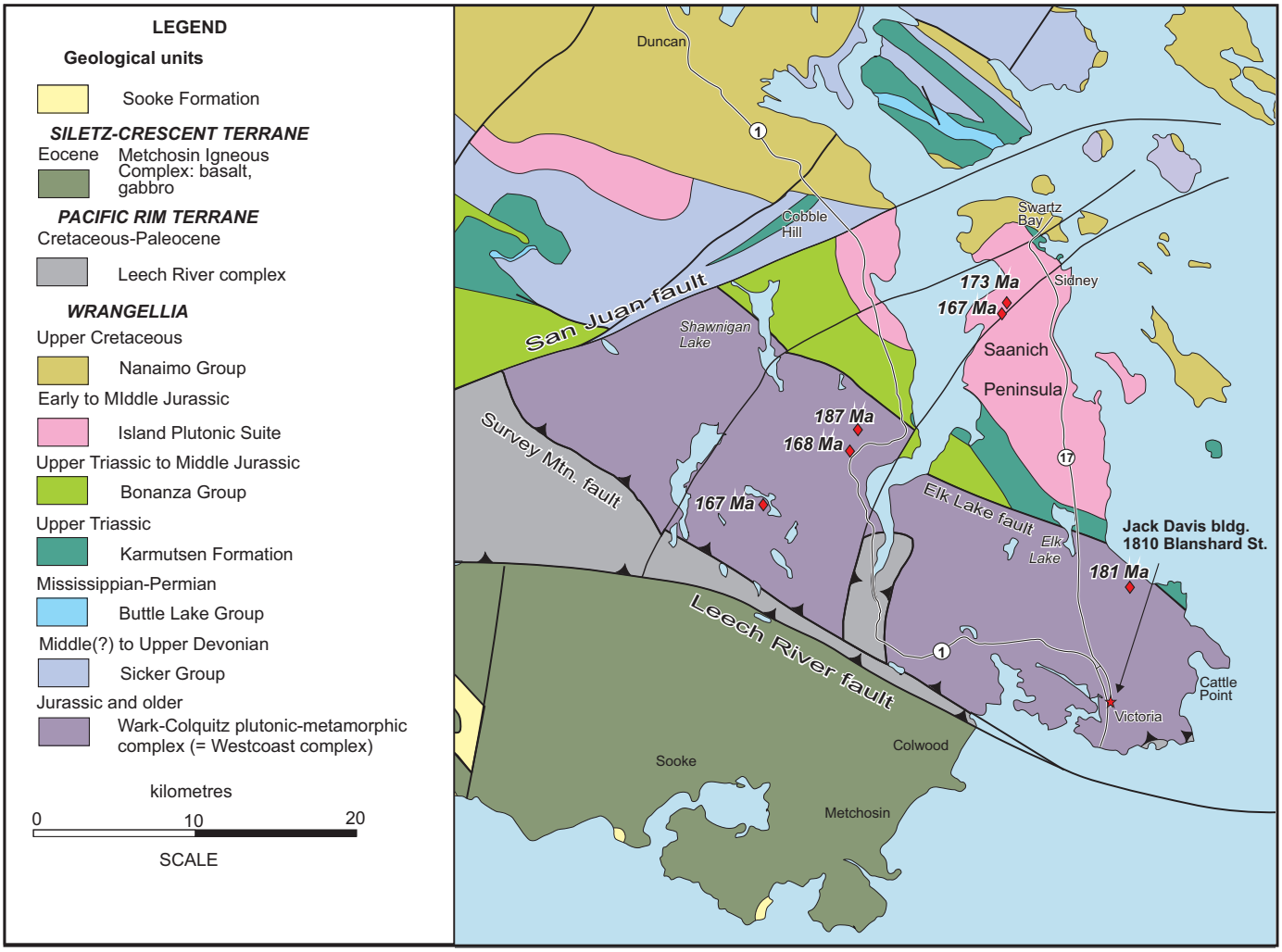


Fig. 2. Geology of the Victoria area, southern Vancouver Island. From British Columbia Geological Survey (2019) with modifications from Harrichhausen et al. (2023). Uranium-lead zircon ages from Isachsen (1984); Breitsprecher and Mortenson (2004); Canil et al. (2013).

for the foundation of a condominium development adjacent to 1810 Blanshard Street, the home of the British Columbia Geological Survey. The data presented here are the sole record of the geology of the 'Jack Davis pit'.

The eastern wall of the pit exposed microporphyritic diorite with a steeply dipping S_1 foliation parallel to contacts with metabasalts that likely originated as sills (Fig. 3). The main foliation is truncated by a gently north-dipping zone of brittle shearing (S_2, Fig. 3). Top-to-the-south, reverse motion is suggested by a set of steeper splays. The foliation is defined by wispy trains of fine-grained matrix minerals albite+actinolite+chlorite (Figs. 4a, b). A finer-grained, unfoliated leucotonalite cuts the foliated diorite, and contains xenoliths of foliated diorite and metabasalt (Figs. 4c, d).

3.1. Geochronology

Samples of the foliated diorite (JDP-5) and crosscutting unfoliated tonalite (JDP-6) were taken for U-Pb zircon geochronology. CA-TIMS analyses were performed by Richard Friedman at the Pacific Centre for Isotopic and Geochemical Research at The University of British Columbia (PCIGR) in 2009.

3.1.1. Methods

Zircon was separated from rock samples using conventional crushing, grinding and Wilfley table techniques, followed by final concentration using heavy liquids and magnetic separations. Mineral fractions for analysis were selected based on grain morphology, quality, size and magnetic susceptibility. Except where noted, all zircon fractions were abraded before dissolution to minimize the effects of post-crystallization Pb-loss (Krogh, 1982). Samples were dissolved in concentrated hydrofluoric acid (HF) and nitric acid (HNO_3) in the presence of a mixed $^{233\text{-}235}U$-^{205}Pb tracer. Separation and purification of Pb and U employed ion exchange column techniques modified slightly from those described by Parrish et al. (1987). Pb and U were eluted separately and loaded together on a single Re filament using a phosphoric acid-silica gel emitter. Isotopic ratios were measured using a modified single collector VG-54R thermal ionization mass spectrometer equipped with

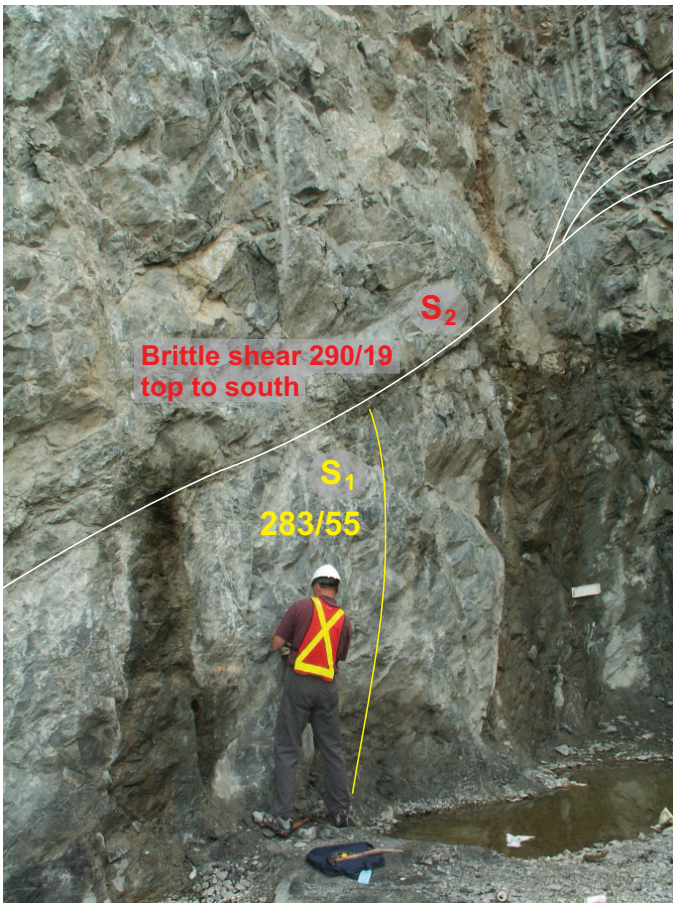


Fig. 3. East wall of the 'Jack Davis pit'. Main foliation (S_1) is parallel to contacts of metadiorite and metabasalt. Cut by brittle shear (290/19); UTM 473129E, 5364229N.

a Daly photomultiplier. Measurements were done in peak-switching mode on the Daly detector. U and Pb total procedural blanks were in the range of 1 pg and 3 to 5 pg, respectively, during this study. U fractionation was determined directly on individual runs using the $^{233\text{-}235}$U tracer, and Pb isotopic ratios were corrected for a fractionation of 0.37%/amu for Faraday and Daly runs, respectively, based on replicate analyses of the NBS-981 Pb standard and the values recommended by Thirlwall et al. (2000). All analytical errors were numerically propagated through the entire age calculation using the technique of Roddick (1987). Concordia intercept ages and associated errors were calculated using a modified version of the York-II regression model (wherein the York-II errors are multiplied by the mean square of weighted deviates (MSWD) and the algorithm of Ludwig (1980). All errors are quoted at the two-sigma level. Results are plotted on standard concordia diagrams (Fig. 5) and listed in Table 1.

3.1.2. Results

Sample 08JDP-5 yielded five concordant zircon fractions. A weighted mean of the three younger fractions is 192.5 ±0.24 Ma (Fig. 5). The two older fractions are ca. 195 Ma and probably represent xenocrysts or antecrysts. Sample 08JDP-6 yielded four concordant fractions. A weighted mean of the three younger fractions is 192.66 ±0.59 Ma (Fig. 5), with a single ca. 195 Ma fraction representing xenocrysts or antecrysts. The two dates agree within analytical error (±0.6 Ma 2σ). The two populations of xenocrysts/antecrysts are remnants of a slightly older zircon crystallization.

4. Discussion

With dates of 192.59 ±0.24 Ma and 192.6 ±0.6 Ma, the two plutonic phases at the 'Jack Davis pit' were emplaced during a <1 Ma time interval, between 193 and 192 Ma. This age corresponds to the oldest intrusive ages reported elsewhere in the Westcoast complex (Canil et al., 2012), and to the Early Jurassic (Hettangian-Sinemurian) LeMare Lake volcanic unit, the older of the two predominantly volcanic units in the Bonanza Group on northern Vancouver Island (Nixon et al., 2011). It may coincide with the earliest stages of Jurassic magmatism in the Bonanza arc on southern Vancouver Island.

The contrast in foliation development in the two phases, from early foliated diorite to later unfoliated leucotonalite, demonstrates that this brief intrusive episode was accompanied by ductile deformation that waned before emplacement of the leucotonalite. Coexisting ca. 192-194 Ma foliated and unfoliated phases also occur in the Westcoast complex near Port Renfrew (Canil et al., 2012), indicating a similar short-lived episode of localized strain accompanying plutonic emplacement. A significantly younger foliated phase (ca. 183 Ma) has also been identified, a banded meta-quartz diorite from Meares Island near Tofino (Isachsen, 1984). Episodic, localized deformation may have accompanied intrusion at various times throughout the development of the Bonanza arc infrastructure.

In developing magmatic arcs, both orogen-normal and strike-slip episodic deformation occur (de Saint Blanquat et al., 1998; Buritica et al., 2019; Gehrels et al., 2025), as well as less common episodes of orogen-normal extension linked to megathrust events (Acocella, 2014). The extensive exposures of the Wark-Colquitz and Westcoast complexes present an opportunity for detailed study of linked deformation and plutonism in the mid-crustal region of an active magmatic arc. Future work should focus on geochronology of coexisting deformed and undeformed intrusive phases as well as kinematic observations to establish prevailing strain regimes.

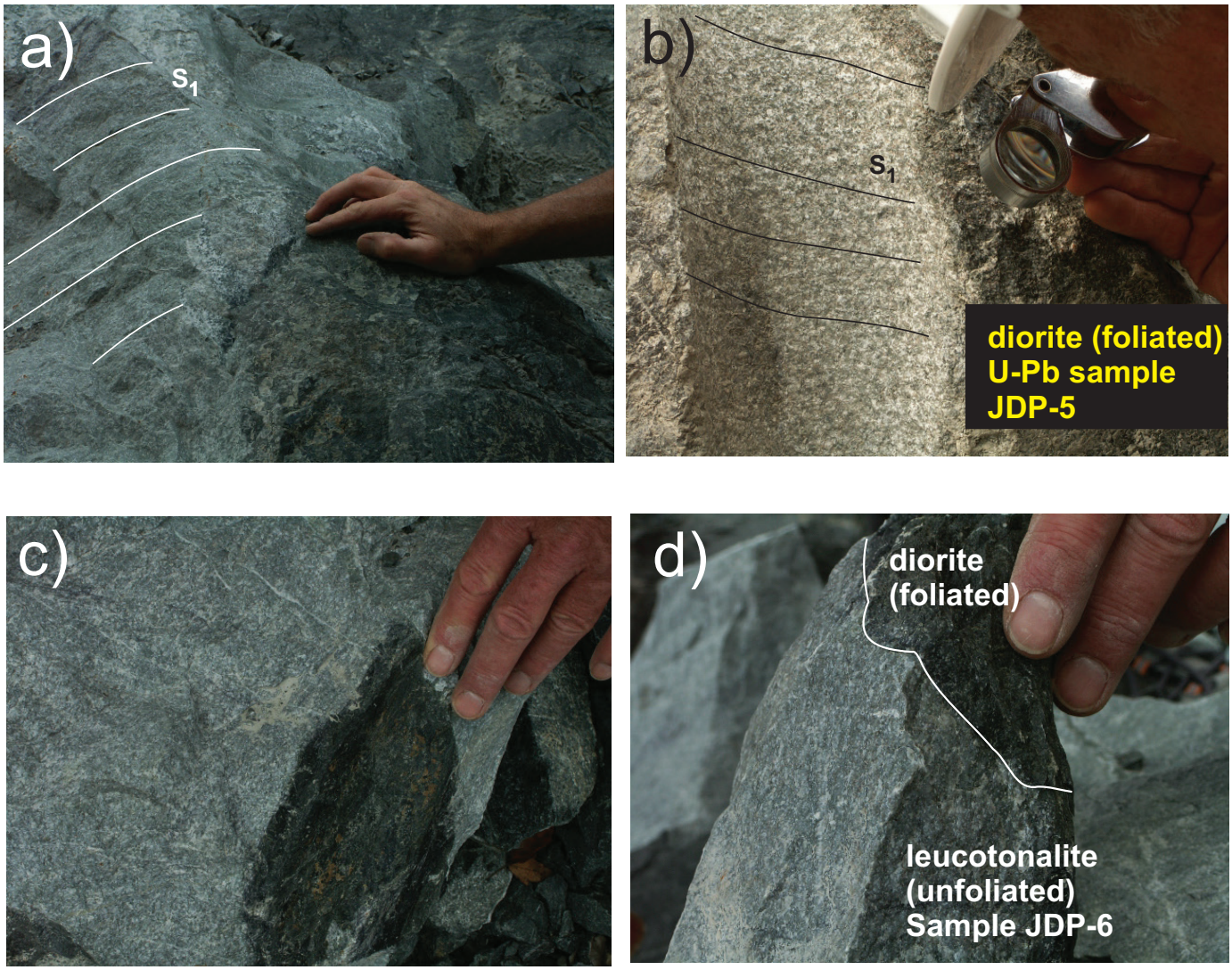


Fig. 4. Intrusive phases in the 'Jack Davis pit'. **a)** Ductile fabrics in metadiorite-metabasalt; UTM 473111E, 5364229N. **b)** Foliated diorite, U-Pb sample 08JDP-5, UTM 473111E, 5364229N. **c)** Pale green leucotonalite, unfoliated but with discrete brittle shears and well-foliated metabasalt inclusion, UTM 473190E, 5364262N; **d)** Unfoliated leucotonalite, U-Pb sample 08JDP-6 cutting foliated diorite, UTM 473190E, 5364262N.

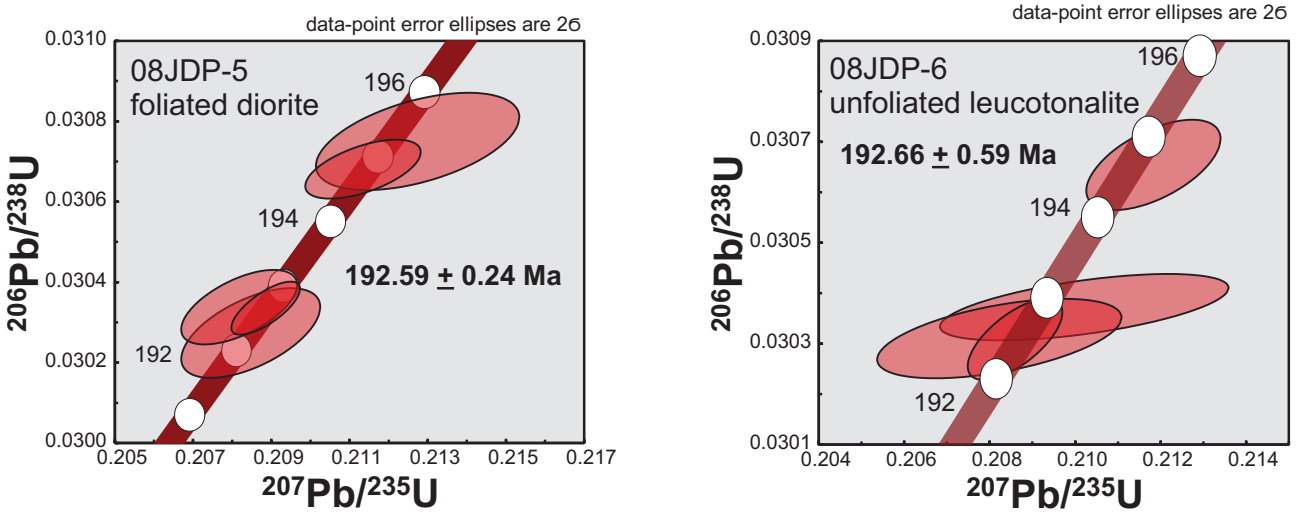


Fig. 5. U-Pb concordia plots for Wark-Colquitz complex intrusive phases.

Table 1. U-Pb zircon geochronological results for samples 08JDP-5 and 08JDP-6.

U-Th-Pb isotopic data

					Compositional Parameters					Radiogenic Isotope Ratios							Isotopic Ages					
Sample	Wt. mg	U ppm	$\frac{Th}{U}$	Pb ppm	$^{208}Pb^*$ x10^{-13} mol	mol % $^{206}Pb^*$	$\frac{Pb^*}{Pb_c}$	Pb_c (pg)	$\frac{^{206}Pb}{^{204}Pb}$	$\frac{^{208}Pb}{^{206}Pb}$	$\frac{^{207}Pb}{^{206}Pb}$	% err	$\frac{^{207}Pb}{^{235}U}$	% err	$\frac{^{206}Pb}{^{238}U}$	% err	corr. coef.	$\frac{^{207}Pb}{^{206}Pb}$	±	$\frac{^{207}Pb}{^{235}U}$	±	$\frac{^{206}Pb}{^{238}U}$	±
(a)	(b)	(c)	(d)	(c)	(e)	(e)	(e)	(e)	(f)	(g)	(g)	(b)	(g)	(b)	(g)	(b)		(i)	(b)	(i)	(b)	(i)	(b)
08JDP-5																							
A	0.005	192	0.286	5.8	1.2140	99.43%	50	0.57	3263	0.091	0.049941	0.245	0.208895	0.342	0.030337	0.177	0.730	192.26	5.69	192.62	0.60	192.65	0.34
B	0.005	263	0.415	8.7	1.6831	98.20%	16	2.53	1030	0.132	0.050181	0.876	0.212753	0.990	0.030749	0.320	0.498	203.39	20.32	195.86	1.76	195.24	0.61
C	0.005	188	0.340	5.9	1.1893	98.78%	23	1.21	1514	0.108	0.049775	0.470	0.208215	0.573	0.030339	0.249	0.596	184.51	10.94	192.05	1.00	192.67	0.47
D	0.005	377	0.291	11.5	2.3786	99.16%	34	1.65	2215	0.093	0.049953	0.573	0.208517	0.692	0.030275	0.301	0.579	192.80	13.32	192.31	1.21	192.27	0.57
E	0.005	364	0.317	11.5	2.3280	98.74%	23	2.44	1469	0.101	0.049966	0.482	0.211367	0.567	0.030681	0.194	0.575	193.40	11.20	194.70	1.00	194.81	0.37
08JDP-6																							
A	0.005	419	0.275	12.8	2.6526	99.26%	38.03	1.64	2483	0.088	0.050196	1.219	0.210217	1.313	0.030374	0.177	0.580	204.08	28.28	193.73	2.32	192.89	0.34
B	0.005	666	0.355	20.5	4.2055	99.48%	55.72	1.81	3553	0.113	0.049913	0.331	0.208590	0.433	0.030310	0.216	0.667	190.93	7.70	192.37	0.76	192.49	0.41
D	0.005	954	0.355	30.5	6.0987	98.76%	23.23	6.30	1490	0.113	0.050117	0.509	0.211832	0.607	0.030656	0.237	0.577	200.40	11.81	195.09	1.08	194.65	0.45
E	0.005	423	0.383	14.7	2.6736	96.07%	7.17	9.01	470	0.121	0.049822	1.028	0.208224	1.124	0.030312	0.212	0.527	186.70	23.92	192.06	1.97	192.50	0.40

(a) A, B, etc. are labels for fractions composed of single zircon grains or fragments; all fractions annealed and chemically abraded after Mattinson (2005).

(b) Nominal fraction weights estimated from photomicrographic grain dimensions, adjusted for partial dissolution during chemical abrasion.

(c) Nominal U and total Pb concentrations subject to uncertainty in photomicrographic estimation of weight and partial dissolution during chemical abrasion.

(d) Model Th/U ratio calculated from radiogenic $^{208}Pb/^{206}Pb$ ratio and $^{207}Pb/^{235}U$ age.

(e) Pb* and Pb_c represent radiogenic and common Pb, respectively; mol % $^{206}Pb^*$ with respect to radiogenic, blank and initial common Pb.

(f) Measured ratio corrected for spike and fractionation only. Daly analyses, based on analysis of NBS-982.

(g) Corrected for fractionation, spike, and common Pb; up to 3 pg of common Pb was assumed to be procedural blank: $^{206}Pb/^{204}Pb = 18.50 \pm 1.0\%$; $^{207}Pb/^{204}Pb = 15.50 \pm 1.0\%$; $^{208}Pb/^{204}Pb = 38.40 \pm 1.0\%$ (all uncertainties 1-sigma). Excess over blank was assigned to initial common Pb employing Stacey and Kramers model Pb at 195 Ma.

(h) Errors are 2-sigma, propagated using the algorithms of Schmitz and Schoene (2007) and Crowley et al. (2007).

(i) Calculations are based on the decay constants of Jaffey et al. (1971). $^{206}Pb/^{238}U$ and $^{207}Pb/^{206}Pb$ ages corrected for initial disequilibrium in $^{230}Th/^{238}U$ using Th/U [magma] = 3

(j) Corrected for fractionation, spike, and blank Pb only.

5. Conclusion

Precise 192.6 ±0.6 Ma U-Pb TIMS zircon dates from coexisting synkinematic and post-kinematic intrusive phases of the Wark-Colquitz complex in downtown Victoria document a brief deformation episode within the much longer, ca. 25 Ma history of the complex as the roots of the Triassic-Jurassic Bonanza magmatic arc. Given abundant outcrops in Victoria, oopportunities to unravel the history of the complex abound, and it is hoped that this very limited study will be succeeded by more thorough work to investigate of the magmatic and structural evolution of the complex, which will provide insight into subduction dynamics along the developing Cordilleran plate margin.

Acknowledgments

Philippe Erdmer instigated and led the field foray into the pit. Richard Friedman conducted the U-Pb zircon geochronology at Pacific Centre for Isotopic and Geochemical Research, University of British Columbia (Vancouver).

References cited

Acocella, V., 2014. Structural control on magmatism along divergent and convergent plate boundaries: Overview, model and problems. Earth-Science Reviews, 136, 226-288. <https://www.sciencedirect.com/science/article/abs/pii/S0012825214000907>

Breitsprecher, K., and Mortensen, J.K., 2004. B.C. Age 2004-1 (release 3, October 2004) - A database of isotopic age determinations for rock units from British Columbia. British Columbia Ministry of Energy and Mines, British Columbia Geological Survey Open File 2004-03, MS-Access database.

British Columbia Geological Survey, 2019. British Columbia Digital Geology. British Columbia Ministry of Mining and Critical Minerals, British Columbia Geological Survey. Data version 2019-12-19. <https://www2.gov.bc.ca/gov/content/industry/mineral-exploration-mining/british-columbia-geological-survey/geology/bcdigitalgeology>

Buritica, L.F., Schwartz, J.J., Klepeis, K.A., Miranda, E.A., Tulloch, A.J., Coble, M.A., and Kylander-Clark, A.R.C., 2019. Temporal and spatial variations in magmatism and transpression in a Cretaceous arc, Median Batholith, Fiordland, New Zealand. Lithosphere, 11. 652-682. <https://doi.org/10.1130/L1073.1>

Canil, D., Styan, J., Larocque, J., Bonnet, E., and Kyba, J., 2010. Thickness and composition of the Bonanza arc crustal section, Vancouver Island, Canada. Geological Society of America Bulletin, 122, 1094-1105.

Canil, D., Johnson, S.T., Larocque, J., Friedman, R., and Heaman, L.M., 2013. Age, construction, and exhumation of the mid-crust of the Jurassic Bonanza arc, Vancouver Island, Canada. Lithosphere, 5, 82-91.

Colpron, M., 2020. Yukon terranes-A digital atlas of terranes for the northern Cordillera. Yukon Geological Survey. <https://data.geology.gov.yk.ca/Compilation/2#InfoTab>

deBari, S., Anderson, R.G., and Mortensen, J.K., 1999. Correlation among lower to upper crustal components in an island arc: The Jurassic Bonanza arc, Vancouver Island, Canada. Canadian Journal of Earth Sciences, 36, 1371-1413.

de Saint Blanquat, M., Tikoff, B., Teyssier, C., and Vigneresse, J.L., 1998. Transpressional kinematics and magmatic arcs. In: Holdsworth, R.E., Strachan, R.A., and Dewey, J.F., (Eds.), Continental Transpressive and Transtensional Tectonics. Geological Society of London, Special Publication 135, pp. 327-340.

Gehrels, G., Wang, J., Kapp, P., and Pecha, M., 2026. Sinistral shear zones along the central and southern portions of coastal British Columbia, Canada. In: Gordon, S.M., Miller, R.B., Rusmore, M.E., and Tikoff, B., (Eds.), Jurassic-Paleogene Tectonic Evolution of the North American Cordillera, Geological Society of America Special Paper 565. <https://doi.org/10.1130/2025.2565(07)>

Harrichhausen, H., Finley, T., Morell, K.D., Regalla, C., Bennett, S.E.K., Leonard, L.J., Nissen, E., McLeod E., Lynch, E.M., Salomon, G., and Sethanant, I., 2023. Discovery of an active forearc fault in an urban region: Rupture on the XEOLXELEK-Elk Lake fault, Victoria, British Columbia, Canada. Tectonics, 42, article e2023TC008170. <https://doi.org/10.1029/2023TC008170>

Isachsen, C., 1984. Geology, geochemistry and geochronology of the Westcoast Crystalline complex and related rocks, Vancouver Island, British Columbia. M.Sc. thesis, The University of British Columbia, 155 p.

Krogh, T.E., 1982. Improved accuracy of U-Pb zircon ages by the creation of more concordant systems using an air abrasion technique. Geochimica et Cosmochimica Acta, 46, 637-649.

Larocque, J., 2008. The role of amphibole in the evolution of arc magmas and crust: The case from the Jurassic Bonanza arc section, Vancouver Island, Canada. M.Sc. thesis, University of Victoria, 160 p.

Ludwig, K.R., 1980. Calculation of uncertainties of U-Pb isotope data. Earth and Planetary Science Letters 46, 212-220.

Muller, J.E., 1983. Geology of Victoria. Geological Survey of Canada Map 1553A, 1:100,000 scale.

Nixon, G.T., and Orr, A.J., 2007. Recent revisions to the early Mesozoic stratigraphy of Vancouver Island and metallogenetic implications, British Columbia. In: Geological Fieldwork 2006, British Columbia Ministry of Energy, Mines and Petroleum Resources, British Columbia Geological Survey Paper 2007-1, pp. 163-177.

Nixon, G.T., Hammack, J.L., Koyanagi, V.M., Snyder, L.D., Payie, G.J., Panteleyev, A., Massey, N.W.D., Hamilton, J.V., Orr, A.J., Friedman, R.M., Archibald, D.A., Haggart, J.W., Orchard, M.J., Tozer, E.T., Tipper, H.W., Poulton, T.P., Palfy, J., and Cordey, F., 2011. Geology, geochronology, lithogeochemistry and metamorphism of the Holberg-Winter Harbour area, northern Vancouver Island (parts of NTS 92L/05, 12, 13; 102I/08, 09 and 16). British Columbia Ministry of Energy and Mines, British Columbia Geological Survey Open File 2011-01, 1:50,000 scale.

Parrish, R., Roddick, J.C., Loveridge, W.D., and Sullivan, R.W., 1987. Uranium-lead analytical techniques at the geochronology laboratory, In: Radiogenic Age and Isotopic Studies, Report 1, Geological Survey of Canada, Paper 87-2, pp. 3-7.

Roddick, J.C., 1987. Generalized numerical error analysis with application to geochronology and thermodynamics. Geochimica et Cosmochimica Acta, 51, 2129-2135.

Thirlwall, M.F., 2000. Inter-laboratory and other errors in Pb isotope analyses investigated using a ^{207}Pb-^{204}Pb double spike. Chemical Geology, 163, 299-322.

Age and geochemistry of middle to late Paleozoic volcanism along the western edge of Ancestral North America in north-central British Columbia

Filippo Ferri[1, a], and Richard Friedman[2]

[1] Emeritus Scientist, British Columbia Geological Survey, Ministry of Mining and Critical Minerals, Victoria, BC, V8W 9N3
[2] Pacific Centre for Isotopic and Geochemical Research, Earth and Ocean Sciences, The University of British Columbia, Vancouver, BC, V6T 1Z4
[a] corresponding author: Filippo.Ferri@gov.bc.ca

Recommended citation: Ferri, F., and Friedman, R., 2026. Age and geochemistry of middle to late Paleozoic volcanism along the western edge of Ancestral North America in north-central British Columbia. In: Geological Fieldwork 2025, British Columbia Ministry of Mining and Critical Minerals, British Columbia Geological Survey Paper 2026-01, pp. 183-201.

Abstract

Legacy U-Pb zircon analyses from samples collected during systematic mapping in north-central British Columbia in the late 1980s and 1990s yielded ages of ca. 350 to 320 Ma for rocks of the Big Creek Group at the top of the Cassiar terrane (Ancestral North America) section near Germansen Landing and the Osilinka River (Gilliland tuff) and ca. 255 Ma from felsic tuffs occupying the upper part of Big Creek sratigraphy in the north. A sample from the upper part of the Lay Range assemblage, the local basement to the Upper Triassic to Lower Jurassic Nicola Group arc volcanic rocks in Quesnel terrane yielded an age of ca. 275 Ma. Lithogeochemical data (whole rock, trace, and rare earth element) for the Lay Range assemblage are consistent with eruption in an arc setting. Geochemical data for felsic rocks from the Big Creek Group suggest derivation from continental lithosphere. Geochemical results for mafic igneous rocks in the Big Creek Group indicate within-plate affinities. Sm-Nd isotopic geochemistry suggests an older, evolved, continental lithosphere as the source of magma that supplied the Big Creek Group felsic volcanic rocks. Isotopic data from the Lay Range assemblage point to a less evolved, mantle source.

Keywords: U-Pb zircon geochronology, Sm/Nd isotopes, geochemistry, Lay Range assemblage, Big Creek Group, Ingenika Group, Cassiar terrane, Quesnel terrane, Gilliland tuff

1. Introduction

In the late 1980s and 1990s, the British Columbia Geological Survey carried out a systematic mapping program near the Lay Range in the north-central part of the province (Fig. 1) focused on a corridor of metal-rich volcanic and intrusive rocks of Quesnel terrane and adjoining rocks of Ancestral North America (Ferri, 1989; Ferri and Melville, 1988a, b, 1989a, b, 1990a, b, 1994; Ferri et al., 1988, 1989, 1992a, b, 1993a, b; Ferri, 1997, 2000; Ferri et al., 2001a, b). In addition, workers examined Alaskan-type ultramafic rocks in the area (Nixon et al., 1993, 1998) and mapped the northern extent of Triassic volcanic rocks in Quesnellia (Schiarizza, 2004; Schiarizza et al., 2004; Schiarizza et al., 2005; Schiarizza and Tan, 2005; MacIntyre et al., 2005). More recently, Ootes et al. (2019a, b, 2020a, b) investigated the northern half of Hogem batholith and provided fossil and detrital zircon U-Pb constrains on the timing of deposition of the lower sedimentary division of the Lay Range assemblage (Ootes et al., 2022).

This paper presents previously unreleased vintage multigrain U-Pb zircon data on samples collected as part of regional mapping. Four samples are from the Big Creek Group at the top of the Cassiar terrane section (Ancestral North America), and one is from the Lay Range assemblage, the local basement to Nicola Group arc volcanic rocks that are predominant in Quesnel terrane. We also present lithogeochemical and Sm-Nd isotopic data from these and other units.

2. Location and geological setting

Regional mapping of the late 1980s and 1990s spanned the area between Manson Creek and the Lay Range (Fig. 2). Road access is afforded by an all-season forestry road network extending from Manson Creek to Germansen Landing and continues north to Aiken and Johanson lakes. Samples were collected near Germansen Landing, Wasi Lake, northeast of Aiken Lake, and in the Lay and Wrede ranges (Fig. 3).

The area straddles the boundary between rocks of Ancestral North America, here represented by the Cassiar terrane, and those of oceanic and arc affinities belonging to the Slide Mountain and Quesnel terranes (Fig. 1). The Cassiar terrane section includes Neoproterozoic siliciclastic and carbonate rocks of the Ingenika Group that are overlain by a predominantly carbonate succession of Cambrian to Middle Devonian rocks (Fig. 4). At the top of the stratigraphic section are Upper Devonian to Permian dark shales of the Big Creek Group that contain felsic volcanic rocks, which we sampled for geochronologic study (Fig. 5). The northward disappearance of the lower and middle Paleozoic succession between the Wrede-Lay ranges section and the Manson Creek-Wasi Lake section (Fig. 4) suggests a

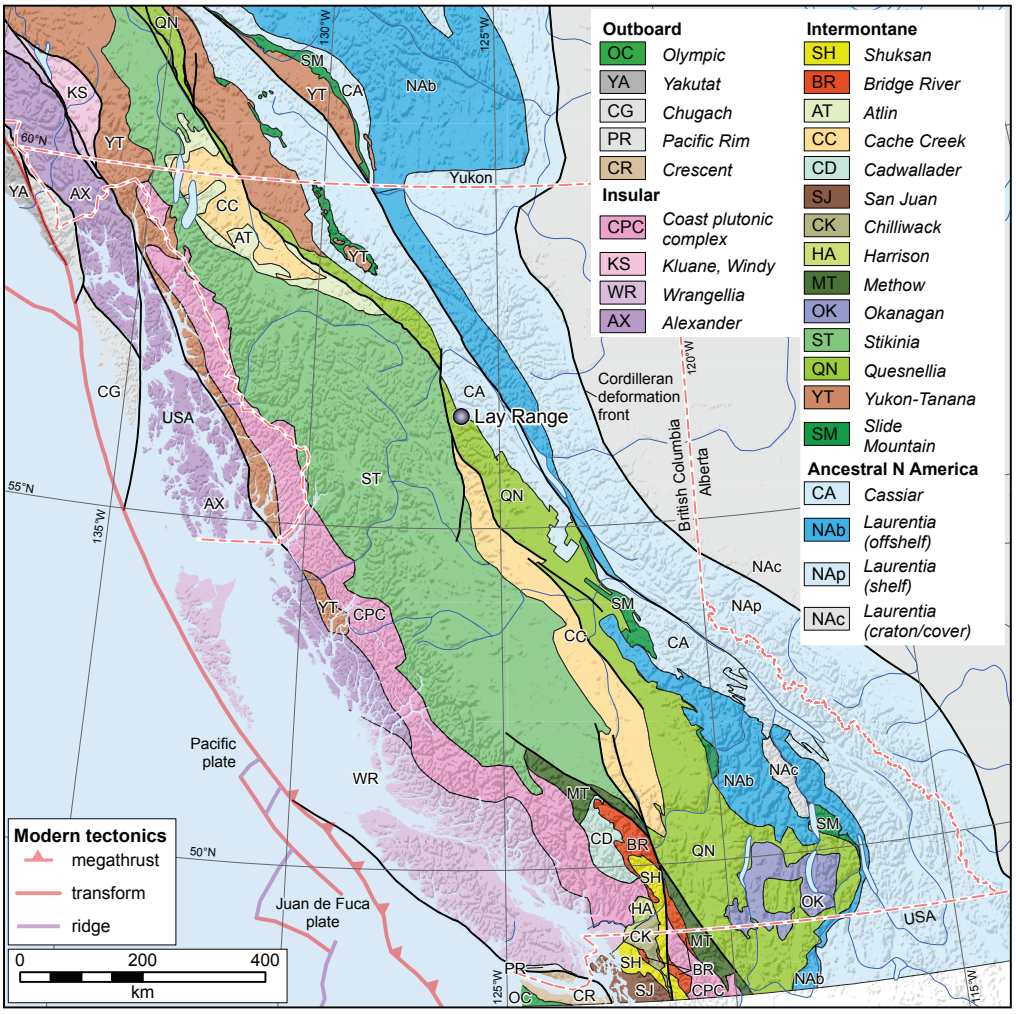


Fig. 1. Tectonic elements of the Canadian Cordillera in British Columbia and location of study area. Terranes after Colpron (2020).

major unconformity at the base of the Big Creek Group in the north. South of Wasi Lake, upper Paleozoic mafic volcanic and sedimentary rocks of the Slide Mountain terrane (Nina Creek Group) sit structurally above Cassiar terrane rocks (Fig. 4). This structurally interleaved sequence represents rocks of oceanic affinity that are considered to have been emplaced onto Cassiar rocks in the Early Jurassic. In the same structural position north of Wasi Lake are upper Paleozoic rocks of the Lay Range assemblage, which constitute basement to the Upper Triassic to Lower Jurassic mafic to intermediate arc volcanic rocks that are predominant in Quesnel terrane (Figs. 2, 4).

The Lay Range assemblage is subdivided into the "lower sedimentary" and "upper mafic tuff" divisions (Fig. 6). The lower sedimentary division is Late Mississippian to Middle Pennsylvanian (Ferri, 1997; Ootes et al., 2022) and consists of siliciclastic, carbonate, and mafic volcanic rocks. The 'upper mafic tuff' division is Middle Pennsylvanian to Permian and contains mafic flows to fragmental volcanic rocks with local felsic units. Above the Lay Range assemblage basement are predominantly volcanic rocks which, as discussed by Ootes et al. (2020a), are referred to in Quesnel terrane as the Nicola Group (Fig. 2); equivalent rocks in Stikine terrane are termed the Takla Group. The multiphase Hogem batholith has Late Triassic to Early Jurassic phases likely comagmatic with the Nicola Group and later post-accretionary Cretaceous intrusions (e.g., Ootes et al., 2020a, b).

3. U-Pb zircon geochronology

We carried out U-Pb zircon geochronology on four samples from the Big Creek Group, and one from the Lay Range assemblage (Fig. 2). Big Creek analyses include two from the Gilliland tuff and two from felsic tuff in the upper part of the unit.

3.1. Methods

Zircons were separated from a ~20 kg sample using conventional crushing, grinding, Wilfley table, heavy liquids and Frantz magnetic separator techniques. U-Pb analyses were done by University of British Columbia using methods for zircon grain selection, abrasion, dissolution, geochemical

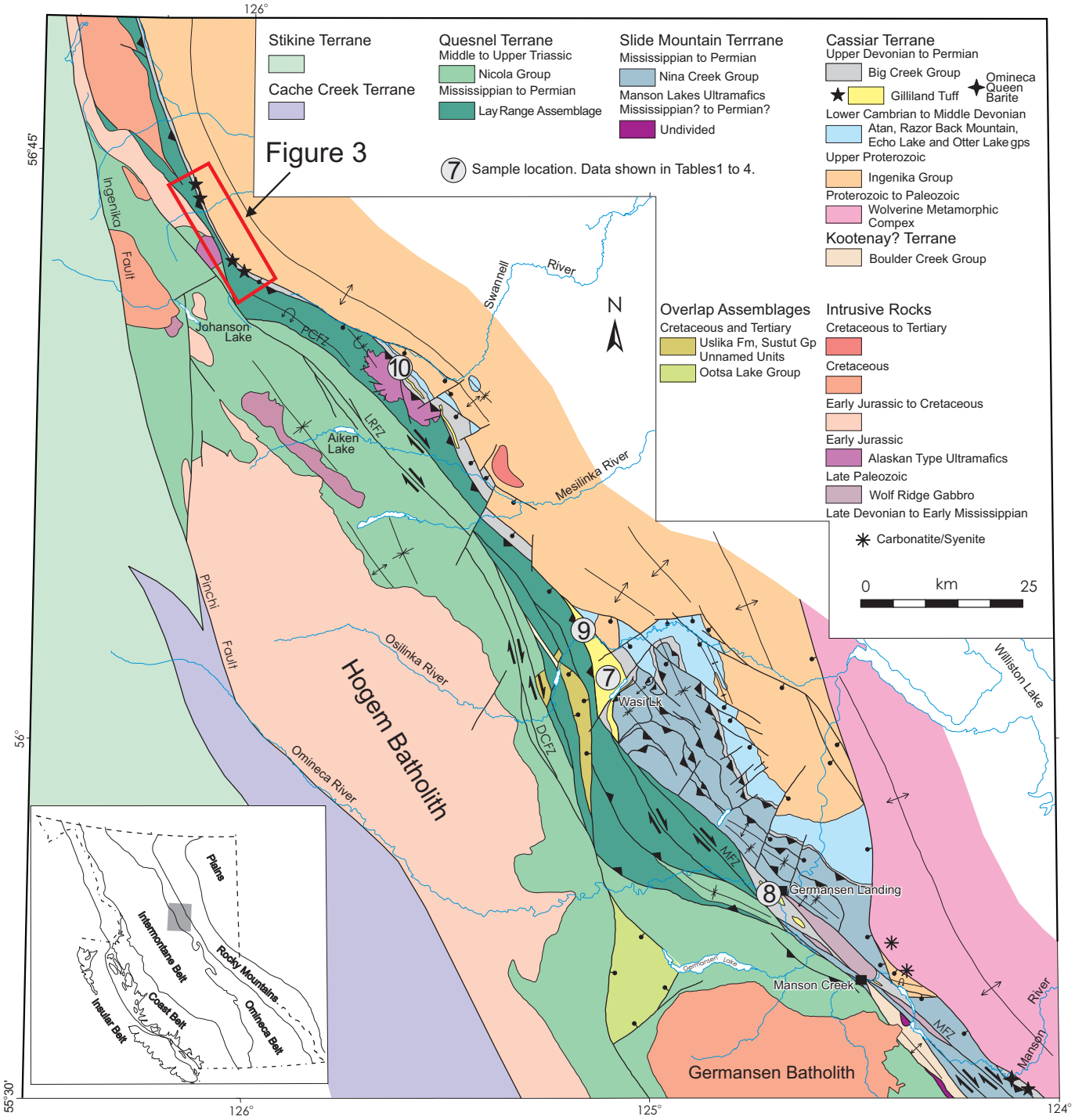


Fig. 2. Regional geological map.

preparation, and mass spectrometry as described by Mortensen et al. (1995). Procedural blanks for Pb and U were 2 and 1 pg, respectively. Errors attached to individual analyses were calculated using the numerical error propagation method of Roddick (1987). Decay constants used are those recommended by Steiger and Jäger (1975). Compositions for initial common Pb were taken from the model of Stacey and Kramer (1975). All errors are given at the 2 sigma level.

3.2. Results

3.2.1. Big Creek Group, Gilliland tuff, sample FFe88-34-2

We resampled rocks at the type locality of the Gilliland tuff near Germansen Landing (Figs. 2, 5) that previously yielded a minimum U-Pb age of 377 ±12 Ma but with evidence of inheritance and lead loss (Ferri and Melville, 1994).

Abundant pale yellow, clear zircon was recovered from the

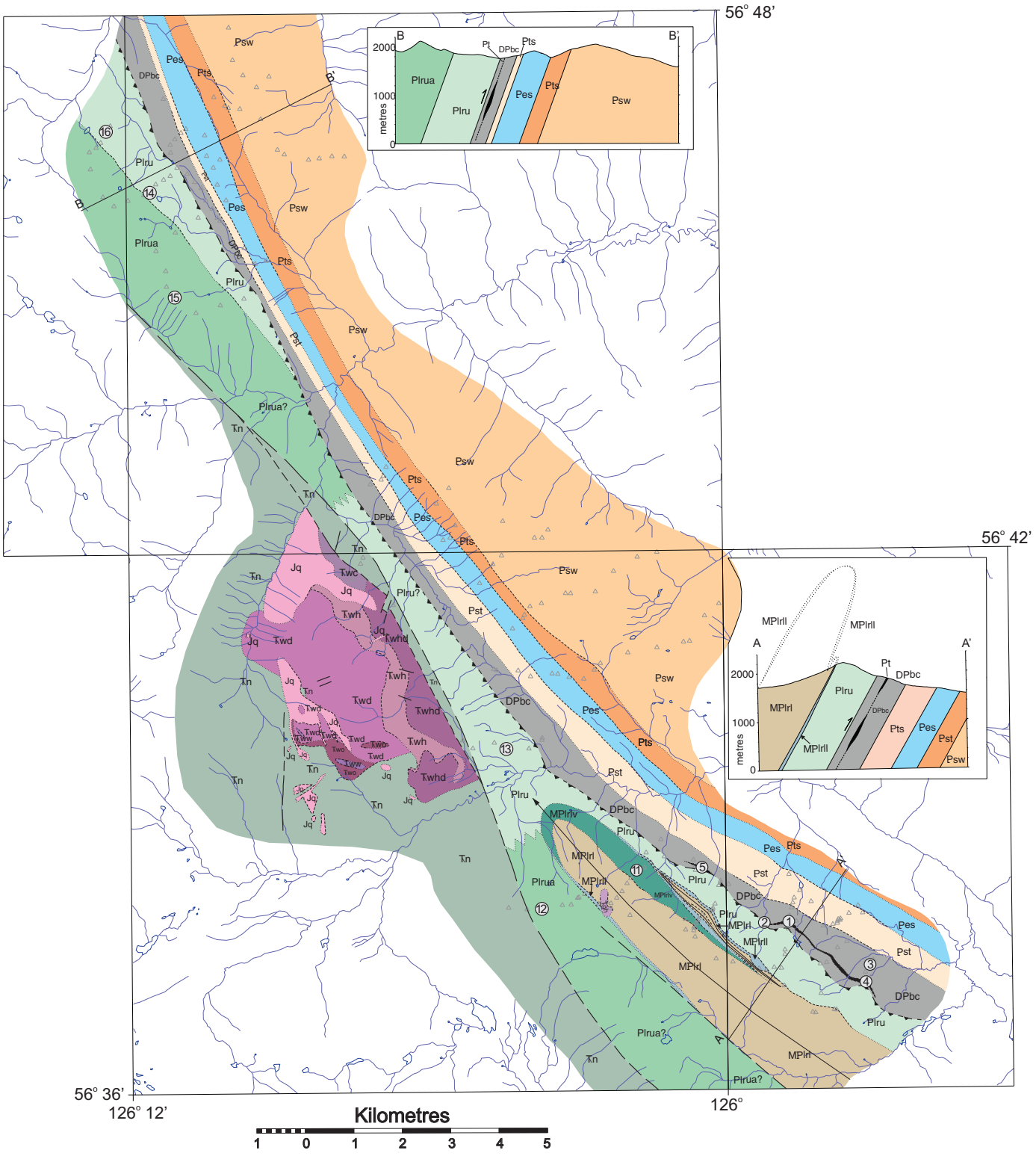


Fig. 3a. Geology of the Lay and Wrede ranges.

MIDDLE JURASSIC

Jq — Buff-white weathering, white to pale grey, medium grained, equigranular hornblende-bearing quartz monzonite/monzonite/quartz diorite/diorite

LATE TRIASSIC

Wrede Complex

Ʇwhd — Pale grey to black weathering, fine to coarse grained hornblende diorite or gabbro/clinopyroxene-hornblende diorite or gabbro plagioclase

Ʇwh — Medium brown weathering, coarse grained hornblende clinopyroxenite

Ʇwc — Dark to medium grey-green weathering, medium to coarse grained undifferentiated clinopyroxenite, includes hornblende clinopyroxenite, olivine clinopryoxenite and olivine-hornblened clinopyroxenite

Ʇwo — Medium to pale grey-green weathering, medium to coarse grained olivine clinopyroxenite

Ʇww — Dark to medium brown weathering predominantly medium grained or medium to coarse grained wehrlite

Ʇwd — Pale buff-orange weathering, dark grey to black, fine to medium grained dunite

Ʇgh — Rusty weathering, grey-green, biotite-bearing gabbro and grey to orange weathering coarsely crystalline hornblendite

Nicola Group

Ʇn — Pale to medium grey-green weathering, dark grey-green augite-feldspar bearing volcanic breccia, tuffs and flows

Lay Range assemblage

MIDDLE PENNSYLVANIAN? TO PERMIAN

Upper Mafic Tuff division

PIrua — Grey-geen or maroon weathering, pale to dark green and maroon, feldspar-pyroxene lapilli tuffs volcanic breccia, flows and lesser crystal tuffs. Rare grey limestone

PIru — Pale greenish grey to green weathering, green to grey green thin to thickly bedded and well laminated tuff. Locally dark green aphanitic basalt with associated lapilli tuff and volcanic breccia. Rare rusty weathering, quartz-bearing tuff to sericite schist

Lower Sedimentary division

LATE MISSISSIPPIAN TO MIDDLE PENNSYLVANIAN

MPIrll — Grey to buff weathering grey limestone. Massive to platy, locally bioclastic with interlayers of beige to pale grey chert. Locally contains maroon and green siltstone or tuffaceous horizons. Tan to buff weathering white to cream recrystallized massive dolomite

MPIrlv — Grey-brown weathering, dark green, aphanitic basalt, lesser volcanic breccia and tuff. Locally spheriolitic. Pale to green, medium to coarsely crysalline gabbro to quartz monzonite, locally foliated

MPIrl — Thick to massively bedded, beige to brown weathering tan to greenish brown calcareous sandstone, very fine to granule conglomerate. Interlayered with black argillite, green tuffaceous siltstone, thin bedded whiite to grey chert and brown to orange weathering grey platy limestone

LATE DEVONIAN TO PERMIAN

Big Creek Group

DPbc — Dark grey, dark blue-grey to black slate and thin to moderately bedded argillite. Minor horizons of dark grey to black quartz-chertz wackes, sandstones and lesser granule conglomerate. ★ Locally contains thin horizons of light coloured quartz-feldspar-bearing felsic tuff and dark green basalt.

Pt — Rusty to tan weathering, pale grey to dark grey or greenish grey, quartz-feldspar tuff to lapilli tuff. Sericitic and locally contains pryrite and ankerite porphyroblasts. Minor argillite clasts. Locally contains tan to grey weathering, very fine to medium crystalline diorite or quartz diorite which can be associated with dark green basalt.

LATE PROTEROZOIC

Ingenika Group

Stelkuz Formation

Pst — Rusty brown weathering, greenish grey slate, lesser thin to massively bedded cream impure quartzite and quartz sandstone and thinly bedded, grey limestone

Espee Formation

Pes — Grey to buff weathering, platy and blocky, finely recrystallized limestone and dolomitic limestone, grey calcareous slate. Cross-cutting zones of orange weathering, coarsely crystalline dolostone are locally present.

Tsaydiz Formation

Pts — Thinly interlayered, grey to orange-brown weathering, grey to green-grey slate, calcareous slate and grey to orange weathering, grey limestone.

Swannell Formation

Psw — Thickly bedded, grey-green to green, feldspar-bearing quartz sandstone to wacke, quartz sandstone, slate, siltstone, impure quartzite and rare grey limestone. Schistose in its lowest parts, locally containing biotite porphyroblasts.

Geologic boundary (approximate, assumed):

Thrust Fault (approximate, assumed):

Fault, unknown displacement (approximate, assumed):

Fold axis, overturned (anticline, syncline):

Field station: △

⑫ Sample location. Data shown in Tables1 to 4.

Fig. 3b. Legend.

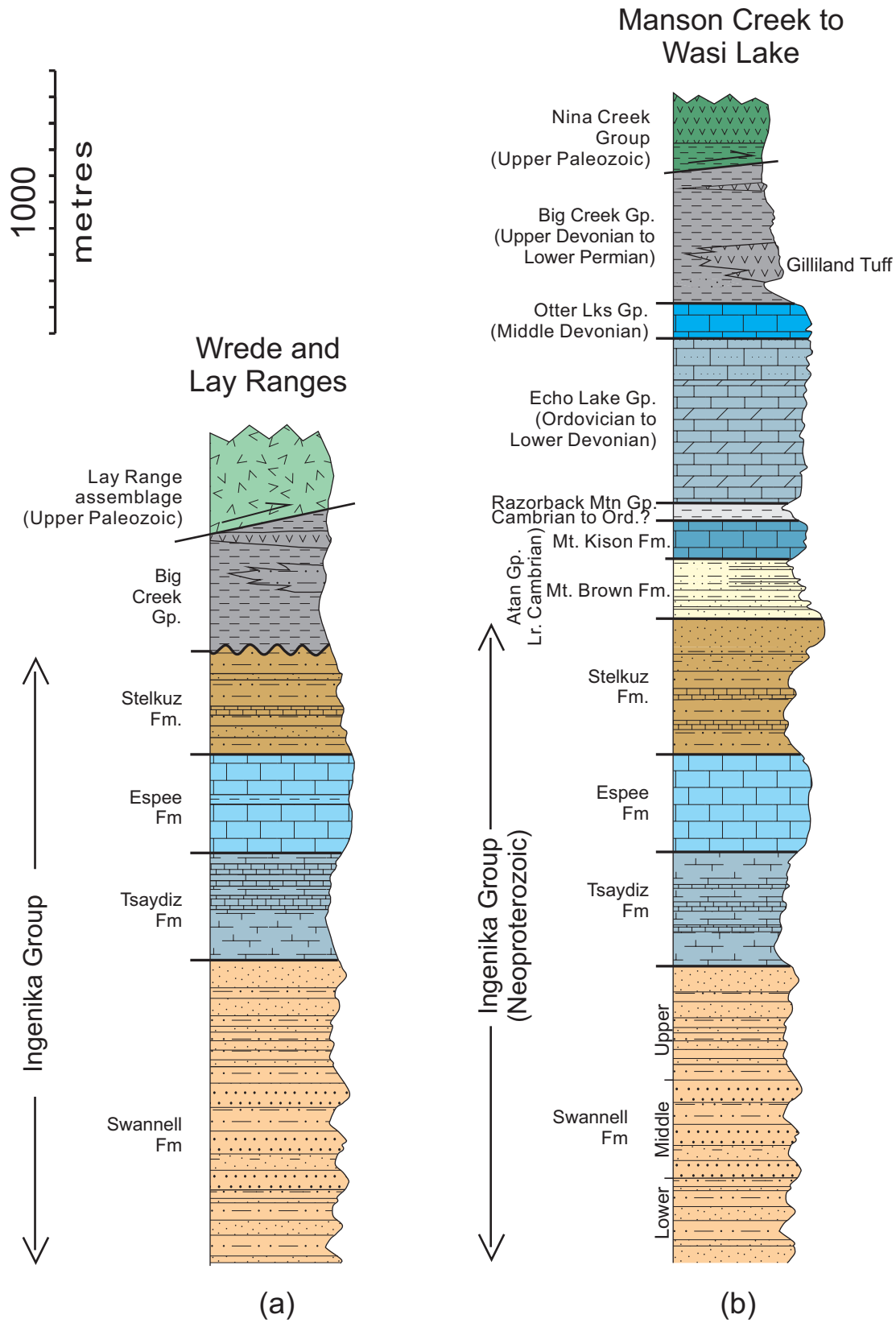


Fig. 4. Cassiar terrane generalized stratigraphic columns. **a)** Wrede and Lay ranges. **b)** Manson Creek to Wasi Lake. The column in b) shows the removal of Lower Paleozoic stratigraphy below the sub-Big Creek unconformity.

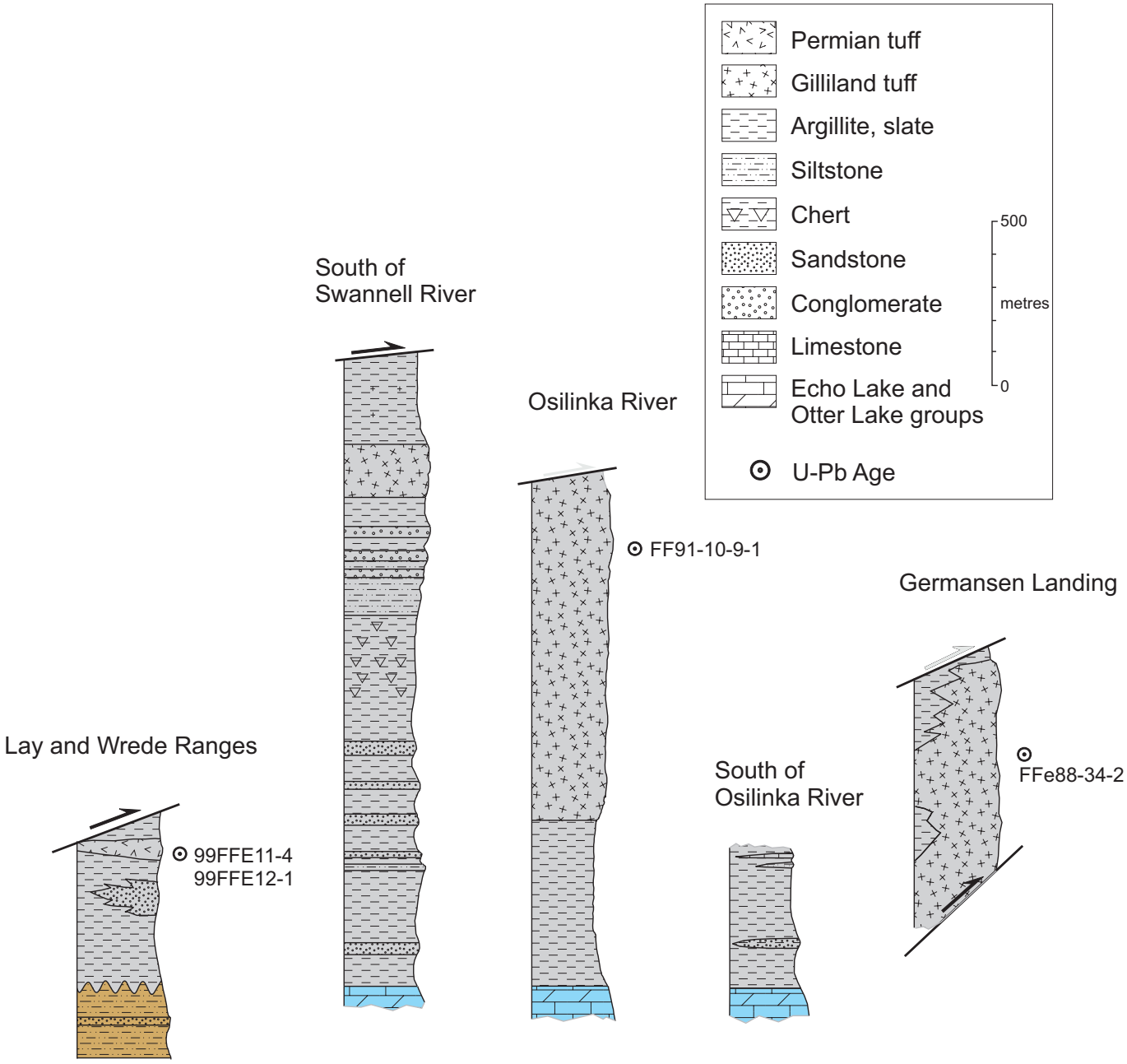


Fig. 5. Local stratigraphic columns and context of Big Creek Group geochronologic samples.

sample. The zircons included stubby to elongate prismatic grains and equant to stubby prismatic multifaceted grains that appeared to represent a single population. Evidence of detrital or xenocrystic components was lacking but cloudy cores were present in a small proportion of the grains. Zircon grains with fractures parallel to the c-axis, and ones with elongate clear tube- or rod-shaped inclusions that passed through the centres of the grains were considered to be least likely to include inherited cores, and these grains were specifically selected for analysis in an attempt to minimize the possibility of inherited zircon. Approximately 30 grains were picked from the coarsest, least magnetic fraction, strongly abraded (Krogh, 1982) to minimize the effects of post-crystallization Pb-loss, and split into five multi-grain fractions for analysis. A sixth fraction comprising fine, clear, elongate prismatic grains was also selected and analyzed without abrasion.

The analytical results (Table 1) indicate that this approach to grain selection was reasonably successful. Selection of grains that contained significant numbers of inclusions results in a somewhat higher proportion of common Pb in the analyses, and consequently slightly less precise analyses. Fraction D gave a slightly younger $^{206}Pb/^{238}U$ age, which is interpreted

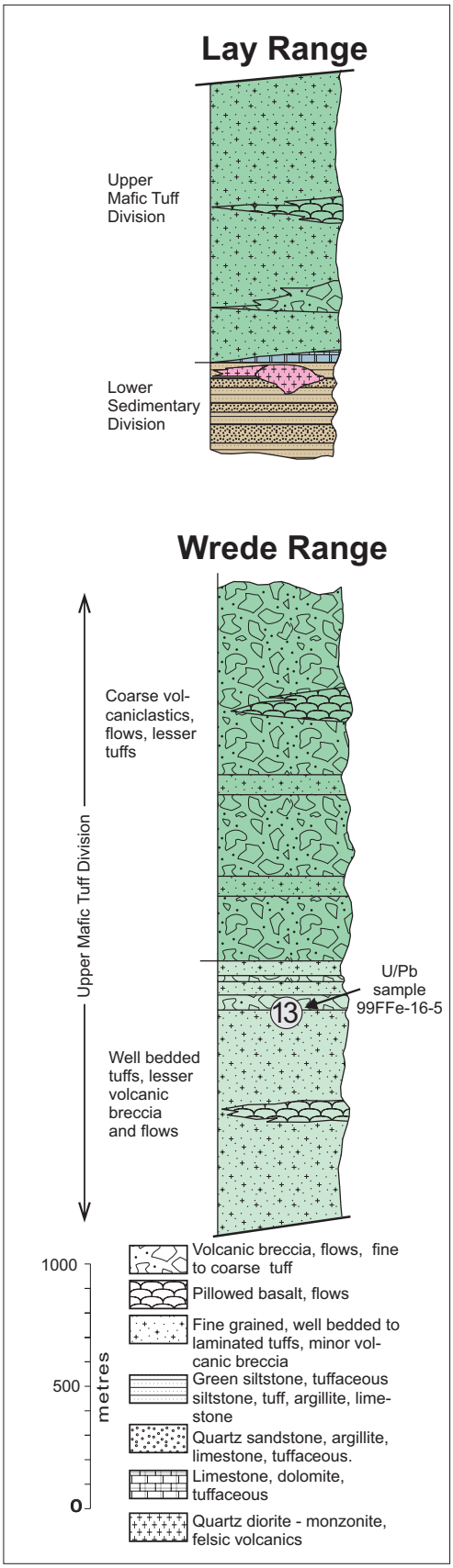


Fig. 6. Generalized stratigraphic columns of the Lay Range assemblage in the Wrede and Lay Ranges.

to indicate minor Pb-loss effects that were not completely eliminated by the strong abrasion. Fraction F, which was not abraded, yielded a much younger $^{206}Pb/^{238}U$ age, indicating significant post-crystallization Pb-loss. Fraction E gave a slightly older $^{206}Pb/^{238}U$ age and fractions A and C give much older $^{206}Pb/^{238}U$ ages, indicating that these fractions contained a significant component of older inherited zircon despite efforts to avoid this complication (Figs. 7a, b). Two-point regressions through fraction B and the two most discordant fractions yield calculated upper concordia intercept ages of 2.06 and 2.71 Ga. This gives an indication of the range of ages of the inherited zircon component in the sample. However, two of the fractions (B and D) yielded concordant analyses (Figs. 7a, b). Fraction B gives the oldest $^{206}Pb/^{238}U$ age of 354.5 ±0.9 Ma, which is considered to be the best estimate for the crystallization age of the sample.

3.2.2. Big Creek Group, Gilliland tuff, sample FF91-10-9-1

Sample FF91-10-9-1 is a slightly foliated quartz and feldspar tuff, collected from the Gilliland tuff unit of the Big Creek Group near Osilinka River (Figs. 2, 5). Five multi-grain zircon fractions were analyzed in 1993 (Table 2; Figs. 7c, d). The coarse fractions C and F (Table 2) are highly discordant due to a large component of inherited zircon. The other three fractions all plot near concordia. Fraction A is concordant at 319 ±31 Ma (Fig. 7d), which is considered the age of crystallization, although an older age should not be ruled out considering the effects of lead loss. An upper limit of 417.1 ±4.0 Ma is the $^{206}Pb/^{238}U$ age of fraction D, the oldest of the three nearly concordant fractions.

3.2.3. Big Creek Group, felsic tuff, sample 99FFE11-4

This felsic tuff yielded clear, pink, euhedral and rarely slightly rounded prismatic grains. Six multi-grain zircon fractions were analyzed (Table 1; Fig. 8a). Fraction F is marginally concordant; it is interpreted to have suffered minor Pb loss and to contain no inherited zircon. Fraction B likely contains inheritance and underwent minor Pb loss. Concordant fraction E and discordant fractions A, D, and C define a linear array of data. The former fraction yielded a $^{206}Pb/^{238}U$ age of 253.6 ±0.5 Ma and also anchors a lower intercept through discordant fractions A-D, and is therefore considered as the best estimate for the age of the rock. The upper intercept of a chord fit to the data gives an upper intercept of 2.5 ±0.3 Ga (mean square weighted deviation=0.56), which provides an estimate for the age of inherited zircon in the latter fractions.

3.2.4. Big Creek Group, felsic tuff, sample 99FFE12-1

This felsic tuff yielded clear, pink, stubby to elongate zircons. Four fractions were analyzed, three of which are strongly discordant (A, B, and C; Table 1; Fig. 8b). Based on the data alone this rock could be as young as ca. 236 Ma.

Table 1. Multigrain U-Pb zircon analyses performed at Pacific Centre for Isotopic and Geochemical Research, Earth and Ocean Sciences, University of British Columbia in 2000.

Fraction[1]	Wt	U[2]	Pb[3]	^{206}Pb[4]	Pb[5]	^{208}Pb[3]	Isotopic ratios (±1-sigma, %)[6]			Apparent ages (±2-sigma, Ma)[6]		
	mg	ppm	ppm	^{204}Pb	pg	%	$^{206}Pb/^{238}U$	$^{207}Pb/^{235}U$	$^{207}Pb/^{206}Pb$	$^{206}Pb/^{238}U$	$^{207}Pb/^{235}U$	$^{207}Pb/^{206}Pb$
99FFE11-4 Big Creek Group felsic tuff[a] (location 4 on Fig. 3)												
A cc,N2,p,1	0.020	364	15	2206	8.4	12	0.04033 (0.13)	0.2881 (0.22)	0.05181 (0.15)	254.9 (0.6)	257.0 (1.0)	276.9(6.8)
B c,N2,p,7	0.030	696	29	224	255	13	0.03983 (0.28)	0.2875 (0.95)	0.05236 (0.77)	251.8 (1.4)	256.6 (4.3)	301(35/36)
C c,N2,p,13	0.050	680	28	2328	38	11	0.04050 (0.11)	0.2932 (0.20)	0.05251 (0.12)	255.9 (0.5)	261.1 (0.9)	307.5(5.3)
D m,M2,p,30	0.040	409	17	3023	14	12	0.04045 (0.10)	0.2913 (0.18)	0.05223 (0.11)	255.6 (0.5)	259.6 (0.8)	295.5(5.1)
E f,N2,p,p,e	0.040	403	16	5614	7.1	10	0.04012 (0.10)	0.2837 (0.18)	0.05129 (0.12)	253.6 (0.5)	253.6 (0.8)	253.8(5.3)
F ff,N2,p,p,e	0.015	331	13	5460	2.2	11	0.03934 (0.20)	0.2782 (0.27)	0.05130 (0.21)	248.7 (1.0)	249.3 (1.2)	254.2(9.6)
99FFE12-1 Big Creek Group felsic tuff[a] (location 5 on Fig. 3)												
A m,N2,p,s,3	0.025	505	52	16530	4.5	12	0.09526 (0.10)	1.5484 (0.16)	0.11789 (0.07)	586.6 (1.1)	949.9 (1.9)	1924.5(2.6)
B f,N2,p,s,15	0.035	385	26	4537	12	11	0.06518 (0.10)	0.7475 (0.17)	0.08319 (0.09)	407.0 (0.8)	566.8 (1.5)	1273.5(3.4)
C f,N2,p,s,23	0.030	215	16	2354	12	15	0.06959 (0.10)	0.8318 (0.18)	0.08669 (0.11)	433.7 (0.8)	614.6 (1.6)	1353.6(4.2)
D ff,N2,p,e,25	0.010	256	9.8	1336	4.5	11	0.03741 (0.15)	0.2646 (0.31)	0.05130 (0.26)	236.7 (0.7)	238.4 (1.3)	254(12)
99FFE16-5 Lay Range assemblage felsic tuff[a] (location 13 on Fig. 3)												
A f,N2,p,na	0.015	113	5.4	1853	2.5	17	0.04356 (0.29)	0.3110 (0.54)	0.05179 (0.47)	274.8 (1.5)	275.0 (2.6)	276(22)
B f,N2,b,na	0.015	176	9.7	3794	2.2	19	0.04967 (0.17)	0.3645 (0.27)	0.05322 (0.22)	312.5 (1.1)	315.6 (1.5)	338(10)
C ff,N2,p,b,na	0.010	357	21	1840	6.5	16	0.05294 (0.13)	0.4864 (0.26)	0.06664 (0.19)	332.5 (0.9)	402.5 (1.7)	826.5(7.9)
D ff,N2,p,na,3	0.007	154	7.1	755	3.8	17	0.04211 (0.38)	0.3196 (0.57)	0.05504 (0.35)	265.9 (2.0)	281.6 (2.8)	414(15/16)
FFe88-34-2 Big Creek Group, Gilliland tuff[b] (location 8 on Fig. 2)												
A N2,+104	0.03	196	26	1014	43	9.8	0.12641(0.11)	1.77115(0.23)	0.10162(0.15)	767.3(1.6)		1653.9(5.5)
B N2,+104	0.01	367	20	663	24	8	0.056533(0.13)	0.41795(0.66)	0.05362(0.60)	354.5(0.9)		355.1(27.2)
C N2,+104	0.02	190	32	930	30	13	0.14854(0.11)	2.98375(0.22)	0.14569(0.14)	892.8(1.9)		2295.9(4.7)
D N2,+104	0.02	361	22	453	43	15	0.05608(0.18)	0.41540(2.08)	0.05372(2.00)	351.7(1.2)		359.5(90.2)
E N2,+104	0.02	256	15	1236	13	13	0.05683(0.12)	0.42474(0.29)	0.05421(0.22)	356.3(0.8)		379.6(10.1)
F N2,62-74,e,u	0.07	398	20	1223	73	7.3	0.05117(0.13)	0.37787(0.65)	0.05356(0.60)	321.7(0.8)		352.5(27.2)

[a]Richard Friedman (2000); [b]Jim Mortensen (2000).

[1] Upper case letter is fraction identifier used in Fig. 7. All zircon fractions air abraded; Grain size, intermediate dimension in micrometres: cc=>149, c=149-134, m=134-104, f=104-74, ff=<74; Magnetic codes: Franz magnetic separator sideslope at which grains are Nonmagnetic (N) or Magnetic (M); e.g., N1=nonmagnetic at 1°; Field strength for all is 1.8A; Front slope for all is 20°; Grain codes: b=broken fragments, e=elongate, eq=equant multifaceted, ov=ovoid, p=prismatic, s=stubby, t=tabular, ti=tips; Additional for detrital grains: colour: co=colourless, pp=pale pink, vp=vivid pink, py=pale yellow, tan=tan; clarity; cl=clear; tr=translucent; Numeral some fractions (listed last) gives number of grains dissolved.

[2] U blank correction of 1pg ±20%; U fractionation corrections were measured for each run with a double ^{233}U-^{235}U spike (about 0.004/amu).

[3]Radiogenic Pb.

[4]Measured ratio corrected for spike and Pb fractionation of 0.0037-0.0043/amu ±20% (Daly collector) and 0.0012/amu (Faraday collector), which were determined by repeated analysis of NBS Pb standard throughout the course of this study.

[5]Total common Pb in analysis based on blank isotopic composition.

[6]Corrected for blank Pb (2-10 pg, zircon; 20 pg, titanite), U (1 pg, all) and common Pb concentrations based on Stacey and Kramers (1975) model Pb at the age or the $^{207}Pb/^{206}Pb$ age of the rock.

Table 2. Multigrain U-Pb zircon analyses performed at Department of Geological Sciences, University of British Columbia in 1993.

Fraction[1,2]	Wt	U[3]	Pb[3]	^{206}Pb[4]	^{208}Pb[3]	Isotopic ratios (±1-sigma, %)			Apparent ages (±2-sigma, Ma)		
	mg	ppm	ppm	^{204}Pb	%	$^{206}Pb/^{238}U$	$^{207}Pb/^{235}U$	$^{207}Pb/^{206}Pb$	$^{206}Pb/^{238}U$	$^{207}Pb/^{235}U$	$^{207}Pb/^{206}Pb$
FF91-10-9-1 Gilliland tuff[a]											
A NM2A/1° abr -104+74m needles	0.44	360	18	427	8.2	0.05004(.119)	0.3642(.723)	0.05277(.675)	314.8(0.7)	315.3(3.9)	319(31)
C NM2A/1° abr +104m	0.35	267	34	3890	12	0.11620(.161)	1.8358(.180)	0.11459(.055)	708.6(2.2)	1058.4(2.4)	1873.4(2.0)
D NM2A/1° abr -74+44m needles	0.26	374	21	1905	9.1	0.05526(.263)	0.4200(.298)	0.05512(.090)	346.7(1.8)	356.0(1.8)	417.2(4.0)
E NM2A/1° abr -44m needles	0.07	395	20	1580	8.7	0.05109(.105)	0.3862(.204)	0.05482(.150)	321.2(0.7)	331.6(1.2)	405.0(6.7)
F M2A/1° abr -104+74m lozenges	0.12	353	36	4295	9.1	0.09731(.086)	1.2811(.119)	0.09548(.055)	598.6(1.0)	837.4(1.4)	1537.6(2.1)

[a]Analyses by J. Gabites, 1993.

IUGS conventional decay constants (Steiger and Jäger, 1977) are: $^{238}Ul=1.55125x10^{-10}a^{-1}$, $^{235}Ul=9.8485x10^{-10}a\text{-}1$, $^{238}U/^{235}U=137.88$ atom ratio.

[1] A, B, C, D, E, F refers to labels in Fig. 7.

[2] Zircon fractions are labelled according to magnetic susceptibility and size. NM = non magnetic at given amperes on magnetic separator, M = magnetic. Side slope is in degrees. Abr = air abraded. The "-" indicates zircons are smaller than, "+" larger than the stated mesh (l).

[3]U and Pb concentrations in mineral are corrected for blank U and Pb. Isotopic composition of laboratory Pb blank is 206:207:208:204 = 17.299:15.22:35.673:1.00, based on ongoing analyses of total procedural blanks of 37 ±5 pg (Pb) and 6 ±0.5 pg (U).

[4]Initial common Pb is assumed to be Stacey and Kramers (1975) model Pb at the $^{207}Pb/^{206}Pb$ date for each fraction.

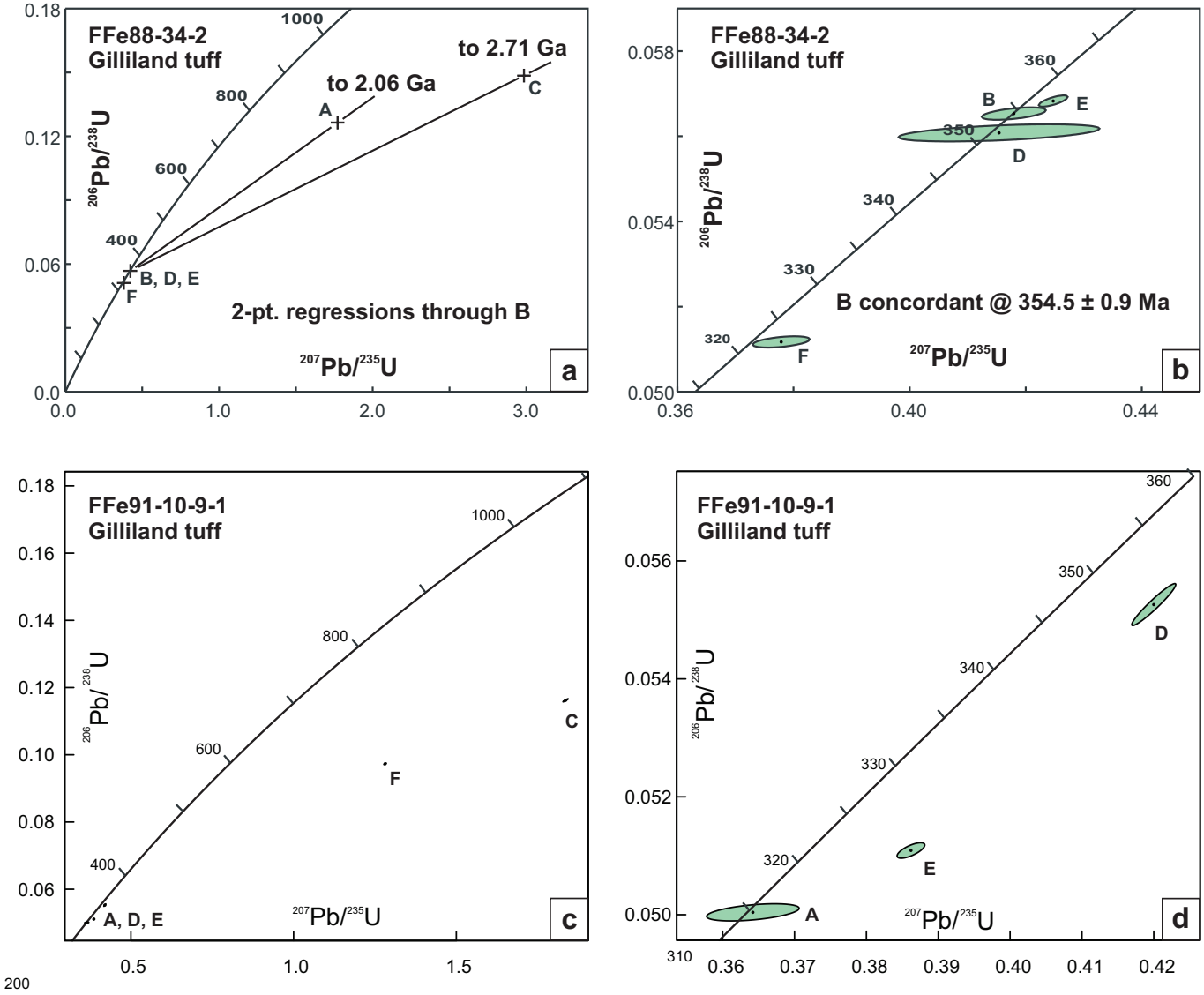


Fig. 7. a) and **c)** U-Pb concordia diagrams for samples collected from the Gilliland tuff of the Big Creek Group. **b)** and **d)** Close ups of the points clustering close to the concordia line, in a) and c), respectively.

Upper intercept ages of about 1.9-2.7 Ga, based on regressions through the quasi-linear data array (chords ABCD, BCD, and ABC), suggest the presence of old inherited zircon in three of the analyzed fractions. Fraction D is only weakly discordant; it yielded a $^{206}Pb/^{238}U$ age of 254 ±12 Ma, which is considered as a good estimate for the age of the rock.

3.2.5. Lay Range assemblage, felsic tuff, sample FFe99-16-5

This felsic tuff yielded a modest quantity of clear, pale tan euhedral to very slightly rounded prismatic zircons. The coarser zircons (>74 mm) were commonly broken euhedral grains. Due to the scarcity of material, abrasion was not carried out. Grains were divided in four multi-grain fractions on the basis of size and shape (euhedral vs. slightly rounded). Three of the four fractions (B-D) yielded discordant results (Table 1; Fig. 8c). Two-point reference chords constructed through AB and AC suggest that inherited zircon components with a range of ages are present. Results for fraction D are consistent with the presence of minor inheritance and subsequent Pb loss. Fraction A is concordant with an $^{206}Pb/^{238}U$ age estimate of 274.8 ±1.5 Ma.

4. Lithogeochemical data

Whole rock, trace and rare earth element analyses were obtained from 16 igneous rock samples from the Big Creek Group and Lay Range assemblage (Table 3). In addition, the Sm-Nd isotopic geochemistry of a subset of these samples was also determined (Table 4).

The Lay Range assemblage contains predominantly mafic volcanic flows and fragmental rocks together with a sub-volcanic intrusion to flow of intermediate composition (Fig. 9).

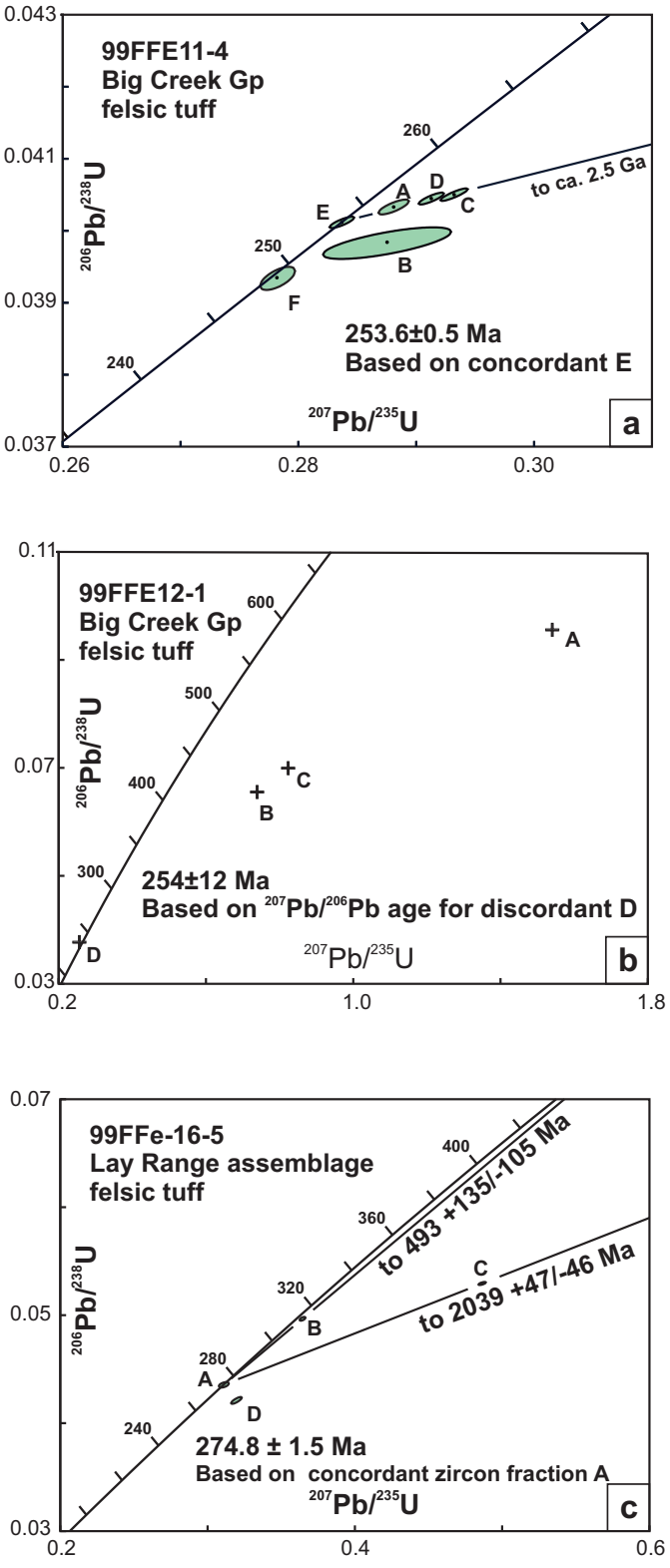


Fig. 8. U-Pb concordia diagrams for samples collected from **a)** and **b)** the Big Creek Group and **c)** the Lay Range assemblage.

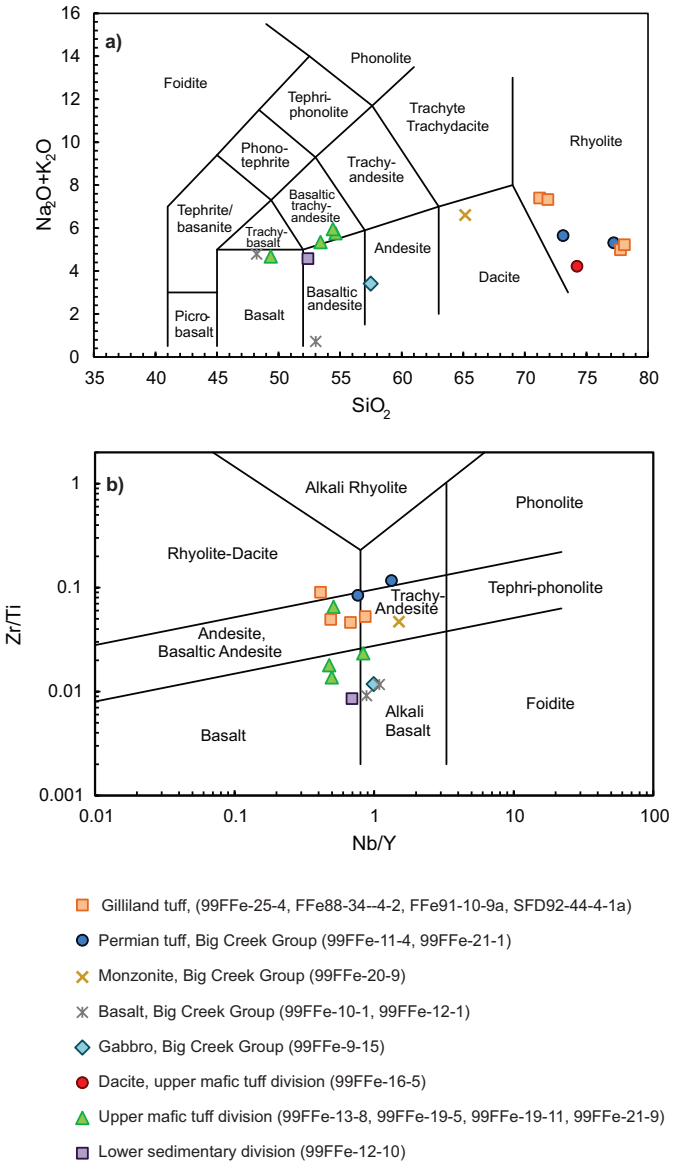


Fig. 9. a) Total alkali-silica plot (Le Bas et al.,1986) re-calculated for water-free compositions. **b)** Rock classification based on Zi/Ti vs. Nb/Y (Pearce, 1996). This plot bypasses any issues related to remobilization of alkali metals.

Compositionally they range from basalt to basaltic andesite. These are calc-alkaline to tholeiitic and predominantly metaluminous, although sample 99FFe-16-5 is strongly peraluminous (Figs. 9, 10). Elemental abundances and REE patterns suggest incipient arc magmatism for rocks in the upper mafic tuff division as indicated by Th/Nb vs. Nb/Yb ratios plotting above the MORB to OIB corridor (Fig. 11a) and the weak but discernable Ti and Nb anomalies (Fig. 11b). Basalt from the lower sedimentary division displays elemental abundances suggestive of an E-MORB setting (Fig. 11). The arc setting for volcanic rocks of the Lay Range assemblage based on geochemical abundances is similar to results for this unit in the southern Lay Range (Ferri, 1997).

Table 3. Major oxide, trace and rare earth element analysis for selected samples of the Big Creek Group and Lay Range assemblage.

Sample	99FFe-9-15 Gabbro	99FFe-10-1 Basalt	99FFe-11-2 Basalt	99FFe-11-4 Tuff	99FFe-12-1 Tuff	99FFe-20-9 Monzonite	99FFe-25-4 Tuff	FFe88-34-2* Flow	FFe91-10-9a Tuff	SFD92-44-4-1a Tuff	99FFe-12-10 Basalt	99FFe-13-8 Volc. Brec.	99FFe-16-5 Tuff	99FFe-19-5 Basalt	99FFe-19-11 Basalt	99FFe-21-9 Basalt
Unit	Big Ck Gp	Big Ck Gp	Big Ck Gp	Big Ck Gp	Big Ck Gp	Big Ck Gp	Gilliland tuff	Gilliland tuff	Gilliland tuff	Gilliland tuff	LRA-LSD	LRA-UMTD	LRA-UMTD	LRA-UMTD	LRA-UMTD	LRA-UMTD
Map No.	1	2	3	4	5	6	7	8	9	10	11	12	13	14	15	16
UTM E	317286[a]	316796[a]	318879[a]	318790[a]	683450[b]	672021[b]	369071[b]	393078[b]	365605[b]	338030[b]	682108[b]	680162[b]	679335[b]	671585[b]	671982[b]	670671[b]
UTM N	6280282	6280271	6279287	6278928	6281435	6295823	6216514	6183563	6223737	6267169	6281324	6280469	6283754	6294998	6292868	6296240
SiO_2	54.15	45.5	40.88	70.52	74.56	61.11	69.12	70.25	74.57	75.97	49.84	49.74	71.02	46.88	52.33	51.34
TiO_2	2.01	0.75	2.25	0.25	0.15	0.43	0.61	0.71	0.32	0.65	3.8	0.89	0.44	1.37	1.37	1.16
Al_2O_3	14.34	11.25	12.64	14.28	14.1	15.5	14.02	14.66	12.00	12.36	14.1	15	12.93	18.75	16.34	16.57
Fe_2O_3	2.77	2.45	6.49	0.68	0.65	1.57	1.96	2.09	-	-	3.55	4.41	1.77	5.51	8.53	4.71
FeO	8.49	9.58	5	2.79	0.43	2.66	1.72	1.27	-	-	7.43	3.31	1.47	4.47	2.24	5.14
$\sum Fe_2O_3$	12.20	13.10	12.05	3.78	1.13	4.53	3.87	3.50	0.68	1.76	11.81	8.09	3.40	10.48	11.02	10.42
MnO	0.07	0.37	0.14	0.01	0.01	0.07	0.02	0.03	0.05	0.04	0.17	0.14	0.05	0.18	0.14	0.15
MgO	6.4	7.32	3.23	2.05	1.41	2.14	1.73	0.83	0.65	0.66	4.86	3.98	3.55	3.85	3.28	5.21
CaO	1.57	6.63	9.25	0.11	0.05	3.63	0.37	0.44	2.68	0.60	5.65	7.78	0.18	8.71	5.67	5.9
Na_2O	3.21	0.11	1.72	2.97	1.72	4.8	1.83	1.46	1.47	1.47	4.09	3.71	0.79	3.43	4.73	3.51
K_2O	0.01	0.51	2.34	2.48	3.42	1.4	5.36	5.71	3.32	3.62	0.27	1.54	3.25	1.02	1	1.63
P_2O_5	0.25	0.3	0.28	0.01	0.01	0.2	0.15	0.17	0.16	0.16	0.56	0.18	0.05	0.31	0.3	0.23
LOI	6.63	14.29	15.33	3.2	2.78	5.75	2.67	2.16	3.70	2.15	5.45	8.95	3.96	5.29	3.87	3.98
SUM	99.91	99.09	99.68	99.46	99.44	99.31	99.64	99.78	99.6	99.44	99.78	99.65	99.54	99.81	99.85	99.59
Cu	15	44	30	<1	<1	30	8	12	9	8	7	39	14	182	53	109
Pb	8	26	8	4	26	2	20	15	16	-	8	6	4	8	8	6
Zn	94	280	82	68	26	96	46	63	45	43	186	64	40	66	90	82
Ni	47	519	76	2	<1	3	12	10	-	-	88	31	<1	22	6	23
Cr	95	1760	242	86	102	32	97	-	-	-	93	123	75	69	23	69
Co	33	68	38	5	2	9	9	24	-	-	39	26	3	28	29	29
Ba	254	292	1329	907	1076	593	988	2400	1174	1369	122	205	860	415	451	428
Rb	<3	25	73	85	167	57	192	190	118	114	4	31	69	21	17	29
Sr	133	169	158	42	34	244	69	110	129	38	174	213	12	416	426	466
Sn	<3	5	<3	<3	4	5	<3	-	-	18	<3	<3	<3	<3	<3	<3
V	166	244	234	9	12	73	49	-	48	32	192	206	62	286	273	260
Nb	19	10	23	14	17	23	19	15	9	16	16	14	13	13	14	13
Zr	142	41	157	126	105	121	192	210	173	179	194	124	172	112	147	122
Y	19.1	11.3	21.1	18.3	12.8	15.2	22.0	30	21	24	23.1	16.7	25.3	26.1	29.4	24.9
La	20.5	1.6	20.6	12.4	27.2	22.3	43.2	26.22	39.50	32.73	12.7	14.0	14.6	12.6	17.5	12.8
Ce	39.3	3.8	46.4	21.7	50.1	46.5	85.5	62.38	80.18	67.66	37.7	30.6	31.5	31.1	40.4	30.0
Pr	5.0	0.6	5.8	2.3	5.0	5.5	9.9	6.40	8.93	7.80	6.5	4.1	3.8	4.2	5.4	4.2
Nd	20.4	3.0	23.3	9.7	16.8	22.2	34.3	24.42	31.97	29.18	33.4	16.0	16.2	19.7	24.1	18.7
Sm	5.8	1.3	6.2	2.9	3.0	5.2	6.8	5.29	6.04	5.53	10.3	4.3	4.2	5.9	6.8	5.3
Eu	1.6	0.5	2.0	0.6	0.5	1.4	1.2	1.09	1.16	0.84	3.2	1.4	0.6	1.7	1.9	1.6
Gd	5.6	1.7	5.9	2.8	2.3	3.1	4.6	4.46	4.88	4.38	8.6	3.9	3.1	4.4	5.3	4.0
Tb	0.9	0.3	0.9	0.5	0.4	0.5	0.7	0.66	0.68	0.62	1.3	0.6	0.6	0.7	0.9	0.7
Dy	4.5	2.3	6.1	3.7	2.4	3.3	4.1	4.24	3.60	3.34	7.3	4.1	4.3	4.6	6.1	4.8
Ho	0.8	0.4	1.0	0.7	0.4	0.6	0.8	0.80	0.63	0.63	1.0	0.7	0.8	0.9	1.1	0.9
Er	2.2	1.3	2.9	2.5	1.4	1.8	2.4	2.25	1.72	1.73	2.5	2.3	3.0	2.7	3.5	2.6
Tm	0.3	0.2	0.3	0.4	0.2	0.3	0.3	0.32	0.23	0.25	0.3	0.3	0.4	0.4	0.5	0.4
Yb	1.5	1.0	2.2	2.4	1.2	1.7	1.9	2.09	1.41	1.51	1.7	1.9	3.1	2.5	3.0	2.5
Lu	0.2	0.2	0.3	0.4	0.2	0.2	0.3	0.31	0.20	0.22	0.3	0.3	0.4	0.3	0.4	0.3
Hf	4.1	1.1	5.8	3.5	3.5	3.6	5.4	4.84	4.25	4.12	6.8	4.2	5.0	3.5	4.9	3.5
Ta	1.3	0.1	1.9	0.3	1.2	1.2	1.4	1.19	0.66	1.01	1.2	0.7	0.5	0.4	0.5	0.4
Th	3.7	0.7	3.1	4.5	21.8	5.8	14.3	14.8	11.6	12.8	0.7	2.2	5.2	1.5	3.0	1.7

LRA: Lay Range Assemblage; UMTD: upper mafic tuff division; LSD: lower sedimentary division. [a]: NAD 83 UTM Zone 9; [b]: NAD 83 Zone 10

Major oxides, U, V, Sn, Sr, Rb, Co, Cs, Nb, Y and Zr determined by x-ray fluorescence at Cominco Laboratories; sample FFe-88-34-2 analyzed at the British Columbia Ministry of Energy, Mines and Petroleum Resources.

Trace elements (Cu, Pb, Zn, Li, Cr, Ni) by atomic absorbtion at Cominco Laboratoires. La to Ta and Th analyses determined by neutron activation analysis at laboratories of Memorial University.

Table 4. Neodymium isotope data for Big Creek Group and Lay Range assemblage.

Unit	Sample Number	Map Label	Age (*T*) (Ma)	Sm (ppm)	Nd (ppm)	$^{147}Sm/^{144}Nd$	$^{143}Nd/^{144}Nd$	$e_{Nd}(T)^1$	$e_{Nd}(0)^1$	$T_{DM}{}^2$ (Ga)
Gilliland tuff	FFe91-10-9-1	9	355	6.02	31.37	0.11858(10)	0.511895(13)	-11.0	-14.5	2.02
Gilliland tuff	FFe88-34-2	8	355	4.97	30.19	0.10160(08)	0.511679(20)	-14.4	-18.7	2.01
Gilliland tuff	SFD91-44-4-1	10	355	5.64	33.98	0.10251(08)	0.511618(21)	-15.6	-19.9	2.11
Gilliland tuff	99FFe-25-4	7	355	6.17	35.50	0.10723(11)	0.511625(15)	-15.7	-19.8	2.19
Big Ck. Gp. Permian tuff	99FFe-11-4	4	254	2.03	9.87	0.12706(12)	0.511964(15)	-10.9	-13.1	2.10
Big Ck. Gp. Permian tuff	99FFe-12-1	5	254	3.13	19.19	0.10073(09)	0.511653(17)	-16.1	-19.2	2.03
Upper mafic tuff division, felsic tuff	99FFe-16-5	13	275	3.20	14.24	0.13572	0.512651(06)	2.4	0.3	1.00
Upper mafic tuff division, basalt	99FFe-19-11	15	275	6.25	26.52	0.14252	0.512861(05)	6.3	4.4	0.65

LA-ICP-MS analysis in laboratories of Memorial University of Newfoundland.

Estimated uncertainties in paranthesis at the 2s level; number in paranthesis is the uncertainty in the last two decimal places.

[1]Calculated using $^{143}Nd/^{144}Nd$ of chondrite reservoir (CHUR) = 0.512638 and $^{147}Sm/^{144}Nd$ = 0.1966 (Hamilton et al., 1983).

[2]Calculated using the values of $^{143}Nd/^{144}Nd$ = 0.513163 and $^{147}Sm/^{144}Nd$ = 0.2137 for the depleted mantle (DM) reservoir (Goldstein et al., 1984).

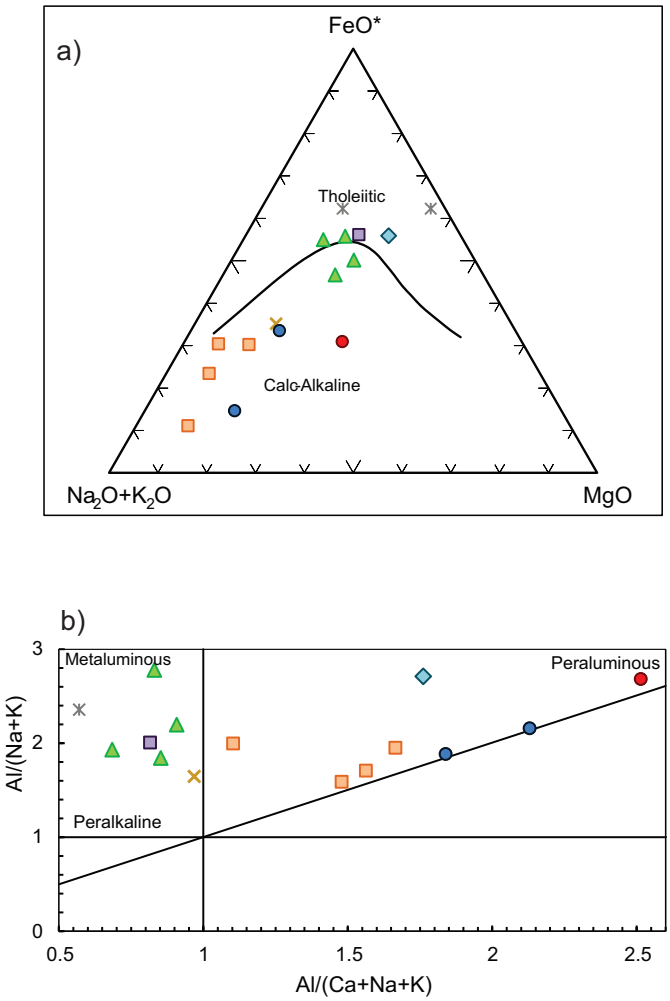


Fig. 10. a) Calc-alkaline to tholeiitic trend from Irvine and Baragar (1971). **b)** Shand's index diagram from Maniar and Piccoli (1989). Symbology is the same as in Figure 9.

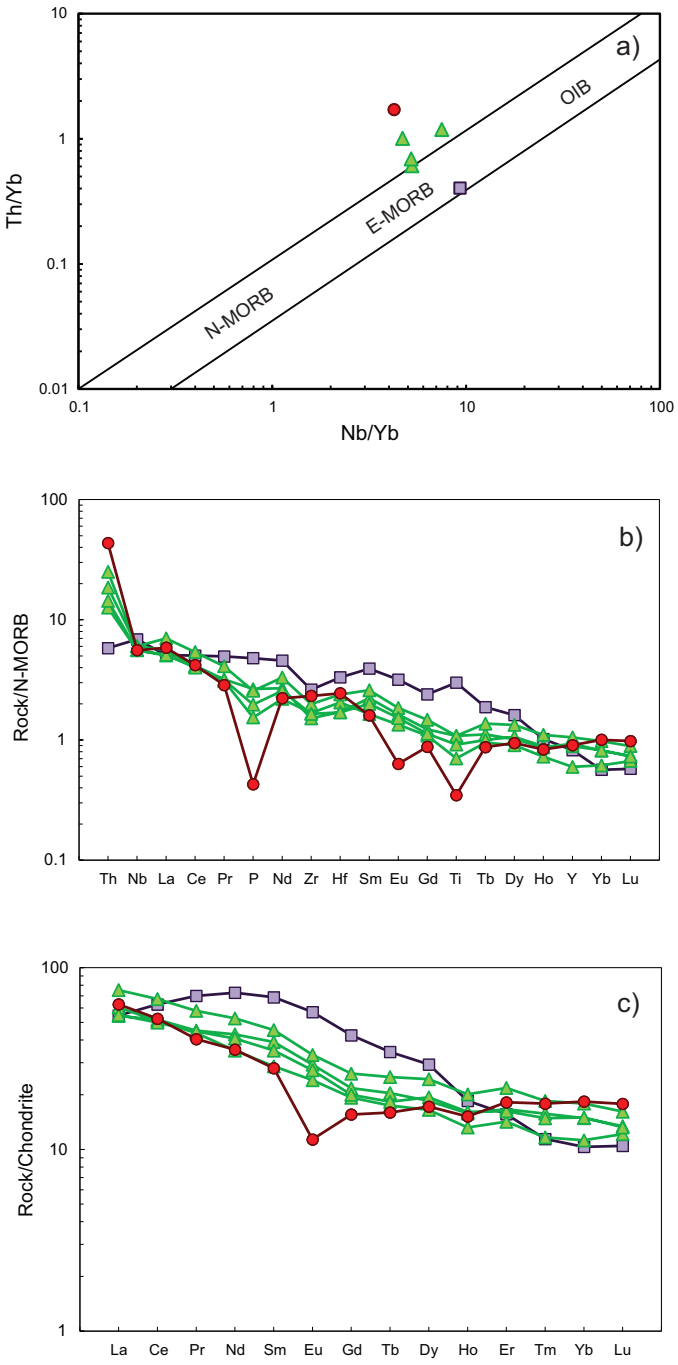


Fig. 11. a) Tectonic discrimination diagram for rocks of the Lay Range assemblage usingTh/Yb vs. Nb/Yb as proposed by Pearce (1998). **b)** Extended rare earth element plot for rocks of the Lay Range assemblage. The Ti and Nb negative anomalies suggest an arc setting for rocks from the upper mafic tuff division. **c)** Rare earth element plot for volcanic rocks of the Lay Range assemblage. Normalizing values from Sun and McDonough (1989). Symbology is the same as in Figure 9.

Igneous rocks of the Big Creek Group have a varied composition. Gilliland tuff and Permian tuff are rhyolitic, calc-alkaline and generally peraluminous (Figs. 9, 10), although the spread of data in Figure 10b may be a function of alteration. Trace and rare earth element abundances, particularly with the Ti and Nb anomalies, are indicative of a volcanic arc setting (Fig. 12).

Rocks of a more mafic nature in the Big Creek Group are basaltic to basaltic-andesite in composition and calc-alkaline to tholeiitic (Figs. 9, 10a, b). Trace and rare earth element data indicate an E-MORB or within-plate tectonic setting for these samples (Fig. 13a). Rare earth element distributions generally support this, although sample 99FFe-10-1 has lower abundances.

Sm-Nd isotopic geochemistry (Table 4) indicates evolved Precambrian continental lithosphere as the source of magma that supplied the felsic volcanic rocks in the Big Creek Group. This contrasts with data from igneous rocks in the Lay Range assemblage that point to a less evolved oceanic mantle source, similar to younger Quesnellia (Table 4; Fig. 14; Ootes et al., 2022).

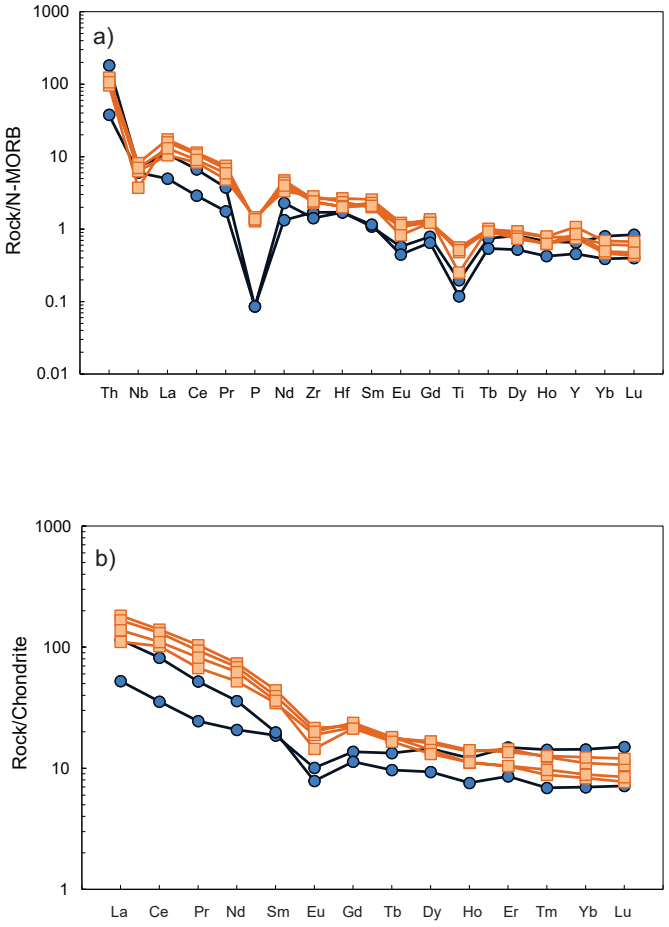


Fig. 12. Extended rare earth element plot **a)** and rare earth element plot **b)** for samples of the Gilliland tuff and felsic Permian volcanics of the Big Creek Group. The strong negative Nb and Ti anomalies suggest arc-related volcanism, although this chemistry could be a reflection of inheritance from continental lithosphere, which is strongly suggested by Nd-Sm isotopic data. Symbology is the same as in Figure 9. Normalized values from Sun and McDonough (1989).

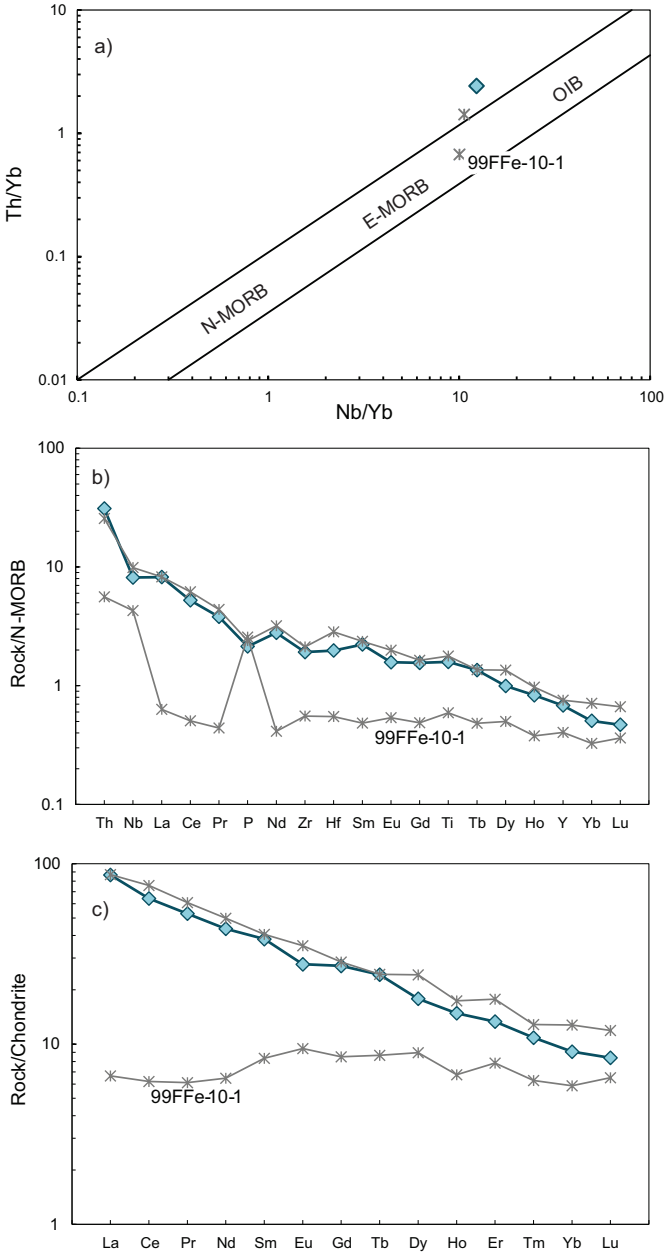


Fig. 13. a) Tectonic discrimination diagram for mafic igneous rocks of the Big Creek Group using Th/Yb vs. Nb/Yb as proposed by Pearce (1998). **b)** Extended rare earth element plot for mafic igneous rocks of the Big Creek Group. **c)** Rare earth element plot for mafic igneous rocks of the Big Creek Group. Normalizing values from Sun and McDonough (1989). Symbology is the same as in Figure 9.

5. Summary

Previously unreleased multigrain U-Pb zircon geochronologic work carried out in 1993 and 2000 from mapping near the Lay Range in the north-central part of the province yielded ca. 350 to 320 Ma ages for the Gilliland tuff in the lower part of the Big Creek Group near Germansen Landing and the Osilinka River in the southern part of the region and ca. 255 Ma from felsic tuffs in the upper part of the unit in the northern Lay Range. Felsic volcanic rocks in the 'upper mafic tuff division' of the Lay Range assemblage, the local basement to the Upper Triassic to Lower Jurassic mafic to intermediate arc volcanic rocks that are predominant in Quesnel terrane (Nicola Group) yielded an age of ca. 275 Ma. Lithogeochemical data from the Lay Range assemblage suggest a volcanic arc setting of these basaltic to andesitic rocks. Similar data from Mississippian and Permian felsic volcanic rocks of the Big Creek Group suggest an origin from partial melting of the continental lithosphere. The arc signature of these felsic rocks may be inherited from the continental lithosphere. Mafic igneous rocks of the Big Creek Group have E-MORB (within-plate) signatures. Sm-Nd isotopic data points to evolved continental lithosphere for the source of felsic volcanics in the Big Creek Group whereas a less evolved oceanic mantle source is suggested for mafic and felsic rocks of the Lay Range assemblage.

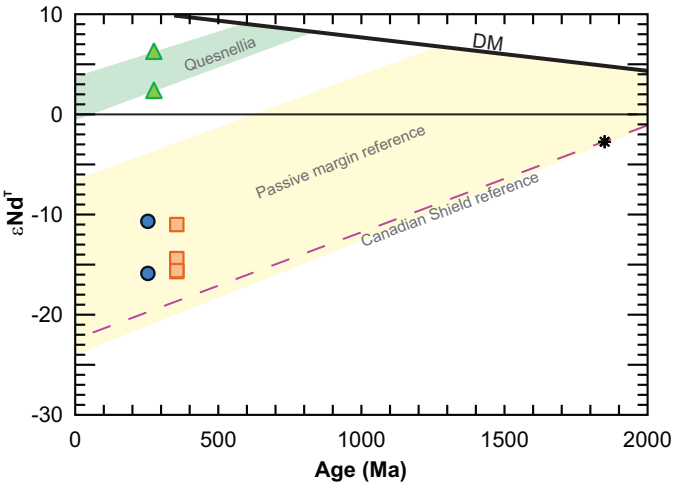


Fig. 14. Age vs. eNd^T for samples in this study (Table 4; symbols follow the key in Figure 9). For comparison, Quesnellia reference (green band) constructed using whole rock Sm-Nd isotopic data from intrusive rocks (n=6 $^{147}Sm/^{144}Nd$=0.112) in Hogem batholith (Jurassic-Cretaceous; 200 to 130 Ma; Ootes et al., 2020c). DM: depleted mantle evolutionary curve as defined by Goldstein et al. (1984). Passive margin reference constructed using whole rock Sm-Nd isotopic data (n=8 $^{147}Sm/^{144}Nd$=0.112) from sedimentary rocks of the Road River Group (Silurian; ca. 425 Ma) in the Mackenzie Mountains (data in Rasmussen et al., 2023). Canadian Shield reference line constructed using whole rock Sm-Nd isotopic data (n=67, average $^{147}Sm/^{144}Nd$=0.11) from igneous rocks in Wopmay orogen of the western Canadian Shield (data from Jackson et al., 2022). Asterix at ca. 1.85 Ga represents youngest intrusive rocks exposed in the western Canadian Shield, where most exposures range between Neoarchean and Paleoproterozoic. The line represents approximate maximum eNd^T at a given time for magmas derived exclusively from Canadian Shield melt sources.

Acknowledgments

We thank L. Ootes and L. Aspler for reviewing several iterations of this paper and providing helpful comments. L. Ootes also provided some of the illustrations.

References cited

Colpron, M., 2020. Yukon terranes-A digital atlas of terranes for the northern Cordillera. Yukon Geological Survey. <https://data.geology.gov.yk.ca/Compilation/2#InfoTab>

Ferri, F., 1989. QCM, 93N/10. In: Exploration in British Columbia 1988, Part B. British Columbia Ministry of Energy, Mines and Petroleum Resources, British Columbia Geological Survey, pp. B139-B142.

Ferri, F., 1997. Nina Creek Group and Lay Range Assemblage, north-central British Columbia: Remnants of late Paleozoic oceanic and arc terranes. Canadian Journal of Earth Sciences, 34, 854-874.

Ferri, F., 2000. Devono-Mississippian felsic volcanism along the western edge of the Cassiar terrane, north-central British Columbia (NTS 93N, 94C and 94D). In: Geological Fieldwork 1999. British Columbia Ministry of Energy and Mines, British Columbia Geological Survey Paper 2000-01, pp. 127-146.

Ferri, F., and Melville, D.M., 1988a. Manson Creek Mapping Project (93N/9). In: Geological Fieldwork 1987, British Columbia Ministry of Energy, Mines and Petroleum Resources, British Columbia Geological Survey Paper 1988-01, pp.169-180.

Ferri, F., and Melville, D.M., 1988b. Geology and geochemistry of the Manson Lake map sheet (NTS 93N/9). British Columbia Ministry of Energy, Mines and Petroleum Resources, British Columbia Geological Survey Open File 1988-12, 1:50,000 scale.

Ferri, F., and Melville, D.M., 1989a. Geology of the Germansen Landing area, British Columbia (93N/10, 15). In: Geological Fieldwork 1988, British Columbia Ministry of Energy, Mines and Petroleum Resources, British Columbia Geological Survey Paper 1989-01, pp. 209-220.

Ferri, F., and Melville, D.M., 1989b. Geochemistry and mineral occurrences of the Germansen Landing area NTS 93N/10 (North Half), 93N/15 (South Half). British Columbia Ministry of Energy, Mines and Petroleum Resources, British Columbia Geological Survey Open File 1989-12, 1:50,000 scale.

Ferri, F., and Melville, D.M., 1990a. Geology between Nina Lake and Osilinka River, North-central British Columbia (93N/15, North Half and 94C/2, South Half). In: Geological Fieldwork 1989, British Columbia Ministry of Energy, Mines and Petroleum Resources, British Columbia Geological Survey Paper 1990-01, pp. 101-114.

Ferri, F., and Melville, D.M., 1990b. Geology between Nina Lake and Osilinka River, British Columbia, 93N/15 (North Half) and 94C/2 (South Half). British Columbia Ministry of Energy, Mines and Petroleum Resources, British Columbia Geological Survey Open File 1990-17, 1:50,000 scale.

Ferri, F., and Melville, D.M., 1994. Bedrock geology of the Germansen Landing-Manson Creek area, British Columbia (NTS 93N/9, 10, 15; 94C/2). British Columbia Ministry of Energy, Mines and Petroleum Resources, British Columbia Geological Survey Bulletin 91, 148 p.

Ferri, F., Melville, D.M., Malensek, G.A. and Swift, N.R., 1988. Geology of the Manson Lakes map sheet, 93N/9. British Columbia Ministry of Energy, Mines and Petroleum Resources, British Columbia Geological Survey Open File 1988-12.

Ferri, F., Melville, D.M., and Arksey, R.L., 1989. Geology of the Germansen Landing area, 93N/10 and 93N/15. British Columbia Ministry of Energy, Mines and Petroleum Resources, British Columbia Geological Survey Open File 1989-12.

Ferri, F., Dudka, S., and Rees, C., 1992a. Geology of the Uslika Lake area, northern Quesnel trough, B.C. (94C/3, 4 and 5). In: Geological Fieldwork 1991, British Columbia Ministry of Energy, Mines and Petroleum Resources, British Columbia Geological Survey Paper 1992-01, pp. 127-146.

Ferri, F., Dudka, S., Rees, C., Meldrum, D.G., and Willson, M., 1992b. Geology and geochemistry of the Uslika Lake area. British Columbia Ministry of Energy, Mines and Petroleum Resources, British Columbia Geological Survey Open File 1992-11.

Ferri, F., Dudka, S., Rees, C., and Meldrum, D.G., 1993a. Geology of the Aiken Lake and Osilinka River areas, northern Quesnel trough (94C/2, 3, 5, 6 and 12). In: Geological Fieldwork 1992, British Columbia Ministry of Energy, Mines and Petroleum Resources, British Columbia Geological Survey Paper 1993-01, pp. 109-134.

Ferri, F., Dudka, S., Rees, C., and Meldrum, D.G., 1993b. Preliminary geology and geochemistry of the Aiken Lake and Osilinka River areas. British Columbia Ministry of Energy, Mines and Petroleum Resources, British Columbia Geological Survey Open File 1993-02.

Ferri, F., Dudka, S., Rees, C., and Meldrum, D., 2001a. Geology of Aiken Lake area, north-central British Columbia. British Columbia Ministry of Energy and Mines, British Columbia Geological Survey Geoscience Map 2001-10, 1:50,000 scale.

Ferri, F., Dudka, S., Rees, C., Meldrum, D., and Willson, M., 2001b. Geology of the Uslika Lake area, north-central British Columbia. British Columbia Ministry of Energy and Mines, British Columbia Geological Survey Geoscience Map 2001-04, 1:50,000 scale.

Goldstein, S.L., O'Nions, R.K., and Hamilton, P.J., 1984. A Sm-Nd isotopic study of atmospheric dusts and particulates from major river systems. Earth and Planetary Science Letters, 70, 221-236.

Gündüz, M., and Asan, K., 2021. PetroGram: An Excel-based petrology program for modeling of magmatic processes. Geoscience Frontiers, 12, 81-92.

Hamilton, P.J., O'nions, R.K., Bridgwater, D., and Nutman, A., 1983. Sm-Nd studies of Archaean metasediments and metavolcanics from West Greenland and their implications for the Earth's early history; Earth and Planetary Science Letters, 62, 263-272.

Irvine, T.N., and Baragar, W.R.A., 1971. A guide to the chemical classification of the common volcanic rocks; Canadian Journal of Earth Sciences, 8, 523-548.

Jackson, V.A., Ootes, L., Pierce, K., Bennett, V., Smar, L., Mackay, D., and Sandeman, H.A., 2022. Geology of the south-central Wopmay orogen, Northwest Territories (parts of NTS 86B, 86C, and 86D); Results from the South Wopmay Bedrock Mapping Project. Northwest Territories Geological Survey, NWT Open File 2017-10.

Krogh, T.E., 1982, Improved accuracy of U Pb zircon ages by the creation of more concordant systems using an air abrasion technique. Geochimica et Cosmochimica Acta, 46, 637-649.

Le Bas, M.J., Le Maitre, R.W., Streckeisen, A., and Zanettin, B., 1986. A chemical classification of volcanic rocks based on the total alkali-silica diagram. Journal of Petrology, 27, 745-750.

Ludwig, K.R., 1980. Calculation of uncertainties of U Pb isotopic data. Earth and Planetary Science Letters, 46, 212-220.

MacIntyre, D.G., Payie, G.J., and Schiarizza, P.A., 2005. Geological setting and economic potential of gold occurrences in the Kliyul Creek-Solo Lake area, north central B.C. In: Geological Fieldwork 2024, British Columbia Ministry of Energy and Mines, British Columbia Geological Survey Paper 2005-01, pp. 131-152.

Maniar, P.D., and Piccoli, P.M., 1989. Tectonic discrimination of granitoids. Geological Society of America Bulletin, 101, 635-643.

Mortensen, J.K., Ghosh, D., and Ferri, F., 1995. U-Pb age constraints of intrusive rocks associated with copper-gold porphyry deposits in the Canadian Cordillera. In: Schroeter, T.G., (Ed.), Porphyry Deposits of the Northwestern Cordillera of North America: Canadian Institute of Mining and Metallurgy, Special Volume 46, pp. 142-158.

Nelson, J.L., Colpron, M., Piercey, S.J., Dusel-Bacon, C., Murphy, D.C., and Roots, C.F., 2006. Paleozoic tectonic and metallogenetic evolution of pericratonic terranes in Yukon, northern British Columbia and eastern Alaska. In: Colpron, M., and Nelson, J.L., (Eds.), Paleozoic Evolution and Metallogeny of Pericratonic Terranes at the Ancient Pacific Margin of North America, Canadian and Alaskan Cordillera. Geological Association of Canada, Special Paper 45, pp. 323-360.

Nixon, G.T., Archibald, D.A., and Heaman, L.M., 1993. ^{40}Ar-^{39}Ar and U-Pb geochronometry of the Polaris Alaskan-type complex, British Columbia: Precise timing of Quesnellia-North America interaction. Geological Association of Canada, Program with Abstracts, page A-76.

Nixon, G.T., Hammack, J.L., Ash, C.A., Cabri, L.J., Case, G., Connelly, J.N., Heaman, L.M., Laflamme, J.H.G., Nuttall, C., Paterson, W.P.E., and Wong, R.H., 1998. Geology and platinum-group-element mineralization of Alaskan-type ultramafic-mafic complexes in British Columbia. British Columbia Ministry of Energy and Mines, British Columbia Geological Survey Bulletin 93, 155 p.

Ootes, L., Bergen, A., Milidragovic, D., Graham, B., and Simmonds, R., 2019a. Preliminary geology of northern Hogem batholith, Quesnel terrane, north-central British Columbia. In: Geological Fieldwork 2018, British Columbia Ministry of Energy, Mines and Petroleum Resources, British Columbia Geological Survey Paper 2019-01, pp. 31-54.

Ootes, L., Bergen, A.L., Milidragovic, D., and Graham, B., 2019b. Preliminary bedrock geology of Notch Peak and Ogden Creek (parts of NTS 094C/04 and 093N/13), northern Hogem batholith, Quesnel terrane, north-central British Columbia. British Columbia Ministry of Energy, Mines and Petroleum Resources, British Columbia Geological Survey Open File 2019-02, 1:50,000 scale.

Ootes, L., Bergen, A.L., Milidragovic, D., Jones, G.O., Camacho, A., and Friedman, R., 2020a. An update on the geology of northern Hogem batholith and its surroundings, north-central British Columbia. In: Geological Fieldwork 2019, British Columbia Ministry of Energy, Mines and Petroleum Resources, British Columbia Geological Survey Paper 2020-01, pp. 25-47.

Ootes, L., Bergen, A.L., Milidragovic, D., and Jones, G.O., 2020b. Preliminary geology of the northern Hogem batholith and its surroundings, north-central British Columbia. British Columbia Ministry of Energy, Mines and Petroleum Resources, British Columbia Geological Survey Open File 2020-02, 1:50,000 scale.

Ootes, L., Jones, G., Schiarizza, P., Milidragovic, D., Friedman, R., Camacho, A., Luo, Y., Vezinet, A., Pearson, D.G., and Zhang, S., 2020c. Geochronologic and geochemical data from northern Hogem batholith and its surroundings, north-central British Columbia. British Columbia Ministry of Energy, Mines and Low Carbon Innovation, British Columbia Geological Survey GeoFile 2020-01, 21 p.

Ootes, L., Ferri, F., Milidragovic, D., and Wall, C., 2022. The age and provenance of the Lay Range assemblage provides an indirect record of basement to north-central Quesnellia, British Columbia. In: Geological Fieldwork 2021, British Columbia Ministry of Energy, Mines and Low Carbon Innovation, British Columbia Geological Survey Paper 2022-01, pp. 31-44.

Pearce, J.A., 1996. A user's guide to basalt discrimination diagrams. In: Wyman, D.A., (Ed.), Trace element geochemistry of volcanic rocks: Applications for massive sulphide exploration. Geological Association of Canada, Short Course Notes, 12, pp. 79-113.

Pearce, J.A., 1998. Geochemical fingerprinting of oceanic basalts with applications to ophiolite classification and the search for Archean oceanic crust. Lithos, 100, 14-48.

Rasmussen, K.L., Falck, H., Elongo, V., Reimink, J., Luo, Y., Pearson, D.G., Ootes, L., Creaser, R.A., and Lecumberri-Sanchez, P., 2023. The source of tungsten-associated magmas in the northern Canadian Cordillera and implications for the basement. Geology, 51, 657-662.

Roddick, J.C., 1987. Generalized numerical error analysis with application to geochronology and thermodynamics. Geochimica et Cosmochimica Acta, 51, 2129-2135.

Schiarizza, P.A., 2004. Geology and mineral occurrences of Quesnel terrane, Kliyul Creek to Johanson Lake. In: Geological Fieldwork 2003, British Columbia Ministry of Energy and Mines, British Columbia Geological Survey Paper 2004-01, pp. 83-100.

Schiarizza, P., and Tan, S.H., 2005. Geology and mineral occurrences of Quesnel terrane between the Mesilinka River and Wrede Creek, north-central British Columbia (94D/8, 9). In: Geological Fieldwork 2004, British Columbia Ministry of Energy, Mines and Petroleum Resources, British Columbia Geological Survey Paper 2005-01, pp. 109-130.

Schiarizza, P.A., Friedman, R., Orchard, M., and Jaswal, H., 2004. Geology of the Kliyul Creek-Johanson Lake area (NTS 94D/08, 09). British Columbia Ministry of Energy and Mines, British Columbia Geological Survey Open File 2004-05, 1:50,000 scale.

Schiarizza, P.A., Tan, S.H.,, Friedman, R., Orchard, M.J., and Rhodes, R., 2005. Geology of the Johanson Lake area. British Columbia Ministry of Energy and Mines, British Columbia Geological Survey Open File 2005-04, 1:50,000 scale.

Stacey, J.S., and Kramer, J.D., 1975. Approximation of terrestrial lead isotope evolution by a two stage model. Earth and Planetary Science Letters, 26, 207-221.

Steiger, R.H., and Jäger, E., 1977. Subcommission on geochronology: Convention on the use of decay constants in geo- and cosmochronology. Earth and Planetary Science Letters, 36, 359-362.

Sun, S.S., and McDonough, W.F., 1989. Chemical and isotopic systematics of oceanic basalts: Implications for mantle composition and processes. In: Saunders, A.D., and Norry, M.J., (Eds.), Magmatism in the Ocean Basins. Geological Society, London, Special Publication, 42, pp. 313-345.

Geochemistry of volcanic rocks in the Snowshoe Group (Neoproterozoic-Cambrian) and geochronology, Sm-Nd isotopic data, and geochemistry of crosscutting Permian intrusions: Episodic back-arc magmatism along the western edge of Ancestral North America in Kootenay terrane

Filippo Ferri[1, a], and Richard Friedman[2]

[1] Emeritus Scientist, British Columbia Geological Survey, Ministry of Mining and Critical Minerals, Victoria, BC, V8W 9N3
[2] Pacific Centre for Isotopic and Geochemical Research, Earth and Ocean Sciences, The University of British Columbia, Vancouver, BC, V6T 1Z4
[a] corresponding author: Filippo.Ferri@gov.bc.ca

Recommended citation: Ferri, F., and Friedman, R., 2026. Geochemistry of volcanic rocks in the Snowshoe Group (Neoproterozoic-Cambrian) and geochronology, Sm-Nd isotopic data, and geochemistry of crosscutting Permian intrusions: Episodic back-arc magmatism along the western edge of Ancestral North America in Kootenay terrane. In: Geological Fieldwork 2025, British Columbia Ministry of Mining and Critical Minerals, British Columbia Geological Survey Paper 2026-01, pp. 203-219.

Abstract

Vintage multigrain U-Pb zircon analysis on three samples of gabbro intruding late Neoproterozoic to Early Cambrian rocks of the Snowshoe Group collected in 2001 from Kootenay terrane (Cariboo subterrane) returned ages of ca. 280 Ma. Geochemical and isotopic data define two suites. One displays elemental levels suggesting derivation from an E-MORB and OIB (within-plate) source and has Sm-Nd isotopic abundances indicating the magmas originated from an immature mantle source. The second suite displays arc-like signatures and Sm-Nd isotopic levels that suggest derivation from more evolved continental lithosphere. These results are consistent with a Permian back-arc along the western margin of Ancestral North America. Lithogeochemical analysis of mafic volcanic rocks in the Snowshoe Group are predominantly alkali basalts indicating a within-plate setting, but some contain basalt to alkali basalt with both E-MORB and arc signatures, and others are alkali basalts displaying within-plate abundances. These results are consistent with an earlier, Neoproterozoic to Cambrian, back-arc.

Keywords: Snowshoe Group, Kootenay terrane, Cariboo subterrane, geochronology, Sm-Nd isotopes, Permian

1. Introduction

In the early 2000s, the British Columbia Geological Survey conducted systematic mapping in the Cariboo Lake area of Kootenay terrane focused on sulphide-bearing mafic volcanic rocks of the Snowshoe Group (Fig. 1), a succession of polydeformed and metamorphosed Neoproterozoic to lower Cambrian siliciclastic, carbonate, and volcanic rocks (Ferri, 2001a, b; Ferri and O'Brien, 2002, 2003). This paper presents previously unpublished multigrain U-Pb zircon ages and Sm-Nd isotopic data from three gabbroic intrusions that cut the Snowshoe Group, together with trace and rare earth element data from a regional suite of mafic to intermediate volcanic samples collected during this mapping. Geochronological data from the three samples return, within error, the same Early Permian age (ca. 280 Ma). Geochemical data from both the Snowshoe Group and crosscutting Permian intrusions are consistent with back-arc basin processes near the western flank of Ancestral North America.

2. Previous work

Our work in the region builds on numerous previous studies. Höy and Ferri (1998a, b) described mineralization in the Wells-Barkerville area, Ferri et al. (1999) detailed the age and geochemistry of the Quesnel Lake gneiss, Bichler and Bobrowski (2001) conducted a till geochemistry survey, and Ray et al. (2001) detailed the geochemistry of mineral deposits in the Wells-Barkerville area. Earlier investigations include Struik (1986, 1988), Campbell (1978), Rees (1987), and Rees and Ferri (1983). Schiarizza and Ferri (2003) and Ferri and Schiarizza (2006) redefined Snowshoe Group stratigraphy based on the recognition of large nappe-like structures that repeat stratigraphy. Investigations of adjoining rocks in Quesnel terrane include Struik (1983a, b), Bloodgood (1990), Panteleyev et al. (1996), and Schiarizza (2024).

3. Geological setting

Straddling the boundary between the Intermontane and Omineca morphotectonic belts, the Cariboo Lake area is in

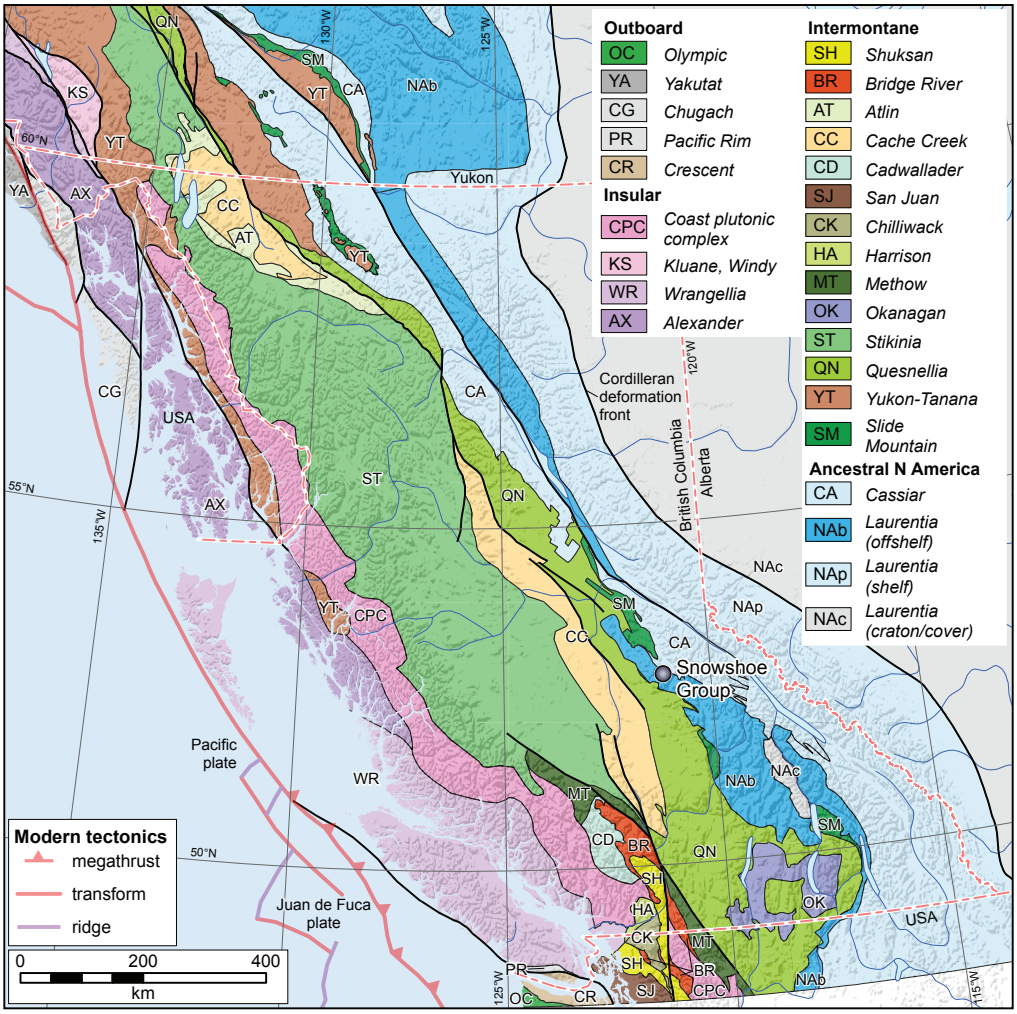


Fig. 1. Tectonic elements of the Canadian Cordillera in British Columbia and location of study area. Terranes after Colpron (2020).

Kootenay terrane, locally represented by Barkerville subterrane (Fig. 2). The Snowshoe Group (Neoproterozoic-lower Cambrian), which consists predominantly of siliciclastic rocks with lesser carbonate and volcanic rocks, represents part of the Ancestral North America clastic wedge that was displaced from the original continental margin. The unit is bounded to the southwest, across the northeast-vergent Eureka thrust, by Late Triassic to Early Jurassic arc volcanic rocks and comagmatic intrusions and siliciclastic rocks of Quesnel terrane (Nicola Group) and late Paleozoic oceanic rocks of Slide Mountain terrane (Crooked amphibolite). To the northeast, across the southwest-vergent Pleasant Valley thrust, are siliciclastic and carbonate rocks of the Cariboo terrane that originated closer to the Ancestral North American continental margin. To the north is a large Slide Mountain terrane klippe consisting of fine-grained siliciclastic rocks, chert, basalt, and mafic intrusive rocks (Slide Mountain Group). The klippe is floored by the Pundata thrust, which is considered to link with the Eureka thrust (Fig. 2; Ferri and O'Brien, 2003).

In the Jurassic-Cretaceous, the Snowshoe Group was polydeformed and metamorphosed to upper amphibolite grade. Ferri and O'Brien (2003) recognized a series of second-phase southwest-vergent nappes (Fig. 3), which enabled simplifying Snowshoe Group stratigraphy (Fig. 4; see also Schiarizza and Ferri, 2003; Ferri and Schiarizza, 2006). Mafic to intermediate volcanic rocks and small gabbroic dikes and sills are interspersed throughout the Snowshoe Group (Fig. 4). The most areally extensive volcanic rocks are exposed along the ridge containing Mount Barker and continuing northwest across the Cariboo River valley (Fig. 3). Grouped with this unit is a belt of doubly folded mafic metavolcanic rocks between Keithley and Rollie creeks (Fig. 3). Mafic to intermediate volcanic rocks are also found southwest of Frank Creek and near Badger Peak. Isolated mafic volcanic rocks also occur throughout the Harveys Ridge succession. Gabbroic dikes and sills are most prevalent in the Downey and Transitional Harveys successions near Keithly and Rollie creeks and in the Downie succession northeast of Mount Barker, one of which forms a mappable unit northeast of Mount Barker (Fig. 3). Two of the samples collected for U-Pb zircon geochronology are from this intrusion; the third is from a smaller sill between Rollie and Keithley creeks (Fig. 3).

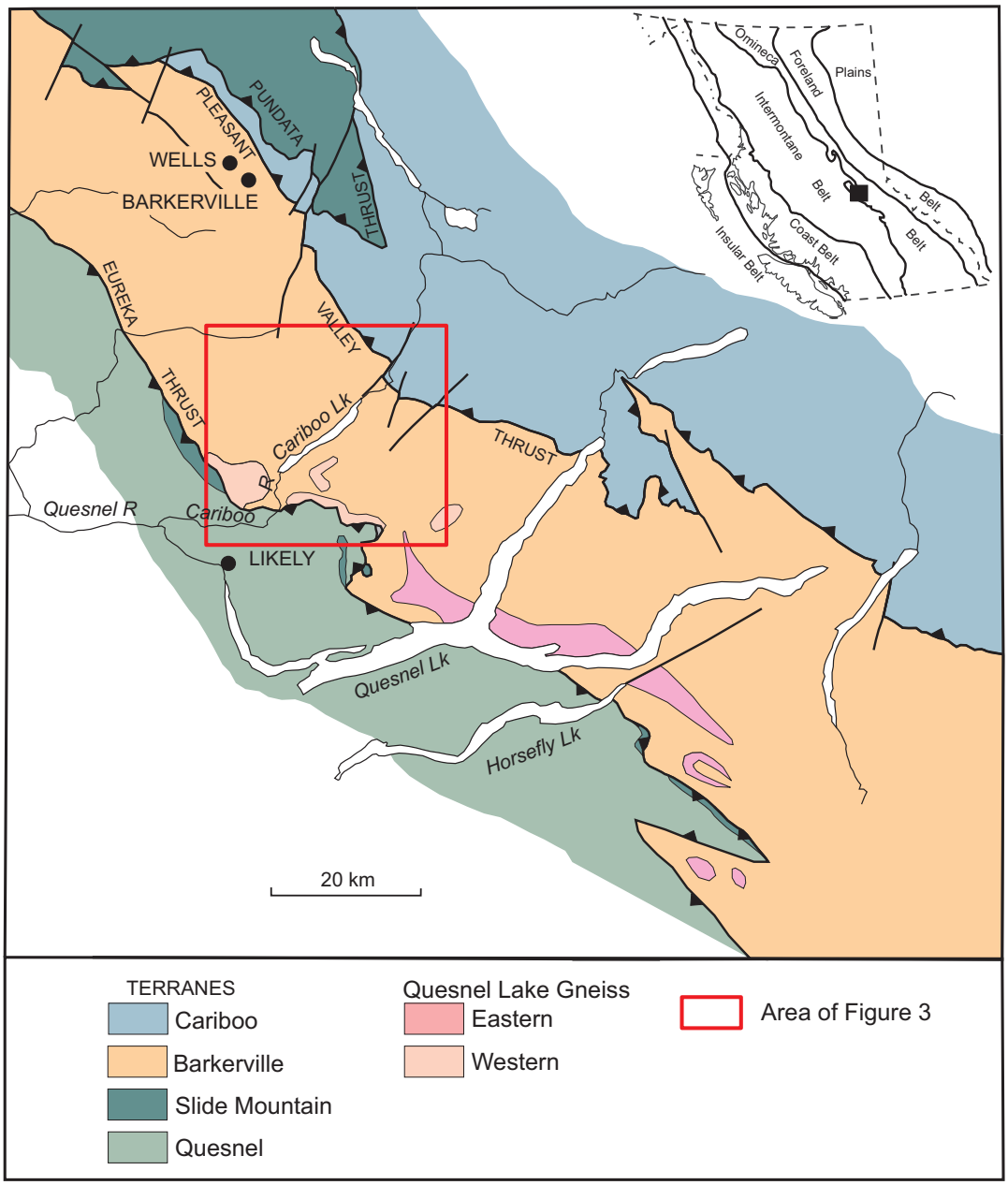


Fig. 2. Regional geological map. Modified after Struik (1986).

4. U-Pb zircon geochronology

During 2001 mapping, three gabbroic intrusions were sampled for geochronological analysis: two from a northwest-trending body northeast of Mount Barker and one from a sill intruding the Transitional Harveys Ridge succession between Rollie and Keithley creeks (Fig. 3). These bodies were chosen as they were relatively coarser grained and contained a few per cent modal quartz.

4.1. Analytical techniques

U-Pb geochronological analysis of the three samples began in late 2001. Multigrain zircon fractions were selected on the basis of zoning patterns observed in cathode luminescence and backscatter images. The portions of grains selected for analysis were broken off and plucked from grain mounts with a probe and surgical forceps under a binocular microscope. These fragments were air abraded before dissolution using the technique of Krogh (1982). This was followed by washing with 3N HNO_3 in an ultrasonic cleaner for 10 minutes and rinsing with deionized water and acetone. Immediately before dissolution, grain fragments were washed in clean 10 ml borosilicate beakers, with ultrapure 3N HNO_3 at 50°C for 20 minutes and rinsed with ultrapure water and sub-boiled acetone. Fragments were tapped onto Al-foil weigh boats and weighed on a Mettler M3

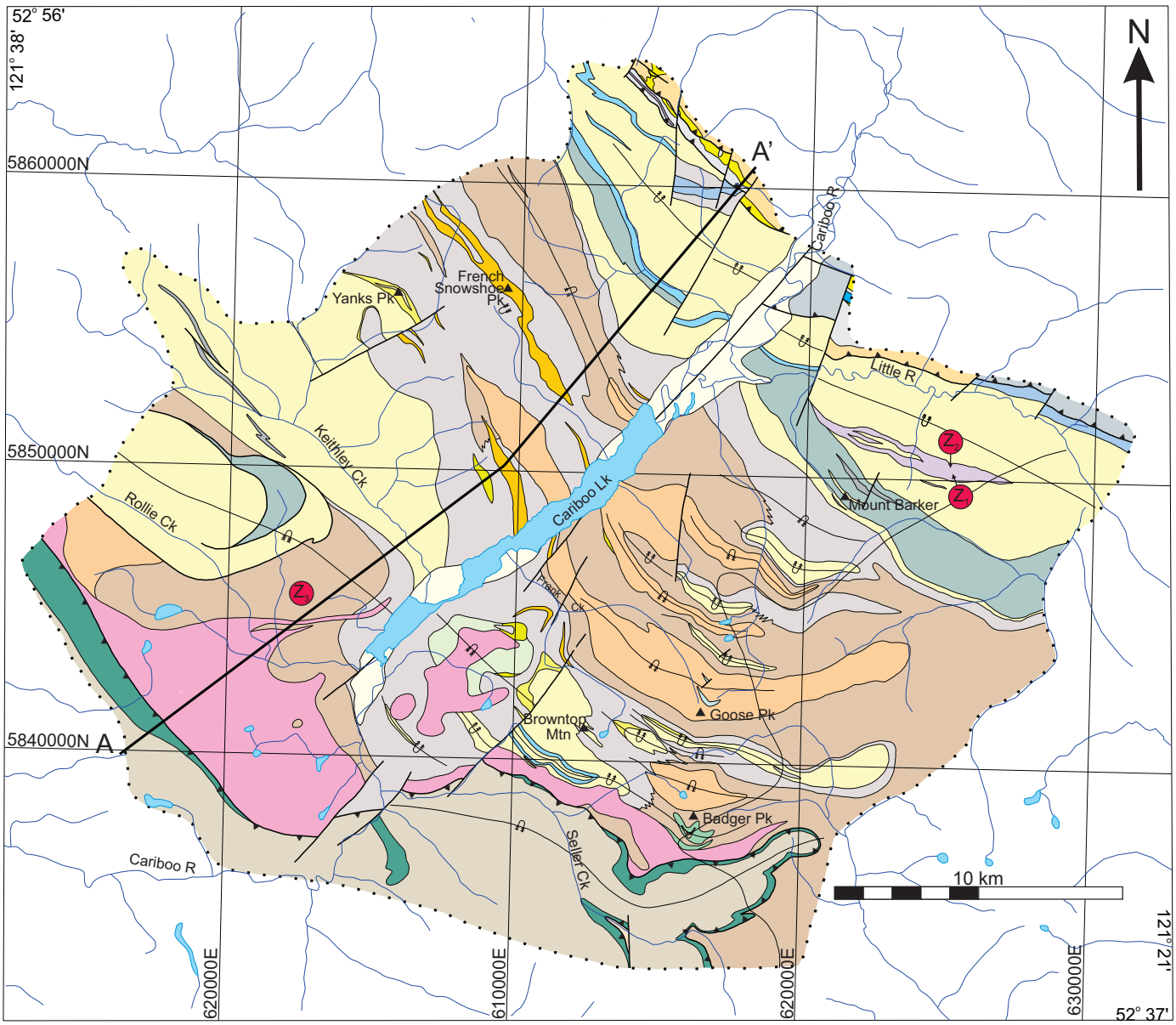
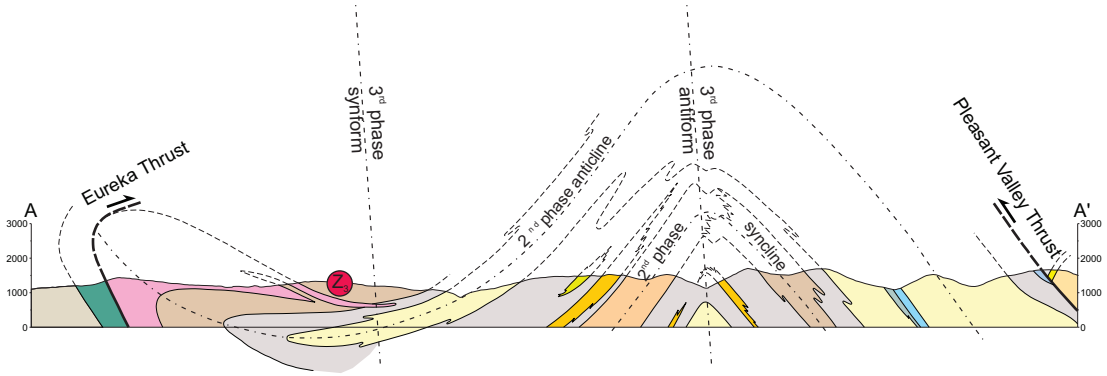


Fig. 3. a) Geology of the Cariboo Lake area. **b)** Legend.

microbalance with an estimated precision of ±2 mg and then loaded into 300 ml teflon or Savillex® PFA Parrish-style microcapsules. Zircon fragments were dissolved in ~100 ml of sub-boiled 29N HF and ~15 ml of sub-boiled 15N HNO_3 in the presence of a mixed $^{233\text{-}235}U$-^{205}Pb tracer for 40 hours at 240°C. Dissolution took place in conventional stainless steel Parr bombs with 250 ml teflon liners, each containing 8-13 microcapsules. Sample solutions were then dried to salts at ~125°C. Approximately 100 ml of ultrapure 3.1N HCl (sub-boiled 6.2N HCl + ultrapure water) was added to microcapsules, which were rebombed and salts were dissolved for 12 hours at 210°C. Separation and purification of Pb and U employed ion exchange column techniques modified slightly from those described by Parrish et al. (1987), using 250 ml resin volume FEP shrink tube columns. Pb and U were eluted sequentially into the same 7 ml Savillex® screwtop beaker followed by the addition of ~10 ml of 0.6N ultra-pure phosphoric acid. Each sample was loaded onto a single zone refined Re filament using a phosphoric acid-silica gel emitter made with silicon tetrachloride. Isotopic ratios were measured using a modified single collector VG-54R thermal ionization mass spectrometer equipped with a Daly photomultiplier. Both U and Pb were run at 1450°C, in peak-switching mode on the Daly detector. U fractionation was determined directly on individual runs using the $^{233\text{-}235}U$ tracer, and Pb isotopic ratios were corrected for a fractionation of 0.37%/amu, based on replicate analyses of the NBS-981 Pb standard and the values recommended by Thirlwall (2000). U and Pb analytical blanks were less than 1 pg and in



Slide Mountain terrane

Quaternary

M. to L. Triassic
SLOCAN GP
Dark grey to black phyllite

Penn. to Permian
SLIDE MOUNTAIN GP
Crooked amphibolite; chlorite schist, amphibolite ultramafite

Kootenay terrane

E. Permian
Gabbro

E. Mississippian
Western Quesnel Lk gneiss; mega crystic orthogneiss

Proterozoic and Cambrian
SNOWSHOE GP
Cambrian
Bralco limestone
Grey to cream limestone

Goose Peak quartzite
Quartzite and quartzite conglomerate

Chloritic phyllite to schist

Agnes conglomerate
Granule to boulder conglomerate

Harveys Ridge succession
Grey to dark grey phyllite

Transitional Harveys Ridge; grey to dark grey phyllite, sandstone.

Frank Creek mafic to intermediate metavolcanic rocks;

Frank Creek mafic metavolcanic rocks

Badger Peak mafic metavolcanic rocks

Neoproterozoic to Cambrian
Downey succession
Quartzite

Micaceous to feldspathic sandstone

Chlorite schist (meta-volcanics)

Dark grey limestone

Grey to white limestone

Neoproterozoic or Cambrian
SNOWSHOE GP undivided

Cariboo terrane

Permian?
Gabbro

L. Ordovician and Devonian or younger
BLACK STUART GP
Black shale, argillite, limestone

Proterozoic and Paleozoic
CARIBOO Gp
Cariboo Gp undivided

E. Cambrian
Midas Fm

Yanks Peak Fm

Neoproterozoic
Yankee Belle Fm

Second phase anticline, syncline

Third phase antiform, synform

Z U-Pb geochronology sample

Fig. 3. b) Legend.

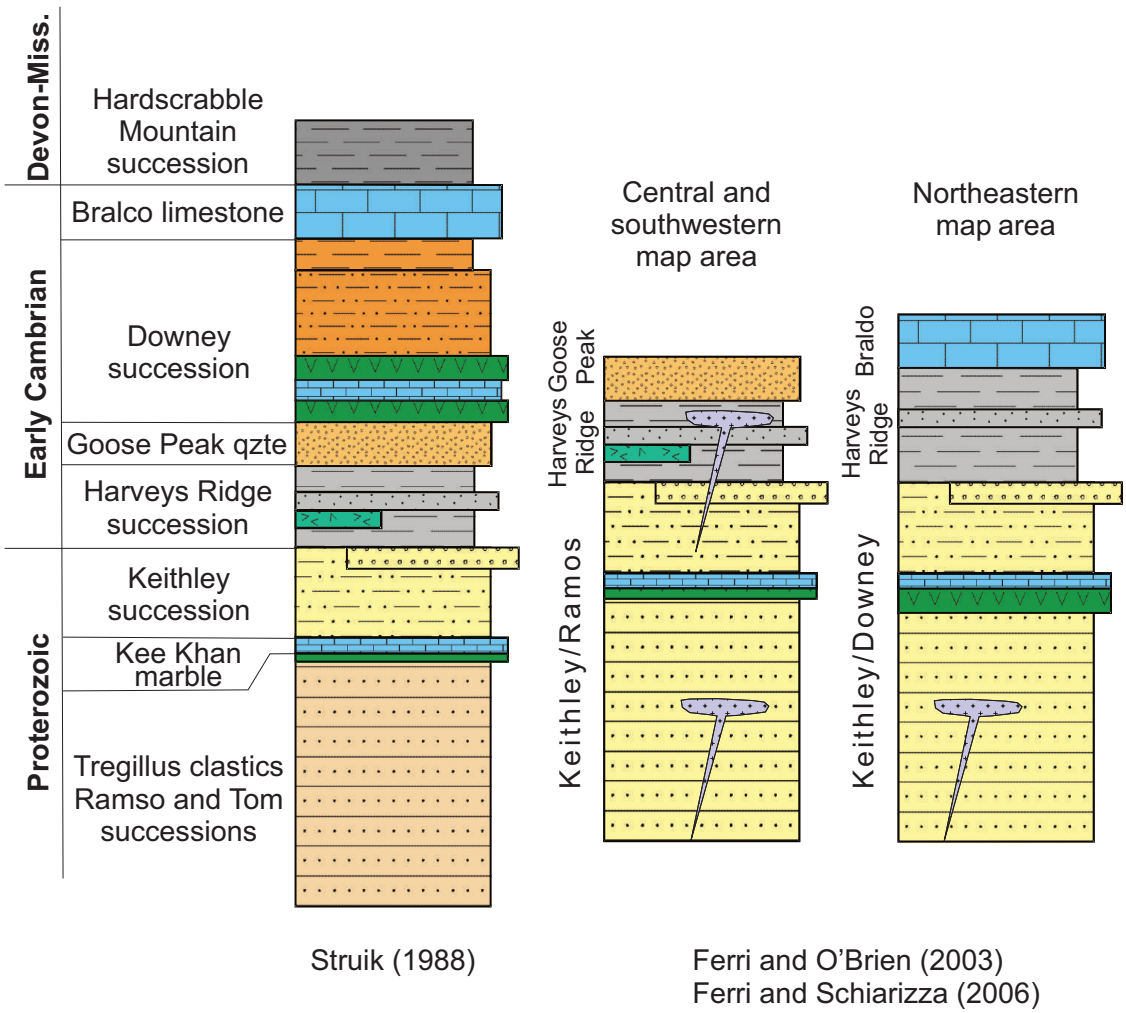


Fig. 4. Generalized stratigraphy of the Snowshoe Group as proposed by Struik (1988) and re-interpretation by Ferri and O'Brien (2003) and Ferri and Schiarizza (2006) based on repetition of units in large F_2 folds.

the range of 1.5-3.5 pg, respectively, during the course of this study. Common Pb isotopic compositions are derived from the model of Stacey and Kramers (1975). Concordia intercept ages and associated errors were calculated using a modified version of the York-II regression model (wherein the York-II errors are multiplied by the MSWD) and the algorithm of Ludwig (1980). All ages are quoted at the 2σ level of uncertainty. Isotopic dates are calculated with the decay constants λ238 = 1.55125E-10 and λ235 = 9.8485E-10 (Jaffey et al., 1971).

4.2. Results

Data from all three multigrain samples (Table 1) indicate significant lead loss; sample BO-06-04 also indicates evidence of inheritance. Regression lines on concordia plots yield upper intercepts that suggest a single crystallization age of ca. 280 Ma (Fig. 5).

5. Lithogeochemistry

Rare earth element data for more than 50 samples of mafic to intermediate metavolcanic and mafic intrusive rocks (Table 2) were determined at Memorial University in St. John's, Newfoundland using peroxide fusion followed by inductively coupled plasma mass spectrometry (ICP-MS) analyses. The corresponding major oxide and trace element compositions for many of these samples are provided in Ferri (2001a) and Ferri and O'Brien (2002). Whole rock Sm-Nd isotopic abundances for selected mafic intrusive bodies, including those analyzed for U-Pb geochronology (Table 3), were generated at the Pacific Centre for Isotopic and Geochemical Research, University of British Columbia in Vancouver.

Based on these analyses, we recognize three broad age groupings of igneous rocks (Fig. 6). One group consists of Mississippian to Permian metavolcanic rocks of the Crooked amphibolite. The second includes several Permian intrusions: 1) a gabbro sill in rocks of Cariboo terrane; 2) gabbroic sills and dikes intruding Snowshoe Group rocks between

Table 1. Multigrain U-Pb zircon analyses.

	Compositional Parameters									Radiogenic Isotope Ratios									Isotopic Ages					
Sample	Wt. mg	U ppm	Th/U	Pb ppm	$^{206}Pb^*$ x10^{-13} mol	mol % $^{206}Pb^*$	Pb^*/Pb_c	Pb_c (pg)	$^{206}Pb/^{204}Pb$	$^{208}Pb/^{206}Pb$	$^{207}Pb/^{206}Pb$	% err	$^{207}Pb/^{235}U$	% err	$^{206}Pb/^{238}U$	% err	corr. coef.	$^{207}Pb/^{206}Pb$	±	$^{207}Pb/^{235}U$	±	$^{206}Pb/^{238}U$	±
(a)	(b)	(c)	(d)	(c)	(e)	(e)	(e)	(e)	(f)	(g)	(g)	(h)	(g)	(h)	(g)	(h)		(i)	(h)	(i)	(h)	(i)	(h)
01FFe39-1																								
A	0.014	14320	0.756	569.4	278.1437	97.79%	14	520.87	805	0.246	0.051745	1.541	0.237406	1.681	0.033275	0.222	0.670	274.17	35.30	216.29	3.27	211.01	0.46
B	0.011	12459	0.918	571.6	201.1978	96.09%	8	678.79	467	0.298	0.051912	0.539	0.252027	0.643	0.035211	0.299	0.553	281.55	12.33	228.22	1.31	223.08	0.65
C	0.013	9517	0.852	376.8	173.2806	99.02%	33	142.30	1859	0.278	0.051816	0.269	0.239983	0.541	0.033590	0.403	0.877	277.31	6.17	218.41	1.06	212.98	0.84
D	0.008	13331	1.046	583.1	154.5681	98.27%	20	224.96	1057	0.339	0.051730	0.322	0.247926	0.472	0.034760	0.237	0.783	273.48	7.37	224.89	0.95	220.27	0.51
E	0.009	9767	0.766	473.1	132.9370	94.13%	5	689.22	308	0.249	0.051997	1.826	0.260040	1.926	0.036271	0.379	0.357	285.26	41.74	234.70	4.04	229.68	0.85
01FFe39-2																								
A	0.007	13774	0.972	621.3	139.8978	96.67%	10	399.09	542	0.316	0.051825	1.096	0.248661	1.219	0.034799	0.262	0.555	277.70	25.08	225.49	2.46	220.51	0.57
B	0.023	2111	0.727	91.9	75.7651	98.40%	20	102.91	1115	0.235	0.051875	0.938	0.267701	1.051	0.037428	0.313	0.490	279.89	21.47	240.85	2.25	236.87	0.73
C	0.016	13362	0.900	567.6	313.2660	98.51%	22	393.80	1180	0.292	0.051714	1.374	0.250583	1.599	0.035143	0.592	0.539	272.79	31.48	227.05	3.25	222.66	1.29
D	0.016	11949	0.927	527.2	280.9968	97.55%	13	585.13	745	0.301	0.051891	0.391	0.252196	0.538	0.035249	0.279	0.716	280.60	8.94	228.36	1.10	223.32	0.61
E	0.019	8121	0.918	342.3	225.7390	98.89%	30	210.22	1642	0.298	0.051895	0.261	0.251055	0.502	0.035087	0.354	0.871	280.76	5.96	227.43	1.02	222.31	0.77
BO-06-04																								
A	0.005	460	1.530	32.0	4.3137	97.97%	21	7.43	889	0.637	0.071386	0.657	0.442824	0.805	0.044990	0.399	0.583	968.50	13.42	372.24	2.51	283.69	1.11
B	0.011	399	2.556	32.9	8.1341	97.30%	18	18.72	673	0.976	0.064388	0.429	0.394412	0.504	0.044427	0.262	0.526	754.40	9.06	337.59	1.45	280.21	0.72
C	0.010	369	3.310	27.1	5.9649	97.99%	26	10.14	902	1.064	0.051884	0.494	0.277254	0.568	0.038757	0.214	0.511	280.28	11.30	248.48	1.25	245.12	0.51
D	0.010	1211	3.141	91.5	18.8701	93.57%	8	107.40	284	1.016	0.052021	0.724	0.267986	0.697	0.037362	0.440	0.252	286.31	16.56	241.08	1.50	236.46	1.02

(a) A, B, etc. are labels for fractions composed of air abraded zircon grains.

(b) Fraction masses determined on Mettler M3 microbalance to ±2 micrograms.

(c) U and total Pb concentrations subject to uncertainty in fraction mass.

(d) Model Th/U ratio calculated from radiogenic $^{208}Pb/^{206}Pb$ ratio and $^{207}Pb/^{235}U$ age.

(e) Pb* and Pbc represent radiogenic and common Pb, respectively; mol % $^{206}Pb^*$ with respect to radiogenic, blank and initial common Pb.

(f) Measured ratio corrected for spike and fractionation only. Mass discrimination of 0.37%/amu based on analysis of NBS-982; all Daly analyses.

(g) Corrected for fractionation, spike, and common Pb; up to 300 pg of common Pb was assumed to be procedural blank: $^{206}Pb/^{204}Pb = 17.40 \pm 3.0\%$; $^{207}Pb/^{204}Pb = 15.80 \pm 2.0\%$; $^{208}Pb/^{204}Pb = 36.40 \pm 1.0\%$ (all uncertainties 1-sigma). Excess over blank was assigned to initial common Pb with S-K model Pb composition at 280 Ma.

(h) Errors are 2-sigma, propagated using the algorithms of Schmitz and Schoene (2007) and Crowley et al. (2007).

(i) Calculations are based on the decay constants of Jaffey et al. (1971). $^{206}Pb/^{238}U$ and $^{207}Pb/^{206}Pb$ ages corrected for initial disequilibrium in $^{230}Th/^{238}U$ using Th/U [magma] = 3.

(j) Corrected for fractionation, spike, and blank Pb only.

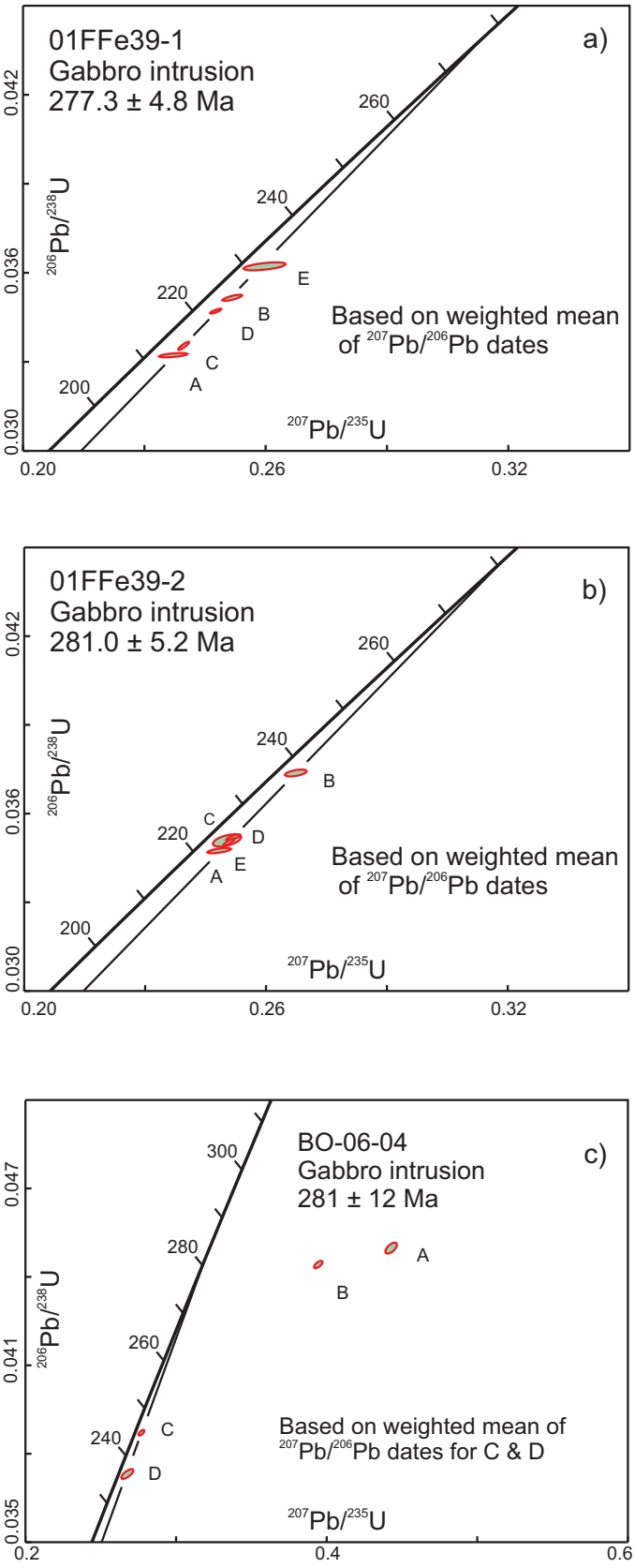


Fig. 5. Multigrain U-Pb zircon concordia plots for samples of gabbro that intrudes the Snowshoe Group north of Mount Barker (**a**, **b**) and northwest of southern Cariboo Lake (**c**).

Keithley and Rollie creeks; and 3) gabbroic intrusions in the Downey succession north of Mount Barker. The third includes Neoproterozoic to Cambrian metavolcanic rocks comprising: 1) metavolcanic rocks along Badger Peak; 2) metavolcanic rocks in the Harveys Ridge succession southwest of Frank Creek; 3) metavolcanic rocks in the Harveys Ridge succession north of Cariboo Lake; 4) sheared gabbro and metavolcanic rocks southwest of Keithley Creek; and 5) metavolcanic rocks along the ridge containing Mount Barker and that extend northwestward across the Cariboo River.

5.1. Mississippian to Permian

5.1.1. Crooked amphibolite

Metavolcanic rocks of the Crooked amphibolite consist primarily of chlorite schist to finely crystalline amphibolite. Analyzed samples define a cluster of basaltic composition (Fig. 6a). A tectonic discrimination diagram using Th/Yb versus Nb/Yb defines a cluster straddling the E-MORB-N-MORB transition along the mantle array corridor (Fig. 7a). The MORB nature of these samples is further exemplified by flat REE and extended-REE patterns (Figs. 8a, b).

5.2. Permian

5.2.1. Gabbro in Cariboo terrane

A gabboic sill intrudes rocks of the Midas Formation in the far northern part of the map area (Fig. 3). This body is an alkaline basalt (Fig. 6a) plotting near the OIB area of the MORB-OIB (Fig. 7b), which is supported by REE abundances (Figs. 8c, d). This sill has textural, modal and geochemical attributes similar to gabbro intruding Snowshoe rocks between Keithley and Rollie creeks and are assumed to be of the same age.

5.2.2. Gabbro sills and dikes intruding Snowshoe Group rocks between Keithley and Rollie creeks

Fine-grained gabbro sills and/or dikes up to 10s of m thick intrude rocks of the Downey, Harveys Ridge, and Transitional Harveys Ridge successions between Keithley and Rollie creeks. One of these was dated by U-Pb geochronology and returned an age of ca. 280 Ma. Based on similar textural, modal, and geochemical characteristics we consider that all are of the same age. These rocks form two bulk compositional clusters: basalt and alkali basalt (Fig. 6a). The basaltic rocks plot within the E-MORB portion of the MORB- OIB array whereas the alkali basalts plot near the OIB field, suggesting within-plate affinities (Fig. 7a). Similarly, the basaltic rocks display typical flat MORB profiles in extended REE plots whereas the alkali basalts show enrichment in the light rare earth elements and depletion in the heavy rare earth elements (Figs. 8e, f).

5.2.3. Gabbro intrusions in the Downey succession north of Mount Barker

Fine- to medium-grained gabbro sills and dikes intrude the Downey succession north of Mount Barker. Two samples from a large (~5 km long, up to 1 km wide), northwest-trending

Table 2. Rare earth element geochemistry of selected igneous rocks.

Station No.	Easting	Northing	Unit	Lithology	Th ppm	La ppm	Ce ppm	Pr ppm	Nd ppm	Sm ppm	Eu ppm	Gd ppm	Tb ppm	Dy ppm	Ho ppm	Er ppm	Tm ppm	Yb ppm	Lu ppm	Hf ppm	Ta ppm
00FFE-23-5	616125	5837760	BP	Chlorite schist	4.19	35.92	68.43	7.75	30.70	6.04	1.90	5.60	0.83	4.97	1.01	2.94	0.37	2.24	0.32	4.90	3.49
00FFE-23-6	616164	5837567	BP	Gabbro	1.01	9.56	19.58	2.42	10.53	2.36	0.73	2.37	0.35	2.11	0.43	1.23	0.16	0.95	0.14	2.13	1.08
00FFE-15-9	610828	5839105	CA	Chlorite schist	0.55	3.99	9.47	1.53	7.78	2.31	0.84	3.01	0.50	3.37	0.77	2.40	0.32	1.97	0.29	1.83	0.16
00FFE-22-1	614272	5835709	CA	Listwanite	0.48	4.79	12.53	2.01	10.47	3.39	1.23	4.32	0.75	5.04	1.12	3.52	0.47	3.00	0.45	2.99	0.22
00FFE-22-2	614538	5835485	CA	Amphibolite	0.23	5.08	15.77	2.62	14.25	4.72	1.71	6.02	1.03	6.91	1.51	4.71	0.63	3.89	0.58	4.49	0.34
00FFE-24-2	616084	5836461	CA	Amphibolite	0.58	6.73	16.38	2.61	13.33	4.29	1.62	5.60	0.94	6.28	1.38	4.39	0.59	3.76	0.56	3.78	0.30
01BO-29-5	614366	5863133	C-D	Gabbro	1.49	9.15	18.10	2.21	9.33	2.15	0.78	2.56	0.37	2.23	0.40	1.07	0.13	0.80	0.12	2.06	0.87
01BO-31-5	614857	5862407	C-D	Gabbro	1.87	10.27	20.23	2.44	10.53	2.54	0.93	3.06	0.43	2.57	0.47	1.19	0.15	0.92	0.15	2.47	1.01
00FFE-38-1	609864	5841876	FC	Meta-basalt	10.91	31.35	57.14	6.74	24.44	4.31	0.73	3.39	0.48	2.84	0.57	1.72	0.22	1.40	0.20	3.74	1.22
00FFE-4-1	607352	5844008	FC	Meta-basalt	13.35	45.10	77.34	9.48	33.40	5.57	0.72	3.93	0.53	2.99	0.58	1.78	0.24	1.48	0.22	2.75	1.03
00FFE-4-11	609883	5843781	FC	Meta-basalt	10.72	24.47	46.29	5.89	21.94	4.25	0.76	3.34	0.47	2.75	0.56	1.68	0.23	1.41	0.21	3.06	1.03
00FFE-4-14	609712	5842941	FC	Chlorite schist	2.98	19.12	40.56	4.99	20.76	4.73	1.52	4.61	0.67	3.89	0.76	2.19	0.27	1.66	0.25	4.11	2.19
00FFE-4-7	608730	5843209	FC	Meta-basalt	14.20	39.86	71.42	8.54	29.84	4.87	1.07	3.34	0.45	2.54	0.50	1.54	0.21	1.32	0.19	3.70	1.10
00FFE-8-10	610179	5844196	FC	Meta-basalt	2.30	17.91	35.72	4.32	17.55	3.85	0.76	3.58	0.51	2.96	0.57	1.61	0.20	1.19	0.17	3.33	1.22
00FFE-8-11	610090	5844241	FC	Meta-basalt	2.55	20.64	44.10	5.41	22.39	4.55	1.36	4.30	0.62	3.57	0.72	2.05	0.26	1.54	0.21	4.16	2.04
00FFE-8-2	608248	5844719	FC	Meta-basalt	11.94	37.20	66.91	7.88	27.31	4.43	0.81	3.15	0.42	2.43	0.49	1.51	0.20	1.26	0.18	2.97	0.87
00FFE-9-7	608683	5842293	FC	Meta-basalt	0.44	4.60	12.89	2.07	10.83	3.62	1.29	4.78	0.80	5.47	1.20	3.79	0.50	3.16	0.47	3.39	0.23
01FFE-08-08	608950	5849809	HR-V	Chlorite schist	2.24	18.07	36.99	4.78	20.69	4.53	1.55	4.56	0.66	3.76	0.67	1.74	0.23	1.40	0.19	3.47	1.50
01FFE-09-02a	605096	5844003	HR-V	Chlorite schist	2.59	15.16	28.71	3.28	12.79	2.42	0.85	2.46	0.38	2.26	0.44	1.20	0.17	1.08	0.16	2.30	1.56
01FFE-09-4a	605812	5845055	HR-V	Chlorite schist	4.02	28.65	57.81	7.09	29.35	6.00	1.76	5.93	0.86	4.89	0.88	2.31	0.31	1.88	0.26	5.79	2.91
01FFE-09-4b	605812	5845055	HR-V	Chlorite schist	2.86	24.30	41.76	4.45	16.43	2.86	0.44	2.59	0.37	2.05	0.36	0.96	0.13	0.79	0.11	3.81	2.67
01FFe-35-2	615548	5860691	HR-V	Meta-basalt	0.40	4.16	9.35	1.33	5.59	1.38	0.38	1.65	0.24	1.54	0.36	1.00	0.12	0.79	0.10	1.87	0.39
01FFE-11-08	601192	5849676	KC	Chlorite schist	4.59	35.42	70.66	8.50	34.94	7.40	2.39	6.68	0.98	5.47	0.95	2.49	0.33	2.02	0.30	7.31	4.56
01FFE-11-7a	601064	5850147	KC	Chlorite schist	3.24	24.32	48.74	5.96	24.67	4.98	1.48	4.87	0.70	3.94	0.70	1.83	0.24	1.45	0.20	4.46	3.05
01FFE-11-7b	601064	5850147	KC	Chlorite schist	3.09	20.98	42.80	5.25	22.25	5.26	1.73	5.10	0.77	4.43	0.79	2.13	0.28	1.76	0.26	5.46	3.40
01BO-6-4	601826	5848997	KR-D	Gabbro	0.32	3.33	9.35	1.61	8.39	2.94	1.01	3.93	0.70	4.82	1.00	2.84	0.40	2.65	0.38	3.05	0.20
01FFE-03-01	597750	5845225	KR-D	Gabbro	0.40	3.56	9.50	1.57	8.34	2.68	1.00	4.17	0.72	4.86	1.09	3.26	0.51	3.39	0.42	2.59	0.15
01FFE-03-01A	597750	5845225	KR-D	Gabbro	4.29	28.77	59.16	7.32	30.76	6.30	2.08	6.89	0.97	5.66	1.12	3.05	0.43	2.74	0.33	6.14	2.79
01FFE-03-07	597440	5846775	KR-D	Gabbro	2.71	17.67	37.38	4.69	20.05	4.33	1.47	4.82	0.69	3.99	0.79	2.13	0.30	1.89	0.23	4.21	1.82
01FFE-06-09	602549	5845117	KR-D	Gabbro	3.77	26.55	55.85	6.99	29.53	6.02	2.03	6.42	0.88	4.94	0.94	2.50	0.35	2.17	0.26	5.17	3.43
01FFE-07-02	602901	5846038	KR-D	Gabbro	0.63	2.32	5.82	0.90	4.71	1.52	0.58	2.23	0.40	2.79	0.60	1.85	0.28	1.88	0.29	2.09	0.14
01FFE-11-04	603458	5849443	KR-D	Gabbro	1.07	6.83	17.44	2.67	13.66	4.36	1.49	5.60	0.98	6.60	1.34	3.94	0.58	3.80	0.60	4.93	0.36
01FFe-40-7a	602880	5846012	KR-D	Gabbro	0.70	2.90	7.15	1.06	5.26	1.78	0.65	2.31	0.46	3.28	0.67	2.07	0.30	2.08	0.33	2.37	0.17
BO-06-6	603109	5845654	KR-D	Gabbro	2.86	24.34	52.85	6.63	27.63	5.93	2.12	5.22	0.74	4.09	0.70	1.82	0.24	1.44	0.21	5.15	2.51
01FFe-41-1a	596524	5856980	KR-D	Gabbro	0.68	8.92	22.56	3.36	17.06	5.25	1.98	6.52	1.09	7.20	1.40	4.08	0.56	3.83	0.55	5.71	0.59
01FFe-41-1b	596524	5856980	KR-D	Chlorite schist	3.80	24.70	46.50	5.24	20.75	4.07	1.50	3.87	0.62	3.92	0.75	2.17	0.29	2.02	0.29	3.60	2.56
00FFE-34-5	621233	5849302	MB-D	Gabbro	5.15	19.70	39.02	5.06	21.32	5.00	1.41	4.84	0.69	4.01	0.79	2.35	0.30	1.89	0.28	2.80	0.31
00FFE-35-2	621817	5849596	MB-D	Gabbro	4.17	16.35	32.90	4.21	17.90	4.21	1.07	4.09	0.59	3.44	0.69	2.05	0.27	1.65	0.24	2.48	0.28
01BO-33-3a	626161	5849138	MB-D	Gabbro	5.03	19.62	39.56	5.23	22.88	5.33	1.61	5.77	0.81	4.86	0.84	2.31	0.32	2.07	0.30	3.62	0.34
01FFe-38-5	627262	5848373	MB-D	Gabbro	2.98	11.46	23.52	3.08	13.29	3.16	1.01	3.38	0.46	2.82	0.49	1.28	0.18	1.23	0.18	2.16	0.17
01FFe-39-1	625052	5850254	MB-D	Gabbro	1.36	10.49	23.06	3.29	14.00	2.82	0.94	2.91	0.42	2.50	0.58	1.67	0.21	1.35	0.16	1.86	0.16
01FFe-39-2	624956	5850418	MB-D	Gabbro	3.68	24.75	52.23	7.01	29.14	5.31	1.42	4.84	0.66	3.86	0.91	2.59	0.35	2.25	0.28	3.81	0.39
BO-18-03a	624336	5849846	MB-D	Gabbro	3.97	22.75	56.23	8.47	38.17	7.65	2.86	8.00	1.10	6.34	1.47	3.83	0.50	2.82	0.35	5.20	0.50
BO-18-05	625052	5850070	MB-D	Meta-basalt	7.16	32.46	66.06	8.32	34.83	7.93	2.39	8.22	1.06	6.00	0.98	2.48	0.34	2.11	0.32	4.94	0.68
00FFE-34-4	621228	5849252	MB-V	Chlorite schist	4.13	16.21	32.77	4.27	18.04	4.32	1.31	4.20	0.59	3.40	0.66	1.95	0.25	1.56	0.24	2.35	0.25
00FFE-34-6	621300	5849441	MB-V	Chlorite schist	4.39	22.77	46.75	5.93	24.50	5.40	1.72	5.00	0.70	4.00	0.73	1.96	0.23	1.35	0.20	3.92	1.10
00FFE-34-8	621325	5849754	MB-V	Meta-tuff	2.64	22.80	48.82	6.21	25.89	5.84	1.91	5.48	0.78	4.48	0.86	2.46	0.31	1.86	0.27	4.90	1.89
00FFE-36-7	620252	5851854	MB-V	Chlorite schist	4.90	20.87	41.96	5.47	23.22	5.49	1.57	5.22	0.74	4.27	0.83	2.48	0.32	1.96	0.29	2.70	0.29
00FFE-6-1	618855	5852940	MB-V	Chlorite schist	1.15	10.85	23.95	3.09	13.07	2.93	0.82	2.78	0.39	2.26	0.44	1.26	0.16	0.94	0.13	2.42	0.83
01FFE-17-02	613025	5858272	MB-V	Meta-basalt	4.52	29.32	60.54	7.42	30.71	6.62	2.12	6.06	0.89	5.04	0.89	2.32	0.31	1.90	0.29	7.28	3.37
BO-15-7a	613981	5857068	MB-V	Meta-basalt	1.48	24.80	57.45	7.95	34.36	6.24	1.94	6.00	0.83	4.90	1.19	3.12	0.40	2.50	0.29	7.27	2.59

Positive ion mass spectrometry (ICP-MS) at Memorial University of Newfoundland laboratories.
BP - Badger Peak Volcanics; CA - Crooked Amphibolite; DV - Downey Volcanics; FC - Frank Creek Volcanics; HR - Harveys Ridge Volcanics; KC - Sheared metavolcanics and gabbro southwest of Keithley Creek; KR - Gabbro/diorite between Keithley and Rollie creeks; MB-D - Mount Barker Diorite; MB-V - Mount Barker Volcanics; C-D - Cariboo Terrane Diorite/gabbro

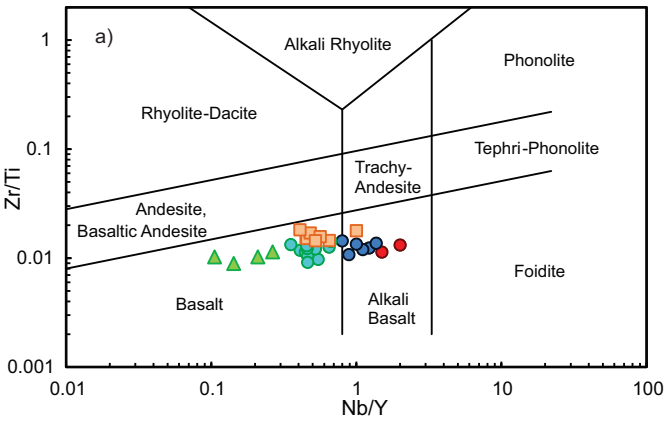
Table 3. Sm-Nd isotope data for gabbro intruding the Snowshoe Group.

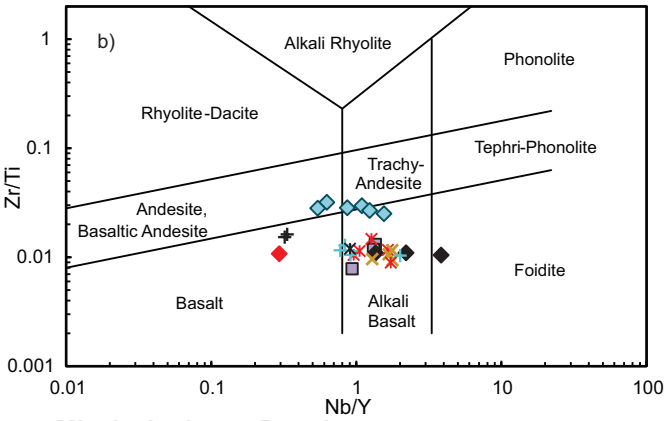
Sample Number	Age(T) (Map)	Sm (ppm)	Nd (ppm)	$^{147}Sm/^{144}Nd$	$^{143}Nd/^{144}Nd$	Error ±2s	$\varepsilon_{Nd}(T)$[1]	$\varepsilon_{Nd}(0)$	T_{DM}[2] (Ga)
01FFe-03-01	280	3.00	8.98	0.2021	0.512967	0.000007	6.2	6.4	N/A
01BO-6-4	280	3.51	10.17	0.2085	0.513012	0.000005	6.9	7.3	N/A
01FFe-39-1	280	3.08	12.95	0.1437	0.512319	0.000007	-4.3	-6.2	N/A
01FFe-39-2	280	5.10	23.98	0.1287	0.512208	0.000008	-6.0	-8.4	1.71

LA-ICP-MS analysis at the Pacific Centre for Isotopic and Geochemical Research, University of British Columbia, Vancouver, BC

[1]Calculated using $^{143}Nd/^{144}Nd$ of chondrite reservoir (CHUR) = 0.512638 and $^{147}Sm/^{144}Nd$ = 0.1966 (Hamilton et al., 1983).

[2]Calculated using $^{143}Nd/^{144}Nd$ = 0.513163 and $^{147}Sm/^{144}Nd$ = 0.2137 for the depleted mantle (DM) reservoir (Goldstein et al., 1984).





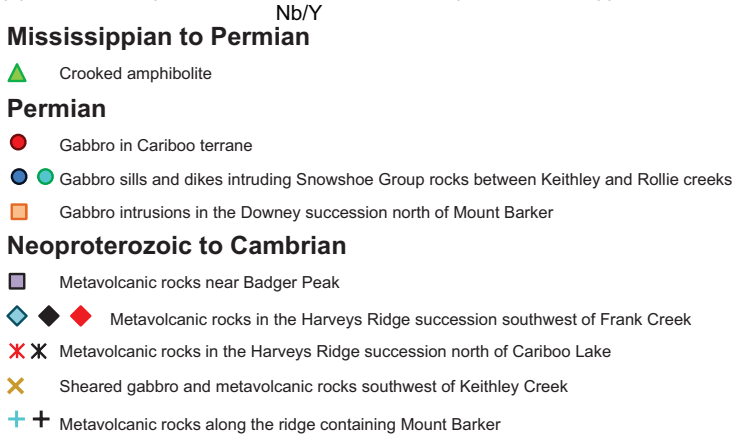


Fig. 6. Rock classification based on Zr/Ti vs. Nb/Y (Pearce, 1996). **a)** Mississippian to Permian rocks of the Crooked amphibolite, Permian gabbro intruding the Cariboo terrane, gabbro sills and dikes between Keithley and Rollie creeks and gabbro intrusions in the Downey succession north of Mount Barker. **b)** Neoproterozoic to Cambrian metavolcanic rocks near Badger Peak, metavolcanic rocks in the Harveys Ridge succession south of Frank Creek, metavolcanic rocks in the Harveys Ridge succession north of Cariboo Lake, sheared gabbro and metavolcanic rocks southwest of Keithley Creek, and metavolcanic rocks along the ridge containing Mount Barker.

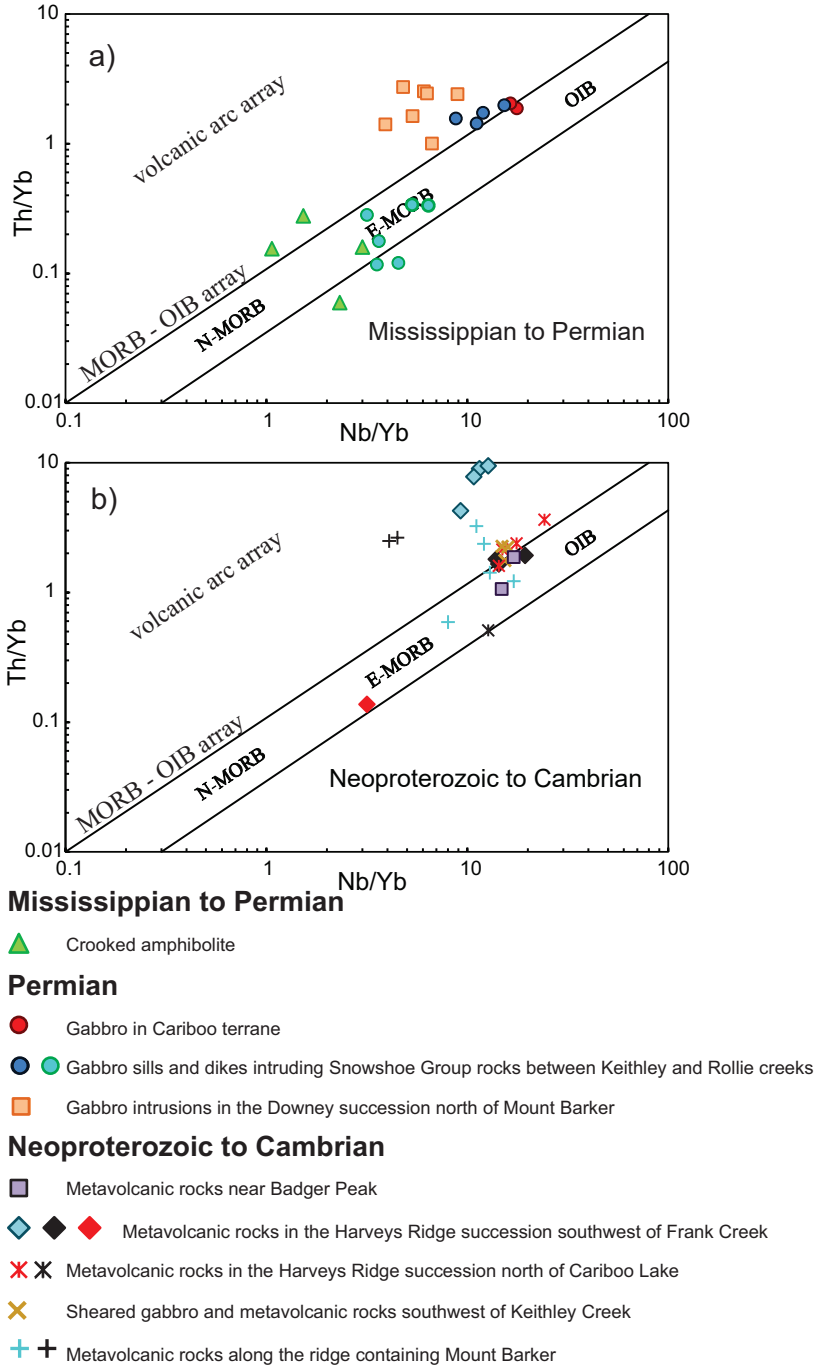


Fig. 7. Tectonic discrimination diagram of Pearce (2008). **a)** Mississippian to Permian rocks of the Crooked amphibolite, Permian gabbro intruding the Cariboo terrane, gabbro sills and dikes between Keithley and Rollie creeks, and gabbro intrusions in the Downey succession north of Mount Barker. **b)** Neoproterozoic to Cambrian metavolcanic rocks near Badger Peak, metavolcanic rocks in the Harveys succession south of Frank Creek, and metavolcanic rocks in the Harveys Ridge succession north of Cariboo Lake, sheared gabbro and metavolcanic rocks southwest of Keithley Creek, and metavolcanic rocks along the ridge containing Mount Barker.

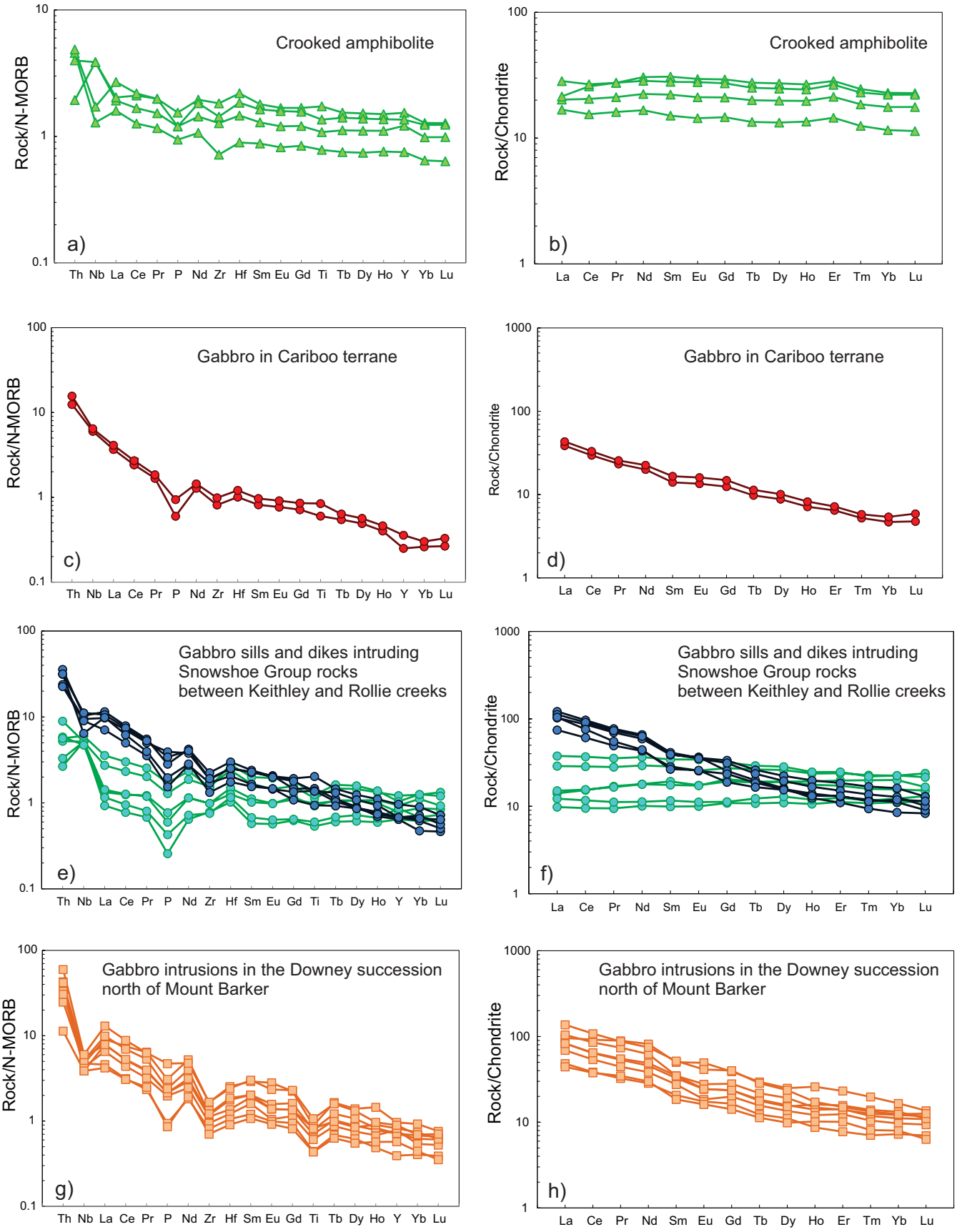


Fig. 8. a-h) Rare earth element plots for igneous and volcanic rocks in Figures 6 and 7.

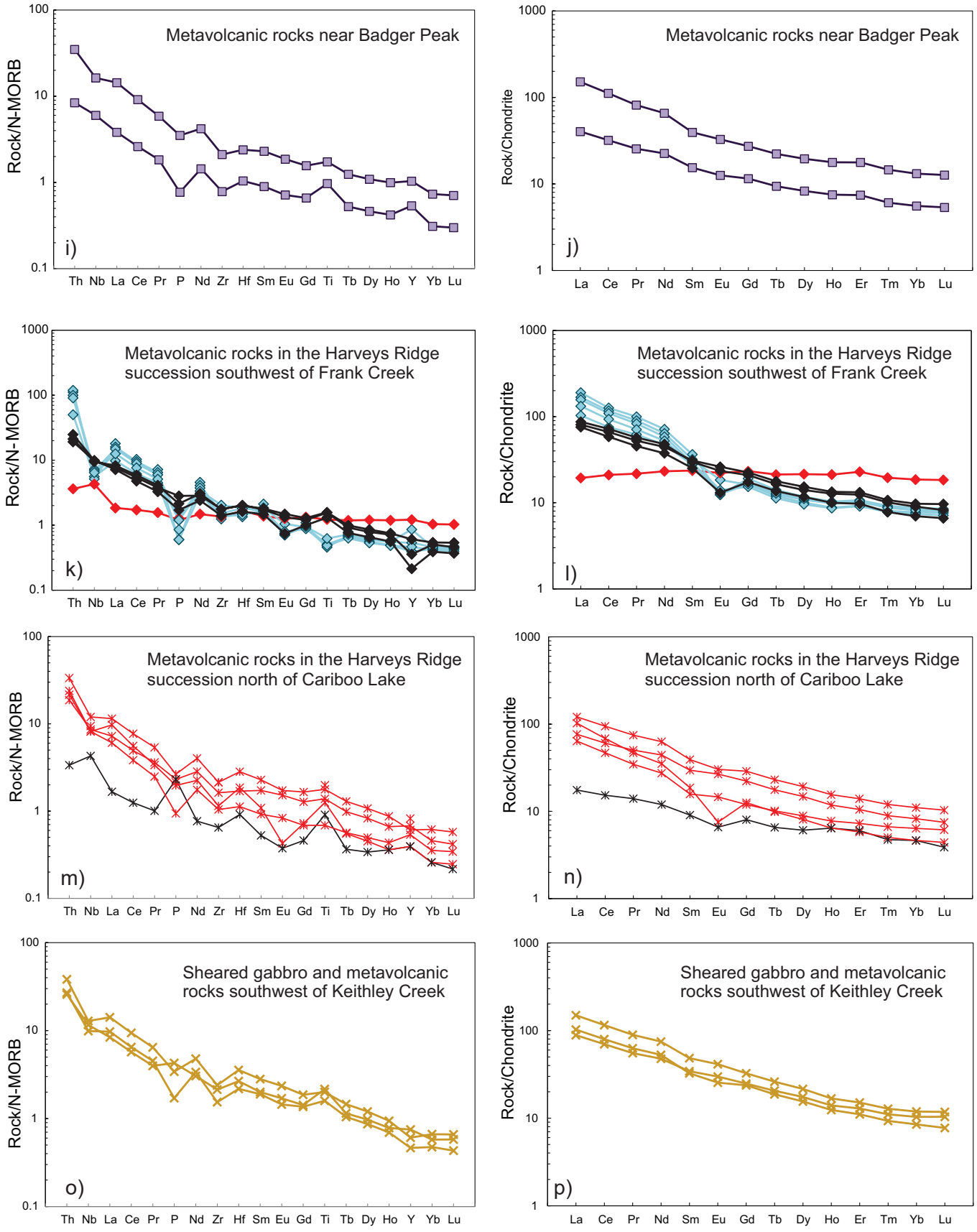


Fig. 8 continued. i-p) Rare earth element plots for igneous and volcanic rocks in Figures 6 and 7.

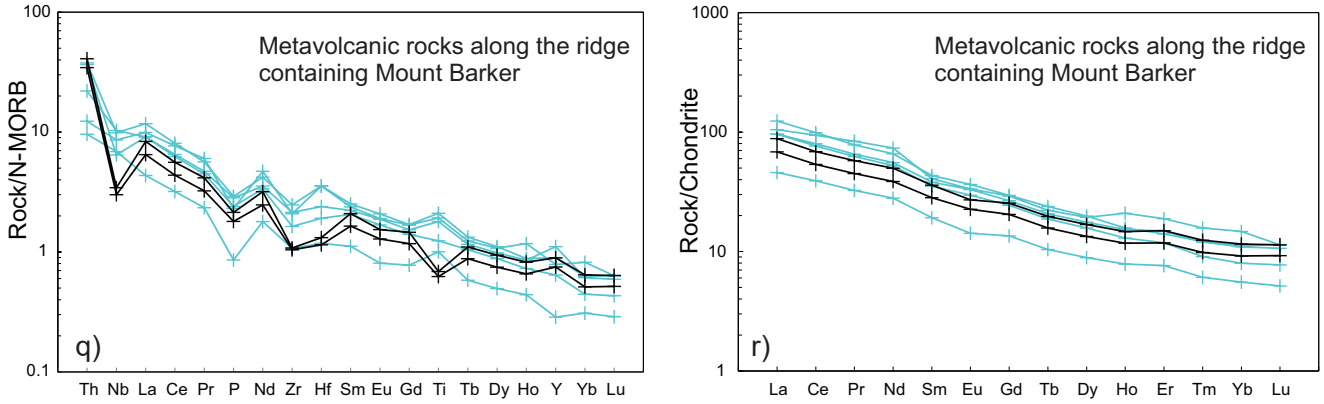


Fig. 8 continued. q-r) Rare earth element plots for igneous and volcanic rocks in Figures 6 and 7.

body (Fig. 3) returned similar ages of ca. 280 Ma. All the gabbros share similar characteristics and are assumed to be of the same age. Trace element data suggest these rocks are predominantly basaltic in composition with one being alkali basalt (Fig. 6a). All samples show similar trends, clustering in the volcanic arc array (Fig. 7a) and displaying arc-like trends on REE and extended REE plots, with negative Nb and Ti anomalies, enriched light REE, and depleted heavy REE (Figs. 8g, h).

5.3. Neoproterozoic to Cambrian

5.3.1. Metavolcanic rocks near Badger Peak

Several horizons of chlorite schist and finely crystalline foliated gabbro outcrop along the ridge immediately south of Badger Peak (Fig. 3) and plot as alkaline basalts (Fig. 6b). Gabbro at Badger Peak has OIB-like REE abundances similar to gabbro in the Cariboo terrane (Fig. 7b) whereas the chlorite schists, here assumed to be metavolcanic, display higher REE abundances (Figs. 8i, j).

5.3.2. Metavolcanic rocks in the Harveys Ridge succession southwest of Frank Creek

Initial mapping of chlorite-actinolite schist, tuffs, lapilli tuffs, and pillowed volcanic rocks in the Harveys Ridge succession southwest of Frank Creek recognized mafic and more felsic varieties, which is borne out by geochemistry. Most straddle the basalt to basaltic andesite fields but one plots as a basalt and there is an alkali basalt cluster (Fig. 6b). The basaltic andesites fall within the volcanic arc array, the one sample of basaltic composition plots in the E-MORB field and the alkali basalts plot as OIB (Fig. 7b). Samples that straddle the basalt to basaltic-andesite composition have REE abundances more compatible with island arc volcanic rocks, particularly as displayed by the negative Ti and Nb anomalies (Figs. 8k, l). The single basalt sample displays flat, MORB-like REE abundances (Figs. 8k, l), whereas the alkali basalts have REE levels compatible with ocean island basalts (Figs. 8k, l).

5.3.3. Metavolcanic rocks in the Harveys Ridge succession north of Cariboo Lake

Dark green metavolcanic rocks in the form of chlorite schist form isolated outcrops to mappable bodies up to several 100 m thick in the Harveys Ridge succession north of Cariboo Lake (Fig. 3). These have similar trace and REE abundances as the alkali basalts southwest of Frank Creek (Figs. 6b, 7b, 8m, n). One sample displays abundances that deviate significantly from the other samples (black symbol, Figs. 6, 7). This sample is highly deformed and altered with SiO_2 less than 40%, alkali metal contents of approximately 0.01% and volatiles of more than 18%.

5.3.4. Sheared gabbro and metavolcanic rocks southwest of Keithley Creek

Southwest of Keithley Creek is a fault-bounded package of highly strained, garnet-bearing chlorite-actinolite schist and gneiss that may have originated as gabbro. Trace element abundances suggest these rocks have compositions consistent with alkali basalt (Fig. 6b) and that they plot in the OIB portion of the MORB-OIB array (Fig. 7b) suggesting a within-plate setting. Rare earth element and extended REE are consistent with these data (Figs. 8o, p).

5.3.5. Metavolcanic rocks along the ridge containing Mount Barker

Dark green chlorite schists of metavolcanic origin exposed along the ridge containing Mount Barker (Fig. 3) display basaltic to alkali basalt bulk compositions (Fig. 6b). These rocks form one cluster within the volcanic arc array (black) and another suggesting within-plate abundances (blue; Fig. 7b). This is supported by REE and extended REE distributions (Figs. 8q, r).

6. Sm-Nd isotopic geochemistry

Using the geochronologic data presented above, we use a crystallization age of ca. 280 Ma for three of the samples and assume that sample (01FFe-3-1) is of the same age (Table 3; Fig. 9). Two samples from gabbro sills and dikes that intrude

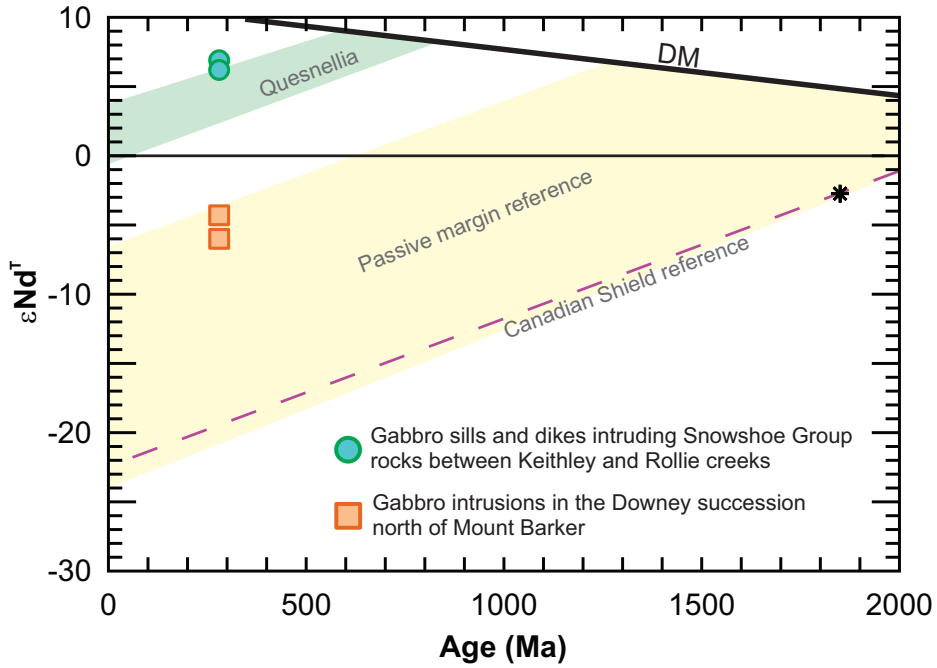


Fig. 9. Age vs. eNd^T. For comparison, Quesnellia reference (green band) constructed using whole rock Sm-Nd isotopic data from intrusive rocks (n = 6 $^{147}Sm/^{144}Nd = 0.112$) in Hogem batholith (Jurassic-Cretaceous; 200 to 130 Ma; Ootes et al., 2020). DM – depleted mantle evolutionary curve as defined by Goldstein et al. (1984). Passive margin reference constructed using whole rock Sm-Nd isotopic data (n = 8 $^{147}Sm/^{144}Nd = 0.112$) from sedimentary rocks of the Road River Group (Silurian; ca. 425 Ma) in the Mackenzie Mountains, NT (data in Rasmussen et al., 2023). Canadian Shield reference line constructed using average of 67 whole rock Sm-Nd isotopic data (n = 67, average $^{147}Sm/^{144}Nd = 0.11$), from igneous rocks in Wopmay orogen of the western Canadian Shield, NT (data from Jackson et al., 2022). Asterix at ca. 1.85 Ga represents youngest intrusive rocks exposed in the western Canadian Shield, where most exposures are Neoarchean to Paleoproterozoic. The line represents approximate maximum eNdT at a given time for magmas derived exclusively from Canadian Shield sources.

Downey succession rocks between Keithley and Rollie creeks have Sm-Nd isotopic ratios that indicate derivation from a mantle source more primitive than Quesnel terrane. In contrast, two samples from the large gabbro body intruding the Downey succession north of Mount Barker has Sm-Nd isotopic ratios that are more evolved, suggesting derivation from continental lithosphere.

7. Discussion

Neoproterozoic to Cambrian rocks in the Snowshoe Group can be grouped into two broad packages: 1) metavolcanic rocks in the Downey succession which include metavolcanic rocks along the ridge containing Mount Barker and sheared gabbro and metavolcanic rocks southwest of Keithley Creek (Fig. 6b); and 2) metavolcanic rocks in the Harveys Ridge succession or Transitional Harveys Ridge succession, which include metavolcanic rocks near Badger Peak, metavolcanic rocks in the Harveys Ridge succession north of Cariboo Lake, and metavolcanic rocks in the Harveys Ridge succession southwest of Frank Creek (Fig. 6b).

Volcanic rocks in the Downey succession generally have trace element levels indicating alkali basalt bulk compositions and trace element and REE abundances that define OIB (within-plate) eruptive settings. The only exception are several localities along Mount Barker that have compositions defining basalt compositions and signatures suggesting derivation from arc-related volcanism. Similarly, volcanic rocks in the Harveys Ridge succession generally have alkali basalt bulk compositions and also show OIB (within-plate) tectonic settings. Although some samples from south of Frank Creek follow this trend, others fall outside this cluster with E-MORB (basalt) and volcanic arc (basaltic andesite) characteristics.

Pearce (2008) noted that modern MORB volcanic rocks erupting at a continental margin can show distributions of data points within Th/Yb versus Nb/Yb space that spread from the MORB array into the volcanic-arc array along a line with a positive slope, similar to what we see with data from volcanic rocks south of Frank Creek. This results from contamination of MORB basalts by continental lithosphere, although it is difficult to maintain a basaltic composition and produce such a magma by mixing with continental lithosphere. Although sparse, our data from volcanic rocks south of Frank Creek do not show the transitional spread such as described by Pearce (2008) but rather define distinct clusters suggesting eruption of discrete magma types. Taken at face value, these data support coeval eruption of MORB and arc lavas, which suggests a Neoproterozoic-Cambrian back-arc setting along this portion of the Ancestral North American margin. Alternatively these volcanic rocks could have been sourced from lithosphere with arc characteristics and not an active arc environment.

Permian gabbros intrude the Snowshoe Group in two areas: between Keithley and Rollie creeks and north and northwest of Mount Barker. Although bulk compositions based on trace element data are identical for these two groups, which suggests they are part of the same igneous suite, other trace and REE data may imply two different magma sources. Gabbros between Keithley and Rollie creeks are of alkali basalts suggesting eruption within an OIB (i.e., within-plate) setting whereas those with basaltic abundances form a grouping of E-MORB affinities. Gabbro in the Mount Barker area displays alkali basalt to predominantly basaltic compositions but defines a cluster in the volcanic arc array and REE abundances that support this. Taken together, the two groups could define a contamination trend from continental lithosphere as proposed by Pearce (2008) and this is supported by the more evolved nature of Mount Barker area gabbros based on Sm-Nd isotopes. Again, as with the volcanic rocks south of Frank Creek, the data points do not define a continuous spread between the two end members, which suggests distinct magma sources. If we simply accept the geochemical and geochronological data, both MORB and arc magmatism appear to have been active during the Early Permian along this part of the Ancestral North American margin. Again, it should be cautioned that this arc signature could also be inherited from a continental lithospheric source. Rocks of the Crooked Amphibolite have a N-MORB signature and are, in part, of similar age. Taken together, this would be consistent with a proposed back-arc setting along the western margin of Ancestral North America during the Permian (Ferri, 1997). Evidence for a late Paleozoic arc immediately outboard of the Ancestral North American margin has been documented elsewhere in the Canadian Cordillera (Nelson and Colpron, 2006; Ferri, 1997; Ferri and Friedman, 2026).

8. Summary

Legacy multigrain U-Pb zircon analysis on three samples of gabbro that intrude the Snowshoe Group (late Neoproterozoic to early Cambrian) in the Cariboo subterrane near Cariboo Lake returned ages of ca. 280 Ma. Geochemical and isotopic data defines two groups. One displays elemental concentrations suggesting derivation from an E-MORB and OIB (within-plate) source and having Sm-Nd isotopic abundances indicating the magmas originated from an immature, mantle source. The second has arc-like signatures and Sm-Nd isotopic levels that suggest derivation from more evolved continental lithosphere. These relationships would be consistent with a Permian back-arc setting along the western margin of Ancestral North America during the Permian. Lithogeochemical analysis of mafic volcanic rocks in the Snowshoe Group support coeval eruption of MORB and arc lavas, are consistent with an older (Neoproterozoic to Cambrian) back-arc setting.

Acknowledgments

We thank L. Ootes for helpful comments and providing the diagram used in Figure 9 and L. Aspler for thorough reviews of early versions of this paper.

References cited

Bichler, A., and Bobrowsky, P.T., 2001. Barkerville Project: Regional till geochemistry (93H/4, 5) and orientation (93A/14) studies. In: Geological Fieldwork 2000, British Columbia Ministry of Energy and Mines, British Columbia Geological Survey Paper 2001-1, pp. 383-396.

Bloodgood, M.A., 1990. Geology of the Eureka Peak and Spanish Lake map area. British Columbia Ministry of Energy, Mines and Petroleum Resources, British Columbia Geological Survey Paper 1990-3, 38 p.

Campbell, R.B., 1978. Quesnel Lake, British Columbia. Geological Survey of Canada Open File 574, 1:125,000 scale.

Colpron, M., 2020. Yukon terranes-A digital atlas of terranes for the northern Cordillera. Yukon Geological Survey. <https://data.geology.gov.yk.ca/Compilation/2#InfoTab>

Crowley, J.L., Schoene, B., and Bowring, S.A., 2007. U-Pb dating of zircon in the Bishop Tuff at the millennial scale. Geology, 35, 1123-1126.

Ferri, F., 1997. Nina Creek Group and Lay Range assemblage, north-central British Columbia: Remnants of Late Paleozoic and arc terranes. Canadian Journal of Earth Sciences, 34, 854-874.

Ferri, F., 2001a. Geological setting of the Frank Creek massive sulphide occurrence near Cariboo Lake, east-central B.C. In: Geological Fieldwork 2000, British Columbia Ministry of Energy and Mines, British Columbia Geological Survey Paper 2000-1, pp. 31-49.

Ferri, F., 2001b. Geology of the Frank Creek-Cariboo Lake area, central British Columbia (NTS 93A/11, 14). British Columbia Ministry of Energy and Mines, British Columbia Geological Survey Open File 2001-11, 1:25,000 scale.

Ferri, F., and Friedman, R., 2026. Age and geochemistry of middle to late Paleozoic volcanism along the western edge of Ancestral North America in north-central British Columbia. In: Geological Fieldwork 2025, British Columbia Ministry of Mining and Critical Minerals, British Columbia Geological Survey Paper 2026-01, pp. 183-201.

Ferri, F., and O'Brien, B., 2002. Preliminary Geology of the Cariboo Lake Area, central British Columbia (093A/11, 12, 13 and 14). In: Geological Fieldwork 2001, British Columbia Ministry of Energy and Mines, British Columbia Geological Survey Paper 2002-1, pp. 59-82.

Ferri, F., and O'Brien, B., 2003. Geology of the Cariboo Lake area, Central British Columbia. British Columbia Ministry of Energy and Mines, British Columbia Geological Survey Open File 2003-01, 1:50,000 scale.

Ferri, F., and Schiarizza, P., 2006. Reinterpretation of the Snowshoe Group stratigraphy across a southwest-verging nappe structure and its implications for regional correlations within the Kootenay terrane. In: Colpron, M., and Nelson, J.L., (Eds.), Paleozoic Evolution and Metallogeny of Pericratonic Terranes at the Ancient Pacific Margin of North America, Canadian and Alaskan Cordillera. Geological Association of Canada, Special Paper 45, pp. 415-432.

Goldstein, S.L., O'Nions, R.K., and Hamilton, P.J., 1984. A Sm-Nd isotopic study of atmospheric dusts and particulates from major river systems. Earth and Planetary Science Letters, 70, 221-236.

Hamilton, P.J., O'Nions, R.K., Bridgwater, D., and Nutman, A., 1983. Sm-Nd studies of Archaean metasediments and metavolcanics from West Greenland and their implications for the Earth's early history. Earth and Planetary Science Letters, 62, 263-272.

Höy, T., and Ferri, F., 1998a. Zn-Pb deposits in the Cariboo subterrane, central British Columbia (93A/NW). In Geological Fieldwork 1997, British Columbia Ministry of Employment and Investment, British Columbia Geological Survey Paper 1998-1, pp.14-1-14-10.

Höy, T., and Ferri, F., 1998b. Stratabound base metal deposits of the Barkerville subterrane, central British Columbia (093A/NW). In: Geological Fieldwork 1997, British Columbia Ministry of Employment and Investment, British Columbia Geological Survey Paper 1998-1, pages 13-1-13-12.

Jackson, V.A., Ootes, L., Pierce, K., Bennett, V., Smar, L., Mackay, D., and Sandeman, H.A., 2022. Geology of the south-central Wopmay orogen, Northwest Territories (parts of NTS 86B, 86C, and 86D); Results from the South Wopmay Bedrock Mapping Project. Northwest Territories Geological Survey, NWT Open File 2017-10, 103 p.

Krogh, T.E., 1982. Improved accuracy of U-Pb zircon ages by the creation of more concordant systems using an air abrasion technique. Geochimica et Cosmochimica Acta, 46, 637-649.

Ludwig K.R., 2003. Isoplot 3.00, A Geochronological Toolkit for Microsoft Excel. University of California at Berkely.

Ootes, L., Jones, G., Schiarizza, P., Milidragovic, D., Friedman, R., Camacho, A., Luo, Y., Vezinet, A., Pearson, D.G., and Zhang, S., 2020. Geochronologic and geochemical data from northern Hogem batholith and its surroundings, north-central British Columbia. British Columbia Ministry of Energy, Mines and Low Carbon Innovation, British Columbia Geological Survey GeoFile 2020-01, 21 p.

Panteleyev, A., Bailey, D.G., Bloodgood, M.A., and Hancock, K.D., 1996. Geology and mineral deposits of the Quesnel River-Horsefly map area, central Quesnel trough, British Columbia. British Columbia Ministry of Employment and Investment, British Columbia Geological Survey Bulletin 97, 156 p.

Parrish, R., Roddick, J.C., Loveridge, W.D., and Sullivan, R.W., 1987. Uranium-lead analytical techniques at the geochronology laboratory, Geological Survey of Canada. In: Radiogenic Age and Isotopic Studies, Report 1, Geological Survey of Canada Paper 87-2, pp. 3-7.

Pearce, J.A., 2008. Geochemical fingerprinting of oceanic basalts with applications to ophiolite classification and the search for Archean oceanic crust. Lithos, 100, 14-48.

Pearce, J.A., 1996. A user's guide to basalt discrimination diagrams. In: Wyman, D.A., (Ed.), Trace Element Geochemistry of Volcanic Rocks: Applications for Massive Sulphide Exploration. Geological Association of Canada, Short Course Notes, 12, pp. 79-113.

Rasmussen, K.L., Falck, H., Elongo, V., Reimink, J., Luo, Y., Pearson, D.G., Ootes, L., Creaser, R.A., and Lecumberri-Sanchez, P., 2023. The source of tungsten-associated magmas in the northern Canadian Cordillera and implications for the basement. Geology, 51, 657-662.

Ray, G.E., Webster, I.C.L., Ross, K., and Hall, R., 2001. Geochemistry of auriferous pyrite mineralization at the Bonanza Ledge, Mosquito Creek mine and other properties in the Wells-Barkerville area, British Columbia. In Geological Fieldwork 2000, British Columbia Ministry of Energy and Mines, British Columbia Geological Survey Paper 2001-1, pp. 135-168.

Rees, C.J., 1987. The Intermontane-Omineca Belt boundary in the Quesnel Lake area, east-central British Columbia: Tectonic implications based on geology, structure and paleomagnetism. Ph.D. thesis; Carleton University, Ottawa, Ontario, 421 p.

Rees, C.J., and Ferri, F., 1983. A kinematic study of mylonitic rocks in the Omineca-Intermontane belt tectonic boundary in east-central British Columbia. In: Current Research, Geological Survey of Canada Paper 83-1B, pp. 121-125.

Schiarizza, P., 2024. Bedrock geology, Bonaparte Lake-Quesnel River parts of NTS 92P, 93A, 93B. British Columbia Ministry of Energy, Mines and Low Carbon Innovation, British Columbia Geological Survey Geoscience Map 2024-01, 1:125,000 scale.

Schiarizza, P., and Ferri, F., 2003. Barkerville terrane, Cariboo Lake to Wells: A new look at stratigraphy, structure and regional correlations of the Snowshoe Group. In Geological Fieldwork 2002, British Columbia Ministry of Energy and Mines, British Columbia Geological Survey Paper 2003-1, pp. 77-98.

Schmitz, M.D., and Schoene, B., 2007. Derivation of isotope ratios, errors, and error correlations for U-Pb geochronology using ^{205}Pb-^{235}U-(^{233}U)-spiked isotope dilution thermal ionization mass spectrometric data. Geochemistry, Geophysics, Geosystems, 8, article Q08006. <https://doi.org/10.1029/2006GC001492>

Stacey, J.S., and Kramer, J.D., 1975. Approximation of terrestrial lead isotope evolution by a two-stage model. Earth and Planetary Science Letters, 26, 207-221.

Struik, L.C., 1983a. Bedrock geology of Spanish Lake (93A/11) and parts of adjoining map areas, central British Columbia. Geological Survey of Canada Open File 920, 1:50,000 scale.

Struik, L.C., 1983b. Bedrock geology of Quesnel Lake (93A/10) and part of Mitchell Lake (93A/15) map areas, central British Columbia. Geological Survey of Canada Open File 962, 1:50,000 scale.

Sun, S.S., and McDonough, W.F., 1989. Chemical and isotopic systematics of oceanic basalts: Implications for mantle composition and processes. In: Saunders, A.D., and Norry, M.J., (Eds.), Magmatism in the Ocean Basins. Geological Society, London, Special Publication, 42, pp. 313-345.

Thirlwall, M.F., 2000. Inter-laboratory and other errors in Pb isotope analyses investigated using a ^{207}Pb-^{204}Pb double spike: Chemical Geology, 163, 299-322.

British Columbia geoscience Spatial Data Infrastructure (BCgSDI): A progress report

Yao Cui[1, a], Jessica Norris[1], and Gabe Fortin[1]

[1] British Columbia Geological Survey, Ministry of Mining and Critical Minerals, Victoria, BC, V8W 9N3
[a] corresponding author: Yao.Cui@gov.bc.ca

Recommended citation: Cui, Y., Norris, J., and Fortin, G., 2026. British Columbia geoscience Spatial Data Infrastructure (BCgSDI): A progress report. In: Geological Fieldwork 2025, British Columbia Ministry of Mining and Critical Minerals, British Columbia Geological Survey Paper 2026-01, pp. 221-226.

Abstract

The British Columbia Geological Survey is modernizing its information systems by developing the British Columbia geoscience Spatial Data Infrastructure (BCgSDI). This modernization addresses the long-standing challenges of managing numerous disparate and legacy databases faced by many public geoscience organizations by introducing a phased transition from siloed applications, to point-to-point system integration and interoperability and, ultimately, towards a canonical data model. This canonical data model will enable the BCgSDI to be the single authoritative source of geoscience data independent of any individual application. Central to the BCgSDI is an end-to-end (from data source to release) approach that streamlines the full geoscience data lifecycle, from data acquisition and updating through validation, integration, and publication. The BCgSDI will be implemented with only a few technologies on a Cloud-native platform, to ensure scalability, while reducing the complexity and cost of developing and maintaining applications. The BCgSDI project can serve as an example of how to modernize a geoscience information infrastructure while maintaining business continuity and enabling future innovation.

Keywords: Spatial Data Infrastructure, SDI, geoscience, mineral resource, architecture, integration, canonical data model, BCgSDI, Cloud-native platform

1. Introduction

The British Columbia Geological Survey (BCGS) integrates research programs with historical data, providing geological and mineral resource information to guide societal decisions centered on the Earth sciences. Although the public-facing end of the Survey databases have been well-received, the back end is a patchwork of legacy systems, largely developed in-house to fulfill specific lines of business and services, which led to siloed applications lacking coherent data management. These systems, many of which are decades-old, have resulted in several enduring challenges including the duplication of efforts to maintain similar data in multiple systems, extra work to prevent data inconsistency for the same information, and added costs of maintaining disparate systems and obsolete technologies. In addition, the systems and applications are not immediately amenable to support artificial intelligence (AI) and large language models (LLM) for advanced data access and modelling.

To eliminate current database-related impediments to delivering Survey programs, the BCGS is developing the British Columbia geoscience Spatial Data Infrastructure (BCgSDI). SDI was defined by the U.S. National Research Council (1993) as a framework of technologies, policies, and institutional arrangements enabling the creation, exchange, and use of geospatial data. In its modernization efforts, the Survey adopted SDI as a concept for a group of logically arranged information systems that are connected via a common interface, link data sources to products, and facilitate data update, sharing, and services (Federal Geographic Data Committee, 2024; Open Geospatial Consortium, 2025). The BCgSDI project aims to establish a coherent, integrated, and interoperable (i.e., easy to share with diverse clients) environment that supports the entire data lifecycle, from geoscience data sources to data products to applications and services. The primary focus is to build a foundation to manage geoscience data as authoritative reusable assets. In practical terms, the BCgSDI provides the database environment, processing workflows, and applications needed to capture, update, validate, integrate, and disseminate geoscience information. It supports both routine operational use and the creation of value-added data products and applications, such as web services and interactive tools, that serve mineral exploration, land-use planning, public safety, and research communities.

2. Context

The analogue to digital transformation in the last half-century created siloed information systems, largely because rapid advancements in computing technology outpaced enterprise-wide planning, system architecture design, and integration standards. Many public geoscience organizations face the same challenge of managing numerous disparate and legacy databases and applications.

Before the widespread adoption of electronic computing, geological and mineral resource information in British Columbia was published as hard-copy documents. Geologists collected

field observations, compiled maps, and released comprehensive reports describing regional geology, mineral deposits, and mineral exploration activities in publications that served as complete records (e.g., Brothers, 1968). Although these reports were comprehensive, they were static, had inconsistent descriptors, and could not readily support comparative analysis. In 1967, British Columbia introduced a paper card system to record mineral deposit information (Fig. 1; Jones and McPeek, 1992). These cards had standardized entries such as location, commodities, mineralogy, claims, status, owners and operators of the property, development work and results, and references. By the early 1970s, these card records were transferred into a computerized database that eventually became MINFILE, the current BCGS online inventory of metallic mineral, industrial mineral, and coal occurrences in British Columbia. Marking a major transformation in information management (Montgomery et al., 1975) this enabled efficient querying and reporting to support advanced data analysis. However, the analogue to digital transformation occurred incrementally in response to emerging new technologies and commonly along independent organizational lines of business. To accommodate specific program needs, individual teams developed dedicated applications with their own back-end databases. Each system was optimized for a particular line of business (e.g., mineral occurrences, exploration tracking, and assessment work reporting) without common feature definitions, data models, computing platforms, and technologies. This approach marked the beginning of systems that were isolated in program-related silos, a practice that has largely persisted to the present not only at the BCGS but at most public geoscience organizations.

Currently, the Survey maintains more than 40 databases and applications, each designed for a specific business purpose. The particularly high-value systems include: MINFILE (mineral occurrences); ARIS (assessment report index system); Property File (historical documents); Publication Catalogue; BC Digital Geology; Surficial Geology; ExploreTrack (tracking mineral exploration and mining activities), and various geochemical and geochronological databases. Our operations commonly require access to data such as topographic base maps and mineral tenures managed by other government agencies. Most of the databases use different technologies, many of which would now be considered obsolete. These systems typically manage subsets of intrinsically related data independently, resulting in multiple copies of similar information stored in siloes lacking connections or interfaces (Fig. 2). Sharing data between systems commonly relies on manual steps or custom computer scripts, which are costly and risk introducing

Appendix C
MINERAL DEPOSIT INVENTORY

EXAMPLE OF COMPLETED CARD

Map No. 93M-106

Property No. ____ Metal ☒ Industrial Mineral ☐ Placer ☐ Coal ☐ Lapidary ☐

Name: Current SAM-DICK; ACE; JOE Previous OLD IRONSIDES; ZEKE ?
C.G. and No. OLD IRONSIDES (L.1206)
Operator/Yr. Old Gold Mines Ltd. 1906-1919

Claim JOE 4-6, 9, 13 Owner ?
Operator Big Co. Ltd. Year '70-

Claim ACE 23 Owner H. Clamestaker
Operator Ace Expl. Year '60

Claim SAM 6, DICK 3 Owner New Gold M. L.
Operator owner Year '54-'59

Location: N.T.S. 93M/4E Lat. 55°13.2' Long. 127°39.5' U.T.M.
M.D. Omineca In park E. & N. ☐ El. 4000 ft. ±
Location plotted Shaft on ACE 23, from Ass. Rpt. 268 Precision 1

Status: Producer ☒: Active ☐ Inactive ☒ L+ ☐ L ☐ M ☐ S ☒ S− ☐
Non-producer ☐: Pot. prod. ☐ Under exploration ☐ Prospect ☐ Occurrence ☐
Reserves: L+ ☐ L ☐ M ☐ S ☐ S− ☐ Tons Grade
Est. potential: L+ ☐ L ☐ M ☐ S ☐ S− ☐ Grade

Development: Surface Approx. 15 pits; 6 trenches
Underground Shaft; adit (350 ft.)

Product(s) Au

Fig. 1. Part of a standardized mineral deposit inventory card that was used by the BCGS in the late 1960s and early 1970s. The inventory cards were the template for what eventually became MINFILE.

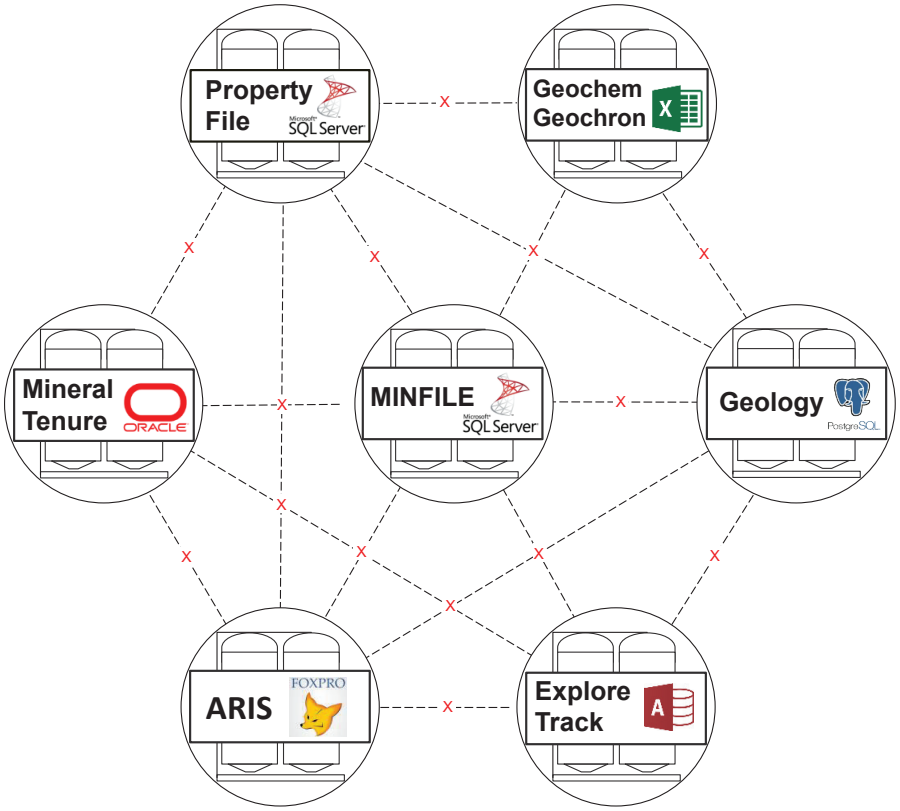


Fig. 2. Siloed legacy systems lacking coherent data management. Black dashed lines refer to intrinsic dependencies; red crosses indicate no connections or interfaces between databases.

errors. This fragmentation not only increases operational and maintenance efforts but also limits the ability to capture and update the data efficiently.

The siloed systems also impede managing and linking source data with derived data products after processing and interpretation. Field observations, laboratory analyses, instrumental measurements, and supporting documentation are not always traceable to derived datasets or published interpretations. As a result, it is difficult to track data provenance, apply consistent validation rules, or make comprehensive datasets readily available for modern analytics, including mineral potential modelling and emerging data-driven approaches.

Together, these issues increase the effort required to ensure data currency, consistency, and authority, while complicating data integration, analysis, and reuse across programs and clients. The Survey BCgSDI project is working toward resolving these issues.

3. Overview of the BCgSDI architecture

The BCgSDI system architecture is multi-tiered (Fig. 3). The lower level is for managing and updating the raw data in what we refer to as the geoscience operational database environment. The next level, which we refer to as the geoscience application database environment is for derived data products and application-level functions. The third level is for geospatial web services and data dissemination.

Serving as the foundation, the operational environment includes: 1) an observational database for capturing and compiling raw data that retains provenance information; 2) a staging database for data transformation (validation, standardization, review, approval, and integration); and 3) an archival database for preserving consistent and standardized results from the staging database (for details see Cui, 2011). Applications create derived data products from the operational environment and integrate them in the application database environment to support queries, reporting, business intelligence, data downloads, web interfaces, and interoperable data sharing to ensure the data and services can be broadly consumed.

Interoperable data sharing is achieved by adopting open standards such as the Open Geospatial Consortium (OGC) standards GeoSciML (GeoSciML Modeling Team, 2017), EarthResourceML (CGI-IUGS EarthResourceML Working Group, 2013), and OGC Web Map Service (WMS) and Web Feature Service (WFS). The BCgSDI will be extended for ready access to the British Columbia Geographic Warehouse (BCGW) and will include a document management system to access many historical and current technical documents. To reduce the complexity and cost of maintenance, the BCgSDI will be implemented in a Cloud-native platform using open-source software.

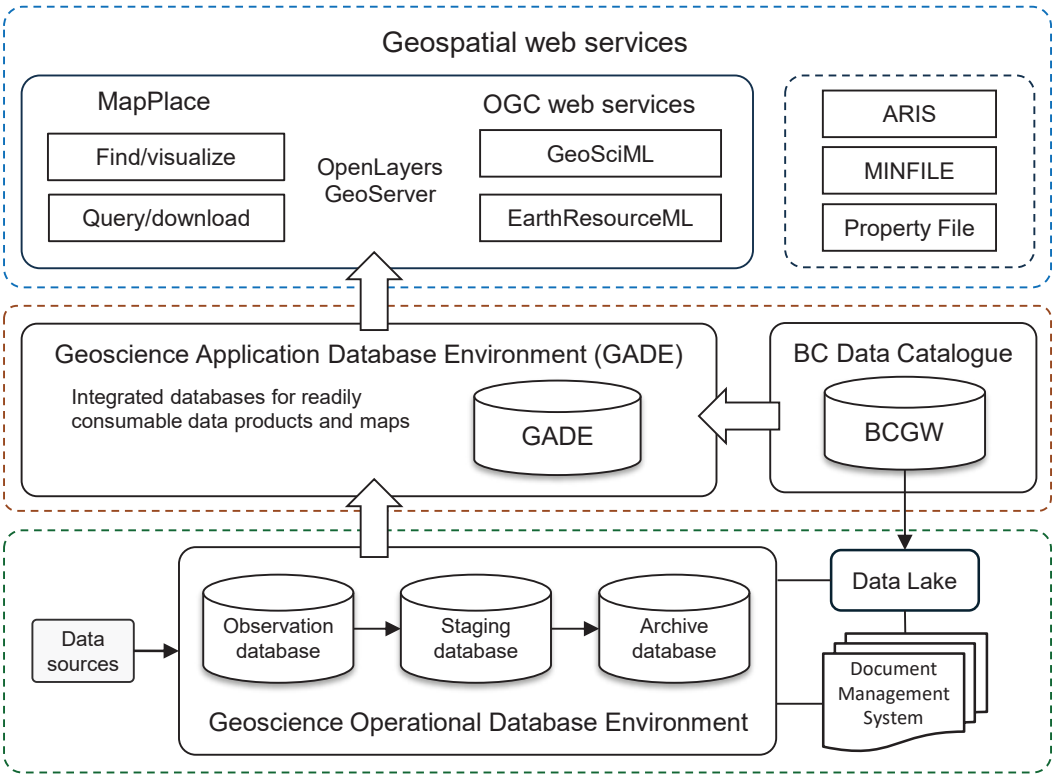


Fig. 3. High-level overview of the BCgSDI system architecture; BCGW refers to British Columbia Geographic Warehouse.

4. Progress

Modernization of the British Columbia information systems will take many years. Thus, we have adopted an incremental approach that ensures continuity of services while progressively improving data management practices. In the first phase, individual applications and their back-end databases are being upgraded to meet current security, performance, and supportability standards. This initial work, which is currently underway, focuses on high-value systems that anchor the broader integration including MINFILE, ARIS, Property File, Publication Catalogue, BC Digital Geology, Surficial Geology, ExploreTrack, and other essential geological and geochemical datasets. Where data need to be shared, we are introducing database to database (or point-to-point) interfaces to reliably exchange information (Fig. 4). This phase reduces the most urgent technical risks and delivers immediate improvements to usability and data currency, while allowing existing business processes to continue.

In the second phase of implementation, our focus will shift from connecting systems to consolidating and managing data more effectively. To reduce the complexity of point-to-point integrations and to improve efficiency and data consistency, we aspire to a canonical data model (Hohpe and Woolf, 2003), a standardized way of representing shared information in the BCgSDI. Modern practice treats the canonical data model as a universal translation layer that supports interoperability and governance across large enterprise environments (e.g., California Learning Resource Network, 2025). At the conceptual level, the canonical data model acts as the authoritative semantic layer defining key feature types and relationships between them. It establishes common and standardized data definitions, vocabularies, and data quality specifications, with each of the datasets recognized as the single authoritative source, independent of any individual application (Fig. 5). Importantly, although the canonical model provides a single source of truth for shared data definitions and datasets, it does not require a single physical database. Individual applications may maintain their own operational data stores, but they access and update shared information through the canonical layer. This ensures that data remains consistent and coherent across the system rather than fragmented into isolated silos. The BCgSDI will use the canonical data model concept to guide how data are structured, shared, and governed. In practice, synchronization mechanisms can be implemented to keep datasets aligned across environments and preserve a single authoritative source of record. In time, successful implementation of this phase will reduce duplication, enforce consistent definitions and validation rules, and streamline the full data lifecycle from collection and update through to publication and dissemination. It will also strengthen data exchange and data sharing with external partners and data providers, enabling analytic capabilities, including business intelligence and mineral potential modelling.

5. Conclusion

The BCgSDI modernization aims to transition BCGS information systems from isolated legacy databases and

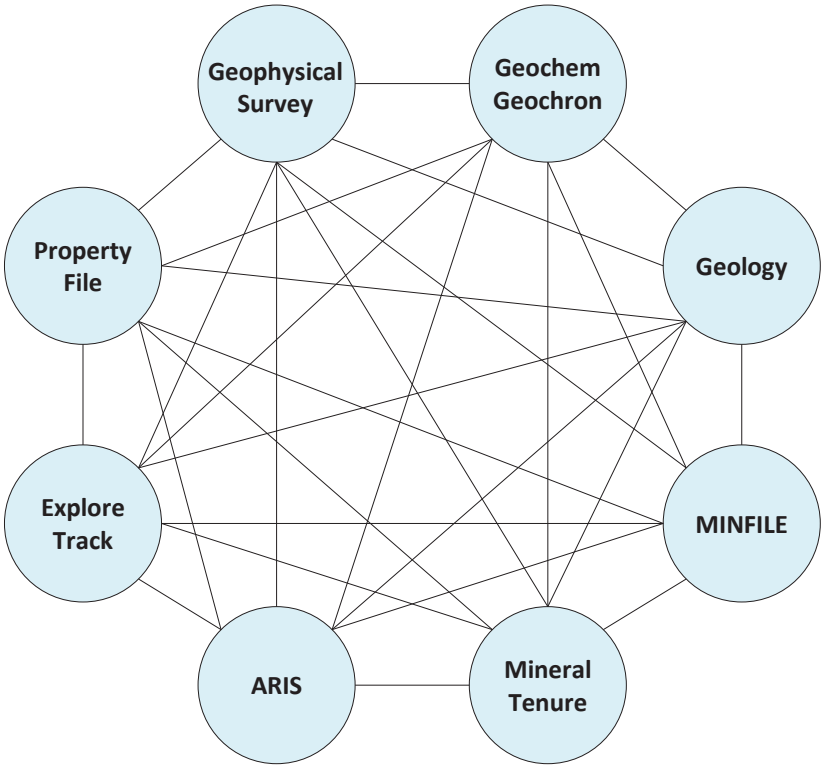


Fig. 4. Point-to-point integration showing individually deployed applications that interface with one another yet operate on separate back-end databases.

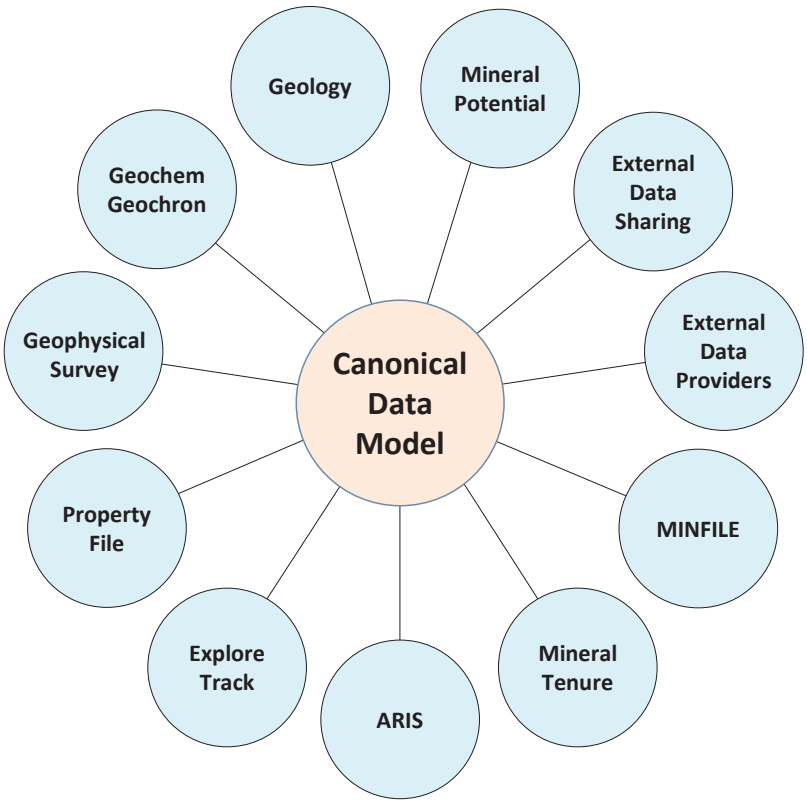


Fig. 5. Conceptual canonical data model as the single authoritative data source that can be used by all applications including data exchange and sharing with external partners.

applications to a sustainable and service-oriented Cloud-based platform. Although the initial goal is to complete point-to-point system integration, the long-term vision is to achieve a single authoritative source of data by adopting a canonical data model. By streamlining the full data lifecycle from data sources to derived products and enabling interoperable access, we are improving the efficiency, reliability, timeliness, and usability of provincial geoscience information. The BCgSDI architecture is designed to be scalable, supporting advanced analytics and emerging technology such as large language models and artificial intelligence. Beyond the BCGS, the BCgSDI modernization approach provides a practical template for other agencies seeking to update their information systems. Ultimately, the BCgSDI architecture enhances the publication of analytic-ready datasets and maps, strengthens discoverability through standardized metadata and services, and reduces friction in collaborative, cross-jurisdictional geoscience initiatives.

Acknowledgments

This work has benefitted from the support and inspiration of many people. We appreciate Tina Qin and David Bayne for their contributions to improving and advancing the business case, and Dylan Dawson, Brian Gillespie, and Abigail Michel for strengthening the system architecture and shaping the decision on the Cloud-native platform. Yao Cui is grateful to Michael Ross, David Skea, Martin Davis, and Paul Ramsey, whose guidance, shared expertise, and thoughtful conversations have elevated my understanding of geospatial data systems and inspired key elements of this BCgSDI initiative. We thank Adrian Hickin and Marc-André Brideau for comments that helped improve this paper.

References cited

Brothers, D.L., 1968. Annual Report of the Mineral Industry of the Province for the year 1967. Department of Mines and Petroleum Resources, Province of British Columbia, 290 p.

California Learning Resource Network, 2025. What is a Canonical Data Model? <https://www.clrn.org/what-is-a-canonical-data-model/> (last accessed February 2026).

CGI IUGS EarthResourceML Working Group, 2013. EarthResourceML v2.0: An XML based data transfer standard for mineral occurrences, mines, and mining activities. IUGS Commission for the Management and Application of Geoscience Information (CGI). <https://earthresourceml.org> (last accessed February 2026).

Cui, Y., 2011. Improving the efficiency in the maintenance of the provincial geological database. British Columbia Ministry of Forests, Mines and Lands, British Columbia Geological Survey Fieldwork Paper 2011-1, pp. 159-168.

Federal Geographic Data Committee, 2024. Building the geospatial future together-The NSDI strategic plan 2025-2035: Reston, Virginia, Federal Geographic Data Committee, 10 p. <https://www.fgdc.gov/nsdi-plan/NSDI2035>

GeoSciML Modeling Team, (Eds.), 2017. OGC Geoscience Markup Language 4.1 (GeoSciML). Wayland, MA: Open Geospatial Consortium, 247 p. (OGC 16-008). <http://www.opengis.net/doc/geosciml/4.1> (last accessed February 2026).

Hohpe, G., and Woolf, B., 2003. Canonical data model. In: Enterprise Integration Patterns. <https://www.enterpriseintegrationpatterns.com/patterns/messaging/CanonicalDataModel.html> (last accessed February 2026).

Jones, L.D., and McPeek, C.B., 1992. MINIFILE-A mineral deposit information system for British Columbia. British Columbia Ministry of Energy, Mines and Petroleum Resources, British Columbia Geological Survey Information Circular 1992-02, 26 p.

Montgomery, J.H., Sinclair, A.J., Wynne-Edwards, H.R., Fox, A.C.L., and Giroux, G.H., 1975. Data capture in the construction of MINDEP's computer-based, mineral deposits files. Canadian Journal of Earth Sciences, 12, 698-703.

Open Geospatial Consortium, 2025. National Spatial Data Infrastructure (NSDI) Modernization Project. <https://www.ogc.org/initiatives/national-spatial-data-infrastructure-modernization-project> (last accessed February 2026).

U.S. National Research Council, 1993. Toward a coordinated Spatial Data Infrastructure for the Nation. Report of the Mapping Sciences Committee, National Academy Press, Washington, DC, 1993, 171 p. <https://openlibrary.org/books/OL10357307M/Toward_a_Coordinated_Spatial_Data_Infrastructure_for_the_Nation> (last accessed February 2026).

Interior Plateau surficial geology compilation: Selection and standardization of maps and data

Easton A. Elia[1, a], and Travis Ferbey[1]

[1] British Columbia Geological Survey, Ministry of Mining and Critical Minerals, Victoria, BC, V8W 9N3
[a] corresponding author: Easton.Elia@gov.bc.ca

Recommended citation: Elia, E.A., and Ferbey, T., 2026. Interior Plateau surficial geology compilation: Selection and standardization of maps and data. In: Geological Fieldwork 2025, British Columbia Ministry of Mining and Critical Minerals, British Columbia Geological Survey Paper 2026-01, pp. 227-237.

Abstract

The British Columbia Geological Survey is producing a digital compilation of surficial geology for the Interior Plateau, a region in central British Columbia where thick packages of glacial drift can add complexity to mineral exploration, land-use planning, forestry, and infrastructure projects. To build the compilation, data from ~100 sources, which include multiple map types (e.g., surficial geology, terrain, soils), must be converted to a uniform standard. Converted data are validated through automated and manual QA/QC procedures to ensure geometric and topological consistency before admission into the final compilation database. Final compilation datasets will be in analytical-ready formats that may be applied, for example, to find subglacial tills and sand and gravel deposits or to investigate landslide and flood hazards.

Keywords: Digital compilation, surficial geology, Interior Plateau

1. Introduction

Maps describing British Columbia's surficial sediments and features have been produced for decades by provincial and federal governments (e.g., Fulton, 1995; Plouffe, 2000; Ferbey et al., 2016), universities (e.g., Hashmi et al., 2015; Sauvé et al., 2025), and industry (e.g., Bobrowsky et al., 1992; Lewis, 1987; McGregor and Sacco, 2021). Catalogued in British Columbia Geological Survey spatial indexes (Arnold and Ferbey, 2019; Veness et al., 2024), these maps provide information about surficial deposits and distribution of bedrock exposures (e.g., Plouffe, 2000; Ferbey et al., 2016), terrain (e.g., Dixon-Warren et al., 1997) and soils (e.g., Farstad, 1979; Jungen, 1980). However, inconsistency in mapping methods, labelling schema, and storage locations hinders accessibility to a broad audience that may be unfamiliar with interpreting different map types.

The British Columbia Geological Survey is developing a topologically consistent digital dataset of surficial geology for the Interior Plateau (Fig. 1) that allows units and features to be queried. Equivalent to BC Digital Geology for bedrock (British Columbia Geological Survey, 2019), this compilation will be similar to surficial geology products provided from Yukon (Yukon Geological Survey, 2023) and Alberta (Fenton et al., 2013). Building on initial work in which Veness et al. (2024) scanned, catalogued, and re-released the physical collection of surface materials maps in a spatial index, we are now focusing on translating selected datasets to current BCGS mapping specifications. In this paper, we describe how we selected, ranked, and compiled source maps, present methods for converting surficial data to a uniform standard, and provide details about how the compilations may be used. Compilation data will retain original unit labels and scale, in addition to their converted label, to ensure they maintain their intended function and level of detail.

2. Study area

The Interior Plateau, the major physiographic division of central British Columbia (Holland, 1976), extends across ~200,000 km^2, or roughly 20% of the province by area (Fig. 1). The plateau extends from the Omineca and Skeena mountains in the north to the southern Canada-United States border (Fig. 2). It is flanked by the Coast and Cascade mountains to the west and by the Rocky and Columbia mountains to the east. The region is characterized by subdued, rolling topography, and is covered by glacial drift deposited during and directly following the last glaciation (e.g., Holland, 1976; Clague and Ward, 2011) that can locally be up to 200 m thick in well-developed river valleys (Kerr and Levson, 1997). Due to decades of forestry and mineral exploration activity, the Interior Plateau has the highest density of surficial geology maps in the province, and data gaps are minimal.

3. Map types

Three general map types have been used to describe surficial features in British Columbia (Fig. 3). Conventional surficial geology maps describe geological units based on material type (e.g., till, colluvium, or glaciofluvial) and surface expression (e.g., veneer, fan, or terrace). Terrain maps are similar, but units can be further divided by geomorphological processes, slope gradient, sediment texture, drainage, and/or slope stability. Soils maps focus on describing the materials produced or affected by pedogenic processes (A-, B-, and organic horizons), but they also contain descriptions of parent materials (C-horizon).

Sediment packages in maps are described using unit labels consisting of groups of letters, symbols, and numbers (components). Components are arranged so that each represents a particular characteristic of the geology or terrain (Table 1; Howes and Kenk, 1997). The components available to build a

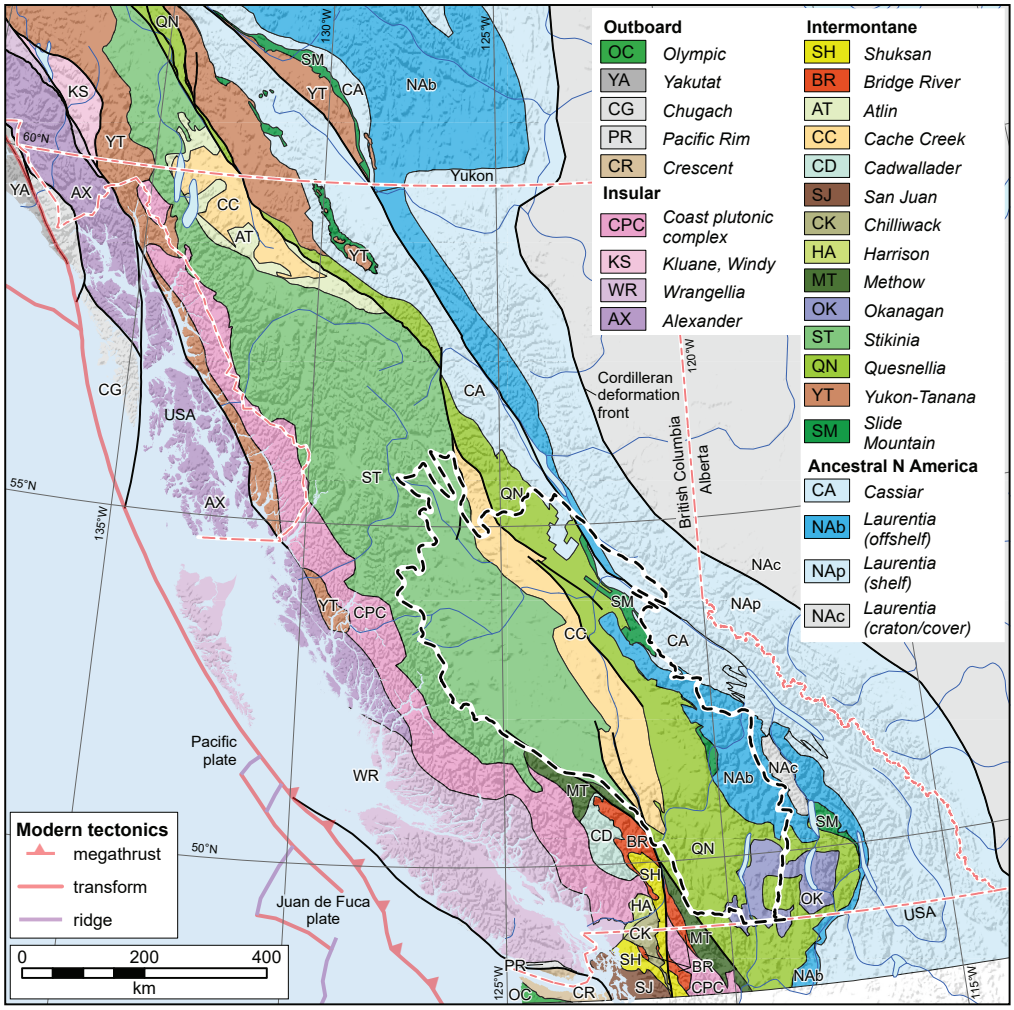


Fig. 1. Interior Plateau surficial geology compilation area. Terranes after Colpron (2020).

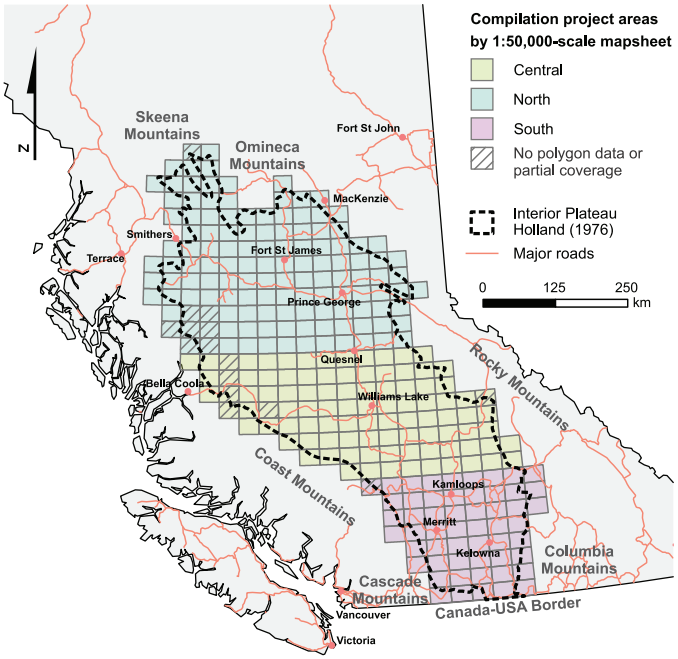


Fig. 2. Interior Plateau of British Columbia (Holland, 1976) divided into central, north, and south project areas. Project areas are subdivided into National Topographic System (NTS) 1:50,000-scale map sheets, the working scale for the compilation.

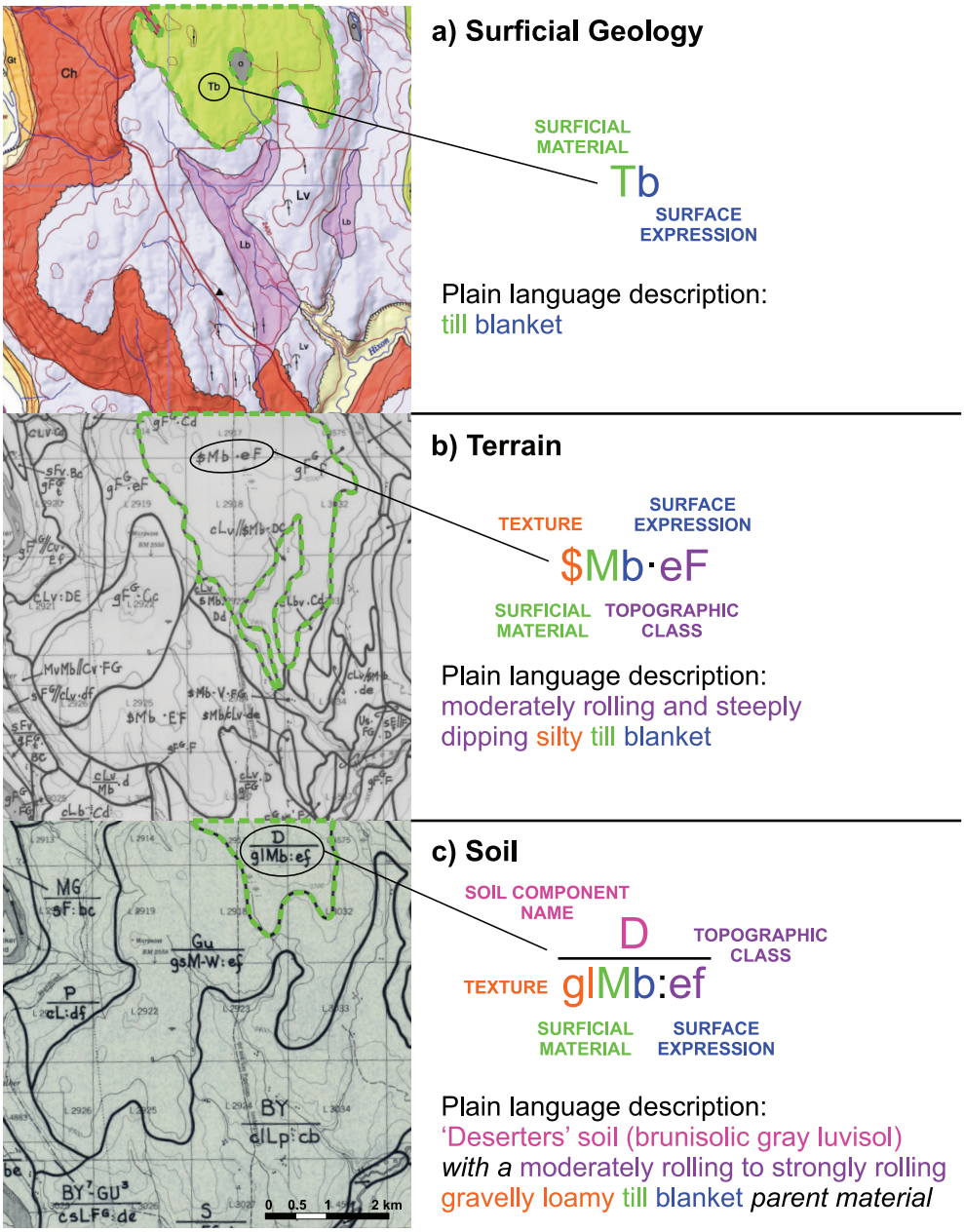


Fig. 3. Example of different map types for the same area at 1:50,000 scale. An equivalent unit in each map type is outlined with a green dashed line. Coloured words link plain language descriptions to components of the map unit label. **a)** Conventional surficial geology (Blais-Stevens and Clague, 2007). **b)** Terrain (Ministry of Environment, 1973). **c)** Soils (Farstad, 1979).

unit label depend on map type. Unit labels in terrain and soils maps can be converted to surficial geology labels with reasonable accuracy for general reconnaissance because they contain the main components of a conventional surficial geology map: surface expression and parent material type. However, maps made for different purposes, such as terrain maps for assessing slope stability, may have a greater focus on subdividing surface expressions compared to a conventional surficial geology map, and soil maps concentrate on soil associations rather than parent materials and thus influence where unit contacts are drawn. Differences in the mapping purpose may also influence addition of symbols (e.g., striations, eskers, and flutings) or create variations in unit labels and descriptions (Fig. 3).

3.1. Legend types

British Columbia's surficial materials maps either have open legends or closed legends. In open legends, geological unit labels are built from combining components of a classification system (e.g., Howes and Kenk, 1997; Canada Soil Survey Committee, 1978; E.L.U.C. Secretariat, 1978). A map user must reference the corresponding classification system to find detailed definitions for each label component. Separate maps built using the same classification system have identically defined units, for example Chr-F (hummocky ridged colluvium with slow mass movement; Howes and Kenk, 1997) units have the same meaning regardless of the map source or study area.

Table 1. Unit label components contained in surficial geology map types.

Unit label component	Description	Examples
Material type	Non-lithified, unconsolidated sediments (surficial materials) classified according to mode of deposition (Howes and Kenk, 1997).	T – Till (Deblonde et al., 2024) / M – Till (Howes and Kenk, 1997) GF – Glaciofluvial (Deblonde et al., 2024) C – Colluvium (Deblonde et al., 2024)
Surface expression	The form (shape) of the land surface or the thickness of the materials (Howes and Kenk, 1997).	b – Blanket (Deblonde et al., 2024) v – Veneer (Deblonde et al., 2024) t – Terrace(s) (Deblonde et al., 2024) h – Hummock(s) (Deblonde et al., 2024)
Geomorphological process	Geomorphological processes that are modifying, or have modified, surficial materials or landforms.	E – Channeled by meltwater (Howes and Kenk, 1997) R – Rapid mass movements (Howes and Kenk, 1997) H – Kettled (Howes and Kenk, 1997)
Texture	The size, roundness and sorting of particles in mineral sediments and the fibre content of organic materials (Howes and Kenk, 1997).	s – Sand (Howes and Kenk, 1997) g – Gravel (Howes and Kenk, 1997) $ – Silt (E.L.U.C. Secretariat, 1978) x – Angular fragments (Howes and Kenk, 1997)
Soil component/class/ association	A natural grouping of soil associates based on similarities in climatic or physiographic factors and soil parent materials. It may include a number of soil associates provided that they are all present in significant proportions (Canada Department of Agriculture, 1976).	Specific names and their relative proportions based on map or region. $BY^{7}GU^{3}$ – 70% Beverly soils, 30% Gunniza soils (e.g., Farstad, 1979)
Topographic class/ Slope class	Describes simple and/or complex topography to quantify the dominant slopes within a unit or landform.	A – Depressional to level (Canada Department of Agriculture, 1974) c – Undulating (Canada Department of Agriculture, 1974) 8 – Extreme slopes (Soil Classification Working Group, 1998)
Terrain stability class	A relative ranking of the likelihood of a landslide occurring after timber harvesting or road construction (Forest Practices Code, 1999).	I – No significant stability problems exist V – Expected to contain areas with a high likelihood of landslide initiation following timber harvesting or road construction.
Qualifying descriptor/ qualifier	Used where appropriate to provide additional information about surficial materials and geomorphologic processes (Howes and Kenk, 1997).	A – Active (Howes and Kenk, 1997) I – Inactive (Howes and Kenk, 1997) G – Glacial (Howes and Kenk, 1997)

Closed legends are attached to the map and contain only the units and symbols in the mapped area. Authors can customize a legend by including direct observations (e.g., unit thicknesses, sediment textures, or sorting), thus making closed legends unique to a particular map. As a consequence, different closed legends could lead to differences in how units are portrayed. For example, although similar, landslide deposits (Cz) in Sauvé et al. (2025) and Ferbey et al. (2016) have different closed legend descriptions, which could affect placement of unit contacts.

3.2. Map formats

Inputs for the compilation are available as attributed vector data (digital points, lines, or polygons) and scanned maps (raster files). Vector data are available from modern maps produced in a geographic information system (GIS; e.g., Hashmi et al., 2015; Ferbey et al., 2016; Sauvé et al., 2025) or in regional data assembly projects and compilations (e.g., Forest Renewal BC (FRBC), Morfitt, 1999; MacIntyre and Struik, 2000; Struik et al., 2007). Maps produced before computer-aided mapping (approximately 1995 or earlier) need to be manually converted to vector data by tracing unit boundaries and geologic symbols in a GIS (i.e., vectorization).

3.3. Modern BCGS surficial geology maps

The BCGS produces surficial geology maps for a general audience with a broad range of applications. Modern BCGS maps are commonly published at 1:50,000 scale with a closed legend and descriptive notes (e.g., Ferbey, 2014a; Ferbey and Elia, 2025). Unit descriptions in the legend are simple, commonly containing one surface expression and material type per unit. In addition to geological units (presented as polygons), these maps contain geological and geomorphological point and line features. These features can include ice-flow indicators, moraines, field stations, sample locations, eskers, kettles, deltas, rock glaciers, pits, or quarries. Overlays (polygons with a transparent component) are used to show additional, commonly secondary, processes or features such as mine tailings, reworked sediments, and large kettles. All BCGS maps are published as PDF maps with accompanying spatial files.

The BCGS uses the Geological Survey of Canada's (GSC) Surficial Data Model (Deblonde et al., 2024) to standardize symbols and colour geological units. This allows integration with existing GSC mapping in British Columbia, and simplifies decisions related to choosing appropriate symbols or classes. BCGS maps can contain entries that deviate from Deblonde et al. (2024), like Rs (rock steep; Ferbey and Elia, 2025), although these types of polygons are rare. Custom symbols are also rare (e.g., landslide toe; Sauvé et al., 2025), except for mineral occurrences, which are included in finished maps.

4. Map selection

To build the Interior Plateau compilation, we selected 67 vector data sources and 38 scanned maps (extending across 281 NTS 50,000-scale grid cells). The density, coverage, type, and scale of surficial materials maps are not consistent across the Interior Plateau. In many instances, maps include the same area or overlap, requiring us to manually select the best source data for the compilation. Some map sheets have incomplete coverage of point or line data, and full data gaps are most common in and around Provincial parks or at the edges of the Interior Plateau bordering more mountainous topography (Fig. 2).

For each of the NTS grid cells intersecting the Interior Plateau boundary, we visually inspected all available surficial data and maps to select sources for compilation components that best resemble those in modern BCGS surficial geology maps. We considered the map type, scale, and publication agency to guide our selection (Table 2).

5. Surficial data standard and storage

Surficial data are converted to a modified version of the BCGS geospatial frame data standard (GFD, Cui, 2021), a data model that stores the components of a geology map in point and line geometry (Table 3; Fig. 4). Using points and lines in place of polygons simplifies modification by allowing us to easily manage gaps, overlaps, or slivers between adjacent geologic units (topological errors). Storing mapping data as points and lines can improve usability and loading times on geospatial web services like MapPlace 2 by only producing polygons for specific areas or zoom levels (Cui et al., 2018; Cui, 2021). Although data are stored as points and lines, geologic polygon data will be available in compilation releases.

We developed a specifications manual to ensure all project data are compiled consistently to meet GFD standards and can be immediately integrated into the compilation database. The specifications manual is referenced during vectorization of scanned maps to avoid inconsistency when recording unit labels, drawing features, and creating digital legends. Feature Manipulation Engine (FME) is used to transform existing vector data to the modified GFD standard (i.e., converting polygons to points and lines) and enforce topology rules (Table 4). The output is stored in a PostgreSQL/PostGIS database where it undergoes secondary quality control processes to check data for adherence to database standards and proper coding. Features that fail quality control tests are corrected automatically using PostgreSQL queries or manually in QGIS.

6. Standardization of unit labels and symbols

To be used in the compilation, unit labels must be standardized across the different map types. We converted unit labels on a map-by-map basis to be consistent with Deblonde et al. (2024). For closed map legends, we interpreted unit descriptions and used regional context to determine an equivalent Deblonde et al. (2024) unit label.

Open legend maps are commonly more complex and require rules for consistent conversion and to capture the most compilation-relevant information. Original unit labels may include information not captured in Deblonde et al. (2024) such as sediment texture, geomorphological process, and stability class (E.L.U.C. Secretariat, 1978; Howes and Kenk, 1997). We

Table 2. Map priority system for selecting surficial map components for each NTS 1:50,000-scale grid cell.

Hierarchy	Scale	Producer	Type	Notes
1	1:50,000 – 1:249,999	Geological Survey	Conventional surficial geology (raster or vector)	Maps in Arnold and Ferbey (2019). Unit labels commonly use versions of Deblonde et al. (2024).
2	1:50,000 – 1:249,999	Geological Survey or Natural Resources Ministry	Terrain (raster or vector)	Maps found in Veness et al. (2024) or Arnold and Ferbey (2019). Unit labels commonly use versions of E.L.U.C. Secretariat (1978) or Howes and Kenk (1997).
3	≤1:250,000	Geological Survey	Conventional surficial geology (raster or vector)	These maps may be used over a 1:50,000-scale terrain map (e.g., GSC A-Series; Plouffe, 2000) based on visual assessment by compiler. Unit labels commonly use versions of Deblonde et al. (2024).
4	1:50,000	Natural Resources Ministry or Industry	Soils (raster or vector)	Maps in Veness et al. (2024) or Knowledge Management (2011). Unit labels commonly use versions of Canada Soil Survey Committee (1978).

Table 3. Components of surficial geology maps and their frame data geometries in database back-end.

Map component	Frame data geometry	Feature examples
point symbols	point	Striations, field stations, outcrop locations.
line symbols	line	Eskers, flutes, meltwater channels.
geologic polygons	line	Edges of geologic and overlay polygons (contacts) or limits of mapping.
	point	Data stored in geologic (Tb, Cv, etc.) or overlay (e.g., mine tailings, reworked sediments, etc.) polygons.

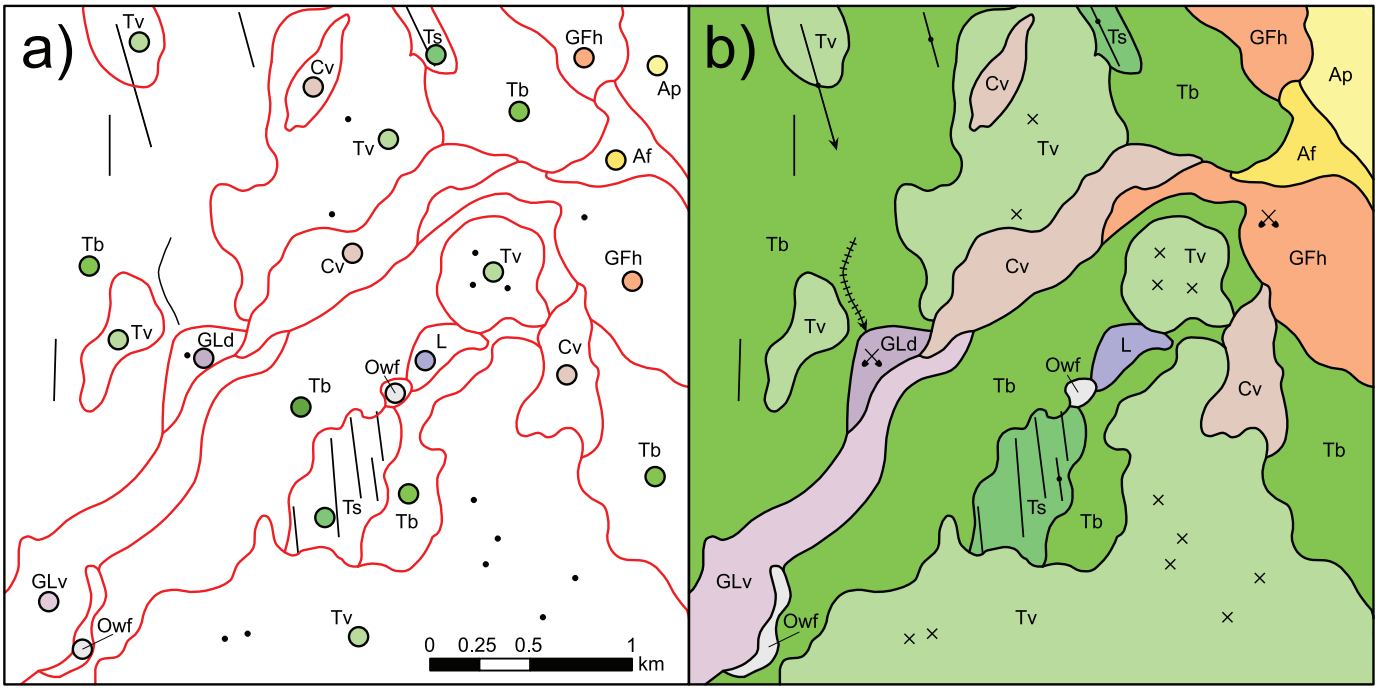


Fig. 4. Geospatial frame data. **a)** Frame data components. Coloured circles are map unit centroids, black points are point symbols (e.g., bedrock outcrops, active pits), black lines are line symbols (e.g., crag-and-tails, flutes, drumlins, meltwater channels), and red lines are geologic contacts. **b)** Client-facing data of the same map extent symbolized using Deblonde et al. (2024).

Table 4. Geospatial frame data specifications on geometric and topological consistency (modified after Cui, 2021).

Specification	Description
Allowable geometry	Single, simple, and valid LineString and LinearRing compliant to OGC Simple Features Specification (Open Geospatial Consortium, 1999) are allowed for planar geological features and topographic boundaries. A single point is allowed for centroids and point symbols.
Unit of precision	The unit of precision is at decimal m (nearest 10 cm) and can be rounded to the nearest m for coordinates in UTM or BC Albers, and rounded to the 6th floating point for coordinates in geographic.
Duplicate and overlap	Duplication and partial overlapping of LineStrings is not allowed; LineStrings within 1 m of each other are checked to be valid. Only applies to LineStrings in the same file/data type (i.e., contacts or line symbols).
Noding	All LineStrings must be noded at intersections. Only applies to LineStrings in the same file/data type (i.e., contacts or line symbols).
Connectivity	There must be no dangling nodes for contact LineStrings.
Continuity	LineStrings are not fragmented by pseudo nodes (non-node intersections), abnormal change of directions, and abnormal change of feature types.
Minimum length of LineString	All LineStrings should be digitized. Lines <10 m will be checked for validity; lines <1 m are simplified.
Distance between vertices	Distance for a line segment between two sequential coordinates should be greater than 1 m and less than 500 m (to facilitate accurate coordinate transformations).
Coordinate density	A minimum number of coordinates should be used to accurately delineate the geological boundaries at a given map scale. LineStrings with too many redundant coordinates should be simplified (1 m), and LineStrings with too few coordinates are densified (greater than one node per 500 m).
Geometric irregularity	Sharp spikes along a linear LineString are checked and removed; sharp wedges in a LinearRing are checked to be valid; sharp angles between two LineStrings are checked, validated as real, or fixed.

omitted these details to simplify the unit labels and ensure they are consistent across the compilation. The soils maps we used in our compilation are categorized as 'soils and surficial geology' or 'soils and landforms' (Veness et al., 2024). After omitting the soil associations from these maps, the remaining unit labels are similar to terrain mapping, commonly coded with material type and surface expression in a comparable classification system, and can be converted using the same methods.

Point and line symbols were converted directly to symbol codes in Deblonde et al. (2024). If not specified in the original map, all symbols became their 'defined' version as opposed to 'poorly defined' or 'buried'. Point and line symbols not available in Deblonde et al. (2024) were recorded as a 'feature to be defined' and will be omitted from the public-facing data (e.g., slump direction line symbol; McCuaig, 2009). Locational confidence of geologic contacts is inconsistently defined, so all contacts were converted to a 'defined' version even if originally mapped as 'approximate' or 'inferred'.

All project data contain a 'src_featur' column populated with the original unit label or symbol description. Closed map legends unmodified from original source maps are stored in separate tables and can be joined with spatial data to obtain original unit descriptions. Open legend unit labels from source maps commonly contain too many components to include full descriptions. Map users must reference the original classification system to understand these units in detail.

6.1. Unit label conversion from Howes and Kenk (1997) to those in Deblonde et al. (2024)

To demonstrate how unit label conversion is performed, we convert the unit codes in Howes and Kenk (1997), a mapping scheme that has been used extensively in the province, to those in Deblonde et al. (2024). Unit labels coded in Deblonde et al. (2024) can have one or two map units, each including a material type and surface expression. In the case of two map units, they are separated by either a complex (.) or stratigraphic (/) designator. Complex designators are used if units extend across an area too small, or their relationship is too complex to be mapped individually. The dot (".") separates the first more extensive unit from the less extensive secondary unit. In Howes and Kenk (1997), this designator is a forward slash ("/") but holds a similar meaning. In Deblonde et al. (2024), stratigraphic designators with a forward slash ("/") separate superposed units; the unit to the left of the designator is stratigraphically above the unit to the right. Howes and Kenk (1997) show this relationship through a physical separation where the upper unit(s) is placed on top of a separator (horizontal line) and the lower unit below is placed below (i.e., $\frac{Cb}{Mp}$).

Unit labels from terrain maps (Fig. 3b) may be converted directly after removing components not captured in Deblonde et al. (2024) (e.g., $Mb-eF → Tb). In instances where an original label contains more than two material types, we only retain the two most extensive ones (e.g., Mb/Cv/GFt → Tb.Cv). In classification systems such as Howes and Kenk (1997), a material type can have up to three corresponding surface expressions. In these cases, the most extensive expressions are kept (e.g., Cba/Tb → Cb.Ca). We only maintain stratigraphic relationships if the underlying material was in the first two most extensive material types (e.g., $\frac{Cb}{Mp}$ → Cb/Tp). If a unit contains two material types exposed at surface, the stratigraphic relationship is not kept (e.g., $\frac{Cb/Af}{Mp}$ → Cb.Af).

Areas with the surface expressions blanket (>1 m) and veneer (<1 m) commonly include discontinuous bedrock outcrop. If an original unit label has a blanket or veneer, bedrock, and an additional unit, the bedrock component can be omitted to capture a less extensive unit (e.g., Mv/R/GFb → Tv.GFb). If the most extensive unit is bedrock, then both the bedrock and blanket/veneer unit are kept (e.g., R/Mv/GFb → R.Tv). Similarly, if a single material type is linked with both blanket and veneer expressions, we can simplify the unit to be described using only the more extensive one to capture a less extensive unit (e.g., Mbv.Cv → Tb.Cv). Both expressions are kept if a unit contains a single material type and only blanket and veneer expressions (i.e., Mbv → Tb.Tv).

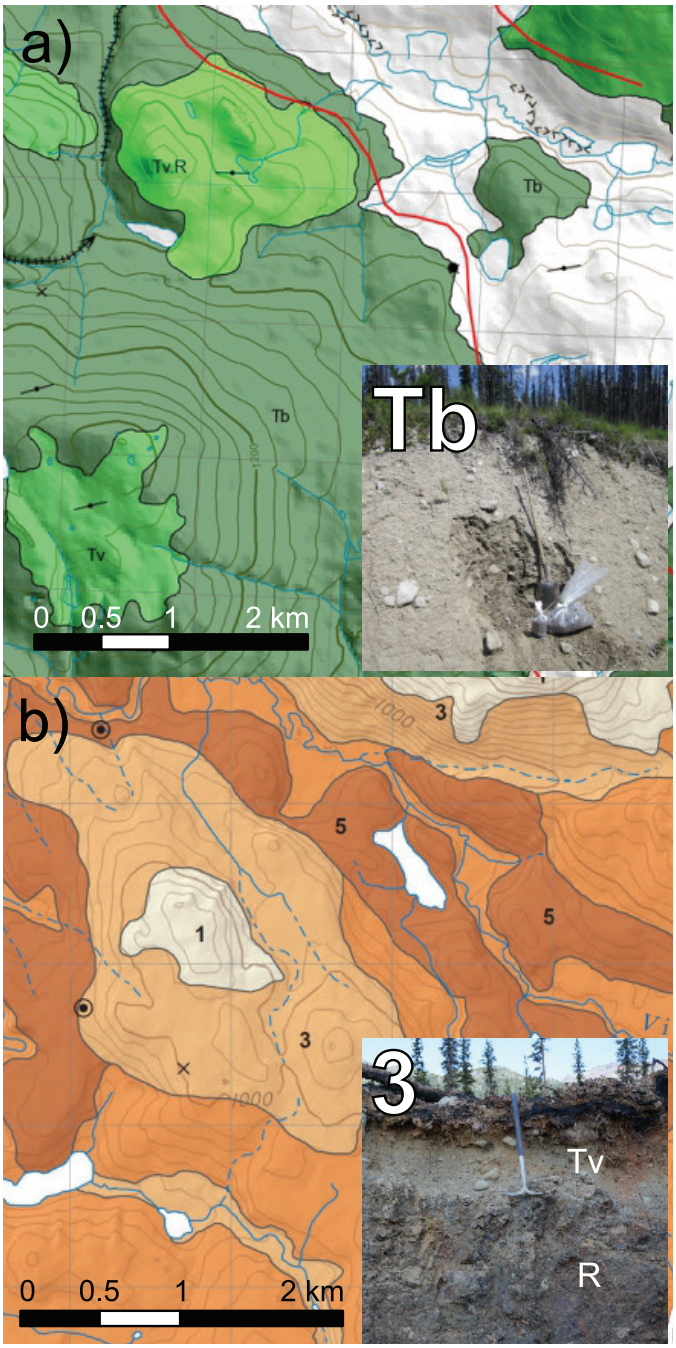
7. Compilation uses

The surficial geology compilation will be a comprehensive map of sediment type across the Interior Plateau of British Columbia. The compilation can be used to target specific material types (e.g., alluvial or glaciofluvial units) and features (e.g., eskers) that can inform aggregate exploration (e.g., Huntley and Hickin, 2010; Huntley et al., 2013). Sediments that are known to produce unstable terrain can be targeted for assessing ground conditions (e.g., peat, clay, groundwater) related to earthquakes (Monahan and Levson, 2000; Monahan et al., 2000a; Monahan et al., 2000b) or mass wasting (e.g., glaciolacustrine sediments; British Columbia Ministry of Forests and British Columbia Ministry of Environment, 1999; Brideau et al., 2026a, b). Parent materials derived from surficial geology maps can help inform silviculture, agriculture, and viticulture sectors. For example, surficial geology maps can help viticulture sectors by targeting specific Quaternary deposits used to grow grapes like glacial outwash or shoreline terraces (Hamblin, 2018).

The surficial geology compilation will be important to users interested in understanding sediment thickness or depth to bedrock. Surficial geology maps provide locations of extensive bedrock units and isolated outcrops. These locations can be used as surface inputs for depth to bedrock models (Arnold, 2021). Understanding the thickness and distribution of sediments is important for interpreting geochemical and geophysical results and for hazard risk assessment, agriculture, hydrology, and infrastructure engineering (Shangguan et al., 2016). Along with bedrock locations, units like veneers and blankets can be reclassified to build derivative maps for estimating drift thickness (Sacco et al., 2022; Wolter et al., 2022). These maps may be used to help determine suitable locations of bedrock outcrop for traditional mineral prospecting or to select sampling locations for drift prospecting.

This compilation will contain ice-flow indicators (e.g., striations, flutes, and crag-and-tails) and other glacial landforms (e.g., cirques, moraines, kettles) that contribute to the understanding of ice movement or behaviour during the Late Pleistocene (Arnold and Ferbey, 2020). Knowledge of ice flow and material type is important for designing or interpreting geochemical or mineralogical sediment samples (e.g., till or soil samples) for mineral exploration (Kerr and Levson, 1997; Plouffe and Ferbey, 2016).

Data in the Interior Plateau surficial geology compilation can be added to other compilations or used to build derivative maps. Features recorded in surficial geology maps can be added to other databases, for example landslides from this compilation can be an input for the Preliminary Canadian Landslide Database (Brideau et al., 2026a, b). Compiled digital data may be used to build derivative maps like subglacial till potential or aggregate resource maps (Fig. 5a; Ferbey, 2014b; Fig. 5c; Buchanan and Hora, 1992). The existence of these data in an analytical-ready format makes them easily applied to machine-learning (Latifovic et al., 2018; Odom and Doctor, 2023).



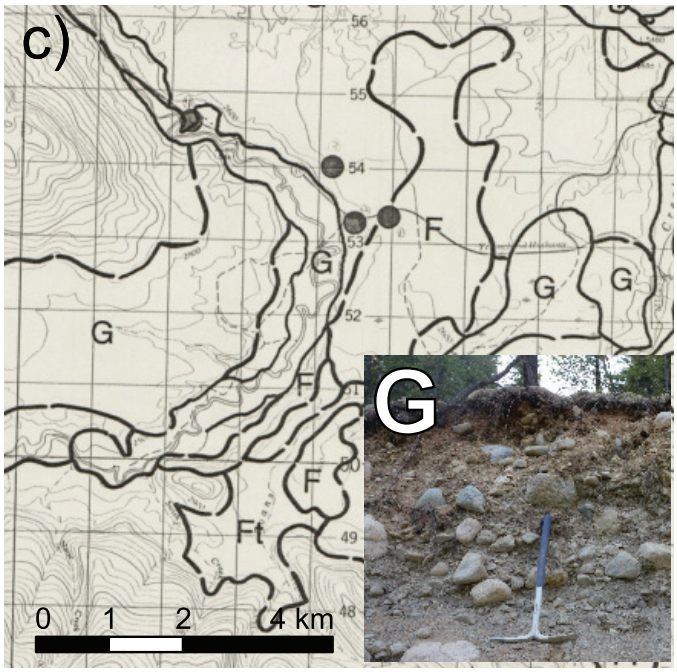


Fig. 5. Derivative maps with inset photos displaying related exposures. **a)** Basal till potential map from Ferbey (2014b); inset shows a till blanket (Tb) with till samples (Tb=high basal till potential, dark green). **b)** Till thickness map from Wolter et al. (2022); inset shows a till veneer above bedrock (Tv/R=drift thickness class 3, light orange). **c)** Aggregate resources map from Buchanan and Hora (1992); inset shows a glaciofluvial unit (G). Map plots all glaciofluvial (G) and fluvial (F, Ft) units with potential for aggregate. Black points represent gravel pit locations.

8. Conclusion

Analogous to BC Digital Geology (Cui et al., 2017), this compilation will improve public access to decades of surficial materials mapping in the Interior Plateau for multidisciplinary use. Consistent conversion to a single legend will allow users to compare multiple areas that were originally in incompatible classification systems. By presenting data using simple plain language descriptions, inexperienced users can immediately understand geological unit labels and feature symbology.

Acknowledgments

M-A. Brideau, Y. Cui, and B.I. van Straaten provided input into data and compilation standards. Reviews by D.J. Utting and A.C. Graham improved the manuscript.

References cited

Arnold, H., 2021. Depth to bedrock dataset for the Interior Plateau. British Columbia Ministry of Energy, Mines and Low Carbon Innovation, British Columbia Geological Survey GeoFile 2021-13, 6 p.

Arnold, H., and Ferbey, T., 2019. British Columbia surficial geology map index. British Columbia Ministry of Energy and Mines, British Columbia Geological Survey Open File 2019-03, 2 p.

Arnold, H., and Ferbey, T., 2020. Ice-flow indicator database, British Columbia and Yukon. British Columbia Ministry of Energy, Mines and Petroleum Resources, British Columbia Geological Survey Open File 2020-03, 1 p.

Blais-Stevens, A., and Clague, J.J., 2007. Surficial geology, Hixon, British Columbia. Geological Survey of Canada Open File 5272, 1:50,000 scale.

Bobrowsky, P.T., Giles, T., and Jackaman, W., 1992. Surficial geology map index of British Columbia. British Columbia Ministry of Energy, Mines and Petroleum Resources, British Columbia Geological Survey Open File 1992-13, 13 p.

Brideau, M-A., Brayshaw, D., Hancock, C.A., Lipovsky P., Cronmiller, D., Lewkowicz, A., Geertsema, M., McGregor, C., Tannant, D., Friele, P., Clarke, J., Steelquist, A., Wong-Teichroeb, H., Ring, C., and Wells, G., 2026a. Preliminary Canadian Landslide Database (13.0). <https://doi.org/10.5281/zenodo.10271431>

Brideau, M-A., Brayshaw, D., and Hancock C-A., 2026b. Highlights for British Columbia from the preliminary Canadian Landslide Database. In: Geological Fieldwork 2025, British Columbia Ministry of Mining and Critical Minerals, British Columbia Geological Survey Paper 2026-01, pp. 239-245.

British Columbia Geological Survey, 2019. British Columbia Digital Geology. British Columbia Ministry of Mining and Critical Minerals, British Columbia Geological Survey. Data version 2019-12-19. <https://www2.gov.bc.ca/gov/content/industry/mineralexploration-mining/british-columbia-geological-survey/geology/bcdigitalgeology>

British Columbia Ministry of Forests and British Columbia Ministry of Environment, 1999. Mapping and assessing terrain stability guidebook, 2nd ed. Forest Practices Code of British Columbia, Victoria.

Buchanan, R., and Hora, Z., 1992. Aggregate Resources, Dome Creek. British Columbia Ministry of Transportation and Highways and British Columbia Ministry of Energy, Mines and Petroleum Resources, 1:50,000 scale.

Canada Department of Agriculture, 1974. The system of soil classification for Canada. Publication 1455, 255 p.

Canada Department of Agriculture, 1976. Glossary of terms in soil science. Agriculture Canada Research Branch Publication 1459, 44 p.

Canada Soil Survey Committee, 1978. The Canadian system of soil classification. Agriculture Canada Research Branch Publication 1646, 164 p.

Clague, J.J., and Ward, B.C., 2011. Pleistocene glaciation of British Columbia. In: Ehlers, J., Gibbard, P.L., and Hughes, P.D., (Eds.), Developments in Quaternary Sciences Volume 15, pp. 563-573. <https://doi.org/10.1016/B978-0-444-53447-7.00044-1>

Colpron, M., 2020. Yukon Terranes-A digital atlas of terranes for the northern Cordillera. Yukon Geological Survey. <https://data.geology.gov.yk.ca/Compilation/2#InfoTab>

Cui, Y., 2021. A geospatial frame data model to simplify digital map compilation and integration. British Columbia Ministry of Energy, Mines and Low Carbon Innovation, British Columbia Geological Survey Paper 2021-03, 20 p.

Cui, Y., Zhao, S., Fortin, G., Meredith-Jones, S., and Jones, L.D., 2018. Development of MapPlace 2 geospatial web service to disseminate geoscience in British Columbia. In: Geological Fieldwork 2017, British Columbia Ministry of Energy, Mines and Petroleum Resources, British Columbia Geological Survey Paper 2018-01, pp. 183-195.

Deblonde, C., Campbell, J.E., Chow, W., Cocking, R.B., Huntley, D.H., Parent, M., Rice, J.M., Robertson, L., Smith, I.R., Weatherston, A., and Zawadzka, K., 2024. Surficial Data Model: The science language of the integrated Geological Survey of Canada data model for surficial geology maps. Natural Resources Canada, Geological Survey of Canada Open File 8236, ver. 2.5.1. <https://doi.org/10.4095/332530>

Dixon-Warren, A.B., Bobrowsky, P.T., Leboe, E.R., and Ledwon, A., 1997. Terrain geology map of Adams Plateau area (NTS 82M/4). British Columbia Ministry of Employment and Investment, British Columbia Geological Survey Open File 1997-07, 1:50,000 scale.

E.L.U.C. Secretariat, 1978. Terrain Classification System, British Columbia Ministry of the Environment, Resource Analysis Branch, 56 p.

Farstad, L., 1979. Soils & Surficial Geology, Hixon. Agriculture Canada, 1:50,000 scale.

Fenton, M.M., Waters, E.J., Pawley, S.M., Atkinson, N., Utting, D.J., and Mckay, K., 2013. Surficial Geology of Alberta. Alberta Energy Regulator, AER/AGS Map 601, 1:1,000,000 scale.

Ferbey, T., 2014a. Surficial geology of the Nadina River map area (NTS 093E/15), British Columbia. British Columbia Ministry of Energy and Mines, British Columbia Geological Survey Geoscience Map 2014-01, Geoscience BC Map 2014-09-01, 1:50,000 scale.

Ferbey, T., 2014b. Basal till potential of the Colleymount map area (93L/01), British Columbia. British Columbia Ministry of Energy and Mines, British Columbia Geological Survey Open File 2014-04, 1:50,000 scale.

Ferbey, T., and Elia, E.A., 2025. Surficial geology of the Nanitsch Lake area (NTS 94D/1), British Columbia. British Columbia Ministry of Mining and Critical Minerals, British Columbia Geological Survey Geoscience Map 2025-02, 1:50,000 scale.

Ferbey, T., Levson, V.M., and Plouffe, A., 2016. Surficial geology, Moffat Creek area, British Columbia (Parts of NTS 93A/3, 4, 5, 6). British Columbia Ministry of Energy and Mines, British Columbia Geological Survey Geoscience Map 2016-01, Geological Survey of Canada Geoscience Map 252, 1:50,000 scale.

Forest Practices Code, 1999. Mapping and assessing terrain stability guidebook. British Columbia Environment, Forest Service British Columbia, 36 p.

Fulton, R.J., 1995. Surficial materials of Canada. Geological Survey of Canada Map 1880A, 1:5,000,000 scale.

Hamblin, A.P., 2018. Message in a bottle: The wine terroir concept in Canada, from an earth sciences perspective. Natural Resources Canada, Geological Survey of Canada Open File 8365, 62 p. <https://doi.org/10.4095/308492>

Hashmi, S., Plouffe, A., and Ward, B.C., 2015. Surficial geology, Bootjack Mountain area, British Columbia, Parts of NTS 93-A/5, NTS 93-A/6, NTS 93-A/11, and NTS 93-A/12. Geological Survey of Canada Canadian Geoscience Map 209 (preliminary); British Columbia Geological Survey Geoscience Map 2015-02, 1:50,000 scale.

Holland, S.S., 1976. Landforms of British Columbia: A physiographic outline. British Columbia Ministry of Energy, Mines and Petroleum Resources, British Columbia Geological Survey Bulletin 48, 138 p.

Howes, D.E., and Kenk, E., 1997. Terrain Classification System for British Columbia: A system for the classification of surficial materials, landforms and geological processes of British Columbia. British Columbia Ministry of Environment and British Columbia Ministry of Crown Lands, Ministry of Environment Manual 10 (version 2), 102 p.

Huntley, D.H., Hickin, A.S., Chow, W., and Mirmohammadi, M., 2013. Surficial geology, Trail Lake, British Columbia (prelim. ed.). Natural Resources Canada, Canadian Geoscience Map 123, 1:50,000 scale. <https://doi.org/10.4095/292400>

Huntley, D.H., and Hickin, A.S., 2010. Surficial Deposits, Landforms, Glacial History and Potential for Granular Aggregate and Frac Sand: Maxhamish Lake Map Area NTS 94O, British Columbia. Natural Resources Canada, Geological Survey of Canada Open File 6430, 17 p.

Jungen, J.R., 1980. Soil resources of the Nelson map area (82 F). British Columbia Ministry of Environment, British Columbia Soil Survey Report No. 28, 217 p.

Kerr, D.E., and Levson, V.M., 1997. Drift prospecting activities in British Columbia: An overview with emphasis on the Interior Plateau. In: Diakow, L.J., Matcalfe, P., and Newell, J., (Eds.), Interior Plateau Geoscience Project: Summary of geological, geochemical and geophysical studies. British Columbia Ministry of Employment and Investment, British Columbia Geological Survey Paper 1997-2, pp. 159-172.

Knowledge Management, 2011. Terrestrial ecosystem information scanned map boundary. <https://catalogue.data.gov.bc.ca/dataset/terrestrial-ecosysteminformation-scanned-map-boundary> (last accessed August 2024).

Latifovic, R., Pouliot, D., and Campbell, J., 2018. Assessment of Convolution Neural Networks for Surficial Geology Mapping in the South Rae Geological Region, Northwest Territories, Canada. Remote Sensing, 19 p.

Lewis, T., 1987. TFL 24-MORESBY British Columbia Geographic System (BCGS) 81.3, Ecosystem-Terrain Classification. Western Forest Products Limited map, 1:10,000 scale.

MacIntyre, D.G., and Struik, L.C., 2000. Nechako NATMAP Project, Central British Columbia-1999 Overview. In: Geological Fieldwork 1999, British Columbia Ministry of Energy and Mines, British Columbia Geological Survey Paper 2000-01, pp. 7-14.

McCuaig, S.J., 2009. Surficial Geology, Deka Lake, British Columbia. Geological Survey of Canada Open File 6173, 1:50,000 scale.

McGregor, C., and Sacco, D.A., 2021. Surficial geology of the Saxton Lake map area (NTS 093J/03), British Columbia. Geoscience BC map 2021-03-06a, 1:50,000 scale.

Ministry of Environment, 1973. Surficial Geology (Provisional), Hixon, 1:50,000 scale.

Monahan, P.A., and Levson, V.M., 2000. Quaternary Geological Map of Greater Victoria. British Columbia Ministry of Energy and Mines, British Columbia Geological Survey Geoscience Map 2000-2, 1:25,000 (approximate) scale.

Monahan, P.A., Levson, V.M., McQuarrie, E.J., Bean, S.M., Henderson, P., and Sy, A., 2000a. Relative Earthquake Hazard Map of Greater Victoria, Showing Areas Susceptible to Amplification of Ground Motion, Liquefaction and Earthquake-Induced Slope Instability. British Columbia Ministry of Energy and Mines, British Columbia Geological Survey Geoscience Map 2000-1, 1:25,000 (approximate) scale.

Monahan, P.A., Levson, V.M., Henderson, P., and Sy, A., 2000b. Relative liquefaction and amplification of ground motion hazard maps of greater Victoria (TRIM 92B.043, 044, 0 53, 054). British Columbia Ministry of Energy and Mines, British Columbia Geological Survey Geoscience Map 2000-3. 1:25,000 (approximate) scale.

Morfitt, G.L., 1999. Forest Renewal BC: Planning and Accountability in the Corporation, The Silviculture Programs. Office of the Auditor General of British Columbia Report 1999/2000: 6, 123 p.

Odom, W., and Doctor, D., 2023. Rapid estimation of minimum depth-to-bedrock from lidar leveraging deep-learning-derived surficial material maps. Applied Computing and Geosciences. 11 p.

Open Geospatial Consortium, 1999. OpenGIS® Simple Features Specification for SQL, Revision 1.1; Open Geospatial Consortium, Inc. OpenGIS® Project Document 99-049, Release May 5, 1999, 78 p.

Plouffe, A., and Ferbey, T., 2016. Till geochemistry, mineralogy, and textural data near four Cu porphyry deposits in British Columbia. Geological Survey of Canada Open File 8038, British Columbia Ministry of Energy and Mines, British Columbia Geological Survey GeoFile 2016-10, 44 p.

Plouffe, A., 2000. Surficial geology, Manson River, British Columbia. Natural Resources Canada, Geological Survey of Canada "A" Series Map 1987A, 1:250,000 scale. <https://doi.org/10.4095/211398>

Sauvé, M., Ward, B., and Ferbey, T., 2025. Surficial geology of the Kinaskan Lake area, British Columbia (parts of NTS 104G/08, 09, 16 and 104H/12, 13). British Columbia Ministry of Mining and Critical Minerals, British Columbia Geological Survey Geoscience Map 2025-01, 1:50,000 scale.

Sacco, D.A., Janzen, B., and Jackaman, W., 2022. Mineral exploration in the Central Interior Copper-Gold Research projects area, central British Columbia (parts of NTS 093A, B, G, J, K, O): New tools for a proven approach to exploration under cover. In: Geoscience BC Summary of Activities 2021: Minerals, Geoscience BC Report 2022-01, pp. 1-10.

Shangguan, W., Hengl, T., Mendes de Jesus, J., Yuan, H., and Dai, Y., 2017. Mapping the global depth to bedrock for land surface modeling. Journal of Advances in Modeling Earth Systems, 9, 65-88.

Soil Classification Working Group, 1998. The Canadian system of soil classification. Agriculture and Agri-Food Cananda Publication 1646 (Revised), 187 p.

Struik, L.C., MacIntyre, D.G., and Williams, S.P., 2007. Nechako NATMAP Project: A digital suite of geoscience information for central British Columbia. Natural Resources Canada, Geological Survey of Canada Open File 5623. <https://doi.org/10.4095/224578>

Veness, H., Elia, E.A., and Ferbey, T., 2024. A digital update of Open File 1992-13: Surficial geology map index of British Columbia. British Columbia Ministry of Mining and Critical Minerals, British Columbia Geological Survey Open File 2024-09, 2 p.

Wolter, A., Sacco, D.A., and McGregor, C., 2022. Drift thickness of the Swift River and Quesnel River map areas (Parts of NTS 093A/13 and 093B/16), British Columbia. Geoscience BC Map 2021-08-01c, 1:50,000 scale.

Yukon Geological Survey, 2023. Surficial Geology dataset. Yukon Geological Survey. <https://data.geology.gov.yk.ca/Compilation/33> (last accessed August 2025).

Highlights for British Columbia from the preliminary Canadian Landslide Database

Marc-André Brideau[1, a], Drew Brayshaw[2], and Carie-Ann Hancock[3]

[1] British Columbia Geological Survey, Ministry of Mining and Critical Minerals, Victoria, BC, V8W 9N3
[2] Statlu Environmental Consulting Ltd., Chilliwack, BC, V2P 6L9
[3] BGC Engineering Inc., Vancouver, BC, V6Z 0C8
[a] corresponding author: Marc-Andre.Brideau@gov.bc.ca

Recommended citation: Brideau, M-A., Brayshaw, D., Hancock, C-A., 2026. Highlights for British Columbia from the preliminary Canadian Landslide Database. In: Geological Fieldwork 2025, British Columbia Ministry of Mining and Critical Minerals, British Columbia Geological Survey Paper 2026-1, pp. 239-245.

Abstract

The preliminary Canadian Landslide Database is a publicly available compilation of existing landslide inventories and new mapping. Version 13 of the database contains 28,000 national entries of which 14,520 are from British Columbia. These entries include both landslide events (discrete recorded periods of movement) and landslide features (e.g., slopes with a morphology consistent with past or ongoing movement). The occurrence and distribution of different types of landslides reflect the interaction between geological materials, relief, and other contributing factors (e.g., river erosion, timing with respect to wildfires), and triggers (e.g., weather events, seismicity, and anthropogenic activity). The database fills a gap in our overall understanding of landslide processes and provides common baseline knowledge to local governments, practitioners, and researchers. It also provides interested parties with initial desktop-level information of known landslides in an area and helps to identify priorities for further work.

Keywords: Landslide, hazard, mass movement, lidar, InSAR, inventory

1. Introduction

It is important to understand the distribution of landslides in British Columbia because they represent a risk to infrastructure (e.g., Hungr et al., 1999) and public safety (Strouth and McDougall, 2024). Four types of landslide maps are recognized in the professional practice guidelines on landslide mapping developed by Engineers and Geoscientists British Columbia: inventory, susceptibility, hazard, and risk (EGBC, 2025). The guidelines define inventory maps as depicting the locations or spatial extents of past and active landslide occurrences, or the distribution of morphological features within a single landslide or landslide complex. Landslide inventories provide basic data that, when used in conjunction with other terrain, material, and trigger information, can be used to identify susceptible terrain where future events could occur. Landslide inventories are typically compiled for a specific area (e.g. Bornaetxea et al., 2022) but they can also be prepared for specific triggers such as earthquakes (Barth et al., 2020) and storms (Hancock and Wlodarczyk, 2025) or type (e.g., glaciomarine, Geertsema and Millard, 2025).

Although the need for a Canadian landslide database has long-been recognized (Cave et al., 1992), and efforts were initiated to develop a database structure (Grignon et al., 2004), it was not until September 2022 that the initial version of the preliminary Canadian Landslide Database was made publicly available. The database, being developed by a group of volunteer geohazard experts from the public, private, and academic sectors, is available at no cost at the open data repository Zenodo (Brideau et al., 2026). It contains landslide point locations and attributes as a .csv file which can be imported in GIS software and as a .kmz file for visualization using Google Earth. While it represents the best information currently available, the database should be considered a preliminary characterization of landslides in British Columbia because it is not based on systematic mapping across the province and it is predominantly based on remote sensing observations. This paper introduces the methods used to compile the database, outlines the landslide classification used, presents highlights for British Columbia, and discusses potential applications and limitations.

2. Methods

Landslide locations in the database are provided as point features and include attributes for a unique landslide identifier, landslide name, location coordinates (latitude and longitude), landslide type (see section 3 for more details), material type (surficial, rock, anthropogenic), point location type (headscarp, source, transport, deposit), qualitative location confidence (low, moderate, high), and an attribute for tracking the database version when an entry was last updated. Where available, additional attributes such as volume estimate, date of occurrence, trigger, contributing factors, interpreted historical interferometric synthetic aperture radar (InSAR)-based displacement, and reference to previous work are also provided.

Most landslides in the database were identified using Google

Earth and publicly available imagery and lidar. Online mapping applications such as HazMapper (Scheip and Wegman, 2021) and Arctic Landscape EXplorer (ALEX; Lübker et al., 2024) have also been used to identify landslides based on the changes in multi-spectral indices derived from satellite-acquired datasets. Starting with Version 12 of the database, InSAR-based displacement information from publicly available regional projects (e.g., Choe et al., 2021) was incorporated in the reference and comment attributes for individual entries. The recent availability of NASA's Observational Products for End-Users from Remote Sensing Analysis (OPERA; NASA, 2025) and Natural Resources Canada's pilot national-scale maps of active deformation processes (NRCan, 2024) allowed for the addition of deformation information to existing database entries along with the identification of new landslides.

3. Landslide types mapped

Following an approach similar to Varnes (1978) and Hungr et al. (2014), landslide types in the database are classified based on material type (bedrock, debris, soil/earth, water/ice) and predominant transport mechanism (fall, topple, slide, flow, spread, deformation). This basic classification was modified to incorporate landslide types specific to regions underlain by permafrost (e.g., Wolfe et al., 2025). Where associated with events of significant magnitude or impact, large ice falls resulting in cascading hazards and glacial lake outburst floods (GLOF) have been included (Table 1).

Snow avalanches, common in mountain areas of British Columbia, are not included, and debris cones that may form at the base of snow avalanche paths are not mapped because they are assumed to be deposited by snow. Rock glaciers are only included if their geomorphology indicates they originated as a consequence of a landslide or if material in the rock glacier subsequently failed as a landslide. Alluvial fans are formed by a combination of processes, including rock falls, debris flows, debris floods, and floods (e.g., de Haas et al., 2024). Although alluvial fans are distinct landforms that can be mapped, they are only included in the database where specific events have been observed and documented (e.g., debris flows).

4. Highlights for British Columbia

Due to its landslide-prone mountainous terrain, British Columbia accounts for about half of the Canada-wide entries in Version 13 of the database. This may also reflect an observational bias because most contributors have regional expertise in the province.

The spatial distribution of landslide occurrences and types (Fig. 1) reflects the interaction between geological material, relief, climate, and seismicity and has long-been recognized (Eisbacher, 1979; British Columbia Geological Survey, 1993; Guthrie, 2005). In the Insular Mountains (Haida Gwaii, Vancouver Island) and Coast Mountains, debris flows, debris floods, debris avalanches and debris slides are prevalent (Fig. 1), which we attribute to the combination of steep terrain and wet climate. In particular, the wettest coastal areas have steep organic soil failures not observed elsewhere (e.g., Campbell et al., 2010). In the central Interior Plateau and northeastern British Columbia, earth slides are spatially associated with glaciolacustrine deposits (Geological Survey of Canada, 2014), which are particularly susceptible to failure (e.g., Bobrowsky and Dominguez, 2012). Earth flows in the central Interior Plateau are spatially associated with the weathered Cretaceous to Eocene sedimentary and volcanic geological units (Bovis, 1985). Rock slides (undifferentiated, translational, irregular, and rotational) and rock falls in the Purcell and Rocky mountains are spatially associated with layered sedimentary units.

Bovis and Evans (1996), Hensold et al. (2010), and Clayton et al. (2017) have described mountain and rock slope deformation (as defined in Hungr et al., 2014) in British Columbia. The province-scale distribution (Fig. 1) shows mountain and rock slope deformation in all mountainous regions of the province, consistent with the global literature indicating that they develop by a range of mechanisms (Kinakin and Stead, 2005; Agliardi et al., 2012). Although mountain and rock slope deformation can occur in unglaciated landscapes, formerly glaciated mountains are especially susceptible (Panek et al., 2015).

The role of wildfires contributing to increased landslides in British Columbia has previously been recognized (e.g., Jordan, 2016), particularly in cases where a recently burnt region was affected by atmospheric rivers (Hancock and Wlodarczyk, 2025). The increased landslide susceptibility of post-wildfire landscape is due to changes in soil properties which in turn impact water infiltration and the rainfall thresholds at which landslides occur (Gartner et al., 2024). Version 13 of the database contains 1300 entries with wildfires interpreted as a contributing factor.

Version 13 of the database is levering ongoing interpretation of InSAR-based deformation maps (NASA, 2025; NRCan, 2024) to identify 344 slopes with landslide morphology that were likely active between 2016 and 2024 (Fig. 2). Although province-scale deformation areas had previously been generated using multiple SAR sensors (ALOS-1, Sentinel-1, RADARSAT-2) to identify potential landslides (Pichierri et al., 2019), the previous deformation areas were not publicly available and had not been reviewed to confirm they corresponded to landslide morphology.

5. Applications and limitations

Even in a preliminary form being continuously updated, the database provides a starting point for desktop-level landslide hazard and risk assessments. Reference to the database can provide non-specialists with regional overviews of geohazards. Other applications for the database include geospatial analysis to investigate attributes (e.g., geology, slope, aspect) at landslide initiation zones. Preliminary exposure assessments have been facilitated by cross-referencing the database with specific asset and infrastructure layers such as roads, transmission lines, railways, or pipelines (e.g., Journeay et al., 2022). Although the absence of mapped features does not indicate an absence of

Table 1. Landslide classification scheme used in the preliminary Canadian Landslide Database (Version 13).

		Rock	Surficial		Water
			Debris[1]	Earth[1]	
Movement Type	Fall	Rock fall	Debris fall	Earth fall	Ice fall[2]
	Topple	Rock topple			
	Slide	Rock slide undifferentiated			
		Rock translational slide	Debris slide		
		Rock rotational slide		Earth slide	
		Rock irregular slide			
		Deep-seated permafrost landslide[3]			
	Flow	Rock avalanche	Debris avalanche	Flowslide	
			Debris flow	Earth flow	
			Debris flood	Mud flow	Flood[2]
			Glacial lake outburst flood[2]		
			Active layer detachment[3]	Retrogressive thaw slump[3]	
	Slope deformation	Mountain slope deformation			
		Rock slope deformation			
	Spread	Rock spread		Earth spread	
	Complex	Rock complex[4]			

[1] 'Debris' contains between 20% and 80% material coarser than 2 mm, with the remainder being less than 2 mm, and 'Earth' contains greater than 80% material finer than 2 mm (Varnes, 1978).
[2] Geomorphic processes that resulted in cascading hazards including landslides.
[3] Permafrost-specific landslide type.
[4] Complex failure refers to slopes where multiple movement types are present.

landslides, the known features provide a baseline that additional assessments can improve on.

Observational biases include those imposed by the quality of imagery and sensor data and by proximity to populated areas. The use of Google Earth imagery results in a bias towards more recent events. Large landslides persist as landforms that may be visible on imagery for hundreds to thousands of years, particularly in low-vegetation areas such as Arctic and alpine environments. In contrast, on the Pacific coast of British Columbia, debris slides and debris flows may only remain visible for several years before becoming revegetated and hard to discern (Guthrie and Evans, 2007). Historical event inventories taken from media sources such as Septer (2007a, b) have biases towards places where people lived or worked relative to remote or uninhabited places. Historic air photos provide important documentation of historical events, but it can be costly and time consuming to generate comprehensive databases from them. Consequently, many of the debris flows, debris avalanches, and debris slides recorded in the database are relatively young (<30 years) and older events are underrepresented.

The recent availability of InSAR-based deformation information provides improved interpretation of slope processes that can be used to update landslide inventories and hazard characterizations. Nonetheless, InSAR techniques have limitations (e.g., Wu and Madson, 2024) and hazard characterization needs to consider the impact of radar wavelength, stack depth, processing algorithm, topography, vegetation, snow cover, satellite line-of-sight relative to slope movement, and rate of surface displacement. This means that

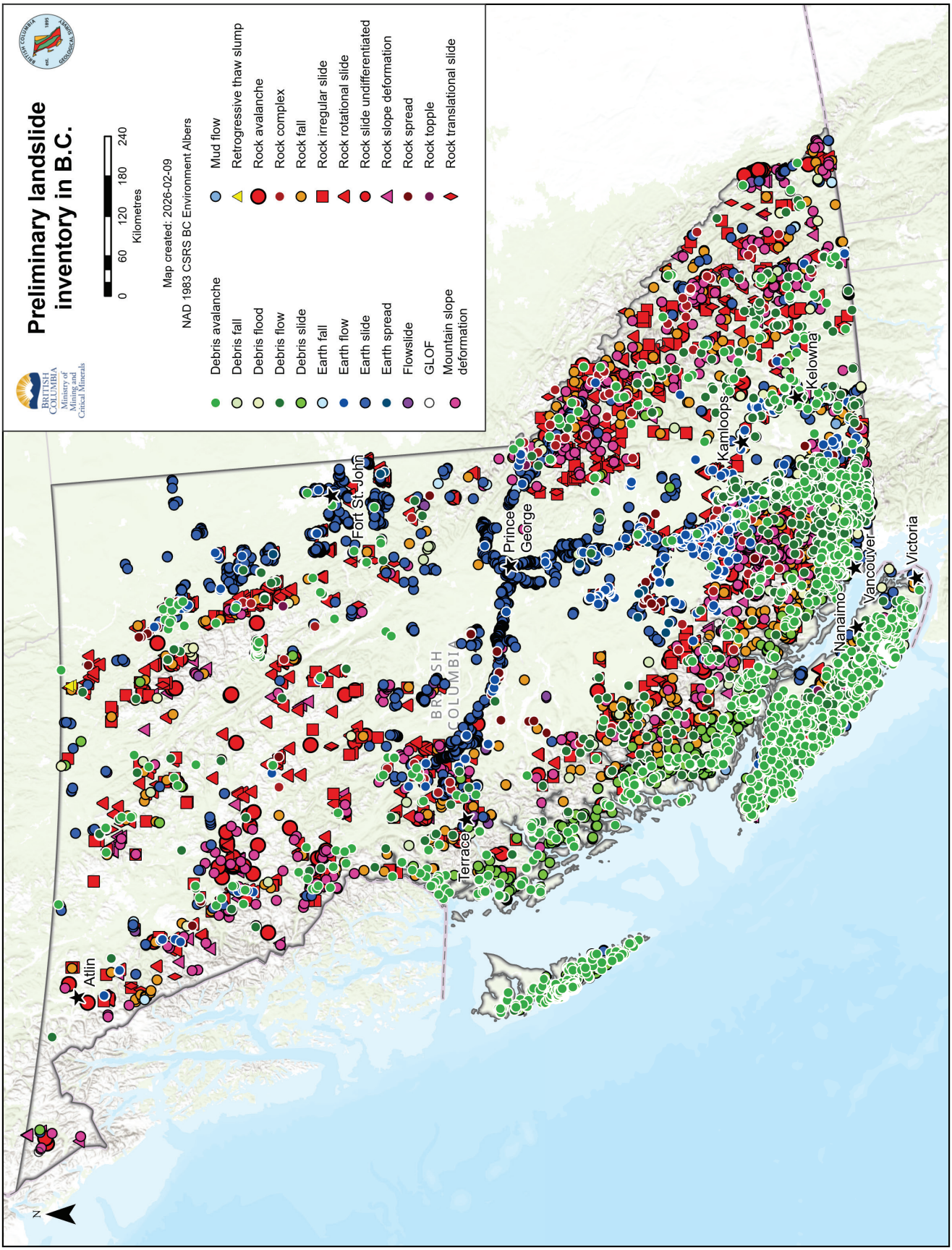


Fig. 1. Map of 14,520 British Columbia landslides from Version 13 of the preliminary Canadian Landslide Database. Points are symbolized according to landslide type. Data from Brideau et al. (2026).

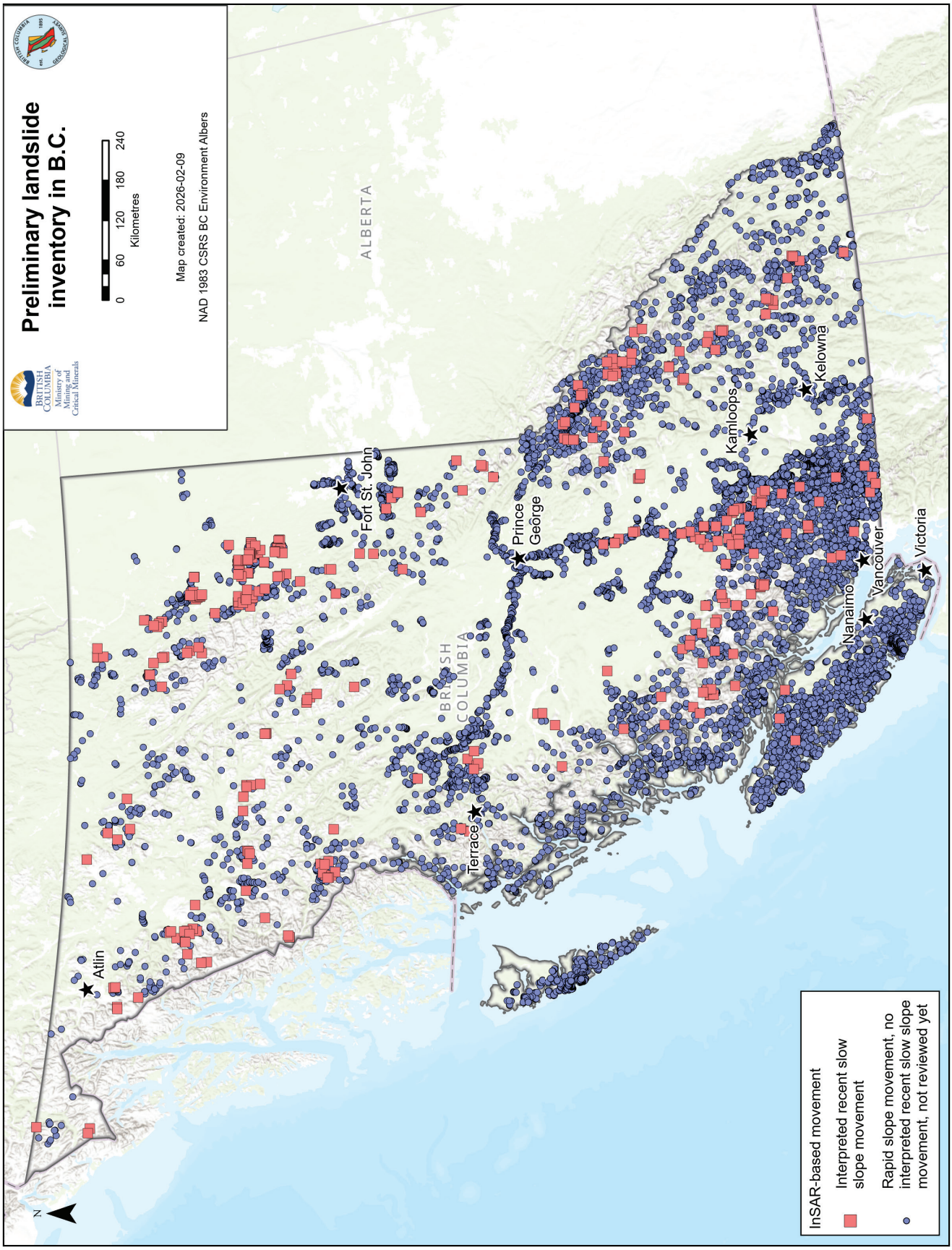


Fig. 2. Map of 14,520 British Columbia landslides from Version 13 of the preliminary Canadian Landslide Database. Points are symbolized based on interpreted slow slope movement from InSAR-based deformation maps. Uncertainties and limitations of this in-progress interpretation are discussed in the text. Data from Brideau et al. (2026).

large (>100,000 m^3), very slow (<160 mm/year; Porter 2023), unvegetated, east-west moving landslides are preferentially captured in the InSAR data. As a result, the number of presently moving slopes in the province with the potential to cause damage is expected to be significantly greater than captured in the database. The database entries with attributes recording interpreted historical InSAR-based deformation pattern are also based on records that stopped in 2024 (NASA, 2025; NRCan, 2024) or earlier (Choe et al., 2021). Their current state of activity and hazard needs to be confirmed by site-specific investigations.

6. Conclusion

The preliminary Canadian Landslide Database is a freely and publicly accessible inventory of landslide point locations across Canada compiled since September 2022 on a volunteer basis by a group of geohazard experts from the public and private sectors. Version 13 of the database contains 28,000 entries including 14,520 in British Columbia. Although the database currently provides the best publicly available characterization of landslide distribution at the national and provincial scales, it has temporal and spatial biases such as recent landslides near infrastructure being better represented than old landslides in remote locations. The current database supports previous experienced-based interpretations of landslide distribution and type in British Columbia. InSAR-based deformation maps of 344 slopes have identified movements at very slow rates between 2016 and 2024.

Acknowledgments

This overview benefitted from contributions by Panya Lipovsky and Derek Cronmiller (Yukon Geological Survey), Antoni Lewkowicz (Carleton University), Andrée Blais-Stevens (Geological Survey of Canada), Rick Guthrie (Stantec), Marten Geertsema, Hazel Wong-Teichoeb, and Gareth Wells (British Columbia Ministry of Forests), Jason Goetz (Wilfrid Laurier University), Cory McGregor (British Columbia Ministry of Water, Land and Resource Stewardship), Dwayne Tannant (University of British Columbia Okanagan), Pierre Friele (Cordilleran Geoscience), Jennifer Clarke (Clarke Geoscience), Aaron Steelquist (Stanford University), Caleb Ring (BGC Engineering Inc.), and from discussions with Phil Lesueur (Geological Survey of Canada), Ben Mirus and Dennis Staley (United States Geological Survey), Kris Holm, Richard Carter, Corey Scheip, and Derek Kinakin (BGC Engineering Inc.), Scott McDougall and Dominique Austin (University of British Columbia). A constructive review and comments by Travis Ferbey (British Columbia Geological Survey) helped improve the paper.

References cited

Agliardi, F., Crosta, G., and Frattini, P., 2012. Slow rock-slope deformation. In: Clague, J.J., and Stead, D., (Eds.), Landslides: Types, Mechanisms and Modeling. Cambridge University Press, pp. 207-221.

Barth, S., Geertsema, M., Bevington, A.R. Bird, A.L., Clague, J.J., Millar, T., Bobrowsky, P.T., Hasler, A., and Liu, H. 2020. Landslide response to the 27 October 2012 earthquake (MW 7.8), southern Haida Gwaii, British Columbia, Canada. Landslides 17, 517-526.

Bobrowsky, P.T., and Dominguez, M.J., 2012. Landslide susceptibility map of Canada, Geological Survey of Canada, Open File 7228, 1:6,000,000 scale.

Bornaetxea, T., Blais-Stevens, A., and Miller, B., 2022. Landslide inventory map of the Valemount area, British Columbia, Geological Survey of Canada, Open File 8926.

Bovis, M.J., 1985. Earthflows in the Interior Plateau, southwest British Columbia. Canadian Geotechnical Journal, 22, 313-334.

Bovis, M.J., and Evans, S.G., 1996. Extensive deformations of rock slopes in southern Coast Mountains, southwest British Columbia, Canada. Engineering Geology, 44, 163-182.

Brideau, M-A., Brayshaw, D., Hancock, C-A., Lipovsky, P., Cronmiller, D., Lewkowicz, A., Blais-Stevens, A., Guthrie, R., Geertsema, M., Goetz, J., McGregor, C., Tannant, D., Friele, P., Clarke, J., Steelquist, A., Wong-Teichroeb, H., Ring, C., and Wells, G., 2026. Preliminary Canadian Landslide Database (Version 13.0) [Dataset]. Zenodo. <https://doi.org/10.5281/zenodo.18216956>

British Columbia Geological Survey, 1993. Landslides in British Columbia. British Columbia Ministry of Energy, Mines and Petroleum Resources, British Columbia Geological Survey Information Circular 1993-07, 2 p.

Campbell, D., Millard, T., Schwab, J., and Roberts, B., 2010. Landslides in organic soils on forested slopes. Extension Note 99, British Columbia Ministry of Forests and Range, 7 p.

Cave, P.W., Church, M., Jackson, L.E., Jr., Lister, D.R., and Skermer, N., 1992. Recommendations of the Geologic Hazard Workshop-by the steering committee on geologic hazards. In: Bobrowsky, P., (Ed.), Geological Hazards in British Columbia. British Columbia Ministry of Energy, Mines and Petroleum Resources, British Columbia Geological Survey, Open File 1992-15, pp. 1-6.

Choe, B-H., Blais-Stevens, A., Samsonov, S., and Dudley, J., 2021. Sentinel-1 and RADARSAT Constellation Mission InSAR assessment of slope movements in the southern interior of British Columbia, Canada. Remote Sensing, 13, article 3999, 17 p. <https://www.mdpi.com/2072-4292/13/19/3999>

Clayton, M.A., Stead, D., Kinakin, D., and Wolter, A., 2017. Engineering geomorphological interpretation of the Mitchell Creek Landslide, British Columbia, Canada. Landslides 14, 1655-1675.

de Haas, T., Hancock, C-A., and Ventra D., 2024. Debris-flow watersheds and fans: morphology, sedimentology and dynamics. In: Jakob, M., McDougall, S., and Santi, P., (Eds.), Advances in Debris-Flow Science and Practice, Springer-Verlag, pp. 9-73.

EGBC (Engineers and Geoscientists British Columbia), 2025. Professional practice guidelines, landslide mapping. Version 1.0, July 16, 2025, 78 p. <https://tools.egbc.ca/Registrants/Practice-Resources/Guidelines-Advisories#natural-hazards>

Eisbacher, G.H., 1979. First-order regionalization of landslide characteristics in the Canadian Cordillera. Geoscience Canada, 6, 69-79.

Gartner, J.E., Kean, J.W., Rengers, F.K., McCoy, S.W., Oakley, N., and Sheridan, G., 2024. Post-wildfire debris flows. In: Jakob, M., McDougall, S., Santi, P., (Eds.), Advances in Debris-flow Science and Practice, pp. 309-345.

Geertsema, M., and Millard, T., 2025. Sensitive clay landslides in British Columbia-an update. Earth and Environmental Science 1523, article 012015, 15 p. <https://doi.org/10.1088/1755-1315/1523/1/012015>

Geological Survey of Canada, 2014. Surficial geology of Canada. Geological Survey of Canada, Canadian Geoscience Map 195, 1:5,000,000 scale.

Grignon, A.G., Bobrowsky, P.T., and Coultish, T., 2004. Landslide database management philosophy in the Geological Survey of Canada. Proceedings of the 57th Canadian Geotechnical Conference, 5th Joint CGS/IAH-CNC Conference, GeoQuebec2004. Session 3C, pp. 37-41.

Guthrie, R.H., 2005. Geomorphology of Vancouver Island: Mass wasting potential. British Columbia Ministry of Environment, Victoria, British Columbia. Research Report No. RR01, 24 p.

Guthrie, R.H., and Evans, S.G., 2007. Work, persistence, and formative events: The geomorphic impact of landslides. Geomorphology, 88, 266-275.

Hancock, C-A., and Wlodarczyk, K., 2025. The role of wildfires and forest harvesting on geohazards and channel instability during the November 2021 atmospheric river in southwestern British Columbia, Canada. Earth Surface Processes and Landforms, 50, article e6065, 15 p. <https://onlinelibrary.wiley.com/doi/10.1002/esp.6065>

Hensold, G., Stead, D., Clague, J., Moretti, D., and Sturzenegger, M., 2010. Deep-seated gravitational slope deformation at Handcar Peak in the southern Coast Mountains of British Columbia. Proceedings of the GeoCalgary 2010 Conference. pp. 922-931.

Hungr, O., Evans, S.G., and Hazzard, J., 1999. Magnitude and frequency of rock falls and rock slides along the main transportation corridors of southwestern British Columbia. Canadian Geotechnical Journal, 36: 224-238.

Hungr, O., Leroueil, S., and Picarelli, L., 2014. The Varnes classification of landslide types, an update. Landslides, 11, 167-194.

Jordan, P., 2016. Post-wildfire debris flow in southern British Columbia, Canada. International Journal of Wildland Fire, 25, 322-326.

Journeay, J.M., LeSueur, P., Chow, W., and Wagner, C., 2022. Physical exposure to natural hazards in Canada. Geological Survey of Canada Open File 8892, 95 p.

Kinakin, D., and Stead, D., 2005. Analysis of the distributions of stress in natural ridge forms: implications for the deformation mechanisms of rock slopes and the formation of sacking. Geomorphology, 65, 85-100.

Lübker, T., Nitze I., Laboor S., Irrgang A., Lantuit H., and Grosse G., 2024. Presenting land surface changes through the web-based Arctic Landscape EXplorer (ALEX) to permafrost communities-a permafrost service. Proceedings of the International Conference on Permafrost (ICOP 2024), pp. 43-44. <https://epic.awi.de/id/eprint/58864/1/LuebkerEtAl-2024_ICOP-Whitehorse_ALEX.pdf>

NASA, 2025. OPERA Surface Displacement from Sentinel-1 validated product (Version 1) [Data set]. NASA Alaska Satellite Facility Distributed Active Archive Center. <https://doi.org/10.5067/SNWG/OPL3DISPS1-V1 (last accessed December 2025)>

Natural Resources Canada (NRCan), 2024. Pilot national scale maps of active deformation processes in Canada. Government of Canada; Natural Resources Canada; Canada Centre for Mapping and Earth Observation (CCMEO). <https://app.geo.ca/en-ca/map-browser/record/1da588c1-0dc6-45e4-9e63-9acf2fdc353a (last accessed December 2025)>

Panek, T., Mentlik, P., Dichburn, B., Zondervan, A., Norton, K., and Hardecky, J., 2015. Are sackungen diagnostic features of (de) glaciated mountains? Geomorphology, 248, 396-410.

Pichierri, M., Pon, A., Mackenzie, D., Alipour, S., and Guman, P., 2019. A landslide inventory for British Columbia (Canada) using SAR interferometry. American Geophysical Union, Fall Meeting 2019, Abstract H11H-1574.

Porter, M., 2023. Predicting annual displacement probability of slow-moving landslides through Markov chain and Monte Carlo simulation. Proceedings of the 3rd JTC1 Workshop on Impact of Global Changes on Landslide Hazard and Risk, 4 p.

Scheip, C.M., and Wegmann, K.W., 2021. HazMapper: A global open-source natural hazard mapping application in Google Earth Engine. Natural Hazards Earth System Sciences, 21, 1495-1511.

Septer, D., 2007a. Flooding and landslide events, northern British Columbia, 1820-2006. British Columbia Ministry of Environment, 216 p.

Septer, D., 2007b. Flooding and landslide events, southern British Columbia, 1808-2006. British Columbia Ministry of Environment, 140 p.

Strouth, A., and McDougall, S., 2021. Historical landslide fatalities in British Columbia, Canada: Trends and implications for risk management. Frontiers in Earth Science, 9, article 606854, 8 p. <https://doi.org/10.3389/feart.2021.606854>

Varnes, D.J., 1978. Slope movement types and processes. In: Schuster, R.L., and Krizek, R.J., (Eds.), Landslides, Analysis and Control. Transportation Research Board, Special Report 176, pp. 11-33.

Wolfe, S.A., Duchesne, C., O'Neill, H.B., Parker, R.J.H., Young, J.M., Rudy, A.C.A., Steedman, A.E., Lantz, T.C., and Kokelj, S.V., 2025. A database of thermokarst and related landform observations in Canada (1961 to 2024). Geological Survey of Canada, Open File 9296e.

Wu, Y-Y., and Madson, A., 2024. Error sources of interferometric synthetic aperture radar satellites. Remote Sensing, 16, Paper 354, 37 p.

Geoscience knowledge density map of British Columbia, Version 1.0

Peng Zhang[1, a], Marc-André Brideau[1], and Kaleigh Szponarski[2]

[1] British Columbia Geological Survey, Ministry of Mining and Critical Minerals, Victoria, BC, V8W 9N3
[2] British Columbia Geological Survey, Ministry of Mining and Critical Minerals, Cranbrook, BC, V1C 3P9
[a] corresponding author: PengDavid.Zhang@gov.bc.ca

Recommended citation: Zhang, P., Brideau, M-A., and Szponarski, K., 2026. Geoscience Knowledge Density Map of British Columbia, Version 1.0. In: Geological Fieldwork 2025, British Columbia Ministry of Mining and Critical Minerals, British Columbia Geological Survey Paper 2026-01, pp. 247-251.

Abstract

Maps depicting the spatial distribution of geoscience information are of value for establishing information needed for making land-use decisions, planning new projects, mineral potential modelling, and increasing public awareness of geoscience activities. Although the British Columbia Geological Survey, Geological Survey of Canada and Geoscience BC have a long history of generating public geoscience data, geospatial distributions at the province-wide level have not previously been compiled. Grouping datasets into five categories (maps, thematic, geophysical, geochemical and geochronological, and mineral resource), Version 1.0 of the geoscience knowledge density map of British Columbia represents the first iteration. Using a Python script, data were aggregated using an existing 1:5000 map sheet grid to produce category specific density maps along with a cumulative map. Geoscience information is not equally distributed across the province. High information-density zones correspond to regions of extensive exploration and mining activities and corresponding multidisciplinary public geoscience initiatives.

Keywords: Geoscience knowledge density, compilation

1. Introduction

Publicly funded geological surveys generate large amounts of geoscience data and have long histories of releasing these data in print or online. However, with rare exceptions (e.g., Brazil, de Abreu Cunha et al., 2025; Québec, Daubois and Solgadi, 2025; SIGÉOM, 2026), few jurisdictions provide compilations showing the geospatial distribution of these data. Such compilations are valuable for establishing what and where information is needed for making land-use decisions, planning new projects, mineral potential modelling, and increasing public awareness of geoscience activities. For almost 30 years, the public has been able to access bedrock, surficial, and thematic maps, along with geophysical, geochemical, geochronological, mineral deposit, and mineral potential modelling data generated by the British Columbia Geological Survey (BCGS), the Geological Survey of Canada (GSC) and Geoscience BC (GBC) through MapPlace, the BCGS geospatial web service. Nonetheless, a province-wide spatial compilation of these different types of data has hitherto been lacking. This paper introduces a prototype of the first series of geoscience knowledge density maps for British Columbia. These maps display the spatial distribution of map, thematic, geophysical, geochemical, geochronological, and mineral resource information and we include a derivative cumulative density map that provides a first-order characterization of all geoscience information in the province.

2. Methods

Geoscience knowledge density maps only consider the geospatial location of the information, not the information itself. This means that a feature is counted by its location independent of its attribute information (e.g., geological unit, map scale, geochemical concentration, age, mineral occurrence type). Following the structure used by de Abreu Cunha et al. (2025), we organized British Columbia geoscience into five categories: map, thematic, geophysical, geochemical and geochronological, and mineral resource (Table 1). We prioritized geological survey datasets because they are extensive, capture more than 100 years of geoscience knowledge, and are stored in formats that can be readily incorporated into geospatial analysis. In some cases, map footprints were available (e.g., Arnold and Ferbey, 2019) and only needed to be updated for recent work. In other cases, such as for continental Lithoprobe seismic lines, no single compilation existed and digitizing from various sources was required.

After compiling and categorizing publicly accessible datasets, we used the British Columbia Geographical System 1:5000 map sheet grid as the framework to aggregate data occurrences. Extending across the entire province, this represents 109,141 map sheets or cells. Following the approach by Daubois and Solgadi (2025), all data categories were assigned an equal weighting. For points and line features, an item was counted if it was partly or fully present in a grid cell. For polygon features, an intermediate dataset was first generated by identifying areas of overlap and counting the features within them. The intermediate dataset was then overlaid on grid cells and assigned a count based on the value occupying the largest area in the grid cell.

Table 1. Summary of the geoscience information considered for generating Version 1.0 of the geoscience knowledge density map of British Columbia.

Category	Description	Source
Geological maps	Surficial geology map	BCGS, GSC, GBC
	Bedrock geology map	BCGS, GSC, GBC
Thematic geoscience	Mineral potential modelling	BCGS, GSC
	Aggregate potential mapping	BCGS, GSC
	Ice flow indicator	BCGS
	Drift thickness	BCGS, GSC
	Landslide inventory map	BCGS, GSC
	Earthquake hazard map	BCGS, GSC, University of Western Ontario
	Geothermal potential map	BCGS
	Karst potential map	BC Ministry of Forests
Geophysics	Airborne gravity	GSC, GBC
	Airborne magnetic	GSC, GBC
	Borehole geophysics	GSC
	Rock petrophysical properties	GSC, BCGS
	Seismic	GSC
Geochemistry and geochronology	Rock geochemistry	BCGS
	Till geochemistry	BCGS, GBC
	Assessment report-sourced surface-sediment geochemistry	BCGS
	Ash geochemistry	BCGS
	Rock geochemistry	BCGS
	Rock geochronology	BCGS
	Regional geochemistry survey (RGS)	BCGS
Mineral resource	Mineral inventory (MINFILE)	BCGS
	Coal inventory (COALFILE)	BCGS
	Assessment report indexing system (ARIS)	BCGS
	Assessment report-sourced drillhole database	BCGS

A data count was prepared for each information category to produce category-specific density maps, which we then combined to produce a cumulative map. To perform the data aggregation, we developed a Python script using ArcPy and Pandas libraries. Three data classification methods were evaluated: equal intervals, natural breaks, and geometric intervals. Given the skewed distribution of knowledge density, we considered the geometric intervals approach to be the most informative for distinguishing between areas with low, moderate, and high knowledge density. For geoscience knowledge categories where several grid cells had a low (<2) knowledge density, the lowest classification category was manually set to 0 to create a distinction between low and no information available.

3. Results

The geoscience knowledge density maps (Figs. 1, 2) provide easy-to-understand representations of where and what types of geoscience data are available across the province. The geochemical and geochronology category (Fig. 1d) has the highest knowledge density because it includes 86,000 rock geochemistry sample locations, 65,000 regional geochemistry survey locations, 10,000 till geochemistry sample locations, and the location of 8700 samples with age determinations. Cumulative geoscience information is not equally distributed (Fig. 2), with high-density areas in the south-central and northwestern parts of the province related to past and current intensive mining and exploration activities and in the East Kootenay and Peace River coalfields of the Rocky Mountains.

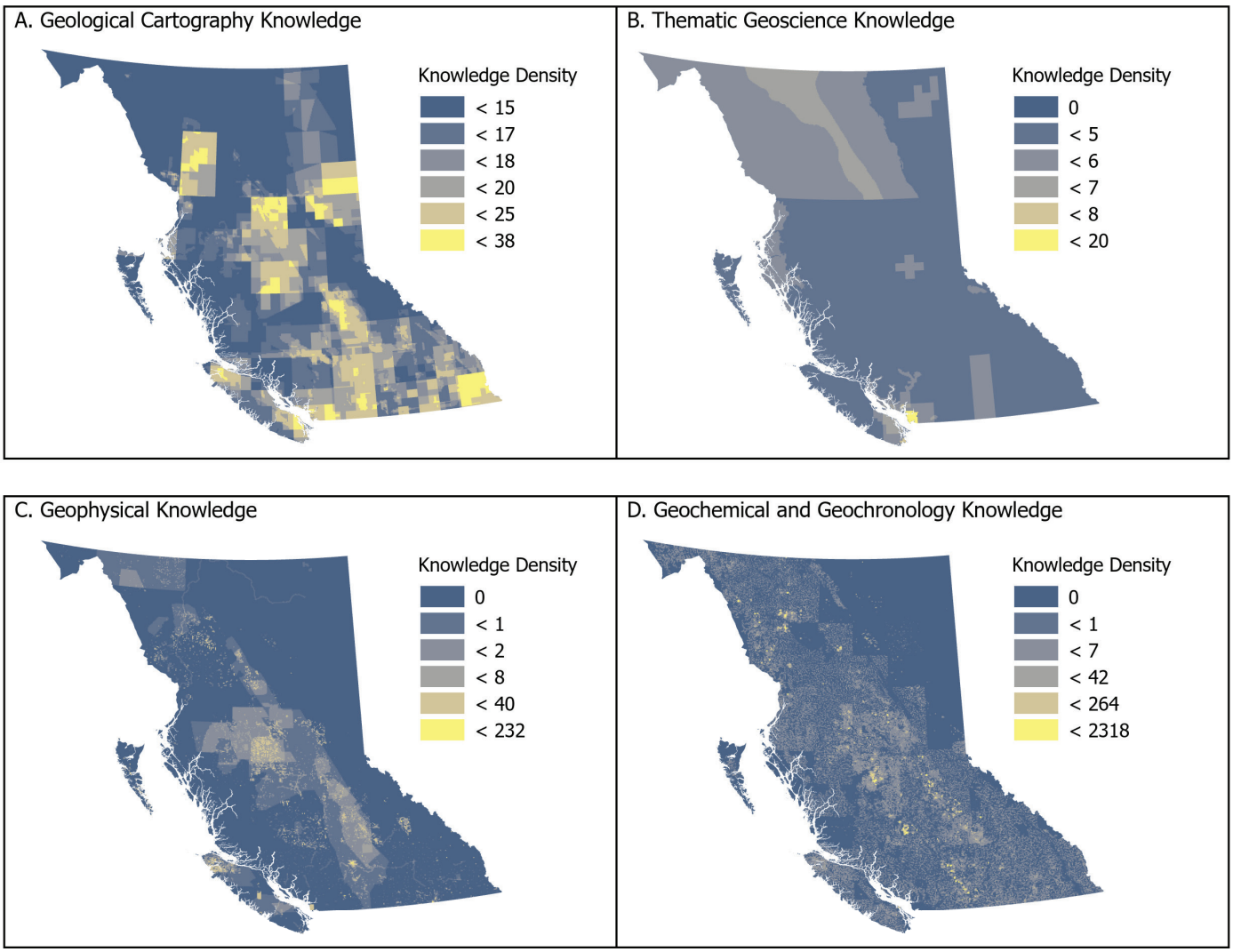


Fig. 1. Geoscience knowledge density map for five data categories. The knowledge density scale refers to the number data occurrences per 1:5000 grid cell using a geometric interval classification.

4. Discussion: applications and limitations

The knowledge maps can be used in planning exercises to identify priority areas for future work. They can also be used to help interpret mineral potential modelling maps (e.g., Wearmouth et al., 2024) and establish if an area appears to have low mineral potential because knowledge is limited. Both maps can be used in engagement and outreach activities to demonstrate the different types of geoscience information available and their distribution.

Limitations of Version 1.0 include lack of comprehensive sourcing, information overlap, and indiscriminate weighting. First, the focus for the initial maps was on geoscience generated by geological surveys and in accessible databases. Sources not currently incorporated include BCGS paper publications, scientific journal publications, and university theses because spatial compilations of these discrete geoscience contributions are lacking. For example, approximately 2600 BCGS publications other than maps are currently undergoing footprint

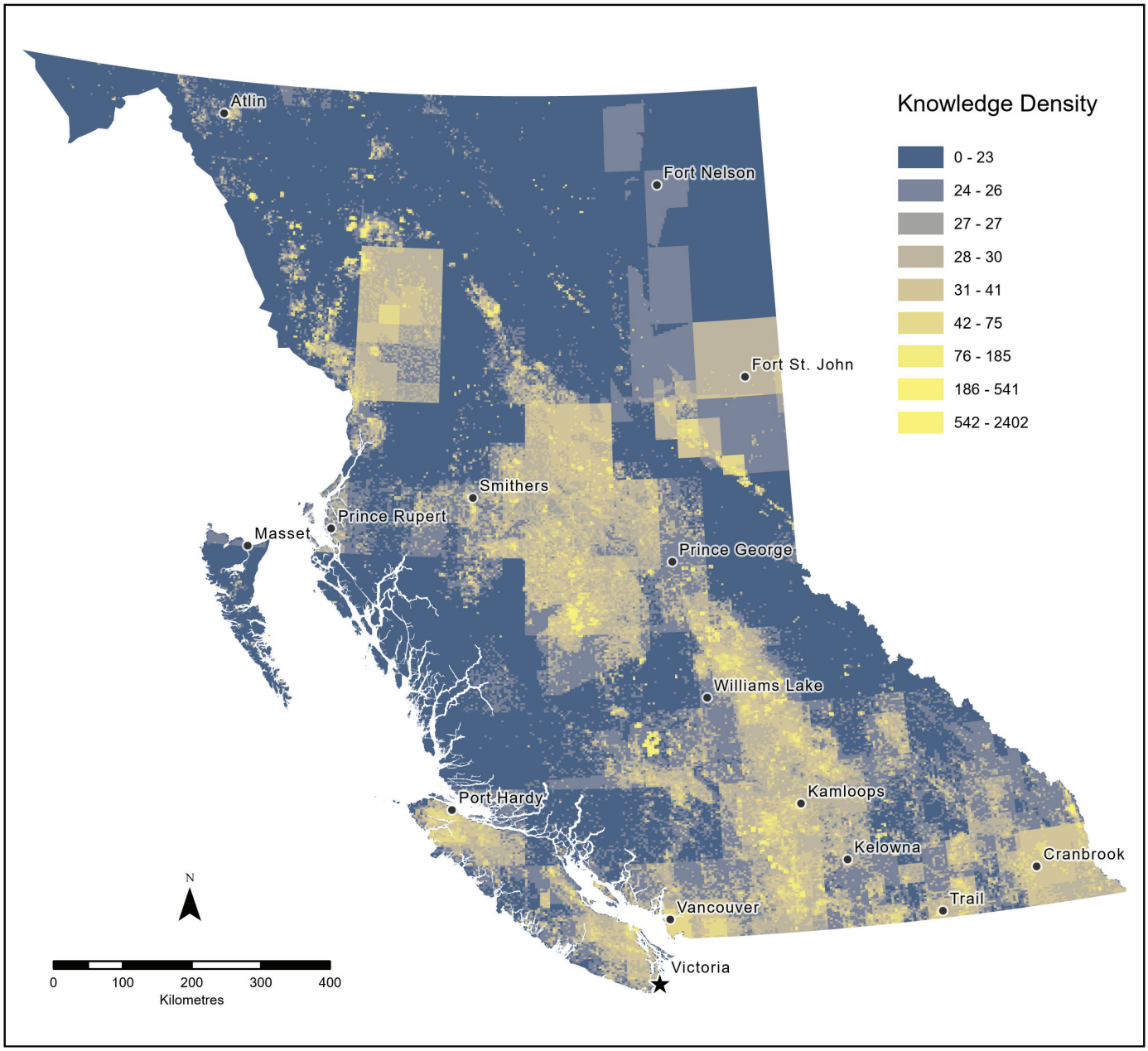


Fig. 2. Version 1.0 of the geoscience knowledge density map for British Columbia. This map is the cumulative version of the five categories shown in Figure 1. The knowledge density scale refers to the number of data occurrences per 1:5000 grid cell using a geometric interval classification.

digitization. Furthermore, much geological, geochemical, and geophysical data from exploration and mining companies is privately held. Moreover, Version 1.0 does not include any data from oil and gas companies held by the British Columbia Energy Regulator (BCER); if these data were included, the knowledge density in the northeastern part of the province would increase dramatically. Second, considerable overlap between the datasets was noted during the compilation of information from different sources. For example, Assessment Report Indexing System reports are represented by a single point location in the mineral resources knowledge category, but data from these reports are also included as separate surface-sediment geochemistry sample points (Norris and Fortin, 2019) or drill hole location points (Fortin and Silva, 2025). Although efforts were made to reconcile such overlaps, some may persist, potentially skewing knowledge density in some areas. Third, we did not discriminate weighting between and within categories; a point occurrence is given the same weight as a polygon representing a study area. This has potential to skew density on the maps toward point data such as in the case of geochemical or geochronological point data in a single map area.

5. Future work

There are many opportunities to expand and improve on Version 1.0. Current plans for the next version include incorporating additional datasets such as the provincial groundwater wells database, which contains approximately 130,000 entries with information about the type and thickness of surficial geology units and depth to bedrock (British Columbia Ministry of Water, Land and Resource Stewardship, 2026), the British Columbia Energy Regulator well database (2026), which contains approximately 39,000 entries with geological and production information, and the footprints for BCGS publications other than maps. Future work could also consider varied weighting for the different datasets. For example, a map that represents the compilation and interpretation of multiple data sources (desktop, field, laboratory) could have a higher weighting than a single geochemical sample point. Similarly, different weighting could be applied to map footprints based on their scale.

6. Conclusion

This study represents the first attempt in understanding the spatial distribution of geological information in British Columbia. Version 1.0 of the geoscience knowledge density map illustrates the spatial distribution of publicly accessible geoscience data generated by BCGS, GSC and GBC. High information-density zones correspond to areas of extensive exploration and mining activities and corresponding large multidisciplinary public geoscience programs. Future versions could be improved by incorporating additional datasets, further eliminating overlapping entries, and developing a weighting formula that accounts for data sources and geometry.

Acknowledgments

This project benefited from discussions with Travis Ferbey, Bram van Straaten, Luke Ootes, Jessica Norris, Gabe Fortin, and Adrian Hickin of the British Columbia Geological Survey along with Étienne Girard and Nathan Hayward of the Geological Survey of Canada. Constructive comments by Adrian Hickin helped improve the paper.

References cited

Arnold, H., and Ferbey, T., 2019. British Columbia surficial geology map index. British Columbia Ministry of Mining and Critical Minerals, British Columbia Geological Survey Open File 2019-03 version 2020-01.

British Columbia Energy Regulator (BCER), 2026. Data centre. <https://www.bc-er.ca/data-reports/data-centre/> (last accessed February 2026).

British Columbia Ministry of Water, Land and Resource Stewardship (WLRS), 2026. British Columbia groundwater wells and aquifer. <https://apps.nrs.gov.bc.ca/gwells/> (last accessed February 2026).

de Abreu Cunha, I., de Almeida, R.C., Brod, E.R., de Souza Santos, N.P., Cabral-Neto, I., Queiroz, L., Ferreira da Silva, G., Rodrigues da Silva, A.D., de Souza Gaia, S.M., Justo, A.P., Rodrigues da Silva, A.D., de Rezende, E.S., Uchoa, E., Costa, F.G., Lages, G.A., de Oliviera Polo, H.J., Costa, I., Santana, J., de Sales Macedo Carneiro, J., Cunha, L.M., Takehara, L., Motta, M., Almeida, M.E., Ferreira, M., Santos, M.E.M., Maurutto, P.C., Lima, R.B., Silva dos Santos, R.L.M., Loreti, R., Cavalcante, R., Abdallah, S., Guimaraes, S.B., Manfredi, T.R., de Castro Paes, V.J., and Abram, M.B., 2025. An overview of critical minerals and potential of Brazil, 2025 Edition. <https://rigeo.sgb.gov.br/handle/doc/25452>

Daubois, V., and Solgadi, F., 2025. Two decades of mineral potential modelling in Québec: Geoscientific knowledge at the core of Géologie Québec's work. In: Pan-Canadian workshop on mineral potential modelling, September 23, 2025, program with extended abstracts. British Columbia Ministry of Mining and Critical Minerals, British Columbia Geological Survey GeoFile 2025-24, pp. 20-23.

Fortin, G., and Silva, P.L., 2025. Assessment report drillhole database: Development and initial data release. British Columbia Ministry of Mining and Critical Minerals, British Columbia Geological Survey GeoFile 2025-11, 9 p.

Norris, J., and Fortin, G., 2019. Assessment report-sourced surface sediment geochemical database: Development and initial data release from the Interior Plateau. British Columbia Ministry of Energy, Mines and Petroleum Resources, British Columbia Geological Survey GeoFile 2019-04, 10 p.

SIGÉOM, 2026. Système d'information géominière-carte interactive. Ministère des Ressources nature et des Forêts. <https://sigeom.mines.gouv.qc.ca/signet/classes/I1108_afchCarteIntr?l=F> (last accessed February 2026).

Wearmouth, C.D., Peters, K.J., Czertowicz, T.A., and Orovan, E.A., 2024. Mineral potential modelling results for northwestern British Columbia, a comparison between past and current work at the British Columbia Geological Survey. In: Geological Fieldwork 2023, British Columbia Ministry of Energy, Mines and Low Carbon Innovation, British Columbia Geological Survey Paper 2024-01, pp. 79-95.

British Columbia Geological Survey Publications 2025
including peer-reviewed external papers co-authored by BCGS staff

All BCGS publications are available for download, free of charge, from www.BCGeologicalSurvey.ca

To receive notification of our latest releases email Geological.Survey@gov.bc.ca



Papers

Geological Fieldwork 2024. British Columbia Ministry of Mining and Critical Minerals, British Columbia Geological Survey Paper 2025-01, 207 p.

Hickin, A.S., Cui, Y., Clarke, G., Ootes, L., and van Straaten, B.I., 2025. British Columbia Geological Survey annual program review 2024-2025. In: Geological Fieldwork 2024, British Columbia Ministry of Mining and Critical Minerals, British Columbia Geological Survey Paper 2025-01, pp. 1-15.

Miller, E.A., Ferri, M.D., van Straaten, B.I., and Wall, C., 2025. Stratigraphic framework, structural setting, and timing of VMS, epithermal, and porphyry mineralization in the Kitsault River area, northwest British Columbia. In: Geological Fieldwork 2024, British Columbia Ministry of Mining and Critical Minerals, British Columbia Geological Survey Paper 2025-01, pp. 17-47.

Campbell, R.W., and van Straaten, B.I., 2025. New data on Late Triassic to late Early Jurassic plutonic suites in the northern Golden Triangle region of northwest British Columbia. In: Geological Fieldwork 2024, British Columbia Ministry of Mining and Critical Minerals, British Columbia Geological Survey Paper 2025-01, pp. 49-72.

Orovan, E.A., Ebert, S., Baldazzi, P., Saxton, D., and Goudie, D.J., 2025. Critical minerals at the Berg and Huckleberry porphyry deposits, British Columbia, using scanning electron microscropy-mineral liberation analysis (SEM-MLA). In: Geological Fieldwork 2024, British Columbia Ministry of Mining and Critical Minerals, British Columbia Geological Survey Paper 2025-01, pp. 73-84.

Wang, X., Jiao, R., and Ootes, L., 2025. Apatite fission track data from northern Hogem batholith, Quesnel terrane, north-central British Columbia: A progress report. In: Geological Fieldwork 2024, British Columbia Ministry of Mining and Critical Minerals, British Columbia Geological Survey Paper 2025-01, pp. 85-91.

Morris, R., Canil, D., and Lacourse, T., 2025. An optimized rapid analytical workflow for applying magnetite as an indicator mineral for porphyry copper deposits. In: Geological Fieldwork 2024, British Columbia Ministry of Mining and Critical Minerals, British Columbia Geological Survey Paper 2025-01, pp. 93-103.

Mihalynuk, M.G., Wall, C., and Zagorevski, A., 2025. Time of deposition refinements for key stratigraphic intervals of the Nicola Group, southern British Columbia. In: Geological Fieldwork 2024, British Columbia Ministry of Mining and Critical Minerals, British Columbia Geological Survey Paper 2025-01, pp. 105-118.

Rukhlov, A.S., Ootes, L., Creaser, R.A., Cunningham, Q.F., de Waal, F.S., and Wenger, D.K., 2025. British Columbia carbonatites revisited: New whole rock Sr-Pb-Nd isotopic insights and drainage prospectivity trends. In: Geological Fieldwork 2024, British Columbia Ministry of Mining and Critical Minerals, British Columbia Geological Survey Paper 2025-01, pp. 119-139.

Graham, A.C., Wearmouth, C.D., Northcote, B., and Ootes, L., 2025. A preliminary assessment of critical companion elements in SEDEX deposits of eastern British Columbia: Examples from the historic Sullivan mine and the Cirque project. In: Geological Fieldwork 2024, British Columbia Ministry of Mining and Critical Minerals, British Columbia Geological Survey Paper 2025-01, pp. 141-152.

Bain, W.M., de Waal, F., and Goudie, D.J., 2025. Co-Te mineralization in iron skarns on Vancouver Island and Texada Island. In: Geological Fieldwork 2024, British Columbia Ministry of Mining and Critical Minerals, British Columbia Geological Survey Paper 2025-01, pp. 153-175.

Rukhlov, A.S., Ootes, L., and Han, T., 2025. British Columbia radiogenic isotope compilation (Sr-Nd-Hf-Pb): Introduction and examples of utility. In: Geological Fieldwork 2024, British Columbia Ministry of Mining and Critical Minerals, British Columbia Geological Survey Paper 2025-01, pp. 177-188.

Piercey, S.J., Pietruszka, D., and Goudie, D., 2025. Critical metals in volcanogenic massive sulphide (VMS) deposits in British Columbia: A progress report. In: Geological Fieldwork 2024, British Columbia Ministry of Mining and Critical Minerals, British Columbia Geological Survey Paper 2025-01, pp. 189-201.

Appendix: British Columbia Geological Survey Publications 2024, including peer-reviewed external papers co-authored by BCGS staff, pp. 203-207.

Wearmouth, C., Czertowicz, T.A., Peters, K.J., and Orovan, E., 2024. Mineral potential modelling at the British Columbia Geological Survey: Renewed methods with application to northwestern British Columbia. British Columbia Ministry of Energy, Mines and Low Carbon Innovation, British Columbia Geological Survey Paper 2024-02, 28 p.

Geoscience Maps

Sauvé, M., Ward, B., and Ferbey, T., 2025. Surficial geology of the Kinaskan Lake area, British Columbia (parts of NTS 104G/08, 09, 16, and 104H/12, 13). British Columbia Ministry of Mining and Critical Minerals, British Columbia Geological Survey Geoscience Map 2025-01, 1:50,000 scale.

Ferbey, T., and Elia, E.A., 2025a. Surficial geology of the Nanitsch Lake area (NTS 94D/1), British Columbia. British Columbia Ministry of Mining and Critical Minerals, British Columbia Geological Survey Geoscience Map 2025-02, 1:50,000 scale.

Ferbey, T., and Elia, E.A., 2025b. Surficial geology of the Carruthers Pass area (NTS 94D/8), British Columbia. British Columbia Ministry of Mining and Critical Minerals, British Columbia Geological Survey Geoscience Map 2025-03, 1:50,000 scale.

Open Files

Mihalynuk, M.G., Zagorevski, A., Campbell, R.W., Vaillancourt, A., and Haji Egeh, A., 2024. Geology of the western Gladys Lake area (NTS 104N/13E, 14). British Columbia Ministry of Mining and Critical Minerals, British Columbia Geological Survey Open File 2024-02, 1:50,000 scale.

Wearmouth, C., Czertowicz, T.A., Peters, K.J., and Orovan, E., 2024. Preliminary mineral potential maps for the porphyry, volcanic massive sulphide, and magmatic mafic-ultramafic mineral systems, northwestern British Columbia. British Columbia Ministry of Energy, Mines and Low Carbon Innovation, British Columbia Geological Survey Open File 2024-05, 1:800,000 scale.

Wearmouth, C., Czertowicz, T.A., and Peters, K.J., 2024. Preliminary mineral potential maps for the SEDEX and MVT mineral systems, northeastern British Columbia. British Columbia Ministry of Energy, Mines and Low Carbon Innovation, British Columbia Geological Survey Open File 2024-11, 1:500,000 scale.

Clarke, G., Northcote, B.K., Corcoran, N.L., Pothorin, C., Heidarian, H., and Hancock, K., 2025. Mines, mine development, selected proposed mines, and selected exploration projects in British Columbia, 2024. British Columbia Ministry of Mining and Critical Minerals, British Columbia Geological Survey Open File 2025-01.

Höy, T., and DeFields, G.M., 2025. Geology of the Lightning Peak map area (NTS 082E/15). British Columbia Ministry of Mining and Critical Minerals, British Columbia Geological Survey Open File 2025-02, 1:50,000 scale.

GeoFiles

Clarke, G., Northcote, B.K., Corcoran, N.L., Pothorin, C., Heidarian, H., and Hancock, K., 2025. Exploration and Mining in British Columbia, 2024. British Columbia Ministry of Mining and Critical Minerals, British Columbia Geological Survey GeoFile 2025-01 (poster).

Corcoran, N.L., 2025. Exploration and mining highlights, Northwest Region, 2024. British Columbia Ministry of Mining and Critical Minerals, British Columbia Geological Survey GeoFile 2025-02 (poster).

Heidarian, H., 2025. Exploration and mining highlights, North Central and Northeast regions, 2024. British Columbia Ministry of Mining and Critical Minerals, British Columbia Geological Survey GeoFile 2025-03 (poster).

Pothorin, C., 2025. Exploration and mining highlights, South Central Region, 2024. British Columbia Ministry of Mining and Critical Minerals, British Columbia Geological Survey GeoFile 2025-04 (poster).

Hancock, K., 2025. Exploration and mining highlights, Southeast Region, 2024. British Columbia Ministry of Mining and Critical Minerals, British Columbia Geological Survey GeoFile 2025-05 (poster).

Northcote, B.K., 2025. Exploration and mining highlights, Southwest Region, 2024. British Columbia Ministry of Mining and Critical Minerals, British Columbia Geological Survey GeoFile 2025-06 (poster).

Wallace, B., Grundy, R., and Harrison, D., 2025. Assessment report summary: Expenditures and activities 2022. British Columbia Ministry of Mining and Critical Minerals, British Columbia Geological Survey GeoFile 2025-07 (poster).

British Columbia Geological Survey, 2025. British Columbia radiogenic isotope compilation (Sr-Nd-Hf-Pb). British Columbia Ministry of Mining and Critical Minerals, British Columbia Geological Survey GeoFile 2025-08, 1 p.

Rukhlov, A.S., Ootes, L., Creaser, R.A., Cunningham, Q.F., de Waal, F.S., and Wenger, D.K., 2025. Supplementary data for British Columbia carbonatites revisited: New whole rock Sr-Pb-Nd isotopic insights and drainage prospectivity trends. British Columbia Ministry of Mining and Critical Minerals, British Columbia Geological Survey GeoFile 2025-09, 4 p.

Morris, R., Canil, D., and Lacourse, T., 2025. LA-ICP-MS data files for optimized workflow analyses and reproducibility of hydrothermal magnetite as an indicator for porphyry copper deposits. British Columbia Ministry of Mining and Critical Minerals, British Columbia Geological Survey GeoFile 2025-10, 1 p.

Fortin, G., and Silva, P.L., 2025. Assessment report drillhole database: Development and initial data release. British Columbia Ministry of Mining and Critical Minerals, British Columbia Geological Survey GeoFile 2025-11, 9 p.

Piercey, S.J., 2025. Assay data for volcanogenic massive sulfide (VMS) deposit samples from British Columbia. British Columbia Ministry of Mining and Critical Minerals, British Columbia Geological Survey GeoFile 2025-12, 3 p.

Graham, A.C., and Ootes, L., 2025. Geochemical analyses of SEDEX deposits in eastern British Columbia. British Columbia Ministry of Mining and Critical Minerals, British Columbia Geological Survey GeoFile 2025-13, 9 p.

Bailey, L., Kim, R., Takaichi, M., Logan, J., Crowley, J., Friedman, R., Wall, C., van Straaten, B.I., and Campbell, R., 2025. U-Pb geochronological data for intrusive rocks near the Schaft Creek and Galore Creek deposits (southern Telegraph Creek area, NTS 104G), northwestern British Columbia. British Columbia Ministry of Mining and Critical Minerals, British Columbia Geological Survey GeoFile 2025-14, 16 p.

Mihalynuk, M.G., Friedman, R.M., and Wall, C., 2025. U-Pb geochronologic data from samples collected as part of the Southern Nicola Arc Project. British Columbia Ministry of Mining and Critical Minerals, British Columbia Geological Survey GeoFile 2025-15, 7 p.

Gabites, J.E., and Mihalynuk, M.G., 2025. $^{40}Ar/^{39}Ar$ geochronologic data from samples collected as part of the Southern Nicola Arc Project. British Columbia Ministry of Mining and Critical Minerals, British Columbia Geological Survey GeoFile 2025-16, 9 p.

Cordey, F., Zagorevski, A., and Mihalynuk, M.G., 2025. Report on samples collected for radiolaria identification, Atlin area, northwest British Columbia. British Columbia Ministry of Mining and Critical Minerals, British Columbia Geological Survey GeoFile 2025-17, 3 p.

Mihalynuk, M.G., Wall, C., and Zagorevski, A., 2025. Volcanic evolution and refinement of stratigraphy hosting porphyry systems in the southern Nicola arc. British Columbia Ministry of Mining and Critical Minerals, British Columbia Geological Survey GeoFile 2025-18 (poster).

Northcote, B.K., 2025. Sedimentary hosted lead-zinc deposits in British Columbia. British Columbia Ministry of Mining and Critical Minerals, British Columbia Geological Survey GeoFile 2025-19, 23 p.

Miller, E.A., van Straaten, B.I., Ferri, M.D., and Hunter, R., 2025. Preliminary bedrock geology of the Kitsault River area, northwestern British Columbia: GIS data. British Columbia Ministry of Mining and Critical Minerals, British Columbia Geological Survey GeoFile 2025-20, 3 p.

Miller, E.A., Ferri, M.D., Wall, C., Creaser, R.A., van Straaten, B.I., and Graham, A.C., 2025. New geochronologic data, Kitsault River area, northwestern British Columbia: Igneous zircons (high-precision CA-TIMS), detrital zircons (LA-ICP-MS), and molybdenite (Re-Os). British Columbia Ministry of Mining and Critical Minerals, British Columbia Geological Survey GeoFile 2025-21, 6 p.

Bacha, R.R.B., 2025. Field trip guidebook to the geology near Merritt, south-central British Columbia, for the Citxw Nlaka'pamux Assembly. British Columbia Ministry of Mining and Critical Minerals, British Columbia Geological Survey GeoFile 2025-22, 14 p.

Graham, A.C., Orovan, E., Wall, C., Goudie, D., Creaser, R., Layton-Matthews, D., and Ootes, L., 2025. Data release from critical mineral studies of the Kitsault, Huckleberry, and Berg porphyry deposits. British Columbia Ministry of Mining and Critical Minerals, British Columbia Geological Survey GeoFile 2025-23, 7 p.

British Columbia Geological Survey, 2025. Pan-Canadian workshop on mineral potential modelling, September 23, 2025, program with extended abstracts. British Columbia Geological Survey GeoFile 2025-24, 37 p.

Information Circulars

Clarke, G., Northcote, B.K., Corcoran, N.L., Pothorin, C., Heidarian, H., and Hancock, K., 2025. Provincial Overview of Exploration and Mining in British Columbia, 2024. British Columbia Ministry of Mining and Critical Minerals, British Columbia Geological Survey Information Circular 2025-01, 170 p.

Clarke, G., Northcote, B.K, Corcoran, N.L., Pothorin C., Heidarian, H., and Hancock, K., 2025. Exploration and Mining in British Columbia, 2024: A summary. In: Provincial Overview of Exploration and Mining in British Columbia, 2024. British Columbia Ministry of Mining and Critical Minerals, British Columbia Geological Survey Information Circular 2025-01, pp. 1-60.

Corcoran, N., 2025. Exploration and mining in the Northwest Region, British Columbia. In: Provincial Overview of Exploration and Mining in British Columbia, 2024. British Columbia Ministry of Mining and Critical Minerals, British Columbia Geological Survey Information Circular 2025-01, pp. 61-91.

Heidarian, H., 2025. Exploration and mining in the North Central and Northeast regions, British Columbia. In: Provincial Overview of Exploration and Mining in British Columbia, 2024. British Columbia Ministry of Mining and Critical Minerals, British Columbia Geological Survey Information Circular 2025-01, pp. 93-113.

Pothorin, C., 2025. Exploration and mining in the South Central Region, British Columbia. In: Provincial Overview of Exploration and Mining in British Columbia, 2024. British Columbia Ministry of Mining and Critical Minerals, British Columbia Geological Survey Information Circular 2025-01, pp. 115-143.

Hancock, K., 2025. Exploration and mining in the Southeast Region, British Columbia. In: Provincial Overview of Exploration and Mining in British Columbia, 2024. British Columbia Ministry of Mining and Critical Minerals, British Columbia Geological Survey Information Circular 2025-01, pp. 145-156.

Northcote, B.K., 2025. Exploration and mining in the Southwest Region, British Columbia. In: Provincial Overview of Exploration and Mining in British Columbia, 2024. British Columbia Ministry of Mining and Critical Minerals, British Columbia Geological Survey Information Circular 2025-01, pp. 157-170.

British Columbia Geological Survey, 2025. British Columbia Geological Survey. British Columbia Ministry of Mining and Critical Minerals, British Columbia Geological Survey Information Circular 2025-02, 14 p. (brochure)

British Columbia Geological Survey, 2025. Mineral Development Office. British Columbia Ministry of Mining and Critical Minerals, British Columbia Geological Survey Information Circular 2025-03, 4 p. (brochure)

British Columbia Geological Survey, 2025. Online databases at the British Columbia Geological Survey. British Columbia Ministry of Mining and Critical Minerals, British Columbia Geological Survey Information Circular 2025-04, 14 p. (brochure)

British Columbia Geological Survey, 2025. Geoscience engagement at the British Columbia Geological Survey. British Columbia Ministry of Mining and Critical Minerals, British Columbia Geological Survey Information Circular 2025-05, 4 p. (brochure)

British Columbia Geological Survey, 2025. Critical minerals research at the British Columbia Geological Survey. British Columbia Ministry of Mining and Critical Minerals, British Columbia Geological Survey Information Circular 2025-06, 4 p. (brochure)

British Columbia Geological Survey, 2025. Mineral potential modelling at the British Columbia Geological Survey. British Columbia Ministry of Mining and Critical Minerals, British Columbia Geological Survey Information Circular 2025-07, 4 p. (brochure)

British Columbia Geological Survey, 2025. British Columbia Geological Survey publications, 2020 to 2024. British Columbia Ministry of Mining and Critical Minerals, British Columbia Geological Survey Information Circular 2025-08, 8 p. (brochure)

British Columbia Geological Survey, 2025. High-resolution aeromagnetic compilations of British Columbia. British Columbia Ministry of Mining and Critical Minerals, British Columbia Geological Survey Information Circular 2025-09, 2 p. (brochure)

British Columbia Geological Survey, 2025. Tahltan Land Use Planning area mineral potential map for porphyry, volcanogenic massive sulphide (VMS), and magmatic mafic-ultramafic deposits. British Columbia Ministry of Mining and Critical Minerals, British Columbia Geological Survey Information Circular 2025-10, 2 p.

British Columbia Geological Survey, 2025. Kaska Land Use Planning area mineral potential map for porphyry, volcanogenic massive sulphide (VMS), magmatic mafic-ultramafic, sedimentary exhalative (SEDEX) and Mississippi Valley Type (MVT) deposits. British Columbia Ministry of Mining and Critical Minerals, British Columbia Geological Survey Information Circular 2025-11, 2 p.

British Columbia Geological Survey, 2025. Meziadin Land Use Planning area mineral potential map for porphyry, volcanogenic massive sulphide (VMS), and magmatic mafic-ultramafic deposits. British Columbia Ministry of Mining and Critical Minerals, British Columbia Geological Survey Information Circular 2025-12, 2 p.

British Columbia Geological Survey, 2025. TRT Land Use Planning area mineral potential map for porphyry, volcanogenic massive sulphide (VMS), and magmatic mafic-ultramafic deposits. British Columbia Ministry of Mining and Critical Minerals, British Columbia Geological Survey Information Circular 2025-13, 2 p.

External peer-reviewed journal and volume publications

Abazu, G., Brook, M.S., Druskovich, B., Brideau, M.-A., and Hayward, B.W., 2025. Rainfall-triggered landslides from the January 2023 1-in-200 year storm at Maungakiekie/One Tree Hill, Auckland, New Zealand. New Zealand Journal of Geology and Geophysics, 68, 1049-1063.
<https://doi.org/10.1080/00288306.2025.2479699>

Abdale, L., Millonig, L., Nelson, J., Groat, L.A., and Gerdes, A., 2025. Temporal evolution of enriched mantle sources in the southeastern Canadian Cordillera revealed by zircon geochronology and Hf isotopes in carbonatites. Chemical Geology, 695, article 123044.
<https://doi.org/10.1016/j.chemgeo.2025.123044>

Hardman, M.F., Pearson, D.G., DuFrane, S.A., Cabral-Neto, I., Azzone, R.G., Shu, Q., Hinde, J., and Rukhlov, A.S., 2025. Improved trace element discrimination of kimberlitic and carbonatitic zircon: implications for zircon origin in kimberlite and the search for superdeep diamonds. Mineralogy and Petrology, 119, 583-605.
<https://doi.org/10.1007/s00710-025-00916-2>

Heidarian, H., Lentz, D.R., Thorne, K.G., and McFarlane, C.R.M., 2025. Mineralogy, geochronology, and stable isotope geochemistry of gold mineralization in the Belleisle Bay and Annidale groups, southwestern New Brunswick, Canada. Ore Geology Reviews, 186, article 106899.
<https://doi.org/10.1016/j.oregeorev.2025.106899>

Orchard, M.J., Friedman, R.M., and Mihalynuk, M.G., 2025. Conodonts identify the lower-middle Norian boundary in association with ~224 Ma U-Pb dates from the Nicola Group, southern British Columbia, Canada. Journal of the Geological Society, 182.
<https://doi.org/10.1144/jgs2024-299>

Lawley, C.J.M., Petts, D.C., Lee, W.-S., Cajal, Y., Carrasco-Godoy, C., Campbell, I., Dlugosz, J., Larson, K., Savard, D., Kjarsgaard, I., and van Straaten, B., 2025. Critical raw material potential of porphyry copper-gold deposits in the Golden Triangle, British Columbia, Canada, Ore Geology Reviews, 178, article 106463.
<https://doi.org/10.1016/j.oregeorev.2025.106463>

Lockie, J., Ielpi, A., Canam, R., Perrot, M.G., Davies, J.H.F.L., and Ootes, L., 2025. Orogenic unroofing of the Taltson and Thelon orogens depicted through detrital zircon geochronology of the Sosan Group, Great Slave Lake Supergroup (Northwest Territories, Canada). Precambrian Research, 419, article 107706.
<https://doi.org/10.1016/j.precamres.2025.107706>

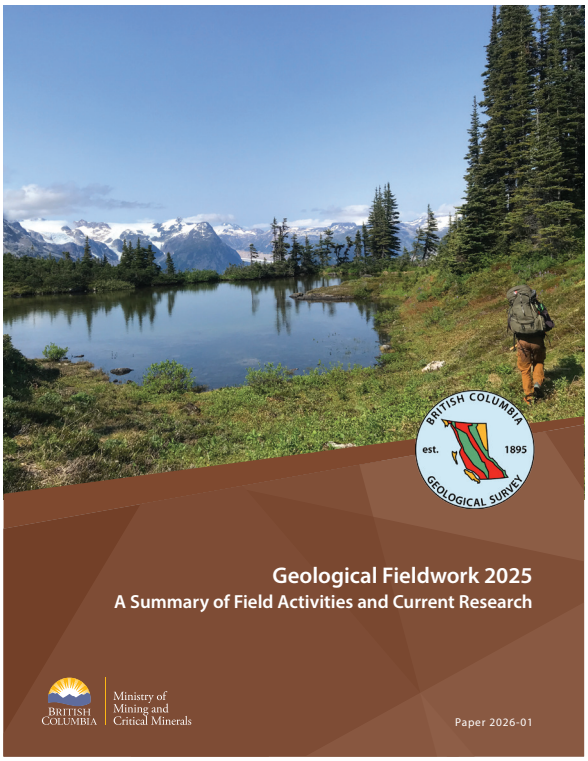
Mashyanov, N.R., Rukhlov, A.S., Sholupov, S.E., Ryzhov, V.V., Shashko, A.D., Perkins, E., and Barnes, W., 2025. New methodology for air mercury surveys over mineralization. Explore, 208, 1-19.
<https://doi.org/10.70499/ZXZS8433>

Contributions to partner publications

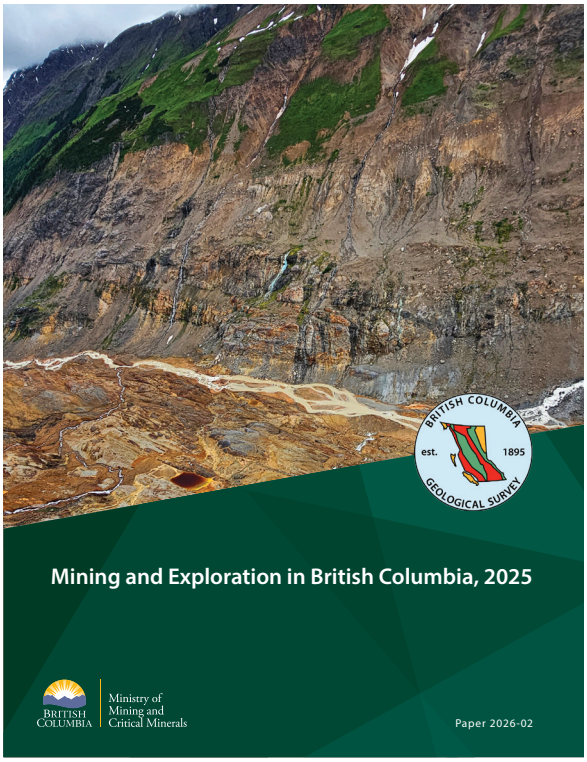
Abdale, L., Nelson, J.L., Millonig, L.J., and Groat, L.A., 2025. Preliminary insights into carbonatite genesis, and future directions using uranium-lead zircon ages and hafnium isotopic signatures of alkaline rocks from the Canadian Cordillera, southeastern British Columbia. In: Geoscience BC Summary of Activities 2024, Geoscience BC, Report 2025-01, pp. 47-56.

Brideau, M.-A., Brayshaw, D., Hancock, C.-A., Lipovsky, P., Cronmiller, D., Lewkowicz, A., Geertsema, M., McGregor, C., Tannant, D., Friele, P., Clarke, J., Steelquist, A., Wong-Teichroeb, H., Ring, C., and Wells, G., 2025. Preliminary Canadian landslide database (13.0), Zenodo dataset.
<https://doi.org/10.5281/zenodo.17219072>

Each year, the British Columbia Geological Survey publishes Geological Fieldwork, a Summary of Fieldwork and Current Research (this volume), and Mining and Exploration in British Columbia. All British Columbia Geological Survey publications can be downloaded, at no cost, from www.BCGeologicalSurvey.ca



Geological Fieldwork volume, British Columbia Geological Survey Paper 2026-01



Mining and Exploration in British Columbia volume, British Columbia Geological Survey Paper 2026-02



BRITISH COLUMBIA

Ministry of Mining and Critical Minerals

BRITISH COLUMBIA est. 1895 GEOLOGICAL SURVEY